DASA-1259

CIVIL ENGINEERING STUDIES
STRUCTURAL RESEARCH SERIES NO. 243

INVESTIGATION OF RESISTANCE AND BEHAVIOR OF REINFORCED CONCRETE MEMBERS SUBJECTED TO DYNAMIC LOADING
PART III

by
A. Feldman
W. A. Keenan
C. P. Siess

A Technical Report to
THE OFFICE OF THE CHIEF OF ENGINEERS
DEPARTMENT OF THE ARMY
Contract DA 49-129-Eng-344

This Research was Sponsored by the
DEFENSE ATOMIC SUPPORT AGENCY

1 FEBRUARY 1962
UNIVERSITY OF ILLINOIS
URBANA, ILLINOIS

DASA-1259

INVESTIGATION OF RESISTANCE AND BEHAVIOR OF REINFORCED CONCRETE MEMBERS SUBJECTED TO DYNAMIC LOADING

PART III

By

A. Feldman

W. A. Keenan

C. P. Siess

A Technical Report to

THE OFFICE OF THE CHIEF OF ENGINEERS
DEPARTMENT OF THE ARMY

Contract DA 49-129-Eng-344

This Research was Sponsored by the
DEFENSE ATOMIC SUPPORT AGENCY

1 February 1962

University of Illinois

Urbana, Illinois

TABLE OF CONTENTS
of
INVESTIGATION OF RESISTANCE AND BEHAVIOR OF REINFORCED CONCRETE MEMBERS SUBJECTED TO DYNAMIC LOADING-PART III

(Final Report on Contract DA-49-129-Eng 344)

LIST OF TABLES

LIST OF FIGURES

APPENDIX FIGURES

FIGURES A1-A34, LOAD AND STRAIN VS. TIME AND LOAD VS. STRAIN FOR BAR SPECIMENS

FIGURES A37-A72, LOAD AND RESPONSE FOR BEAM TESTS

FIGURES A73-A95, STRAIN VS. TIME FOR BEAM TESTS

FIGURES A96-A133, RESISTANCE AND REACTION VS. DEFLECTION

I INTRODUCTION

1.1 General Remarks

The behavior of structures subjected to dynamic forces has been a topic of importance in engineering for many years. Before the advent of atomic weapons the dynamic forces to be considered were those arising primarily from wind, earthquakes, moving loads, and dynamite explosions. The first three categories are characterized by loads whose rate of application is relatively slow compared with that of the last. Also, the loading produced by a dynamite explosion is relatively short and of small magnitude compared with that produced by an atomic explosion (1)*. Therefore, in the case of atomic explosions, there must be considered a dynamic loading of magnitude and speed of application far removed from engineering experience previous to the development of atomic weapons. This blast loading represents a complicated problem in the analysis of structures involving among other things the fact that the material properties of the structure are affected by the rate of loading (2,3,4). Of especial interest is the behavior of reinforced concrete members subjected to blast loading, since reinforced concrete, by reason of its flexibility of shape, is suitable for use in a wide variety of structures whose primary purpose is the protection of their contents from the effects of nuclear detonation.

Tests have been made by various investigators using small scale reinforced concrete beams subjected to various types of rapid loading (5,6,7,8). In all of these tests, the scale of the specimens was limited by the approximately 10,000-lb capacity of the testing machines used. Little other work has been done in connection with the testing of reinforced concrete members or structures subjected to blast where the environmental conditions permit

* Numbers in parentheses refer to items in the Bibliography.

the type of test control possible in a laboratory. A dynamic testing machine with a capacity of 60,000-lb is available in the Structural Research Laboratory at the University of Illinois, and it was deemed desirable to make use of it to test larger scale reinforced concrete beams under rapid loading.

It is a well known characteristic of metals, particularly low carbon steels, that the dynamic yield strength increases with increasing strain rates. This is of practical importance because materials such as concrete reinforcing bars in structural concrete members can be subjected to considerably higher stresses than the static yield stress before yielding when dynamically loaded. In under-reinforced concrete beams, the strength increase exhibited by the reinforcing will increase the load-carrying capacity of the member.

The dependence of yield strength on strain rate and the mechanism of yielding in low carbon steels has been discussed by several investigators (9). However, most of these investigations have been carried out on standard test specimens conforming to ASTM Specification E8-54T. In reviewing the literature concerning this behavior, it has been found that little attention, if any, has been given to the effect of rapid strain rates on the tensile properties of unmachined specimens of deformed reinforcing bars. Therefore, this report is also concerned with the time sensitive stress-strain characteristics of intermediate grade deformed reinforcing bars subjected to rapidly applied loads.

1.2 Object

The ultimate objectives of the investigation, of which the data reported herein are a part, was to obtain, by means of tests, information which will contribute to a better understanding and more accurate prediction of the strength and behavior of reinforced concrete structures subjected to dynamic loading.

The immediate objective of the work at hand was the determination of the resistance and behavior of simple-span reinforced concrete beams subjected to impulsive loading. To accomplish this objective, tests of beams and of reinforcing bar coupons have been made and the resulting data analyzed. It was also the purpose of this work to check the practicability of an existing method of computing the resistance of dynamically loaded reinforced concrete beams. To this end, comparisons have been made between the test results and the predictions of the method of analysis.

1.3 Acknowledgment

This investigation was conducted in the Structural Research Laboratory of the Engineering Experiment Station at the University of Illinois, under the sponsorship of the Office of the Chief of Engineers, Department of the Army, Contract DA-49-129-eng-344 and the Department of the Air Force, Contract No. AF 29(601)-468.

Work on this project was under the general direction of Dr. N. M. Newmark, Professor and Head, Department of Civil Engineering, and Dr. C. P. Siess, Professor of Civil Engineering, and was under the immediate supervision of A. Feldman, Assistant Professor of Civil Engineering. W. A. Keenan, Research Assistant in Civil Engineering, was primarily responsible for the investigation of the dynamic strength of reinforcing bars. Appreciation is expressed to H. S. Hamada, Research Assistant, for his aid in fabricating and testing. Appreciation is also expressed to V. J. McDonald, Associate Professor of Civil Engineering, and his staff, for their help with instrumentation and the conduct of the tests, the mechanical reduction of data, and the development of the circuits for the analog computer used in the analysis, and to W. E. McKenzie and E. Crawford, Junior Laboratory Mechanics, for their aid in the experimental phases of the project.

This report is based on dissertations by A. Feldman and W. A. Keenan submitted to the Graduate College of the University of Illinois in partial fulfillment of the requirements for the degrees of Doctor of Philosophy and Master of Science, respectively (10,11).

1.4 Notation

The following notation has been used in this report. Reference is made to Fig. 1 for those terms relating to the dynamic bar tests.

a = distance from support to nearest load point, divided by L

A = area of cross-section of an ideal laterally vibrating bar

A_o = nominal cross-sectional area of the bar specimen given by ASTM Specification A15-58T

A_s = area of tension reinforcement

A_s' = area of compression reinforcement

b = width of beam

C = coefficient of damping, or analog computer symbol for capacitance

C_e = coefficient of damping of equivalent SDF system

C_{cre} = critical coefficient of damping of equivalent SDF system

d = distance from top of beam to centroid of tension reinforcement

d' = distance between centroids of the compression and tension reinforcement

e = analog computer symbol for voltage

E = modulus of elasticity of ideal homogeneous beam

E_c = initial static tangent modulus of concrete determined from tests of 6 by 12-in. control cylinders

E_d = dynamic modulus of elasticity of the bar specimen

E_s = static modulus of elasticity of the bar specimen corresponding to an average strain rate of 2 to 2.5 x 10^{-5} in./in./sec, also static modulus of elasticity of reinforcement, in general

f'_c = static compressive strength of concrete determined from 6 by 12-in. control cylinders

f'_{cd} = dynamic compressive strength of concrete

f_e = frequency of vibration of equivalent SDF system

f_f = fundamental frequency of lateral vibration of a bar in the "free-free" condition

f_r = static modulus of rupture of concrete determined from 6 by 6 by 20-in. control beams under third-point loading on an 18-in. span

f_s = fundamental frequency of lateral vibration of a bar on simple supports

f_w = static yield strength of stirrups

f_y = static yield strength of tension reinforcement

f'_y = static yield strength of compression reinforcement (obtained from tests in tension)

f_{yd} = dynamic yield strength of tension reinforcement

f'_{yd} = dynamic yield strength of compression reinforcement

g = acceleration of gravity

h = beam height

H = constant relating deflection and curvature, defined by $H = \Delta_c/(\Phi_c L^2)$

I = moment of inertia of ideal homogeneous beam

I_a = average moment of inertia

I_g = gross moment of inertia

I_t = transformed moment of inertia

I_y = transformed moment of inertia at yield

j = distance between tension force and center of compression of the concrete in compression on the cross-section of a reinforced concrete beam, divided by d and equal to $(1 - k'/3)$

k' = depth of neutral axis, divided by d (straight-line theory)

k'' = d'/d

k_e = elastic slope of resistance function of equivalent SDF system

k_1 = slope of elastic portion of static resistance function

k_{1d} = slope of elastic portion of dynamic resistance function

k_{2d} = slope of inelastic portion of dynamic resistance function

k_1k_3 = ratio of average compressive concrete stress in beam at failure to f'_c

K_L = load factor for SDF analysis, equal to P_e/P

K_{LM} = load-mass factor for SDF analysis, equal to K_M/K_L

K_M = mass factor for SDF analysis, equal to M_e/mL

K_Q = resistance factor for SDF analysis, equal to k_e/k_1

ℓ = longitudinal distance measured along beam

L = length of beam span

m = distributed mass of beam

M = applied moment due to P, or general symbol for mass

M_e = equivalent mass concentrated at midspan

M_m = maximum applied beam moment

M_{me} = modified equivalent mass for SDF analysis, equal to $K_{LM}(mL)$

M_p = dynamic plastic resisting moment

M_y = static yield moment capacity

n = E_s/E_c, modular ratio

p = A_s/bd

p' = A'_s/bd

P = magnitude of applied load

$P(t)$ = tensile load in the bar specimen at any time t

P_{dy} = dynamic yield load of the bar specimen, equal to $P(t)$ at $t = t_y$

P_e = force applied to equivalent SDF system

P_{sy} = static yield load of the bar specimen corresponding to an average strain rate of 2 to 2.5 x 10^{-5} in./in./sec

q = pf_y/f'_c

q' = $(pf_y - p'f'_y)/f'_c$

Q = general symbol for dynamic resistance

q_{cr} = $k_1k_3\epsilon_u/(\epsilon_u + \epsilon_y)$, static critical reinforcement parameter

q_{crd} = dynamic critical reinforcement parameter, equal to $102/(120 + f_{yd})$

Q_e = yield resistance level of equivalent SDF system

Q_y = static yield resistance level

Q_{yd} = dynamic yield resistance level

r = percent of web reinforcing

R = dynamic reaction, also analog computer symbol for electrical resistance

SDF = single-degree-of-freedom

T = natural period of vibration

t_d = $t_y - t_s$ = delay time to yield

t_o = time of beginning of load on beam specimens

t_s = time elapsed from beginning of load on bar specimens to $P(t) = P_{sy}$*

t_y = time elapsed from beginning of load on bar specimens to $\frac{P(t)}{A_o\ \epsilon\ (t)} = 20 \times 10^6$ psi*

t_1 = time of ending of load on beam specimens

v = nominal shear stress

V = shearing force

v_y = allowable nominal shear stress

---

* In Tables 1a, 1b, and 1c the values of t_s and t_y listed correspond to the slashes on the figures in the Appendix. However, some of the time axes in these figures were shifted so as not to obscure the initial portions of the plots. See, for example, Fig. A19.

w	=	unit weight of concrete
W_e	=	work done on equivalent SDF system
Z	=	Δ_ℓ/Δ_c
Z_a	=	Δ_a/Δ_c
β	=	ratio of damping coefficient to critical damping coefficient
β_e	=	damping factor of equivalent SDF system, equal to C_e/C_{cre}
γ	=	density of an ideal laterally vibrating bar
Δ	=	general symbol for deflection, displacement, or response
Δ_a	=	deflection at a load point distance aL from a support
Δ_c	=	deflection at midspan
$\dot{\Delta}_c$	=	velocity at midspan
$\ddot{\Delta}_c$	=	acceleration at midspan
Δ_d	=	damped maximum displacement
Δ_ℓ	=	deflection at point ℓ
Δ_m	=	static maximum midspan deflection
Δ_{md}	=	dynamic maximum midspan deflection
Δ_u	=	undamped maximum displacement
Δ_y	=	static midspan yield deflection
Δ_{yd}	=	dynamic midspan yield deflection
$\epsilon(t)$	=	strain in the bar specimen at any time t
ϵ_c	=	strain in tension reinforcement at midspan
$\dot{\epsilon}_c$	=	strain rate at midspan
$\dot{\epsilon}_e$	=	equivalent average strain rate corresponding to a constant loading rate, equal to $(\frac{P_{dy} - P_{sy}}{A_o t_d})/E_d$
ϵ_u	=	concrete compressive crushing strain
ϵ_y	=	static yield strain in tension reinforcement
ϵ_{yd}	=	dynamic yield strain in tension reinforcement

$\dot{\sigma}_e$ = equivalent average stress rate, equal to $\dfrac{P_{dy} - P_{sy}}{A_o t_d}$

σ_{su} = static ultimate stress

σ_{sy} = static yield stress

Φ_c = curvature at midspan

Φ_m = curvature at crushing, at midspan

Φ_y = curvature at yield, at midspan

The No. 6, No. 7, and some of the No. 9 bar specimens are designated by a combination of two numbers such as 6-16. The first number, 6, is the bar size, and the second number, 16, is the serial number of the particular length of bar from which the specimen was cut. Some of the No. 9 specimens are designated by a combination of three numbers such as 9-69-4. The third number, 4, is used to identify the particular specimen cut from a given length of bar.

PART A TESTS OF REINFORCING BAR COUPONS

II SCOPE

A total of thirty-four two-foot specimens, consisting of ten No. 6 bars, fourteen No. 7 bars, and ten No. 9 bars, were tested at room temperature under uniaxial tension. The deformations on all the bar specimens were of the Hi-Bond type manufactured by Inland Steel Company. All specimens met the requirements of ASTM Specification A15-58T. The static yield strength of all specimens, based on an average strain rate of 2 to 2.5 x 10^{-5} in./in./sec, ranged between 40,500 psi and 48,900 psi.

The main variables were the static yield strength, the size of the bar specimen, the maximum applied stress level, and the duration of the load pulse. The tensile stress in the specimen was developed by the 60-kip capacity pneumatic loading machine described in Section 3.1. In most of the tests the maximum load level was applied in 6 milliseconds and then held nearly constant at this maximum until the yielding process had been completed. The mean value of the maximum load level ranged between 102 and 149 percent of the static yield strength. On six specimens the load was rapidly applied to a nearly constant value and after an arbitrary time interval the load level was suddenly increased to a higher value. The lower mean load level ranged between 83 and 102 percent of the static yield strength. The second load level was maintained nearly constant until the yielding process had been completed. The purpose of these double load pulse tests was to determine if the stress-time history had any effect on the dynamic yield strength and the delay-time to yield.

III EQUIPMENT AND INSTRUMENTATION

3.1 Loading Equipment

A schematic diagram of the 60-kip capacity pneumatic loading machine (12) used to apply a tensile stress to the bar specimen is shown in Fig. 2. A photograph of the machine with top external chamber in place is contained in Fig. 21. Basically, the machine is a piston loading device which may be operated as an explosion machine, as an implosion machine, or as an explosion-implosion machine.

Most of the specimens were stressed by using the loading unit as an explosion machine. When used as an explosion machine, the load is applied and removed by the sudden release (explosion) of compressed gas to the atmosphere. Before a test, the trigger mechanism is set and the top and bottom orifices are closed by hydraulic jacking of the slide valves. Equal forces, corresponding to the maximum desired stress level to be developed by the specimen, are then applied to each side of the main piston by the introduction of compressed nitrogen gas into the main chambers. The pressures in the two main chambers are adjusted so that no load is applied to the specimen through the main shaft. The top auxiliary lift system which provides the force necessary to move the slide valve away from the orifices is then pressurized. A photograph of the control panel of the pressurizing system is shown in Fig. 3. Energizing the top solenoid then releases the top trigger. This causes the slide valve restraining link to be pushed aside and moves the top slide valve away from the orifices at the desired time. As the slide valve clears the orifices, there is a sudden release of pressure from the top main chamber to the atmosphere. This causes a differential pressure on the main piston which loads the test specimen. After the test is completed, the specimen is unloaded by opening a bleeder valve on the control panel which is connected to the bottom main chamber.

When the pneumatic loading unit is used as an implosion machine, use is made of the external storage chamber or manifold surrounding the bottom slide valve orifices. All gas movements are confined within the machine (implosion). Again, the orifices are closed and the trigger mechanism is set. Now the external storage chamber (manifold) is pressurized. At the desired time the lower solenoid is energized, releasing the lower trigger which causes the lower slide valve to move. As the orifices open, the bottom main chamber is suddenly pressurized and the unbalanced force on the piston loads the specimen. Only six specimens were loaded by using the pneumatic loading unit as an implosion machine because of the large oscillations in the load it applied to the specimen.

It is possible to apply a double load pulse to the specimen by using the pneumatic loading unit as an explosion-implosion machine. First, the orifices are closed and the triggers set. Next, the top and bottom main chamber and the external storage chamber are pressurized. The top solenoid is then energized, releasing the top trigger. As the orifices on the top main chamber open, the pressure on the bottom side of the piston loads the specimen. At a predetermined time interval after the top solenoid has been energized, a sequence control device energizes the bottom solenoid. This trips the bottom trigger causing the gas in the manifold to be imploded into the bottom main chamber resulting in a sudden increase in the level of the load on the specimen.

The pneumatic loading unit permits the application of a loading pulse that may begin from a static level ranging from 60 kips tension to 60 kips compression, to undergo a rapid change of plus or minus 60 kips maximum (with the restriction that the prepulse load plus the dynamic change in load cannot exceed the limits of plus or minus 60 kips), and then return rapidly to zero load. The rise time of the load is approximately 6 milliseconds and is practically independent of the load level. The duration of the peak load level may be varied from a few milliseconds to several hours. When the device is used to apply a double load pulse, the time interval between the application of the first load and the start of the second load level can be varied from 18 milliseconds, minimum, to several hours.

3.2 Measuring Equipment

3.2.1 General

For all the tests included in Part A of this report, the following measurements were recorded with time as the independent variable:

(1) The output of an SR-4 gage load cell which recorded the tensile resisting force developed at one end of the bar specimen due to a rapidly applied load at the other end.

(2) The average of the outputs from two SR-4, Type A12-2, strain gages mounted diametrically opposite one another on the ribs of the specimen midway between the ends of the bar.

On specimens 7-2, 7-10, 7-15, 7-18, 7-24, 9-51-2, and 9-69-4, (see notations, Section 1.4) the individual output was recorded from two additional SR-4, Type A12-2, strain gages mounted in the same fashion on the lower half of the specimen, 2 1/2 in., center to center, below the two gages already described. The purpose of these two strain gages was to determine the rate at which the plastic yield front propagated across the specimen and the magnitude of the bending strains due to possible non-alignment of the specimen in the grips. Further, this series of tests gave some indication of the error in assuming that general yielding had initiated under the gages of those specimens which had only two strain gages and thus some indication of the error in the computed delay-time.

On specimens 6-14, 7-2, and 9-69-4, the output was also recorded from a Hathaway Type AMS-20A Electric Accelerometer Head placed at the mid-span of the reaction beam. These measured accelerations were later used to determine their effect on the recorded load cell output of apparent resisting stress developed in the bar specimen.

The signal output from all the measuring devices was recorded on film by a Hathaway Type S-14 magnetic oscillograph shown in Fig. 4. A circuit diagram of the load cell and strain bridges is shown in Fig. 5. A typical oscillogram of the load and strain obtained during a rapid tension test is shown in Fig. 6. The period of the timing trace is two milliseconds per cycle.

3.2.2 Load

The resisting force developed at the lower end of the bar specimen was measured with a Wheatstone Bridge circuit of SR-4 strain gages mounted on an aluminum load cell. There were two bridge circuits, each consisting of four SR-4, Type AD-7, strain gages. The strain output for each circuit was increased approximately 2.6 times and the effect of eccentric loading compensated for by the arrangement of the gages. One circuit was a "static" bridge and the other was a "dynamic" bridge. A circuit diagram of the "dynamic" bridge is shown in Fig. 5. The "static" bridge was used to calibrate the "dynamic" bridge and to measure any pre-load during the pressurization of the pneumatic loading unit. The "dynamic" bridge was used to measure the transient tension in the bar specimen during a rapid test. A hollow aluminum cylinder was used in order to increase the sensitivity of the load cell and to minimize the inertia forces developed by any vibrations of the load cell. The approximate sensitivity of this load cell is 20 kips per 1000 microin./in. of indicated strain.

The lower end of the load cell was enlarged and threaded onto a turnbuckle which was directly attached to a reaction beam. The upper end of the load cell was solid and threaded. It was threaded directly to a steel cone which encased the babbitt grip for the specimen. A photograph of the load cell connected to the turnbuckle is shown in Fig. 7.

3.2.3 Strain

Strains in the bar specimen were measured with SR-4, Type A12-2, strain gages. The longitudinal rib on the bar specimen provided ample area for mounting the A12-2 gages since the grid pattern of the filament consists of a single strand of wire. The effective gage length of these gages is 1.0 in. Two gages were placed diametrically opposite one another on the ribs midway between the ends of the specimen and connected together in series to form one arm of the bridge. Three additional dummy gages (Type A7) made up one Wheatstone Bridge circuit. For seven specimens, two additional SR-4, Type A12-2, strain gages were mounted diametrically opposite one another on the lower half of the specimen. These gages were 2 1/2 in., center to center, from the gages at the midpoint of the specimen. Each of these two strain gages was part of an individual Wheatstone Bridge circuit together with three dummy gages of the same type. The circuit diagram for these strain bridges is shown in Fig. 5.

3.2.4 Calibration of Load and Strain

The following procedure was used to calibrate the load cell which measured the resistance developed by the specimen. The load cell was first placed in a 120,000-lb capacity Baldwin Universal Testing Machine and an SR-4 strain indicator was connected to the "static" bridge. All electrical leads and connections were such that they could be exactly duplicated later. Load was applied to the cell and the strain output from the "static" bridge was recorded by an SR-4 strain indicator as a function of the axial load. The load cell was then fastened to the turnbuckle in the test setup. A No. 9 bar, strong enough to be strained only within its elastic range under the capacity of the machine, was then cast in babbitt grips and the steel cone sleeves were screwed onto the main piston shaft above, and onto the supporting load cell below. Care was taken to assure that the wiring between the "dynamic" bridge and recording oscillograph was exactly the same as that used in a bar test. Load was then slowly applied to the bar in distinct increments by gradually bleeding gas into the lower main chamber of the loading machine. Simultaneously, the signal output from the "dynamic" bridge was recorded on film by the oscillograph while the signal output from the "static" bridge was read from an SR-4 strain indicator. Along with the signals due to the actual load, those signals resulting from placing shunt resistors across a vertical arm of the "dynamic" Wheatstone Bridge circuit were recorded. It was then possible to obtain an equivalent load for each of the resistors, later to be used in establishing the scale of the load record obtained during a test. These calibrating resistors were switched into the "dynamic" bridge circuit of the load cell and their effect recorded on film by the oscillograph at the beginning of each test.

The standard calibration resistances for the strain bridges were the same as those used for the load cell, except that their equivalent values were now expressed in strain units of microinches per inch. These equivalent values were obtained by shunting the resistors across the appropriate arm of each strain bridge circuit and recording the equivalent strain by an

SR-4 strain indicator. All leads, connections, and switching units were the same as those used in a test. As with the load cell, any reactive unbalance due to long leads was compensated for by placing a variable capacitance in the appropriate arm of each bridge before calibrating or testing. Again, these calibrating resistors were switched into each strain bridge circuit to be calibrated and their effect was recorded on film by the oscillograph at the beginning of each test. These calibration marks on the film were later used in establishing the scale of the strain records obtained during a test.

3.2.5 Acceleration

In some of the tests the acceleration of the midspan of the reaction beam was measured with a Hathaway Type AMS-20A Electric Accelerometer Head. It is capable of measuring accelerations up to 500 g. It was placed on the reaction beam, directly in front of the base plate. The mounted accelerometer can be seen in Fig. 7.

Before the test, the accelerometer was given a simple "2g calibration." This was accomplished by first holding the accelerometer in the upright position and recording the signal output on the oscillograph. The accelerometer was then rotated through 180 deg. and again the signal output was recorded on the oscillograph. This provided calibration marks on the film paper corresponding to +1.0g and -1.0g, later to be used in establishing the scale of the records obtained during a test.

3.2.6 Recording Equipment

The signal output from the "dynamic" bridge of the load cell, the steel strain bridges of the bar specimen, and the accelerometer were recorded on film with a Hathaway Type S-14c magnetic oscillograph operating with an MRS-18 carrier amplifying system. This system is essentially flat in response up to 450 cycles per second. The timing trace was marked on the film of the oscillograph with the 500 cps output of an electronic oscillator. A block diagram of the Hathaway equipment is shown in Fig. 5. A typical oscillogram of the load and strain obtained during a rapid tension test is shown in Fig. 6. The period of the timing trace was two milliseconds per cycle.

IV DESCRIPTION OF TEST SPECIMENS AND TEST PROCEDURE

4.1 Physical and Geometric Properties

All specimens used in this investigation were cut from deformed reinforcing bars of intermediate grade steel meeting the requirements of ASTM Specification A15-58T. Three different bar sizes were used, Nos. 6, 7, and 9. The total length of each specimen, including grip length, was 24 in. The specimens tested statically in a 120,000-lb Baldwin Universal Testing Machine, at an average strain rate of 2 to 2.5 x 10^{-5} in./in./sec, had yield stresses ranging from 40,500 psi to 48,900 psi. The yield strength, ultimate strength, and modulus of elasticity (for some bars) for each specimen are listed in Tables 1a, 1b, and 1c.

The surface deformations on all bars were of the Hi-Bond type manufactured by Inland Steel Company and were left intact on all test specimens. Photographs of typical No. 6, 7, and 9 bars are shown in Fig. 8. The geometric properties of the No. 6, 7, and 9 bars were determined from five bars of each size selected at random. The average spacing, height, and gap of the deformations were measured by the procedures recommended by ASTM Specification A305-56T. Each bar was also weighed and the average cross-sectional area was determined. The average spacing, height, and gap of the deformations and the cross-sectional area for each bar size are listed in Table 2. The geometric properties listed in Table 2 are not necessarily typical for all the bars tested since all bars used in the investigation were not contained in the same shipping order.

4.2 Method of Gripping

The manner of gripping the specimen was very important because high stress concentrations had to be avoided and slipping of the specimen in the gripping device minimized. The method of attachment eventually adopted consisted of molding the ends of the bar specimen in babbitt metal. This method was effective and there was no tendency for the specimens to fracture at a reduced strength at the grips. With reference to Fig. 9a, the steel cone (A) and then the cone plug (B) were slipped over each end of the bar specimen. Finally, the casting rig (C) was screwed onto each end of the specimen and securely fastened to the steel cone by two set pins. The casting rig aligned the cone with the bar, thus reducing the possibility of eccentrically loading the specimen during a test. The steel cone served as a mold for the babbitt. With the steel cones in position, the total distance between the ends of the two cones was 10 in. The bar-cone arrangement was then held in a vertical position, and the cone was heated with a torch to drive off any moisture and prevent popping of the babbitt. The babbitt was then poured into the cone up to within 3 3/4 in. of the end of the specimen. A pyrometer applied to the bar between the ends of the two cones showed that the temperature of the bar due to heat transfer from the hot babbitt never exceeded 200 deg. F. After the babbitt had cooled, the casting rig was removed from each end of the specimen and a nut and a washer were screwed onto each end. The babbitt was a Hoo-Hoo brand with a high grade tin base. It had a pouring temperature of 810 deg. F. At 68 deg. F. it had an elastic limit of 2,900 psi, a yield strength of 5,750 psi, and an ultimate compressive strength of 13,875 psi. Figure 9b shows the specimen after the babbitt grips had been cast. The specimen was cooled at room temperature. The bar specimen was now ready to be tested dynamically. The total distance between the near ends of the grips was measured before and after several tests. The maximum recorded relative movement of the bar with respect to the cone grips was 3/16 in.

4.3 Preparation of Specimens

Two adjacent 24-in. test specimens were cut from each 24 ft length of bar stock in order that the specimen material for the static and dynamic tests would be as similar as practicable. One specimen from each pair was then tested statically without further preparation.

The specimens tested under rapid loading were prepared as follows: First, the ends of each specimen were threaded to take a nut and washer (see Fig. 10). The nut and washer arrangement was part of a safety measure to prevent the specimen from failing by bond in the babbitt grip. The threaded ends also served as a means of connecting the casting rig to the specimen. After the ends of the bar had been threaded, the longitudinal ribs of the specimen were prepared for mounting the strain gages. At each gage location the longitudinal rib was draw filed and then hand sanded to a final finish with emery paper for a length of about 3 in. Care was taken to remove a minimum amount of material. This rib width provided ample area for mounting Type A12-2 strain gages since the grid pattern of the filament consists of a single strand of wire. These gages have a 1-in. effective gage length. The surface at each gage location was cleaned and the strain gages were mounted with Duco cement. The test specimens were then oven-dried at 170 deg. F. On all specimens tested under rapid loading, two strain gages were mounted diametrically opposite one another on the longitudinal ribs, midway between the ends of the specimen. On specimens 7-2, 7-10, 7-15, 7-18, 7-24, 9-51-2, and 0-60-4, two additional strain gages were mounted in a similar fashion 2 1/2 in. center to center from the midpoint gages. A typical test specimen before pouring the babbitt grips is shown in Fig. 11. After the ends of the specimen had been threaded and all gages mounted, the ends of the specimen were ready to be placed in steel cones and molded in babbitt grips.

4.4 Slow Tests

For each specimen tested under rapid loading, a static test was made on a 24-in. specimen cut from the same bar. For those No. 9 bars in which four specimens were cut from the same length of bar, only one static test was made. All slow tests were conducted in a 120,000-lb Baldwin Universal Testing Machine. Standard wedge grips provided a satisfactory method of gripping the specimen. The average distance between grips for each test was 10 in. This distance corresponded to the distance between the near ends of the cone grips used in the dynamic tests. The testing machine was equipped with a pacing device for the measurement and control of the rate of straining. Each specimen was tested at an average strain rate of 2 to 2.5 x 10^{-5} in./in./sec. This rate is within the limits specified by ASTM Specification A15-58T. On some specimens, an 8-in. extensometer connected to an autographic recording device was used. After a strain of 3 to 4 percent was recorded, the extensometer was removed and the test carried to failure. Typical stress-strain diagrams for No. 6, 7, and 9 bar specimens are shown in Figs. 12, 13 and 14, respectively. The results of the static tests are given in Tables 1a, 1b, and 1c. The resulting tensile properties of all specimens conformed to the requirements of ASTM Specification A15-58T.

4.5 Rapid Tests

The test setup is shown in Fig. 15. A horizontal wide flange steel member spanning between columns provided the reaction for the applied load. The four tie rods connecting the stop plate to the reaction beam were a safety measure to prevent damage to the machine if the specimen fractured. The height of the stop plate could be adjusted to limit the piston travel, and thus the elongation of the specimen, to any desired amount.

After the strain gages were mounted and the babbitt grips had been poured and cooled to room temperature, each end of the specimen was fitted with a nut and washer. The nut and washer prevented the bar from failing by bond in the babbitt grips. The threaded steel cone at one end of the specimen was screwed onto the main piston shaft and the other cone was screwed onto the load cell. The leads from the strain bridges were then soldered to the strain gages on the bar. The specimen was now ready to be tested dynamically.

First, the gain of each amplifier was set so that the calibrating step representing the largest trace deflection (which in turn represented a value of strain or load greater than that applied in a test) would remain on the film of the oscillograph. Next, the appropriate chambers of the pneumatic loading machine were pressurized to a pressure corresponding to the maximum desired load level. As the chambers were pressurized, the load in the specimen was monitored with an SR-4 strain indicator connected to the static bridge of the load cell. Thus, it was possible to ensure that there was no load on the specimen prior to the dynamic test. The auxiliary chambers were then pressurized to activate the slide valve when the triggers were tripped by the solenoid. Immediately before the test, the calibrating resistors were switched into the Wheatstone Bridge circuit of each measuring device and their effect recorded on film by the oscillograph. In order to assure that the specimen was aligned with respect to the loading axis of the machine and to remove any slack from the system, a very small preload or initial tension was applied. However, this load was negligible relative to the static yield load of the specimen. After the specimen had finished yielding under the rapidly applied load, the load was removed by bleeding the bottom main chamber.

In most of the rapid tests the load was applied rapidly to a nearly constant stress level. The load was then maintained at this stress level until the yielding process had been completed. In six tests the load was applied rapidly to a nearly constant load level and, before sufficient time had elapsed to allow general yielding, the load level was rapidly increased to a higher load level. The load was then maintained nearly constant at this second load level until the yielding process had been completed. In one test the area of the orifices in the machine was reduced in an effort to apply a stress to the specimen that increased at a constant rate throughout the stress history of the bar.

4.6 Machine Vibration Tests

During the initial stages of load application, particularly under high load levels, the load cell recorded fluctuations in the apparent resistance developed by the specimen. These vibrations damped out very quickly and uniform measurements of the tension in the bar were always possible after an elapsed time of approximately 25 milliseconds. These oscillations in resistance could have been the result of variations in the load applied to the specimen by the machine or could have been produced by the inertia of the load cell and the bottom grip. If these oscillations were due to the latter, it meant that the load cell was not giving an exact measurement of the varying tension in the specimen. Therefore, an investigation was made to determine if the inertia of the load cell and the bottom grip was giving rise to forces large enough to affect significantly the load cell output.

In order to determine the magnitude of the inertia forces, an accelerometer was placed at the midspan of the reaction beam as shown in Fig. 7. The recorded accelerations as a function of time during the initial stages of the loading for tests 6-14, 7-2, and 9-69-4, are shown in Fig. 16. The peak accelerations recorded by the accelerometer were +8g and -11g. Assuming that the deformations in the turnbuckle, load cell, and bottom bar grip during a test are negligible, thus making the acceleration of the reaction beam and the load cell the same, the maximum computed inertia force was 0.45 kips. This was based on the mass of one-half of the bar specimen, the bottom grip, and the portion of the load cell above the section at which the tension in the cell was being recorded. Since this is within the accuracy of the recording equipment, the load cell output was considered an accurate enough measurement of the varying tension in the test specimen.

The oscillations of the tension in the specimen were attributed to the vibration of the testing apparatus. Although the accelerations were not large enough to affect the accuracy of the load cell, the amplitude of the vibrations was large enough to cause large fluctuations in the applied load. Any small oscillations of the recorded tension in the bar were probably due to the pulsating gases in the machine.

V TEST RESULTS

5.1 Definition of Terms

5.1.1 Yield Criterion

It is evident from the results of the tests presented in this report that the time at which general yielding was initiated was not a well defined point. As illustrated in Fig. 1, after the maximum load level in the bar had been reached, a certain amount of inelastic "microstrain"* developed in the specimen. The rate at which this strain increased with time gradually increased, at a nearly constant load level, until general yielding was initiated. Because there was no distinct time corresponding to a sudden change in the rate of strain, and thus the beginning of general yielding, the time t_y at which general yielding began was arbitrarily defined as the time at which the ratio of nominal stress to strain $\left[\frac{P(t)}{A_o\ \epsilon(t)}\right]$ decreased to a value of 20 x 10^6 psi. This yield criterion is that which has been suggested by other investigators (13).

5.1.2 Delay-Time

As illustrated in Fig. 1, the stress under rapid loading exceeds the static yield point before general yielding is initiated. Thus, a delay-time elapses between the attainment of the static yield stress and general yielding, irrespective of the definition used to define the time when general yielding occurs. This delay-time to yield, t_d, for any loading pattern, P(t), was arbitrarily defined as the interval between the time t_s when the stress first reached the static yield stress, and the time t_y when the ratio of nominal stress to strain decreased to 20 x 10^6 psi. Delay-time, so

---

* In this report the term microstrain is defined as all inelastic straining preceding the development of the general yielding condition.

defined, has engineering significance because it is related at one end to a stress level which would result in yielding under static loading and at the other end to general yielding.

5.1.3 Dynamic Yield Stress

Owing to the characteristics of the testing apparatus, the load in the bar tended to oscillate for several milliseconds after the maximum load level was reached. Because of these oscillations in the load, the mean value of the maximum load level was usually slightly higher or lower than the instantaneous load level in the bar when general yielding occurred. Any large initial elastic oscillations in the load could have caused the mean stress level at the time of general yielding to be significantly different from the instantaneous load level. Therefore, in the interest of consistency, the dynamic yield stress, P_{dy}, was arbitrarily defined as the instantaneous stress in the bar when the ratio of nominal stress to strain decreased to 20 x 10^6 psi, as illustrated in Fig. 1.

5.2 Experimental Results

The results of the dynamic tension tests are presented in both curves and tables. The results of the tests are plotted in Figs. A1-A34. Figures A1-A27 show the results of the first series of tests in which the load was rapidly applied to a nearly constant load level and maintained at this load level until yielding had been completed. Figures A28-A33 show the results of the double load-pulse tests. Figure A34 shows the results of an effort to apply a load which increased at a constant rate throughout the stress-time history of the bar. In each figure, the measured strain, $\epsilon(t)$, and the corresponding tension in the specimen, $P(t)$, are plotted as a function of time for each specimen tested under rapid loading. The strain-time traces labeled "A" represent the output from the SR-4 strain gages mounted midway between the ends of the specimen. The traces labeled "B" represent the output from the SR-4 strain gages mounted 2 1/2 in., center to center, below the "A" gages. The resulting dynamic load-strain curves are also shown. The load-strain curves are based on the strains recorded midway between the ends of the specimen. The varying tension in the specimen, P(t), was recorded as a function of time until yielding under the applied load level was completed. However, the plots of load vs. time have been terminated when the strain in the bar exceeded the capacity of the strain gages or the strain trace went off the edge of the film record. The slash marks on the plots correspond to the values of load and time listed in the tables described below. (See footnote to t_s and t_y in Section 1.4, Notation).

The time to reach the static yield load, t_s; the time to initiate general yielding, t_y, (as defined in Section 5.1.1); the delay-time to yield, t_d, (as defined in Section 5.1.2); the dynamic yield stress, P_{dy}, (as defined in Section 5.1.3); and the dynamic modulus of elasticity, E_d, were taken from the figures and are presented in Tables 1a, 1b, and 1c. The static yield stress, static ultimate stress, and static modulus of elasticity (for some bars) are also listed in Tables 1a, 1b, and 1c. It is important to note that these static properties are based on an average strain rate of 2 to 2.5×10^{-5} in./in./sec.

VI DISCUSSION OF RESULTS

6.1 General

Because of the limitations of the strain gages, this investigation was confined to the tensile properties of each specimen up to approximately one percent strain. The initial rate at which tensile stress was applied to each specimen ranged between 5×10^6 and 10×10^6 psi/sec. As the load on the specimen was rapidly increased, there was a proportionate increase in the strain. After the load exceeded the static yield load, the specimen continued to behave elastically. When the maximum load level was reached, usually in 5 to 10 milliseconds, the load started to oscillate. An explanation of these oscillations is given below. In this stage of behavior, any measured change of tension in the bar produced a corresponding increase or decrease in the strain, regardless of the load level. The mean level about which the load oscillated was then maintained at a nearly constant value throughout the remainder of the test. At this load level a definite time elapsed during which no straining took place. Just before general yielding was initiated, some inelastic straining (microstrain) occurred. Once this non-recoverable strain had started, the rate at which strain changed with time gradually increased, until general yielding began. The time required to initiate general yielding increased as the relative dynamic to static yield load decreased. In every test, the maximum load level applied to the specimen was less than the static ultimate load. No specimen fractured under the applied load.

Immediately after the maximum load level had been reached, the tensile stress in the bar tended to oscillate during the initial stages of the loading. The major cause of this has been attributed to the vibrations of the testing apparatus. It was explained in Section 4.6 that the accelerations produced by these vibrations did not introduce significant error in the load cell output measuring tensile load in the bar, but that the amplitude of the vibrations was large enough to cause large oscillations in the applied load. However, these large vibrations of the load generally damped out very quickly relative to the delay-time. Any remaining small oscillations of the recorded tension in the bar were probably due to the vibration of the gases in the machine caused by the sudden change in volume, resulting in an erratic differential load on the main piston.

In every test in which two sets of strain gages were used, the strain-time records indicated that general yielding was initiated toward one end of the specimen. For those tests in which the dynamic load level was only slightly above the static yield load (e.g. Fig. A27) the strain gages showed that the time required for the onset of general yielding at a point 2 1/2 in. below the midpoint of the specimen was approximately half the time required at the center of the specimen. This difference in time to yield increased as the relative dynamic to static yield stress decreased. This indicates that for only slight increases in the dynamic yield level, the velocity at which the yield front propagates across the length of the specimen is relatively slow. For very high dynamic yield levels, the velocity of the plastic yield front is so great that uniform yielding over the length of the specimen appears to have occurred, at least within the sensitivity of the recording apparatus used. This phenomenon was also observed by Taylor (14) in an investigation concerning the non-uniform yield in a mild steel under dynamic straining. Taylor found that yield was initiated at one end of the specimen and the amplitude of the permanent strain increased at this point of initiation until a critical value was reached and a definite yield front then progressed along the gage length.

6.2 Dynamic Load-Strain Diagram

For each specimen tested under rapid loading there was a pronounced "spike" in the load-strain diagram as shown in Fig. 17b. The magnitude of this "spike" was a function of the magnitude of the oscillations in load immediately after the maximum load level was reached. This behavior can best be explained by reference to Fig. 17. After the load on the specimen reached point A, the load oscillated for several cycles between points A and B. Since the specimen was still acting elastically, there was a proportionate oscillation in the strain between points a and b. On the load-strain diagram, this corresponded to an oscillation along the elastic slope between A, a and B, b. After the oscillations in the load had damped out at point C, the load and strain in the specimen were represented by point C, c until a time corresponding to point D was reached. At this time, the strain in the specimen began to increase at a nearly constant load level along line de. This behavior is clearly illustrated by tests 6-22 and 9-69-2 shown in Fig. A10 and Fig. A26, respectively. Therefore, the point corresponding to point A, a in the load-strain diagrams of Figs. A1-A34 should not be interpreted as the dynamic upper yield point.

It is interesting to note in Tables 1a, 1b, and 1c that the modulus of elasticity was always less under rapid loading than under static loading. Freudenthal (15) suggests that this phenomenon is due to the thermal softening of the material by the energy dissipated in inelastic deformation and not carried away. However, this difference between the static and dynamic moduli may be due to the distinctly different procedures used to measure load and strain in the static and dynamic tests and the inherent inaccuracies in each.

6.3 Delayed-Yield Effect

With reference to Fig. 1, the specimen did not yield in the rapid-load tests when the tension in the bar reached the static yield load. As the tension in the bar continued to increase, the specimen continued to behave elastically and a finite time, the delay-time, elapsed before the onset of general yielding. The delay-time to yield (as defined in Section 5.1.2) for each test is listed in Tables 1a, 1b, and 1c. This delay-time to yield was found to be a function of the amount by which the maximum load level exceeded the static yield load. The percentage by which the dynamic yield load, P_{dy}, exceeded the static yield load for each test is listed in Col. 1 of Tables 3a, 3b, and 3c. In Fig. 18 the percentage increase in the yield stress is plotted against the delay-time to yield. There are only a few points corresponding to $t_d < 4$ milliseconds because of the limited load capacity of the testing machine and the limited loading rate imposed by the structural flexibility of the testing apparatus. Figure 18 confirms the results of other investigators (9), that the delay-time to yield decreases with increasing yield strength.

The scatter in Fig. 18 may be attributed to the following factors:

(1) The static yield strength of each specimen was different. Uzhik and Voloshenko-Klimovitsky (16) found that the dynamic yield strength is dependent not only upon the loading pattern, which influences the delay-time, but also upon the value of the static yield strength. Their tests confirmed that, for a given loading rate, the ratio of dynamic to static

yield strength increases as the static yield strength decreases. It was impossible to determine the magnitude of the effect of the static yield stress on the dynamic yield strength of the bar specimens because the loading pattern on each specimen prior to general yielding was different.

(2) The measured delay-time is based on the assumption that first yielding in the specimen occurred at the location of the strain gages. This is not necessarily true. Therefore, the delay-time for a given increase in yield stress may have been less than that indicated by the strain gages. The tests in which the strain, $\epsilon(t)$, was recorded at two different points on the specimen indicate that this error decreases as the relative dynamic to static yield stress increases.

6.4 Effect of Stress-Time History on Behavior

An investigation was made to determine if the stress-time history on the bar prior to the time t_s had any effect on the delay-time to yield and the dynamic yield stress. This was accomplished by applying two different loading patterns to the specimens. Each pattern had a different stress-time history prior to the time t_s and a similar stress-time history after time t_s. For the first pattern of loading (Figs. A1-A27) a stress greater than the static yield stress was rapidly applied to the specimen in 5 to 10 milliseconds and then maintained at a nearly constant stress level until yielding had been completed. The stress-time histories of each specimen of this series were very similar prior to the time t_s when the dynamic stress exceeded the static yield stress. The second pattern of loading (Figs. A28-A33) was applied to six specimens. Each was subjected to a stress which increased to a maximum stress level less than the static yield stress in 5 to 10 milliseconds and was then held nearly constant.

After an arbitrary time interval had elapsed at this stress level, the stress was rapidly increased to a higher level and maintained nearly constant until yielding under this higher stress level had been completed. The lower mean stress level ranged between 83 and 102 percent of the static yield stress. The measured delay-time, t_d, and the computed increase in the yield stress are plotted in Fig. 18. The results of these tests showed that the stress-time history on the specimen prior to the time t_s when the dynamic stress, P(t), exceeded the static yield load, had no noticeable effect on the delay-time to yield (at least within the limits of the investigation, $t_s < 108$ milliseconds). This would imply that the increased strength exhibited by a specimen under rapid loading depends only on the stress history during the elapsed delay-time.

6.5 Equivalent Average Stress Rate

In the literature (9,14), the phenomenon of increase in yield point under rapid loading is usually related to a time parameter such as delay-time to yield, t_d, or time to reach yield, t_y. Although this method of presenting experimental data on increased yield point is convenient, it is of little practical value in the analysis of reinforced concrete beam tests. In the reinforced concrete beam tests of this investigation, records of strain as a function of time for both the tension and compression steel do not show finite times during which no straining takes place. (See Figs. A73-A95). The strains, and thus the stresses, generally tend to increase continuously with time. Thus, relating the increase in yield stress to either a stress rate or strain rate has practical value in the analysis of reinforced concrete beam tests. It has been shown in Section 6.3 that the delay-time to yield can be fairly well correlated with the percent increase in yield stress. If the delay-time to yield can now be related to an equivalent average stress or strain rate, then each can in turn be related to the percent increase in yield stress. Thus, the following method of relating the experimental values of delay-time to yield to an equivalent average stress rate is presented.

With reference to Fig. 1, the equivalent average stress rate, $\mathring{\sigma}_e$, in time t_d, is equal to $(P_{dy}-P_{sy})/t_d A_c$. The computed equivalent average stress rate, $\mathring{\sigma}_e$, for each specimen is listed in Col. 2 of Tables 3a, 3b, and 3c. In Fig. 19, the percent increase in the yield stress is plotted against the equivalent average stress rate for each specimen. The curve shown in this figure is drawn as a lower bound to the experimental points because the delay-time to yield for a given increase in yield stress may have been less than the time indicated by the strain gages (see Section 6.3).

This method of relating the experimental values of delay-time corresponding to a load which is rapidly applied and then held at a constant stress level, to an equivalent average stress rate is based on the following assumption: For a particular metal, the delay-time to yield is a unique quantity in that it depends only on the total change in the magnitude of the load level during the elapsed delay-time to yield. This assumption could not be validated by tests on this project because of the limitations of the testing apparatus. In fact, the results of an experimental investigation by Vigness, Krafft, and Smith (9) indicates that this assumption is not completely valid. Vigness, et al., found that for the same steel stock, the delay-time for a load rapidly applied and then held constant is less than the delay-time for a load which increases linearly with time. It is suggested (9) that this difference in delay-time to yield for the two loading patterns is due to the lower average stress during the elapsed delay-time for the constant rate of loading. This difference in the delay-time for the two loading patterns suggests that the computed equivalent average stress rate corresponding to the points shown in Fig. 19 may be approximately 12 percent larger than would be expected if the bars were actually loaded at a constant loading rate during the elapsed delay-time. Thus, for a given stress rate the corresponding increase in yield stress may be greater than that indicated by Fig. 19.

The above discussion concerning the test results reported by Vigness, et al., assumes that the delay-time is independent of the stress-time history of the specimen prior to the time t_s. It has already been shown in Section 6.2 that within the scope of these tests, the stress-time history prior to the time t_s appeared to have no influence on the delay-time to yield.

6.6 Equivalent Average Strain Rate

For the reasons stated in Section 6.5, it would be of practical value if the increase in yield stress under rapid loading could also be related to an equivalent average strain rate. The equivalent average strain rate, $\mathring{\epsilon}_e$, is defined as the equivalent average stress rate, $\mathring{\sigma}_e$ (explained in Section 6.5), divided by the dynamic modulus of elasticity, E_d, listed in Tables 1a, 1b, and 1c. The equivalent average strain rate for each specimen is listed in Col. 3 of Tables 3a, 3b and 3c. The percent increase in the yield stress is plotted against the equivalent average strain rate in Fig. 20. The curve shown in this figure is drawn as a lower bound to the experimental points because the delay-time to yield for a given increase in yield stress may have been less than the time indicated by the strain gages (see Section 6.3). For the same reasons stated in Section 7.5, for a given equivalent average strain rate, the corresponding increase in yield stress may be greater than that indicated by Fig. 20. For purposes of comparison, the experimental curve obtained by Manjoine (17,18) in which test specimens were subjected to a nearly constant strain rate is also shown in Fig. 20. As shown, the two curves agree fairly well. However, one should not expect the two curves to be the same since the physical properties of the specimens used by Manjoine were different. Manjoine's tests were performed at room temperature on 0.2-in. diameter specimens machined from a commercial low carbon open hearth steel. The yield point of this steel was 28,400 psi, when tested at a strain rate of 10^{-5} in./in./sec.

This method of relating the experimental values of delay-time corresponding to a load which is rapidly applied and then held at a nearly constant stress level, to an equivalent average strain rate is based on the same assumption presented in Section 6.5. In addition, it assumes that no inelastic microstraining occurs prior to the time when general yielding is initiated.

VII SUMMARY AND CONCLUSIONS - PART A

The behavior of intermediate grade deformed reinforcing bars at room temperature under rapid rates of loading to a constant stress level has been determined experimentally and the following conclusions are drawn.

(1) The yield strength of intermediate grade reinforcing steel is much greater under rapid rates of loading to a constant stress level than under ordinary static loadings. The yield strength may be expected to increase as much as 50 percent under dynamic loadings of the types used in this investigation.

(2) There appears to be a relationship between the delay-time to yield and the dynamic yield stress in excess of the static yield stress as shown in Fig. 18. The delay-time to yield decreases with increasing yield strength of intermediate grade reinforcing steel. Load levels which correspond to very little increase in the yield strength generally result in delay-times greater than about 2 seconds. Load levels corresponding to increases in yield strength of as much as 45 percent generally result in delay-times of 1 to 3 milliseconds.

(3) Within the scope of the investigation, the stress-time history prior to the time t_s has no apparent influence on the delay-time to yield. This would imply that the increased strength exhibited by the bars under rapid loading depends primarily on the stress-time history during the elapsed delay-time.

(4) The yield strength of intermediate grade reinforcing steel increases with increasing equivalent average stress rate as shown in Fig. 19. At at equivalent average stress rate of 10^7 lb/in.^{2}/sec, the yield strength of the material may be expected to be 45 percent greater than under static rates of loading.

(5) The yield strength of intermediate grade reinforcing steel increases with increasing equivalent average strain rate as shown in Fig. 20. At an equivalent average strain rate of 1 in./in./sec, the yield strength of the material may be expected to be 45 to 50 percent greater than under static rates of straining.

PART B - TEST OF REINFORCED CONCRETE BEAMS

VIII SCOPE AND OUTLINE OF TESTS

8.1 Scope

The objectives set forth in Section 1.2 were pursued through a program of testing reinforced concrete beams and coupons of reinforcing bars. In all, ten beams were tested under loads applied at midspan, and 33 beams were tested under two-point loading. The tests of the first ten beams were reported in Ref. 19 and the tests of the reinforcing bars were presented in Part A of this report. Part B is concerned with the 33 tests of beams under two-point loading.

The beams were approximately half-scale models, being 6 by 12 in. in cross-section with an effective depth of 10 in. The spans were 9 ft and 12 ft-8 in. The loads were placed 18 in. each side of midspan, resulting in shear span-to-depth ratios of 3.6 and 5.8. Two percentages of tension reinforcement were employed using intermediate grade steel. Some beams also had compression and/or shear reinforcement. Concrete strength, beam width and depth, and yield strength of reinforcement were essentially constant.

Eight of the two-point loaded beams were tested statically, requiring from about two to six minutes each to reach collapse deflection. In the dynamic tests of the other 25 beams, loads were applied in from 0.1 to 0.8 times the natural period of vibration. Some of the dynamic loads were of "infinite" duration, while others were terminated at from one-half to three times the beam period. The load levels varied from less than static yield capacity to more than dynamic ultimate capacity.

The analysis of the test results consisted of determining the dynamic resistance characteristics of the test beams. This was accomplished by considering the beam to be a single-degree-of-freedom system and analyzing its behavior on an analog computer. The measured load pulse was fed into the computer along with an arbitrary resistance function for the beam. This resistance function was then changed until its response matched the response measured in the test. Dynamic resistance functions were also determined using the strain rates measured in some of the tests together with the results of the reinforcing bar tests and information from Ref. 2. The resistance functions determined with the analog computer are compared with those computed functions and with the static resistance deflection characteristics.

The test results and the resistance functions determined with the analog computer are also compared with the results of computations based on the procedures and formulas of the Manual of the Corps of Engineers, U. S. Army, entitled, "Design of Structures to Resist the Effects of Atomic Weapons" (20).

8.2 Outline of Tests

The beam properties and configurations tabulated in Table 4 were chosen to satisfy certain considerations. The 6 by 12 in. cross-section and 9 ft span coincide with the size of beams previously tested statically on another project in Talbot Laboratory at the University of Illinois (Ref. 21). The Series 4 beams represent a somewhat typical design which might be arrived at using the American Concrete Institute Building Code. The Series 3 beams were an attempt to increase the strength of the beams while maintaining the ductility. This required the addition of compression reinforcement. Series 2 beams were designed to have the same strength as the Series 3 beams but the compression reinforcement was left out to determine its effect under dynamic loading. The beams of Series 5, 6, and 7 were essentially a duplication of those in Series 2, 3, and 4 but with a longer span. This provided variations in the ratio of moment to shear and the ratio of rise-time-of-load to period of the beam. Within each series, variations in web reinforcing were provided to study its effect on the mode of failure. Within Series 3, there was also variation in the configuration of the ties that hold the compression reinforcement in place.

It was felt that at least one static test in each series would be desirable for comparison with dynamic behavior. Variations in the scheme for operating the loading device were also introduced in an attempt to vary the rise time and further extend the ratio of rise time to period. This attempt was unsuccessful. In order to keep the program within manageable limits, it was decided to maintain concrete strength, steel yield strength, and beam width, height, and depth constant.

IX EQUIPMENT AND INSTRUMENTATION

9.1 Loading Equipment

The pneumatic loading device and its associated pressurizing and control equipment are rather completely described in Reference 12 and in Chapter III of this report.

Some of the beams were tested using an arrangement of gas movement described as "explosion" though most were tested using an arrangement described as "implosion." (See Chapter III.) It was hoped that the implosion procedure would give faster rise times of loading but this did not prove to be the case; there was no significant difference in rise times between the two procedures. In addition, the implosion procedure introduced an oscillation into the load trace with a frequency of about four milliseconds that was considerably more pronounced than any oscillations appearing in the traces of the beams tested using the explosion procedure. Attempts were made to eliminate these oscillations by inserting specially designed vibration absorbing rubber pads in various parts of the test setup. All such arrangements, however, appeared to have no appreciable effect. Nevertheless, the implosion procedure was quieter, safer, and easier to use.

The load from the pneumatic device was transferred to the beam through a steel distributing beam which applied the load at two points 18 in. each side of midspan. This beam can be seen in Fig. 21. For dynamic testing, the natural period of the distributing beam should be small compared to the natural period of the test beam. The computed period of the distributing beam was approximately one millisecond, while the computed period of the test beams was generally greater than 18 milliseconds. The distributing beam was equipped with a load measuring cell at each load point to measure directly the pulse applied to the test specimen. The sum of the outputs of these two cells was considered to be the load applied to all beams tested dynamically. In the static tests, the load was taken as the output of the load cell located between the distributing beam and the pneumatic loading device.

9.2 Measuring Equipment

9.2.1 Load

The load applied to the distributing beam by the pneumatic device was measured with the load cell described in Section 3.2.2. There were two bridge circuits on this cell. One circuit was a "static bridge," and the other was a "dynamic bridge." The static bridge was used to calibrate the dynamic bridge, the load cells on the distributing beam, and those built into the reactions; to monitor the slow or static tests; and to measure any preload during the pressurization of the pneumatic unit. The dynamic bridge was used to measure the load applied to the distributing beam during a dynamic test. One end was threaded directly onto the piston shaft of the pneumatic loading device and the other end was fitted into the swivel cap mounted on the top of the distributing beam.

The load applied by the distributing beam to the test beam was measured at each load point by a hollow cylindrical load cell of T-1 steel. The cells were rigidly mounted to the distributing beam and were threaded at the bottom into half-rounds of mild steel, which in turn rested on bearing plates attached to the top surface of the test beams. The cells were designed to resist as much load laterally as axially without yielding. This design criterion was dictated by the manner in which the load cells were wedged between the distributing beam and the test beam as the test beam deflected and the top surface shortened. Each cell was instrumented with four SR-4 Type AD-7 strain gages mounted and connected in the same manner as those on the aluminum load cell. The approximate sensitivity of these cells in the axial direction was 30 kips per 1000 microin./in. of strain.

9.2.2 Reactions

The reactions at each end of a beam specimen were measured in terms of the strain in load cell groups built into the roller support assemblies. The entire assembly is visible in Fig. 21. These load cell groups each consisted of three hollow aluminum cylinders with enlarged ends firmly attached at each end to 2-in. thick steel plates. Four SR-4 Type A-7 strain gages were mounted in a symmetrical pattern on the outside of each cylinder, two parallel to the axis of the cylinder and two circumferential. The section of the cylinders where strains were measured has an outside diameter of 1.3 in. and an inside diameter of 0.9 in. The three cylinders were arranged symmetrically around the center points of the end plates to which they were attached. One Wheatstone Bridge circuit was made up from all twelve gages in each cylinder group. Each leg of the bridge contained a gage from each cylinder. This arrangement eliminated the effect of any eccentricity of load and resulted in a signal output from the bridge equal to 2.6 times the average of the vertical gages. The approximate sensitivity of these groups was 10 kips per 1000 microin./in. of strain.

9.2.3 Calibration of Load and Reaction Cells

In order to insure that mechanical and electrical conditions during calibration of the load and reaction cells were the same as during a test, the following procedure was followed for calibrating these devices. The aluminum load cell was placed in a 120,000-lb capacity Baldwin Universal Testing Machine and a relation was obtained for axial compressive load vs. static strain bridge output as read with an SR-4 indicator. All leads and connections were such that they could be duplicated exactly in subsequent tests. This load cell was then threaded on the main shaft of the pneumatic loading device and the distributing beam attached to it. A steel beam, strong enough to be strained only within its elastic range under the capacity of the machine, was then placed under the distributing beam and its associated load cells and supported on the reaction-measuring supports. Load monitored by the static bridge on the aluminum cell and read with an SR-4 indicator was applied slowly to the beam in distinct increments by gradually bleeding gas into the loading machine. Simultaneously, the signals from the dynamic bridge, the distributing beam cells, and the reaction cells were recorded on film by the oscillographs later to be used in the dynamic tests. The wiring between load cells and the recording oscillographs was exactly the same as that used in the beam tests. Along with the signals due to actual load, those signals resulting from placing shunt resistors across a vertical gage leg of the Wheatstone Bridge in each measuring device in turn were also recorded. It was then possible to obtain equivalent load and reaction values for each of the resistors, later to be used in establishing the scale of the records obtained during a test. These resistors were switched into each circuit to be calibrated and their effect recorded at the beginning of each test.

9.2.4 <u>Deflection</u>

Deflection of the beam specimens was measured by slide-wire deflection gages. Each gage consisted of a 22-in. length of nickel-chromium alloy (nichrome) wire mounted in a frame of aluminum plates and thin wall conduit. A plastic block was connected to the beam at mid-height by a length of conduit. This block contained the sliding contact which was a thick strip of copper. At the bottom end of the conduit was a ball and socket joint which had a threaded bolt on the ball side of the joint. This bolt was attached to an angle-shaped bracket by two nuts, the bracket in turn being attached to the test beam by a bolt threading into a lead cinch anchor. The maximum possible travel was 18 in.

Each gage was connected to the test frame by a separate truss. In Fig. 21 are photographs showing gages and trusses. As the beam deflected, the sliding contact moved with it and changed the lengths of nichrome wire in adjacent legs of the deflection gage circuit. A rod mounted on the gage frame parallel to the nichrome wire contained pegs at a given spacing and was used to set the deflection gage at any given deflection. Thus, the deflection gages were calibrated before each test by setting the gage at various deflections and recording the signal output. A set of calibration resistances was used to set the range of the oscillograph for each deflection gage.

9.2.5 <u>Strain</u>

Strains in the tension and compression reinforcement were measured with SR-4 Type A-7 gages. Strains in the concrete on the top surface of the beam were measured with SR-4 Type A-1 gages. Each strain gage was part of an individual Wheatstone Bridge circuit together with three dummy gages of the same type. The standard calibration resistance for the strain bridges were the same as those used for the load and reaction bridges, except that their equivalent values were now expressed in strain units of microinches per inch. These equivalent values were obtained by shunting the resistors across actual gage installations on a beam and noting the equivalent strain on an SR-4 indicator. All leads, connections, and switching units were the same as those used in a test. Again, these resistors were switched into each bridge circuit to be calibrated and their effect recorded at the beginning of each test.

9.3 Recording Equipment

The signals from the load, reaction, and strain bridges were recorded on film with Hathaway S-14 magnetic oscillographs operating with an MRS-18 carrier amplifying system. This system is essentially flat in response up to 450 cycles per second. The timing trace was marked on the records of these oscillographs with a timing trace generator employing a Hewlett-Packard 200C audio oscillator.

The signals from the deflection gages were recorded with Hathaway S-14 OC 2 Group 23 galvanometers, also with a flat response up to 450 cps. The time trace was established by the same instrument as above. There was a gang switch through which the time trace circuits of the Hathaway equipment passed. A break in the traces achieved by suddenly opening and closing this switch provided a means of positively tying together, with respect to time, the records from the various oscillographs.

X TESTS OF REINFORCED CONCRETE BEAMS

10.1 Description of Test Beams

10.1.1 Configuration

The 33 specimens tested were reinforced concrete beams 6 by 12 in. in cross-section with a span of 108 or 152 in., loaded symmetrically at two points 18 in. each side of midspan. They were cast in lengths of 120 or 164 in. and were variously reinforced in tension, compression, and shear. Tables 4, 5, and 6 and Figs. 22 and 23 contain all the pertinent data regarding beam properties, configuration, and gage location. Several points should be emphasized. The shear reinforcement given for Beams 6b1 and 6b2 consisted only of the ties which were required to contain the compression steel. Since these ties were required throughout the length of the beam, they probably contributed, though slightly, to the shear resistance in the end regions. The values given for f_y and f'_y are the average values for the two bars used in each case. The values given for f'_c and E_c were determined from standard 6 by 12-in. cylinders and are those associated with the batch of concrete placed in the upper half of the beam. The values of f_r were determined from a 6 by 6 by 20-in. beam loaded at the third-points on an 18-in. span and are those for the concrete placed in the lower half of the beam. In Tables 4 and 6, stirrups refer to vertical steel placed in the end regions of the beam and intended primarily to resist inclined tension stresses. Of course, these stirrups also served to confine the compression steel if there was any present. Ties, on the other hand, were placed in the middle region with the primary purpose of confining the compression steel. Since, in Beams 6b1 and 6b2, no stirrups were used, it was necessary to place ties in the end spans, where they also served as shear reinforcement.

10.1.2 Materials

Marquette or Alpha brand Type I cement was used in all beams. The aggregate was Wabash River sand with a fineness modulus of 3.0 to 3.2 and Wabash River gravel with a maximum size of 1 in. The concrete mix was 1:3.8:5.5 by weight, with a water-cement ratio of from 8 to 9 gallons per sack, depending on the moisture content of the aggregates. All reinforcing steel was intermediate grade Inland Hi-Bond deformed bars except for the No. 2 bars which were plain round. The bars were received in 24-ft lengths and a sufficient amount was cut from each length to provide coupons for both static and dynamic testing. All static testing of the coupons was completed before the bars were used in the beams; thus, it was possible to match bars on the basis of their static yield strengths.

10.1.3 Attachment of Strain Gages

The first step in the fabrication of a test beam was the preparation of the reinforcing bars for the attachment of SR-4 strain gages. The location of the gages was determined and the mill scale was brushed off for a distance of several inches each side of this location. One longitudinal rib and parts of the connecting transverse lugs were ground off only enough to provide a smooth surface just slightly wider than the gage for a length of about 1 1/2 in. at each gage location. The gages used on the reinforcement were Type A-7 with an effective gage length of 1/4 in. and an overall width of 5/16 in. The ground area was then filed and sanded with No. 120 emery cloth. The gages were mounted and allowed to dry. Drying was accelerated by the use of infra-red lamps. After drying, the gages were covered with electrical tape and the leads soldered to them. The bars were then heated and entirely covered in the vicinity of the gages with Petrolastic, and asphaltic waterproofing compound. (This waterproofing procedure destroys the bond between the steel and the concrete over a distance of about 2 1/2 in. at each gage location.) The bars were then immersed in water overnight and the gages were checked for leakage resistance. Gages with leakage resistance less than 5000 megohms were replaced. (This, however, was no guarantee against loss of gages due to mechanical damage during casting.) The bars were then assembled into a reinforcement cage and placed in the form.

10.1.4 Casting and Curing of Beams

All beams were cast right side up in a steel form with a movable side plate to facilitate their removal. The reinforcing cage was held in position by three chairs made of 1/4-in. mild steel bars. Two hooks of 1/4-in. mild steel bars were embedded in the top of the beams near the ends to facilitate handling.

All concrete was mixed from three to eight minutes in a non-tilting drum-type mixer of 6 cu ft capacity. Each beam was cast from two batches of concrete of approximately the same proportions. The first batch was placed along the bottom of the beam and the second batch was evenly distributed over it. Three 6 by 12-in. control cylinders and one 6 by 6 by 20-in. flexure beam were cast from each batch. The concrete was placed in the forms and cylinder molds with the aid of a high-frequency internal vibrator.

Several hours after casting, the top surface of the beam was troweled smooth and all cylinders were capped with neat cement paste. The specimens were removed from the forms the day after they were cast and stored under moist conditions for an additional six days. They were then stored in the air of the laboratory until tested.

10.1.5 Beam Preparation

The preparation of the beam for testing was the same whether the test was to be made dynamically or statically. The beam was marked to indicate the positions of the SR-4 gages for measuring concrete strains, the deflection targets, and the reactions. Shortly before the initial set of the concrete occurred, the top surface of the beam had been struck smooth with a finishing trowel. When this surface was later ground and polished with a portable grinder, it was suitable for mounting SR-4 gages. Type A-1 gages with an effective gage length of 1 in. were used on the concrete. Only the small area necessary for the gage was ground. A thin layer of Duco Cement was applied and allowed to dry before placing the gages. The gages were then attached with Duco Cement and light weights were placed on the felt-covered gages while the cement dried. Heat was not used to hasten the drying since it could be detrimental to the concrete. To protect the gages, a coating of wax was applied after the cement was thoroughly dry. The leakage resistance provided with this procedure was generally greater than 50 megohms.

The deflection brackets and load bearing plates were attached to the beam with bolts threaded into cinch anchors. Holes to receive the cinch anchors were formed in the beams at the time of casting.

After the test beam was placed under the distributing beam, the reaction measuring supports were moved to the correct positions under the beam and the beam was lowered and clamped to them. The slide rods of the deflection gages were then connected to the deflection brackets and the electrical leads for the SR-4 gages were soldered to the gages. Next, all the electrical connections required for recording and calibrating the various measuring devices were made, and the distributing beam was brought to bear by bleeding a small amount of gas into the loading device. A beam ready for testing is shown in Fig. 21.

10.2 Test Procedure

Up to the point of actually applying the load, the test procedure used to test a beam statically was the same as that used to test beams dynamically. The zero value of each measuring device was read with an SR-4 indicator by disconnecting the proper cable leading to the instrument room and plugging in the indicator in its place. After the zero readings were taken, all of the cables were replaced.

At this point, the natural frequency of vibration of some of the specimens was determined. For this purpose, the distributing beam was temporarily raised. The procedure for determining the natural period involved the mounting at midspan of a very sensitive velocity pickup made from a headphone. The output of this pickup was observed on an oscilloscope. The beam was excited either by a single blow at midspan with the fist or an electromagnetic linear driver. When a single exciting pulse was used the oscilloscope face was photographed. The driver was merely rested on the top surface of the beam. The frequency of driving was variable and was changed until the pickup revealed that resonance was obtained. The deflection corresponding to this resonant condition was of the order of 0.01 in. The results of these determinations are presented and discussed in Appendix C.

In a static test, the calibrating traces for each measuring device were then put on the records. The gain of each amplifier was first set so that the calibrating step representing the greatest trace deflection--which in turn represented a value of strain, load, or deflection greater than that expected in the test--would remain on the record. The load was monitored with an SR-4 indicator connected to the static bridge of the main load cell while gas was gradually bled into the chamber above the loading piston. At several times during the progress of the test a switch was thrown which simultaneously marked all the records. For each such mark, the time from the beginning of the test was noted as well as the strain in the main load cell and the pressure in the loading device. This procedure tied all the records together and provided a check on the load. Once loading had been started, it was not stopped until the maximum resistance of the beam had been overcome and its downward travel was stopped either by wood blocks placed under the midspan of the beam or safety catches placed under the wings of the distributing beam. After the beam hit bottom, the pressure was bled off and the piston raised. The zero value of each measuring device was read again except for those gages which may have been destroyed in the test.

In a dynamic test, the loading device was pressurized before the calibration traces were put on the records. For an explosion test, pressure was applied to both faces of the loading piston at the same time, care being taken to keep the forces balanced by monitoring the procedure with an SR-4 indicator connected to the main load cell. When the pressure in the top chamber had reached the desired amount, determined from the area of the piston face (78.54 sq. in.) and the desired value of maximum load, the inlet valves to the loading chamber were closed. For an implosion test, the external storage chambers were pressurized to pre-determined values based on previous performance of the machine. Calibration traces were then put on the records and pressure was bled into the chambers controlling the action of the loading and unloading slide valves. The oscillographs were then started and load was applied by throwing a switch which activated the trigger on one side of the machine. If the load were to have a finite duration, unloading was automatically accomplished through the use of an audio oscillator, successive pulses from the output of which tripped the loading and unloading triggers. Then the records were stopped, the loading beam was raised, and zero readings were taken on the load and reaction bridges.

10.3 Results of Static Tests

10.3.1 Presentation of Results

Static tests were made for three purposes. Eight beams were tested statically to destruction to provide a comparison with similar beams tested dynamically. Four beams were loaded statically only to the point where sufficient cracking developed to produce what was felt would be a significant difference in dynamic behavior compared with those beams tested uncracked. Eight beams were tested statically to determine their residual strength after having been loaded one or more times dynamically. The first two cases will be treated here. The latter case will be treated under the discussion of the results of the dynamic tests, Section 10.5.

While the tests to collapse were essentially "static" in nature, the rate of loading was more rapid than in the usual slow test. This rate varied from approximately 5 kips/min for Beams 4cl and 7al to 11 kips/min for Beam 3al.

The most illuminating description of the behavior of a reinforced concrete beam under static test is contained in a graph of load vs. deflection. Figure 24 contains plots of load vs. deflection for the beams tested statically to collapse. Also shown in Fig. 24 are straight line elasto-plastic approximations to the load-deflection curves. The plastic level was chosen to have zero slope and fitted by eye as an "average" value. The slope of the elastic portion was also chosen by eye to be the best representation possible of the measured elastic region. An attempt was made to keep the area under the measured and approximate curves the same.

The results of the static tests to collapse are tabulated in Table 7. The yield level and deflections presented correspond to the elaso-plastic approximations shown in Fig. 24. The initial slope, k_1, was computed as the plastic resistance level, Q_y, divided by the yield deflection, Δ_y.

In Fig. 25 are plotted the initial resistance characteristics of the four beams which were cracked statically before being tested dynamically. In each case, the static loading was carried to the point where the flexural cracks extended to one-third to one-half the height of the beam.

Photographs of the beams tested statically to collapse are included in Figs. 27-32. The vertical arrows drawn on the sides of the beams near midspan indicate the original positions of the loads. The cracks were marked with ink for better photographic contrast.

10.3.2 Discussion of Results

There was nothing out of the ordinary in the static behavior of these beams. At first, the beams exhibited what can be considered elastic behavior with small deflections that increased proportionally with load. Although, in general a small change in the initial slope is expected somewhere in the "elastic" range due to cracking of the concrete, this change cannot be assigned to a distinct point in any of the plots shown in Figs. 24 or 25 because of small uncertainties in the measurement of deflection inherent in the system used, for which the accuracy was limited to 0.05 in.

In the tests of Beams 4c1 and 5b1, the elastic behavior continued to collapse which was triggered by the development of extensive inclined tension cracking in the shear spans of the beams. In the other tests, except for Beam 2b1, yielding of the tension reinforcing initiated a region of inelastic, or plastic behavior, and collapse occurred when the concrete in the compression zone crushed. In the test of Beam 2b1, it appears that yielding of the steel and crushing of the concrete occurred at nearly the same time.

The great degree of destruction evident in the photographs of the beams tested statically to collapse (Figs. 27-32) is due to the fact that for static tests a pneumatic loading device is essentially a "dead-load" machine. Therefore, the beams were forced down, after having achieved their maximum load and deformation resistance, until either they hit the bed of the testing frame or the loading piston was mechanically stopped.

With regard to Series 3 and Series 6 beams, the effectiveness of compression reinforcement, with its associated ties, in holding together a reinforced concrete beam and providing additional ductility is evident in Fig. 24 and in Figs. 27, 28, 30a, 31a and 32a. The effectiveness of stirrups in providing resistance to diagonal tension cracking and splitting along the reinforcement is evident in Figs. 30a, 31a and 32a. Both of these effects are normally expected.

Some of the cracks in the photographs are secondary effects of the test setup. For example, the diagonal crack in Beam 4c1 in the middle region (Fig. 29a) was probably due to the beam striking the wooden block at midspan subsequent to collapse. The vertical crack at the south end of Beam 5b1 (Fig. 30b) was probably a flexure crack resulting from the plain concrete above the reinforcing bar being loaded upward by the debris at midspan as a cantilever while the reaction continued to rotate counterclockwise due to its inertia. The crack in the compression zone at the south end of Beam 2b1, (Fig. 27a), is believed to be due to the south reaction roller assembly being clamped too tightly or being jammed. During the progress of the test of Beam 2b1, distinct jumps in the various measurement traces were recorded on the oscillographs and there were repeated sounds of something "giving."

Additional reference will be made to Figs. 27-32 in Section 10.5.

10.4 Presentation of Results of Dynamic Tests

The results of the dynamic tests are presented in the form of graphs, tables, and photographs. Figures A35-A72 contain plots of the measured load vs. time, indicated by P, taken as the sum of the outputs of the load cells mounted on the distributing beam, for all tests in which records were obtained. Owing to malfunctioning of the recording equipment, no records were obtained during the tests of Beams 4b2 and 5b2. The load records are plotted only to the point where the load was removed, the beam collapsed, or the load achieved a relatively constant value. In some instances, the load graph does not start at zero load; for example, Beam 2b3 in Fig. A38. The reason for this is that the pressure which was used to bring the distributing beam to bear against the test specimen before the test began, and which was usually quite small, was in these cases large enough to affect the output of the load cells.

Also shown in Figs. A35-A72 are plots of the measured midspan response, indicated by Δ, the response computed as described in Section 11.1.4, indicated by ACR (analog computer response) and the response computed as described in Section 13.1, indicated by OCE. These plots are carried beyond the point of maximum displacement or collapse, as the case may be. In those tests where a beam was subjected to more than one blow, the responses shown for blow other than the first have been adjusted by subtracting any permanent deflection remaining from the first blow. (If it is the third blow that is under consideration then the permanent deflection from the second blow was subtracted, and so on.) For the same reason that the load trace does not start at zero, as explained above, the deflection trace does not start at zero in the case of Beam 4c2, Blow 1 (Fig. A52).

The point of collapse, where appropriate, was determined approximately for the purpose of establishing the range of these plots by noting the time at which the load experienced a considerably drop-off if this drop-off occurred prior to the time when the load was deliverately removed. In other cases the collapse point was determined approximately from inspection of drop-off in the reaction records or in the strain records. This point is indicated in Figs. A35-A72 by a short slash and the notation C. Yield deflection and collapse deflection as determined in Sections 11.1.4 and 13.1 are also shown in Figs. A35-A72 by short slashes and the notation Y and ACC (analog computer collapse), respectively.

Several of the figures merit special attention. In Fig. A47 (Beam 3b3) it is noticed that the deflection continues to increase. It was intended to remove the load after 20 milliseconds. However, an error in wiring the triggers allowed the load to remain. Although it was immediately apparent to the investigating team that the load had not been removed, it was not apparent that the beam was still moving after the dynamic test.

Therefore the recording equipment was stopped. However, the beam collapsed after about 30 seconds of slowly increasing deflection. In Fig. A72 it is seen that Beam 7a3 under the third blow may still have been deflecting beyond the confines of the graph. Actually a small amount of recovery occurred. However, the beam had already failed, for all practical purposes. This is evident from the residual static strength shown in Fig. 26. The response beyond 80 milliseconds, therefore, is not of immediate interest.

In some instances it appears that load remained even after the beam collapsed; for example, Figs. A48 and A50. In these cases, the distributing beam followed the collapsed test beam downward and continued pushing it against the bed of the testing frame even after failure. This phenomenon did not occur after stops had been installed to catch the distributing beam in the event of specimen collapse.

Two marks, indicating what is considered to be the beginning (t_o) and ending (t_1) of the load pulse, are to be found on the time scale of Figs. A35-A72. The mark for the beginning of loading was established by projecting the primary initial slope of the load pulse backward. The second mark was established in those instances where collapse occurred by projecting the primary final slope of the load pulse forward. When collapse did not occur, the end of the pulse was taken as the time at which the load returned to zero.

Figures A73-A95 contain plots of measured strain vs. time for all tests where records were obtained. In some of the cases where more than one blow was applied to a beam, the strains for other than the first blow may not be reported since the gages were often damaged under the first or second blow.

The strain plots in Figs. A73-A95 are not carried beyond the point in time where the gages were destroyed, the beam collapsed, maximum deflection was passed, or the strain trace loses significance. A short vertical line at the end of a curve indicates that the trace disappeared from the paper. This is indicative of destruction of the gage or its connections. An arrow at the end of a curve indicates the trace went off the edge of the recording paper. This is generally also indicative of gage destruction since the ranges of calibration were such as to keep any meaningful output signal on the oscillograph paper. A plus sign shown with a trace designation indicates that the normal direction of strain was tensile and a minus sign indicates compressive strains.

Figures A96-A133 contain plots of the sum of the measured reactions, indicated by R, vs. the measured midspan deflection for all tests in which records were obtained. These plots are carried to the point where the reactions approached zero, the beam collapsed, or the reactions achieved a relatively constant value. Also shown in these figures are plots of the resistance, indicated by Q, determined as described in Section 11.1.4, and plots of the static load-deflection characteristics, indicated by S, computed as explained in Section 11.2. In some of these figures plots of the dynamic resistance (OCE-Q) and sum of reactions (OCE-R), computed as described in Chapter XIII, are given. These figures will be discussed in subsequent chapters.

Static load-deflection curves, obtained after the dynamic tests, are shown in Fig. 26 for all the beams which did not experience total collapse under dynamic loading. The graphs start at the value of permanent set exhibited by the various beams under the dynamic loading and continue to collapse as indicated by the short vertical line.

Photographs of typical failures of beams which collapsed under dynamic loading are included in Figs. 27-32. The photographs will be discussed in Section 10.5.

Tables 8 and 9 contain those data which were readily tabulated. In Table 8, the response characteristics, characteristics of the applied load, and mode of failure are indicated. As a part of the response characteristics are included the deflections under static loading which may have been applied prior to the dynamic test to crack the specimen, or subsequently to determine its residual static strength. The cumulative maximum deflection in each case equals the incremental deflection plus whatever permanent deformation may have resulted from a previous loading. When the cumulative maximum deflection represents collapse it is an estimate made as indicated in the beginning of this section and corresponds to the "estimated collapse" deflections shown in Figs. A35-A72.

The load characteristics given in Table 8 are presented only as a guide to the magnitude and duration of the loading applied. The duration corresponds to the two marks on the time scale described above. The magnitude is the maximum value recorded. These quantities have no computational value in themselves since it is the variation of load with time that is important.

The mode of failure given in Table 8 was determined from visual inspection of the manner of collapse. When the collapse was accompanied by severe inclined cracking in the end regions and a general lack of crushing in the middle region, indicating an overriding influence of shear forces, the failure was termed shear. On the other hand, when collapse was accompanied by considerable crushing in the middle region and less cracking in the end spans, indicating that flexural deformation was the dominant factor, it was termed flexure. This is in general accord with the practice in the field of reinforced concrete research (22). With regard to the indication of detected crushing it should be noted that this refers especially to those instances when crushing occurred but was not accompanied by collapse. Collapse, on the other hand, was always accompanied by crushing for the flexural failures.

In Table 9 the rates of strain deemed critical for the analyses in Chapters XI and XII are presented. Where the rate shown was determined from the output of only one gage, the gage used is indicated. The steel strain rates were chosen from that region of the strain-time plots just beyond the static yield strain value, taken as the yield strength given in Table 4 divided by 30,000,000 psi. This region was chosen because the analysis presented in Part A of this report indicates that the strain rate in this region may be the most significant for determining the increased yield strength of the reinforcing steel. The value of strain rate for the compression steel for the third blow on Beam 3b2 is indicated by a question mark because the strain-time relation shown in Fig. A78 cannot at present be explained by the writers.

The research on the effect of strain rate on concrete strength summarized in Ref. 2 generally involved testing under constant rates of strain. Since the strain rates measured in the tests herein reported could hardly be considered constant, it was assumed that the rate just prior to what was felt to be crushing would probably have the most influence on what the crushing strength would be. If the concrete did not crush under a particular blow, then the rate of strain had no significance for the purpose of determining increases in crushing strength. In several instances, indicated by (d) in Table 9, a visual inspection of the test beam revealed some crushing. However, the strain gages were not so located that it was recorded. Paradoxically, in the case of Beam 7a2 no crushing was recorded by gage CC yet the gage was destroyed by the first blow.

Crushing at midspan was detected visually after the second blow on Beam 3b2. However, the concrete strains in Fig. A77 do not lead themselves to a readily acceptable determination of strain rate just prior to crushing. This uncertainty is reflected in the question mark shown for this case and for the third blow in Table 9. It can be seen in Table 9 that two values are given in the concrete column for Beam 7a2. The reason is that, though it would appear from Fig. A94 that the concrete at the location of gage CB crushed under the fourth blow, gage CB seems to have maintained its integrity even for the fifth blow. Since it was not known which case would be significant for the analysis of this beam both values are given.

Also presented in Table 9 are values of maximum recorded concrete strain for beams when crushing was detected, either visually or by the gages. The choice of these values and their significance are discussed in Section 10.5.3.

10.5 Discussion of Results of Dynamic Tests

This section is concerned with qualitative aspects of the behavior of the beams tested. A detailed quantitative analysis is presented in Chapter XI.

10.5.1 Details of Individual Tests

Before discussing the general patterns of behavior of the test beams and making comparisons of gross results, it is necessary to point out some considerations which help to evaluate those results more objectively. Before and after each test, notes were taken on details of the test procedure, beam behavior, instrumentation behavior, etc., that were at the time thought to be pertinent to a proper evaluation of the test. Some of these notes were incorporated into the presentation of results in Section 10.4. The others of importance are presented below.

After the dynamic tests of Beam 3a4, it was noticed that the bracket holding the deflection gage slide rod to the test beam had twisted. This twisting was probably due to the inertia of the rod when the beam started to recover from the maximum dynamic deflection. The bracket was straightened and tightened before the static test to collapse. Nevertheless, some doubt is cast on the response for Beam 3a4 shown in Fig. A41.

After the first blow on Beam 3b2, it was noticed that the "L" - shaped fingers used to calibrate the deflection traces were not turned out. A careful examination of the top of Fig. 21b will reveal this device mounted on the bottom of the plastic slide block. In Fig. 21b, it is shown in the position employed to engage protrusions on the calibrating rod, which is just visible. Normally, just before a test this finger is turned away so as to clear the protrusions. However, this was overlooked before the test of Beam 3b2 and on all five gages this finger probably dragged along the calibrating rod, perhaps causing some slip in the slide rod-slide block connection or some twisting of the block out of the horizontal plane. In any case there is some question as to the validity of the response shown in Fig. A44.

As with the test of Beam 3a4, the midspan deflection gage bracket twisted during the first blow on Beam 5b4 casting doubt on the accuracy of the response given in Fig. A59. Also, the response as recorded on the oscillograph was very "hashy," probably due to poor contact between the slide wire and sliding contact. The curve given in Fig. A59 represents a "faired-in" and smoothed estimate of the response as recorded.

In Fig. 31d a crack can be seen in the middle region of Beam 6b2 that extends throughout the depth of the beam. This crack should be shown also in Fig. 31c, but it was not noticed until after the photograph was taken. It represents the effect of rebound, the action of the beam recovering more than the downward deflection. This behavior is produced, of course, by the elastic nature of the material and the inertia possessed by the beam when it reaches the position of zero deflection during recovery. It is possible only if the load has been removed or greatly reduced. The crack is caused by the tensile stresses produced in the top regions of the beam by the upward deflection. This cracking was also observed after the first blow on Beams 5b4 and 7a2. These cracks did not always occur at midspan. One can be seen in Fig. 32b just north of the north load position.

It may be noted in Table 8 that collapse is indicated for Beam 4b3 at two values of deflection, approximately 2.07 in. and 3.26 in. It may also be noted that collapse is indicated for this beam in Fig. A51, but that a curve of residual static capacity is shown in Fig. 26. The explanation lies in the fact that the dynamic load was removed from the beam just as collapse was occurring. The phenomenon of collapse appears to require several milliseconds at least to take place. If the load does not follow the beam down, it might not complete the collapse action, in which case there is required some finite reapplication of static load to complete the destruction of the beam. This argument applies also to the behavior of Beam 7a3 (Figs. 32c and d). It is felt that this sequence of events could be made to involve several stages of imminent collapse if one were able to remove the load at just the right time at each stage, in essence coaxing the beam downward.

10.5.2 Dynamic Modes of Failure

The photographs in Figs. 27-32 are arranged to permit convenient comparisons of, among other things, the appearance after failure of similar beams loaded statically and dynamically. The general impression is that the type of loading did not affect the configuration of the beams after collapse. In Figs. 27a, b, and 28c, d, the areas of destruction and manner of concrete breakup are quite similar for the short span beams without compression reinforcement under the two types of loading. In Figs. 27c, d, and 28a, b, the short span beams with compression reinforcement exhibited the same characteristic buckling of the top steel and well-confined crushing of the concrete away from the buckling zone. In Figs. 29a, b, the inclined cracking and horizontal splitting generally associated with failure in shear is evident in both tests. The primary difference between the tests is the lack of flexural cracking in Beam 4cl. The shear failures illustrated in Figs. 30a, b, and c again exhibit similar configurations, especially with regard to the location of the inclined cracks and the splitting along the reinforcing steel. The configuration of Beam 5b2 shown in Fig. 30d is somewhat different in that there are two major inclined cracks at each end. Though still classified as a shear failure, the mechanism of collapse may not have been quite the same as that undergone by Beams 5bl and 5b4. A detailed discussion of the distinctions associated with various modes of shear and flexural failure is presented in Ref. 22. As in the case of the Series 3 beams, the Series 6 beams shown in Figs. 31a, b exhibit similar behavior under static and dynamic loading. The Series 7 beams under static and dynamic loading also exhibited comparable collapse configurations as shown in Figs. 32a, b. The failure of Beam 7a3 shown in Figs. 32c, d lacks the splitting along the reinforcing bars experienced by Beams 7a1 and 7a2. This may have been due to the fact that the depth of crushing was greater just before Beam 7a3 collapsed, thus permitting a greater concentration of rotation at midspan.

There are two notable exceptions to the impression that the manner of loading did not affect the mode or manner of collapse. These exceptions are Beams 4c2 and 6b2. Beam 4c2, Fig. 29, failed in flexure while the companion specimens, Beams 4c1 and 4c3, failed in shear. There was little difference in properties of the beams, as can be seen from Table 4, except that Beam 4c2 had a slightly higher concrete strength than either of the other beams and a lower yield strength of steel than Beam 4c3. Both of these factors would tend to favor a flexural failure. There was some tendency for Beam 4c2 to fail in shear as can be seen from the well developed inclined crack in Fig. 29e. It can only be concluded that the shear and flexural strengths were very nearly the same.

Beam 6b2 failed in shear under dynamic loading while the companion specimen, Beam 6b1, failed in flexure under static loading (Fig. 31). The relative strength of the materials, Table 4, would favor a flexural failure for Beam 6b2. It is possible, as in the case of the Series 4c beams, that these beams were nearly balanced in their shear and flexural capacities. One cannot draw the conclusion, however, that such a balanced beam will fail in shear under a dynamic loading if it failed in flexure statically; at least not on the basis of this one test result.

In several instances, the test beams were subjected to additional blows or to a static test after crushing had already occurred in the compression zone. In the Series 3 and Series 6 beams this was made possible by the presence of the compression reinforcement which carried the major portion of the compressive forces. In the other instances, if crushing was not extensive a redistribution of stress in the beams accompanied by a lowering of the neutral axis made possible the extra loadings. In other words, the occurrence of a small amount of crushing did not necessarily lead to immediate collapse. Crushing had to be extensive and, in the case of the compression reinforced beams, accompanied by buckling of the compression reinforcement. The time-dependent characteristics of the loading and the collapse phenomenon are, of course, important considerations here. As explained in Section 10.5.1, the load had to be maintained long enough for the collapse action to be completed. Even extensive crushing would not cause collapse if the load were diminished or removed at just the right time.

10.5.3 Value of Crushing Strain in Concrete

The values of maximum recorded concrete strain in Table 9 require some explanation. They are presented only for those blows for which crushing was detected since this is the only instance in which they may have some significance regarding the value of crushing strain for concrete loaded dynamically. First, it must be recognized that the strains were measured only at distinct points on the top surface of the beam. Second, when crushing occurs at one point, there is generally a relieving of the compressive strain in adjacent regions. Third, although the strain in the midspan region should theoretically be constant, since the moment is constant under two point loading, it is evident from the concrete strain traces that this was not the case. With these considerations in mind, returning to Table 9, the values followed by a question mark are presented as not being even representative of crushing strain values. In the case of

Beam 3b2, the decreasing values of maximum strain under successive loadings is believed to be a result of the second consideration above. With regard to the questioned values for the first three blows on Beam 7a2, the crushing resulting in the destruction of gage CC and detected visually was so localized as to have practically no effect on the strains in the remainder of the midspan region or on the response.

It is maintained that the remaining values in Table 9 are generally the minimum values at which the concrete crushed in each case. Assuming that the concrete was of uniform quality in the midspan region it probably did not crush at a location where there was no gage at a value less than that recorded by the gages, since it would have crushed at the gage location first when this location reached the hypothesized lesser value. Moreover, if the gage output drops off, indicating a relief of strain, but the gage was not destroyed, it is likely that the strain at the location of crushing was greater than that recorded by the gage. The average of the unquestioned values in Table 9 is 4071 microin./in. This is in good agreement with values of Ref. 23, which is a report of work having as a main objective the evaluation of the crushing strain for static test conditions. Reference 23 also contains a compilation of important previous work in this area. The scatter of the results reported in Reference 23, within which the results given in Table 9 fall, is believed to justify the conclusion that the rate of loading does not have a definite influence on the crushing strain.

10.5.4 Effect of Reinforcement Configuration on Dynamic Behavior

In Table 10 are retabulated various data presented in previous tables but combined here for convenience. The symbols have the same meaning as before.

Considering first the effect of compression reinforcement on ductility, comparisons of the collapse deflections in Series 2 and Series 3, and in Series 5 and Series 6, provide dramatic evidence of the increased deformation before collapse made available by the use of compression reinforcement. This effect, of course, is to be expected. The degree to which compression reinforcement is useful for increased ductility is dependent somewhat on the spacing and configuration of the ties which hold it in place. These ties generally act to confine the compression reinforcement and prevent it from buckling. The persistence with which the tie maintains the possible buckling length depends on the manner in which it is formed. If, for some reason, a tie should open up, the possible buckling length would be increased and the tendency to buckle would be increased, perhaps decreasing the beam ductility.

Based on the above reasoning, it was felt that welded ties should develop the maximum potential ductility for a given spacing. Furthermore, ties hooked in the tension region of the beam (around the bottom steel) should provide more beam ductility than ties hooked in the compression region (around the top steel) for a given tie spacing. However, the data of Table 10 do not necessarily bear this out. Although Beam 3a3 has a smaller collapse deflection than Beam 3a4, which in turn is smaller than that for Beam 3a2, the result is reversed in the Series 3b beams. Also, the slightly wider spacing in Beam 3a5, (though it is admitted a heavier bar was used for the ties) did not decrease the ductility. It is felt that perhaps other factors, such as rate of collapse, degree of concrete crushing, and time-dependent characteristics of the load may have an influence on collapse deflection that obscures the effect of ties configuration and small differences in tie spacing.

Figure 33 contains photographs of Beams 3a2, 3a3, and 3a4 in the region of compression steel buckling. The opening of the tie in Beam 3a3 and the resulting increase in possible buckling length is evident. The ability of ties hooked around the bottom steel to confine the compression steel as well as the welded ties did is also evident. Nevertheless, it can be seen in Fig. 33d that Beam 3b3 had a higher collapse deflection in spite of the tie opening up.

One other variation in the reinforcing details to be considered is the percentage of web reinforcement and its effect on the mode of failure. The questions of capacity in shear and minimum amount of web reinforcement necessary to prevent shear failure are still in a state of flux in the field of reinforced concrete research. However, several general ideas are fairly well established. Shear failure is more likely with increased values of q and q', decreased values of moment/shear or span/depth ratios, and decreased percentages of web reinforcement, or its absence. None of these trends is refuted by the data in Table 10, but boundary values or general relations for dynamically loaded beams cannot be established from these meager data.

10.5.5 Collapse Deflection

Returning to Table 10, a close examination of the values of collapse deflection indicates a small but consistent increase in collapse deflection under dynamic loading. This holds as well for the shear failures as for the flexural failures. Compare 2b2 and 2b3 with 2b1, 3a2 with 3a1, 3b2 with 3b1, 4b3 with 4b1, 4c3 with 4c1, 5b3 and 5b4 with 5b1, and 7a2 and 7a3 with 7a1. There does not seem to be a consistent variation with concrete strength although in most of the cases the concrete strength of the statically loaded beam was higher. Concrete strains were not measured on the statically loaded beams to permit a direct comparison of collapse strains. However, in Section 10.5.3, this question was discussed and the conclusion that the collapse strains under dynamic loading were not higher than those under static loading is still felt to be valid. The increase in collapse deflection under dynamic loading may be due to an upward shift in the neutral axis. This would require the tensile steel strains at collapse to be greater under dynamic loading than under static loading. There is no direct way to check this possibility on the basis of the tests in this program since the strain gages on the tension reinforcement were generally rendered useless before collapse occurred.

10.5.6 Reactions

The sum of the measured reactions, indicated by R, is presented in Figs. A96-A133 plotted as a function of measured midspan deflection. Several details are to be noted. It is believed that the oscillations in the reactions are due to oscillating accelerations in the testing apparatus. These accelerations manifested themselves with little attenuation in all of the force measuring devices employed in the setup, since force is directly proportional to acceleration. The oscillations do not appear as pronounced in the measured deflections since deflection is proportional to the double integral of acceleration and the integrating process is inherently "smoothing." (This explanation applies with equal validity to the loads plotted in Figs. A35-A72).

It will be noticed that in any case where collapse occurred the deflection continues to increase as the reactions drop off. On the other hand, if a beam did not collapse under the load in question then the deflection decreases as the reactions drop off. The previous statements can be used as criteria to determine whether collapse occurred under a particular loading.

For those beams which were subjected to more than one blow, the plot for a given blow starts at the deflection corresponding to the cumulative permanent set from previous blows.

XI ANALYSIS OF TEST RESULTS

11.1 Computation of Dynamic Resistance

11.1.1 Introduction

When a prismatic beam is subjected to a rapid load it will generally vibrate as a system with an infinite number of degrees of freedom. The analysis of such a system, however, is too complicated to be used in design. This difficulty is increased when the inelastic behavior of the member is to be considered. Therefore, in this study the beam is approximated as a single-degree-of-freedom (SDF) system and the dynamic response of the system is computed.

The behavior of a reinforced concrete beam when subjected to a slow rate of loading can be defined by its load-deflection characteristics which are represented by a resistance diagram. The shape of this resistance diagram depends on such properties as yield strength of steel, concrete strength, and percentage of reinforcement. When a reinforced concrete member is subjected to rapid loading, both the concrete compressive strength and the yield point of the reinforcing steel are increased. As a result, the resistance diagram of the member under rapid loading is different from that corresponding to static loading. In addition, the resistance diagram is not represented by a plot of load vs. deflection, as in the static loading case, because the accelerations involved result in substantial inertia forces in the initial stages of loading.

11.1.2 Equivalent Single-Degree-of-Freedom System

As stated above, the exact analysis of a flexible beam with distributed mass subjected to impulsive loadings is too complicated for use as a design tool, especially when inelastic as well as elastic behavior is to be considered. Therefore, it is desirable to modify the system to one to which a simplified analysis can be applied. To accomplish this it is assumed that at any one time the beam vibrates in some definite deflection configuration. This assumption, in effect, reduces the system to a SDF system, since only a single value is needed to define its position at any one time. As a result, if the motion of any one point is known, the motion of any other point can be found by simple proportion. It is convenient to consider only the motion of a point at the midspan of the beam.

A SDF replacement for the original beam may be represented as shown in Fig. 34. The mass and all forces are concentrated at midspan. It is required that this equivalent system exhibit the same behavior at midspan with respect to time as the original beam. The equation of motion of the equivalent system is

$$M_e \ddot{\Delta}_c + C_e \dot{\Delta}_c + k_e \Delta_c = P_e \tag{1}$$

where the dot indicates a derivative with respect to time.

Equation 1 can be rewritten

$$\ddot{\Delta}_c + \frac{C_e}{M_e} \dot{\Delta}_c + \frac{k_e}{M_e} \Delta_c = \frac{P_e}{M_e} \tag{2}$$

Letting $\beta_e = \frac{C_e}{C_{cre}}$, where C_{cre} is the critical coefficient of damping for the equivalent system

$$\ddot{\Delta}_c + \beta_e \frac{C_{cre}}{M_e} \dot{\Delta}_c + \frac{k_e}{M_e} \Delta_c = \frac{P_e}{M_e} \tag{3}$$

But $C_{cre} = 2f_e M_e$, where $f_e = \sqrt{k_e/M_e}$ (24).

So

$$\ddot{\Delta}_c + 2\beta_e f_e \dot{\Delta}_c + \frac{k_e}{M_e} \Delta_c = \frac{P_e}{M_e} \tag{4}$$

As stated above, it is desired to have the behavior in terms of the deflection, velocity, acceleration, frequency or vibration, f, and percentage of critical damping, β, the same for the equivalent system and the beam. To achieve this correspondence it is necessary to relate by factors the equivalent quantities in Eq. 4 (those with subscripts e) to the parameters associated with the beam.

11.1.3 Computation of Equivalent Factors

11.1.3.1 Mass. The generally accepted procedure for computing the equivalent mass is to equate the kinetic energies of the original and equivalent systems (24). This equivalent mass is a function of the deflection configuration the original beam is assumed to have at any one time. The shape assumed herein is the static deflection curve of a beam loaded at two points symmetrically placed with respect to midspan (Fig. 34). Then denoting by Δ_c the displacement at midspan during vibration, the relative displacement of any element $m\,d\ell$ of the beam, distance ℓ from the support, will be

$$\frac{\Delta_\ell}{\Delta_c} = Z \tag{5}$$

For $\ell \leq a\,L$

$$Z = \frac{4\ell}{aL^3} \frac{(3L^2 a - 3a^2 L^2 - \ell^2)}{(3 - 4a^2)} \tag{6}$$

For $aL \leq \ell \leq L/2$

$$Z = \frac{4}{L^2} \frac{(3\ell L - 3\ell^2 - a^2 L^2)}{(3 - 4a^2)} \tag{7}$$

If it is assumed that the shape of the deflection curve is constant throughout the cycle of vibration, then the velocity varies along the beam as the deflection, and Eqs. 6 and 7 for Z are also valid for the velocity at ℓ. The kinetic energy of the beam itself will be

$$K.E._{beam} = 2\int_0^{L/2} \frac{1}{2}\, m\, (\dot{\Delta}_\ell)^2 d\ell = 2\int_0^{L/2} \frac{1}{2}\, m\, (Z\dot{\Delta}_c)^2 d\ell \tag{8}$$

The kinetic energy of the equivalent SDF system is

$$K.E._e = \frac{1}{2} M_e (\mathring{\Delta}_c)^2 \tag{9}$$

Equating Eqs. 8 and 9

$$\frac{1}{2} M_e (\mathring{\Delta}_c)^2 = m (\mathring{\Delta}_c)^2 \int_0^{L/2} Z^2 d\ell \tag{10}$$

and letting

$$K_M = \frac{M_e}{mL} \tag{11}$$

then

$$K_M = \frac{2}{L} \int_0^{L/2} Z^2 \, d\ell \tag{12}$$

Evaluating the integral,

$$K_M = \frac{2}{L} \left[\frac{4L \, (-64a^5 + 112a^4 - 70a^2 + 21)}{35 \, (3 - 4a^2)^2} \right] \tag{13}$$

The two loadings used on this program are a = 1/3 and a = 29/76.

For a = 1/3, $K_M = \frac{5576}{11109} = 0.5019$

and for a = 29/76, $K_M = 0.4953$ (14)

For the beams of this program using 150 lb per cu. ft for the unit weight of concrete, and taking only the mass between the supports, one obtains for a = 1/3 and L = 9 ft,

$$M_e = 0.5019 \text{ w L/g} = 0.5019 \times \frac{150 \times 9}{2} \times \frac{1}{386.4} = 0.8768 \text{ lb-sec}^2\text{/in.},$$

and for a = 29/76 and L = 12 2/3 ft,

$$M_e = 0.4953 \text{ w L/g} = 0.4953 \times \frac{150 \times 12\ 2/3}{2} \times \frac{1}{386.4} = 1.218 \text{ lb-sec}^2\text{/in.}$$

11.1.3.2 Load. The procedure for computing the equivalent load is to equate the work done by the applied loads on the original beam to the work done by the applied loads on the SDF System (25). The shape of the assumed deflection curve of the beam during vibration also influences this computation. It is taken the same as before for the computation of the equivalent mass. Evaluating Eqs. 6 and 7 for $\ell = aL$

$$Z_a = \frac{\Delta_a}{\Delta_c} = \frac{4a\ (3 - 4a)}{(3 - 4a^2)} \tag{15}$$

The work done by the loads on the beam is

$$W_{beam} = 2 \times \frac{1}{2} \times \frac{P}{2} \times \Delta_a = P\Delta_a/2 = PZ_a\Delta_c/2 \tag{16}$$

The work done on the equivalent system is

$$W_e = \frac{1}{2} P_e \Delta_c \tag{17}$$

Equating, and letting

$$K_L = \frac{P_e}{P} \tag{18}$$

one obtains

$$K_L = Z_a \tag{19}$$

For $a = 1/3$,

$$K_L = \frac{20}{23} = 0.8696$$

and for $a = 29/76$, (20)

$$K_L = \frac{3248}{3491} = 0.9304$$

11.1.3.3 Stiffness. The procedure for computing the equivalent stiffness is to equate the strain energy of the original beam to the strain energy of the equivalent system (25). Again, the assumed deflection shape influences the result and it is taken the same as for the mass computation. The strain energy of the actual beam for symmetrical loading is

$$S.E._{beam} = 2 \int_0^{L/2} \frac{M^2}{2EI} \, d\ell \tag{21}$$

Since

$$M = -\frac{EId^2\Delta_\ell}{d\ell^2}$$

$$S.E._{beam} = EI\int_0^{L/2}\left[\frac{d^2\Delta_\ell}{d\ell^2}\right]^2 d\ell \qquad (22)$$

The spring constant in terms of the midspan deflection, that is, the static load at location (aL) required to cause unit deflection at midspan, for the deflection configuration under consideration, is

$$k_{1d} = \frac{48EI}{a\ L^3(3 - 4a^2)} \qquad (23)$$

Substituting for EI in Eq. 22

$$S.E._{beam} = \frac{k_{1d}aL^3(3 - 4a^2)}{48}\int_0^{L/2}\left[\frac{d^2\Delta_\ell}{d\ell^2}\right]^2 d\ell \qquad (24)$$

The strain energy of the equivalent system is

$$S.E._e = \frac{1}{2}\, Q_e\Delta_c = \frac{1}{2}\, k_e(\Delta_c)^2 \qquad (25)$$

Equating Eqs. 24 and 25, and letting

$$K_Q = \frac{k_e}{k_{1d}} \qquad (26)$$

then

$$K_Q = \frac{a\ L^3(3 - 4a^2)}{24\ (\Delta_c)^2}\int_0^{L/2}\left[\frac{d^2\Delta_\ell}{d\ell^2}\right]^2 d\ell \qquad (27)$$

$$K_Q = \frac{a\ L^3(3 - 4a^2)}{24}\int_0^{L/2}\left[\frac{d^2Z}{d\ell^2}\right]^2 d\ell$$

$$K_Q = \frac{a\ L^3(3 - 4a^2)}{24}\left[\frac{4 \times 24\ (3 - 4a)}{L^3(3 - 4a^2)^2}\right]$$

$$K_Q = \frac{4a\ (3 - 4a)}{(3 - 4a^2)} \qquad (28)$$

But Eq. 28 is equal to Z_a (Eq. 15) and Z_a is equal to K_L (Eq. 19). Therefore,

$$K_Q = K_L \tag{29}$$

11.1.3.4 Damping. The factor of interest with regard to damping is β, the percent of critical damping. Both the actual damping and the critical damping would have to be related between the original and equivalent systems by some factor if their absolute values were desired. However, since both terms would involve the same factor, as they are measures of the same phenomena, their ratio would be dimensionless and without a factor. Therefore, the β of the equivalent system can be taken as the β of the original beam without modification.

11.1.3.5 Modified Equivalent Mass. Using the relations of Eqs. 11, 18, 26, and 29, Eq. 4 can now be rewritten as

$$\ddot{\Delta}_c + 2\beta f_e \dot{\Delta}_c + \frac{K_L k_{ld}}{K_M (mL)} = \frac{K_L P}{K_M (mL)} \tag{30}$$

Equation 30 defines a system with midspan deflection characteristics equivalent to those of the original beam, with stiffness equal to that of the original beam, with load as applied to the original beam, and with a mass of $K_M(mL)/K_L$. In other words, it is possible to apply all of the factors to the mass and to use all other quantities as they are for the original beam. Terming the combined factor the load-mass factor and designating it as K_{LM}, then

$$M_{me} = \frac{K_M}{K_L} (mL) = K_{LM} (mL) \tag{31}$$

where M_{me} is the modified equivalent mass. Using the values of relations 14 and 20 for a = 1/3,

$$K_{LM} = \frac{0.5019}{0.8696} = 0.577$$

and for a = 29/76, (32)

$$K_{LM} = \frac{0.4953}{0.9304} = 0.532$$

For the beams tested on this program the values of M_{me} are, for a = 1/3 and L = 9 ft,

$$M_{me} = \frac{0.8768}{0.8696} = 1.008 \text{ lb-sec}^2/\text{in.}$$

and for a = 29/76 and L = 12 2/3 ft, (33)

$$M_{me} = \frac{1.218}{0.9304} = 1.309 \text{ lb-sec}^2/\text{in.}$$

The computations for the frequency and period are then made according to the following relations:

$$f_e = \sqrt{k_e/M_e} = \sqrt{k_{1d}/M_{me}} \tag{34}$$

and

$$T = 2\pi \sqrt{M_{me}/k_{1d}} \tag{35}$$

All of the factors of equivalence derived above are based on elastic behavior and the two-point-load deflection configuration. As a reinforced concrete beam deflects, it cracks and the steel reinforcement yields; the deflection configuration changes continuously and all of the above factors change. However, for the purposes of this program, the factors are assumed to remain constant throughout the range of behavior of the test beams. As an indication of the magnitude of the effect of this assumption it can be shown that for the extreme plastic case, considering the deflection configuration to be a triangle, the value of the equivalent mass is 1/3 that of the total mass instead of approximately 1/2 as obtained above. Also, in the plastic range, if the resistance is constant with increasing deflection, the value of the stiffness factor is of no importance. Since, generally, the inertia forces in the plastic range are small, the change in equivalent mass is also felt not to be of primary importance.

11.1.4 Determination of Dynamic Resistance of Test Beams

As illustrated in Fig. 24 the static behavior of the beams falling in flexure are represented by an elasto-plastic resistance diagram. The shear failures are represented completely by an elastic curve. This same type of representation was desired for the dynamic resistance curves since it would make comparison with static behavior a simpler matter. Consequently, the equation defining the behavior of the equivalent system, Eq. 4, defines this behavior in two distinct ranges. In the elastic range, Eq. 4 is simply the equation of a SDF system for which solutions for the response, Δ, as a function of time are available for regular load pulses, such as sinusoidal, rectangular, triangular, etc. (26). In the plastic range, the system is non-oscillating, unless it is specified that any decrease in deflection be along the elastic stiffness curve. Solutions for this case are also available for regular load pulses (26).

If the load pulse is irregular and difficult or impossible to represent by an algebraic function, it becomes necessary to use some numerical procedure to solve for the deflection. Several such procedures are available and require knowledge of the load and the resistance as functions of time or displacement (25). The problem at hand, however, is not the determination of the response. The load and the response were measured in the tests. Rather, the problem is to determine the resistance, and it can only be attacked, with any expectation of success, by assuming a resistance, subjecting it to the measured load, determining the response, and comparing this computed response with the measured response. If the responses match, then the assumed dynamic resistance diagram is considered to belong to a system, which, under the same condition of loading will give a response identical to that of the beam actually tested. If the responses do not match, then the resistance is changed and the problem run through again until a response having the desired degree of agreement with the measured response is achieved.

To follow such a procedure is very time-consuming even using a desk calculator. The problem has been coded for the ILLIAC, the digital computer at the University of Illinois, but even so, the effects of changing various parameters associated with the resistance are not immediately apparent. It is desirable to solve the problem in such a way that trial solutions can be made quickly. An electronic analog computer is ideally suited to this task.

Analog computers have been used before to solve this type of problem (27, 28). The computer used on this program was a Heathkit Electronic Analog Computer Model ES 400. A photograph of the equipment is shown in Fig. 35. An explanation of the various components and the utility of certain interconnections is given in Appendix A. The load function was supplied to the computer by a Moseley "Autograf" Two-Axis Recorder Model No. 3 modified as a curve follower. The load-time relation was plotted by hand, then covered with a thin wire held to the graph paper by wax. When a current was passed through the wire it attracted a magnetic follower whose position determined the voltage output from the follower. Thus the voltage varied with time in the same manner as the load although the time scale for the computer solution was about 300 times that of the actual beam. Where a test took 1/20 sec to run, a computer solution took about 15 sec.

The response of the system in the computer was plotted on another Moseley plotter. The voltage output from the location in the circuit representing deflection was fed to the Y-axis of the plotter. The X-axis, the time scale, was locked in step with the curve follower, each being driven by the same linear time generator.

A method of operation was used which made it unnecessary to read any quantities or values from the computer dials or meter. Instead, a stiffness for a given beam was assumed and a step pulse of known magnitude was fed to the computer, the computer being set to behave as an entirely elastic system. The various knobs controlling time, mass, stiffness, etc., were adjusted until the sinusoidal output agreed in magnitude and period to that computed previously for the step pulse load and stiffness assumed. Generally, the step pulse put in was that which would yield a response of one inch for the assumed stiffness. This, in effect, placed the proper value of equivalent mass into the computer, and calibrated the computer in terms of the scales used on the graph paper in the curve follower and plotter. It was then possible to change the stiffness setting, if necessary to obtain a match with measured response, and have the period and magnitude of response automatically change correspondingly. When a match with measured response was obtained, the measured response having been plotted on the paper in the plotter beforehand, the characteristics of the system in the computer were determined by again applying a step pulse to the elastic portion of the system. This time the step pulse was varied in magnitude until a given magnitude, generally one inch, of sinusoidal response was obtained. From the value of the pulse necessary, it was possible to compute the initial stiffness of the system in the computer. The period could be read directly from the graph paper. These values of stiffness and period were then used to compute the mass. If the mass agreed with the assumed equivalent mass (Section 11.1.3) then the solution was acceptable. If the mass was more than five percent off, indicating serious drift in the computer elements during the course of the trial solutions, the problem was rerun.

There was also a provision in the equipment connections permitting the resistance, Q, to be plotted on the X-axis of the plotter against deflection on the Y-axis. Thus, when the measured response had been matched, the resistance diagram producing that match could be directly plotted, and the yield deflection read from the graph. Having the yield deflection, Δ_{yd}, thus determined, and the stiffness, k_{1d}, obtained as described in the preceding paragraph, the dynamic plastic level was computed as $Q_{yd} = k_{1d}\Delta_{yd}$. If it was necessary to include a point of collapse in the computer solution, because the beam collapsed during the test under consideration, the deflection at which this occurred was also read directly from the plot of Δ vs. Q.

In some instances, it was necessary to introduce some damping into the computer system in order to obtain a match of responses. The amount of damping introduced was determined in the following manner. After a match of satisfactory correspondence was secured, the feedback circuit introducing damping was disconnected. The stiffness of the undamped elastic portion of the solution was determined as above. Then the damping was re-introduced and the response to the step pulse used on the undamped system was plotted. By comparing the maximum deflection of the damped and undamped responses, the percent of critical damping could be determined.

The relation is as follows:

$$\log_e \left[\frac{2\Delta_d}{\Delta_u} - 1\right] = - \frac{\beta\ \pi}{\sqrt{1-\beta^2}} \qquad (36)$$

where Δ_d = damped maximum displacement

Δ_u = undamped maximum displacement, equal to twice the static displacement

An attempt was made to obtain a match for each response with the percent damping equal to zero and the slope of the inelastic region equal to zero. This attempt was successful in most instances, as reflected by the discussion in the next section.

11.1.5 Presentation of Computed Resistance Functions

The resistance functions computed by trial as explained in the preceding section are presented in Table 11 and plotted vs. deflection in Figs. A96-A133. The parameters relating to the resistance function are defined in Fig. 36. The responses which were taken to be the best obtainable matches are shown along with the measured responses in Figs. A35-A72. It is emphasized that these solutions are unique only in the sense that they are the best matches obtainable with an inelastic portion of zero slope and, generally, $\beta = 0$. It was possible to obtain as good a match in many cases with positive values of inelastic slope, or with damping. Of course, this required correspondingly different values of initial slope and yield deflection.

Several remarks are in order concerning the preciseness of fit between the measured and computed responses. In many of the cases, such as the beams of Series 2, the match is excellent up to and even beyond collapse. However, a different situation is encountered with Beam 3a2 (Fig. A39).

The curves labeled A and B represent responses due to the measured load and resistance function which differed so slightly that the difference was indistinguishable when the resistance diagram was plotted by the Moseley plotter. This uncertainty with regard to maximum deflection is a function of the system rather than the computer as can be seen from several of the charts in Ref. 26. It may be noted in Table 11 that the plastic range of the resistance function for Beam 3a2 has a slightly negative slope. However, the uncertainty with regard to maximum deflection was apparent even when the plastic slope was zero, if it was necessary to enter the plastic region very far in order to obtain a match. In a number of instances therefore, the computed response is presented as two responses, labeled A and B, bracketing the measured response, but corresponding to negligibly different resistance functions.

In Fig. A40, Beam 3a3, it is seen that the computed response deviates from the measured response after maximum. Although an attempt was made to match this portion also, the range up to maximum was of primary importance and failure to fit the curve beyond that point did not cause undue concern. In Fig. A41, Beam 3a4, the lack of fit in the region just before maximum is not necessarily the fault of the computer solution. As explained in Section 10.5.1 there is some doubt about the accuracy of the measured response for this beam. In Fig. A42, Beam 3a5, Blow 1, the computed responses shown bracket fairly well the measured response and result from resistance diagrams that were indistinguishably different. The measured response does not exhibit the recovery at 35 milliseconds which is shown for the computer responses. No explanation can be offered.

For Beam 4c3, Fig. A55, it was not possible to tell from the load pulse where collapse probably occurred, although from the appearance of the response of other beams that collapsed, it was assumed to be before 42 msec. Therefore, when a match was obtained to this point, the problem was considered solved. Beam 5b3, Fig. A58, failed in shear and it was felt that the midspan deflection was no longer representative of the behavior of a SDF system when the beam lost its characteristic sinusoidal shape. Therefore, an attempt was made to match the response only up to 35 msec. Beam 6b2, Blow 2, (Fig. A64) also failed in shear and again the response was matched for only part of the way. In order to obtain a response exhibiting the very slow recovery of the measured response, it would appear to be necessary to introduce a great deal of damping at about 30 msec, corresponding to the formation of inclined cracks. Similarly, in Fig. A72, although Beam 7a3 failed in flexure, it was so near complete collapse that the crushed nature of the concrete and presence of extensive cracking again probably introduced a great deal of damping. It was not possible to introduce damping into the computer solution at an intermediate time in such a manner that the results could be interpreted. Repeated attempts to achieve matches to the responses for the first blow on Beam 3b2 and for Beam 3b3 were unsuccessful. The measured response for Beam 3b2 (Fig. A44) under the first blow was questionable as explained in Section 10.5.1. Though the measured response for Beam 3b3 (Fig. A47) is believed to be correct there were other peculiarities associated with the behavior of Beam 3b3 as explained in Section 10.4 which may have caused an atypical response.

The values in Table 11 are generally self-explanatory. The resistance functions given are for the blow under consideration. To obtain the total yield or collapse deflections under a second or third blow, the deflection obtained from the given resistance function must be added to the value of permanent set for the previous blow. In those cases where it was possible to obtain a match for the measured response without the use of an inelastic portion of the resistance diagram, the values of Δ_{yd} and Q_{yd} are preceded by a "greater than" symbol. The values listed correspond to the maximum deflection reached under the blow being considered and were still in the elastic range. For both blows on Beam 5b4, the values of Δ_{yd} and Q_{yd} are the maximum values attained under the dynamic loading. The values of time to reach yield are measured from the first mark (t_o) on the time axes in Figs. A35-A72.

It is noted in Table 11 that only five problems required the introduction of damping. Of these, it is felt that additional effort may have produced acceptable solutions for Beam 3a4 (Fig. A50) and Beam 7a2, Blow 4, (Fig. A68) without damping. However, the relative constancy of values for the three blows on Beam 4c2 (Figs. A52, A53, A54) suggest that there may have been some aspect of the test set-up producing the damping in this particular test. One such condition could have been reaction assemblies that were overly tight.

The values of velocity at yield given in Table 11 are not, strictly speaking, part of the computer solution. These values were taken from the plots of measured response in Figs. A35-A72. The slope in the region of yielding was determined by eye. What constituted the region of yielding was determined from the computer solution.

11.2 Comparison of Dynamic with Static Resistance

As explained in Section 10.3.1, several beams were tested statically to provide a basis of comparison with the dynamic tests. These comparisons cannot be made directly, however, because there are some differences in the yield strength of the steel and the compressive strength of the concrete within each series. The differences in compressive strength of the concrete can generally be ignored since concrete strength has little effect on the resistance at yield. The yield resistance, however, is directly dependent on the yield strength of the tension reinforcement as reflected in the following expression for the moment capacity at yield (21).

$$M_y = A_s f_y jd \tag{37}$$

The static capacity of a particular dynamically loaded beam was determined, therefore, by multiplying the capacity of a similar beam tested statically by the ratio of the respective static yield strengths of the tension reinforcement. The computed static capacities for the beams tested dynamically are given in Table 12 and shown in Figs. A96-A133. Equation 37 holds for beams reinforced only in tension; and for beams reinforced in both tension and compression, if the center of compression in the concrete is taken at the level of the compression steel, a not unreasonable assumption. In the latter case, jd represents the distance between the centers of gravity of the tension and compression reinforcement. Since there was no static test on which to base the computation for Beams 5a1 and 5a2 the capacity was determined from the equations in Ref. 21. These computations are presented in Appendix B. For the purpose of determining the static yield deflection, it was assumed that all beams of a given series would have the same stiffness since their cross-sectional properties were the same.

For Beams 4c3, 5b2, 5b3, and 5b4, which failed in shear, yield level and yield deflection have no particular meaning. Similar failures were exhibited by Beams 4c1 and 5b1, the statically tested beams used as a base. The values given in Table 12 are those for Beams 4c1 and 5b1 at failure in shear, modified by the ratio of the square roots of the concrete strengths. No account was taken of the differences in steel yield strength. The justification for this procedure lies in the formulas for shear strength presented in Ref. 22. Although Beam 6b2 eventually failed in shear in the dynamic test, yield values are given for it because the statically-tested beam used as a basis for the computation, Beam 6b1, failed in flexure and this information was available.

Since the materials exhibit strengths under dynamic loading which are somewhat greater than those exhibited under static loading, as previously pointed out in Section 11.1, it is to be expected that the dynamic resistance function will be different from the static load-deflection relation for a given beam. The difference would be expected to manifest itself in terms of an increased yield resistance, Q_{yd}, and an increased stiffness, k_{1d}, in the elastic range of behavior. The yield deflection, being dependent on both Q_{yd} and k_{1d}, could either increase or decrease.

The percentage changes in the parameters of the resistance diagrams due to dynamic loading are tabulated in Table 13. The values were computed by subtracting the static values in Table 12 from the dynamic values in Table 11 and dividing the difference by the static values. A negative value indicates a decrease in the property due to dynamic loading. In almost every instance the resistance level was increased under dynamic loading, as expected. The yield deflections and elastic slopes usually increased but in a few cases decreased. Generally, it will be noted that a large increase in yield deflection is accompanied by a decrease in slope and vice versa. Also the decreases in slope are associated with second and third blows on a beam while the greatest increases in slope are associated with first blows.

The effects of dynamic loading on yield resistance, stiffness, and yield deflection have been presented above. One parameter defining the resistance function remains to be examined, namely collapse deflection. The pertinent data are gathered in Table 14. The values of collapse deflection, Δ_m, listed under the column headed "static" were measured in static tests. They are given for beams tested statically to collapse and for beams tested dynamically which did not collapse and were subsequently tested statically to collapse.

Before proceeding to the dynamic values, it is worthwhile to examine the values in Col. 1. Comparisons can be made to determine the effect of dynamic damage on static collapse capacity in Series 3 and Series 6. (Series 4 and Series 7 are not considered because of the negligible static capacity of Beams 4b3 and 7a3). In Series 3, the beams damaged dynamically, Beams 3a2, 3a3, and 3a4, exhibit collapse capacities under subsequent static loading that range above and below the values for beams tested only statically. Any effect of dynamic damage is obscured by the possible effects of reinforcement configuration, as discussed in Section 10.5.4. The values for Beams 6a1 and 6b1 are almost identical. (Beam 6b2 failed in shear.) It can be concluded, then, that prior dynamic damage neither enhanced nor diminished the collapse capacity associated with static behavior.

Proceeding now to the collapse deflection exhibited by beams tested dynamically to collapse, the values of Col. 2 are those used in the computer analysis to obtain matches for the measured response, as explained in Section 11.1.4. In general, there appears to be a small increase in collapse deflection under dynamic loading. In Series 2, the average collapse deflection of the beams tested dynamically is approximately 1.04 in. while Beam 2b1 under a static load collapsed at 0.95 in. In

Series 3a, the value of 4.47 in. for Beam 3a5 is to be compared with the value of 4.05 in. for Beam 3a1. In Series 3b, the average of the values for Beams 3b2 and 3b3 is approximately 4.55 in. while Beam 3b1 collapsed at 3.93 in. In Series 4, the average of the collapse deflections of the beams tested dynamically (excluding Beam 4c3 which failed in shear) is 2.32 in. while Beam 4b1 collapsed at 1.98 in. No conclusions can be drawn from Series 5 as the beams tested statically failed in shear. In Series 6, none of the beams collapsed under dynamic loading. The remaining beams which afford a comparison, Beams 7a1 and 7a2, appear to indicate a considerable increase in collapse deflection under dynamic loading. In this instance, however, there may be some question regarding the collapse value for Beam 7a1. From information presented in Fig. A-5 of Ref. 29 the collapse deflection of Beam 7a1 should be about 2.75 in. With regard to the collapse value for Beam 7a2 the coaxing effect of successive loadings on collapse, as discussed in Sections 10.5.1 and 10.5.2, may have had some influence. It can be concluded, therefore, that there appears to be an increase in collapse deflection of approximately ten percent due to dynamic loading for beams failing in flexure. However, so many factors can influence the collapse deflection, such as the reinforcement configuration as discussed in Section 10.5.1, that it appears unwise to depend on this increased deformation capacity for the purpose of design.

While considering the factors influencing collapse deflection, another worthwhile comparison can be made of the values in Cols. 1 and 2 of Table 14. It is noted that there are marked differences between the collapse deflections for various series of beams. This is due to the difference in q value associated with each series. As pointed out in Ref. 29, the value of $q = pf_y/f'_c$ (or $q' = [pf_y - p'f'_y]/f'_c$ for beams reinforced in both tension and compression) has a profound influence on the collapse deflection of a reinforced concrete beam. A high value of q (or q') corresponds to a beam of brittle nature, that is, one having a relatively low collapse deflection. A low value of q, on the other hand, corresponds to a beam of ductile nature, that is, one having a relatively large collapse deflection. This dependence of collapse deflection on q is well illustrated in Table 14 by both the beams that were tested statically and those that were tested dynamically. Referring at the same time to Table 5, where values of q and q' based on the static strengths of the materials are tabulated, the correspondence of q (or q') and collapse deflection is evident and requires no further comment.

The concept of ductility, defined as the ratio of collapse deflection to yield deflection, is often used in dynamic design procedures (25). Consequently, the ductility exhibited by the beams herein discussed deserves some attention and the additional data are also presented in Table 14. The values of yield deflection in Col. 3 are those measured in the static tests. The values in Col. 4 are those determined as part of the analog computer solutions to which have been added any permanent set possibly suffered by the beam due to static preloading. Ratios of collapse to yield deflection are given in Cols. 5 and 6 only for those cases where yield and collapse occurred under the same loading condition, that is static or dynamic. The cases where a dynamic test was followed by static loading to collapse are not considered to be amenable to meaningful interpretation.

Examining the values in Cols. 5 and 6 series by series, it is noted that there is no significant difference between the ductility exhibited under static loading and that under dynamic loading. In Series 2, the average of the dynamic values is 1.62 while the static value is 1.73. In Series 3, the values to be compared are 6.98 for the dynamic ductility and 8.43 for the static ductility. In Series 4, the considerably higher value for Beam 4c2 is computed using a value of yield deflection associated with a damped computer solution. If damping were not used, it is probable that a higher yield deflection would have been necessary to provide a match of measured and computed responses, thus decreasing the value of ductility. In fact, it must be kept in mind that the computation of ductility as the ratio of collapse to yield deflection places great weight on small changes in the yield value, especially if the yield value is small. Since one can hardly be expected to know the yield deflection any closer than a few hundredths of an inch, it seems unreasonable to ascribe any apparent increases in ductility under dynamic loading to anything but chance.

11.3 Effect of Damage on Initial Slope

It is to be expected that a beam which has undergone some damage in the form of cracking of the tension concrete, yielding of the reinforcement, or slight crushing of the concrete in compression, would exhibit a reduced value of initial slope of the resistance diagram upon subsequent loadings. The pertinent data for those beams which were subjected to more than one loading and exhibited an inelastic region of behavior are presented in Table 15.

Since a reinforced concrete beam that has only been cracked but has not yielded is generally considered to be relatively undamaged, it was decided to measure the damage produced by a given loading by the amount of inelastic deformation experienced. However, the inelastic deformation capacity depends on many factors, including percentage of reinforcement. In order to compare the several tests, therefore, the criterion of damage chosen was the cumulative inelastic deformation for a particular blow divided by the total inelastic deformation capacity. This ratio is defined as the damage ratio.

Column 1 in Table 15 contains values of the maximum deflection obtained under a particular blow. These values were taken from Table 8. Column 2 contains the yield deflection for the first blow as determined by the analog computer and given in Table 11. Any permanent set due to static cracking prior to Blow 1 has been included in the values of Δ_{yd} given in Table 15. By subtracting the values in Col. 2 from those in Col. 1 one obtains the cumulative inelastic deflection experienced by the beam under a particular blow. In Col. 4, the collapse deflection is given for each beam. (If the beam collapsed under a dynamic load, the value in Col. 4 is that determined by the analog computer. If the beam collapsed under a static load applied subsequent to dynamic loading, the value given is that recorded in the static test.) By subtracting the values in Col. 2 from those in Col. 4 one obtains the values in Col. 5 which represent the total possible inelastic deformation. The ratio of the cumulative inelastic deflection (Col. 3) to the total possible inelastic deflection (Col. 5) is the damage ratio as defined above and the values are given in Col. 6.

The values of the elastic slope of the resistance diagram for each blow under consideration are given in Col. 7 of Table 15. These are taken from Table 11 and represent the values determined by the analog computer. The ratio of the elastic slope exhibited under subsequent blows to that exhibited under the first blow is given for each such subsequent blow as a percentage in Col. 8. The values to be compared, then, are the damage ratio for a particular blow and the percentage of Blow 1 slope for the next subsequent blow. These values are plotted in Fig. 37. Except for the erratic relation for the damage under Blow 1 for Beam 7a2, the trend is unmistakable and verifies the original expectation. One is cautioned, however, against developing any relation from Fig. 37 which may later be inadvertently extrapolated below an elastic slope value of 0.4. It is believed that even if the damage ratio experienced by a beam under a particular blow is as high as 0.9, the elastic slope under the next blow would probably not be less than about 40 percent of the elastic slope for the undamaged beam. This belief is evoked by the plots in Fig. 26 which represent the static tests to collapse of beams which had previously suffered considerable damage under dynamic loading. Ignoring Beams 4b3 and 7a3, which were destroyed under the dynamic loading for all practical purposes, the least slope is that for Beam 6b2 the value of which is approximately 16.5 kips/in. and is 38 percent of the slope of the undamaged beam, which was 43.6 kips/in.

11.4 Comparison of Dynamic Resistance with Measured Reactions

If the inertia forces generated by the dynamic loading of a beam are ignored, then the determination of the sum of the reactions in the beam supports is reduced to a problem of statics; that is, the sum of the reactions is equal to the load which, in turn, is equal to the resistance of the beam. Recognizing that this is a crude approximation if the inertia forces have any significance whatever, the sum of the reactions as measured in the tests, R, and the dynamic resistance as determined on the analog computer, Q, (Section 11.1.4) are compared in Figs. A96-A133. In these figures the sum of the measured reactions is represented as a solid line and the analog computer solution for resistance by alternating dots and dashes.

Several qualitative generalizations can be drawn regarding the relative shapes of the R and Q curves in Figs. A96-A133. For the short span beams, Series 2, 3 and 4, in the initial phase of the response the R curves exhibit a steeper slope than the Q curves, then break over and are less steep than the Q curves, as though something akin to cracking had occurred. Cracking is not the explanation, however, since the phenomenon appears for the cracked cases and secondary blows as well as for blows on uncracked beams. The second portion of the initial phase then rises to a peak from which it drops sharply, then descends gradually through the inelastic region until either collapse occurred or the load was removed. The peaks are most pronounced in the Series 3 beams, relatively small in the Series 4 beams and difficult to distinguish in the Series 2 beams, being obscured by the close proximity of collapse. Since the Q curves were deliberately programmed as elasto-plastic, they do not exhibit the broken initial slope, the peak, or a descending inelastic region (except for Beam 3a2). In general, within the inelastic region the constant values of the Q curves are equal to or greater than the fluctuating values of the R curves.

For the long span beams, Series 5, 6 and 7, careful examination of the R and Q curves fails to reveal the general qualities described above for the short span beams. Rather, the occurrence of a break in the initial portion of the R curves and the following peak do not appear with consistency. Furthermore, because of several obscuring factors such as lack of an inelastic region due to low ductility, failure in shear, or failure to initiate yielding on a particular blow, it is difficult to ascertain whether there is a tendency for the measured reactions to gradually decrease in the inelastic region of behavior. However, one characteristic does appear with some consistency. Within the inelastic region, the measured reactions are generally greater than the computed resistance.

No attempt has been made to relate the qualities of the measured reactions discussed above to any beam parameters. Whether such an attempt is warranted is open to question in the light of the recommendations for the computation of reaction presented in Section 15.5.

11.5 Effect of Various Parameters on Dynamic Resistance and Behavior

The results of the dynamic tests presented in this report have been rather completely described and discussed in Sections 10.4, 10.5, 11.2, 11.3, and 11.4. In Sections 10.5, 11.2, and 11.3, the effects of several of the variables in the tests, such as tie reinforcement and q', were discussed in connection with the particular topics of interest. However, there are many other parameters which affect the strength and behavior of a reinforced concrete beam subjected to rapid loading which deserve attention.

Although the beam width and depth were not varied in this program there is no reason to believe that the effects of these dimensions on the strength of the beam would be different under dynamic loading than under static loading. It can be seen in Table 11 that the effects of A_s and A_s' on the strength are also the same for dynamic as for static loading. For example, the beams of Series 2 and Series 3 with the same amounts of tension reinforcement, have yield strengths of the same magnitude, whereas the yield strengths for Series 4 are reduced almost in direct proportion to the reduction in steel areas. This substantiates the fact that the strength of an under-reinforced beam is directly related to the amount of tensile reinforcement, while the compressive reinforcement primarily provides ductility as explained in Section 10.5.4. It is not as easy to discern the effect of r, the percent of web reinforcement. As pointed out in Section 10.5.4 it can be seen in several instances that the presence of web reinforcement prevented failure in shear. However, the minimum percentage required to assure failure in flexure is not definitely known for reinforced concrete beams under static loading, and the tests of this program can only hint at the amount required for dynamic loading. The effect of increasing the span length was, of course, to decrease the load carrying capacity, and, since the shear forces consequently drop with respect to moments, to decrease the likelihood of shear failure, as can be seen by comparing the failure modes of Series 4c and 7.

The effect of the strength of the constituent materials, f_y, f_y', f_c', f_r, and E_c, on the beam behavior is somewhat obscured by the effects of dynamic loading on the materials themselves. The combined effects of dynamic loading on material strength, and the resultant effect of material strength on beam strength are treated in Chapter XII. The effects of the material strengths combined into the parameter q' has already been considered with regard to collapse deflection and will be treated quantitatively in Chapter XII.

The phenomenon responsible for the differences in behavior of reinforced concrete beams under static and dynamic loads is, of course, the time-dependent character and impulsive nature of the dynamic load. The effect that dynamic loading has on beam response depends on the characteristics of the load and their relation to the characteristics of the beam. The effect of load characteristics on the response of a beam which can be represented by a single-degree-of-freedom system with a given or known resistance function has been studied extensively for several cases of loadings having regular time dependent variations, that is, load-time relations that can be readily expressed by a small number of characteristic parameters (26). For the irregular loadings applied in these tests, an attempt was made to correlate some measures of the magnitude and time characteristics of the load with various measures of the resistance and response of the beams tested. However, these attempts were unsuccessful because it was not possible to adequately describe the applied loads except by considering the entire load-time function.

The discussion above is concerned with the relation between a dynamic load and a known resistance function. However, for a given reinforced concrete beam, the resistance is itself a function of the load characteristics. The primary effect of load on resistance is that on the strength and stiffness of the beam materials due to the rapid application of the load and the resulting rapid strain rates. For the beams in this investigation the most pronounced effect of rapid loading on resistance appeared to be the increase in the yield strength of the tension reinforcing steel.

In Chapter XII, the measured strain rates are used to determine the increased yield strengths of the reinforcement and, in turn, the dynamic resistance functions of some of the beams tested, from which their behavior can be inferred by comparison with the resistances determined with the analog computer.

XII COMPUTED RESISTANCE BASED ON STRAIN RATE

12.1 Method of Computation

Since strain rates were determined from some of the tests, and since information was available on the change in strength of steel (Part A) and concrete (2) as a function of strain rate, it was deemed worthwhile to attempt to predict the dynamic resistance of the beams tested by means of procedures already available for predicting static resistances, but using strengths of the materials corrected for the rapid rates of strain involved.

12.1.1 Resistance Level

In order to compute the dynamic resistance level it was again assumed that Eq. 37 was valid for beams reinforced in tension only or in tension and compression. Thus it was necessary only to determine the dynamic yield strength of the tension steel. For this purpose, the measured strain rates from Table 9 were used in conjunction with the steel curve in Fig. 38 which is taken from Fig. 20. The steel used for the tests reported in Part A comprised coupons cut from the bars used in the beams described herein. The dynamic yield level was then computed as the static level multiplied by the increase in steel strength,

$$Q_{yd} = Q_y \frac{f_{yd}}{f_y} \tag{38}$$

where the values of Q_y used were those listed in Table 12. The strain rates, increased yield strength of reinforcement, and dynamic resistance levels thus computed are given in Table 16.

12.1.2 Yield Deflection

The determination of yield deflection is essentially a computation of elastic deflection. The deflection at midspan of a beam loaded symmetrically at two points by loads P/2 is

$$\Delta_c = \frac{PaL^3(3 - 4a^2)}{48\ EI} \tag{39}$$

where aL is the distance from a reaction to the nearest load point. The moment at midspan is

$$M = \frac{PaL}{2} \tag{40}$$

and the curvature at midspan is

$$\Phi_c = \frac{M}{EI} \tag{41}$$

Therefore

$$\Delta_c = \frac{\Phi_c L^2}{24}(3 - 4a^2) \tag{42}$$

For $a = 1/3$,

$$\Delta_c = \frac{23}{216}\Phi_c L^2 = 0.1063\ \Phi_c L^2 \tag{43}$$

For $a = \frac{29}{76}$,

$$\Delta_c = \frac{3491}{34656}\Phi_c L^2 = 0.1007\ \Phi_c L^2 \tag{44}$$

If it is assumed that strain through the cross-section of the beam varies linearly with depth, then, at yielding

$$\Phi_y = \frac{\epsilon_y}{(1-k')d} \tag{45}$$

where ϵ_y is the yield strain of the tension reinforcement and k'd is the depth to the neutral axis. If the modulus of elasticity of the steel is taken as 30,000,000 psi, then

$$\Phi_y = \frac{f_y}{30 \times 10^6(1-k')d} \tag{46}$$

The expression used to determine k' is

$$k' = \sqrt{2\,[np + (1-k'')(n-1)p'] + [(n-1)p' + np]^2} - [(n-1)p' + np] \tag{47}$$

where

$$k'' = d'/d$$

$$n = 30 \times 10^6/E_c$$

This formula reduces to

$$k' = \sqrt{2pn + (pn)^2} - pn \tag{48}$$

for beams reinforced in tension only, and is based on a linear distribution of strain.

The midspan deflection at yield can then be computed from Eqs. 43 and 44 with $\Phi_c = \Phi_y$ as given by Eq. 46. The value of f_y in Eq. 46 is replaced by f_{yd} from Table 16. The value of k' in Eq. 46 is obtained from Eq. 47 or 48 using values of E_c given in Table 4. Values of Δ_{yd} thus computed are given in Table 16.

It may be noted that the above procedure for computing deflections yields results identical to those obtained from the conventional expressions for deflection of a beam of constant cross-section involving the use of a moment of inertia for the transformed section with no tension in the concrete and corresponding values of E_c. The two procedures are based on identical assumptions.

12.1.3 Ductility

In Ref. 29 the following formula (A34) is advanced as a reasonable approximation to the ductility developed by two-point loaded beams.

$$\frac{\Delta_m}{\Delta_y} = \frac{q_{cr}}{0.75\, q'} \tag{49}$$

where Δ_m is the collapse deflection, and

$$q_{cr} = \frac{k_1 k_3 \epsilon_u}{\epsilon_u + \epsilon_y} \quad (50)$$

$$q' = \frac{pf_y - p'f'_y}{f'_c} \quad (51)$$

The quantity ϵ_u is the crushing strain in the concrete, and k_1k_3 relates the compressive strength of the concrete in the beam to that measured by the control cylinders. Assuming $\epsilon_u = 0.004$, $k_1k_3 = 0.85$, and $\epsilon_y = f_y/30 \times 10^3$,

$$q_{cr} = \frac{102}{120 + f_y} \quad (52)$$

where f_y is in ksi.

If it is assumed further that the gain in strength under dynamic loading is the same for the concrete and for the steel, then the values of q' (Eq. 51) would be the same for both static and dynamic loadings.

The values of q_{cr}, computed according to Eq. 52 and using f_{yd} in place of f_y, are listed in Table 16 and designated q_{crd}. In the next column of this table, the ductility factor computed according to Eq. 49 is given. The collapse deflection, designated Δ_{md}, is the dynamic yield deflection multiplied by the ductility factor. The slope of the initial portion of the curve, $k_{1d} = Q_{yd}/\Delta_{yd}$, is given in the last column of Table 16.

12.1.4 Direct Computation of Collapse Deflection

Instead of computing collapse deflection as the product of yield deflection and ductility, as is done in Section 12.1.3, it is possible and perhaps more desirable to make the computation directly, utilizing fundamental properties of the beams. From the equations in the Appendix of Ref. 29 it can be shown that

$$\Phi_m = \frac{k_1 k_3 \epsilon_u}{q' d} \tag{53}$$

where Φ_m is the curvature at midspan at crushing of the concrete. If it is again assumed, as in Section 12.1.2, that curvature varies as the moment, then substituting Φ_m for Φ_c and Δ_m for Δ_c into Eqs. 43 and 44 yields, for a = 1/3,

$$\Delta_m = 0.1063\ \Phi_m L^2 \tag{54}$$

and for a = 29/76,

$$\Delta_m = 0.1007\ \Phi_m L^2 \tag{55}$$

Replacing Φ_m in Eqs. 54 and 55 by the expression in Eq. 53 one obtains for a = 1/3,

$$\Delta_m = \frac{0.1063\ k_1 k_3 \epsilon_u\ L^2}{q' d} \tag{56}$$

and for a = 29/76,

$$\Delta_m = \frac{0.1007\ k_1 k_3 \epsilon_u\ L^2}{q' d} \tag{57}$$

It is probable that the values of the terms $k_1 k_3$, ϵ_u, and q' are all influenced by rapid loading. However, the scatter in the values of the terms $k_1 k_3$ and ϵ_u for static loading only, presented in the literature of research in reinforced concrete (23), hardly warrants an attempt to differentiate between static and dynamic values of these parameters. With regard to q' it may again be assumed, as in Section 12.1.3, that the values would be the same for both static and dynamic loadings. In view of the discussion in Section 11.2 regarding the unimportant differences between measured static and dynamic collapse deflections it does not appear to be unreasonable to use

Eqs. 56 and 57 for both static and dynamic loading conditions. Further simplification can be achieved by substituting 0.1 for the values 0.1063 and 0.1007 in Eqs. 56 and 57. Then, assuming $k_1k_3 = 0.85$ and $\epsilon_u = 0.004$, Eqs. 56 and 57 reduce to

$$\Delta_m = \frac{3.4}{10^4}\frac{L^2}{q'd} \tag{58}$$

The values of Δ_m computed by Eq. 58, using values of q' from Table 5, are given in Table 17 for all the beams tested. It must be remembered, however, that Eq. 58 is valid only for flexural failures. (These computed values of Δ_m are different from those in Table 16 because Eq. 58 does not involve the effect of strain rate on the strength of the materials in the beams.) Also given in Table 17 are the measured values of Δ_m and the ratio of computed to measured values. These ratios will be discussed in Section 12.2. Other information is repeated in Table 17 for convenience.

12.2 Comparison with Analog Computer Solutions

In Table 18 the values of the resistance parameters obtained using the analog computer (A.C.) and those computed from strain rates (Str.) according to Section 12.1 are listed in adjacent columns. Also given are the ratios of the computed values to those obtained from the analog computer analysis.

With regard to the dynamic yield level, Q_{yd}, the value based on strain rate is always higher than the value from the analog solution. This consistent error could be due to a misinterpretation of the strain-time curves, a misapplication of the curve in Fig. 38, neglect of the influence of the concrete strength on the yield capacity, neglect of a possible shift in the neutral axis at yielding due to dynamic loading, and perhaps to other unknown factors. In any case, the scheme used in Section 12.1 to compute Q_{yd}

is slightly but consistently on the unsafe side. Probably the easiest way to correc this discrepancy is to shift the curve shown in Fig. 38 so that it yields values of dynamic yield strength of steel about ten percent smaller.

The yield deflections determined from strain rates are in general agreement with those determined with the analog computer except for Beams 4a1 and 5a2, although they are consistently too low for the short beams. In Ref. 21, the static yield deflections are given for beams having the same span and overall dimensions as those of Series 2, 3 and 4 and loaded at the third-points. Computations for the yield deflections of these beams using the procedure described in Section 12.1.2, which is identical with the procedure of Ref. 21, gave values that averaged 22 percent below the measured values for the beams of Ref. 21 reinforced only in tension, and 29 percent below the measured values for the beams reinforced in both tension and compression. The range of error was 4 to 56 percent. The average of the errors in the computed values of Δ_{yd} for the short beams in Table 18 is approximately 9 percent. However, if the values of f_{yd} used in the computation are actually 10 percent too high, as is indicated above for the computation of Q_{yd}, then the error in Δ_{yd} due to the method of computation, disregarding the influence of material strengths, is actually of the order of 20 percent, which is in agreement with the results of Ref. 18. No explanation can be offered for this discrepancy, especially since the computation assumes a fully cracked section throughout the length of the beam, which should result, it would seem, in the highest values of Δ_y computable using a "straight-line" procedure.

Gaston (Ref. 21) attempts to explain this discrepancy by questioning the use of his measured values of E_c, which were what might be called initial tangent moduli, and questioning the measured value of yield deflection. He explains that the load was applied in distinct increments and the yield deflection could have been consistently over-estimated since deflection readings were taken at the end of an increment while yielding may have occurred during the load increment.

Regarding the use of the initial tangent value of E_c, if one inspects Eq. 39 in Section 12.1.2 it appears that E has a direct effect on Δ. However, this is true only for homogeneous cross-sections. It can be shown that the computation of the transformed moment of inertia of reinforced concrete beams also involves the use of the value of E_c, as does the computed value of yield capacity. These effects tend to cancel each other. A more direct method of determining the effect of E_c on the value of the yield deflection is to consider Eqs. 43, 45, and 47. In these equations it can be seen that E_c is involved only in the computation of k' and cannot possibly have enough influence to change the values of Φ_y by 15-20 percent. Changes in E_c of as much as 500,000 psi change k' by only 0.02. The explanation regarding the use of load increments and the influence of this procedure on the measured values of yield deflection may be valid. The data of the tests herein described were continuously recorded, and the errors in computed values appear to be of a somewhat smaller magnitude.

The fact that the computed values of yield deflection for the longer beams are in slightly better agreement with "measured" values (those determined from the analog computer solution) suggests some effect of span length or load distribution. This could take the form of shear deflection, which would be more important in the short span beams; distribution of yield strain in the tension reinforcement, which extends over a relatively greater portion of the span in the short beams; and other unknown factors.

Examining the expression for Δ_c, Eq. 43, and that for Φ_y, Eq. 45, it is seen that Δ_c could be increased if, for the short beams, the constant

0.1063 were increased, ϵ_y were increased, or k' were increased. However, it is not expected, in general, that k' will vary a great deal. In fact, it is quite close to 0.4 for a range of normal values of p, p', and E_c. In addition, any increase in ϵ_y is a correction in the wrong direction so far as Q_{yd} is concerned, as explained above. The only quantity remaining is the constant 0.1063. A change in this value can be justified on the grounds that the distribution of curvature in a reinforced concrete beam does not vary as the moment, as was assumed in deriving Eq. 42. The value of the constant would have to be approximately 0.125 to give computed values of Δ_{yd} in general agreement with the measured values if ϵ_y were decreased the amount necessary to provide agreement also between measured and computed values of Q_{yd}.

The next values compared in Table 18 are those of Δ_{md}/Δ_{yd}, the dynamic ductility. Only four comparisons are made because collapse occurred in only these four instances, as noted in Table 18. In the other cases, a static test or other dynamic blows followed those reported. No computations are shown in Table 18 for these additional tests because the strain gages were destroyed.

Except for Beam 2b2, the computed values of ductility based on strain rates are too high. One probable cause is the use of too high a value of ϵ_u in the computation of q_{crd}. If $\epsilon_u = 0.003$ were used instead of 0.004, the value of q_{crd}, and therefore Δ_{md}/Δ_{yd}, would be reduced 12 percent for $f_{yd} = 60$ ksi. Another possible source of error is the use of the static value of q' (or q) which may be too low. It may be that the increase in strength of the concrete is not as great as that of the reinforcement, in which case the value of q should be increased. At least, the curves in Fig. 38 indicate that for the same strain rate the concrete does not increase in strength as much as the steel.

By a combination of the errors discussed in this section for the computed values of Δ_{yd} and Δ_{md}/Δ_{yd}, the computed values of Δ_{md} compare remarkably well with the measured values given in Table 18. This is a fortuitous circumstance and is not to be taken as confirmation of the procedure for computing Δ_{md} as the product of Δ_{yd} and the ductility factor.

In Table 17, values are given for measured and computed collapse deflection where the computed values were determined according to Section 12.1.4. Comparisons are made only for beams which failed in flexure. In general, the computed values are too low, sometimes strikingly so. The primary reason is that Eq. 58 assumes collapse to occur when the concrete crushes. It has been pointed out in various places in Sections 10.4 and 10.5 that this was often not the case. In many instances crushing was detected visually and by the strain gages before collapse occurred. This was especially true of the beams of Series 3 which had compression reinforcement. Nevertheless, in spite of the apparently better agreement between measured and computed values of Δ_{md} achieved by multiplying the yield deflection by the ductility, it is believed that the additional deformation capacity which may be available after crushing of the concrete should not be relied on in design and that a conservative approach to the computation of collapse indicates the use of the procedure of Section 12.1.4; that is, a direct computation of Δ_{md} based on the assumption that collapse occurs when the concrete crushes.

Since k_{ld} was computed from Q_{yd}/Δ_{yd}, any errors in these latter terms will be reflected in the former. In general, the computed values of k_{ld} are too high. This is simply a result of too high values of Q_{yd} in combination with too low values of Δ_{yd}. Of course, the use of too high a value of k_{ld} is unsafe since it would yield too low a value of computed response, but it is felt that greater effort should be expended toward the development of more accurate methods of computing Q_{yd} and Δ_{yd}, if possible, and that the value of k_{1d} should then be allowed to fall where it may.

Several of the comparisons made in Tables 17 and 18 are shown graphically in Fig. 39. The resistance function from the analog computer solution has been taken as the "measured" resistance. The measured values of Q and Δ have been expressed as proportions of the measured values of Q_{yd} and Δ_{yd}. This results in a single "measured" resistance function up to yield, having coordinates $Q_{yd} = 1$ and $\Delta_{yd} = 1$. In the inelastic range, the values of collapse deflection Δ_{md}, are also expressed as ratios of the value at yield, Δ_{yd}; thus the abscissas of the points representing collapse correspond to the "measured" ductility. The ordinates are of course constant at $Q = 1$. Using this representation of the measured values as a base, the resistance functions computed from strain rates are shown in Fig. 39 as dashed lines. These curves were also obtained by expressing the computed resistance as a proportion of the measured value of Q_{yd} and the computed deflections both at yield, Δ_{yd}, and at collapse, Δ_{md}, as proportions of the measured value of Δ_{yd}. The four comparisons made are for those beams listed in Table 18 which experienced collapse under the first blow and which, incidentally, generally represent the widest range of variation between computed and measured values.

12.3 Discussion of Usefulness

A question may be raised regarding the usefulness in design of the information presented in Sections 12.1 and 12.2, since the strain rates are not known prior to a test or at the design stage. However, with the use of an analog computer or a numerical method of computation such as the Newmark β Method (30), it is possible to compute the response of a beam to an applied impulsive load. It is then necessary only to relate this response to the strain rate.

From Section 12.1.2 it is seen that the deflection at midspan is

$$\Delta_c = H\Phi_c L^2 \tag{59}$$

where H is a constant depending on the loading. For third-point loading, H = 0.1063; for two-point loading with a = 29/76, H = 0.1007; for midspan loading, H = 0.0833; for uniform loading, H = 0.1042. Substituting,

$$\Phi_c = \frac{\epsilon_c}{(1-k')d} \tag{60}$$

Eq. 59 becomes

$$\Delta_c = HL^2\ \epsilon_c/(1-k')d \tag{61}$$

Taking the derivative with respect to time of both sides of Eq. 61

$$\mathring{\Delta}_c = HL^2\ \mathring{\epsilon}_c/(1-k')d \tag{62}$$

where $\mathring{\Delta}_c$ is the deflection rate, or velocity; and rearranging,

$$\mathring{\epsilon}_c = \mathring{\Delta}_c\ (1-k')d/HL^2 \tag{63}$$

Values of $\mathring{\Delta}_c$, taken from the measured responses in Figs. A35-A72 at the point at which yielding occurred as determined by the analog computer for those beams for which $\mathring{\epsilon}_c$ was measured, are given in Table 19. The values of $\mathring{\epsilon}_c$, computed from Eq. 63 using the value of k' computed as in Section 12.1.2 and the appropriate values of H and L^2, are also given. In the next column the values of $\mathring{\epsilon}$ taken from the strain vs. time plots are given. There are some glaring differences between measured and computed values. However, the important consideration is the effect of strain rate on the yield strength of the steel. In the last two columns of Table 19, the increases in yield strength as determined from Fig. 38 are given for both the measured and computed values of $\dot{\epsilon}_c$. In only one case, Beam 7a2, Blow 4, is the difference more than five percent. It can be concluded, therefore, that the use of strain rate determinations is feasible as one step in the design and analysis of beams subjected to blast loadings. In summary, the design procedure might follow these steps:

(1) Select a beam cross-section. This would be the result of experience, judgment, previous designs, etc.

(2) Assume an increase in yield strength due to dynamic loading and compute the pertinent properties of the beam, such as Q_{yd}, Δ_{yd}, k_{1d}, Δ_{md}, T, etc.

(3) Compute the response to a predetermined dynamic loading, using some iterative procedure, or an analog computer.

(4) Scale off the velocity at yield.

(5) Compute the strain rate in the tension reinforcement.

(6) Check the value of f_{yd}/f_y assumed in Step 2 using a relation such as that shown in Fig. 38.

(7) If the assumed and computed values of f_{yd}/f_y do not check, then return to Step 2 with the new value of f_{yd}/f_y. If they do check, then it must be decided whether the maximum response of the selected cross-section is acceptable. If so, the problem is finished. If not, then the cross-section assumed in Step 1 must be changed and the process gone through again.

This is not presented as the only way to accomplish a design of reinforced concrete under impulsive loads, nor is it necessarily the most efficient way. Of course, the errors between measured and computed values discussed in Section 12.2 must be handled in some manner, perhaps by arbitrary coefficients applied to the dynamic yield strength as previously suggested. Also, it must be realized that the process of computing strain rates from velocity involves the assumption that the strain varies directly as the moment. This can be far from the truth in a cracked reinforced concrete beam, and the only saving factor is the relatively small, though important, change in influence that strain rate has on f_{yd}/f_y within the range of rates that occurred in these tests. It is felt that this will also cause the trial and error process of Steps 2-6 to converge to compatible values of $\dot{\epsilon}_c$ and f_{yd}/f_y rather quickly.

XIII PREDICTED BEHAVIOR USING PRESENT O.C.E. METHOD

13.1 Method of Calculation

The current edition of Design of Structures to Resist the Effects of Atomic Weapons, (20) contains information and examples regarding the behavior and design of reinforced concrete beams subjected to rapid loading. Several equations and methods presented therein have been used to predict the resistance, response, reactions and mode of failure of some of the beams described in this report. Only those beams are considered which had strain gages on the steel permitting strain rates to be determined, which in turn defined the dynamic properties of the materials.

13.1.1 Material Properties

Before considering the particular methods and equations it is necessary to define the procedures used to determine the properties of the steel and concrete which are required by the equations.

It is explained in Section 12.1.1 how the dynamic yield strength of the tension steel was determined. These yield strengths are retabulated in Col. 1 of Table 20 for convenience. The yield strengths of the compression steel were similarly computed, which assumes that the compressive strength of the steel is affected by dynamic loading in the same manner as the tensile strength. The values are tabulated in Col. 2 of Table 20. For Beams 3b2 and 6a1, where the strain gages indicated that yielding did not take place, the values tabulated are the maximum measured strains multiplied by 30,000 ksi. Since no measurements were made of strains in the web reinforcing, the static yield strengths given in Table 4 will be used. The pertinent quantities are retabulated in Col. 3 of Table 20.

The values of dynamic concrete strength to be used were determined on the basis of the strain rates tabulated in Table 9. These strain rates were used with Fig. 38 to determine the percent increase in concrete strength. The strain rates and percent increase, expresses as a ratio of dynamic to static strength, are tabulated in Cols. 4 and 5 of Table 20. In several instances there are values in Table 20 where there were none in Table 9 because no crushing was detected. In these cases the concrete strain rate values in Table 20 represents an estimate of the strain rate exhibited by the major portion of the concrete strain versus time curves. The corresponding dynamic strengths are tabulated in Col. 6. For Beams 2a1, 4a1, and 4a2, where there were no gages on the concrete to record strain, the increase in compressive strength of the concrete was estimated by comparison of the behavior of the beams in question with that of similar beams, namely Beams 2b2 and 4c2. The estimate was arrived at by increasing the values of the ratio of f'_{cd}/f'_c for Beams 2a1, 4a1, and 4a2 over the values for Beams 2b2 and 4c2 as much as the values of f_{yd}/f_y were greater for Beams 2a1, 4a1, and 4a2 than for Beams 2b2 and 4c2. The other property of the concrete required by the equations is the modulus of elasticity. The values used are those tabulated in Table 4 which were determined from tests of 6 x 12-in. cylinders and represent the tangent modulus. The pertinent values are repeated in Table 20 for convenience.

13.1.2 Equations for Capacity

In Ref. 20 the following equation is given as the plastic resisting moment, in bending only, under dynamic loading (Eq. 4-18), Equation 64 assumes

$$M_P = A'_s f_{yd} d' + (A_s - A'_s) f_{yd} d \left[1 - \frac{(A_s - A'_s) f_{yd}}{1.7 f'_{cd} bd}\right] \qquad (64)$$

that the dynamic yield strengths of the tension and compression reinforcing are the same. In order to consider different values for these strengths Eq. 64 was modified as follows,

$$M_P = A_s' f_{yd}' d' + (A_s f_{yd} - A_s' f_{yd}')d \left[1 - \frac{(A_s f_{yd} - A_s' f_{yd}')}{1.7 f_{cd}' bd}\right] \tag{65}$$

For $A_s' = 0$, Eq. 65 reduces to

$$M_P = A_s f_{yd} d \left[1 - \frac{A_s f_{yd}}{1.7 f_{cd}' bd}\right] \tag{66}$$

For the purposes of comparison with measured values is it more convenient to express the resistance in terms of a force. Thus, the following conversion must be made:

For the short beams (shear span = 36 in.)

$$Q_{yd} = M_P/18 \tag{67a}$$

For the long beams (shear span = 58 in.)

$$Q_{yd} = M_P/29 \tag{67b}$$

The computed yield capacities of the test beams according to Eqs. 65 and 67, using the material properties of Table 20, are tabulated in Col. 1 of Table 21.

In Ref. 20 the following statement is made in regard to shear, ".... beams should be designed so that the nominal shear stress calculated by equation (4.23) does not exceed the values obtained by equations (4.24a) and (4.24b)." With some minor changes in notation, the equations are:

$$v = \frac{8V}{7bd} \qquad (4.23) \tag{68}$$

For beams with web reinforcement:

$$v_y = 0.04\ f'_c + 5000\ p + rf_w \qquad (4.24a) \qquad (69a)$$

For beams with no web reinforcement:

$$v_y = 0.04\ f'_c + 5000\ p \qquad (4.24b) \qquad (69b)$$

In Col. 2 of Table 21 the values of $\underline{v}$ according to Eq. 68 are tabulated using $Q_{yd}/2 = V$. In Col. 3 of Table 21 the values of v_y according to Eq. 69 are tabulated using the static concrete strength for f'_c, as recommended in Ref. 20. In Col. 4 of Table 21, the symbol "S" represents the cases for which $v > v_y$; that is, for which shear governed the design. The symbol "F" corresponds to $v < v_y$; that is, flexure governs the design.

13.1.3 Equations for Deformation

In Ref. 20 it is recommended that the deflection at yield be computed using an elastic method involving the "theoretical load causing plastic deflection," (Q_{yd}), the initial tangent modulus for the concrete, (E_c), and a moment of inertia, I_a, equal to the average of the gross (I_g) and transformed (I_t) values (Eq. 4.25). Thus, from Eq. 39,

$$\Delta_{yd} = \frac{Q_{yd}\ a\ L^3\ (3-4a^2)}{48\ E_c\ I} \qquad (70)$$

where

$$I_a = \frac{I_g + I_t}{2} \qquad (4.25) \qquad (71)$$

For a rectangular section, $I_g = bh^3/12$. For the beams of this program $I_g = 864$ in.^{4}. The transformed moment of inertia depends on the properties of the cross-section and is given by

$$I_t = b\ (k'd)^3/3 + pn\ bd^3(1-k')^2 + p'(n-1)bd^3\ (k'+k''-1)^2 \qquad (72)$$

(See Ref. 21, Eq. 34). The value of k' is given by Eq. 47 of this report. The values of Δ_{yd} determined from Eqs. 70, 71, 72, and 47, and using values of E_c from Table 20, are given in Col. 5 of Table 21.

In Ref. 20 it is explained that the ductility can be estimated, with some changes in notation, as

$$\frac{\Delta_{md}}{\Delta_{yd}} = \frac{0.1}{p-p'} \qquad (4.17) \qquad (73)$$

The values of Δ_{md} determined from Eq. 73 are tabulated in Col. 6 of Table 21, using the values of Δ_{yd} from Col. 5.

Also tabulated in Table 21 are the computed initial slope, k_{1d}, equal to Q_{yd}/Δ_{yd}, and the computed period, T, from Eq. 35. These values are needed in the computation of the response, discussed below.

13.1.4 Computation of Response

The quantities Q_{yd}, Δ_{yd}, and Δ_{md}, as given in Table 21, define the dynamic resistance of the beams being considered, according to Ref. 20. These quantities are plotted in certain of Figs. A96-A133 as a series of crosses and are identified as OCE-Q. The small circle which appears on the initial slope in several of the plots (See Fig. A105) represents the point where $v = v_y$, and, thus, where failure in shear could be expected if the methods of determining v and v_y were without error.

These resistance diagrams were subjected to the actual measured load pulses and the response determined on an analog computer. The equipment used was the same as that described in Section 11.1.4. The procedure was straight-forward since a resistance was now given and the response could be determined in one run on the computer. The responses thus determined are plotted as dashes in certain of Figs. A35-A72 and identified as OCE. The plots are terminated at the measured collapse deflection in those cases where collapse occurred in the test.

13.1.5 Computation of Reactions

In Table 6.1A of Ref. 20, two equations are given, depending on the range of behavior, for the computation of the dynamic reactions for a simply-supported beam loaded at the third-points. These equations are, with some modification of notation:

In the elastic range,

$$R = 0.62\ Q - 0.12\ P \qquad (74a)$$

and in the plastic range,

$$R = 0.75\ Q_{yd} - 0.25\ P \qquad (74b)$$

The sum of the two reactions for a simply-supported beam would then be:

In the elastic range,

$$\Sigma R = 1.24\ Q - 0.24\ P \qquad (75a)$$

and in the plastic range,

$$\Sigma R = 1.50\ Q_{yd} - 0.50\ P \qquad (75b)$$

In Figs. A96-A116 the sum of the reactions computed according to Eq. 75, for the short-span beams, are plotted as dashed lines and identified as OCE-R. The actual values of load were used for P at each point of time. The resistance functions used for Q were those determined on the analog computer (See Section 11.1) and identified as Q in Figs. A96-A116. The resistance functions determined above in this chapter were not used because it was felt that those determined on the computer better represented the behavior of the beams tested. There were no determinations of ΣR made for the long-span beams as they were not loaded at the third-points and, consequently, Eq. 75 would not be valid.

13.2 Comparison of Measured and Computed Resistance and Behavior

13.2.1 Resistance and Mode of Failure

Table 22 contains values of the resistance parameters and an indication of the mode of failure as determined directly from the tests or on the analog computer (measured) and as determined above in Section 13.1 (computed). Several of the comparisons to be discussed are graphically illustrated by the pertinent figures among Figs. A96-A133.

First considering the dynamic yield level, Q_{yd}, the values computed according to Section 13.1 are generally somewhat higher than those determined with the analog computer, though the discrepancy here is not as great as that noted in Section 12.2 where the analog computer values are compared with those determined from measured strain rates. Several possible reasons are given in Section 12.2 for the high computed values of Q_{yd} as well as a method of correcting for this tendency. It is noted that the OCE values of Δ_{yd} given in Table 22 are always less than those determined by the computer. This should be expected since Δ_{yd} was determined by dividing the yield load by k_{1d}. Because k_{1d} is nonlinear, the OCE manual evaluates it by deflection equations using the average of the gross and cracked section moments of inertia. Better results will be obtained by the OCE method if the average moment of inertia is used for design purposes where beams are subjected to loads that vary with time, since k_{1d} is large prior to cracking but decreases rapidly after crack formation. However, it appears that, if desired, the actual value Δ_{yd} could be more accurately predicted when k is determined by use of the moment of inertia of the cracked section. This is compatible with relationships shown in Fig. 421, EM 1110-345-414.

In Table 22 the tabulated values of measured Δ_{md} are actual test values. Comparing them with the computed values indicates that the computed values are low in most cases and high in others. (No values are shown for

Beam 5b4 as Δ_{md} has no meaning for a beam failing in shear. However, a value is shown for Beam 6b2 as the failure in this case was nearly balanced between shear and flexure and the analog computer determination of the resistance has an inelastic portion.) Since Δ_{md} as computed in Section 13.1 involves the computation of Δ_{yd} it is difficult to tell whether the discrepancy between measured and computed values of Δ_{md} is due to errors in the calculation of Δ_{yd} or to some mistake in Eq. 73. The results of using measured values of Δ_{yd} in Eq. 73 in order to compute Δ_{md} are also shown in Table 22. There does not seem to be any improvement in the ratio of computed to measured values; in fact, the computed values are now generally unsafe.

In several instances the design by the OCE method was governed by shear whereas failure actually occurred in flexure. This is desirable and would be expected if the method used provides a higher factor of safety in shear than in flexure, as it presumably does. However, in one case, Beam 6b2, shear did not govern the design by the OCE method although failure actually occurred in shear. This is unexpected and deserves further scrutiny. First, though the predicted capacity of Beam 6b2 for failure in shear computed from Eq. 68 with $v = v_y$, is 44.0 kips, using the concrete strength from Table 4, inspection of Fig. 31 leads to the observation that distress in bond and initiation of inclined tension cracking occurred in the lower half of the beam. The strength of the concrete in this section of the beam was 2.32 ksi (not reported elsewhere). Recomputing the capacity in shear using this value of f'_c, instead of 4.44 ksi as given in Table 4, yields a value for v_y of 334 psi. Comparing this value with the value of v given in Table 20 for this beam, the conclusion would be that failure could have occurred in either flexure or shear. Second, the behavior of Beam 6b2 under the dynamic loading was such that the resistance diagram used with the analog computer had to have an inelastic portion in order to match the measured response. Thus, though the crack pattern for this beam is unmistakeably that for a shear failure, the beam did exhibit considerably more ductility than is normally associated with such behavior. It is felt therefore, that one may safely conclude that the error on the part of the OCE method in predicting the governing design condition for this case is not serious.

13.2.2 Response

The measured responses indicated by Δ, and the responses computed using the OCE resistances, indicated by OCE, may be compared by inspecting the pertinent figures among Figs. A35-A72. The differences between the measured and computed curves may be related in every instance to differences in the measured (by the analog computer) and computed resistance diagrams. Where the computed response is too small the computed values of Q_{yd} and/or k_{1d} are too large. A comparatively small computed response with a period similar to that of the measured response is associated with a too high computed value of Q, whereas a too high value of k_{1d}, resulting from low computed values of Δ_{yd}, is associated with both a small response and a comparatively small period. The differences in the times of initiation between measured and computed response are unimportant as they are due to differences in establishing zero times on the test records. For example, the OCE curve in Fig. A59 may be shifted 5 msec. to the right to give a better comparison between measured and computed curves. This shift had already been taken into account in the curve plotted by the computer (ACR).

13.2.3 Reactions

The measured and computed reactions can best be compared by referring to Figs. A96-A116. In eight of the nineteen cases where comparisons can be made the computed curves exhibit strong peaks or dips in a direction opposite to that exhibited by the measured curves. In nine of the cases the computed curves are much too high in the inelastic range of behavior, while in eight of the cases the computed curves tend to increase in value in the inelastic range of behavior while the measured curves generally decrease in value in this range. In only three cases can the computed curves be said to approximate the measured curves reasonably well.

XIV SUMMARY AND CONCLUSIONS - PART B

The object of this investigation was to obtain information on the strength and behavior of reinforced concrete beams subjected to rapid loading. To this end, 33 beams of various strengths, 6 by 12-in. in cross-section and 9 ft or 12 ft-8 in. in span, were tested under static and dynamic loads, using a pneumatic loading device. The results are presented in the form of graphs, tables, and photographs and are interpreted by means of comparisons between static and dynamic properties, and in terms of the effects of several of the variables on the behavior of the test beams. An analytical procedure for the determination of the dynamic resistance of reinforced concrete beams is proposed which involves the use of deflection rates at yield and their correlation with changes in material strengths.

As a consequence of the study, interpretation, and analysis of the test results presented in this report, several conclusions can be drawn regarding the resistance and behavior of reinforced concrete beams subjected to rapid loading. Before enumerating these conclusions the limited scope of the tests should be brought to mind. Limitations on the scope include: the use of only one grade of reinforcement with one type of deformation pattern; one value each of width and depth of beam cross-section; one type of concrete aggregate; one general form of load-time relation; one type of load distribution; only two span lengths; only two percentages of tension reinforcement; and only one percentage of compression reinforcement; limited variation in percentage of web reinforcement; and only ten beams where computed and "measure" values could be compared. Within the bounds of these limitations, the conclusions and findings presented below are relieved to be valid.

With regard to the dynamic resistance of reinforced concrete beams, the level of yield resistance was increased over the static level in direct proportion to the increase in strength of the tensile reinforcement. In most cases, the yield deflection and elastic slope also increased with respect to the values for beams loaded statically. Generally, a large increase in yield deflection was accompanied by a decrease in elastic slope, and vice versa. The dynamic resistance level could be maintained through successive dynamic loadings; however, a decrease in elastic slope was generally exhibited with each successive loading. A small increase in capacity between the yield and collapse stages of reinforced concrete beams under two point loading, and the existence of damping, were recognized; nevertheless, it was possible to match the measured response of the beams tested using resistance diagrams with zero slope in the region beyond yield and neglecting damping. The computations involved the assumption that the behavior of the test beams could be adequately represented by a single-degree-of-freedom system, and the results of the analysis support the conclusion that this assumption is reasonable.

With regard to the collapse behavior of the beams tested, it was noted that crushing of the concrete in compression did not necessarily cause collapse. Values of collapse deflection computed for the assumption that crushing and collapse were coincident, were generally too low as compared to measured values, especially for beams reinforced in compression. Measured values of crushing strain in the concrete under dynamic loading were generally the same as those reported by others for static loading. However, a small but consistent increase in collapse deflection under dynamic loading was noted. The effects of the parameter q and of compression reinforcement on collapse deflection were the same under dynamic loading as under static loading; that is, the collapse deflection increased with the use of compression reinforcement and with lower values of q. The effect of tie configuration, however, was obscured by other factors. It appeared that successive blows had a tendency to increase the final collapse deflection of a beam tested statically to collapse. The appearance of comparable beams after collapse was generally the same whether they had been tested statically or dynamically, if the modes of failure were the same. No distinctive visual characteristic could be associated with a beam tested dynamically. The general effect of stirrups was to prevent shear failure, although no limiting value of web reinforcement was established.

An analytical procedure for determining the dynamic resistance of a reinforced concrete beam, based on the rate of deflection at yield, appears feasible. However, certain adjustments must be made in available data on the relation between strain rate and yield strength of reinforcing steel and in the method of computing yield deflection based on the "straight-line" theory. The analytical procedure requires the computation of the entire response curve of a beam subjected to dynamic loading, a task for which an analog computer has been found to be ideally suited.

The test results and the resistance functions determined with the analog computer are also compared with the results of computations based on the procedures and formulas of the Manual of the Corps of Engineers, U. S. Army, entitled "Design of Structures to Resist the Effects of Atomic Weapons" (20). In general, the computation for dynamic resistance level yielded adequate results, and the prediction of the mode of failure was quite accurate. However, computations for the yield deflection resulted in values that were too small, computations for the maximum deflection resulted in values that were too large, and computations for the reactions resulted in curves at wide variance with the measured curves.

PART C RECOMMENDATIONS

XV RECOMMENDATIONS FOR DESIGN AND ANALYSIS

15.1 Introduction

In Parts A and B of this report tests of reinforcing bar coupons and reinforced concrete beams under dynamic loading have been described and interpreted. This material will be used below to support recommendations for the determination of the dynamic resistance of a reinforced concrete beam under two point (or uniform) load, for computing reactions, for estimating the effectiveness of web reinforcement in preventing shear failures under dynamic loading, and for determining the size and spacing of compression reinforcement ties. In those instances where the recommended equation or procedure has not already been compared with the test results reported in Parts A and B, such comparisons will be made below, provided they are feasible.

15.2 Dynamic Resistance

In Section 12.3 a design procedure is suggested for reinforced concrete beams under dynamic loading. This procedure will be repeated here with some changes reflecting the differences between some of the equations below and those considered previous to Section 12.3.

(1) Select a beam cross-section, based on judgment, experience, previous designs, etc.

(2) Assume an increase in yield strength of the longitudinal reinforcing steel and compute the pertinent properties of the beams, such as Q_{yd}, Δ_{yd}, Δ_{md}, k_{ld}, T, etc., according to the equations below.

(3) Compute the response to a predetermined dynamic loading, using some iterative procedure, or an analog computer.

(4) Scale off the velocity at yield.

(5) Compute the strain rate in the tension reinforcement.

(6) Determine the increase in yield strength from Fig. 20 and check against the value assumed in Step 2.

(7) If the assumed and computed values of the increase in yield strength do not check, then return to Step 2 with the new value from Step 6. If they do check, then it must be decided whether the maximum response of the selected cross-section is acceptable. If so, the problem is finished. If not, then the cross-section assumed in Step 1 must be changed and the process gone through again.

15.2.1 Resistance Level

In order to compute the resistance level, Q_{yd}, called for in Step 2, it is necessary to compute the resisting moment. The value of Q is then a linear function of the moment, the function depending on the arrangement of loading. For the purpose of computing the dynamic resisting moment, the equation given as Eq. 4-18 in Ref. 20 is recommended, with the change that the static concrete strength be used. Equation 4-18 then becomes

$$M_P = A_s' f_{yd} d' + (A_s - A_s') f_{yd} d \left[1 - \frac{(A_s - A_s') f_{yd}}{1.7 f_c' bd} \right] \qquad (76)$$

The effect of the concrete strength on the capacity of a reinforced concrete member is of secondary importance if the member is designed to fail by yielding of the steel. It seems unnecessary, therefore, to consider the possible slight increase in beam strength resulting from the effect of the dynamic loading on the plain concrete, especially since this effect is not well defined.

Table 23 contains the values of Q_{yd} computed using Eq. 76, in conjunction with the appropriate parts of Eq. 67, and the measured values from Table 11, for those beams where valid comparisons could be made. (The values in Col. 1 were computed taking into consideration the difference in the yield strengths of the tension and compression reinforcement. However, for design purposes it is recommended that these strengths be considered the same.)

15.2.2 Yield Deflection

The following equation is recommended for the computation of dynamic yield deflection,

$$\Delta_{yd} = \frac{L^2}{d}\,\frac{\epsilon_{yd}}{5} \tag{77}$$

Equation 77 was derived by starting with Eq. 61 for the deflection at midspan,

$$\Delta_c = HL^2\,\epsilon_c/(1-k')d \tag{61}$$

and substituting $H = 0.1$, $k' = 0.5$ and $\epsilon_c = \epsilon_{yd}$. The substitution of 0.1 for H is quite reasonable in the light of the theoretical values given for this quantity in Section 12.3. The value of 0.5 for k' is an average between the straight line design "balanced" value of 0.4 and the value of 0.6 which is approximately the dividing point between compression and tension failures in flexure for materials of ordinary strength. The dynamic yield deflections computed according to Eq. 77, with $\epsilon_{yd} = f_{yd}/30 \times 10^6$ psi, and f_{yd} taken from computed strain rates based on the measured velocity at yield (Table 19), are compared with the measured values in Cols. 4, 5 and 6 of Table 23. The computed strain rates were used to evaluate f_{yd} instead of the rates taken from measured strains in order to follow more closely the suggested procedure at the beginning of this section.

The strain rate is computed from the velocity by the use of Eq. 63, which is

$$\dot{\epsilon}_c = \dot{\Delta}_c \ (1-k')d/HL^2 \tag{63}$$

It is recommended that Eq. 63 be simplified by substituting H = 0.1 and $k' = 0.5$, yielding

$$\dot{\epsilon}_c = 5\dot{\Delta}_c d/L^2 \tag{78}$$

15.2.3 Maximum Deflection and Ductility Factor

It is recommended that the maximum deflection capacity be computed directly from the properties of the beam under consideration utilizing Eq. 58;

$$\Delta_{md} = \Delta_m = \frac{3.4 \ L^2}{10^4 \ q'd} \tag{58}$$

Note that the value of q' for use in Eq. 58 is computed using static strength values for both concrete and steel. Pertinent values from Table 17 where measured and computed maximum deflections are compared, are repeated in Table 23.

Though it is not recommended that the ductility factor be used as a design parameter, an expression for it can be obtained from the above expressions for Δ_{yd} and Δ_{md};

$$\frac{\Delta_{md}}{\Delta_{yd}} = \frac{3.4 \ L^2}{10^4 \ q'd} \frac{d}{L^2} \frac{5}{\epsilon_{yd}} = \frac{17}{10^4 \ q'\epsilon_{yd}} \tag{79}$$

15.3 Reactions

In fourteen of the nineteen cases illustrated by Figs. A96-A116 where comparisons can be drawn, the resistance of the beams tested, as determined with the analog computer, represents a better approximation of the sum of the measured reactions than does the computed sum of reactions according to Eq. 75. In the other five cases there is no decided preference. It is therefore recommended that the sum of the reactions be taken equal to the beam resistance, i.e.,

$$\Sigma R = Q_{yd} \tag{80}$$

or

$$R = Q_{yd}/2 \tag{81}$$

Equations 80 and 81 neglect the initial peak often exhibited by the reactions. Since the forces in the supports of a beam under dynamic loading are the loadings on the supports it is necessary to substantiate the safety of ignoring the initial peak. The effect of such a peak in the load-time function on the behavior of a dynamic system is investigated in Ref. 26, in which the peak is represented by a concentrated impulse. On the basis of the material contained therein, it is maintained that peaks of the magnitude of those measured in this program, in relation to the total magnitude of the reactions, will not have a significant effect on the behavior of the supporting structures.

15.4 Shear Reinforcement and Compression Reinforcement Ties

As illustrated in Table 22 and discussed in Section 13.2.1, the present procedure for determining the effect of web reinforcing given in Ref. 20 appears adequate. It is recommended that this procedure and the accompanying equations be retained pending further investigation and publication of results of shear failures in dynamically loaded beams of normal proportions.

The spacings of the ties used in the beams reported in Part B were designed to comply with Section 706a of the 1956 Building Code of the American Concrete Institute (31). In none of the tests can premature collapse or loss of ductility be attributed to the failure of these tests to hold the compression steel in place. Lacking further evidence, it is therefore recommended that tie spacing be designed in compliance with Section 706a of Ref. 31 with the additional stipulation that the hooks for the ties be made in the tension zone of the beam.

BIBLIOGRAPHY

1. The Effects of Nuclear Weapons. United States Atomic Energy Commission. Government Printing Office, Washington, D. C., June 1957.

2. "Review of Data On Effect of Speed in Mechanical Testing of Concrete." Douglas McHenry and J. J. Shideler. Development Department Bulletin D9, Portland Cement Association, Chicago, Illinois, 1956.

3. Proceedings of the Conference on the Properties of Materials at High Rates of Strain. The Institution of Mechanical Engineers (London), 1957.

4. "The Engineering Behavior of Structural Metals under Slow and Rapid Loading." J. M. Massard and R. A. Collins. Civil Engineering Studies, Structural Research Series No. 161, Department of Civil Engineering, University of Illinois, Urbana, Illinois, June 1958.

5. "Elasto-Plastic Response of Beams to Dynamic Loads." J. R. Allgood and W. A. Shaw. Technical Memorandum M-130, U. S. Naval Civil Engineering Research and Evaluation Laboratory, Port Hueneme, California, 3 March 1958.

6. "Impulse Testing of Concrete Beams." F. T. Mavis and F. A. Richards. Journal of the American Concrete Institute, September 1955.

7. "Destructive Impulse Loading of Reinforced Concrete Beams." F. T. Mavis and M. J. Greaves. Journal of the American Concrete Institute, September 1957.

8. Behavior of Structural Elements Under Impulsive Loads, Part I, II, and III. R. J. Hansen, et al. Department of Civil and Sanitary Engineering, Massachusetts Institute of Technology, Cambridge, Mass. April 1950, November 1950, July 1951.

9. "Effect of Loading History Upon the Yield Strength of a Plain Carbon Steel." I. Vigness, J. M. Krafft, and R. C. Smith. Proceedings of the Conference on the Properties of Materials at High Rates of Strain. The Institution of Mechanical Engineers (London), p. 138, 1957.

10. "Resistance and Behavior of Reinforced Concrete Beams Under Rapid Loading." A. Feldman. Ph.D. Thesis, University of Illinois, Urbana, Illinois, 1960.

11. "The Yield Strength of Intermediate Grade Reinforcing Bars Under Rapid Loading." W. A. Keenan. M. S. Thesis, University of Illinois, Urbana, Illinois, 1959.

12. "60 Kip Capacity Slow or Rapid Loading Apparatus." W. Egger. Civil Engineering Studies, Structural Research Series No. 158, Department of Civil Engineering, University of Illinois, Urbana, Illinois, June 1957.

13. "The Stress-Deformation Characteristics of Some Mild Steels Subjected to Various Rapid Uniaxial Stressings." J. M. Massard. Ph.D. Thesis, University of Illinois, Urbana, Illinois, 1955.

14. "Non-uniform Yield in a Mild Steel Under Dynamic Straining." D. B. D. Taylor. Proceedings of the Conference on the Properties of Materials at High Rates of Strain. The Institution of Mechanical Engineers (London), p. 229, 1957.

15. The Inelastic Behavior of Engineering Materials and Structures. A. M. Freudenthal. John Wiley and Sons, Inc., New York, 1950.

16. "On the Elastic-Plastic Strain of Steels Under Longitudinal Impact." G. V. Uzhik and J. J. Voloshenko-Klimovitsky. Proceedings of the Conference on the Properties of Materials at High Rates of Strain. The Institution of Mechanical Engineers (London), p. 239, 1957.

17. "Influence of Rate of Strain and Temperature on Yield Stresses of Mild Steel." M. J. Manjoine. Journal of Applied Mechanics, December, 1944.

18. "High Speed Tension Tests at Elevated Temperatures." M. J. Manjoine and A. Nadai. Part I, Proceedings of American Society for Testing Materials, Vol. 40, p. 822, 1940; Parts II and III, Journal of Applied Mechanics, p. A77, June, 1941.

19. "Investigation of Resistance and Behavior of Reinforced Concrete Members Subjected to Dynamic Loading, Parts I and II." A. Feldman and C. P. Siess. Civil Engineering Studies, Structural Research Series Nos. 125 and 165. Department of Civil Engineering, University of Illinois, Urbana, Illinois, 30 September 1956, 30 September 1958.

20. Design of Structures to Resist the Effects of Atomic Weapons. Manuals - Corps of Engineers, U. S. Army, EM 1110-345-414, 415, 416, Washington, D. C., 15 March 1957.

21. "An Investigation of the Load-Deformation Characteristics of Reinforced Concrete Beams Up to the Point of Failure." J. R. Gaston, et al. Civil Engineering Studies, Structural Research Series No. 40, Department of Civil Engineering, University of Illinois, Urbana, Illinois, December 1952.

22. "Development of Design Criteria for Reinforced Concrete Box Culverts, Part I: Strength and Behavior of Reinforced Concrete Beams and Frames." R. Diaz de Cossio and C. P. Siess. Civil Engineering Studies, Structural Research Series No. 163, Department of Civil Engineering, University of Illinois, Urbana, Illinois, September 1958.

23. "Concrete Stress Distribution in Ultimate Strength Design." Eivind Hognestad, et al. Journal of the American Concrete Institute, December 1955.

24. Vibration Problems in Engineering. S. Timoshenko. Third Ed., D. Van Nostrand, New York, 1955.

25. Structural Design for Dynamic Loads. C. H. Norris, et al. McGraw-Hill, New York, 1959.

26. "Development of Procedures for Rapid Computation of Dynamic Structural Response." N. B. Brooks, J. W. Melin, et al. Civil Engineering Studies, Structural Research Series Nos. 51, 83, 126, 145, and 171. Department of Civil Engineering, University of Illinois, Urbana, Illinois, April 1953, July 1954, July 1956, July 1957, January 1959.

27. "Analog Computers Applied to Elasto-Plastic Systems." L. Schenker and G. Martin. Transactions, Vol. 121, American Society of Civil Engineers, New York, 1956.

28. "Plastic Behavior of Beams Under Long Duration Impulsive Loads." W. T. Thomson. Report No. 54-92, Department of Engineering, University of California, Los Angeles, October 1954.

29. "Load-Deformation Characteristics of Simulated Beam Column Connections in Reinforced Concrete." H. M. McCollister, et al. Civil Engineering Studies, Structural Research Series No. 76, Department of Civil Engineering, University of Illinois, Urbana, Illinois, June 1954.

30. "Computation of Dynamic Structural Response in the Range Approaching Failure." N. M. Newmark. Earthquake and Blast Effects on Structures. Earthquake Engineering Research Institute, Department of Engineering, Berkeley, California, June 1952.

31. "Building Code Requirements for Reinforced Concrete. (ACI 318-56)." Journal of the American Concrete Institute, May 1956.

32. Electronic Analog Computers. G. A. Korn and T. M. Korn. Second Ed., McGraw-Hill, New York, 1956.

33. "Tables of Characteristic Functions Representing Normal Modes of Vibration of a Beam." D. Young and R. P. Felgar, Jr. Engineering Research Series No. 44, Bureau of Engineering Research, University of Texas, Austin, Texas, 1 July 1949.

APPENDIX A

ANALOG COMPUTER CIRCUIT

The analog computer used on this program was a Heathkit Model ES 400, in conjunction with two Moseley Autograf Model 3 Two-axis Recorders, one modified as a curve follower. A schematic diagram of the computer connections is shown in Fig. 40.

The equation of the system under consideration can be written in words as

Inertia Force + Damping Force + Resistance = Applied Force or algebraically as

$$M \overset{\circ\circ}{\Delta} + C\mathring{\Delta} + Q(\Delta) = P \tag{A-1}$$

Rearranging,

$$M \overset{\circ\circ}{\Delta} = P - C\mathring{\Delta} - Q(\Delta) \tag{A-2}$$

The computer elements shown in Fig. 40 can perform the following functions:

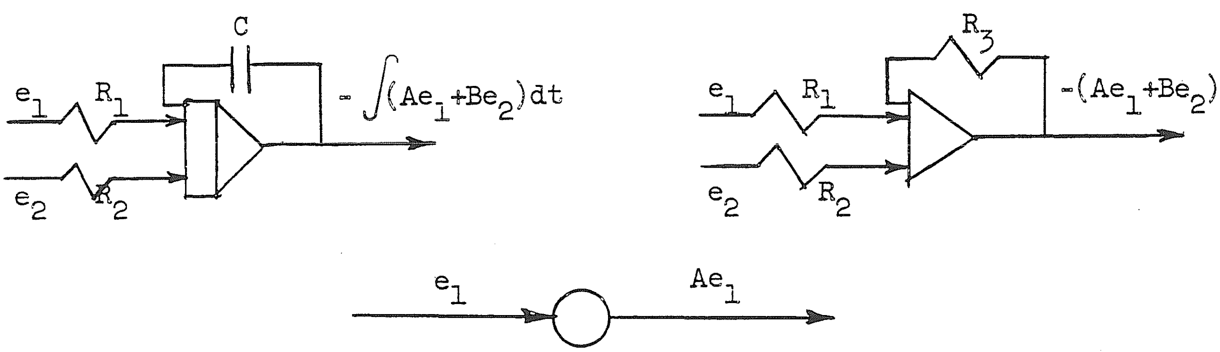

In other words, the triangular elements, symbols for operational amplifiers, can sum and/or integrate depending on whether the signal is fed back through a condenser or a resistor. The value of the "gain" for each input, shown as A and B, depends on the relative values of the input resistors and the feed-back element. An operational amplifier will always change the sign of the signal in this model computer. The circular symbols are potentiometers, used to multiply the signal by a constant value less than one. The switches shown across each integrating amplifier in Fig. 40 are relay contacts, simultaneously activated, to discharge the condensers after each run of a problem. The diodes are used to pass a signal in one direction only. The abbreviation IC stands for "initial condition" and AUX POT stands for "auxiliary potentiometer."

Assuming, for the moment, that the output of amplifier 1 is the inertia, then potentiometer 3A is set for 1/M and its output is the acceleration. By integrating with amplifier 3, $-\mathring{\Delta}$ is obtained. Amplifier 4 changes the sign. Integrating again with amplifier 5, $-\Delta$ is obtained. Amplifier 6 is used to sum the various signals making up the resistance, thus its output is Q. This is fed back into amplifier 1.

Amplifier 2 is fed by the curve follower, which follows the load trace, and a constant signal, (the power supply IC 3), which cancels any output from amplifier 2 when the curve follower is set at zero load position on the graph. The output of amplifier 2 is then -P.

The output of amplifier 4 is also fed through potentiometer 9A back into amplifier 1 and, being proportional to the velocity, represents damping. The sum of the inputs into amplifier 1 represents the inertia. This completes the elastic system. Amplifiers 13, 8 and 11 introduce a change in slope into the resistance diagram while amplifier 10 introduces collapse. Both of these effects are achieved by feeding delayed voltages into amplifier 6 of a sign opposite to that coming from amplifier 5.

Amplifier 14 generates a signal varying linearly with time, and therefore represents time on the horizontal axes of the curve follower and plotter. Amplifiers 7 and 15 introduce sign changes so that oscilloscope display and plotting can be done in conventional directions.

A connection from amplifier 2 to the plotter makes the curve follower and plotter in to a "master-slave" unit and it is thus possible to determine how well the load trace is tracked; imperfect tracking can be improved with a slower time base (control 14A decreased). Relay B permits plotting Q instead of time on the X-axis. With Δ on the Y-axis resistance can be plotted immediately.

An oscilloscope is used for convenience in seeing any function at any time, or any function at any Q. The connections to the X-axis are from amplifiers 15 or 6. The Y-axis is connected to a switch on the computer allowing any amplifier output to be shown.

For detailed information on analog computer components and use, see Ref. 32.

APPENDIX B

STATIC CAPACITY OF BEAMS 5a1 AND 5a2

There was no static test of a beam of the same configuration as Beams 5a1 and 5a2 which would permit the computation of the static resistance for these beams by the same procedure used for the other beams tested dynamically. Therefore, the static capacity of these beams was computed as follows.

The maximum moment resistance of a beam reinforced only in tension can be written

$$\frac{M_m}{bd^2 f'_c} = q(1 - \tfrac{1}{2}q) \qquad \text{(B-1)}$$

if the beam fails by yielding of the tension reinforcement. Whether the beam fails by yielding or experiences crushing of the concrete before yielding depends on the parameter q_{cr} which is derived in Section 12.1.3.

$$q_{cr} = \frac{102}{120 + f_y} \qquad (52)$$

where f_y is in ksi. If $q = pf_y/f'_c < q_{cr}$ then the beam will yield first. If $q > q_{cr}$, the beam will experience crushing first. The capacity in the latter case can be estimated by substituting q_{cr} for q in Eq. B-1.

For Beam 5a1:

$$p = 3.33\%,\ f_y = 49.4 \text{ ksi},\ f'_c = 2.30 \text{ ksi},\ pf_y/f'_c = 0.715,\ q_{cr} = 0.602$$

Therefore, $\dfrac{M_m}{bd^2 f'_c} = 0.602\ (1 - 0.5 \times 0.602) = 0.421$

$$M_m = 0.421 \times 600 \times 2.30 = 581 \text{ in.-kips}$$

$$M_m/29 \text{ in.} = 20.0 \text{ kips}$$

Using the same initial slope as measured for Beam 5b1 (k_1 = 29.9 kips/in.)

$$\Delta_y = 20.0/29.9 = 0.67 \text{ in.}$$

For Beam 5a2:

$p = 3.33\%$, $f_y = 49.4$ ksi, $f'_c = 2.81$ ksi, $pf_y/f'_c = 0.585$, $q_{cr} = 0.602$

Therefore, $\dfrac{M_m}{bd^2f'_c} = 0.585\ (1 - 0.5 \times 0.585) = 0.414$

$M_m = 0.414 \times 600 \times 2.81 = 698$ in.-kips

$M_m/29$ in. $= 24.1$ kips

$\Delta_y = 24.1/29.9 = 0.81$ in.

APPENDIX C

NATURAL FREQUENCY FOR SMALL AMPLITUDES

In Section 10.2 it was explained that the natural frequencies of vibration of some of the beams were determined prior to testing. The results of these determinations are presented in Table 24. The term "simple support" refers to the beam in the frame and clamped to the reaction roller assemblies on a 9 ft span, center to center of reactions. The "free-free" condition refers to a scheme not mentioned in Section 10.2; that of having the beam outside the frame, supported at two points on the corners of pieces of 4-in. steel angle. The positions of support corresponded to the theoretical node points for an elastic bar vibrating in the first mode with free-free end conditions. These positions were determined from Ref. 33 and are 0.224 of the total length of the beam in from each end. For the short beams this was 26.9 in. and for the long beams 36.7 in. The notation "in frame" for Beam 3a1 means that this determination was made with the pieces of steel angle supported on the base rails of the testing frame rather than on the concrete floor as for the other determinations. The terms under "method" refer to the two procedures for inducing vibration described in Section 10.2.

Several things are to be noted in Table 24. Beam 2a2, which was preloaded before dynamic testing to the point where cracks reached the mid-height of the beam, exhibited no difference in behavior under small amplitudes of vibration in the cracked and uncracked states. It is felt that the deflections associated with the period determination would have had to be perhaps 10 to 25 times greater before a difference would have been noticed.

Another interesting observation is the agreement of values for a particular span regardless of material characteristics, reinforcing arrangement, etc. In other words, it appears as though the beams behaved as solid masses of concrete irrespective of the reinforcing and that the major variable is the span, since all of these beams had the same height and width.

From Ref. 24, the fundamental frequency of an elastic, homogeneous bar vibrating laterally with simple supports is,

$$f_s = \frac{\pi}{2L^2}\sqrt{\frac{EIg}{A\ \gamma}} \tag{C-1}$$

and with free-free-supports,

$$f_f = \frac{22.37}{2\pi L^2}\sqrt{\frac{EIg}{A\ \gamma}} \tag{C-2}$$

where
- L = span
- E = modulus of elasticity
- I = moment of inertia
- g = acceleration of gravity
- A = area of cross-section of bar
- γ = density of material

Assuming $\frac{EIg}{A\ \gamma}$ constant for these beams, the ratio of frequencies for the two support conditions can be computed as follows:

For the short beams,

$$f_s = \frac{\pi}{2 \times (108)^2}\sqrt{EIg/A\gamma} = 1.348 \times 10^{-4}\sqrt{EIg/A\gamma}$$

$$f_f = \frac{22.37}{2\pi \times (120)^2}\sqrt{EIg/A\gamma} = 2.472 \times 10^{-4}\sqrt{EIg/A\gamma}$$

$$\frac{f_s}{f_f} = \frac{1.348}{2.472} = 0.545 \tag{C-3}$$

For the long beams, using a simply supported span of 152 in. and a free-free span of 164 in., the ratio is

$$\frac{f_s}{f_f} = 0.514 \tag{C-4}$$

For the short beams, the average frequency in the free-free condition was about 130 cps. This value multiplied by the ratio 0.545 is 71 cps which is somewhat higher than the values obtained using the simple support condition. For the long beams, the ratio 0.514 times the average free-free frequency of 67 cps yields 34.5 cps which agrees rather well with the average of the values obtained with simple supports.

The usefulness of these values of natural frequency obtained for very small amplitudes of vibration is open to question. It is felt that the importance of knowing the period of vibration of a beam lies in its relation to the stiffness of the beam, and stiffness is of interest only where it is considered over the entire elastic region of behavior, elastic here meaning range up to yielding.

Thus, stiffness can be measured only for larger deflections than those employed in these tests for natural frequency, and must surely be affected by the amount, strength, and arrangement of the steel reinforcement.

TABLE 1a

SUMMARY OF UNIAXIAL STRESS TESTS AND RESULTS

NO. 6 BARS

Specimen	Static Properties				Gages*	Dynamic Properties				
	σ_{sy}	P_{sy}	σ_{su}	E_s		t_s	t_y	t_d	E_d	P_{dy}
	ksi	kips	ksi	ksi x 10^3		milliseconds			ksi x 10^3	kips
6-9	40.7	17.9	68.2	29.8	A	4.8	12.8	8.0	27.4	26.7
6-11	40.5	17.8	71.6		A	5.8	9.1	3.7	25.0	24.2
6-12	47.5	20.9	83.2		A	6	107	101	28.6	23.2
6-14	39.5	17.4	69.5		A	5.1	9.1	4.0	27.8	24.4
6-15	41.6	18.3	72.7		A	4.2	10.4	6.2	25.8	24.0
6-16	44.3	19.5	80.5	31.9	A	4.1	5.3	1.2	25.6	26.8
6-18	43.0	18.9	74.3		A	6.0	22.0	16.0	26.9	23.6
6-19	43.0	18.9	75.7	33.8	A	5.0	17.5	12.5	26.6	24.1
6-20	43.4	19.1	81.1		A	4.1	5.5	1.4	26.4	27.2
6-22	43.8	19.3	77.5	35.6	A	12	77	65	25.8	20.0

All stresses are based on the nominal bar area, A_o.

* A = SR-4 strain gages mounted midway between the ends of the specimen.
B = SR-4 strain gages mounted 2 1/2 in. below the "A" gages.

TABLE 1b

SUMMARY OF UNIAXIAL STRESS TESTS AND RESULTS

NO. 7 BARS

Specimen	Static Properties				Gages*	Dynamic Properties				
	σ_{sy}	P_{sy}	σ_{su}	E_s		t_s	t_y	t_d	E_d	P_{dy}
	ksi	kips	ksi	ksi x 10^3		milliseconds			ksi x 10^3	kips
7-2	47.0	28.2	78.7		A	17	454	437	27.9	30.0
					B	17	354	337		30.2
7-4	48.1	28.8	81.0	29.4	A	15	620	605	29.2	30.6
7-6	48.9	29.3	81.8		A	5.6	22.6	17.0	28.3	37.4
7-9**	47.8	28.7	78.5		A	14.5	35.3	20.8	27.9	38.0
7-10**	48.3	29.0	80.3	30.5	A	63.5	98.5	35	27.1	35.1
					B	63.5	89.5	26		34.8
7-12	48.4	29.0	81.2		A	5.5	16.0	10.5	28.8	39.5
7-13	47.5	28.5	78.2	29.2	A	8	82	74	28.4	34.4
7-14	47.9	28.7	81.8		A	10.5	93.5	83	27.9	32.2
7-15	47.6	28.6	80.8		A	6.5	44.5	38	28.4	35.0
					B	6.5	39.5	33		35.0
7-17	47.5	28.5	82.2		A	8	85	77	28.0	33.5
7-18**	46.8	28.1	81.2	30.8	A	96	131	35	26.5	34.9
					B	96	117	21		34.9
7-23**	47.2	28.3	80.0	32.6	A	99.0	107.5	8.5	27.1	37.7
7-24	47.3	28.4	83.2		A	1013	8179	9166	28.3	28.6
					B	1013	2679	3666		28.6
7-25	47.2	28.3	78.5		A	10.5	35.5	25.0	27.4	36.4

All stresses are based on the nominal bar area, A_o.

* A = SR-4 strain gages mounted midway between the ends of the specimen.
B = SR-4 strain gages mounted 2 1/2 in. on centers below the "A" gages.

**Double load pulse test.

TABLE 1c

SUMMARY OF UNIAXIAL STRESS TESTS AND RESULTS

NO. 9 BARS

Specimen	Static Properties				Gages*	Dynamic Properties				
	σ_{sy}	P_{sy}	σ_{su}	E_s		t_s	t_y	t_d	E_d	P_{dy}
	ksi	kips	ksi	ksi x 10^3		milliseconds			ksi x 10^3	ksi
9-48	52.4	52.4	86.3		A	15	253	238	27.0	57.6
9-51-1					A	63	2146	2083	30.0	55.6
9-51-2					A	31	777	746	29.8	55.9
	54.6	54.6	87.9		B	31	227	196		55.8
9-51-3					A	19	349	330	29.0	57.8
9-51-4					A	5.2	8.5	3.3	26.2	66.3
9-61	44.5	44.5	75.5		A	16.5	43.5	27	28.5	58.2
9-69-1**					A	22.8	45.8	23	28.2	58.8
9-69-2	44.0	44.0	78.9		A	13	75	62	27.5	50.1
9-69-3**					A	24.5	58	33.5	28.5	56.0
9-69-4					A	11	6393	6382	29.8	45.0
					B	11	3093	3082		45.0

All stresses are based on the nominal bar area, A_o.

* A = SR-4 strain gages mounted midway between the ends of the specimen.
B = SR-4 strain gages mounted 2 1/2 in. on centers below the "A" gages.

** Double load pulse tests.

TABLE 2

GEOMETRIC PROPERTIES OF REINFORCING BARS*

Bar Size	Area, sq. in.		Deformations, in.				
			Spacing**	Height			Gap***
	Nominal	Measured	Average	Minimum	Average	Maximum	Average
No. 6	0.44	0.51	0.33	.048	.050	.053	0.122
No. 7	0.60	0.60	0.37	.058	.061	.065	0.146
No. 9	1.00	0.99	0.54	.061	.062	.063	0.094

* Geometric properties are based on five bars of each size selected at random.

** The maximum and minimum varied within $\pm$ .001 in.

*** The maximum and minimum varied within $\pm$ .004 in.

TABLE 3a

SUMMARY OF ANALYSIS

NO. 6 BARS

Specimen No.	Gage*	(1) $\frac{P_{dy}-P_{sy}}{P_{sy}}$ percent	(2) $\dot{\sigma}_e$ lb/in.^{2}/sec	(3) $\dot{\epsilon}_e$ in./in./sec
6-9	A	49.1	2.5×10^6	9.2×10^{-2}
6-11	A	35.8	3.9×10^6	1.6×10^{-1}
6-12	A	11.0	5.2×10^4	1.8×10^{-3}
6-14	A	40.2	4.0×10^6	1.4×10^{-1}
6-15	A	31.1	2.1×10^6	8.1×10^{-2}
6-16	A	37.4	1.4×10^7	5.4×10^{-1}
6-18	A	24.8	6.7×10^5	2.5×10^{-2}
6-19	A	27.5	9.5×10^5	3.6×10^{-2}
6-20	A	42.4	1.3×10^7	5.0×10^{-1}
6-22	A	3.6	2.5×10^4	9.4×10^{-4}

* A = SR-4 strain gages mounted midway between the ends of the specimen.

TABLE 3b

SUMMARY OF ANALYSIS

NO. 7 BARS

Specimen No.	Gage*	(1) $\frac{P_{dy}-P_{sy}}{P_{sy}}$ percent	(2) $\dot{\sigma}_e$ lb/in.^{2}/sec	(3) $\dot{\epsilon}_e$ in./in./sec
7-2	A	6.5	6.9×10^3	2.5×10^{-4}
	B	7.1	9.9×10^3	3.5×10^{-4}
7-4	A	6.3	5.0×10^3	1.7×10^{-4}
7-6	A	27.6	7.9×10^5	2.8×10^{-2}
7-9**	A	32.5	7.5×10^5	2.7×10^{-2}
7-10**	A	21.0	2.9×10^5	1.1×10^{-2}
	B	20.0	3.7×10^5	1.4×10^{-2}
7-12	A	36.2	1.7×10^6	5.8×10^{-2}
7-13	A	20.7	1.3×10^5	4.7×10^{-3}
7-14	A	12.2	7.0×10^4	2.5×10^{-3}
7-15	A	22.4	2.8×10^5	9.9×10^{-3}
	B	22.4	3.2×10^5	1.1×10^{-2}
7-17	A	17.5	1.1×10^5	3.9×10^{-3}
7-18**	A	24.0	3.2×10^5	1.2×10^{-2}
	B	24.0	5.4×10^5	2.0×10^{-2}
7-23**	A	33.0	1.8×10^6	6.8×10^{-2}
7-24	A	1.0	4.1×10^1	1.4×10^{-6}
	B	1.0	1.3×10^2	4.4×10^{-6}
7-25	A	28.5	5.4×10^5	2.0×10^{-2}

* A = SR-4 strain gages mounted midway between the ends of the specimen.
B = SR-4 strain gages mounted 2 1/2 in. on centers below "A" gages.

** Double load pulse test.

TABLE 3c

SUMMARY OF ANALYSIS

NO. 9 BARS

Specimen No.	Gages*	(1) $\frac{P_{dy}-P_{sy}}{P_{sy}}$ percent	(2) $\dot{\sigma}_e$ lb/in.^{2}/sec	(3) $\dot{\epsilon}_e$ in./in./sec
9-48	A	10.0	2.2×10^{4}	8.1×10^{-4}
9-51-1	A	1.8	4.8×10^{2}	1.6×10^{-5}
9-51-2	A	2.4	1.7×10^{3}	5.8×10^{-5}
	B	2.2	6.1×10^{3}	2.1×10^{-4}
9-51-3	A	6.0	9.7×10^{3}	3.3×10^{-4}
9-51-4	A	21.5	3.5×10^{6}	1.4×10^{-1}
9-61	A	30.5	5.1×10^{5}	1.8×10^{-2}
9-69-1**	A	33.5	6.4×10^{5}	2.3×10^{-2}
9-69-2	A	14.0	9.8×10^{4}	3.6×10^{-3}
9-69-3**	A	27.0	3.6×10^{5}	1.3×10^{-2}
9-69-4	A	2.0	1.6×10^{1}	5.3×10^{-6}
	B	2.0	3.3×10^{2}	1.1×10^{-5}

* A = SR-4 strain gages mounted midway between the ends of the specimen.
B = SR-4 strain gages mounted 2 1/2 in. on centers below the "A" gages.

** Double load pulse test.

TABLE 4

PROPERTIES OF TWO-POINT LOADED BEAMS

All Beams: b = 6 in., h = 12 in., d = 10 in., d' = 8.5 in.,
Reinforcing steel - Intermediate Grade
Load points - 18 in. each side of midspan
Span: Series 2, 3, 4 - 108 in.; Series 5, 6, 7 - 152 in.

Beam	Reinforcement Tens.	Comp.	Shear	Ties	f_y ksi	f'_y ksi	f_w ksi	f'_c ksi	E_c psi $\times 10^6$	f_r psi	Type of Test (1)	No. of Blows (2)	Age Days
2a1	2-#9	--	#3@3.75	--	49.1	--	55.1	4.14	3.58	665	D	1 I	119
2a2	2-#9	--	#3@3.75	--	47.8	--	50.2	3.40	3.33	590	D*	1 I	38
2b1	2-#9	--	#2@5.5	--	49.0	--	48.2	4.04	3.49	865	S	--	108
2b2	2-#9	--	#2@5.5	--	47.9	--	44.4	3.06	3.30	385	D	1 I	32
2b3	2-#9	--	#2@5.5	--	48.3	--	49.8	3.60	3.33	560	D	1 I	50
3a1	2-#9	2-#7	#3@4.25	#2@12	46.5	46.8	51.6	4.27	4.21	715	S	--	95
3a2	2-#9	2-#7	#3@4.25	#2@12	46.5	47.2	52.4	3.25	3.82	790	DS	1 I	111
3a3	2-#9	2-#7	#3@4.25	#2@12	46.8	47.2	44.1	3.70	4.35	660	DS	1 I	76
3a4	2-#9	2-#7	#3@4.25	#2@12	46.1	47.3	44.1	3.31	3.86	560	DS*	1 I	92
3a5	2-#9	2-#7	#3@4.25	#3@14	45.2	47.5	45.6	3.02	3.76	615	D	2**	86
3b1	2-#9	2-#7	#2@4.25	#2@12	41.0	47.0	43.6	4.09	4.44	540	S	--	112
3b2	2-#9	2-#7	#2@4.25	#2@12	43.7	47.9	43.6	3.26	3.74	740	D	3 E	205
3b3	2-#9	2-#7	#2@4.25	#2@12	42.3	47.6	44.4	3.13	4.54	615	D	1 I	98
4a1	2-#6	--	#3@10	--	44.3	--	55.1	4.28	4.04	725	D	1 I	80
4a2	2-#6	--	#3@10	--	47.5	--	55.1	3.85	3.67	665	D	2 I	78
4b1	2-#6	--	#2@10	--	48.3	--	47.0	4.50	3.68	535	S	--	71
4b2	2-#6	--	#2@10	--	49.4	--	48.0	4.12	3.40	575	D	1 I	70
4b3	2-#6	--	#2@10	--	52.3	--	49.6	3.43	3.38	450	DS	1 I	36
4c1	2-#6	--	--	--	43.4	--	--	2.83	3.17	525	S	--	42
4c2	2-#6	--	--	--	43.4	--	--	3.26	3.49	490	D	3 I	38
4c3	2-#6	--	--	--	43.8	--	--	3.08	3.42	515	D	1 I	40

(1) S-static, D-dynamic to collapse, DS-dynamic followed by static test to collapse.
(2) E-explosion, I-implosion.
* Cracked statically. Any beam subjected to more than one blow was, of course, cracked for the subsequent blows. This refers to beams deliberately cracked statically before the first blow.
** Blow 1-explosion, Blow 2-implosion.

TABLE 4 (Cont.)

Beam	Reinforcement Tens.	Comp.	Shear	Ties	f_y ksi	f'_y ksi	f_w ksi	f'_c ksi	E_c psi $\times 10^6$	f_r psi	Type of Test (1)	No. of Blows (2)	Age Days
5a1	2-#9	--	#3@3.75	--	49.4	--	53.0	2.30	2.92	440	D	1 I	24
5a2	2-#9	--	#3@3.75	--	49.4	--	53.7	2.81	3.71	510	D*	1 I	42
5b1	2-#9	--	--	--	51.6	--	--	3.60	4.65	583	S	--	102
5b2	2-#9	--	--	--	51.6	--	--	3.57	4.06	550	D	1 I	105
5b3	2-#9	--	--	--	54.6	--	--	2.72	2.96	540	DS	1 E	97
5b4	2-#9	--	--	--	52.3	--	--	3.82	3.06	535	D	2 I	49
6a1	2-#9	2-#7	#3@4.25	#2@12	43.6	47.6	53.6	3.76	3.69	465	DS	2 E	72
6b1	2-#9	2-#7	#2@12	#2@12	44.5	48.6	53.4	2.98	4.00	385	S	--	73
6b2	2-#9	2-#7	#2@12	#2@12	44.0	48.2	53.4	4.44	4.00	375	DS	2 E	75
7a1	2-#6	--	--	--	40.8	--	--	2.79	3.25	565	S	--	41
7a2	2-#6	--	--	--	41.5	--	--	2.73	3.83	410	D*	5 I	39
7a3	2-#6	--	--	--	43.0	--	--	3.27	2.78	590	DS	3 E	75

(1) S-static, D-dynamic to collapse, DS-dynamic followed by static test to collapse.

(2) E-explosion, I-implosion.

* Cracked statically. Any beam subjected to more than one blow was, of course, cracked for the subsequent blows. This refers to beams deliberately cracked statically before the first blow.

** Blow 1-explosion, Blow 2-implosion.

TABLE 5

DERIVED BEAM PARAMETERS

Beam	p %	p' %	r %	q	q'
2a1	3.33		0.98	0.395	
2a2	3.33		0.98	0.468	
2b1	3.33		0.31	0.404	
2b2	3.33		0.31	0.521	
2b3	3.33		0.31	0.447	
3a1	3.33	2.00	0.86	0.362	0.143
3a2	3.33	2.00	0.86	0.476	0.186
3a3	3.33	2.00	0.86	0.421	0.166
3a4	3.33	2.00	0.86	0.464	0.178
3a5	3.33	2.00	0.86	0.498	0.184
3b1	3.33	2.00	0.39	0.334	0.104
3b2	3.33	2.00	0.39	0.446	0.152
3b3	3.33	2.00	0.39	0.450	0.146
4a1	1.47		0.37	0.152	
4a2	1.47		0.37	0.181	
4b1	1.47		0.17	0.158	
4b2	1.47		0.17	0.176	
4b3	1.47		0.17	0.224	
4c1	1.47			0.225	
4c2	1.47			0.196	
4c3	1.47			0.209	
5a1	3.33		0.98	0.715	
5a2	3.33		0.98	0.585	
5b1	3.33			0.477	
5b2	3.33			0.481	
5b3	3.33			0.668	
5b4	3.33			0.456	
6a1	3.33	2.00	0.86	0.386	0.133
6b1	3.33	2.00	0.14	0.497	0.171
6b2	3.33	2.00	0.14	0.330	0.113
7a1	1.47			0.215	
7a2	1.47			0.223	
7a3	1.47			0.193	

TABLE 6

LOCATION OF STRAIN GAGES; NUMBER OF DEFLECTION GAGES;
STIRRUP AND TIE CONFIGURATION

(See Fig. 23 for explanation of symbols)

Beam	Strain Gage Location Steel Tens.	Strain Gage Location Steel Comp.	Strain Gage Location Conc. Comp.	Deflection Gages	Stirrups	Ties
2a1	f	-	-	1*	a	-
2a2	-	-	-	5**	a	-
2b1	f	-	-	3***	a	-
2b2	f	-	j	5	a	-
2b3	-	-	-	5	a	-
3a1	-	-	-	5	b	b
3a2	f	h	k	5	c	c
3a3	-	-	-	1	c	d
3a4	-	-	-	1	c	e
3a5	-	-	-	1	c	e
3b1	-	-	-	5	c	c
3b2	f	i	k	5	c	c
3b3	-	-	-	1	c	d
4a1	f	-	-	1	a	-
4a2	f	-	-	1	a	-
4b1	f	-	ℓ	5	a	-
4b2	f	-	ℓ	5	a	-
4b3	-	-	-	5	a	-
4c1	-	-	-	1	-	-
4c2	f	-	m	5	-	-
4c3	-	-	-	5	-	-
5a1	-	-	-	5	a	-
5a2	f	-	n	5	a	-
5b1	-	-	-	5	-	-
5b2	f	-	k	5	-	-
5b3	-	-	-	5	-	-
5b4	g	-	n	5	-	-
6a1	f	h	o	5	b	b
6b1	-	-	-	5	b	b
6b2	f	h	o	5	b	b
7a1	-	-	-	5	-	-
7a2	f	-	n	5	-	-
7a3	-	-	-	5	-	-

* Gage at midspan only.
** Gage at each location shown in Fig. 22.
*** Gages at locations 2, 3, and 4 only as shown in Fig. 22.

TABLE 7

RESULTS OF STATIC TESTS TO COLLAPSE

(PROPERTIES OF ELASTO-PLASTIC APPROXIMATIONS)

Beam	Approximate Loading Rate kips/min	Q_y kips	Δ_y in.	Δ_m in.	k_1 kips/in.	Δ_m/Δ_y	Mode of Failure	T** msec.
2b1	9	45.5	0.55	0.95	82.7	1.73	Flexure - "Balanced"	21.9
3a1	11	45.5	0.48	4.05	94.8	8.43	Flexure - Tension	20.3
3b1	7	41.0	0.54*	3.93*	76.0	7.28	Flexure - Tension	22.9
4b1	7	23.1	0.50*	1.98*	46.2	3.96	Flexure - Tension	29.3
4c1	5	19.4	-	0.38	51.1	-	Shear	27.9
5b1	8	20.9	-	0.70	29.9	-	Shear	41.4
6b1	7	26.9	0.85*	4.98*	31.6	5.86	Flexure - Tension	40.3
7a1	5	11.3	0.60	2.24	18.8	3.74	Flexure - Tension	52.3

* Corrected for difference in deflection at zero load due to making elasto-plastic approximation.

** Computed from $T = 2\pi \; Mme/k_1$.

TABLE 8

RESULTS OF DYNAMIC TESTS

(APPLIED LOADS AND DEFLECTION RESPONSE CHARACTERISTICS)

Beam	Blow	Response Characteristics-inches					Load Characteristics		Mode of Failure
		permanent set		maximum		permanent set	duration	maximum	
		from static preload	from previous blow	incremental	cumulative		msec	kips	(1)
2a1				1.05	1.05*		∞	64.6	F
2a2		0.19		1.02	1.21*		64	54.3	F
2b2				0.98	0.98*		67	57.5	F
2b3				1.06	1.06*		20	58.2	F
3a2				3.86	3.86	2.98	66	59.6	x
3a2	S+		2.98	1.32	4.30*			43.5	F
3a3				2.90	2.90	2.12	39	64.1	x
3a3	S		2.12	1.03	3.15*			45.7	F
3a4		0.08		3.00	3.08	2.40	56	70.1	x
3a4	S		2.40	1.30	3.70*			39.6	F
3a5	1			1.22	1.22	0.55	46	56.2	
3a5	2		0.55	4.18	4.73*		61	59.9	F
3b2	1			1.20	1.20	0.81	42	57.8	x
3b2	2		0.81	1.86	2.67	1.92	42	56.1	x
3b2	3		1.92	2.18	4.10*		32	61.6	F
3b3				~5.00	~5.00*		∞	63.1	F
4a1				2.06-2.21	2.06-2.21*		61	29.7	F
4a2	1			1.23	1.23	1.18	∞	29.0	
4a2	2		1.18	1.42-1.53	2.60-2.71*		∞	30.3	F
4b2	No Records								F
4b3				2.04-2.09	2.04-2.09**	2.78	62	28.7	x
4b3	S		2.78	0.48	3.26**			6.0	F
4c2	1	0.06		0.34	0.40	0.13	∞	18.6	
4c2	2		0.13	0.54	0.67	0.36	∞	23.5	
4c2	3		0.36	2.11-2.37	2.47-2.73**		∞	29.5	F
4c3				0.70-1.00	0.70-1.00*		59	27.2	S

TABLE 8 (Continued)

Beam	Blow	Response Characteristics-inches					Load Characteristics		Mode of Failure
		permanent set		maximum		permanent set	duration	maximum	
		from static preload	from previous blow	incremental	cumulative		msec	kips	(1)
5a1				1.40	1.40*		32	25.1	F
5a2		0.20		1.25	1.45*		33	28.5	F
5b2	No Records								S
5b3				1.05	1.05*		35	19.2	S
5b4	1			1.04	1.04	0.35	49	20.4	
5b4	2		0.35	1.05-1.20	1.40-1.55*		30	26.1	S
6a1	1			1.87	1.87	0.75	54	32.5	
6a1	2		0.75	3.16	3.91	2.75	64	32.9	x
6a1	S		2.75	2.15	4.90*			27.2	F
6b2	1			1.56	1.56	0.55	52	30.6	
6b2	2		0.55	2.25	2.80	1.68	70	29.6	x
6b2	S		1.68	1.32	3.00*			16.0	S
7a2	1	0.16		0.64	0.80	0.65	54	10.8	x
7a2	2		0.65	0.71	1.36	0.84	62	9.3	x
7a2	3		0.84	1.04	1.88	1.24	66	12.1	x
7a2	4		1.24	1.37	2.61	1.96	68	12.5	x
7a2	5		1.96	2.25-2.90	4.21-4.68*		50	14.3	F
7a3	1			1.23	1.23	0.62	53	12.4	
7a3	2		0.62	1.80	2.42	1.64	66	14.2	x
7a3	3		1.64	3.42	5.06	4.90	~57	13.4	x
7a3	S		4.90	0.48	5.38*			3.2	F

\+ S-static test to collapse after dynamic test.
~ Approximately.
* Collapse.
** See explanation in text for two values of collapse deflection.
(1) F-flexure, S-shear, x-crushing detected.

TABLE 9

RESULTS OF DYNAMIC TESTS-CONTINUED

(STRAIN RESPONSE)

Beam	Blow	Critical Strain Rates--Inch/inch/second* Steel Tension	Steel Compression	Concrete Compression	Maximum Recorded Concrete Strain** microin./in.
2a1		SA-0.32	---	b	
2b2		0.24	---	CC-0.72	3760
3a2		SA-0.22	SD-0.29	CB-0.76	5560
3b2	1	SB-0.25	1470 (1)	CB-0.42	3980
3b2	2	a	SD-0.39	?	3040?
3b2	3	a	?	?	1540?
4a1		0.32	---	b	
4a2	1	SB-0.31	---	b	
4a2	2	a	---	b	
4c2	1	0.11	---	c	
4c2	2	0.18	---	c	
4c2	3	a	---	d	2780
5a2		0.12	---	CB-0.16	3380
5b4	1	0.08	---	c	
5b4	2	SB-0.12	---	c	
6a1	1	0.27	1520 (1)	c	
6a1	2	a	SD-0.33	CA-0.18	3700
6b2	1	0.10	SC-0.15	c	
6b2	2	a	SC-0.10	d	2270
7a2	1	SB-0.07	---	d***	1340?
7a2	2	SA-0.06	---	d	1360?
7a2	3	SA-0.10	---	d	2140?
7a2	4	SB-0.55	---	CB-0.14	4820
7a2	5	a	---	CB-0.12	6390
			Average of unquestioned values		4071

* Determined from Figs. A73-A95 Rates for steel chosen in region just beyond static yield level. Rates for concrete chosen in region just prior to crushing.

** Only tabulated for blows when crushing was detected.

*** Gage CC destroyed.

(1) Maximum strain in microin./in., no yielding.

(a) Gage circuit destroyed on previous blow.

(b) No gages.

(c) No crushing detected, visually or with strain gages.

(d) Crushing detected visually but not recorded.

TABLE 10

RESULTS OF DYNAMIC TESTS - CONTINUED

(EFFECT OF REINFORCEMENT CONFIGURATION)

Beam	Type of Test (1)	Compression Reinforcement	Ties	r %	Mode of Failure (1)	Collapse Deflection in.
2a1	D	No	-	0.98	F	1.05
2a2	D	No	-	0.98	F	1.21
2b1	S	No	-	0.31	F	0.95
2b2	D	No	-	0.31	F	0.98
2b3	D	No	-	0.31	F	1.06
3a1	S	Yes	#2 @12 - welded	0.86	F	4.05
3a2	DS	Yes	#2 @12 - welded	0.86	F	4.30
3a3	DS	Yes	#2 @12 - hooked at top	0.86	F	3.15
3a4	DS	Yes	#2 @12 - hooked at bottom	0.86	F	3.70
3a5	D	Yes	#3 @14 - hooked at bottom	0.86	F	4.73
3b1	S	Yes	#2 @12 - welded	0.39	F	3.93
3b2	D	Yes	#2 @12 - welded	0.39	F	4.10
3b3	D	Yes	#2 @12 - hooked at top	0.39	F	~5.00
4a1	D	No	-	0.37	F	2.06-2.21
4a2	D	No	-	0.37	F	2.60-2.71
4b1	S	No	-	0.17	F	1.98
4b2	D	No	-	0.17	F	?
4b3	DS	No	-	0.17	F	2.04-3.26
4c1	S	No	-	0	S	0.38
4c2	D	No	-	0	F	2.47-2.73
4c3	D	No	-	0	S	0.70-1.00
5a1	D	No	-	0.98	F	1.40
5a2	D	No	-	0.98	F	1.45
5b1	S	No	-	0	S	0.70
5b2	D	No	-	0	S	?
5b3	DS	No	-	0	S	1.05
5b4	D	No	-	0	S	1.40-1.55
6a1	DS	Yes	#2 @12 - welded	0.86	F	4.90
6b1	S	Yes	#2 @12 - welded	0.14	F	4.98
6b2	DS	Yes	#2 @12 - welded	0.14	S	3.00
7a1	S	No		0	F	2.24
7a2	D	No		0	F	4.21-4.68
7a3	DS	No		0	F	5.38

(1) S-static, D-dynamic, DS-dynamic followed by static test to collapse.
(2) F-flexure, S-shear.

TABLE 11

SUMMARY OF ANALOG COMPUTER SOLUTIONS FOR DYNAMIC RESISTANCE

Beam	Blow	k_{1d} kips/in.	Δ_{yd} in.	Δ_{md} in.	Q_{yd} kips	β %	T (1) msec.	Time to Reach Yield msec.	Velocity at Yield in./sec
2a1	-	93.0	0.67	1.06	62.4	-	20.4	10	110
2a2	-	82.0	0.63	1.02	51.6	-	22.2	12	100
2b2	-	94.6	0.64	0.95	60.5	-	20.6	11	79
2b3	-	84.6	0.62	1.12	52.5	-	22.0	8	100
3a2 (2)	-	111.4	0.55	-	61.4	-	18.7	8	138
3a3	-	89.6	0.63	-	56.5	-	21.4	10	134
3a4	-	103.0	0.59	-	60.7	4.0	19.7	10	135
3a5	1	95.8	0.64	-	61.3	-	20.3	11	106
3a5	2	80.0	0.76	3.92	60.8	-	22.5	10	151
3b2	1			No Solution					
3b2	2	69.0	0.88	-	60.6	-	23.8	12	104
3b2	3	47.2	1.44	2.19	68.0	-	29.2	20	143
3b3	-			No Solution					
4a1	-	49.8	0.57	2.00	28.4	-	28.5	12	86
4a2	1	61.4	0.47	-	28.9	-	25.5	11	60
4a2	2	46.4	0.62	1.40	28.8	-	29.0	14	79
4b3	-	58.4	0.48	2.00	28.0	-	26.3	11	74
4c2	1	61.2	>0.34	-	>20.8	12.2	25.5	-	-
4c2	2	57.0	0.41	-	23.4	13.0	26.7	15	40
4c2	3	59.0	0.41	2.30	24.2	10.2	26.0	10	58
4c3	-	56.4	0.43	0.80	24.2	-	26.3	12	53
5a1	-	33.2	0.72	1.38	23.9	-	39.5	14	76
5a2	-	31.6	0.83	1.24	26.2	-	40.6	17	83
5b3	-	34.7	0.63	-	21.9	-	38.5	18	49
5b4	1	29.9	1.03 (3)	-	30.8 (3)	-	41.4	-	-
5b4	2	29.9	1.00 (3)	1.00	29.9 (3)	-	41.4	-	-
6a1	1	41.3	0.82	-	33.9	-	35.4	17	91
6a1	2	31.6	1.01	-	31.9	-	40.3	18	109
6b2	1	43.6	0.80	-	34.9	-	34.1	16	88
6b2	2	30.2	1.08	-	32.6	-	41.5	18	114
7a2	1	24.7	>0.64	-	>15.8	-	45.8	-	-
7a2	2	17.2	0.66	-	11.4	-	54.0	27	21
7a2	3	18.8	0.74	-	13.9	-	52.3	24	36
7a2	4	18.2	0.68	-	12.4	4.0	52.5	22	48
7a2	5	18.8	0.69	2.17	13.0	-	52.3	17	74
7a3	1	22.0	0.60	-	13.2	-	47.7	18	50
7a3	2	20.6	0.70	-	14.4	-	49.9	20	61
7a3	3	17.8	0.60	-	10.7	-	53.0	19	50

(1) Undamped.
(2) Slope of inelastic portion, k_{2d} = -2.0 kips/in.
(3) Maximum value attained.

TABLE 12

DERIVED STATIC CAPACITY FOR BEAMS TESTED DYNAMICALLY

Beam	Static Properties			Statically Tested Beam Used as Base
	Q_y kips	Δ_y in.	k_1 kips/in.	
2a1	45.6	0.55	82.7	2b1
2a2	44.4	0.54	82.7	2b1
2b2	44.5	0.54	82.7	2b1
2b3	44.8	0.54	82.7	2b1
3a2	45.5	0.48	94.8	3a1
3a3	45.8	0.48	94.8	3a1
3a4	45.1	0.47	94.8	3a1
3a5	44.2	0.46	94.8	3a1
3b2	43.7	0.58	76.0	3b1
3b3	42.3	0.56	76.0	3b1
4a1	21.2	0.46	46.2	4b1
4a2	22.7	0.49	46.2	4b1
4b2	23.6	0.51	46.2	4b1
4b3	25.0	0.54	46.2	4b1
4c2	20.8	0.45	46.2	4b1
4c3*	20.3	0.40	51.1	4c1
5a1	20.0	0.67	29.9	Appendix B
5a2	24.1	0.81	29.9	Appendix B
5b2*	20.8	0.70	29.9	5b1
5b3*	18.2	0.61	29.9	5b1
5b4*	21.5	0.72	29.9	5b1
6a1	26.4	0.83	31.6	6b1
6b2	26.6	0.84	31.6	6b1
7a2	11.5	0.61	18.8	7a1
7a3	11.9	0.63	18.8	7a1

* Shear failures, no inelastic range in static tests. Values of Q_y and Δ_y correspond to those at failure in shear and do not represent values at yield for these beams.

TABLE 13

PERCENT CHANGE IN RESISTANCE PARAMETERS
DUE TO DYNAMIC LOADING

Beam	Blow	Yield Level $(Q_{yd}-Q_y)/Q_y$ %	Yield Deflection $(\Delta_{yd}-\Delta_y)/\Delta_y$ %	Elastic Slope $(k_{1d}-k_1)/k_1$ %
2a1	-	36.8	21.8	12.4
2a2	-	16.2	16.7	-0.9**
2b2	-	36.0	18.5	14.4
2b3	-	17.2	14.8	2.3
3a2	-	34.9	14.6	17.5
3a3	-	23.4	31.2	-5.5
3a4	-	34.6	25.5	8.6**
3a5	1	38.7	39.1	1.1
3a5	2	37.6	65.2	-15.6
3b2	1	-	-	-
3b2	2	38.7	51.8	-9.2
3b2	3	55.6	148.3	-37.9
3b3	-	-	-	-
4a1	-	34.0	23.9	7.8
4a2	1	27.3	-4.1	32.9
4a2	2	26.9	26.5	0.4
4b3	-	12.0	-11.1	26.4
4c2	1	>0.0	>-24.4	32.5
4c2	2	12.5	-8.9	23.4
4c2	3	16.3	-8.9	27.7
4c3*	-	19.2	7.5	10.4
5a1	-	19.5	7.5	11.0
5a2	-	10.9	2.5	5.7*
5b3*	-	20.3	3.3	16.0
5b4	1	43.3	43.0	0.0
5b4*	2	39.1	38.9	0.0
6a1	1	28.4	-1.2	30.7
6a1	2	20.8	22.9	0.0
6b2	1	31.2	-4.8	38.0
6b2*	2	22.6	28.6	-4.4
7a2	1	>37.4	>4.9	31.4**
7a2	2	-0.9	8.2	-8.5
7a2	3	20.9	21.3	0.0
7a2	4	7.8	11.5	-3.2
7a2	5	13.0	13.1	0.0
7a3	1	10.9	-4.8	17.0
7a3	2	21.0	11.1	9.6
7a3	3	-10.1	-4.8	-5.3

* Shear failures

** Cracked statically

TABLE 14

STATIC AND DYNAMIC
COLLAPSE DEFLECTION AND DUCTILITY

Beam	Type of Test *	Δ_m Static in.	Δ_m Dynamic(1) in.	Δ_y Static in.	Δ_y Dynamic(2) in.	Δ_m/Δ_y Static	Δ_m/Δ_y Dynamic
		(1)	(2)	(3)	(4)	(5)	(6)
2a1	D		1.06		0.67		1.58
2a2	D		1.02		0.63		1.62
2b1	S	0.95		0.55		1.73	
2b2	D		0.95		0.64		1.48
2b3	D		1.12		0.62		1.81
3a1	S	4.05		0.48		8.43	
3a2	DS	4.30			0.55		
3a3	DS	3.15			0.63		
3a4	DS	3.70			0.59		
3a5	D		4.47		0.64		6.98
3b1	S	3.93		0.54		7.28	
3b2	D		4.11		(5)		--
3b3	D		~5.00		(5)		--
4a1	D		2.00		0.57		3.51
4a2	D		2.58		0.47		5.49
4b1	S	1.98		0.50		3.96	
4b2	D		(3)		(3)		--
4b3	DS	3.26	2.04		0.48		4.25
4c1	S	0.38(4)		(6)		(6)	
4c2	D		2.66		0.41		6.49
4c3	D		0.80(4)		0.43		1.86
5a1	D		1.38		0.72		1.92
5a2	D		1.24		0.83		1.49
5b1	S	0.70(4)		(6)		(6)	
5b2	D		(3)		(3)		
5b3	D	1.05(4)			0.63		1.67
5b4	D		1.35(4)		(6)		--
6a1	DS	4.90			0.82		
6b1	S	4.98		0.85		5.86	
6b2	DS	3.00(4)			0.80		
7a1	S	2.24		0.60		3.74	
7a2	D		4.13		0.66		6.26
7a3	DS	5.38			0.60		

* S-static, D-dynamic, DS-dynamic followed by static to collapse.
(1) From analog computer solution, to which is added any previous permanent set.
(2) From analog computer solution.
(3) No records.
(4) Shear failure.
(5) No analog solution.
(6) No inelastic region.

TABLE 15

EFFECT OF DAMAGE ON ELASTIC SLOPE

Beam	Blow	Maximum Cumulative Deflection in.	Δ_{yd} * in.	Maximum Cumulative Inelastic Deflection in.	Δ_{md} in.	Total Possible Inelastic Deflection in.	Damage Ratio	k_{ld} kips/in.	Percent of Blow 1 Slope
		(1)	(2)	(3)	(4)	(5)	(6)	(7)	(8)
3a5	1	1.22	0.64	0.58	4.47	3.83	0.151	95.8	
	2							80.0	83.5
4a2	1	1.23	0.47	0.76	2.58	2.11	0.360	61.4	
	2							46.4	75.6
4c2	1	0.40	**	0.00	2.66	2.19	0.000	61.2	
	2	0.67	0.47				0.091	57.0	93.1
	3							59.0	96.4
6a1	1	1.87	0.82	1.05	4.90	4.08	0.257	41.3	
	2							31.6	76.5
6b2	1	1.56	0.80	0.76	3.00	2.20	0.345	43.6	
	2							30.2	69.3
7a2	1	0.80	**	0.00	4.13	3.31	0.000	24.7	
	2	1.36	0.82	0.54			0.163	17.2	69.6
	3	1.88	0.82	1.06			0.320	18.8	76.1
	4	2.61	0.82	1.79			0.541	18.2	73.7
	5							18.8	76.1
7a3	1	1.23	0.60	0.63	5.38	4.78	0.132	22.0	
	2	2.42	0.60	1.82			0.381	20.6	93.6
	3							17.8	80.9

* Includes any permanent set due to static cracking prior to Blow 1.
** Yielding did not occur in analog computer solution.

TABLE 16

COMPUTED DYNAMIC RESISTANCE BASED
ON MEASURED STRAIN RATES

Beam	Blow	Strain Rate (1) in./in./sec.	$\frac{f_{yd}}{f_y}$	f_{yd} ksi	q_{crd}	$\frac{\Delta_{md}}{\Delta_{yd}}$	k'	Dynamic Resistance			
								Q_{yd} kips	Δ_{yd} in.	Δ_{md} in.	k_{ld} kips/in.
2a1		0.32	1.40	68.7	0.540	1.82	0.52	63.8	0.59	1.07	108.1
2b2		0.24	1.38	66.1	0.548	1.40	0.53	61.4	0.58	0.81	105.9
3a2		0.22	1.38	64.2	0.554	3.97	0.45	62.8	0.48	1.91*	130.8
3b2	1	0.25	1.39	60.7	0.564	4.95	0.45	60.8	0.46	2.28*	132.2
4a1		0.32	1.40	62.0	0.560	4.91	0.37	29.7	0.41	2.01	72.4
4a2	1	0.31	1.40	66.5	0.547	4.03	0.39	31.8	0.44	1.77*	72.3
4c2	1	0.11	1.33	57.7	--	--	0.39	27.7	0.39	--	71.0
4c2	2	0.18	1.36	59.0	0.570	3.88	0.39	28.3	0.40	1.55*	70.8
5a2		0.12	1.34	66.2	0.548	1.25	0.51	32.3	1.05	1.31	30.8
6a1	1	0.27	1.39	60.6	0.565	5.65	0.46	36.7	0.87	4.92*	42.2
6b2	1	0.10	1.32	58.1	0.573	6.76	0.45	35.1	0.82	5.54*	42.8
7a2	1	0.07	1.30	54.0	--	--	0.38	14.9	0.68	--	21.9
7a2	2	0.06	1.29	53.5	--	--	0.38	14.8	0.69	--	22.0
7a2	3	0.10	1.32	54.8	--	--	0.38	15.2	0.67	--	22.1
7a2	4	0.55	1.45	60.2	0.566	3.38	0.38	16.7	0.75	2.54*	22.3

(1) Tension reinforcement.

* Beam did not collapse under this blow in the test.

TABLE 17

COMPUTED COLLAPSE DEFLECTIONS

Beam	Type of Test	Mode of Failure	Δ_m Comp.(1) in.	Δ_m Meas. in.	Comp./Meas.
2a1	D	F	1.00	1.06	0.94
2a2	D	F	0.85	1.02	0.83
2b1	S	F	0.98	0.95	1.03
2b2	D	F	0.76	0.95	0.80
2b3	D	F	0.89	1.12	0.80
3a1	D	F	2.77	4.05	0.68
3a2	DS	F	2.13	4.30	0.49
3a3	DS	F	2.39	3.15	0.76
3a4	DS	F	2.22	3.70	0.60
3a5	D	F	2.15	4.47	0.48
3b1	S	F	3.81	3.93	0.97
3b2	D	F	2.61	4.11	0.63
3b3	D	F	2.71	~5.00	~0.54
4a1	D	F	2.61	2.00	1.30
4a2	D	F	2.19	2.58	0.85
4b1	S	F	2.51	1.98	--
4b2	D	F	2.25	--	--
4b3	DS	F	1.77	2.04	0.87
4c1	S	S	1.76	0.38	--
4c2	D	F	2.02	2.66	0.76
4c3	D	S	1.90	0.80	--
5a1	D	F	1.10	1.38	0.80
5a2	D	F	1.34	1.24	1.08
5b1	S	S	1.64	0.70	--
5b2	D	S	1.63	--	--
5b3	D	S	1.18	1.05	--
5b4	D	S	1.72	1.35	--
6a1	DS	F	5.90	4.90	1.20
6b1	D	F	4.60	4.98	0.92
6b2	DS	S	6.95	3.00	--
7a1	S	F	3.66	2.24	1.63
7a2	D	F	3.52	4.13	0.85
7a3	DS	F	4.06	5.38	0.75

(1) Computed by Eq. 58.

TABLE 18

COMPARISON OF COMPUTED DYNAMIC RESISTANCES

Beam	Blow	Q_{yd}			Δ_{yd}			Δ_{md}/Δ_{yd}			Δ_{md}			k_{1d}		
		A.C. (1) kips	Str. (2) kips	Str./A.C.	A.C. in.	Str. in.	Str./A.C.	A.C.	Str.	Str./A.C.	A.C. in.	Str. in.	Str./A.C.	A.C. k/in.	Str. k/in.	Str./A.C.
2a1		62.4	63.8	1.02	0.67	0.59	0.88	1.58	1.82	1.15	1.06	1.07	1.01	93.0	108.1	1.16
2b2		60.5	61.4	1.01	0.64	0.58	0.91	1.48	1.40	0.95	0.95	0.81	0.85	94.6	105.9	1.12
3a2		61.4	62.8	1.02	0.55	0.48	0.87				(3)			111.4	130.8	1.17
3b2	1	--	60.8	--	--	0.46	--				(3)			--	132.2	--
4a1		28.4	29.7	1.05	0.57	0.41	0.72	3.51	4.91	1.40	2.00	2.01	1.01	49.8	72.4	1.45
4a2	1	28.9	31.8	1.10	0.47	0.44	0.94				(3)			61.4	72.3	1.18
4c2	1	>20.8*	27.7	--	>0.34*	0.39	--				(3)			61.2*	71.0	1.16
4c2	2	23.4*	28.3	1.21	0.41*	0.40	0.98				(3)			57.0*	70.8	1.24
5a2		26.2	32.3	1.23	0.83	1.05	1.27	1.25	1.49	1.19	1.24	1.31	1.06	31.6	30.8	0.97
6a1	1	33.9	36.7	1.08	0.82	0.87	1.06				(3)			41.3	42.2	1.02
6b2	1	34.9	35.1	1.01	0.80	0.82	1.02				(3)			43.6	42.8	0.98
7a2	1	>15.8	14.9	--	>0.64	0.68	--				(3)			24.7	21.9	0.89
7a2	2	11.4	14.8	1.30	0.66	0.69	1.05				(3)			17.2	22.0	1.28
7a2	3	13.9	15.2	1.09	0.74	0.67	0.90				(3)			18.8	22.1	1.18
7a2	4	12.4*	16.7	1.35	0.68*	0.75	1.10				(3)			18.2*	22.3	1.22

(1) A.C. = Analog computer results.
(2) Str. = Results from strain rate determinations.
(3) Beam did not collapse under this blow.
* Damping introduced into solution.

TABLE 19

MEASURED AND COMPUTED STRAIN RATES

Beam	Blow	Velocity at Yield	Strain Rate, $\dot{\epsilon}_c$		f_{yd}/f_y	
			Comp.	Meas.	from Comp. $\dot{\epsilon}_c$	from Meas. $\dot{\epsilon}_c$
		in./sec.	in./in./sec.	in./in./sec.		
2a1		110	0.43	0.32	1.43	1.40
2b2		79	0.30	0.24	1.40	1.38
3a2		138	0.61	0.22	1.45	1.38
3b2	1*	--	--	0.25	--	1.39
4a1		86	0.44	0.32	1.43	1.40
4a2	1	60	0.30	0.31	1.40	1.40
4c2	1**	--	--	0.11	--	1.33
4c2	2	40	0.20	1.18	1.37	1.36
5a2		83	0.18	0.12	1.36	1.34
6a1	1	91	0.21	0.27	1.37	1.39
6b2	1	88	0.21	0.10	1.37	1.32
7a2	1**	--	--	0.07	--	1.30
7a2	2	21	0.06	0.06	1.29	1.29
7a2	3	36	0.10	0.10	1.32	1.32
7a2	4	48	0.13	0.55	1.34	1.45

* No computer solution.

** No yield point in computer solution.

TABLE 20

MATERIAL PROPERTIES USED IN COMPUTING O.C.E.
PREDICTED BEHAVIOR

Beam	Blow	Steel f_{yd} ksi	Steel f'_{yd} ksi	Steel f_w ksi	Concrete Strain Rate in./in./sec	Concrete $\frac{f'_{cd}}{f'_c}$	Concrete f'_{cd} ksi	Concrete E_c psi x 10^6
		(1)	(2)	(3)	(4)	(5)	(6)	(7)
2a1	--	68.7	--	55.1	--	1.46	6.04	3.58
2b2	--	66.1	--	44.4	0.72	1.44	4.41	3.30
3a2	--	64.2	65.6	52.4	0.76	1.44	4.68	3.82
3b2	1	60.7	44.1	43.6	0.42	1.40	4.56	3.74
4a1	--	62.0	--	55.1	--	1.33	5.69	4.04
4a2	1	66.5	--	55.1	--	1.33	5.12	3.67
4c2	1	57.7	--	--	0.06	1.26	4.11	3.49
4c2	2	59.0	--	--	0.10	1.30	4.24	3.49
5a2	--	66.2	--	53.7	0.16	1.33	3.74	3.71
5b4	1	68.5	--	--	0.07	1.27	4.86	3.06
5b4	2	70.1	--	--	0.10	1.30	4.97	3.06
6a1	1	60.6	45.6	53.6	0.28	1.37	5.15	3.69
6b2	1	58.1	65.1	53.4	0.11	1.30	5.78	4.00
7a2	1	54.0	--	--	0.04	1.24	3.38	3.83
7a2	2	53.5	--	--	0.05	1.25	3.41	3.83
7a2	3	54.8	--	--	0.07	1.27	3.47	3.83
7a2	4	60.2	--	--	0.14	1.32	3.60	3.83

TABLE 21

PREDICTED BEHAVIOR OF BEAMS ACCORDING TO O.C.E

Beam	Blow	Q_{yd} kips	v psi	v_y psi	Governing Condition	Δ_{yd} in.	Δ_{md} in.	k_{ld} kips/in.	T msec.
		(1)	(2)	(3)	(4)	(5)	(6)	(7)	(8)
2a1	--	59.3	565	872	F	0.46	1.38	128.4	17.6
2b2	--	51.8	493	426	S	0.44	1.32	118.3	18.3
3a2	--	61.9	590	747	F	0.41	3.08	150.6	16.3
3b2	1	57.4	547	467	S	0.39	2.92	147.2	16.4
4a1	--	27.5	262	449	F	0.23	1.56	118.5	18.3
4a2	1	28.8	274	431	F	0.27	1.84	107.5	19.2
4c2	1	24.8	236	204	S	0.24	1.63	102.5	19.7
4c2	2	25.4	242	204	S	0.25	1.70	102.5	19.7
5a2	--	29.8	284	804	F	0.68	2.04	44.0	34.3
5b4	1	34.2	326	319	S	0.94	2.82	36.3	37.7
5b4	2	35.0	333	319	S	0.96	2.88	36.3	37.7
6a1	1	36.0	343	778	F	0.75	5.62	48.1	32.8
6b2	1	35.2	335	419	F	0.67	5.02	52.2	31.5
7a2	1	14.1	134	183	F	0.38	2.58	37.0	37.4
7a2	2	14.0	133	183	F	0.38	2.58	37.0	37.4
7a2	3	14.3	136	183	F	0.39	2.65	37.0	37.4
7a2	4	15.6	148	183	F	0.42	2.86	37.0	37.4

TABLE 22

COMPARISON OF MEASURED AND COMPUTED RESISTANCE AND MODE OF FAILURE

Beam	Blow	Q_{yd} Meas.	Q_{yd} Comp.	Q_{yd} Comp./Meas.	Δ_{yd} Meas.	Δ_{yd} Comp.	Δ_{yd} Comp./Meas.	k_{1d} Meas.	k_{1d} Comp.	k_{1d} Comp./Meas.	Δ_{md} Meas(1)	Δ_{md} Comp.	Δ_{md} Comp./Meas.	Δ_{md} Comp. from Eq.73 and meas. Δ_{yd}	Δ_{md} Comp./Meas.	Mode of Failure Meas.	Mode of Failure Comp.
		kips	kips		in.	in.		kips/in.	kips/in.		in.	in.		in.			
2a1	-	62.4	59.3	0.95	0.67	0.46	0.69	93.0	128.4	1.38	1.06	1.38	1.30	2.01	1.90	F	F
2b2	-	60.5	51.8	0.86	0.64	0.44	0.69	94.6	118.3	1.25	0.95	1.32	1.39	1.92	2.02	F	S
3a2	-	61.4	61.9	1.01	0.55	0.41	0.74	111.4	150.6	1.35	4.30(4)	3.08	0.72	4.13	0.96	F	F
3b2	1	(2)	57.4	--	(2)	0.39	--	(2)	147.2	--	4.11(4)	2.92	0.71	--	--	F	S
4a1	-	28.4	27.5	0.97	0.57	0.23	0.40	49.8	118.5	2.38	2.00	1.56	0.78	3.88	1.94	F	F
4a2	1	28.9	28.8	1.00	0.47	0.27	0.57	61.4	107.5	1.75	2.58(4)	1.84	0.71	3.20	1.24	F	F
4c2	1	>20.8	24.8	--	>0.34	0.24	--	61.2	102.5	1.68	2.66(4)	1.63	0.61	--	--		S
4c2	2	23.4	25.4	1.08	0.41	0.25	0.61	57.0	102.5	1.80	2.66(4)	1.70	0.64	2.79	1.05	F	S
5a2	-	26.2	29.8	1.14	0.83	0.68	0.82	31.6	44.0	1.39	1.24	1.04	1.64	2.49	2.01	F	F
5b4	1	30.8(3)	33.5(5)	1.09	1.03(3)	0.92(5)	0.89	29.9	36.3	1.21	--	--	--	--	--		S
5b4	2	29.9(3)	33.5(5)	1.12	1.00(3)	0.92(5)	0.92	29.9	36.3	1.21	--	--	--	--	--	S	S
6a1	1	33.9	36.0	1.06	0.82	0.75	0.91	41.3	48.1	1.17	4.90(4)	5.62	1.15	6.15	1.26	F	F
6b2	1	34.9	35.2	1.01	0.80	0.67	0.84	43.6	52.2	1.20	3.00(4)	5.02	1.68	6.00	2.00	S	F
7a2	1	>15.8	14.1	--	>0.64	0.38	--	24.7	37.0	1.50	4.13(4)	2.58	0.62	--	--		F
7a2	2	11.4	14.0	1.23	0.66	0.38	0.58	17.2	37.0	2.15	4.13(4)	2.58	0.62	4.49	1.08	F	F
7a2	3	13.9	14.3	1.03	0.74	0.39	0.53	18.8	37.0	1.97	4.13(4)	2.65	0.64	5.13	1.24		F
7a2	4	12.4	15.6	1.26	0.68	0.42	0.62	18.2	37.0	2.03	4.13(4)	2.86	0.69	4.62	1.12		F
Ave. of flexural failures				1.05													

(1) From Table 17
(2) No computer solution
(3) Maximum value attained
(4) Under final loading
(5) Values for $v = v_y$

TABLE 23

COMPARISON OF MEASURED RESISTANCE WITH RESISTANCE COMPUTED ACCORDING TO CHAPTER XV

Beam	Blow	Q_{yd}			Δ_{yd}			Δ_{md}		
		Meas. kips	Comp. kips	Comp./Meas.	Meas. in.	Comp. in.	Comp./Meas.	Meas. in.	Comp. in.	Comp./Meas.
		(1)	(2)	(3)	(4)	(5)	(6)	(7)	(8)	(9)
2a1	-	62.4	51.5	0.83	0.67	0.55	0.82	1.06	1.00	0.94
2b2	-	60.5	42.3	0.70	0.64	0.53	0.83	0.95	0.76	0.80
3a2	-	61.4	60.6	0.99	0.55	0.52	0.94	4.30	2.13	0.49
4a1	-	28.4	26.6	0.94	0.57	0.49	0.86	2.00	2.61	1.30
4a2	1	28.9	27.7	0.96	0.47	0.52	1.10	2.58	2.19	0.85
4c2	2	23.4	24.3	1.04	0.41	0.46	1.12	2.66	2.02	0.76
5a2	-	26.2	24.6	0.94	0.83	1.03	1.24	1.24	1.34	1.08
6a1	1	33.9	35.0	1.03	0.82	0.92	1.12	4.90	5.90	1.20
6b2	1	34.9	35.0	1.00	0.80	0.93	0.97	Final	failure	in shear
7a2	2	11.4	13.5	1.18	0.66	0.82	1.24			
7a2	3	13.9	13.7	0.98	0.74	0.84	1.14	4.13	3.52	0.85
7a2	4	12.4	14.8	1.19	0.68	0.86	1.26			
			Ave. =	0.98		Ave. =	1.05		Ave. =	0.92

TABLE 24

NATURAL FREQUENCY FOR SMALL AMPLITUDES

Beam	Frequency cycles/sec.	Period millisec.	Method	Place
		Simple Support		
2a1	56	17.9	Single blow	In frame
2a2-Uncracked	59	16.9	Resonance	In frame
2a2-Cracked	59	16.9	Resonance	In frame
2b1	56	18.0	Single blow	In frame
3a1	60	16.7	Resonance	In frame
4a2	59	16.9	Single blow	In frame
4c2	55	18.2	Single blow	In frame
4c2	54	18.5	Resonance	In frame
5a2	35.4	28.2	Resonance	In frame
5b1	34.0	29.4	Resonance	In frame
6b1	35.4	28.2	Resonance	In frame
7a2	32.6	30.6	Resonance	In frame
		Free-Free Support		
3a1	132	7.6	Resonance	Outside frame
3a1	144	6.9	Resonance	In frame
4c2	128.5	7.8	Resonance	Outside frame
5a2	66.5	15.0	Resonance	Outside frame
5b1	68.0	14.7	Resonance	Outside frame
6b1	68.8	14.5	Resonance	Outside frame
7a2	65.2	15.3	Resonance	Outside frame

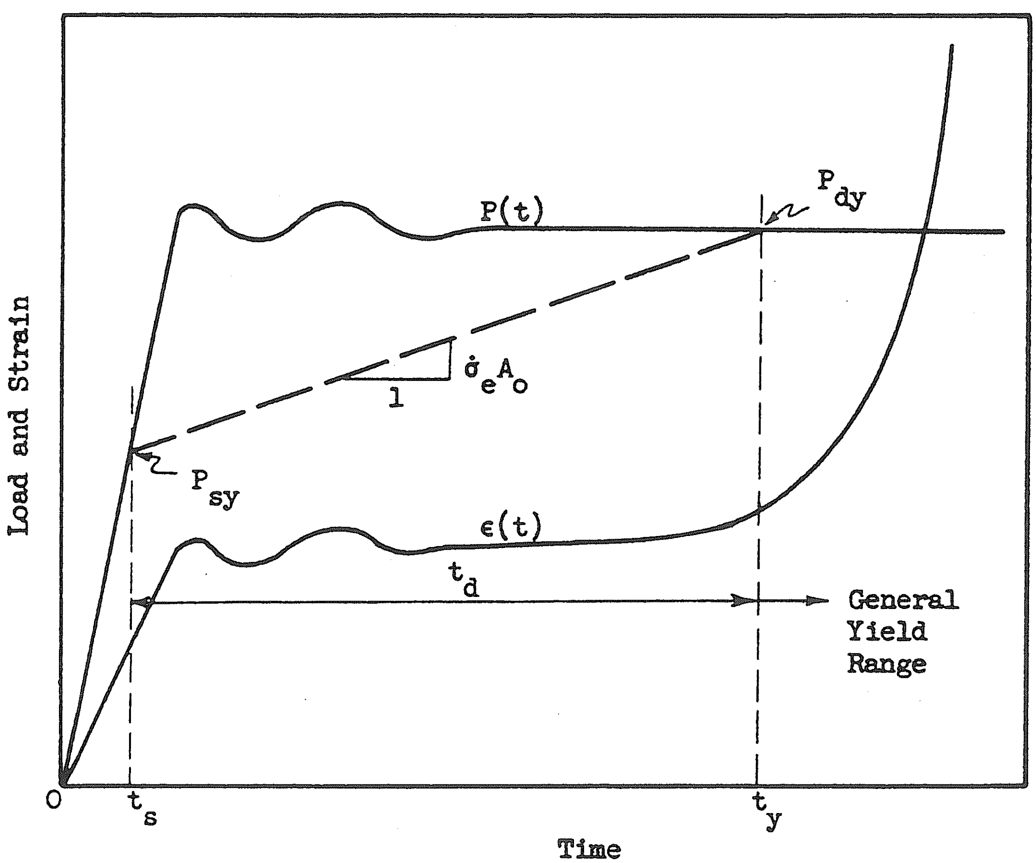

FIG. 1 TYPICAL LOAD AND STRAIN VS. TIME RELATIONSHIPS

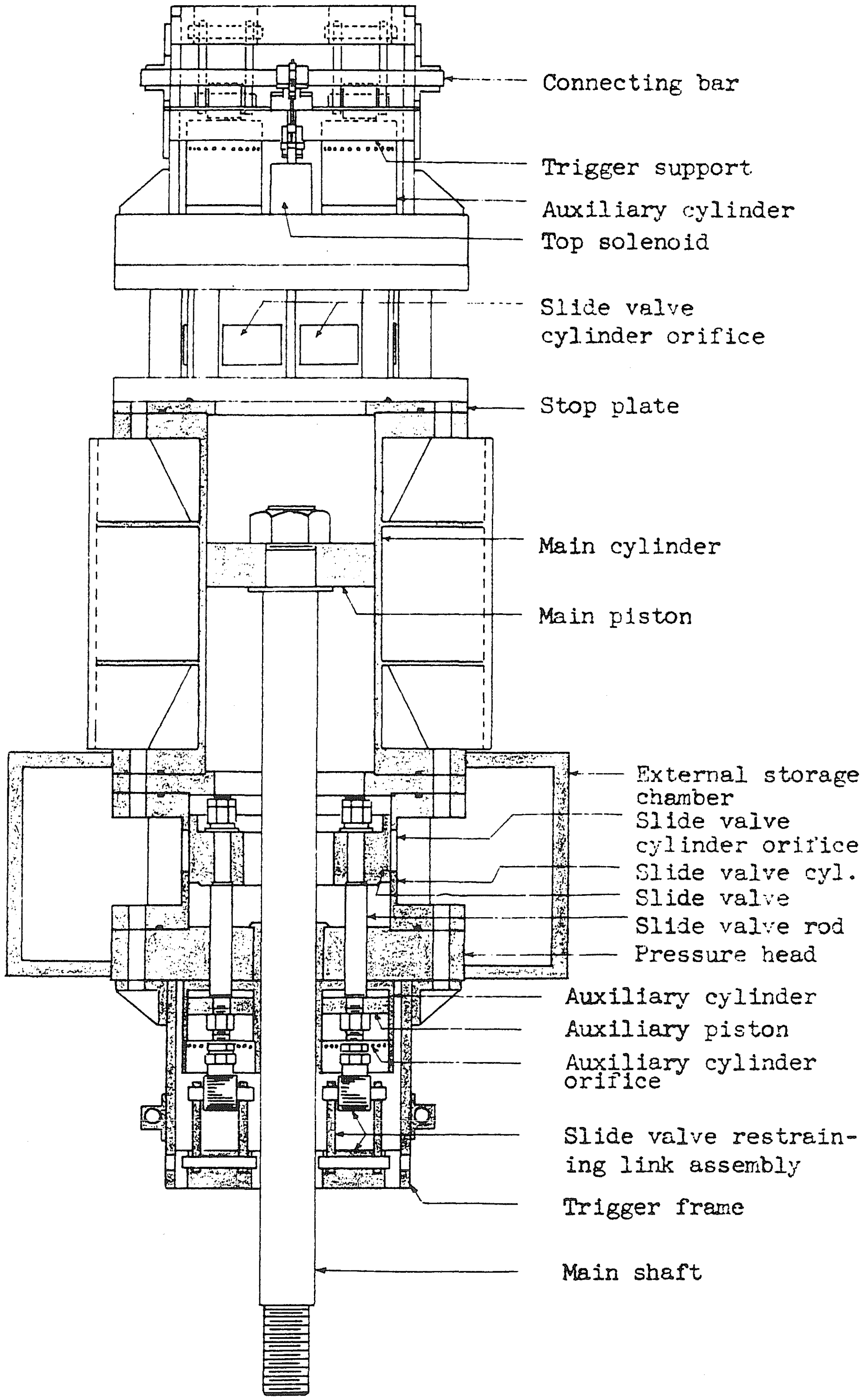

FIG. 2 60 KIP PULSE LOADING MACHINE

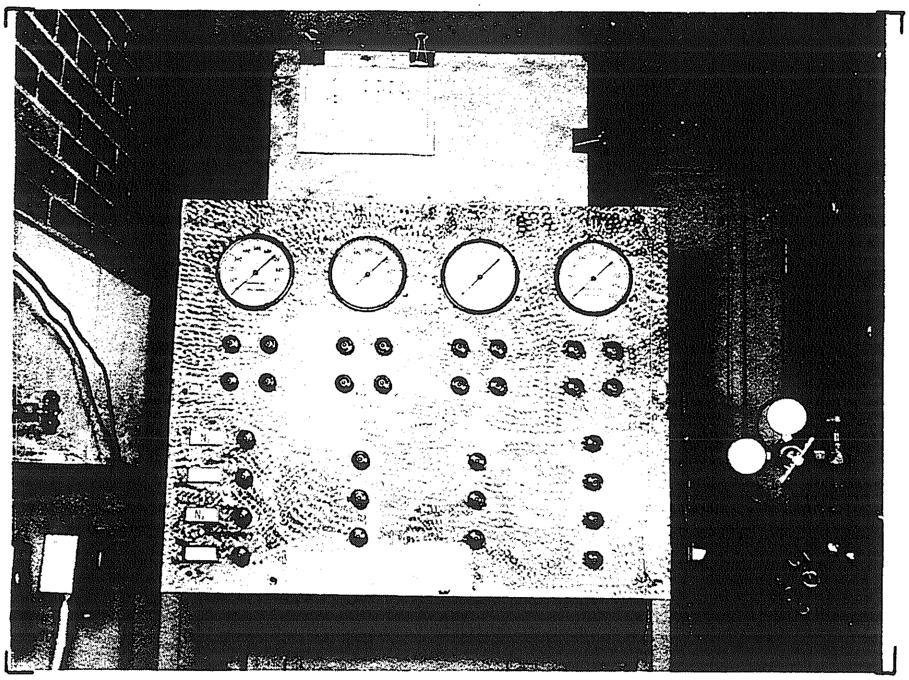

FIG. 3 VIEW OF CONTROL PANEL FOR PRESSURIZATION SYSTEM

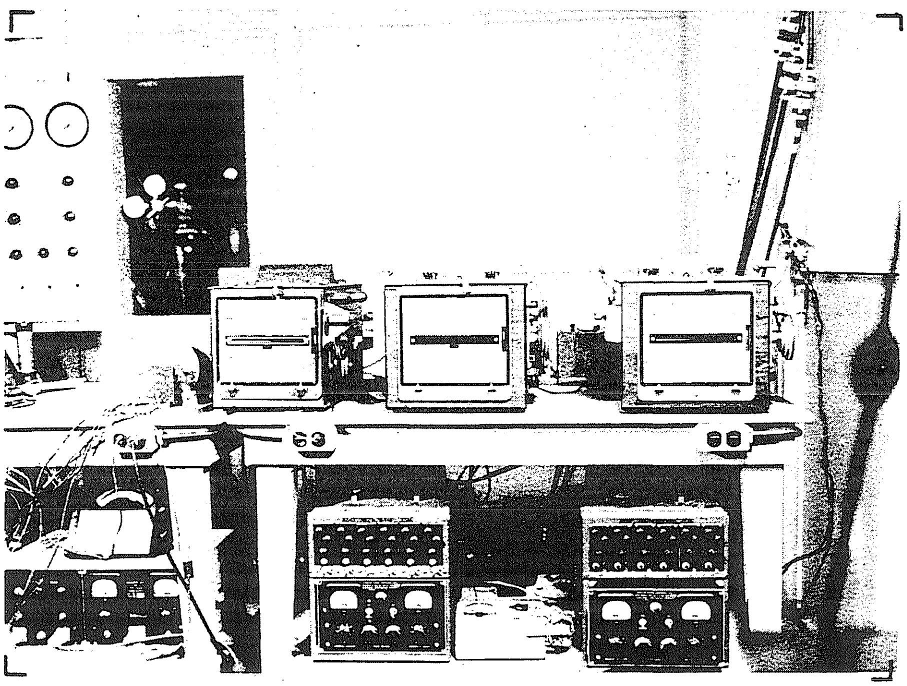

FIG. 4 VIEW OF OSCILLOGRAPHS AND TIMING DEVICE

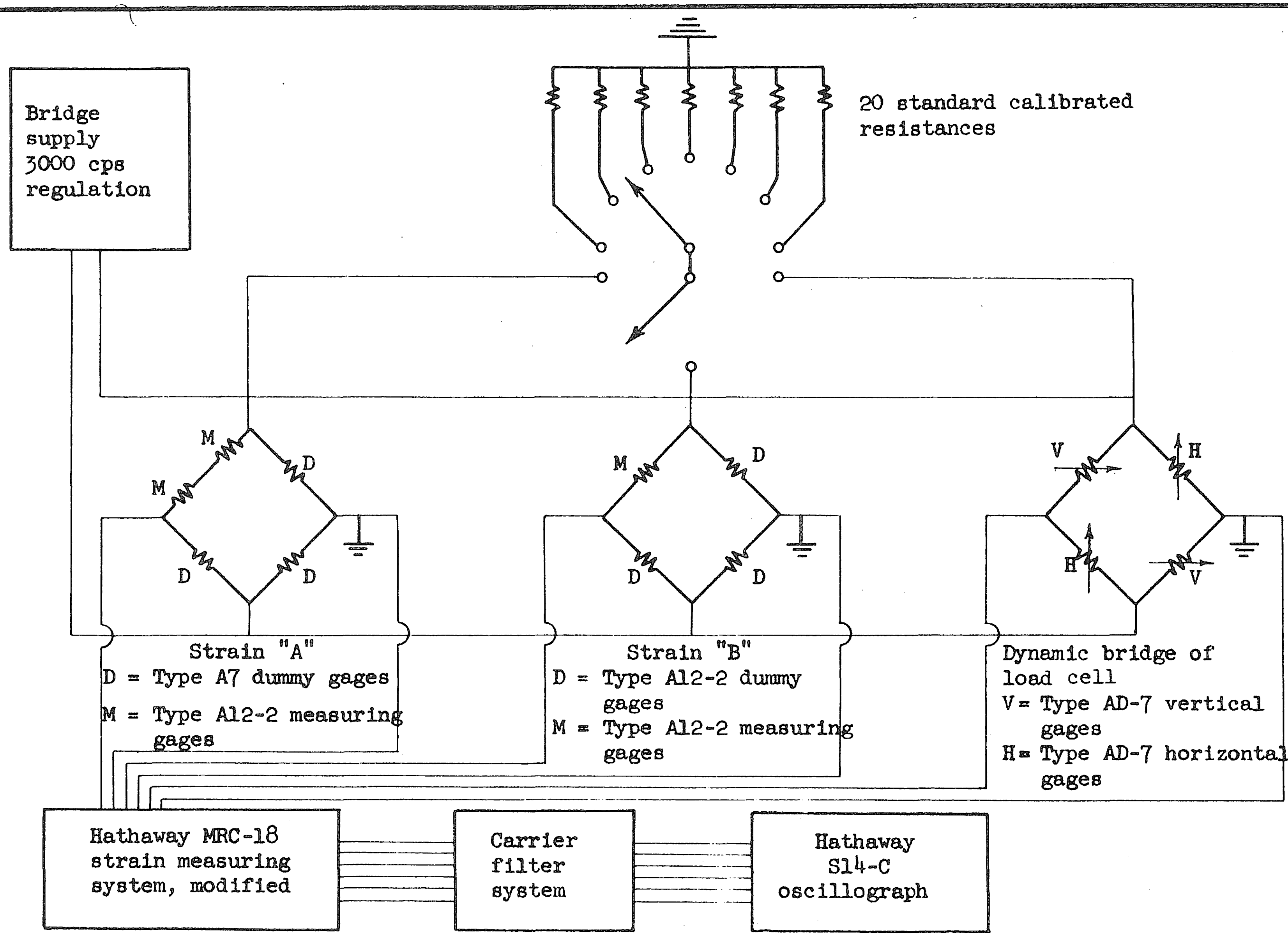

FIG. 5 CIRCUIT DIAGRAM OF LOAD CELL AND STRAIN BRIDGES

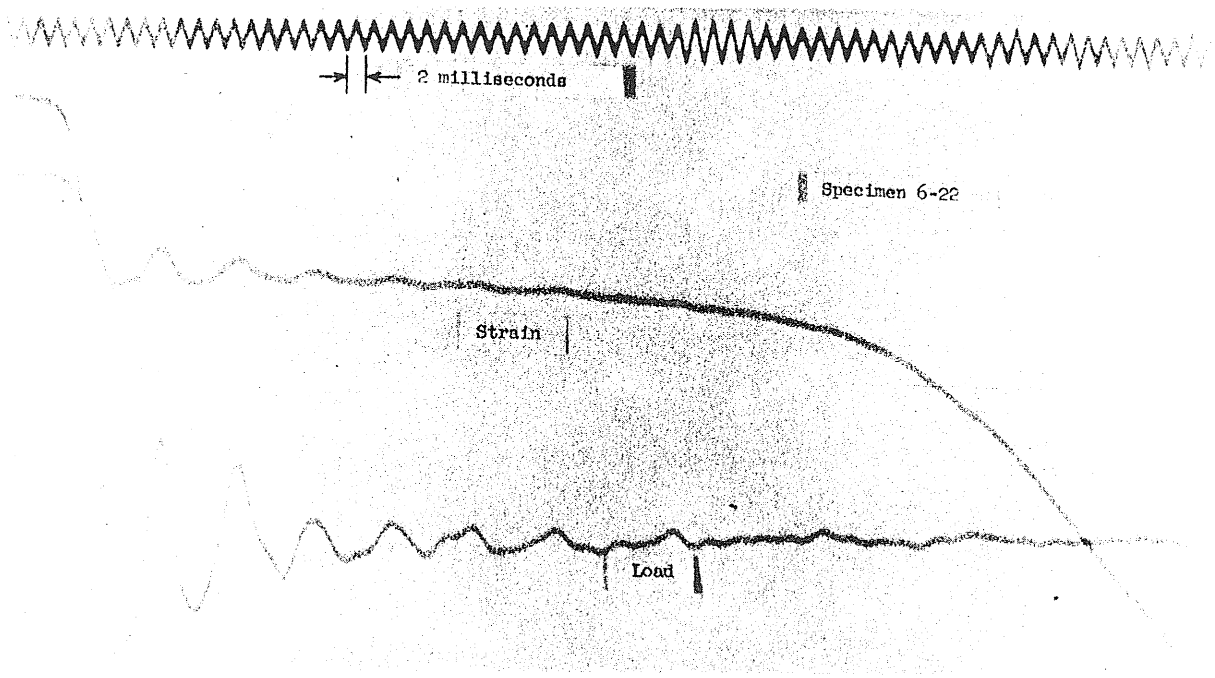

FIG. 6 TYPICAL OSCILLOGRAM OF LOAD AND STRAIN

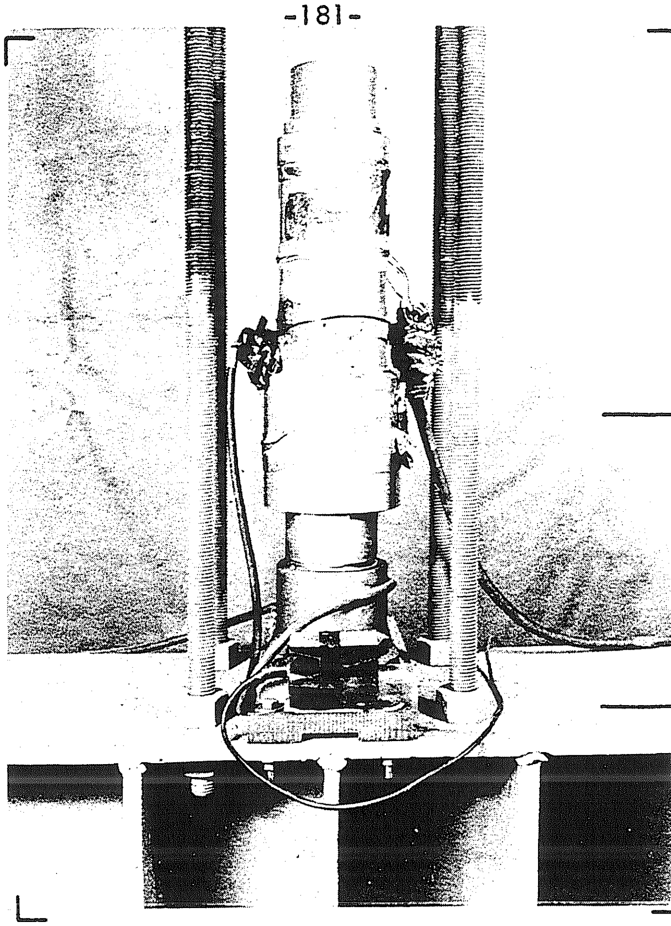

FIG. 7 VIEW OF LOAD CELL AND ACCELEROMETER

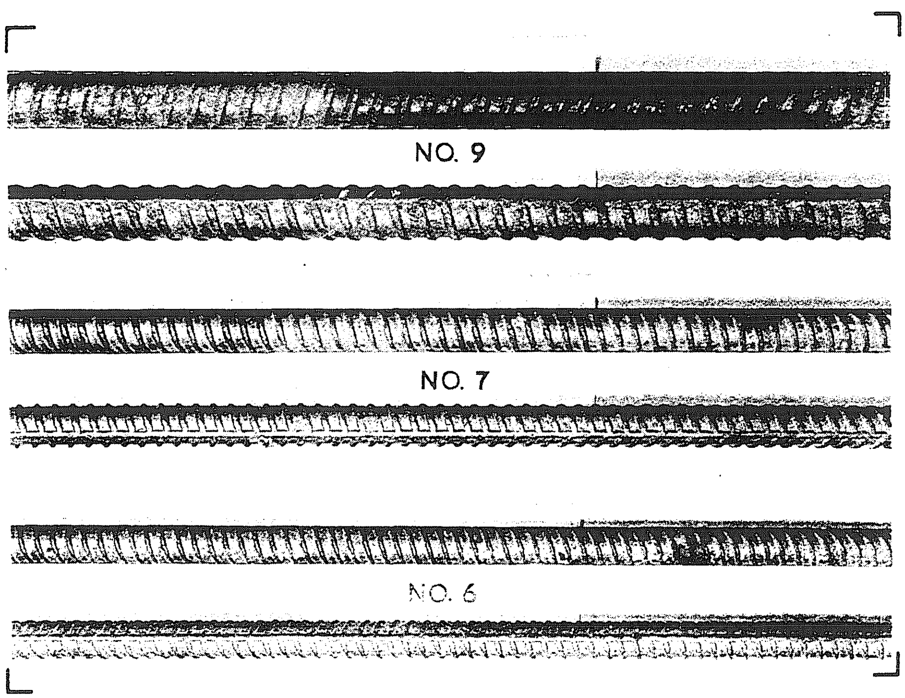

FIG. 8 VIEW OF DEFORMATIONS ON A NO. 6, 7, AND 9 BAR

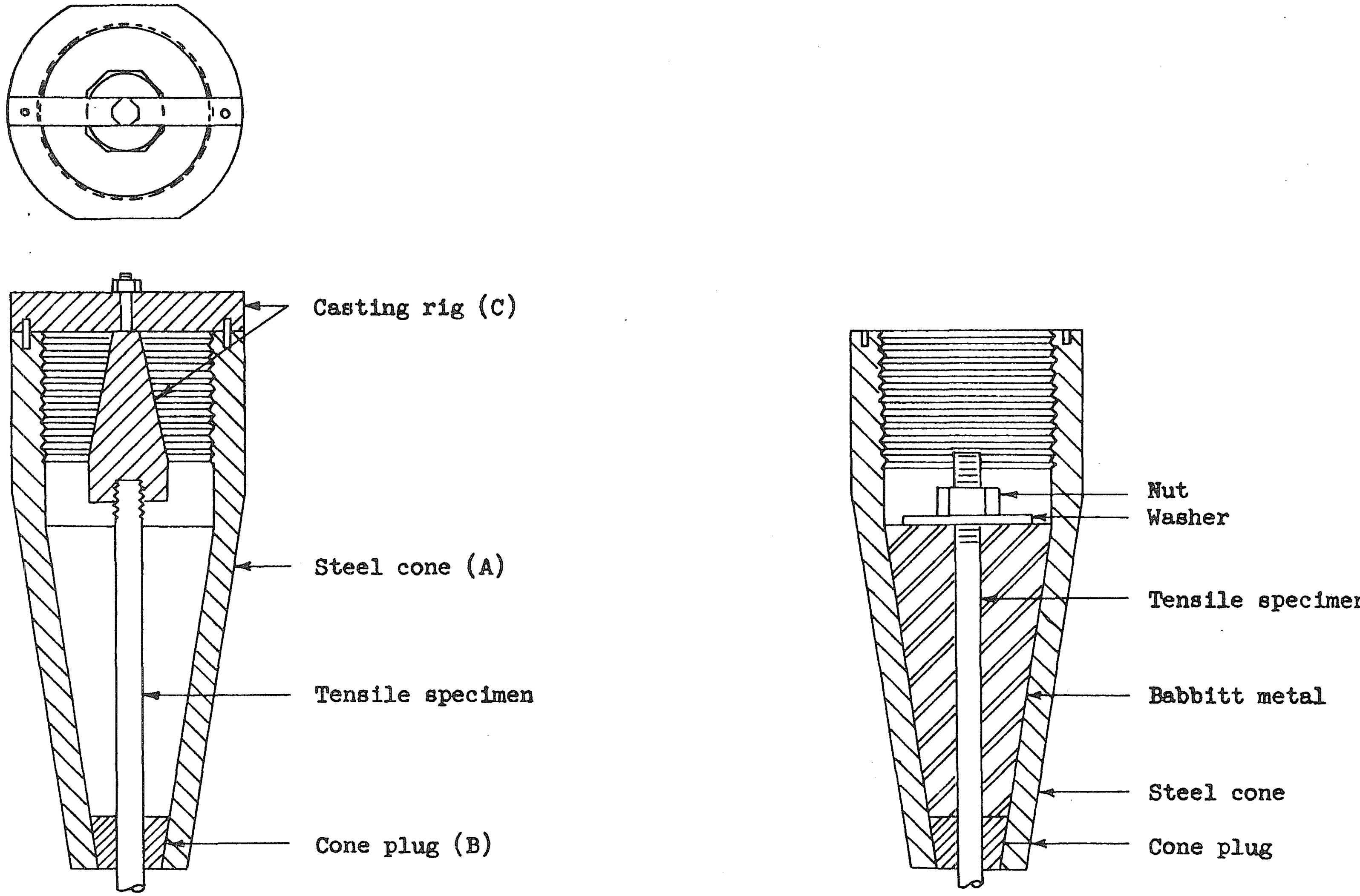

(a) Before Casting

(b) After Casting

FIG. 9 DETAILS OF CASTING THE GRIPS

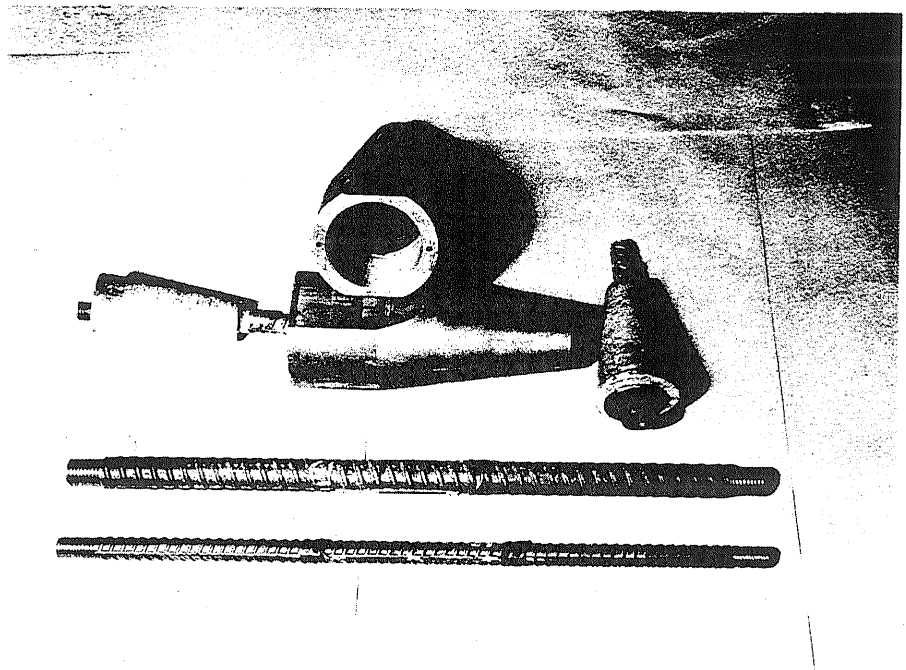

FIG. 10 VIEW OF THREADED SPECIMEN WITH STRAIN GAGES, BABBITT METAL GRIPS, AND STEEL CONES

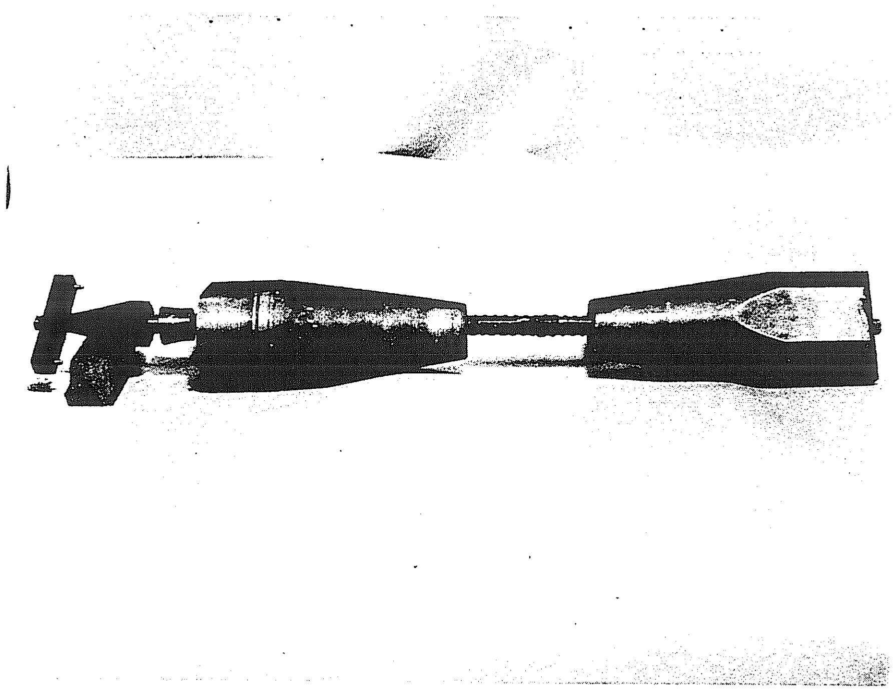

FIG. 11 VIEW OF SPECIMEN BEFORE CASTING THE GRIPS

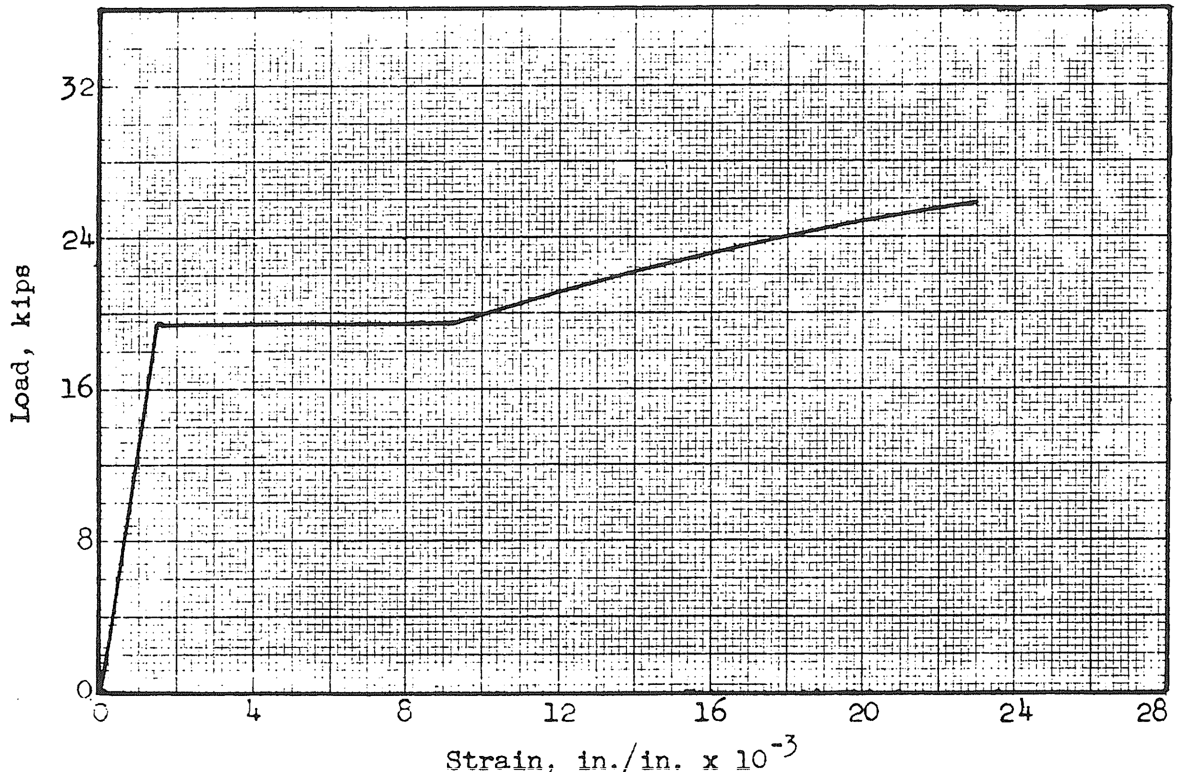

FIG. 12 TYPICAL STATIC LOAD-STRAIN DIAGRAM FOR A NO. 6 BAR

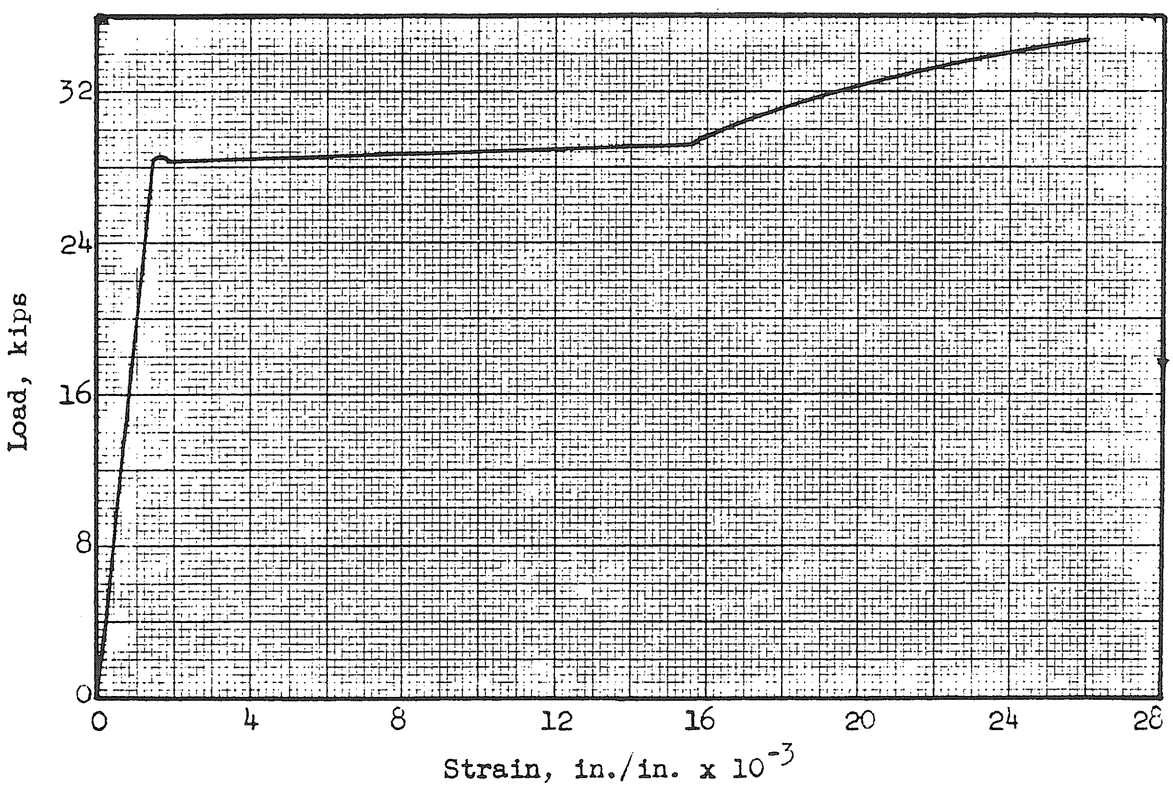

FIG. 13 TYPICAL STATIC LOAD-STRAIN DIAGRAM FOR A NO. 7 BAR

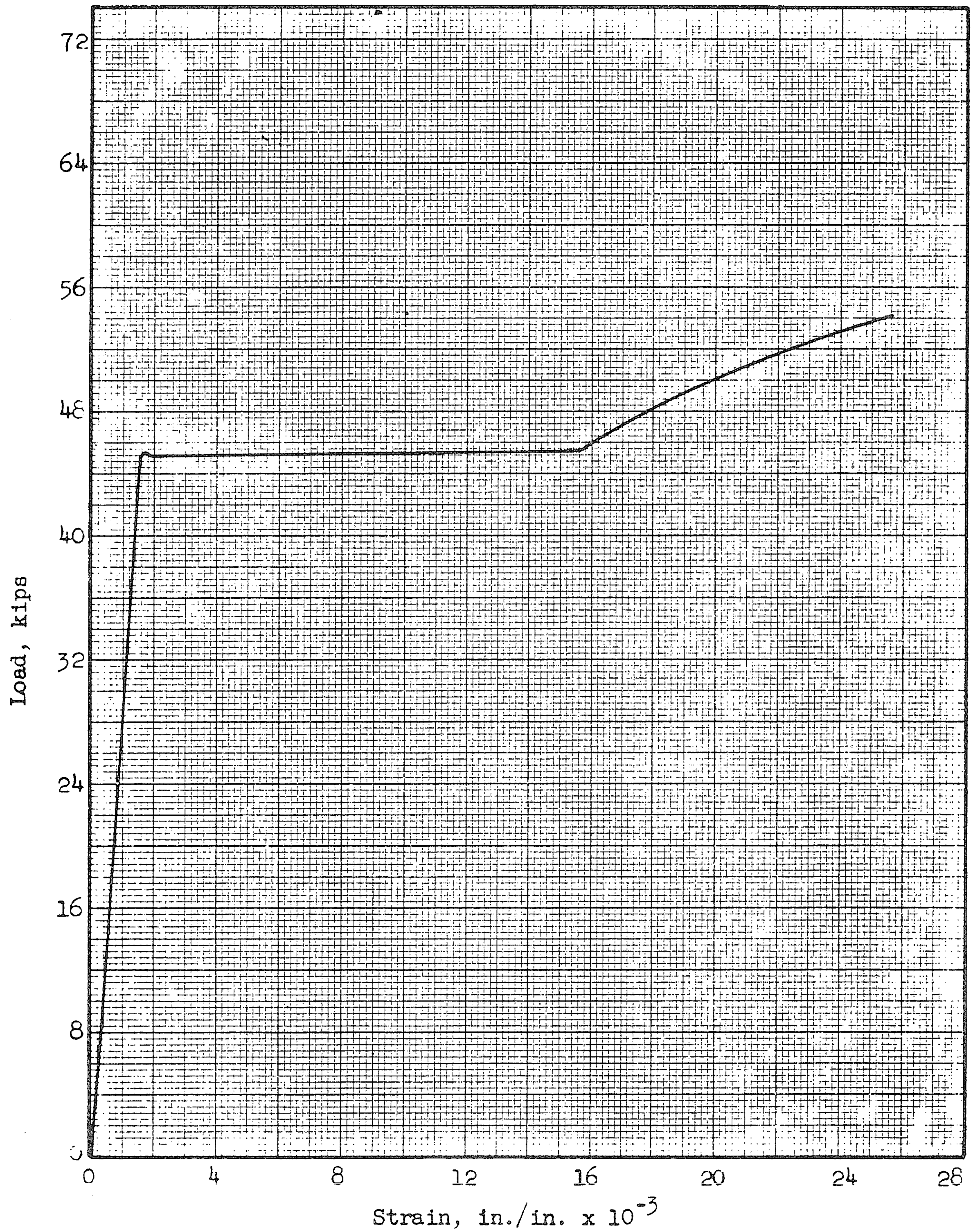

FIG. 14 TYPICAL STATIC LOAD-STRAIN DIAGRAM FOR A NO. 9 BAR

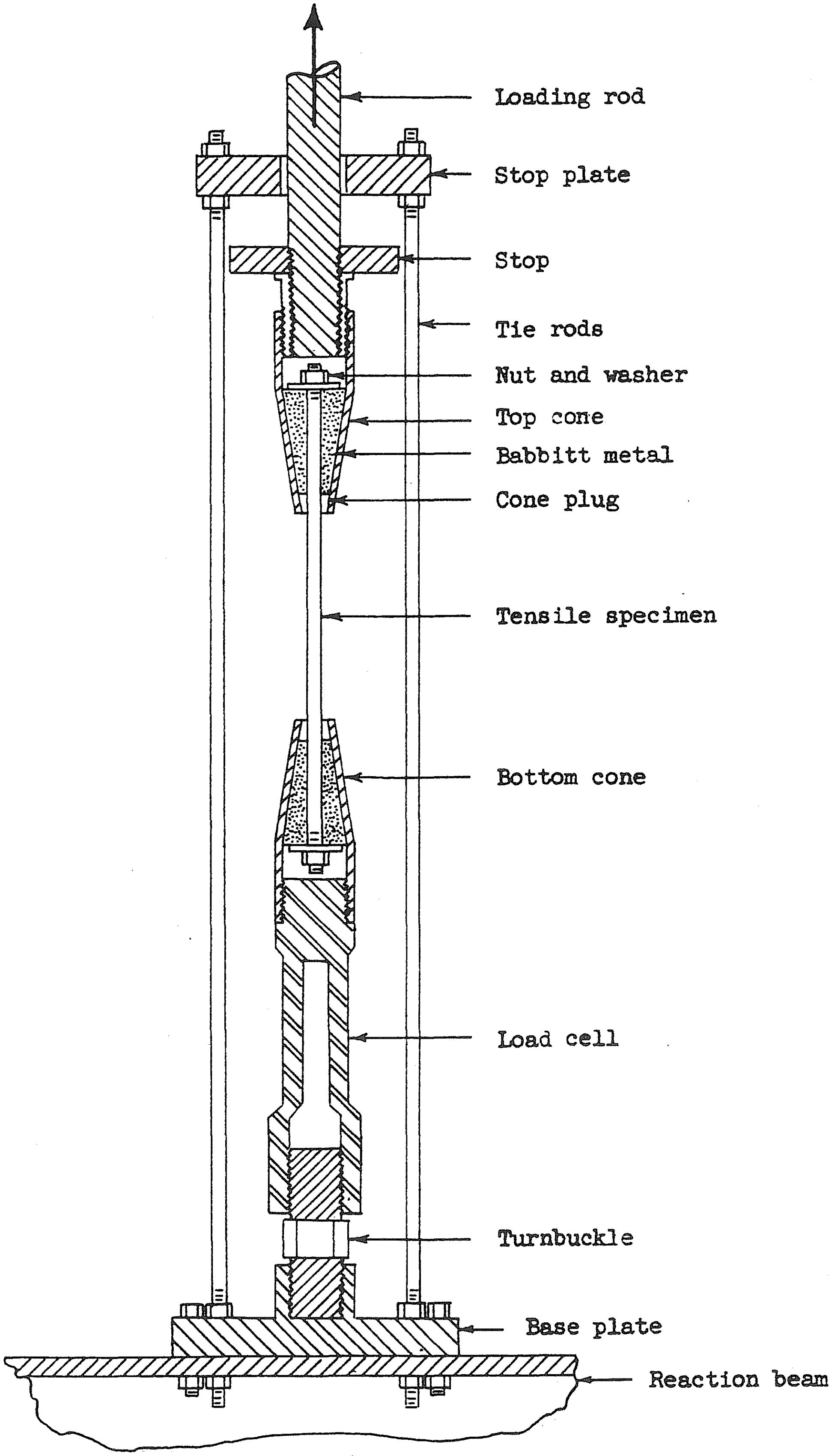

FIG. 15 CONNECTIONS OF TENSILE SPECIMEN TO PNEUMATIC LOADING MACHINE

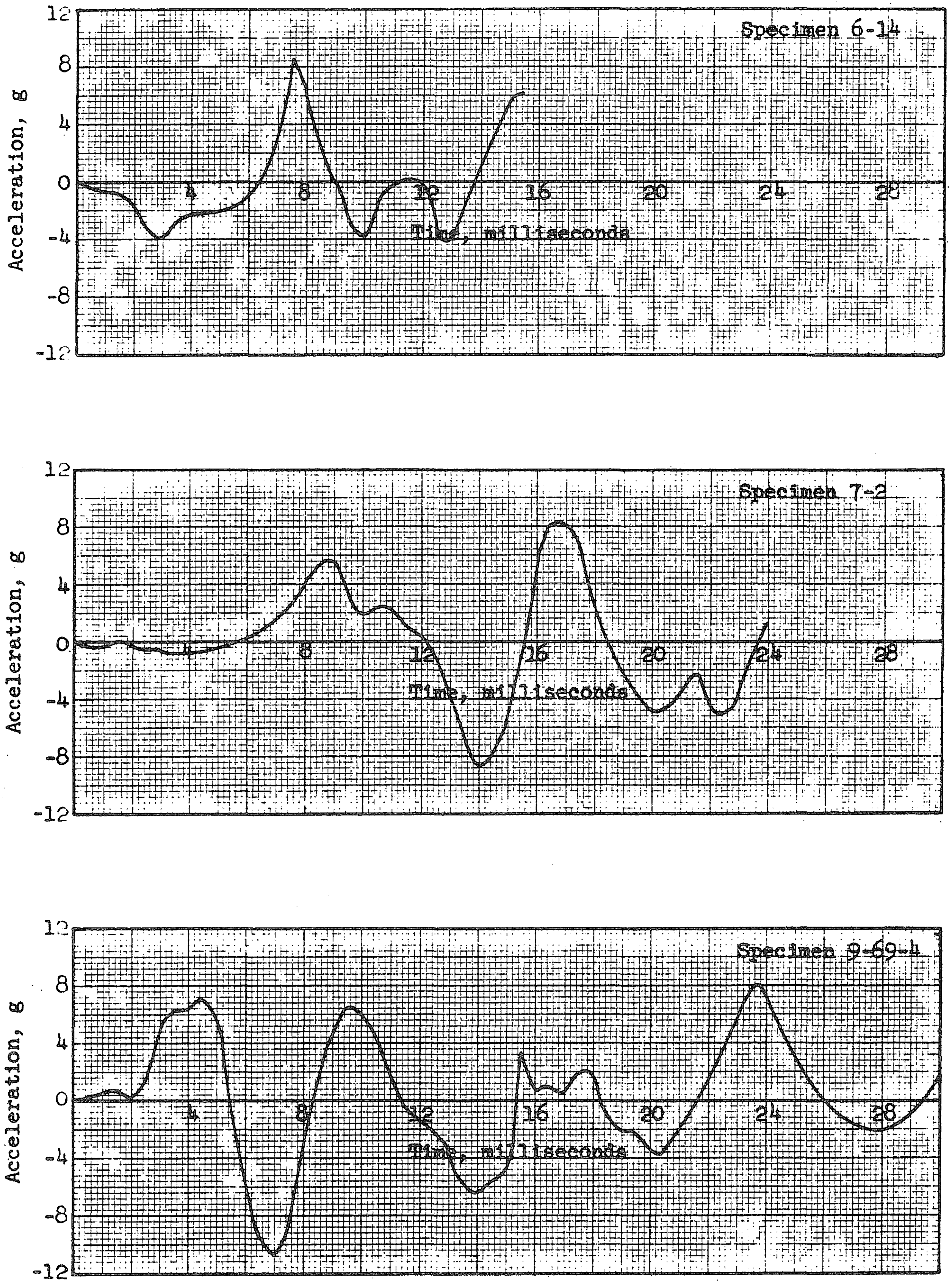

FIG. 16 ACCELERATION-TIME DIAGRAMS AT MIDSPAN OF REACTION BEAM

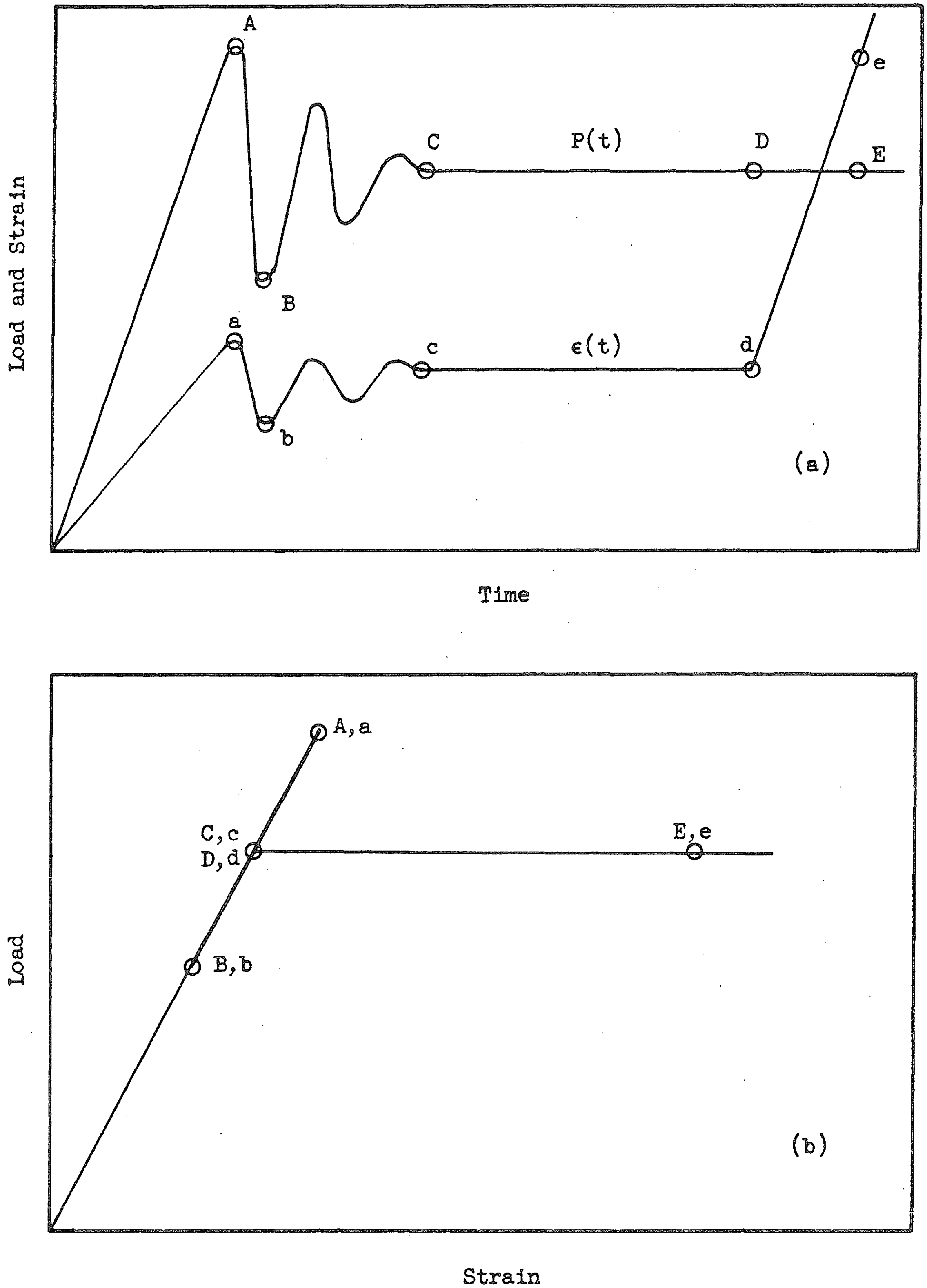

FIG. 17 IDEALIZED DYNAMIC LOAD-STRAIN DIAGRAM

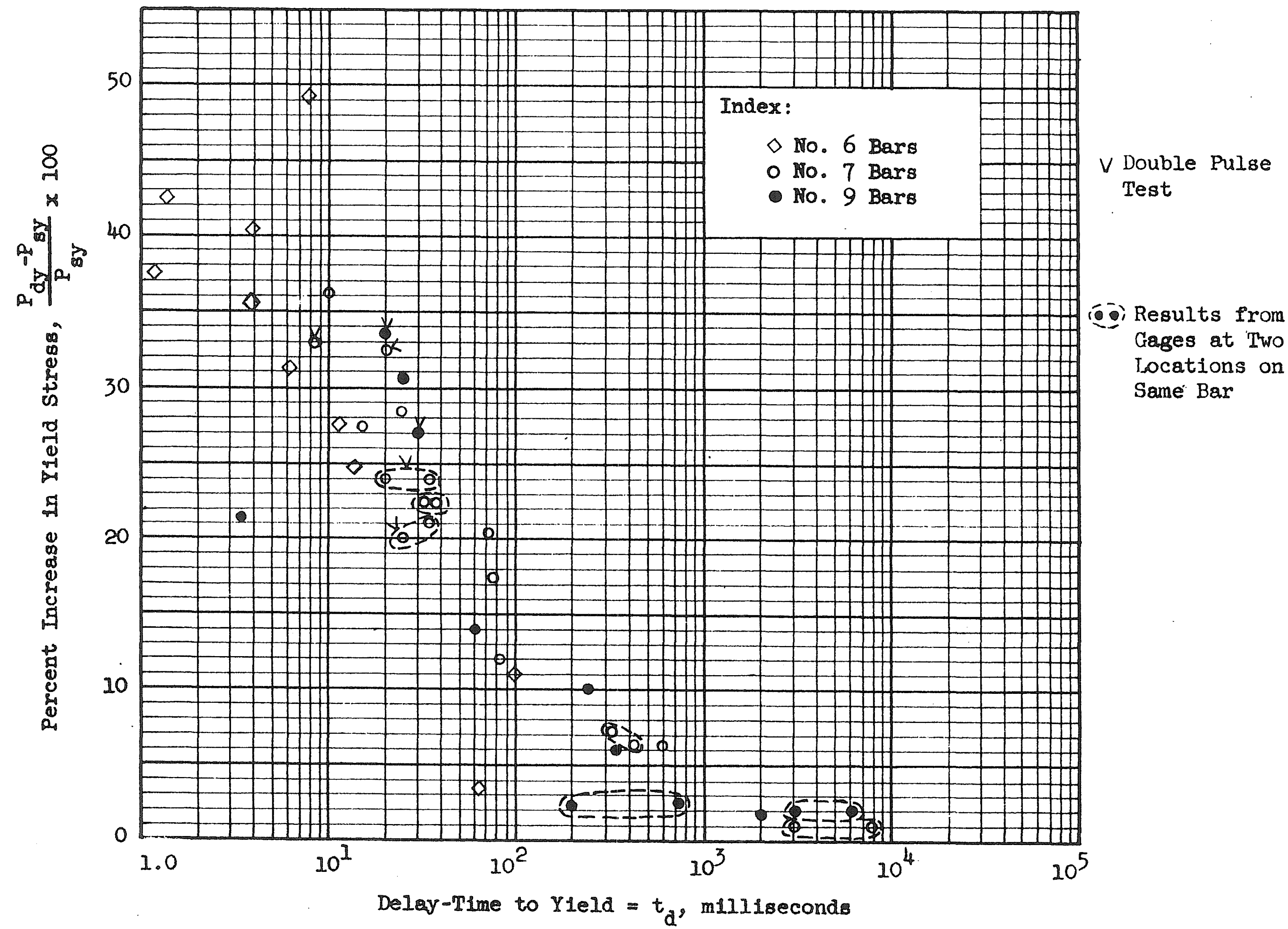

FIG. 18 PERCENT INCREASE IN YIELD STRESS VS. DELAY-TIME TO YIELD

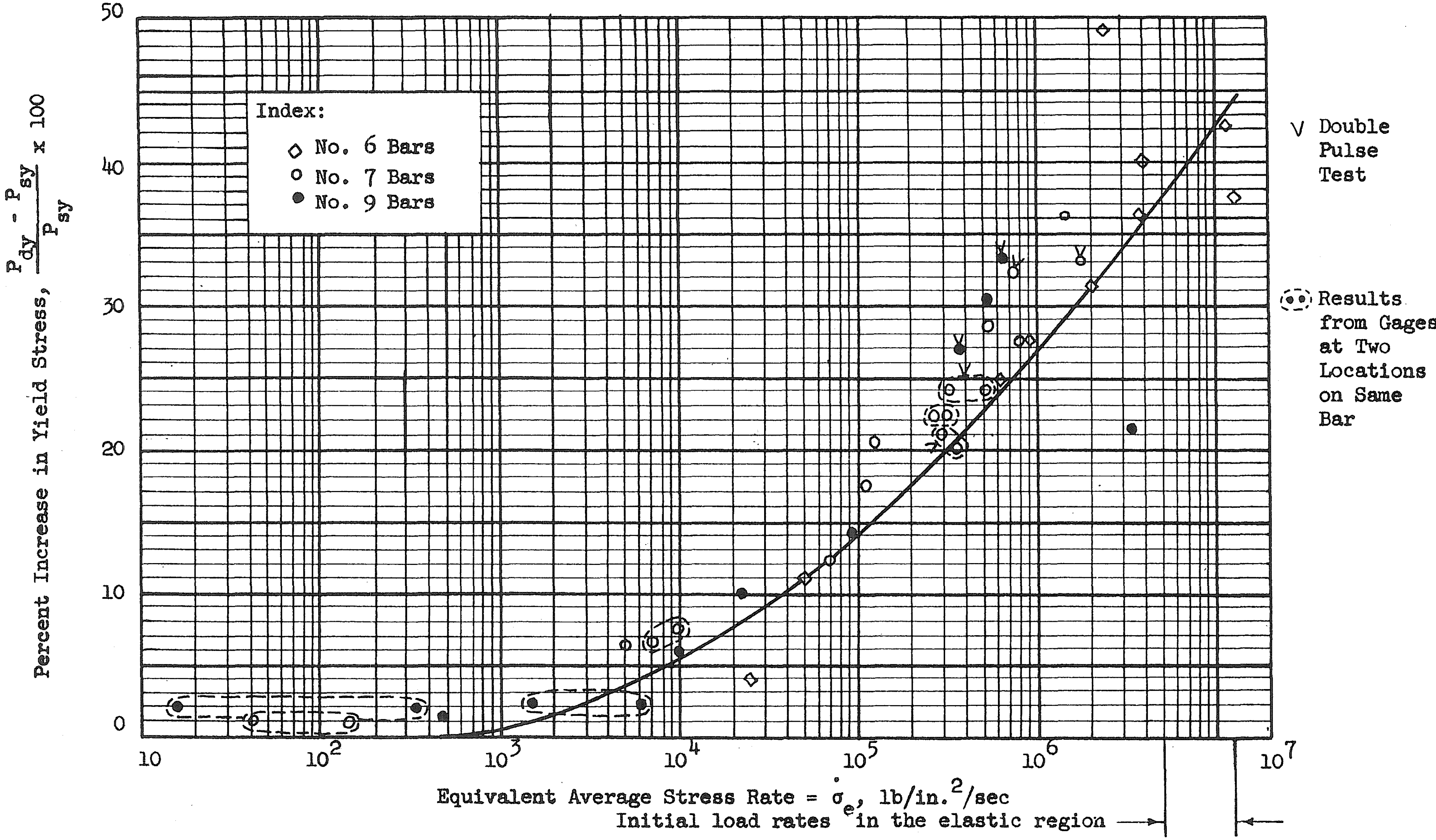

FIG. 19 PERCENT INCREASE IN YIELD STRESS VS. EQUIVALENT AVERAGE STRESS RATE

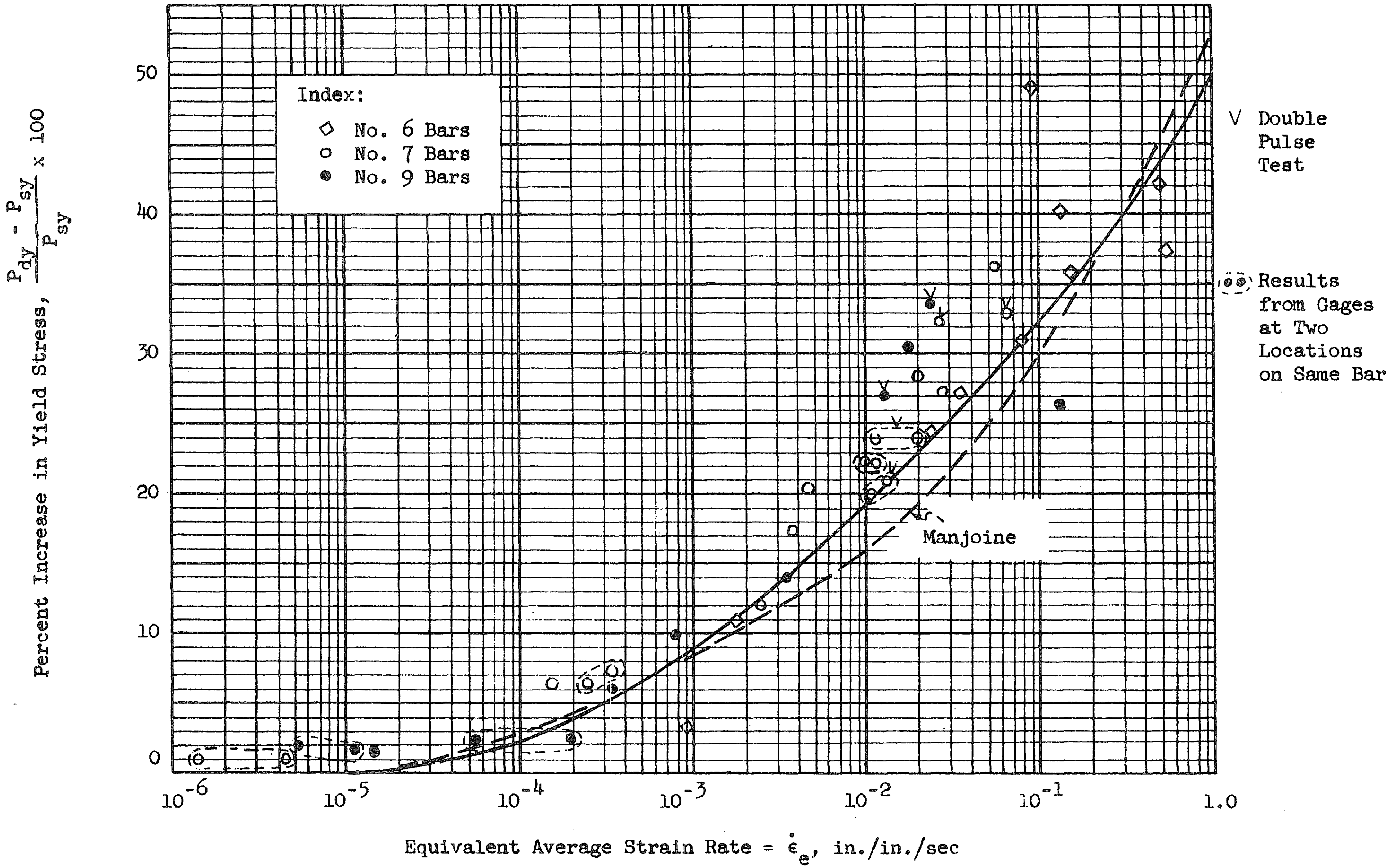

FIG. 20 PERCENT INCREASE IN YIELD STRESS VS. EQUIVALENT AVERAGE STRAIN RATE

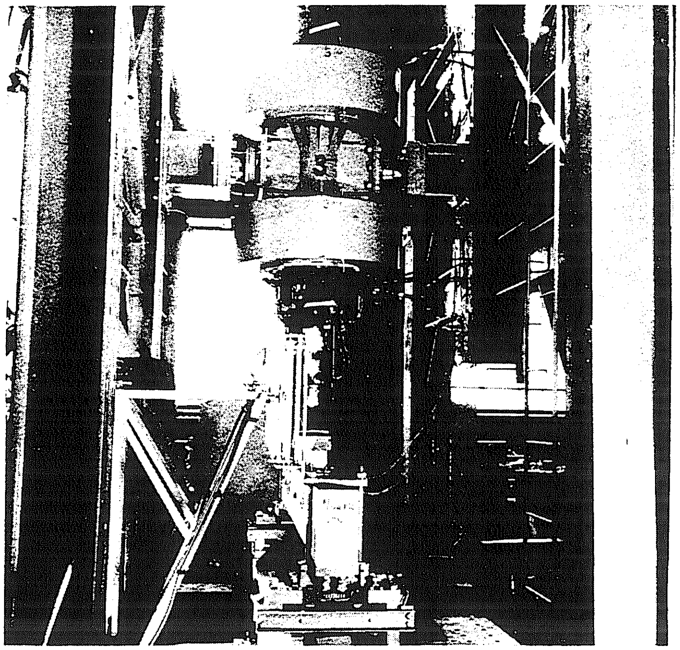

(a) Rapid Load Machine

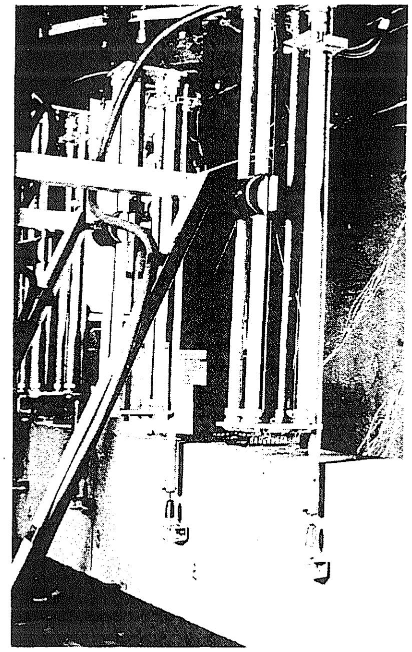

(b) Deflection Gage

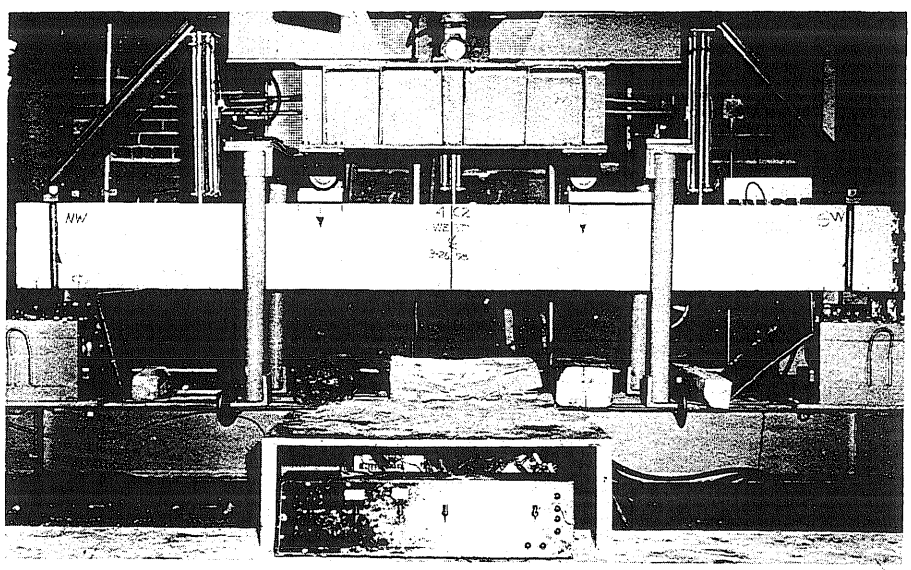

(c) Test Setup

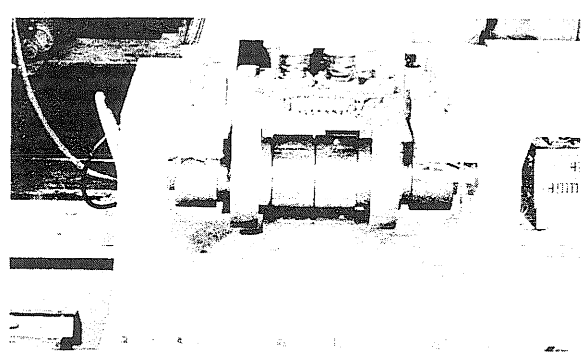

(d) Reaction Measuring Support

FIG. 21 TEST EQUIPMENT AND SETUP

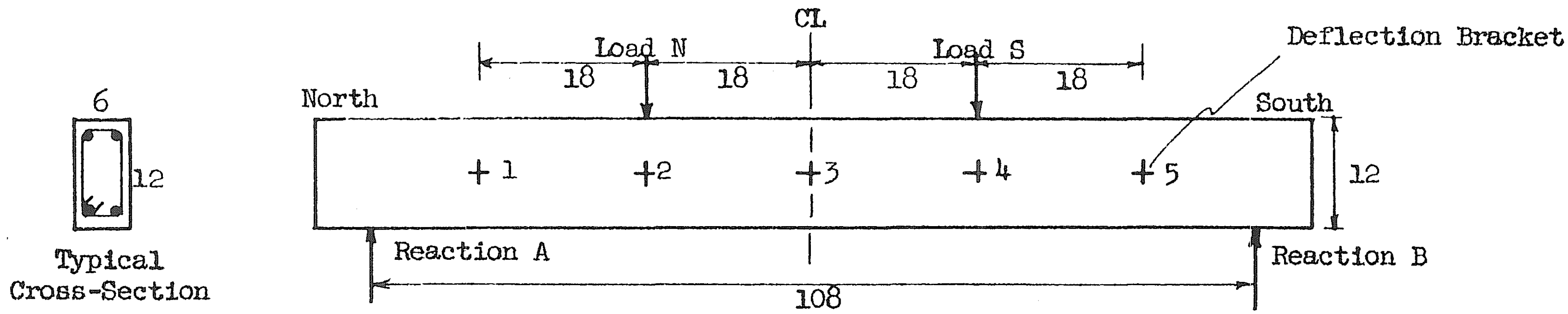

Series 2, 3, and 4
Shear Span = 36 in.

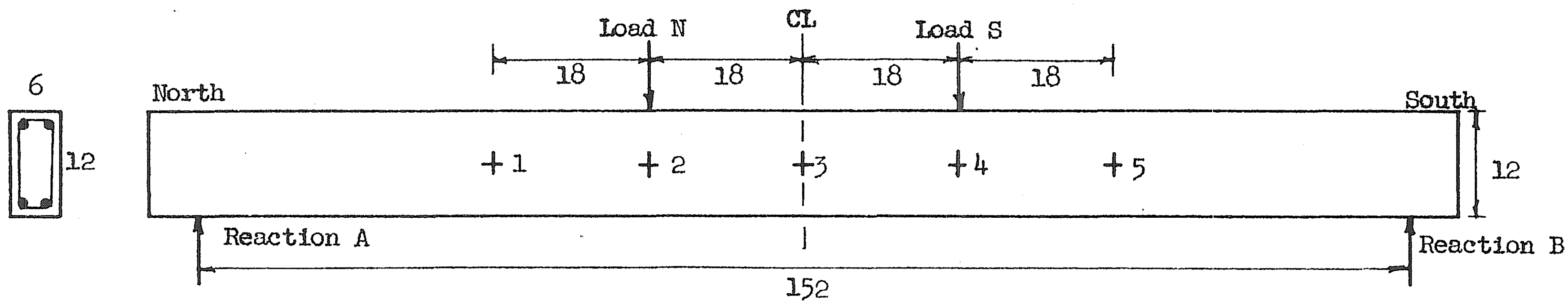

Series 5, 6, and 7
Shear Span = 58 in.

FIG. 22 BEAM CONFIGURATIONS AND DEFLECTION GAGE LOCATIONS

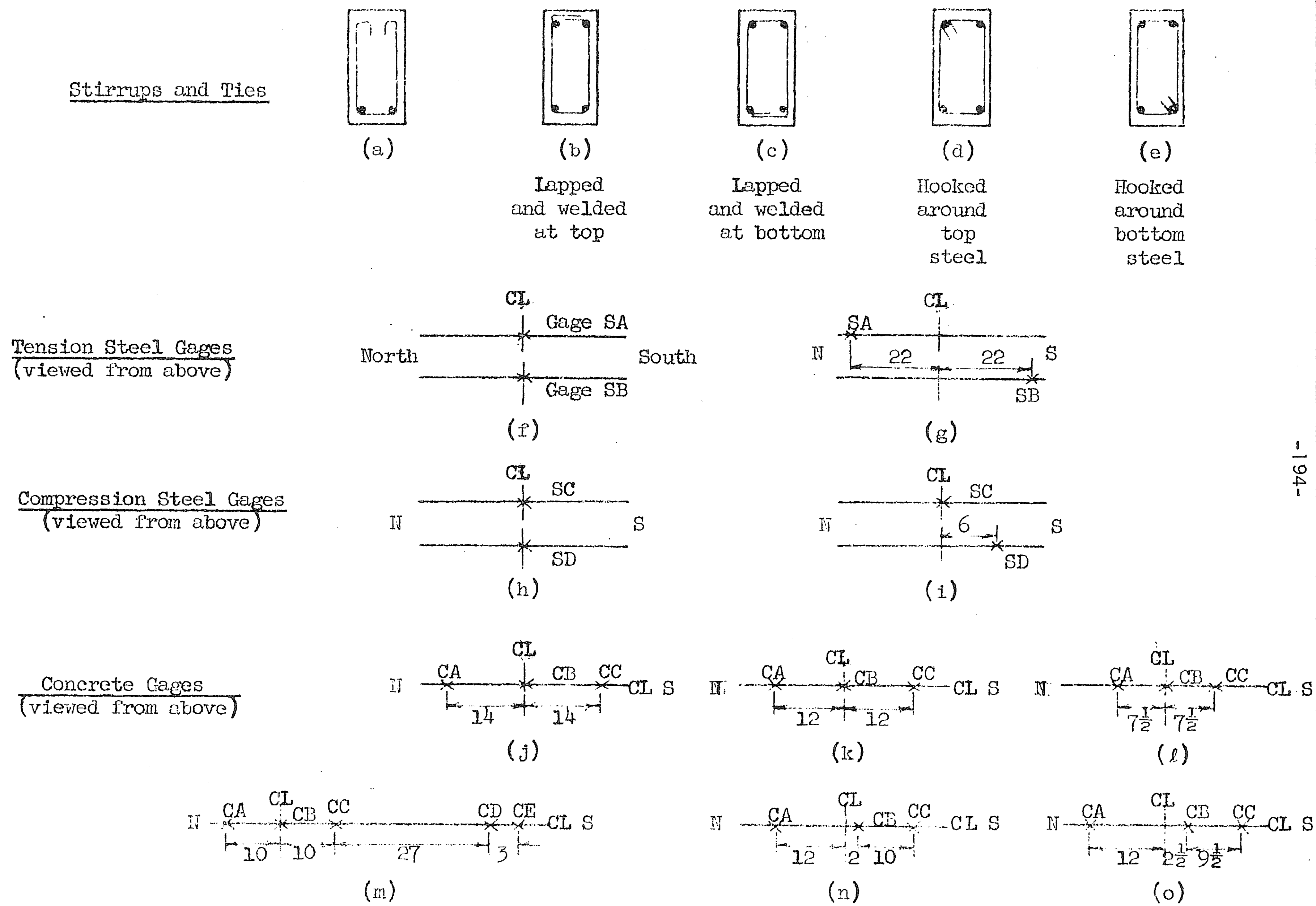

FIG. 23 STIRRUP AND TIE CONFIGURATIONS; LOCATIONS OF STRAIN GAGES

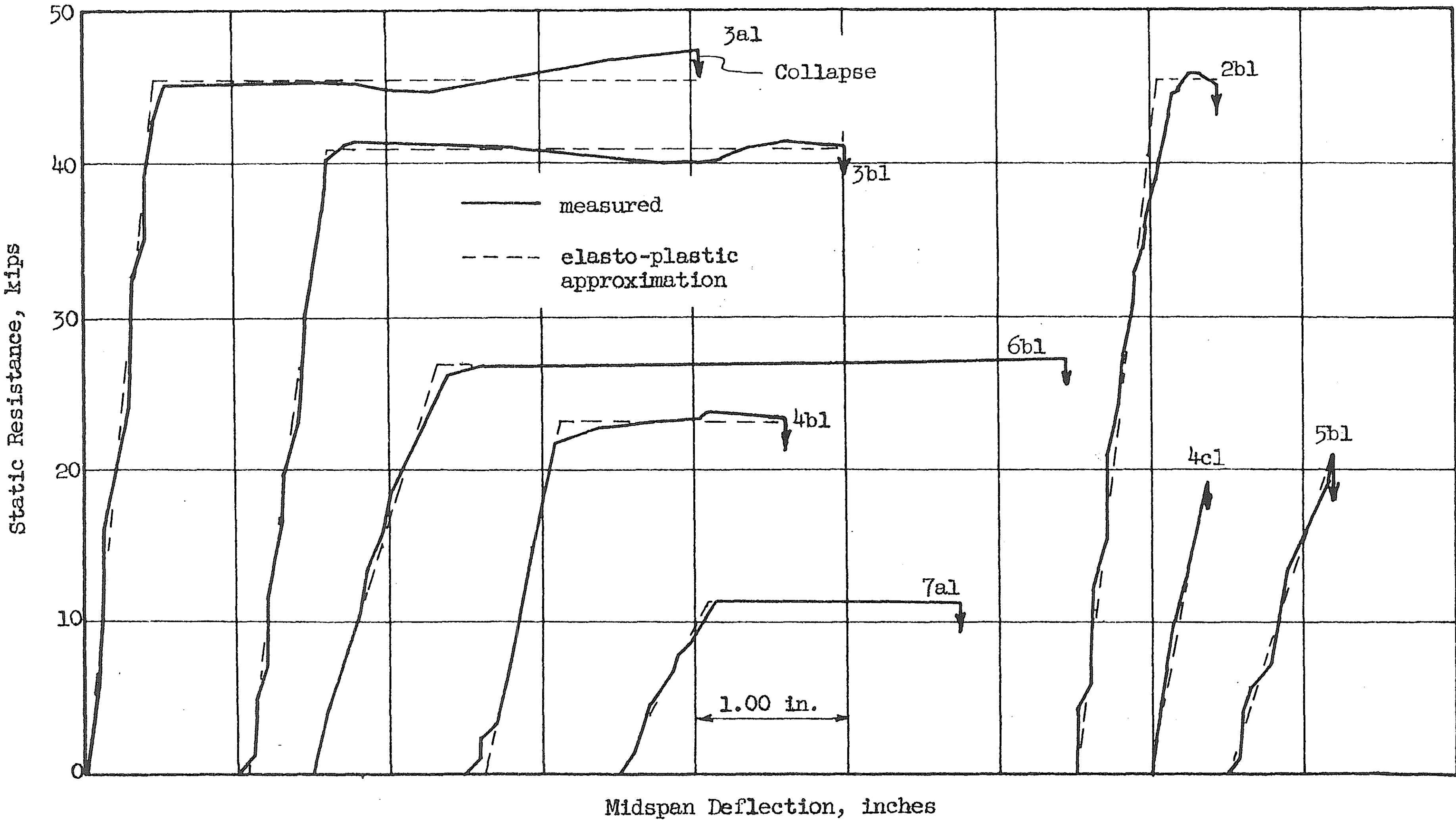

FIG. 24 RESISTANCE-DEFLECTION RELATIONS FOR STATIC TESTS TO COLLAPSE

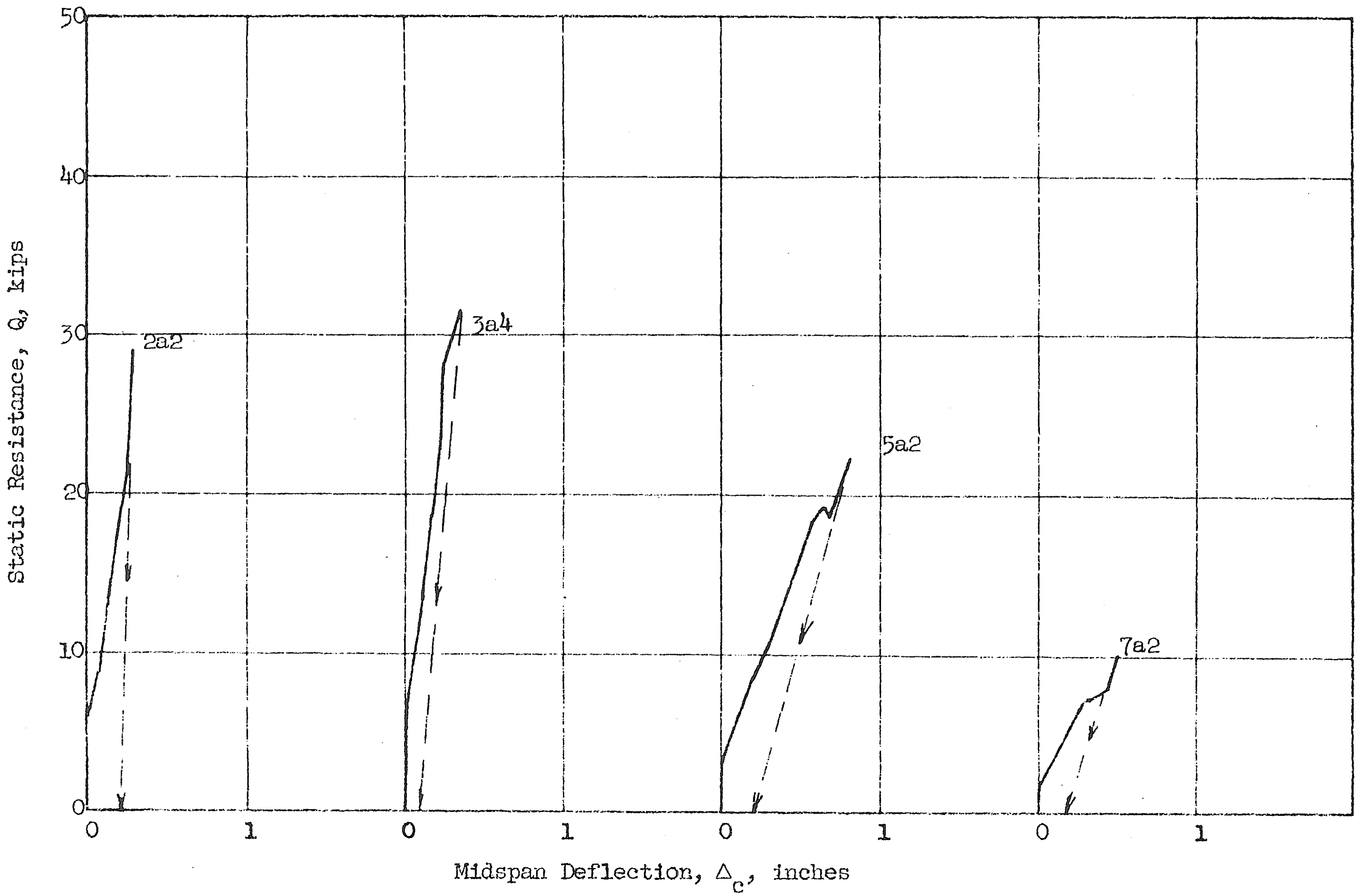

FIG. 25 EXTENT OF STATIC PRE-CRACKING FOR BEAMS 2a2, 3a4, 5a2, AND 7a2

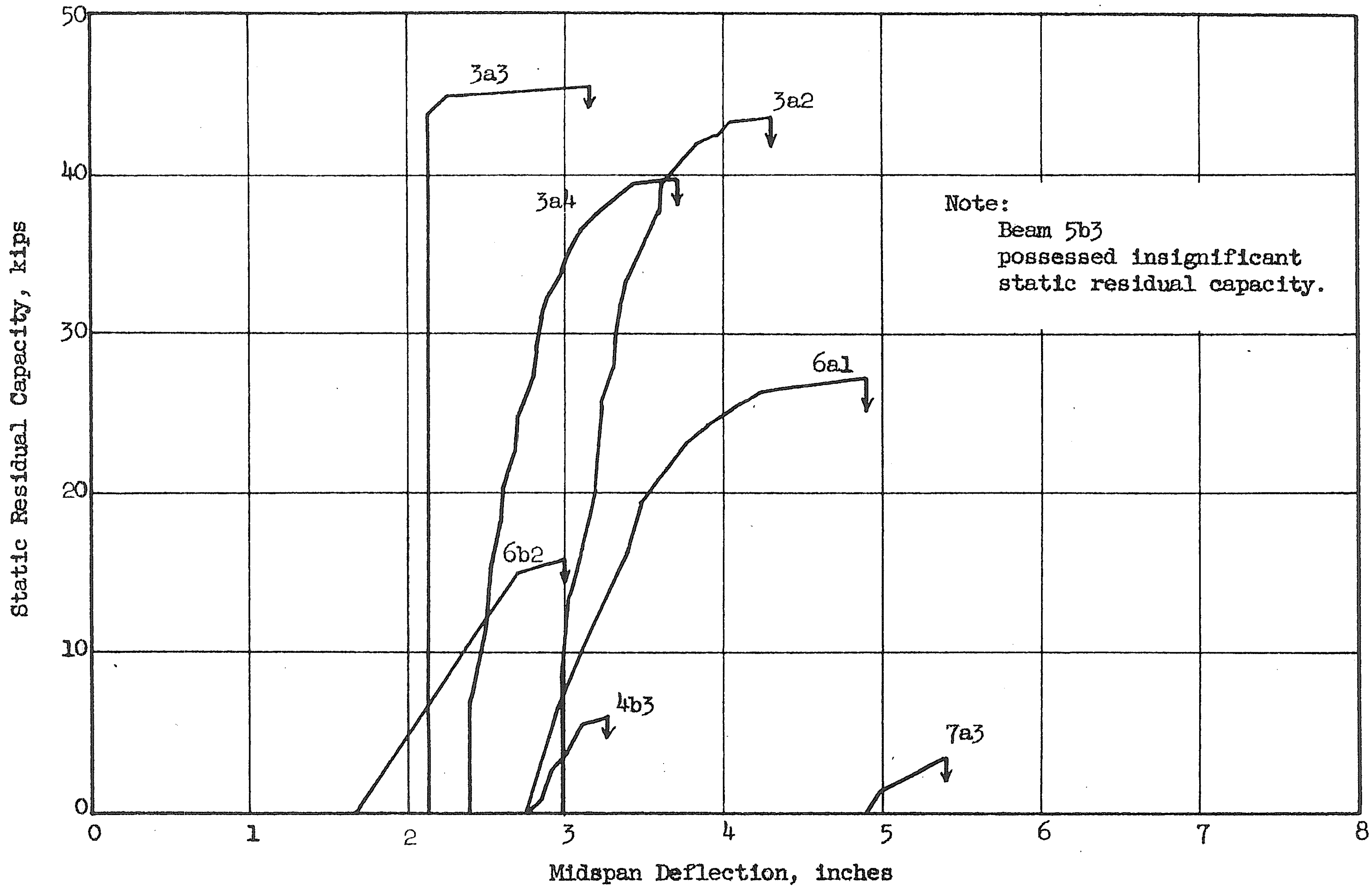

FIG. 26 RESIDUAL STATIC CAPACITY OF DYNAMICALLY LOADED BEAMS

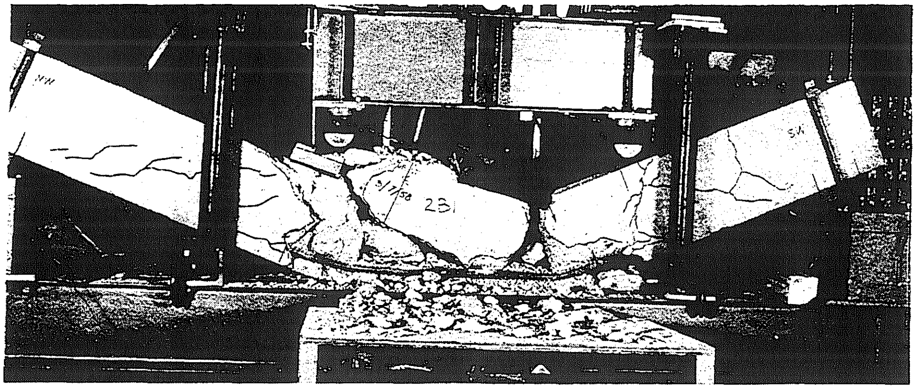

(a)
Beam 2b1
Loaded statically
to collapse

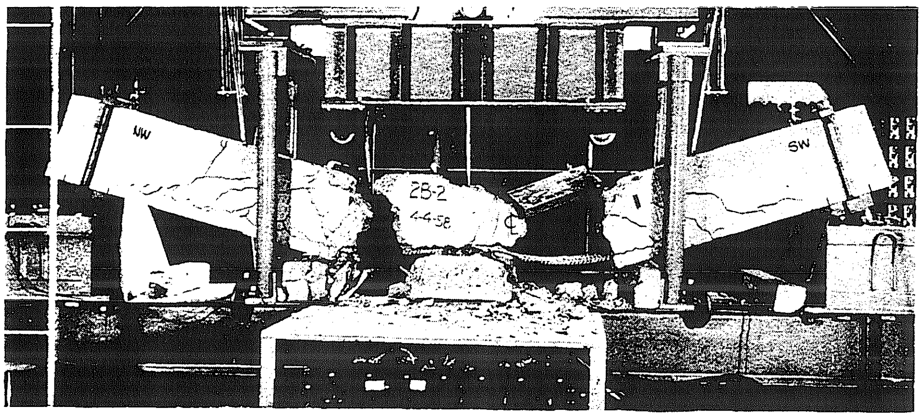

(b)
Beam 2b2
Loaded dynamically
to collapse

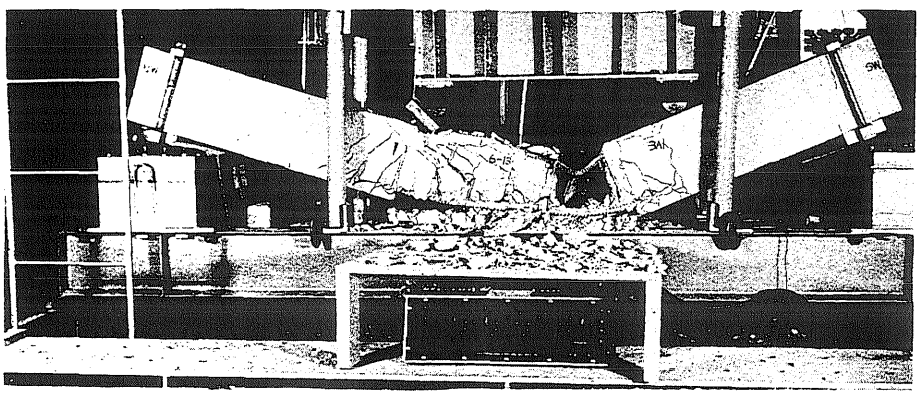

(c)
Beam 3a1
Loaded statically
to collapse

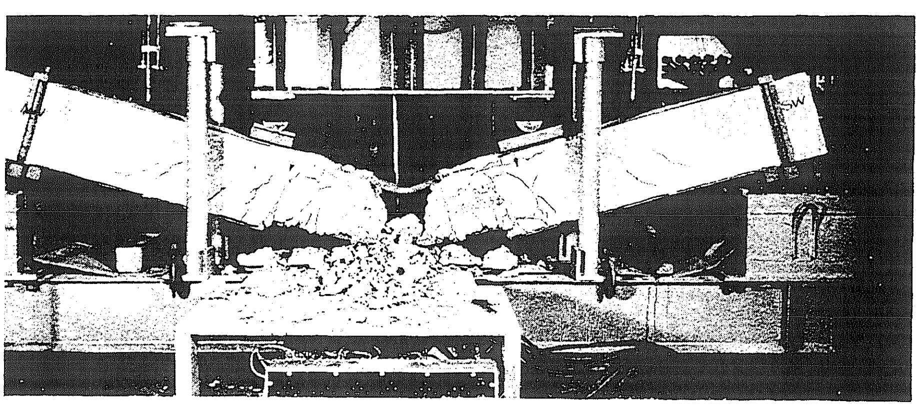

(d)
Beam 3a5
Loaded dynamically
to collapse

FIG. 27 COMPARISON OF STATIC AND DYNAMIC COLLAPSE CONFIGURATIONS, BEAMS, 2b1, 2b2, 3a1, 3a5

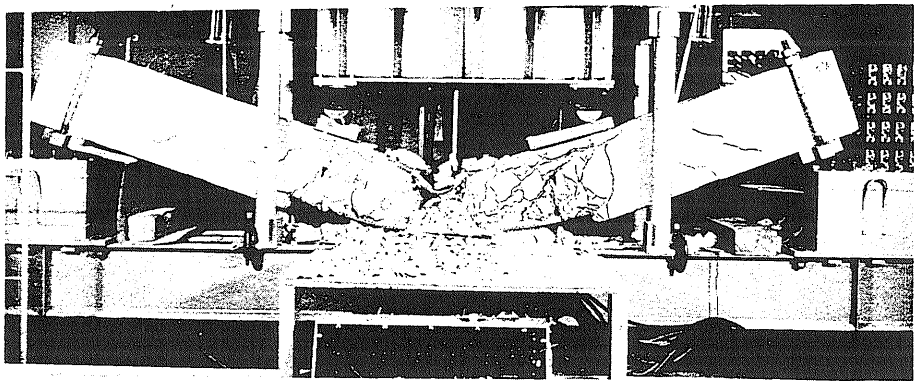

(a)
Beam 3b1
Loaded statically
to collapse

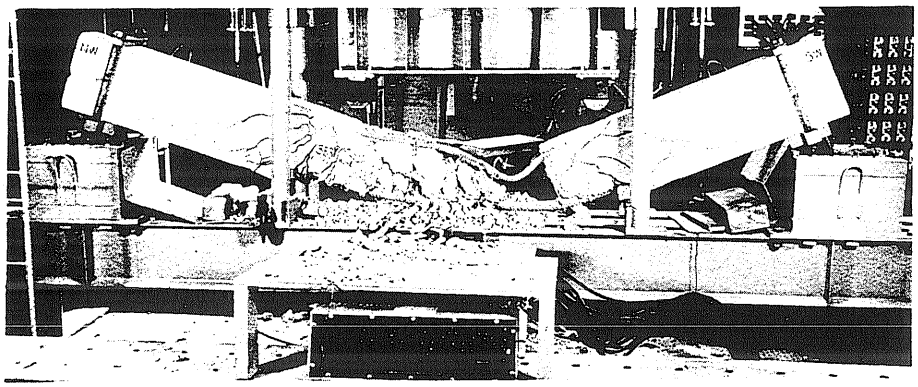

(b)
Beam 3b3
Loaded dynamically
to collapse

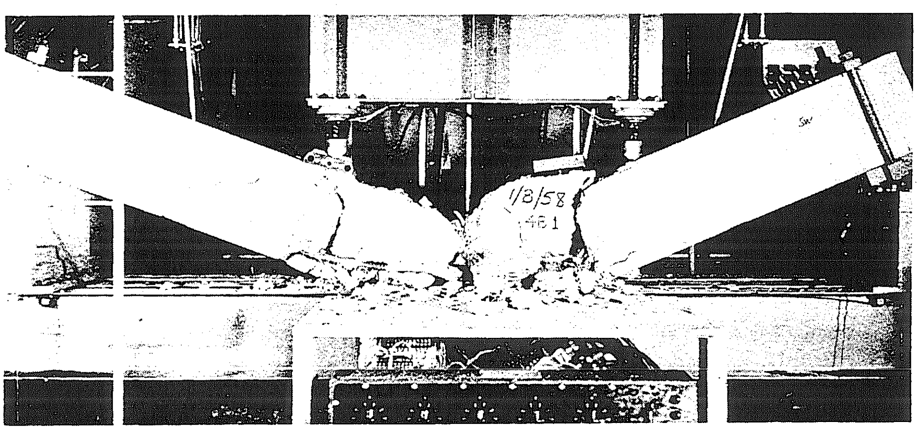

(c)
Beam 4b1
Loaded statically
to collapse

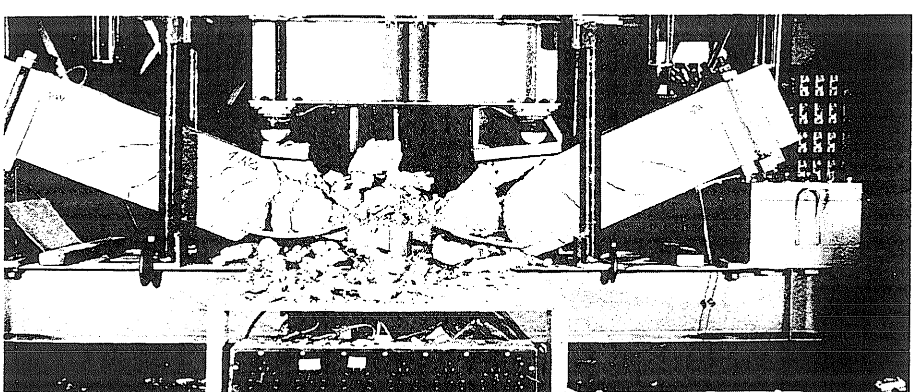

(d)
Beam 4a2
Loaded dynamically
to collapse

FIG. 28 COMPARISON OF STATIC AND DYNAMIC COLLAPSE CONFIGURATIONS, BEAMS 3b1, 3b3, 4b1, 4a2

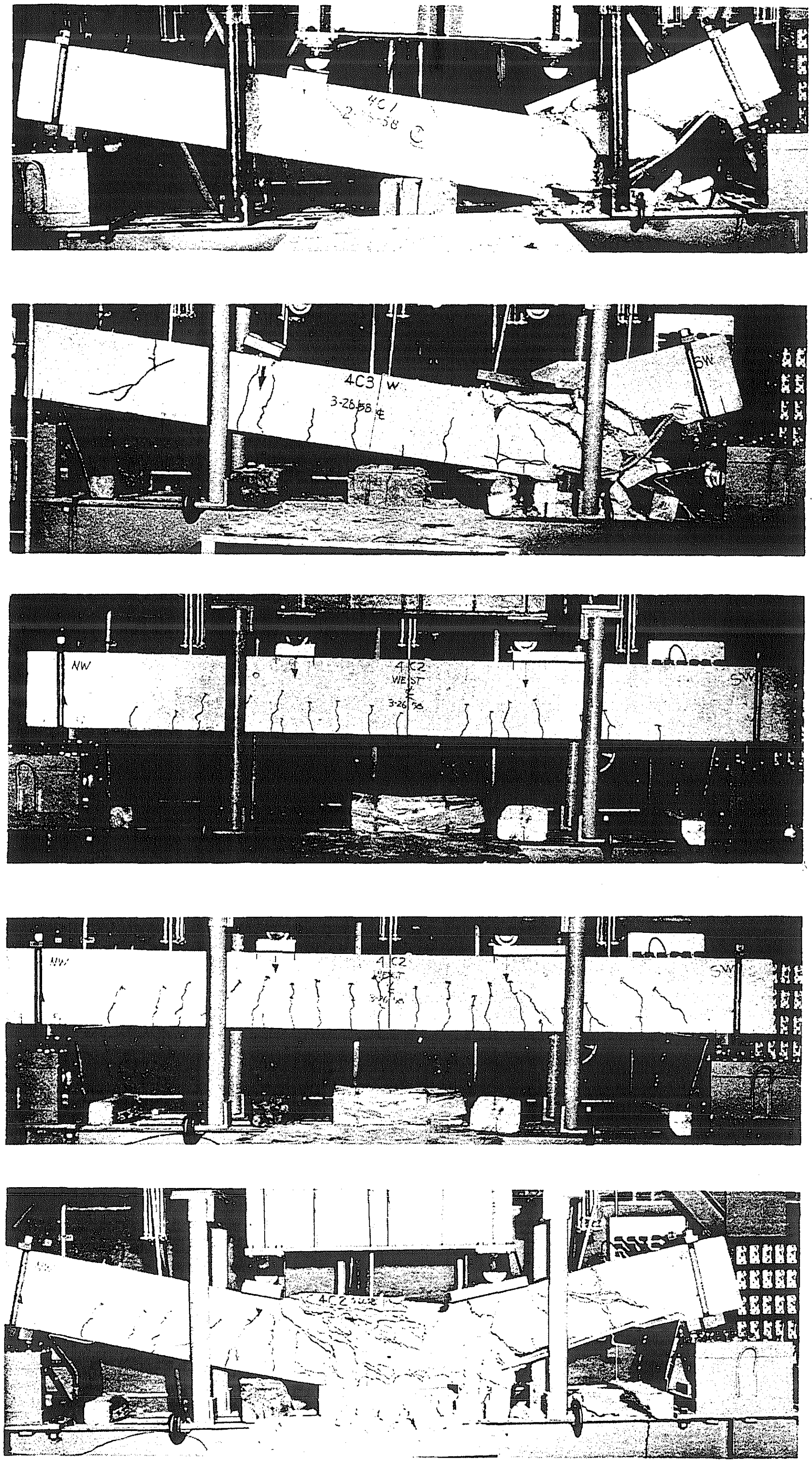

(a)
Beam 4c1
Loaded statically
to collapse

(b)
Beam 4c3
Loaded dynamically
to collapse

(c)
Beam 4c2
After first blow

(d)
Beam 4c2
After second blow

(e)
Beam 4c2
After third blow
(collapse)

FIG. 29 COMPARISON OF STATIC AND DYNAMIC COLLAPSE CONFIGURATIONS, BEAMS 4c1, 4c2, 4c3

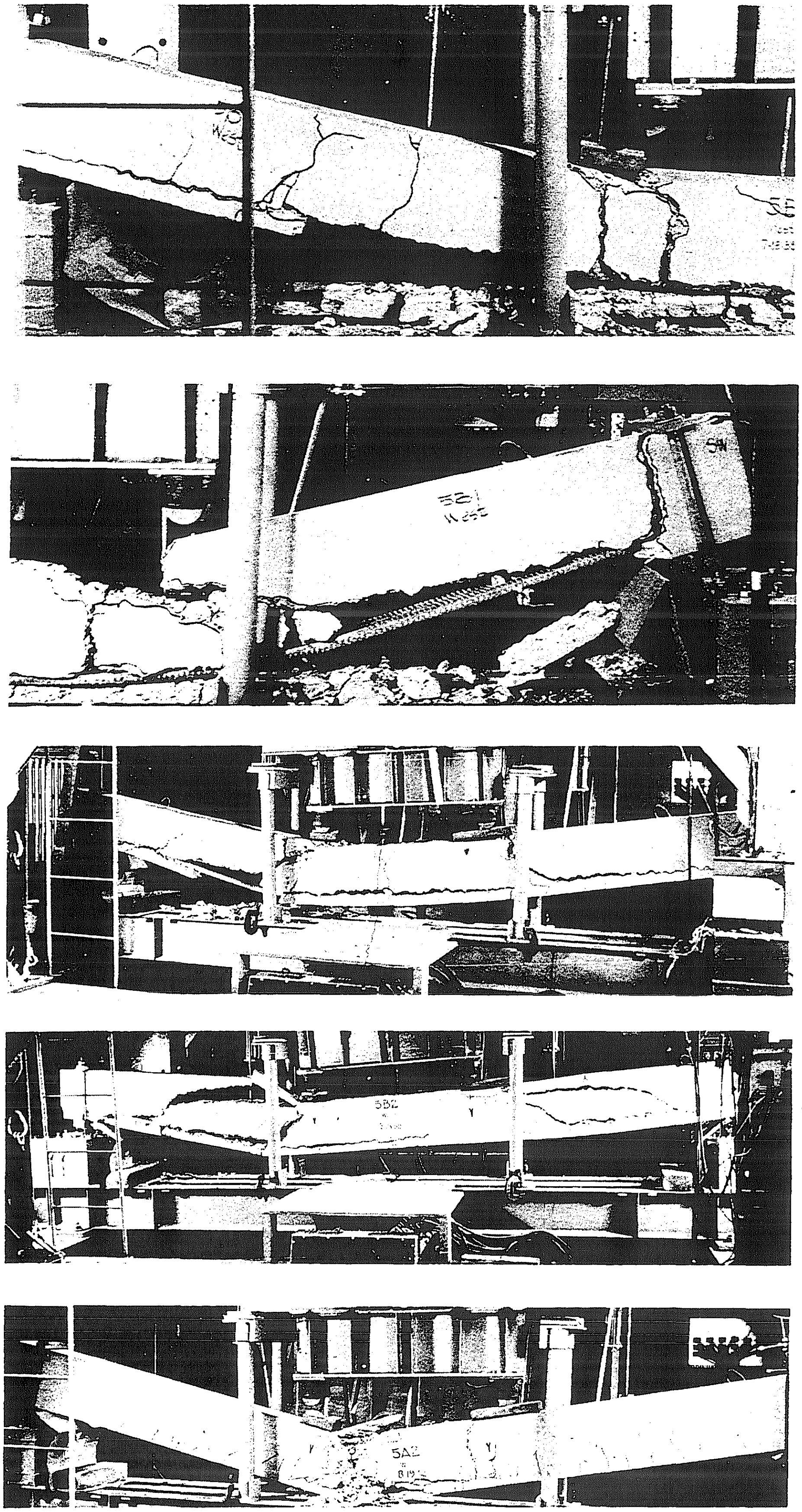

(a)
Beam 5b1
Loaded statically
to collapse
(north end)
(no stirrups)

(b)
Beam 5b1
Loaded statically
to collapse
(south end)
(no stirrups)

(c)
Beam 5b4
Loaded dynamically
to collapse
(no stirrups)

(d)
Beam 5b2
Loaded dynamically
to collapse
(no stirrups)

(e)
Beam 5a2
Loaded dynamically
to collapse
(stirrups - #303.75)

FIG. 30 COMPARISON OF STATIC AND DYNAMIC COLLAPSE CONFIGURATIONS, BEAMS 5b1, 5b4, 5b2, 5a2

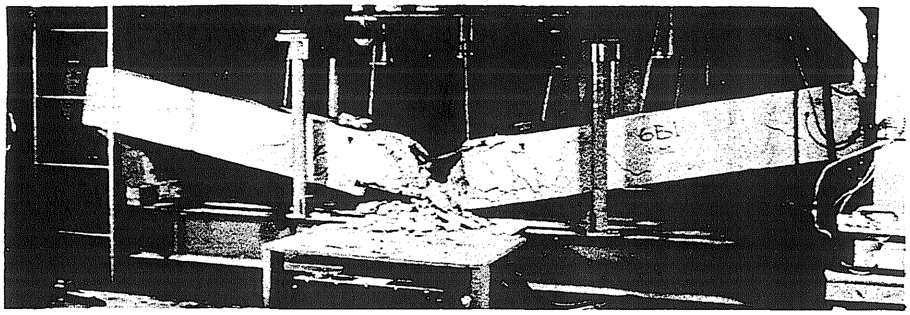

(a)
Beam 6b1
Loaded statically
to collapse
(stirrups - #2@12)

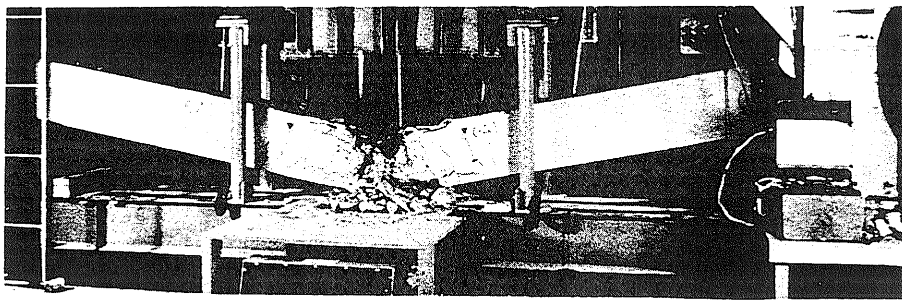

(b)
Beam 6a1
Loaded statically
to collapse after
dynamic test
(stirrups - #3@4.25)

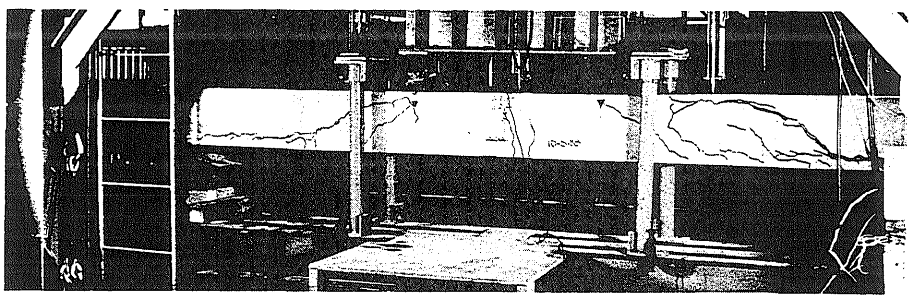

(c)
Beam 6b2
After first blow
(stirrups - #2@12)

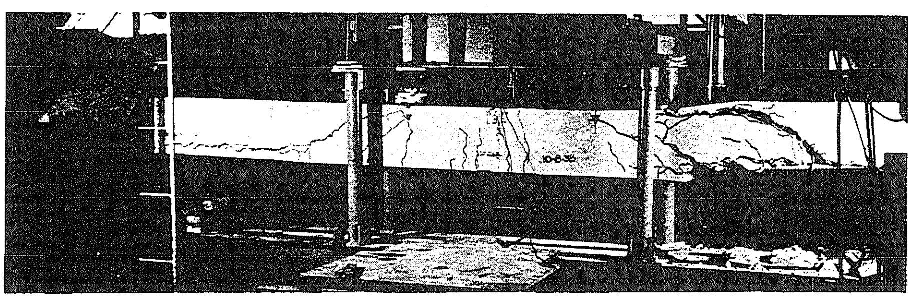

(d)
Beam 6b2
After second blow
(stirrups - #2@12)

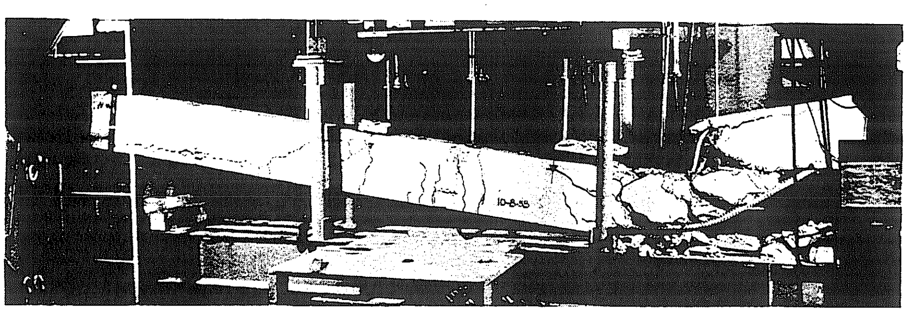

(e)
Beam 6b2
Loaded statically
to collapse
(stirrups - #2@12)

FIG. 31 COMPARISON OF STATIC AND DYNAMIC COLLAPSE CONFIGURATIONS, BEAMS 6b1, 6a1, 6b2

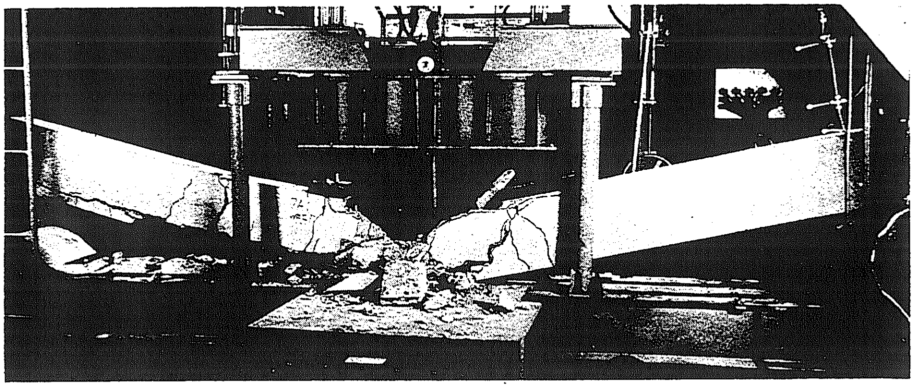

(a)
Beam 7a1
Loaded statically
to collapse

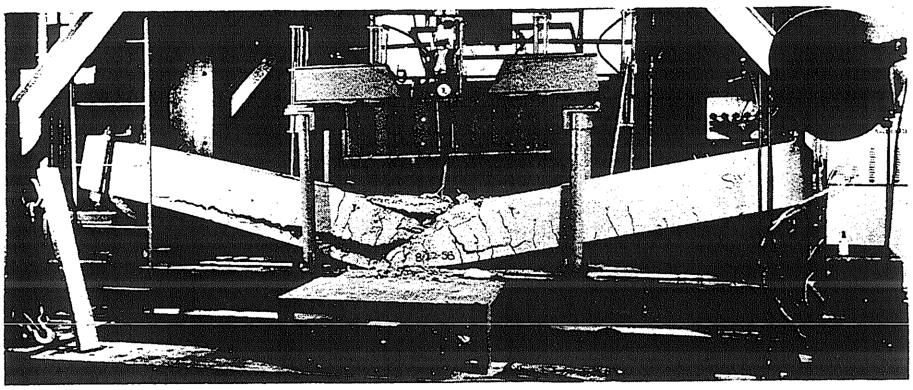

(b)
Beam 7a2
Loaded dynamically
to collapse

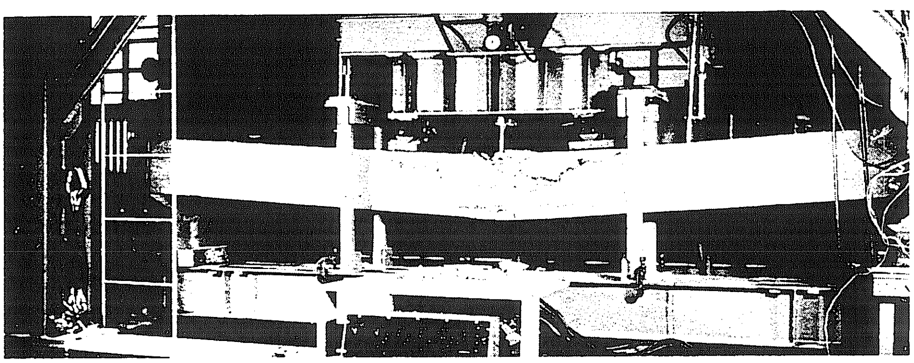

(c)
Beam 7a3
After third blow

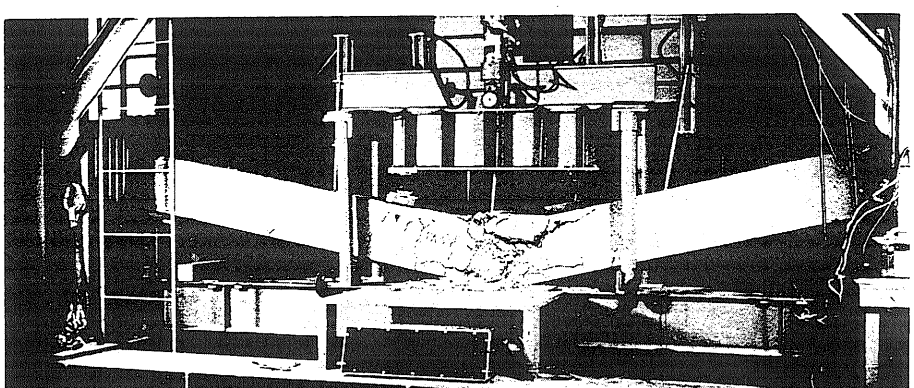

(d)
Beam 7a3
Loaded statically
to collapse

FIG. 32 COMPARISON OF STATIC AND DYNAMIC COLLAPSE
CONFIGURATIONS, BEAMS 7a1, 7a2, 7a3

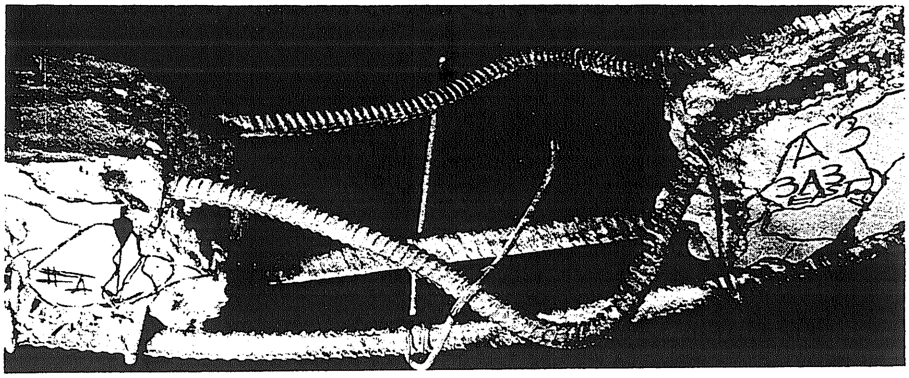

(a)
Beam 3a3
#2 @12
Hooked at top
Δ_{md} = 3.15 in.

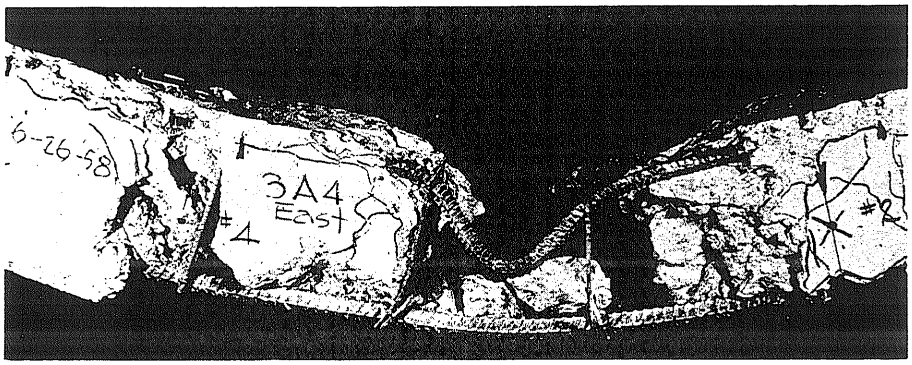

(b)
Beam 3a4
#2 @12
Hooked at bottom
Δ_{md} = 3.70 in.

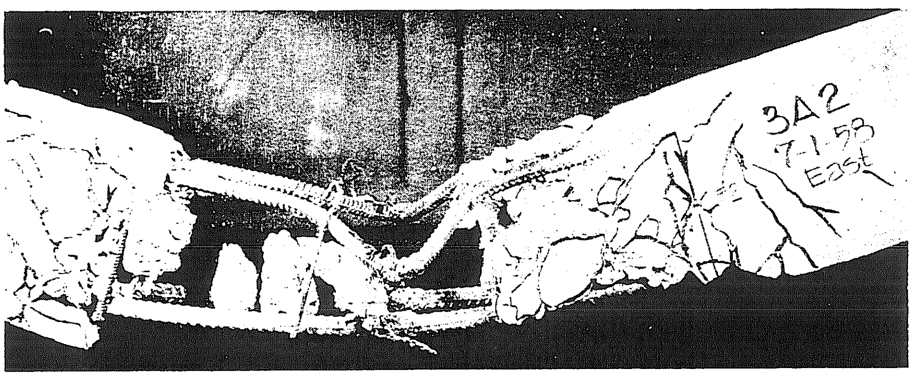

(c)
Beam 3a2
#2 @12
Welded
Δ_{md} = 4.30 in.

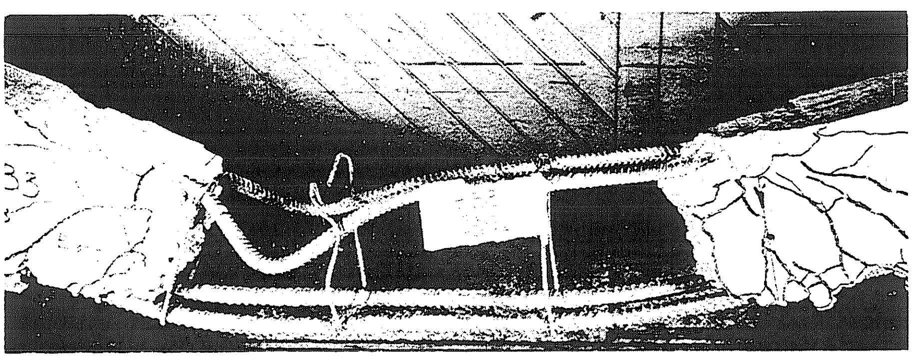

(d)
Beam 3b3
#2 @12
Hooked at top
Δ_{md} = 5.00 in.

FIG. 33 EFFECT OF TIE CONFIGURATION ON BUCKLING LENGTH OF COMPRESSION REINFORCEMENT

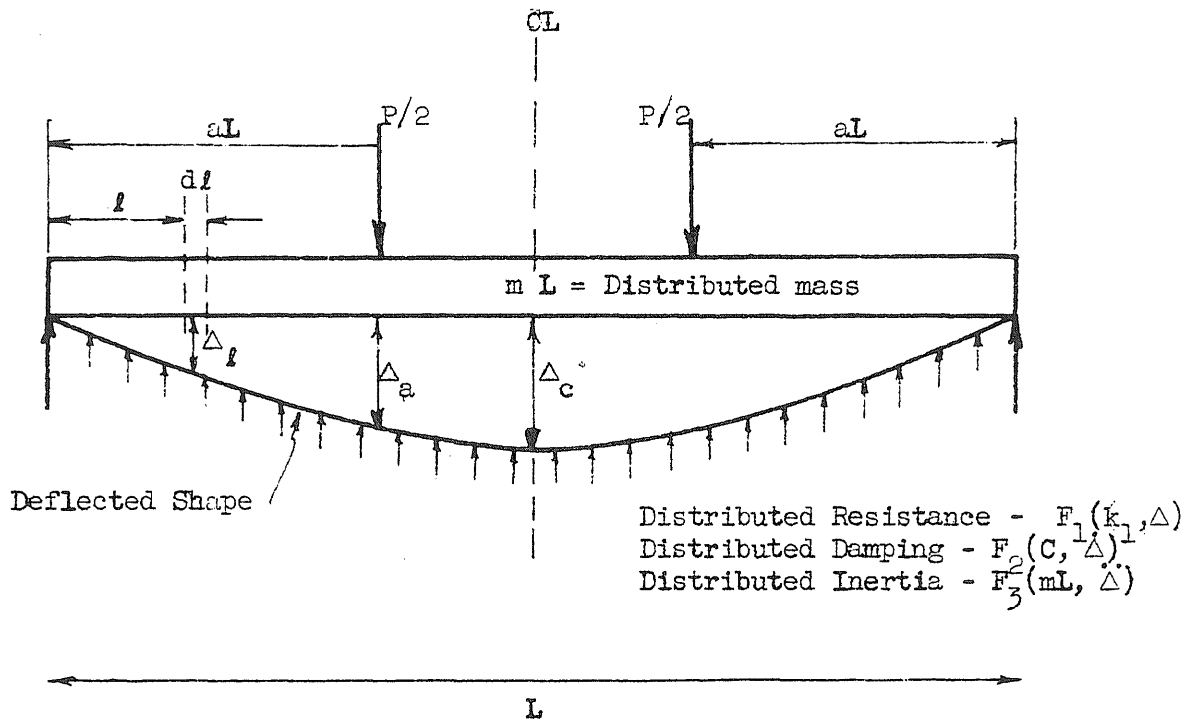

ORIGINAL BEAM

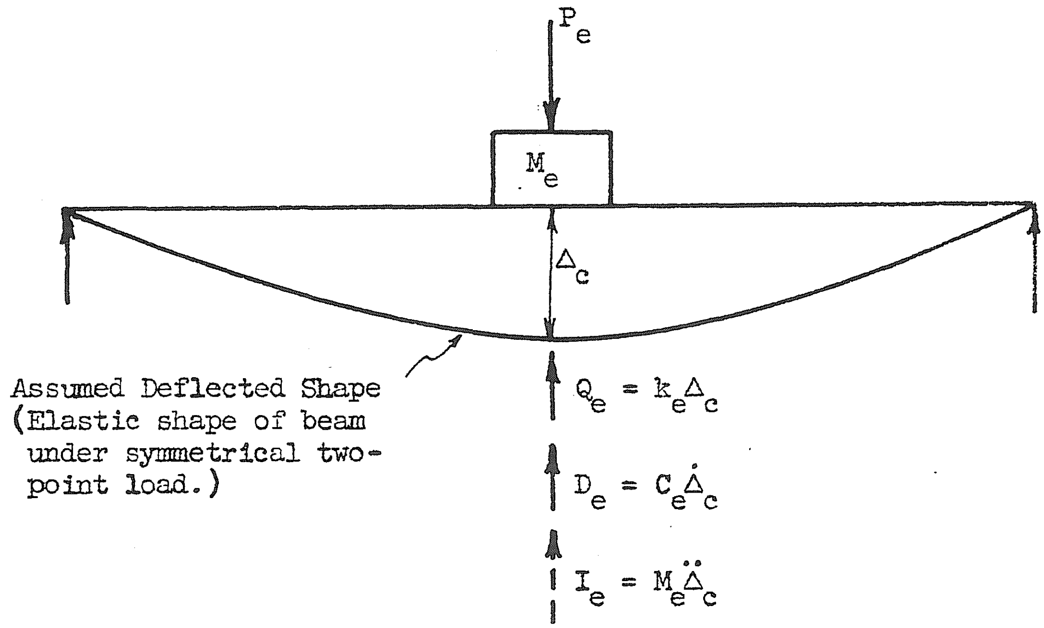

EQUIVALENT SINGLE-DEGREE-OF-FREEDOM SYSTEM

FIG. 34 EQUIVALENT SINGLE-DEGREE-OF-FREEDOM REPLACEMENT FOR TEST BEAMS

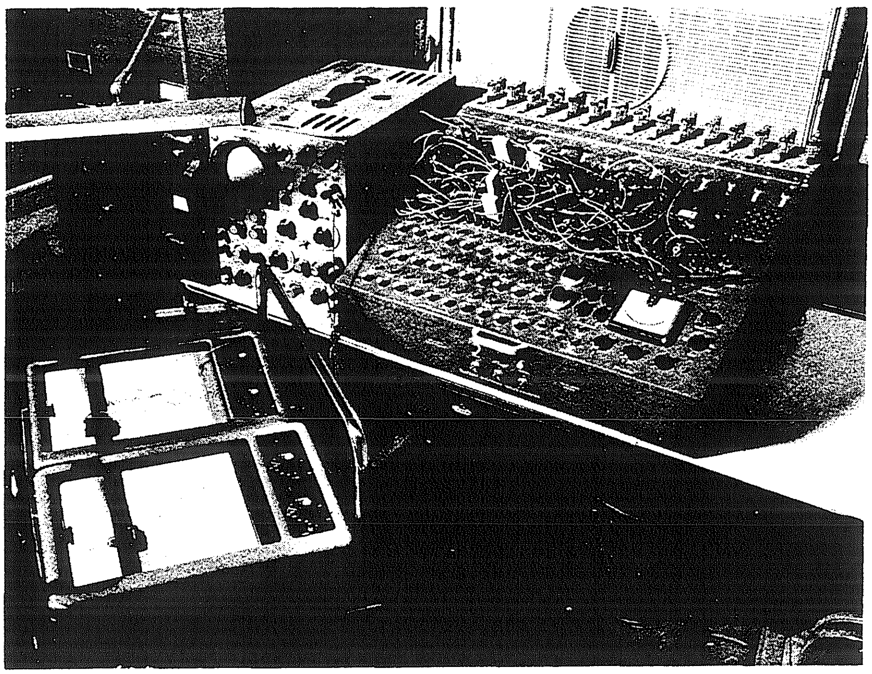

FIG. 35 VIEW OF HEATHKIT ANALOG COMPUTER AND AUXILIARY EQUIPMENT

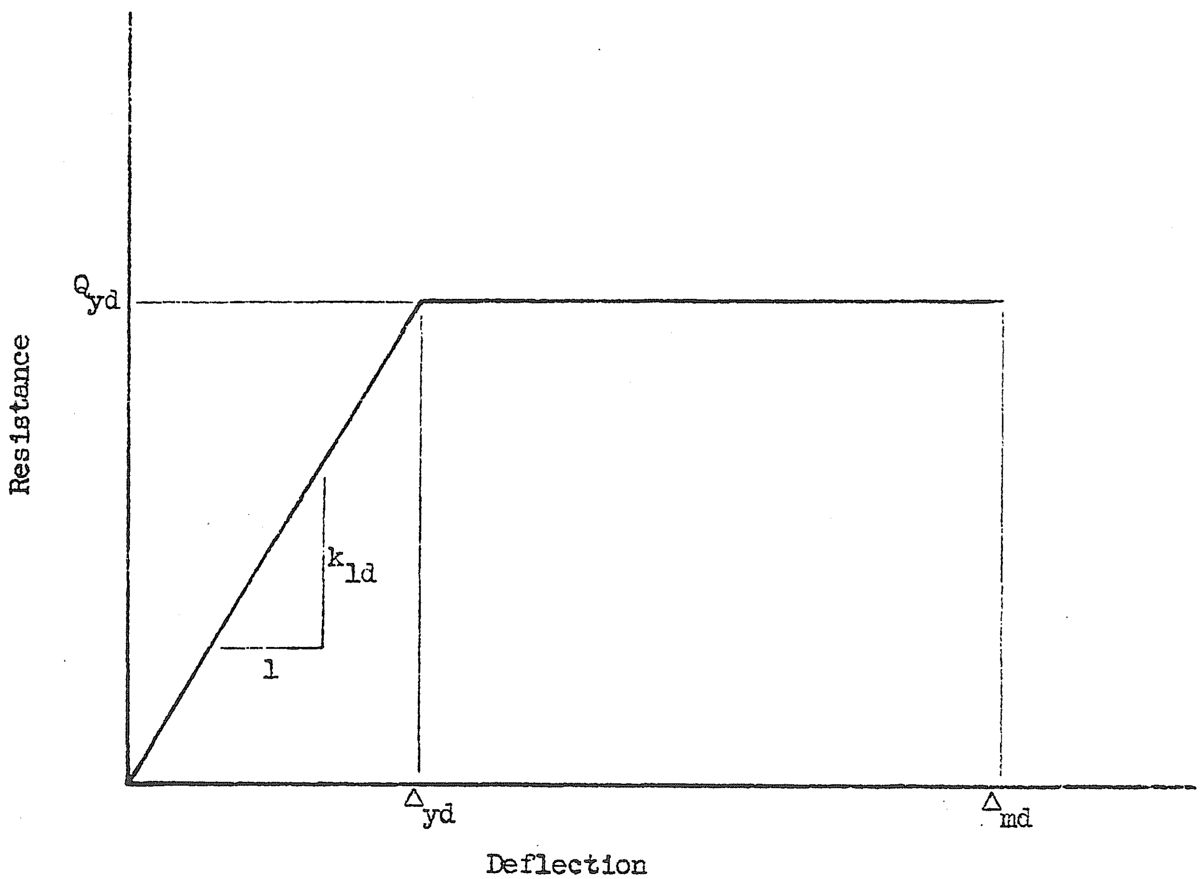

FIG. 36 TYPICAL DYNAMIC RESISTANCE FUNCTION

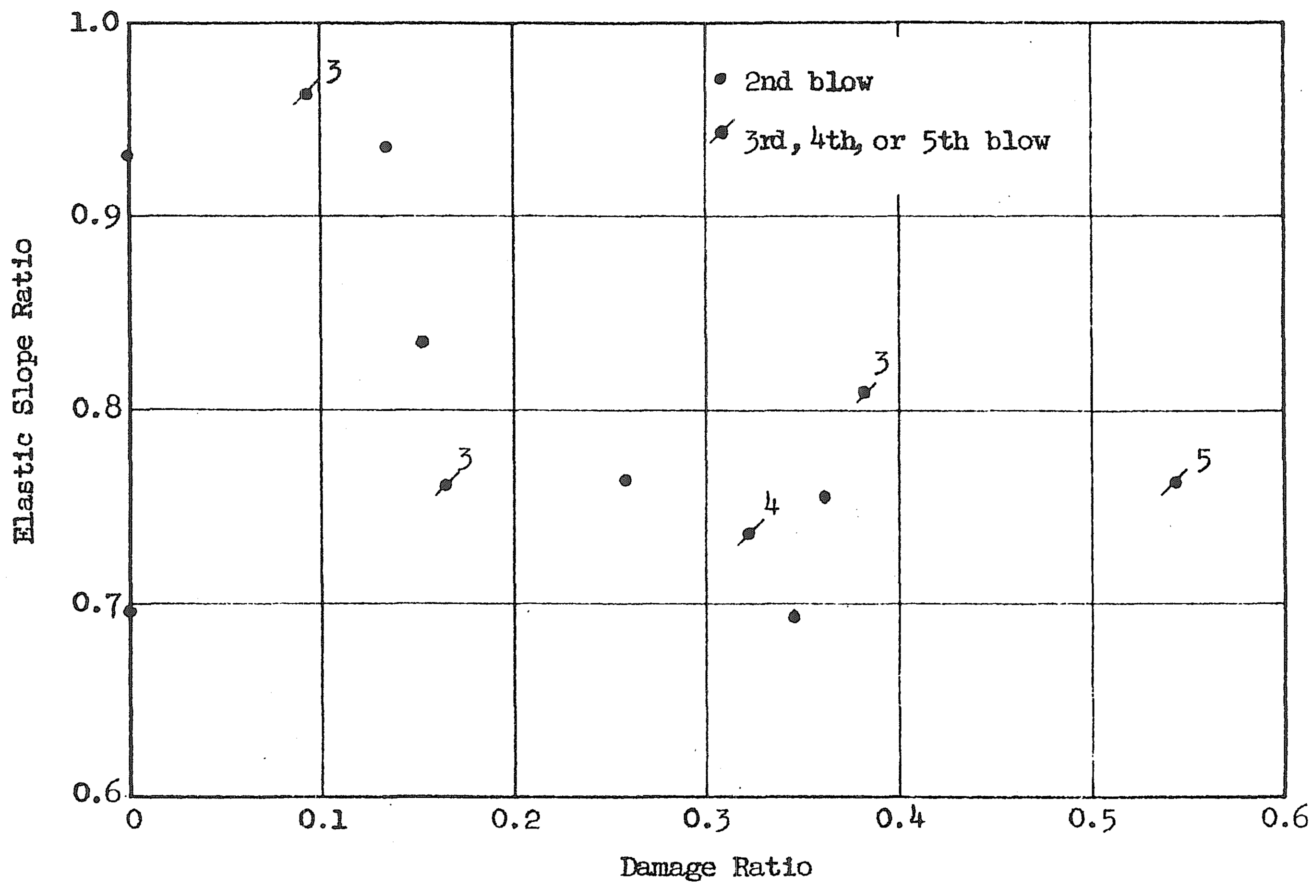

FIG. 37 EFFECT OF DAMAGE ON ELASTIC SLOPE

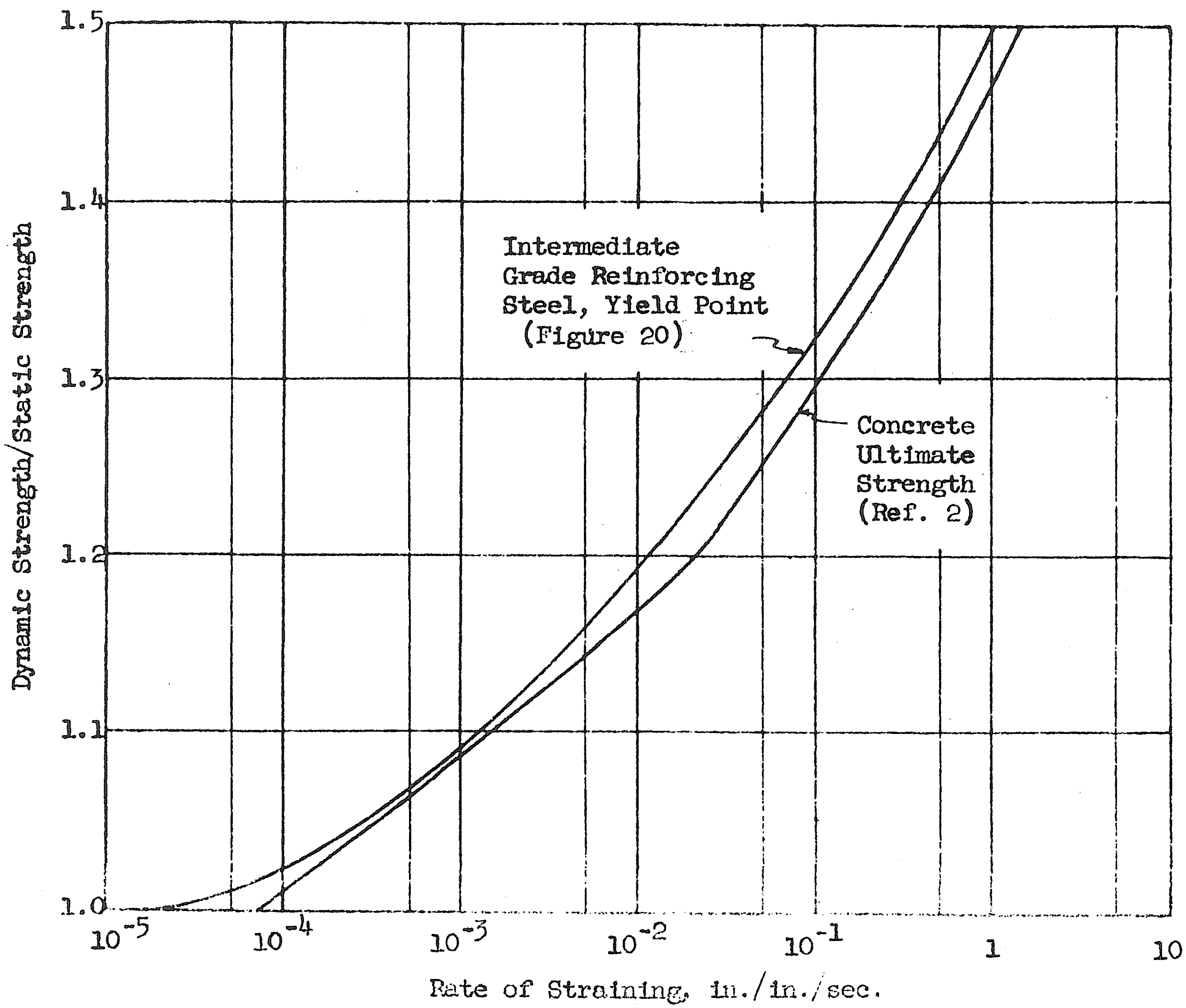

FIG. 38 VARIATION OF MATERIAL PROPERTIES WITH STRAIN RATE

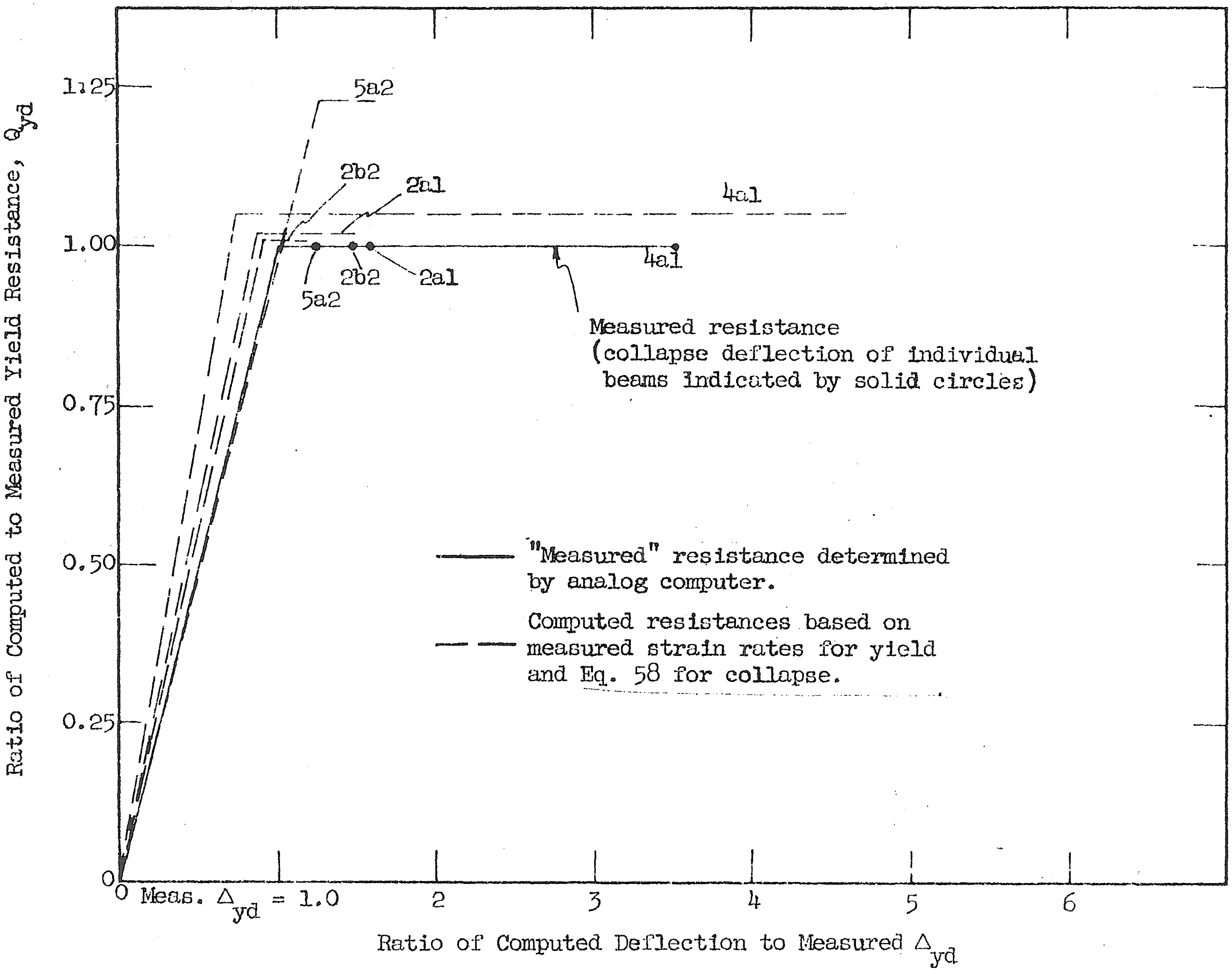

FIG. 39 COMPARISON OF MEASURED AND COMPUTED DYNAMIC RESISTANCE

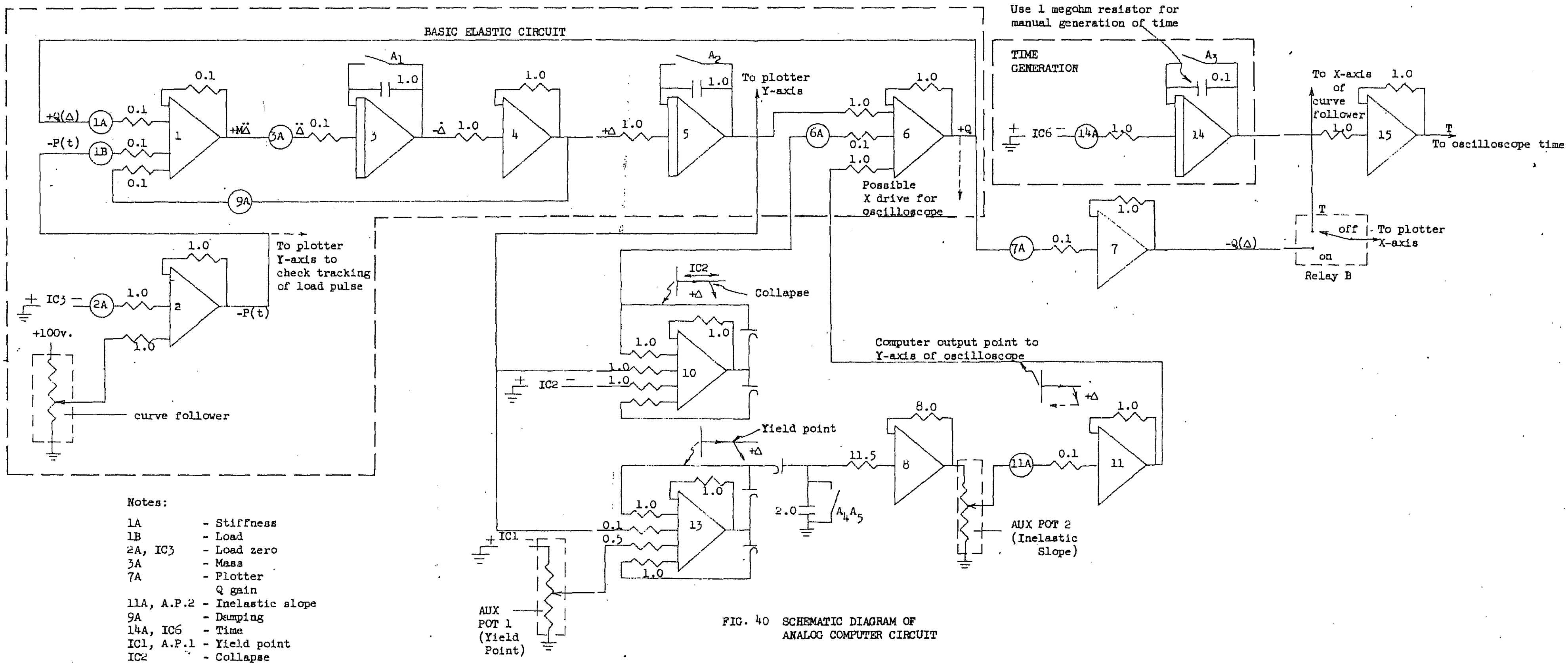

Notes:

1A	- Stiffness
1B	- Load
2A, IC3	- Load zero
3A	- Mass
7A	- Plotter Q gain
11A, A.P.2	- Inelastic slope
9A	- Damping
14A, IC6	- Time
IC1, A.P.1	- Yield point
IC2	- Collapse

FIG. 40 SCHEMATIC DIAGRAM OF ANALOG COMPUTER CIRCUIT

APPENDIX FIGURES

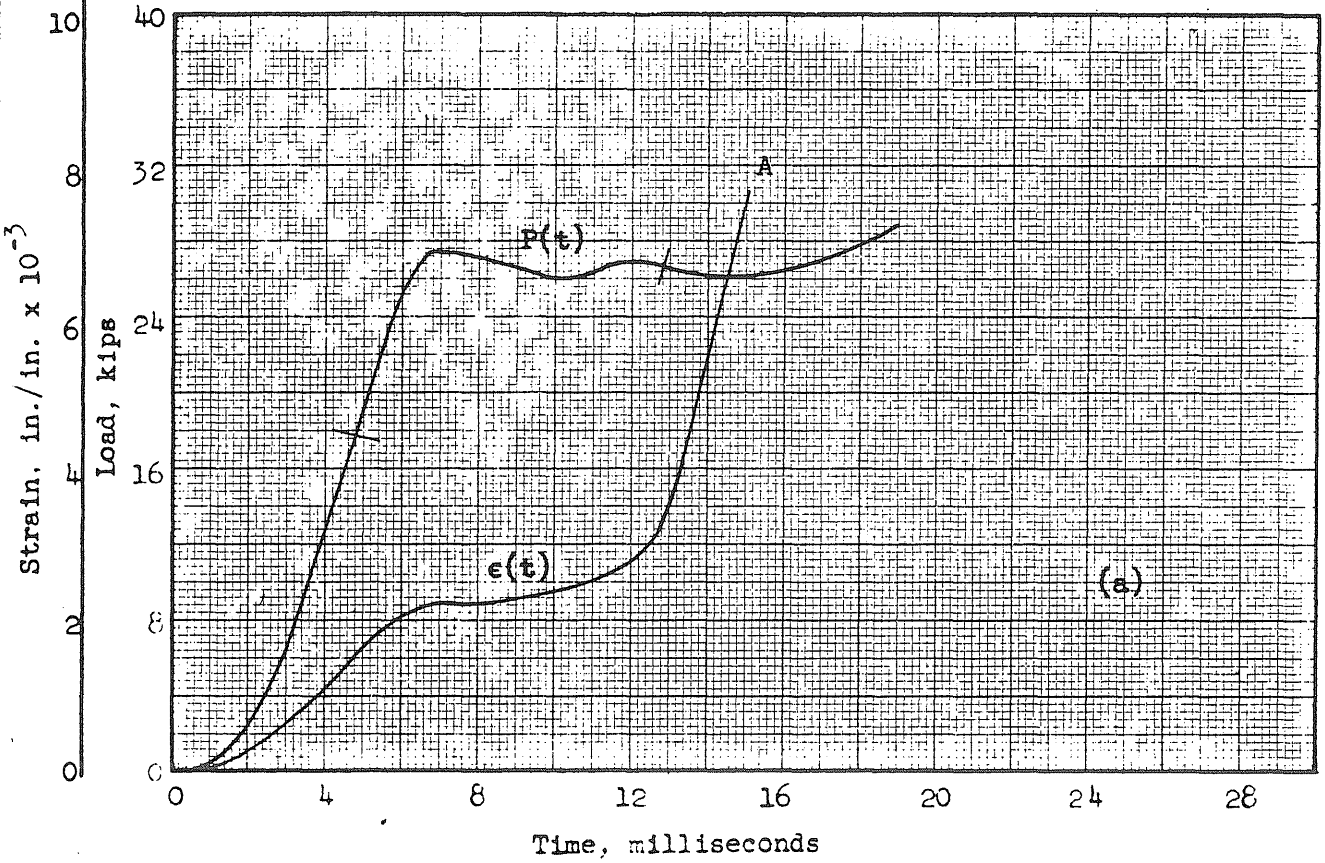

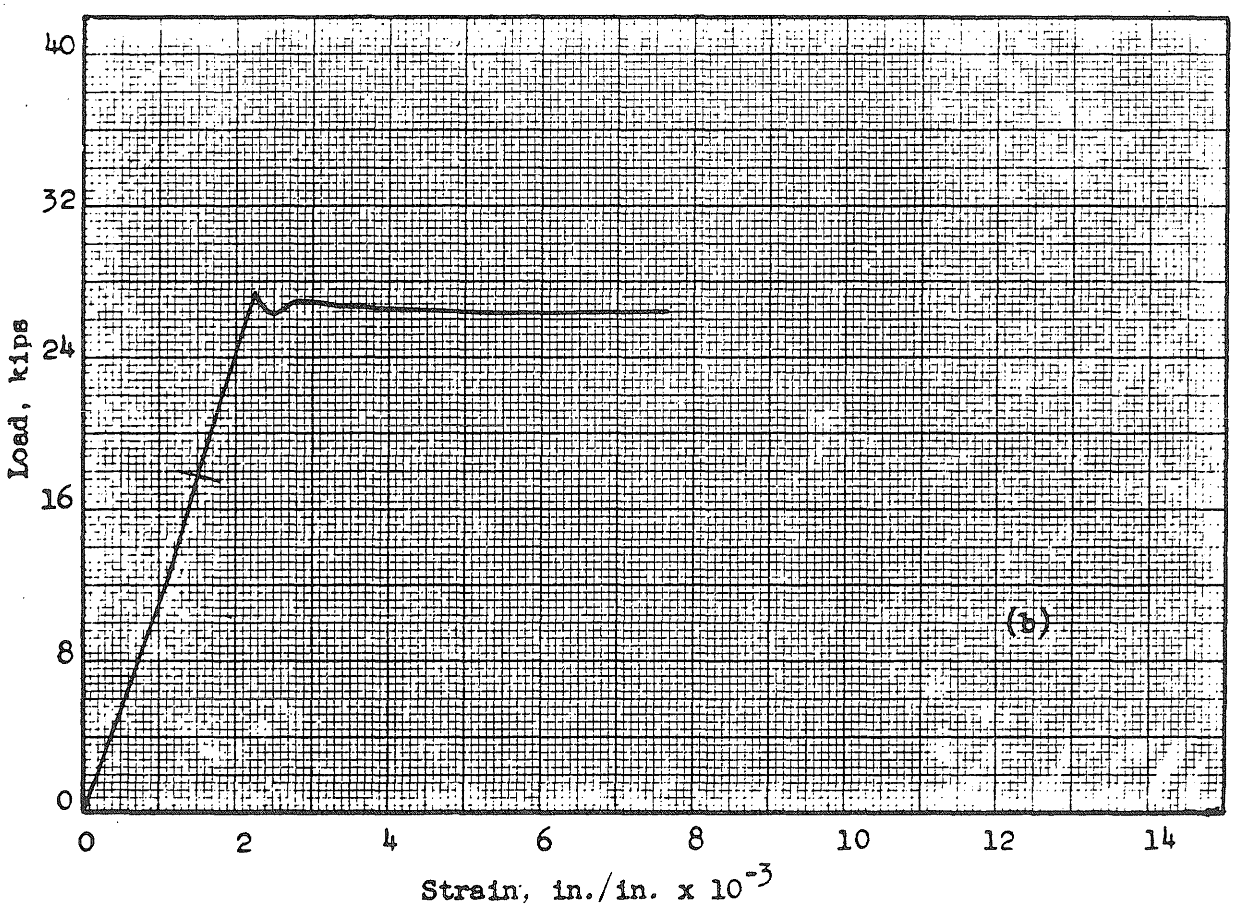

FIG. A1 LOAD AND STRAIN VS. TIME AND LOAD VS. STRAIN
SPECIMEN 6-9

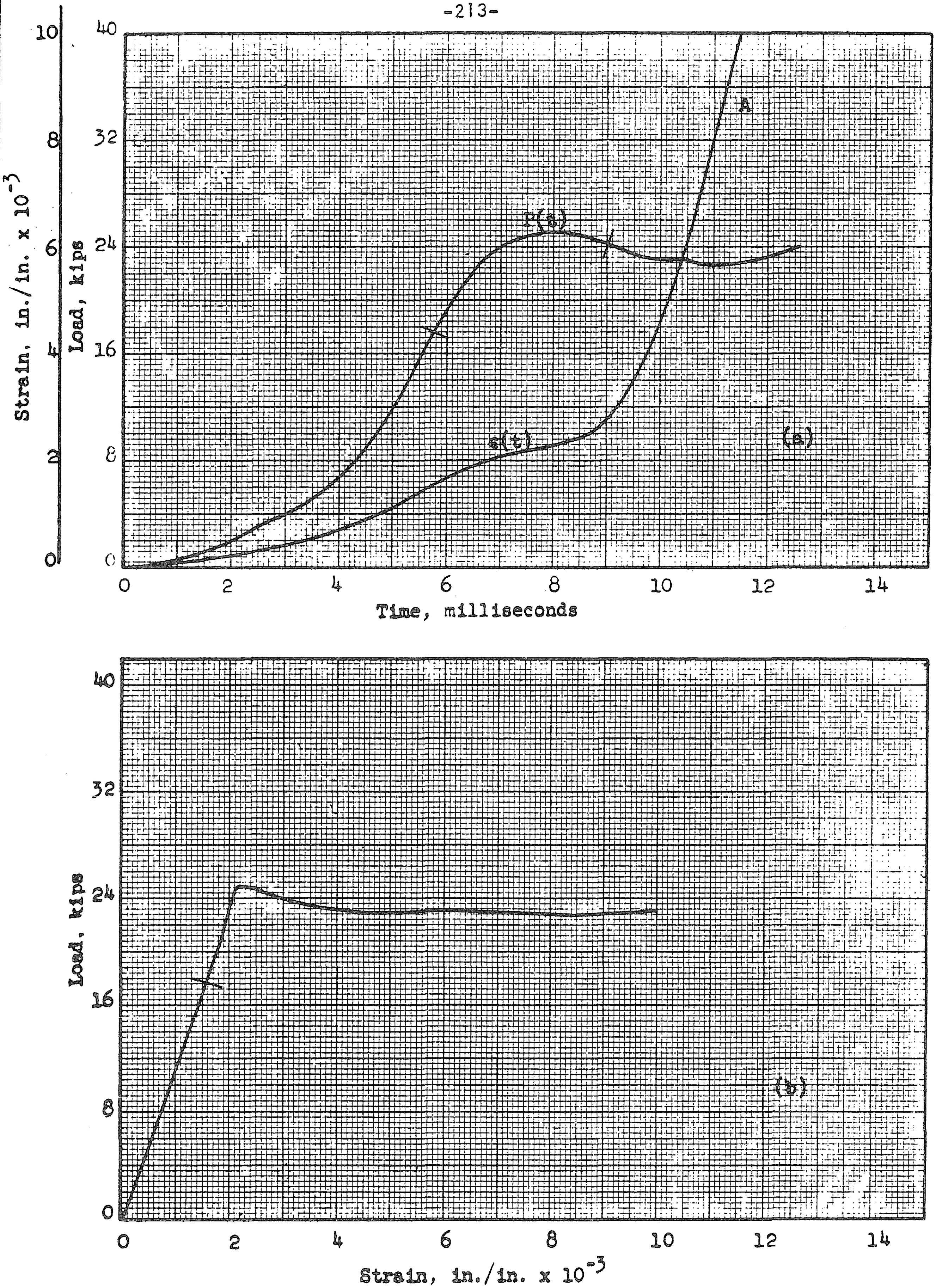

FIG. A2 LOAD AND STRAIN VS. TIME AND LOAD VS. STRAIN
SPECIMEN 6-11

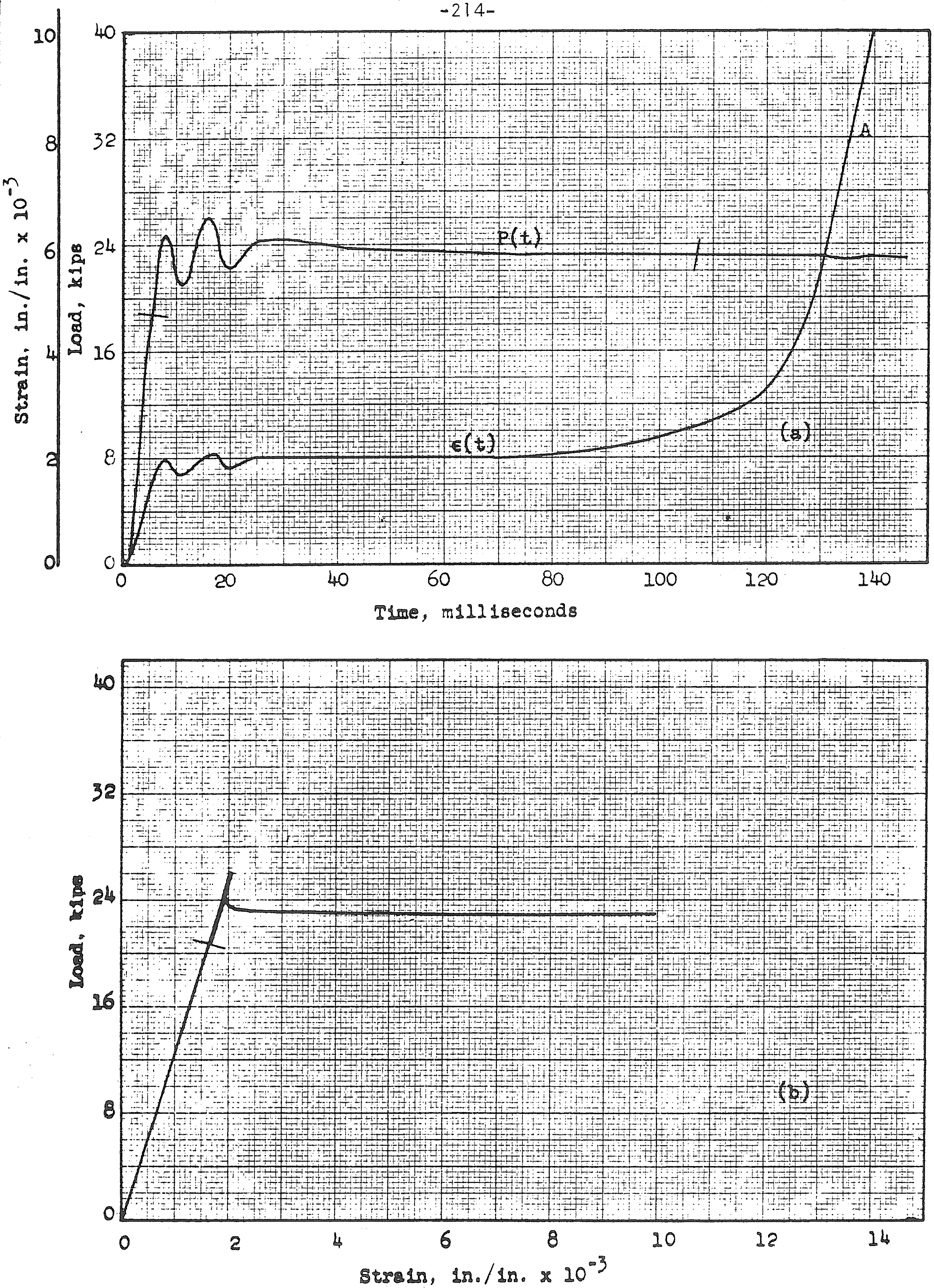

FIG. A3 LOAD AND STRAIN VS. TIME AND LOAD VS. STRAIN
SPECIMEN 6-12

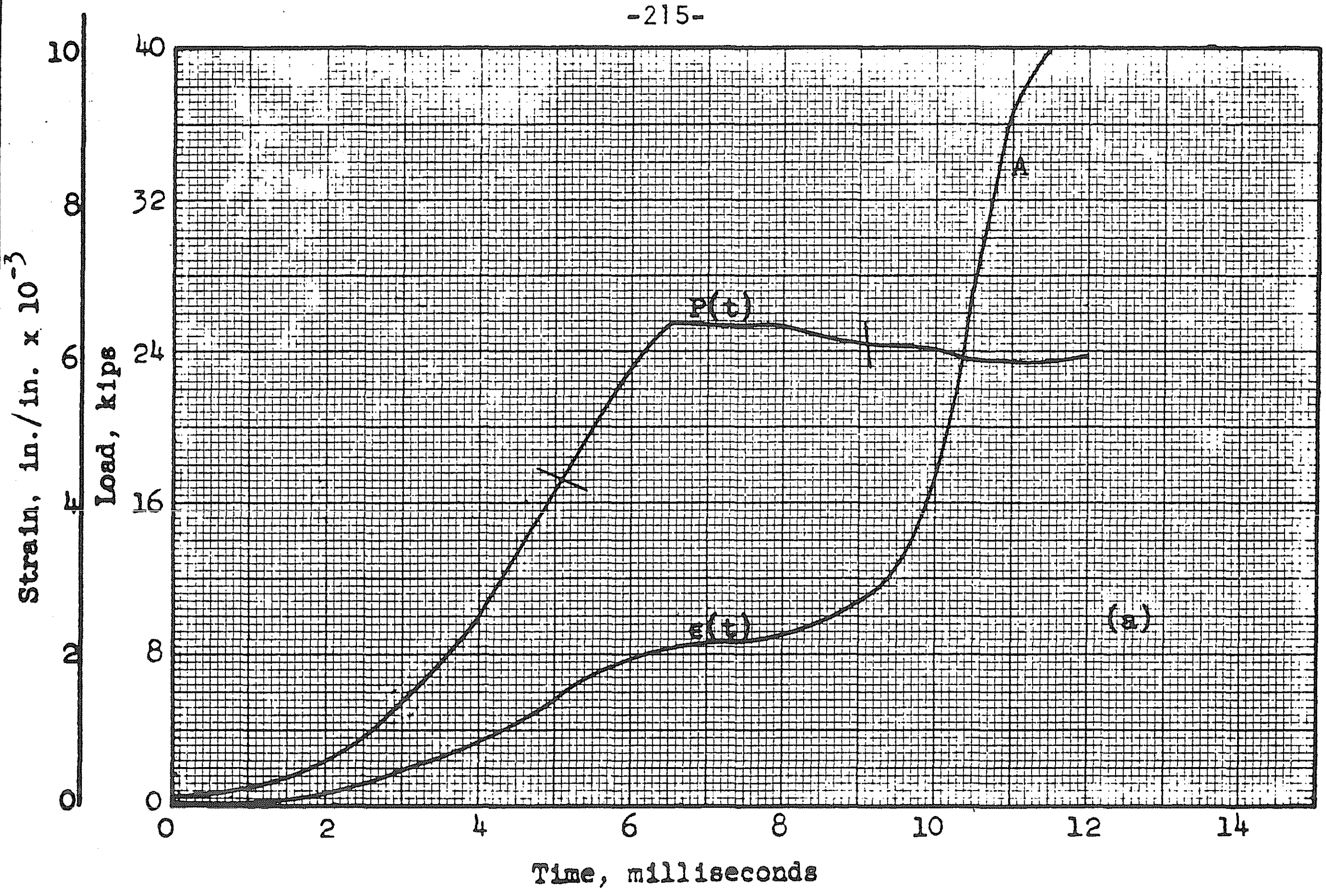

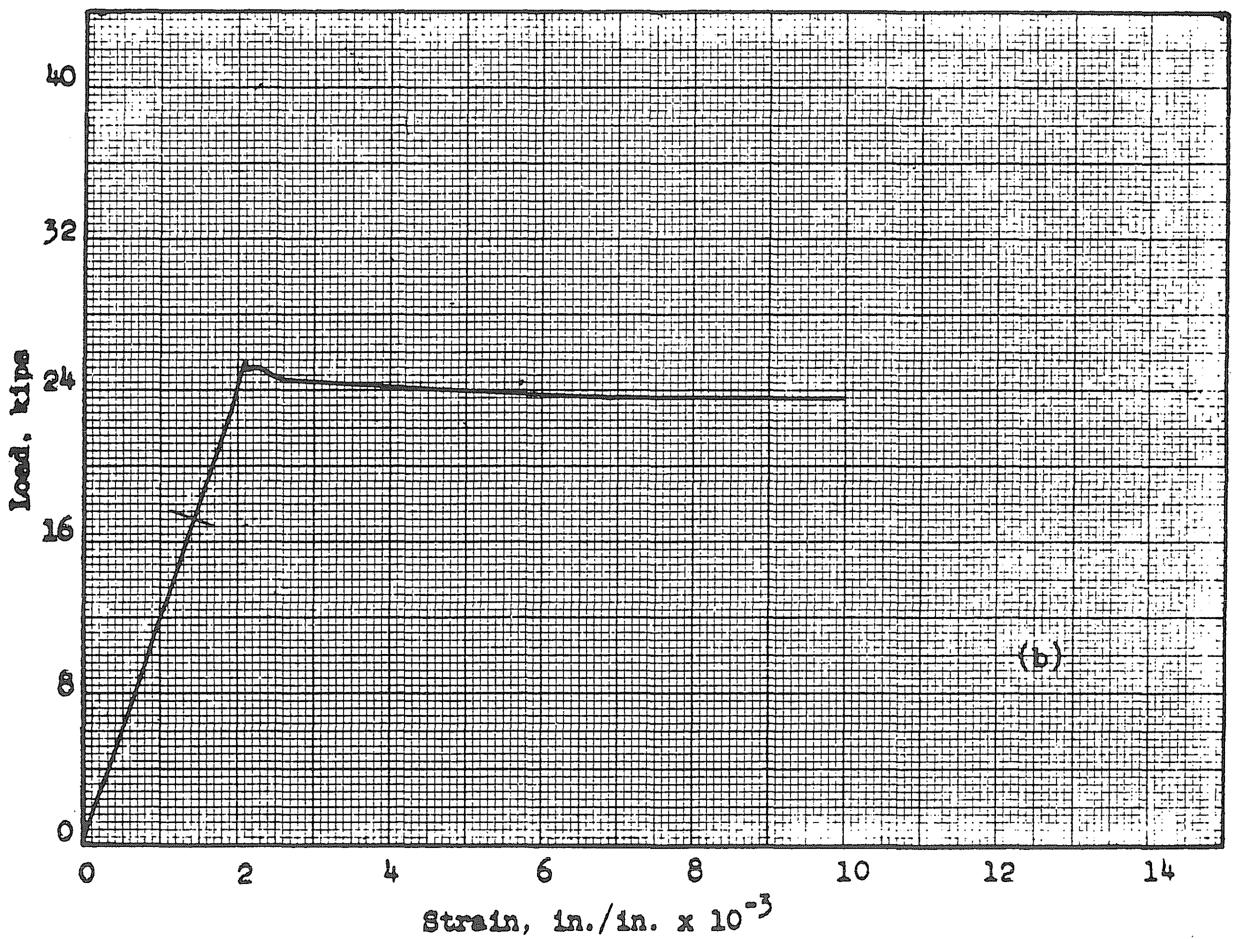

FIG. A4 LOAD AND STRAIN VS. TIME AND LOAD VS. STRAIN
SPECIMEN 6-14

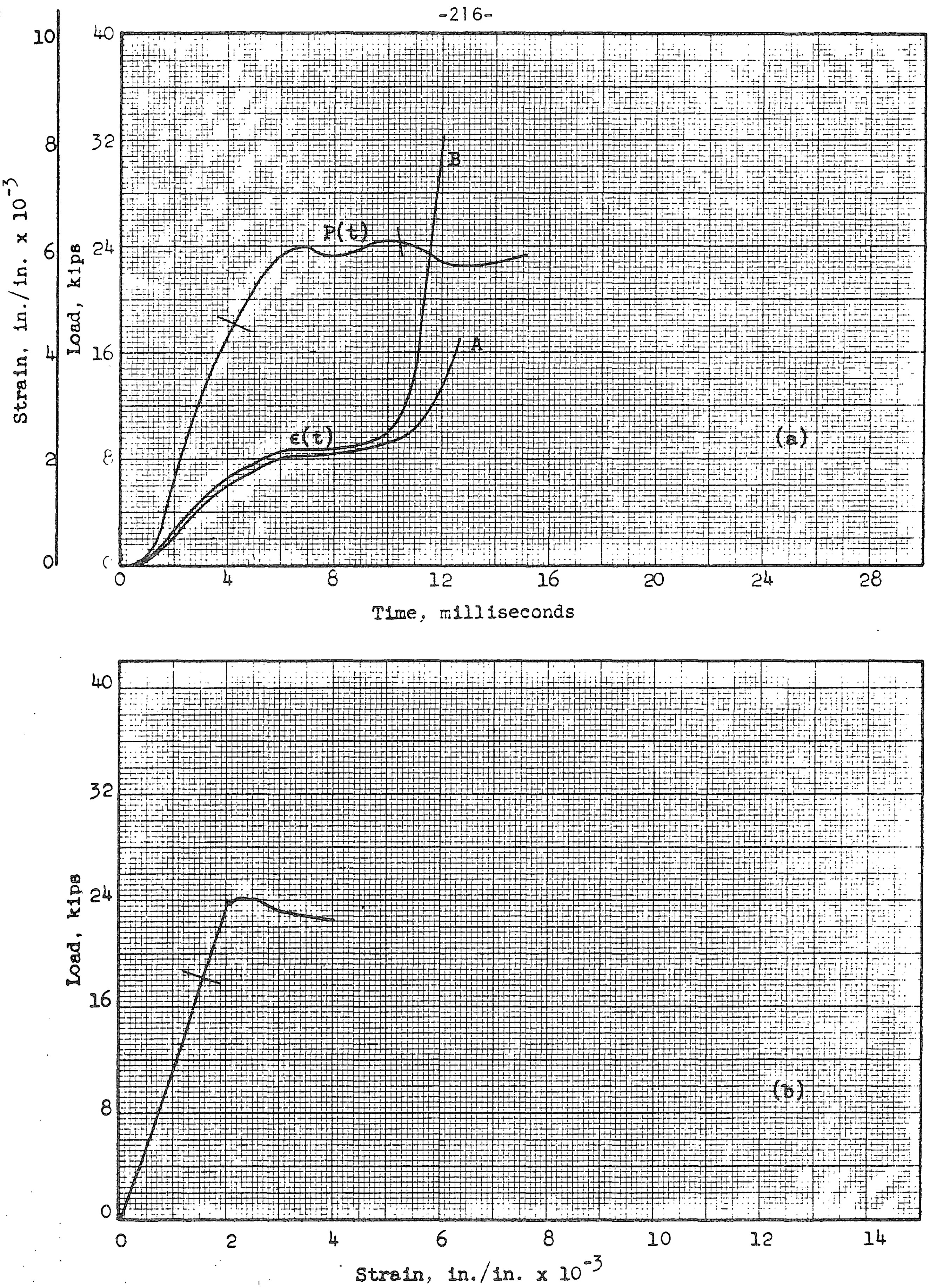

FIG. A5 LOAD AND STRAIN VS. TIME AND LOAD VS. STRAIN
SPECIMEN 6-15

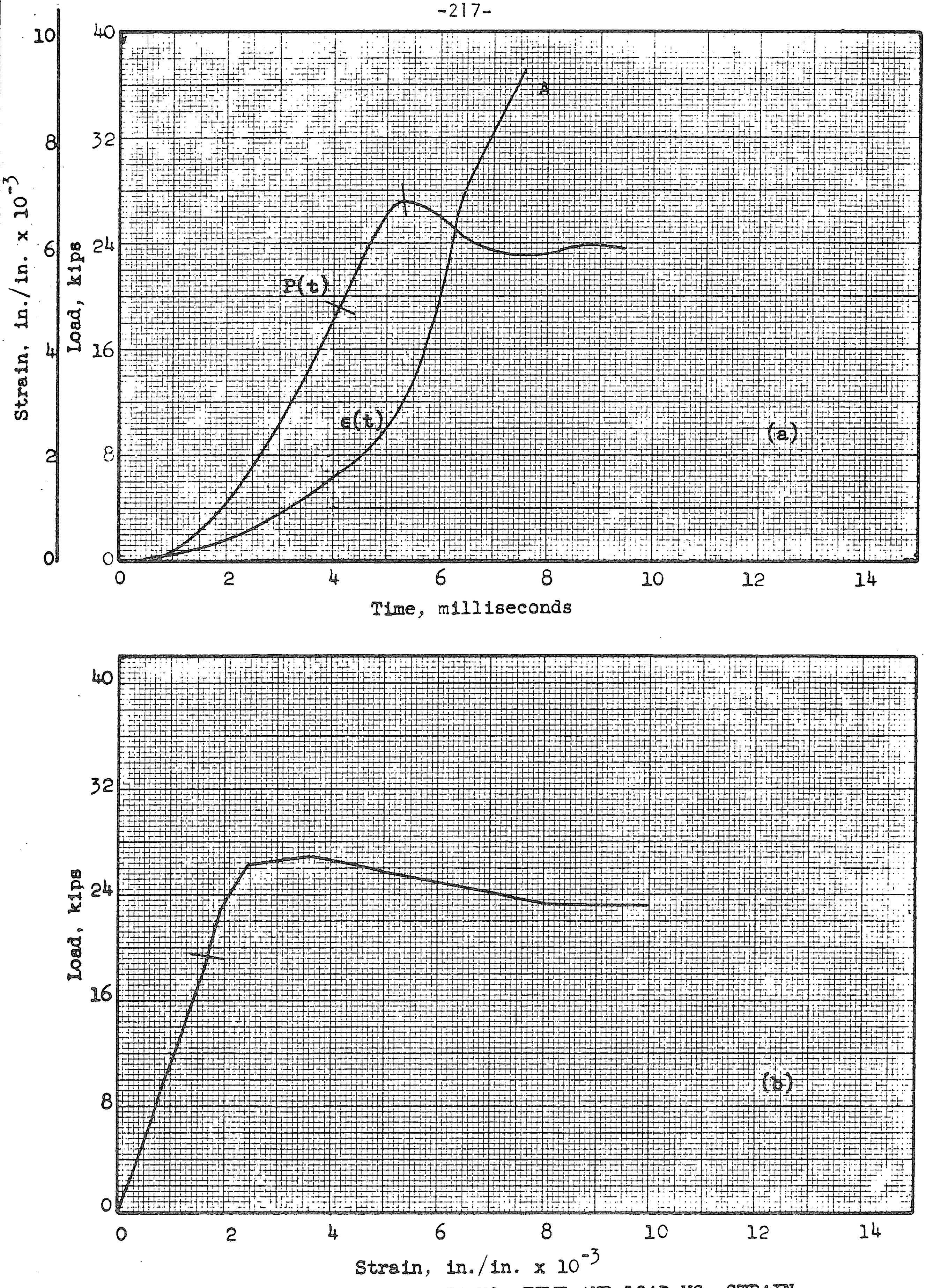

FIG. A6 LOAD AND STRAIN VS. TIME AND LOAD VS. STRAIN
SPECIMEN 6-16

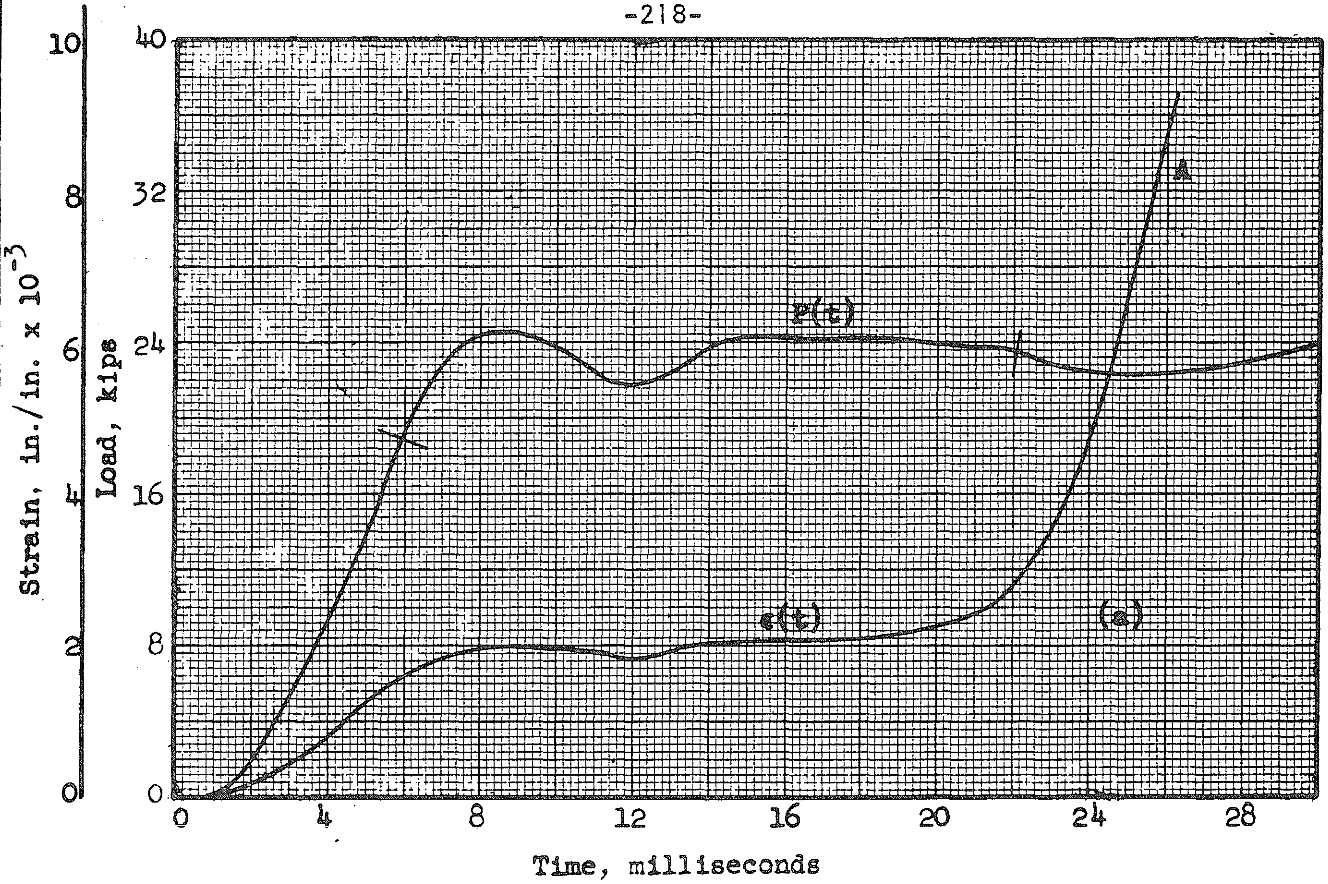

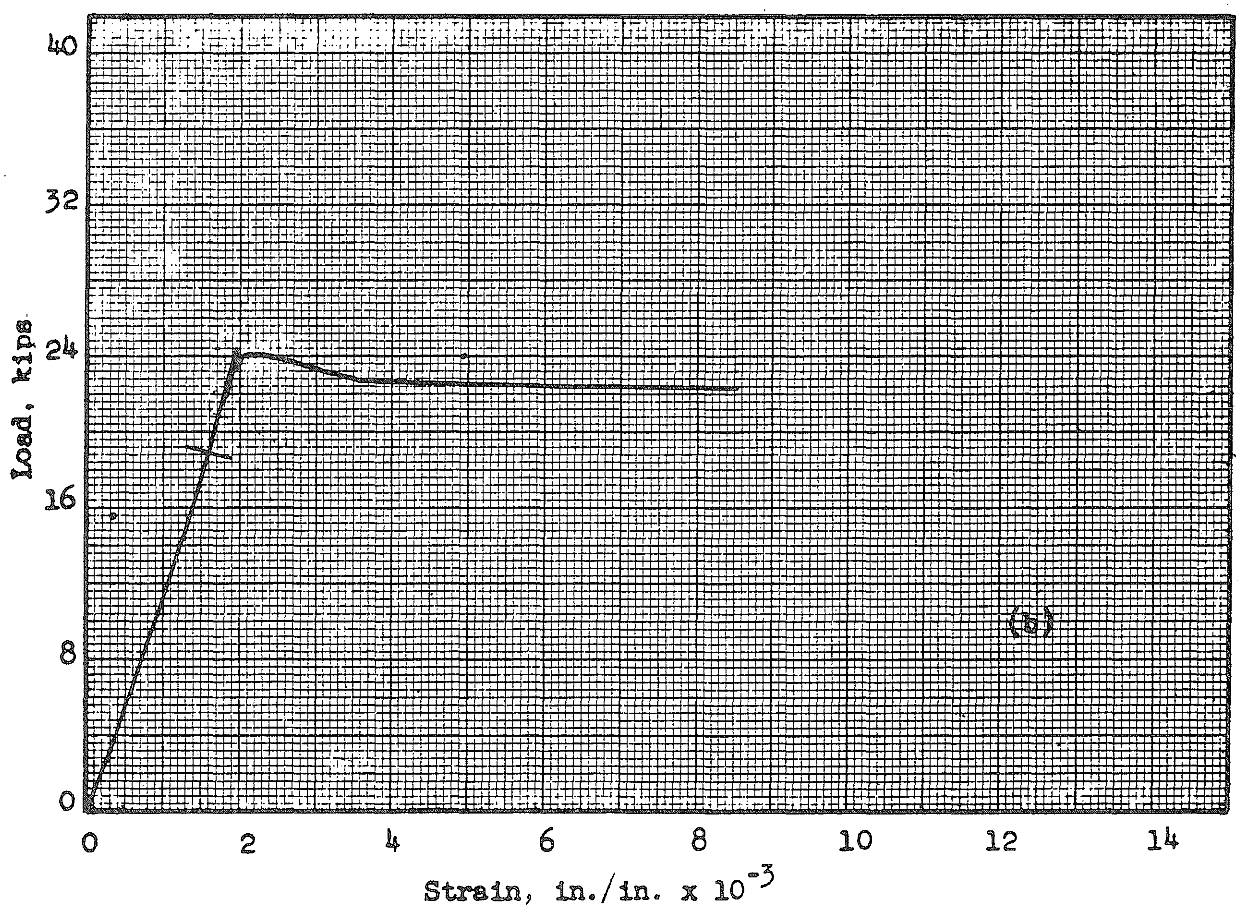

FIG. A7 LOAD AND STRAIN VS. TIME AND LOAD VS. STRAIN
SPECIMEN 6-18

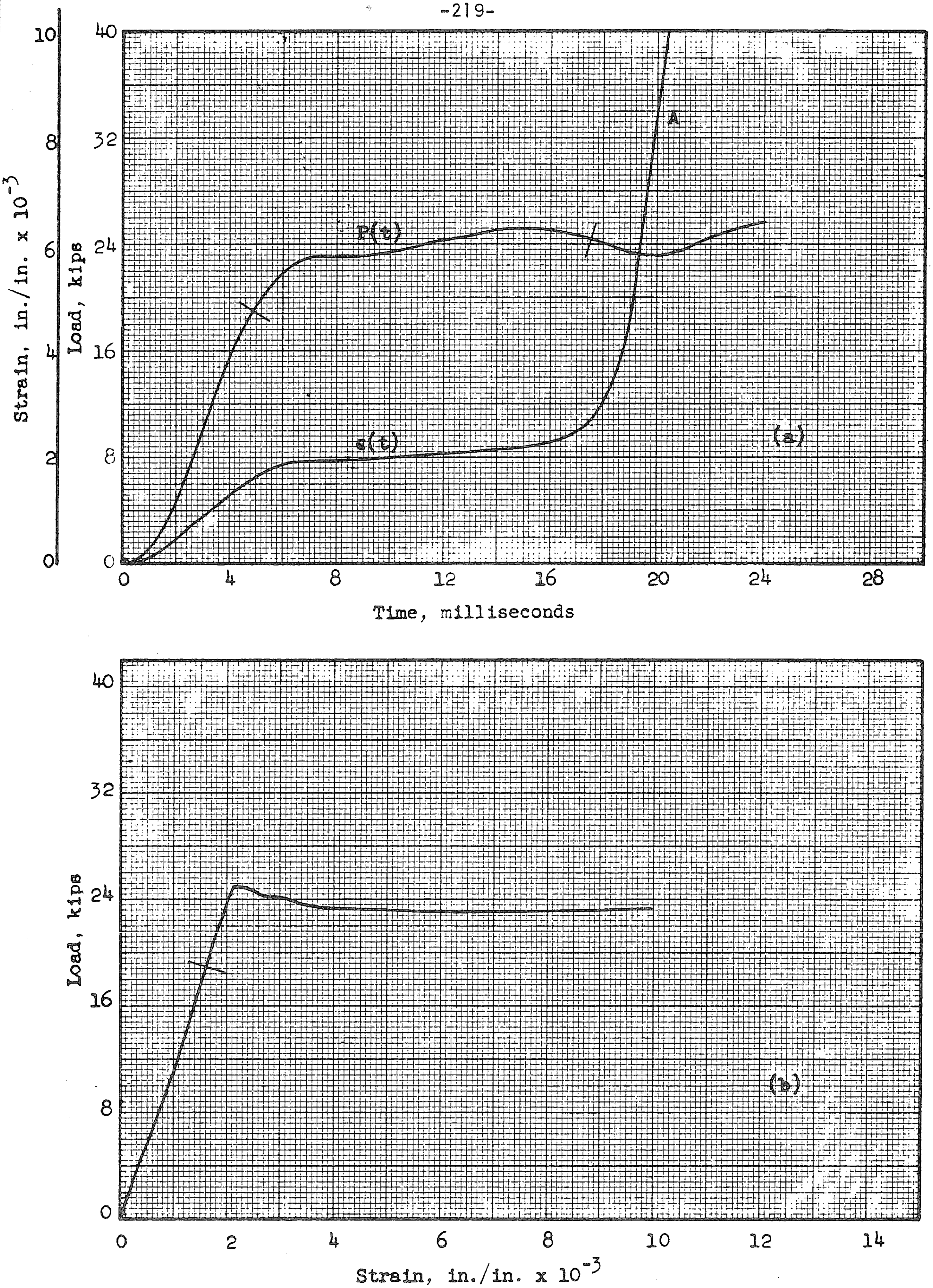

FIG. A8 LOAD AND STRAIN VS. TIME AND LOAD VS. STRAIN
SPECIMEN 6-19

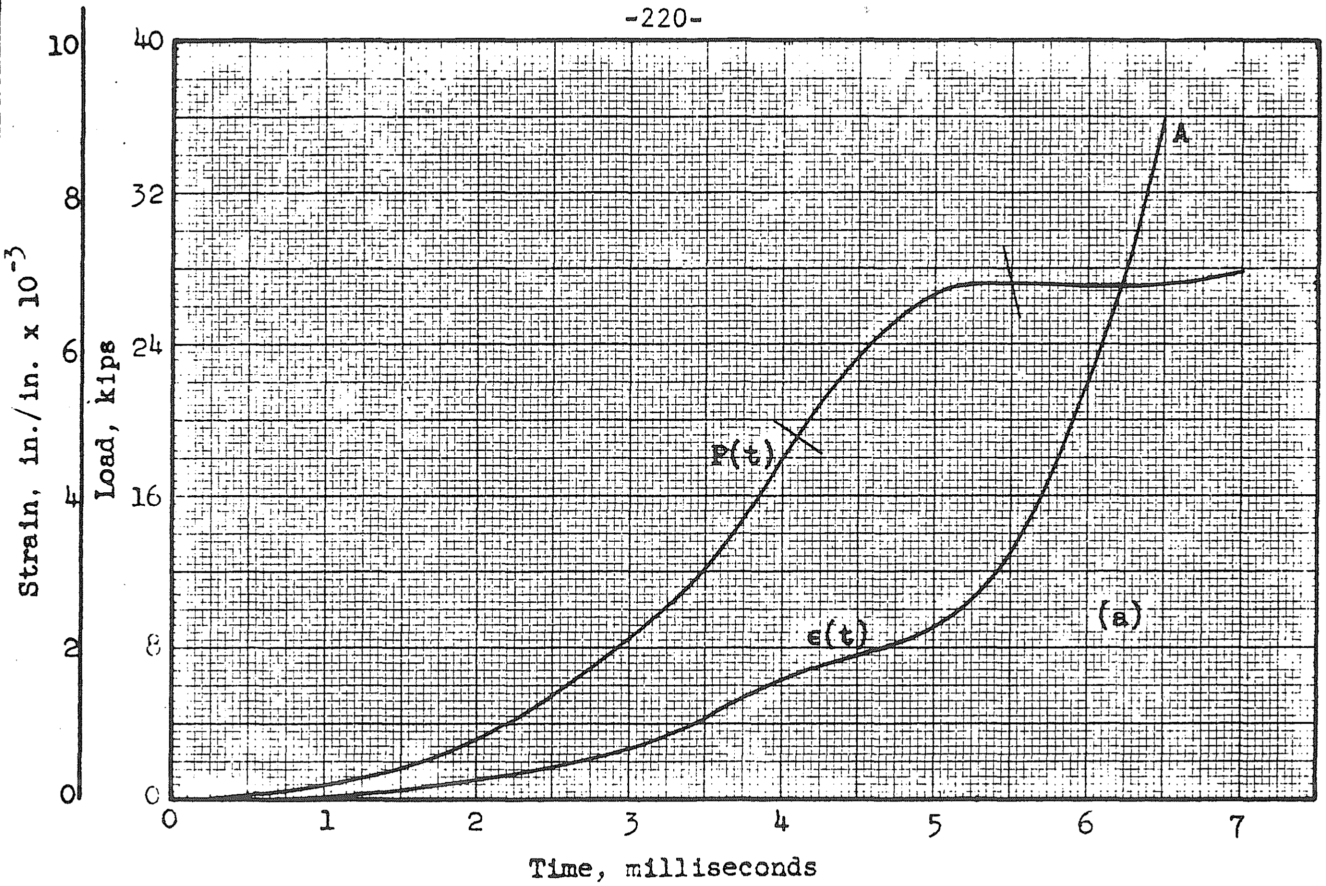

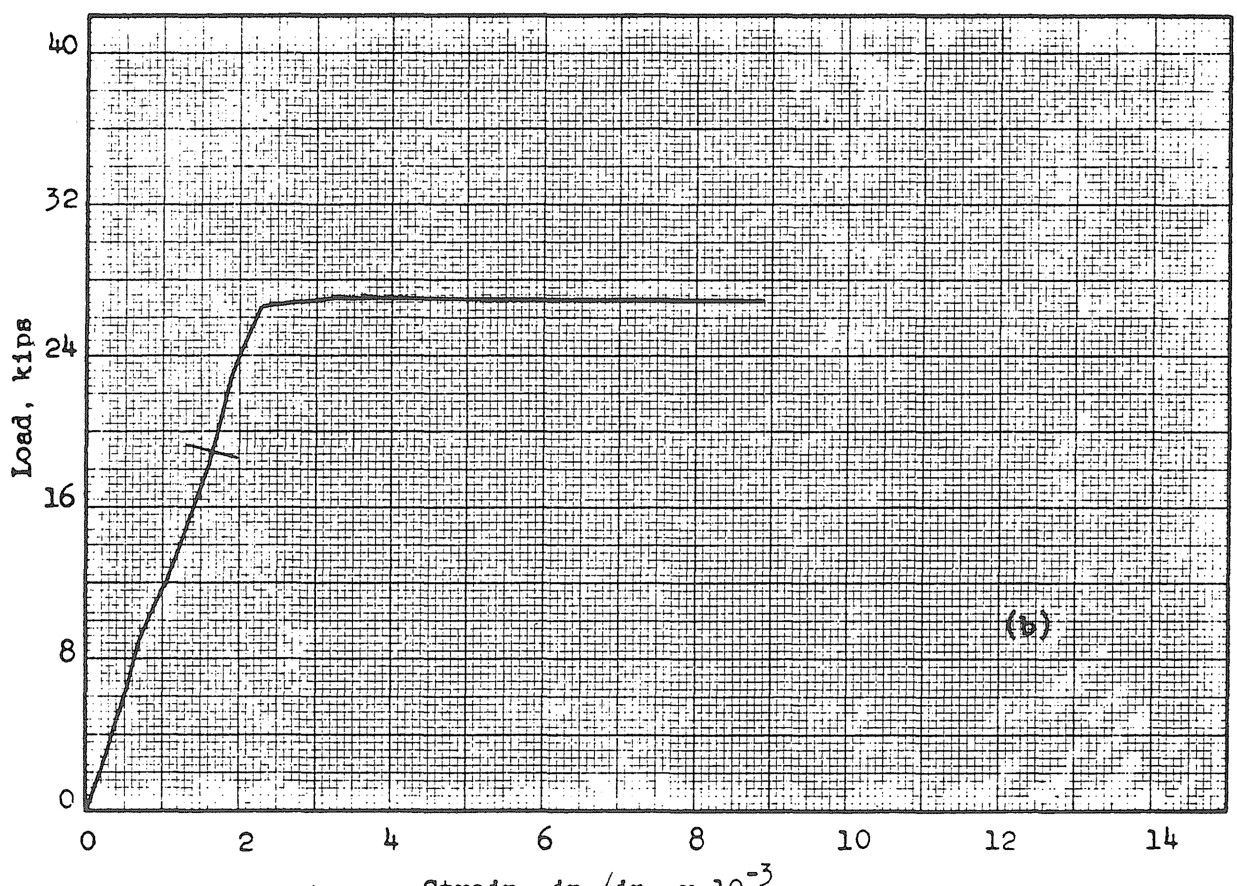

FIG. A9 LOAD AND STRAIN VS. TIME AND LOAD VS. STRAIN
SPECIMEN 6-20

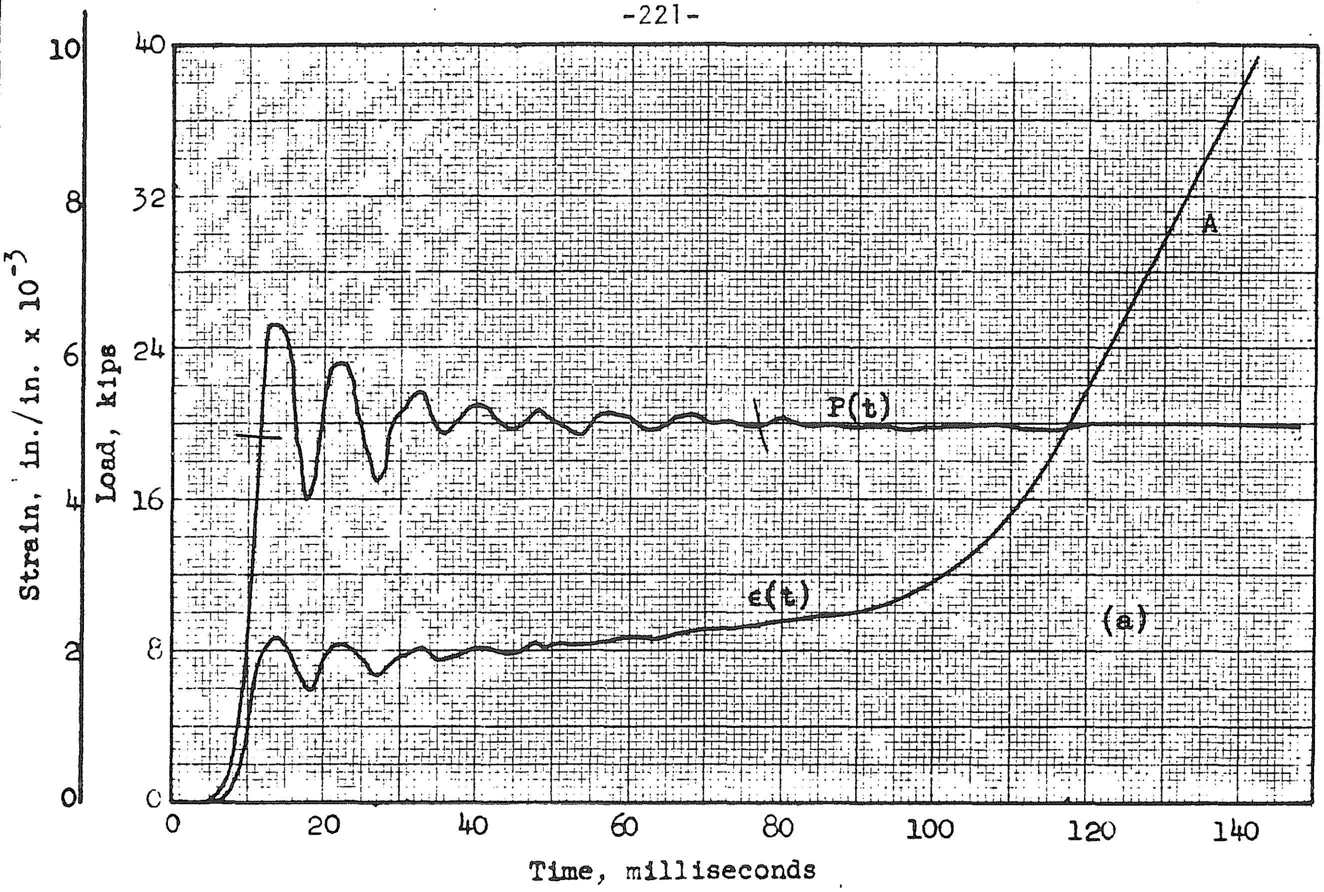

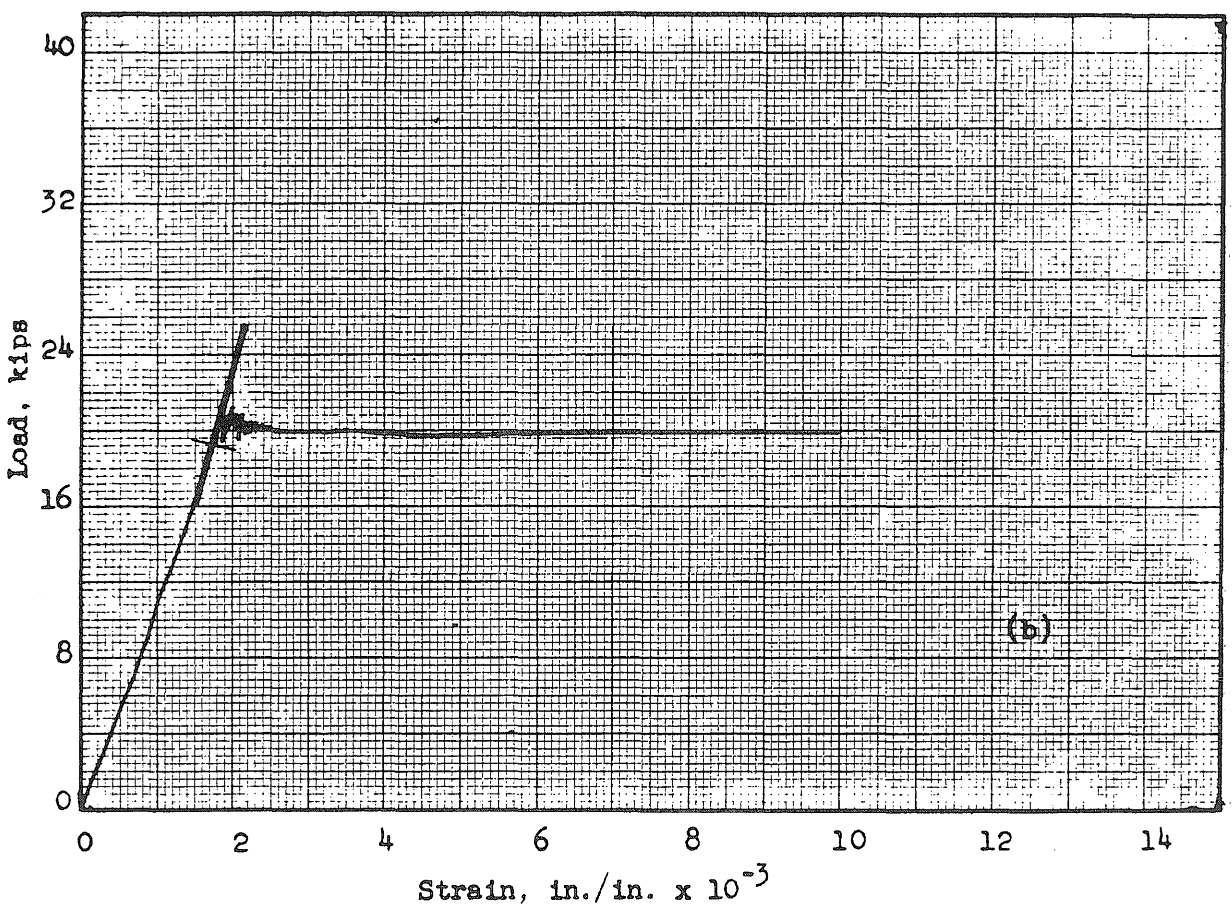

FIG. A10 LOAD AND STRAIN VS. TIME AND LOAD VS. STRAIN
SPECIMEN 6-22

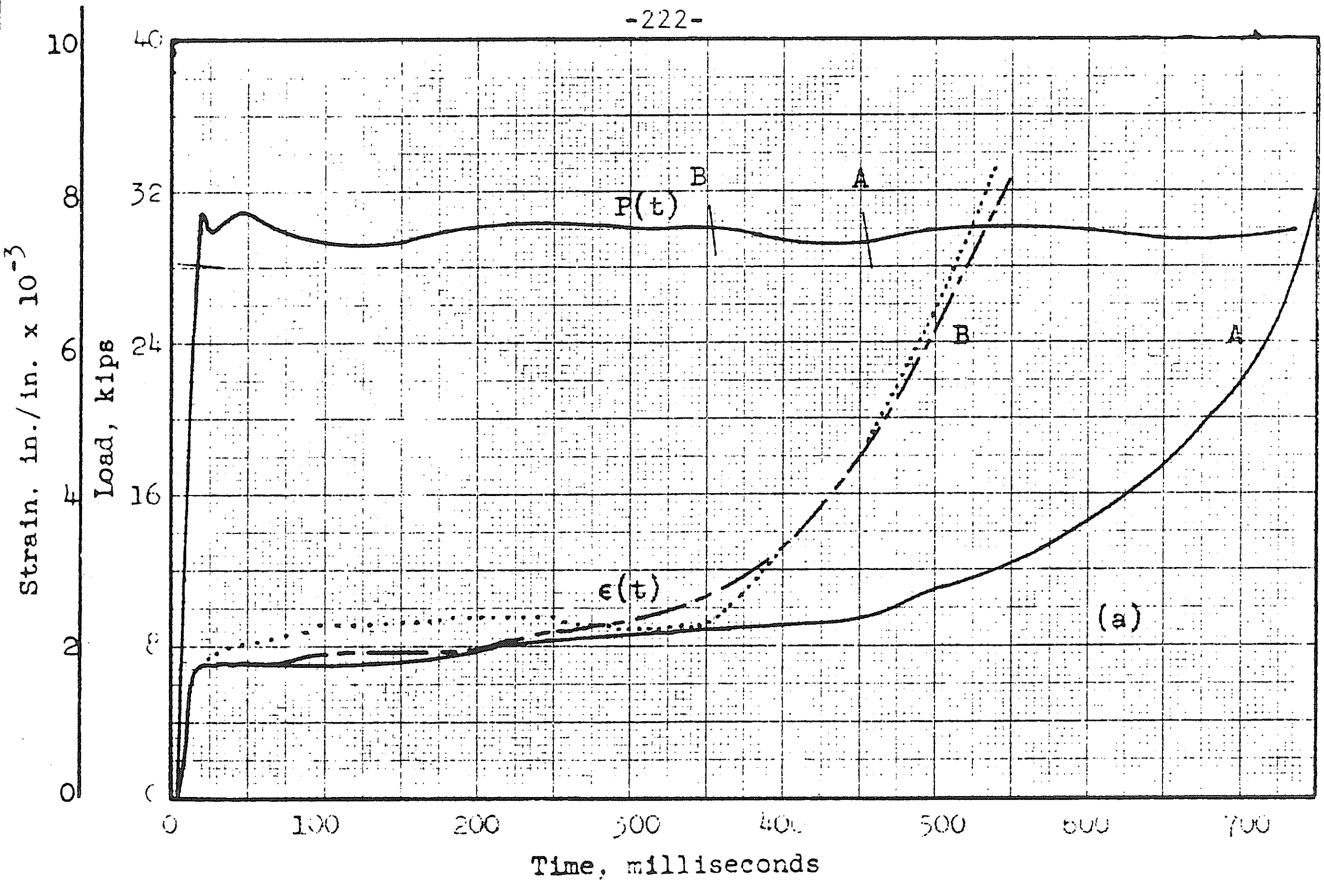

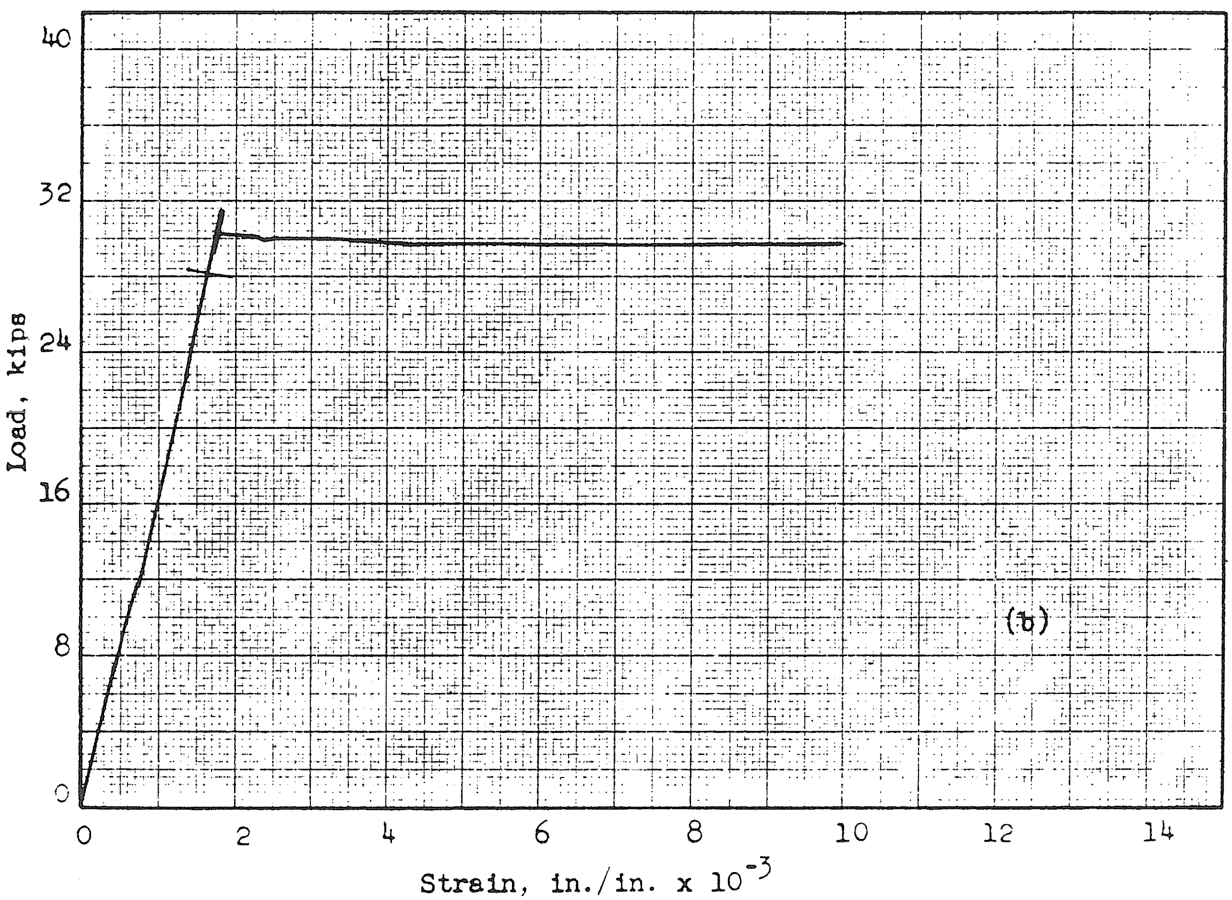

FIG. A11 LOAD AND STRAIN VS. TIME AND LOAD VS. STRAIN
SPECIMEN 7-2

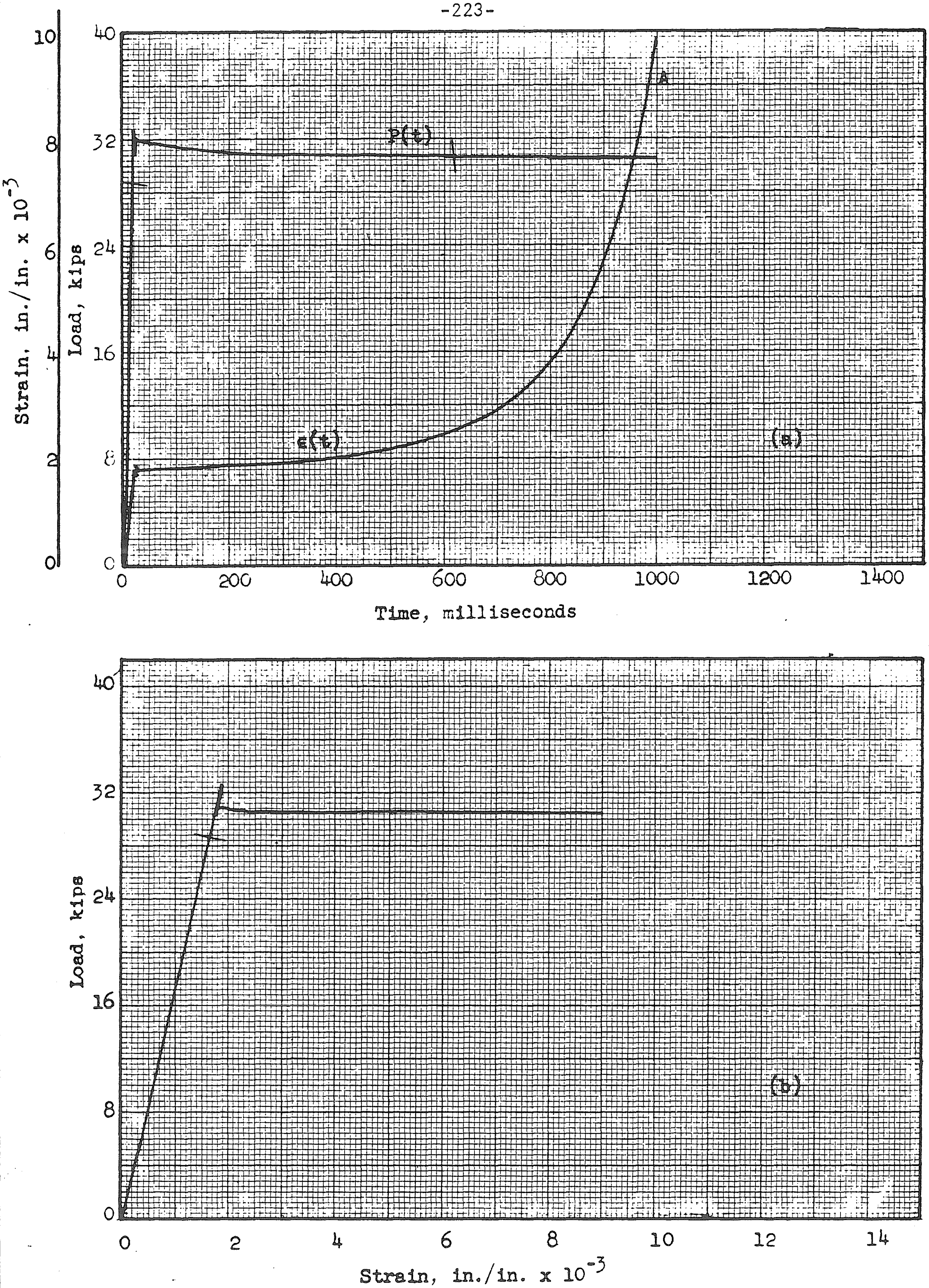

FIG. A12 LOAD AND STRAIN VS. TIME AND LOAD VS. STRAIN SPECIMEN 7-4

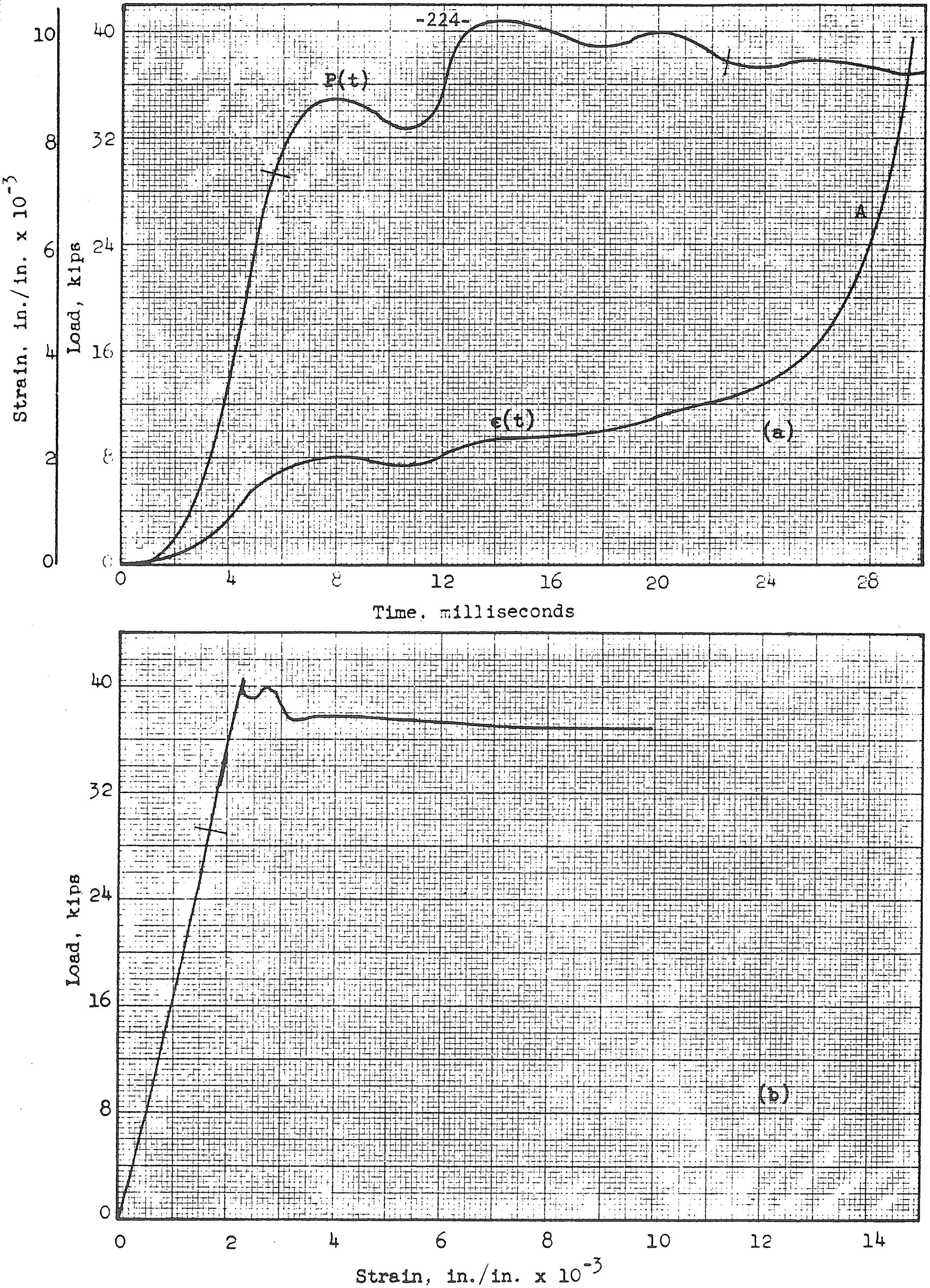

FIG. A13 LOAD AND STRAIN VS. TIME AND LOAD VS. STRAIN
SPECIMEN 7-6

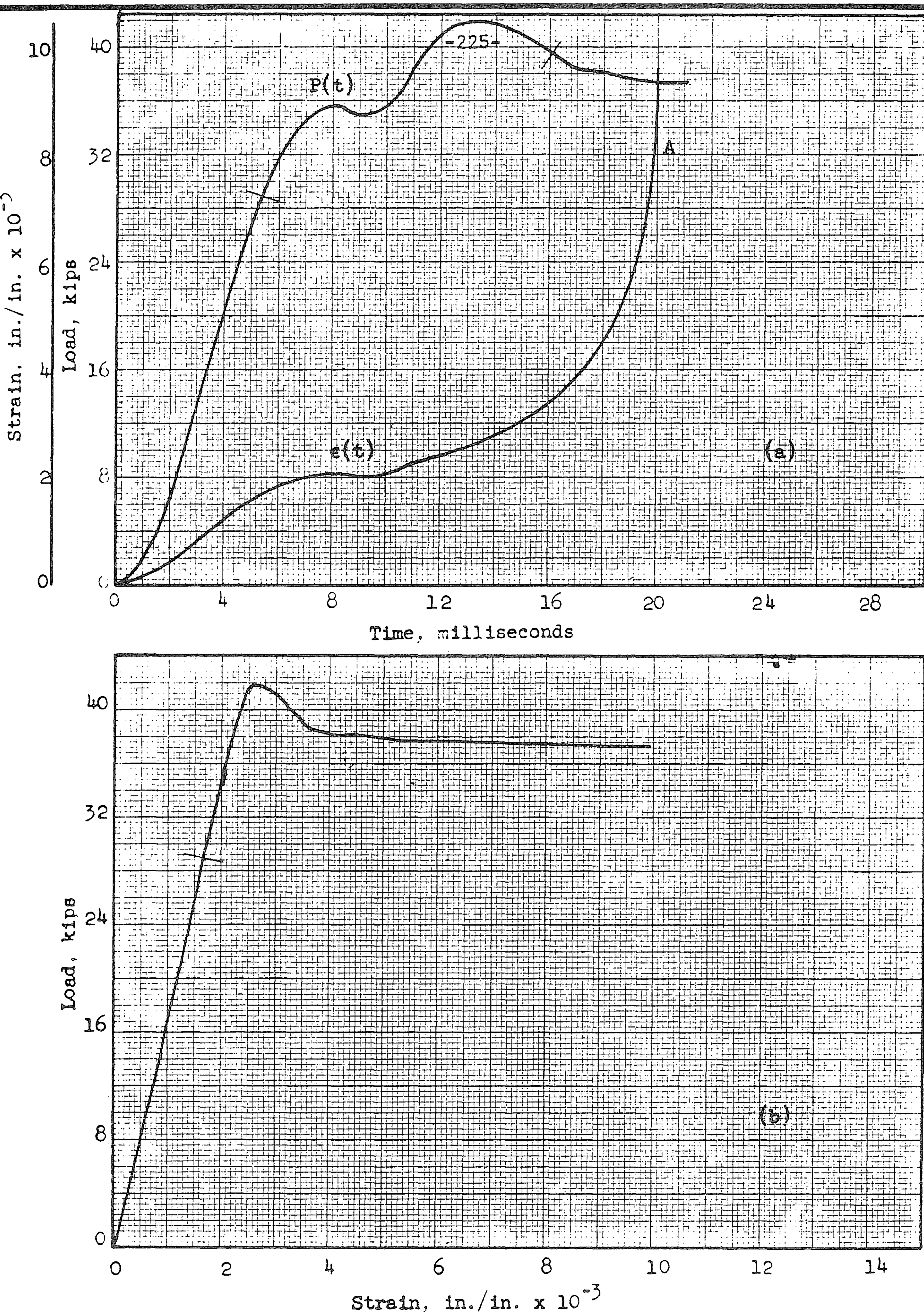

FIG. A14 LOAD AND STRAIN VS. TIME AND LOAD VS. STRAIN
SPECIMEN 7-12

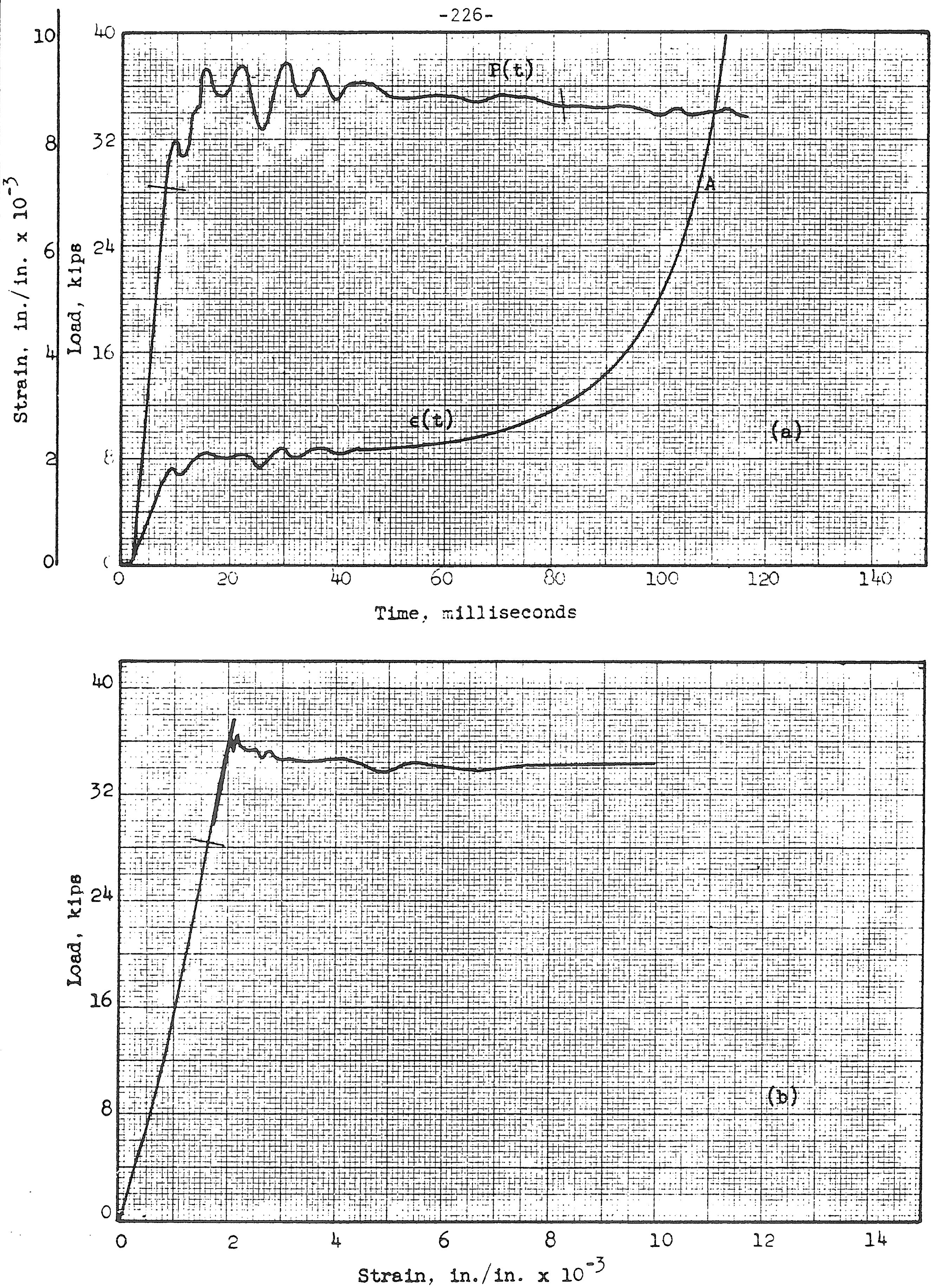

FIG. A15 LOAD AND STRAIN VS. TIME AND LOAD VS. STRAIN
SPECIMEN 7-15

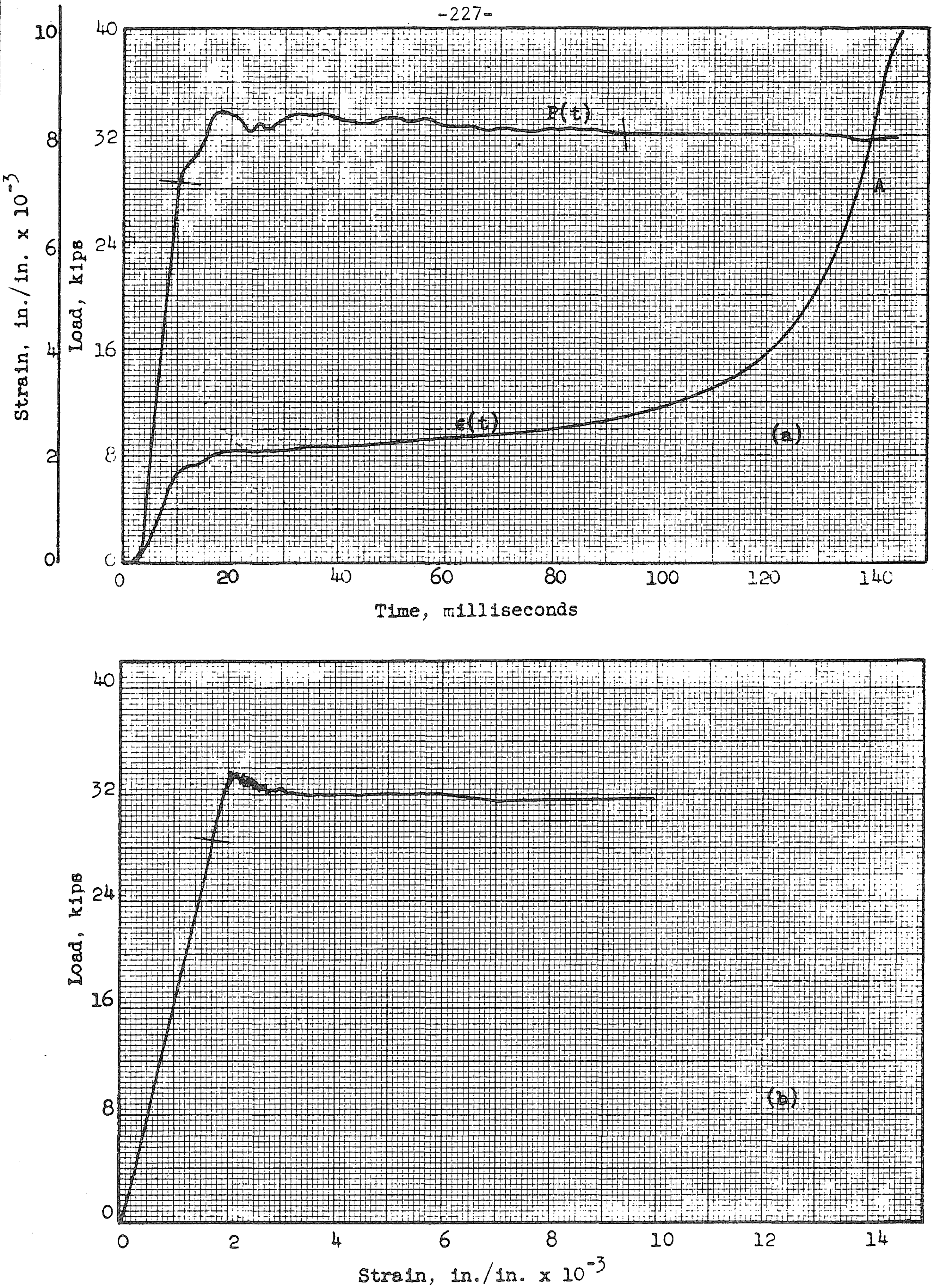

FIG. A16 LOAD AND STRAIN VS. TIME AND LOAD VS. STRAIN
SPECIMEN 7-14

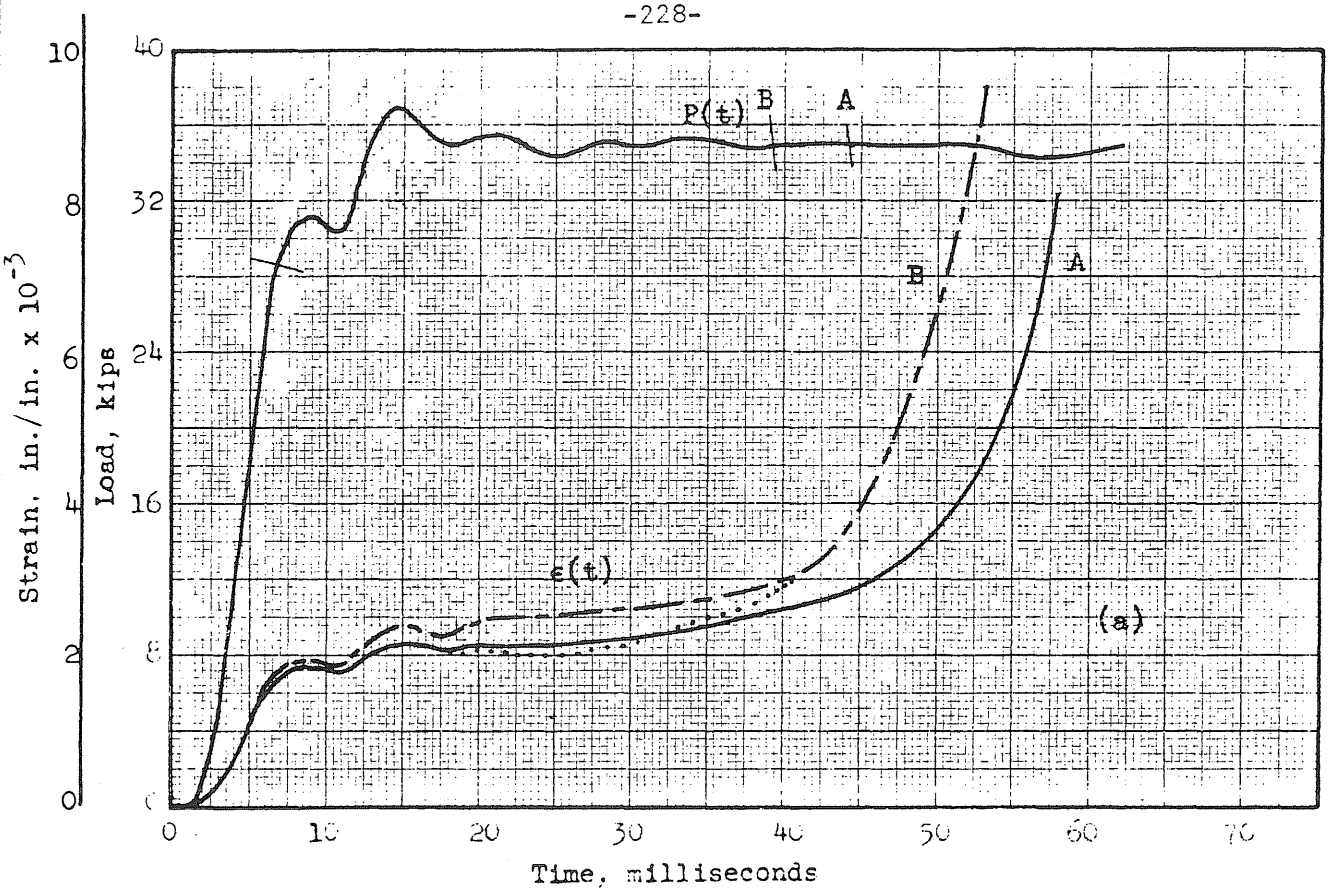

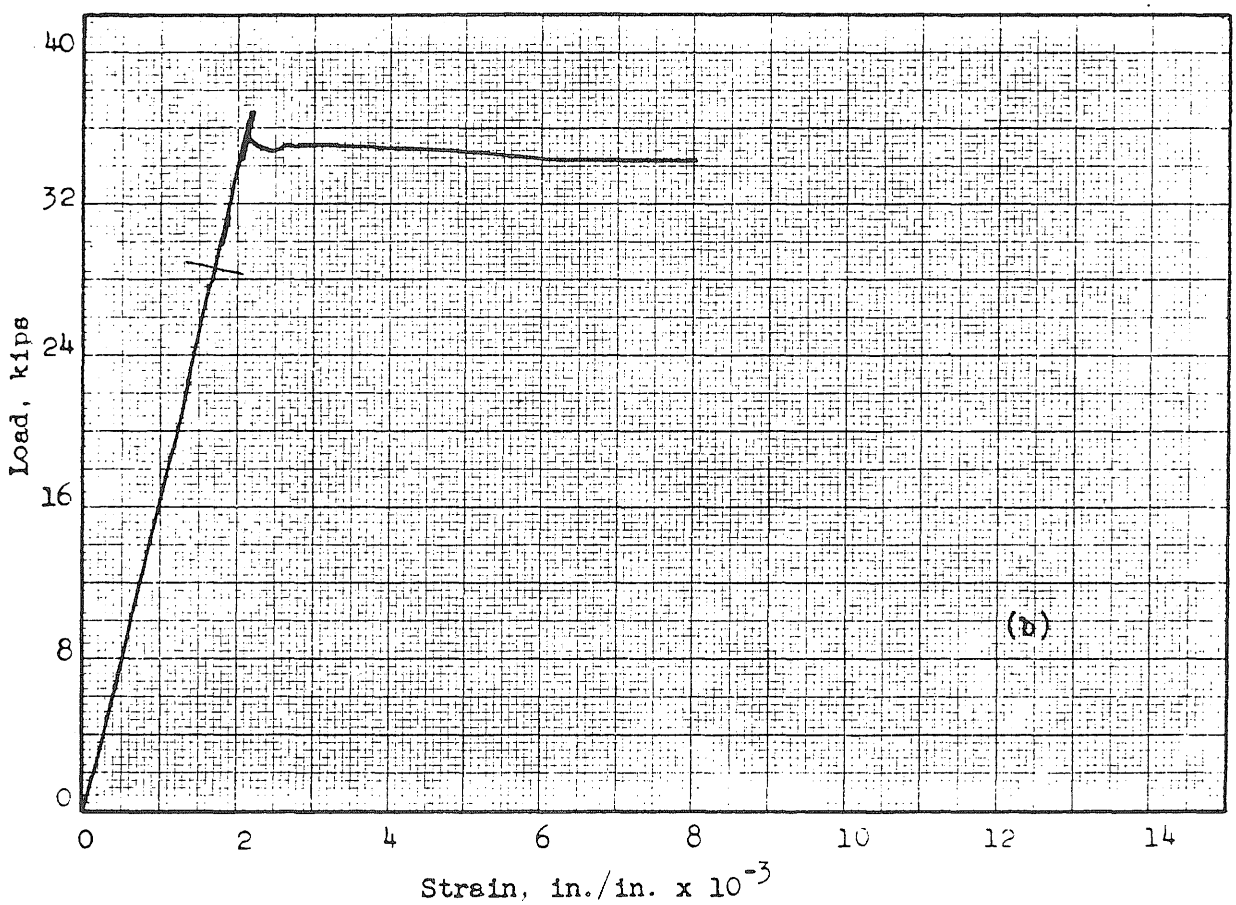

FIG. A17 LOAD AND STRAIN VS. TIME AND LOAD VS. STRAIN
SPECIMEN 7-15

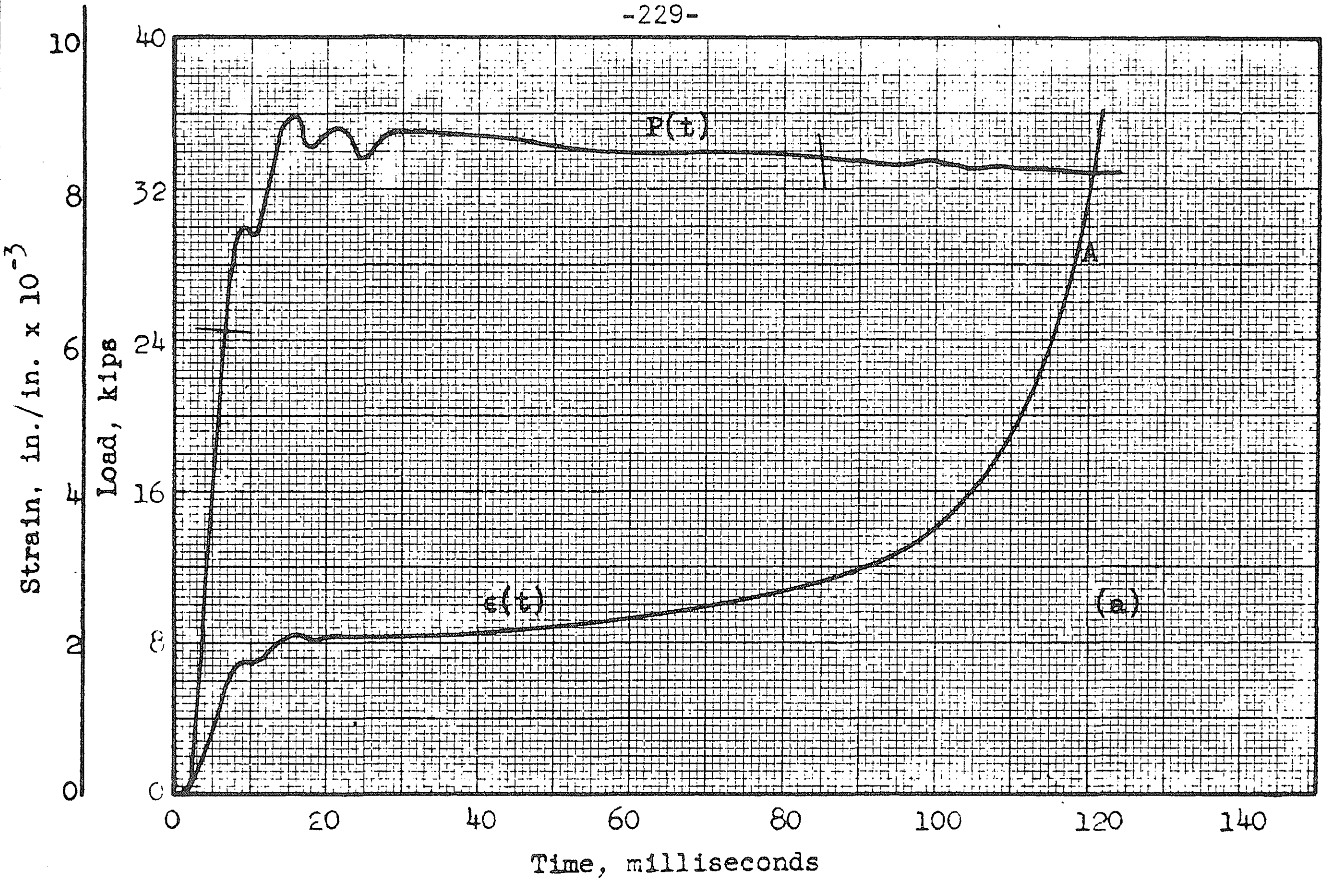

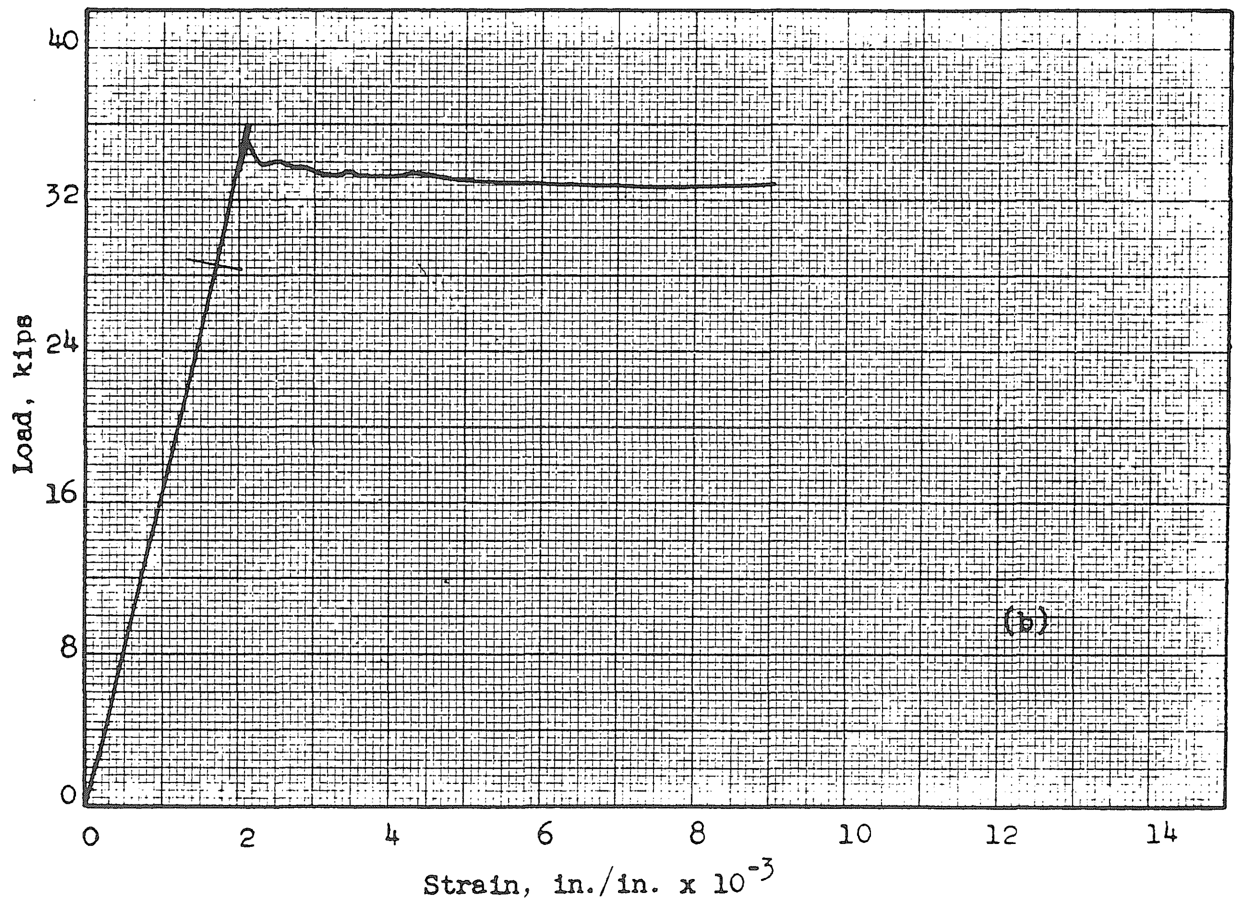

FIG. A18 LOAD AND STRAIN VS. TIME AND LOAD VS. STRAIN
SPECIMEN 7-17

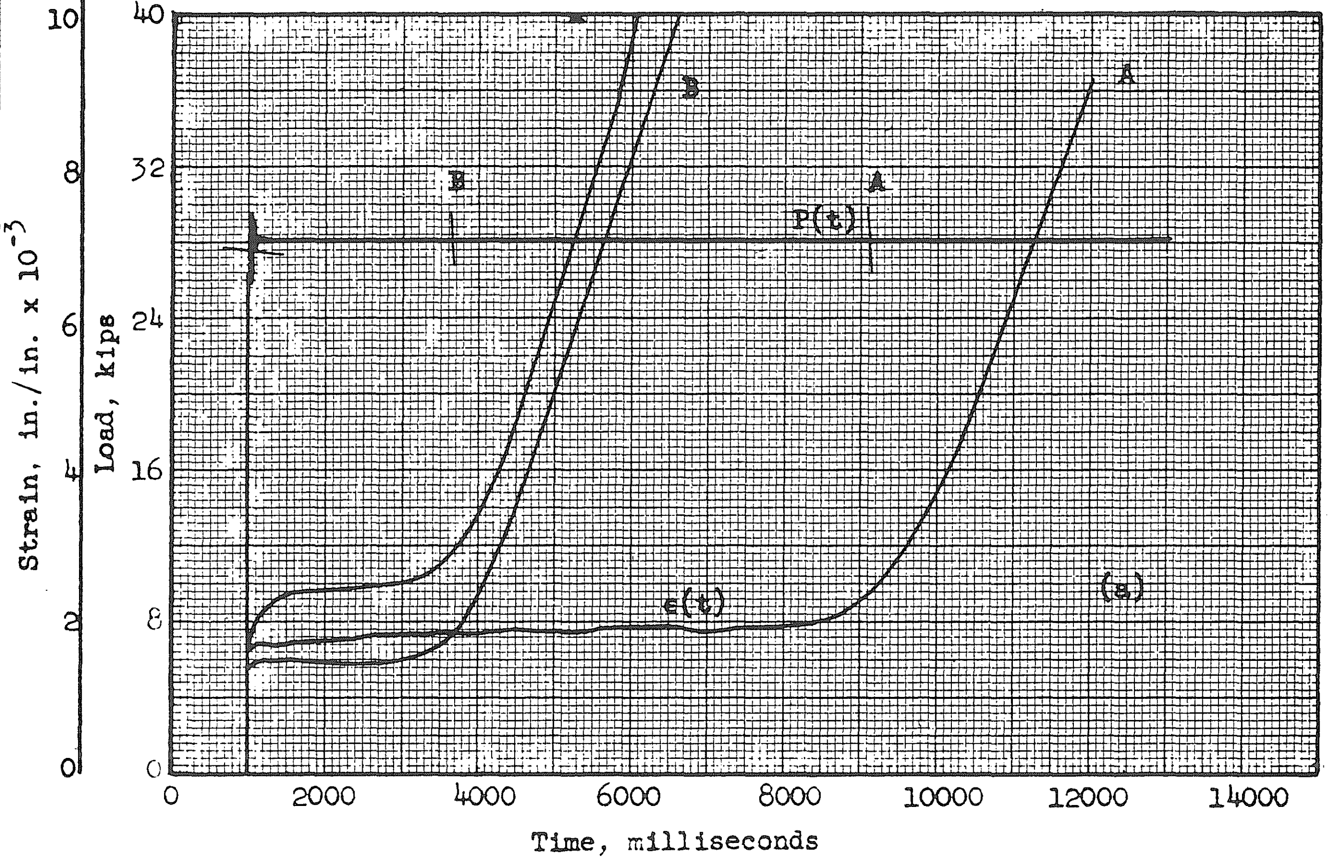

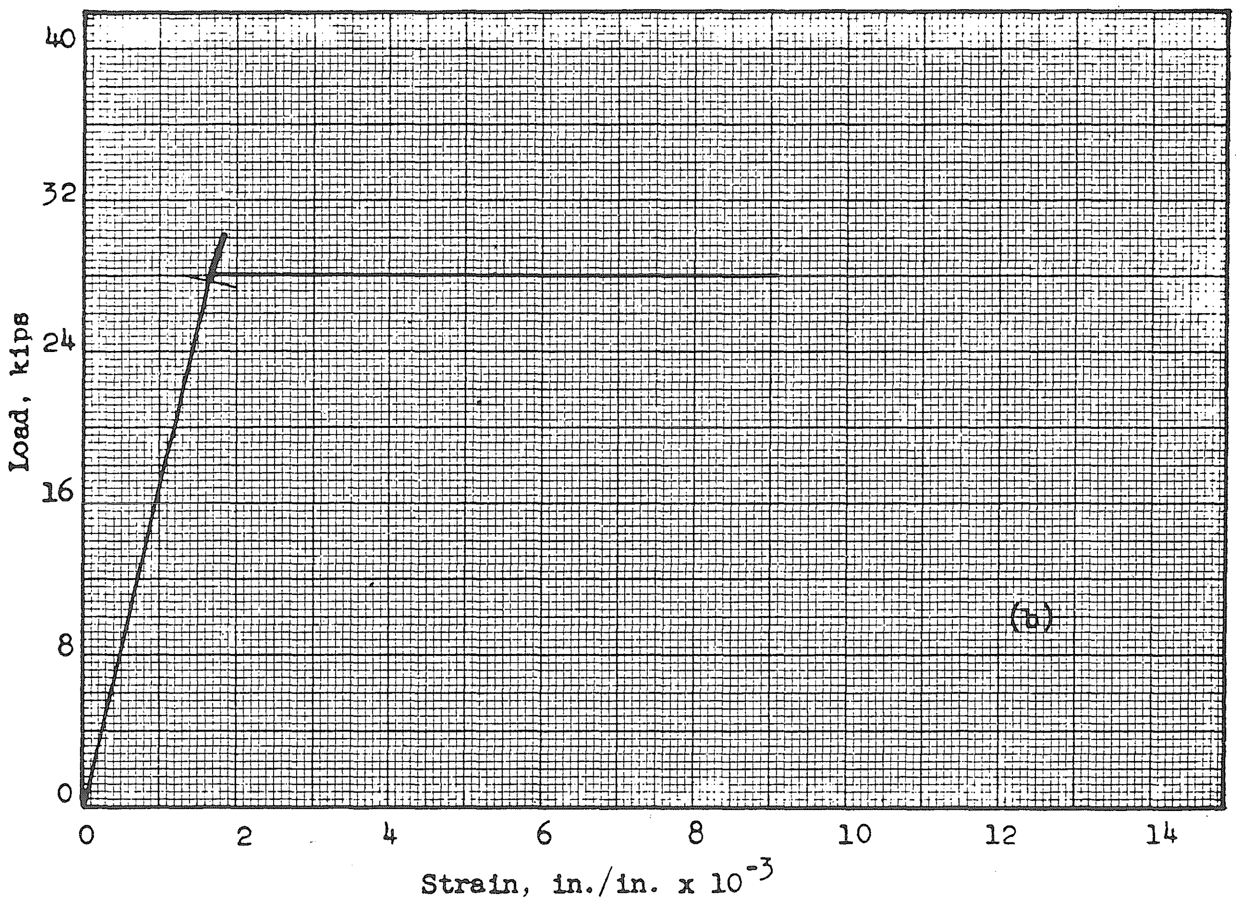

FIG. A19 LOAD AND STRAIN VS. TIME AND LOAD VS. STRAIN
SPECIMEN 7-24

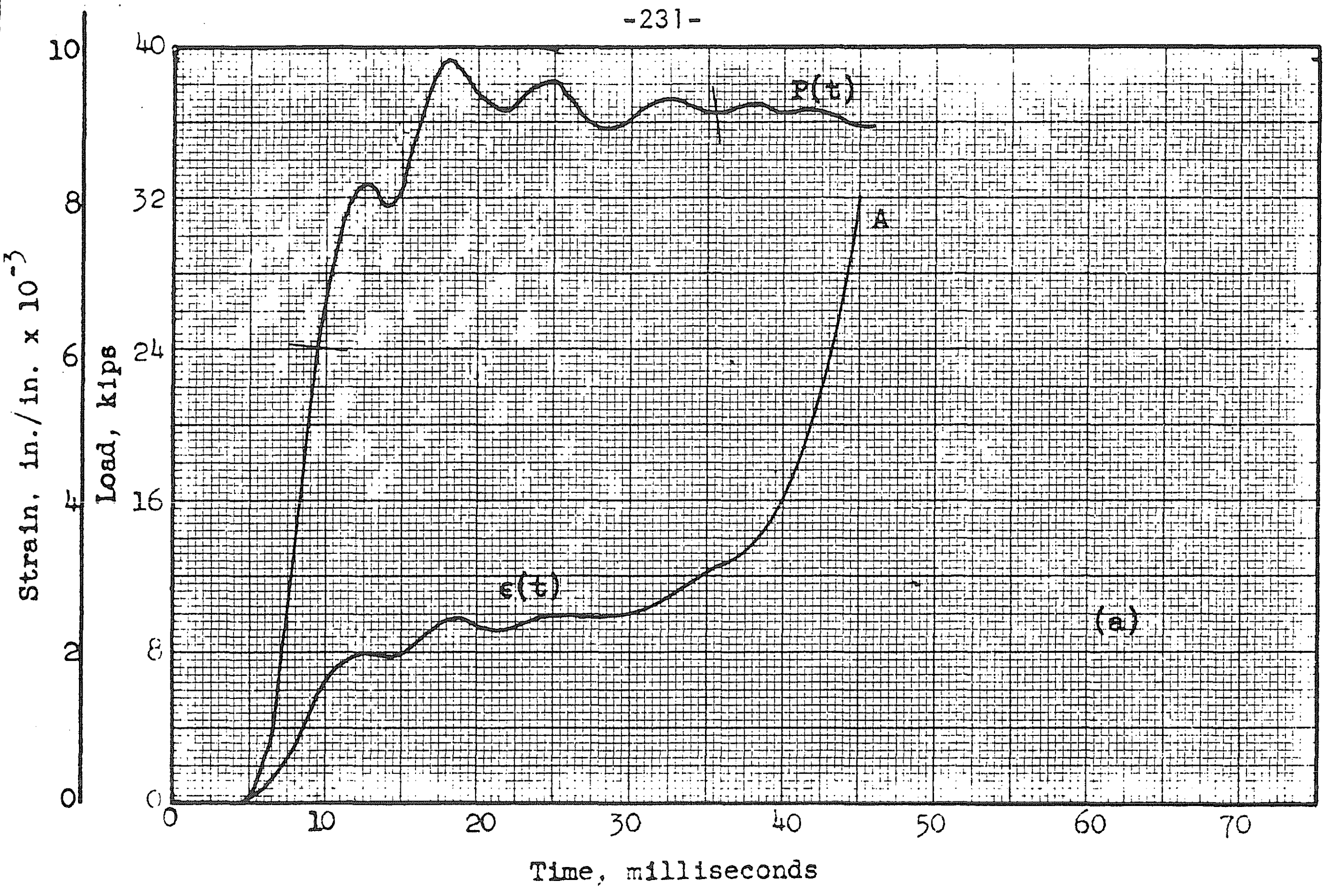

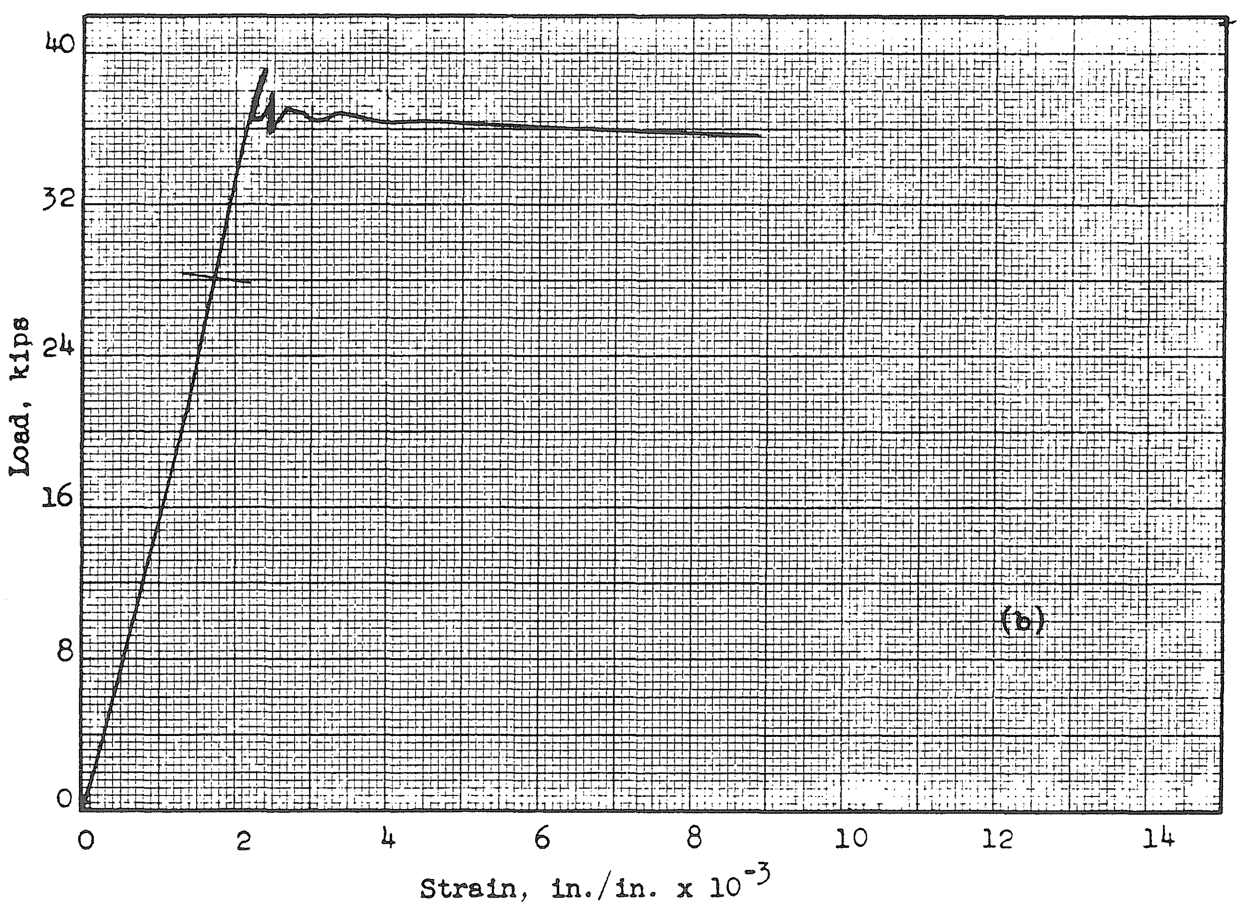

FIG. A20 LOAD AND STRAIN VS. TIME AND LOAD VS. STRAIN
SPECIMEN 7-25

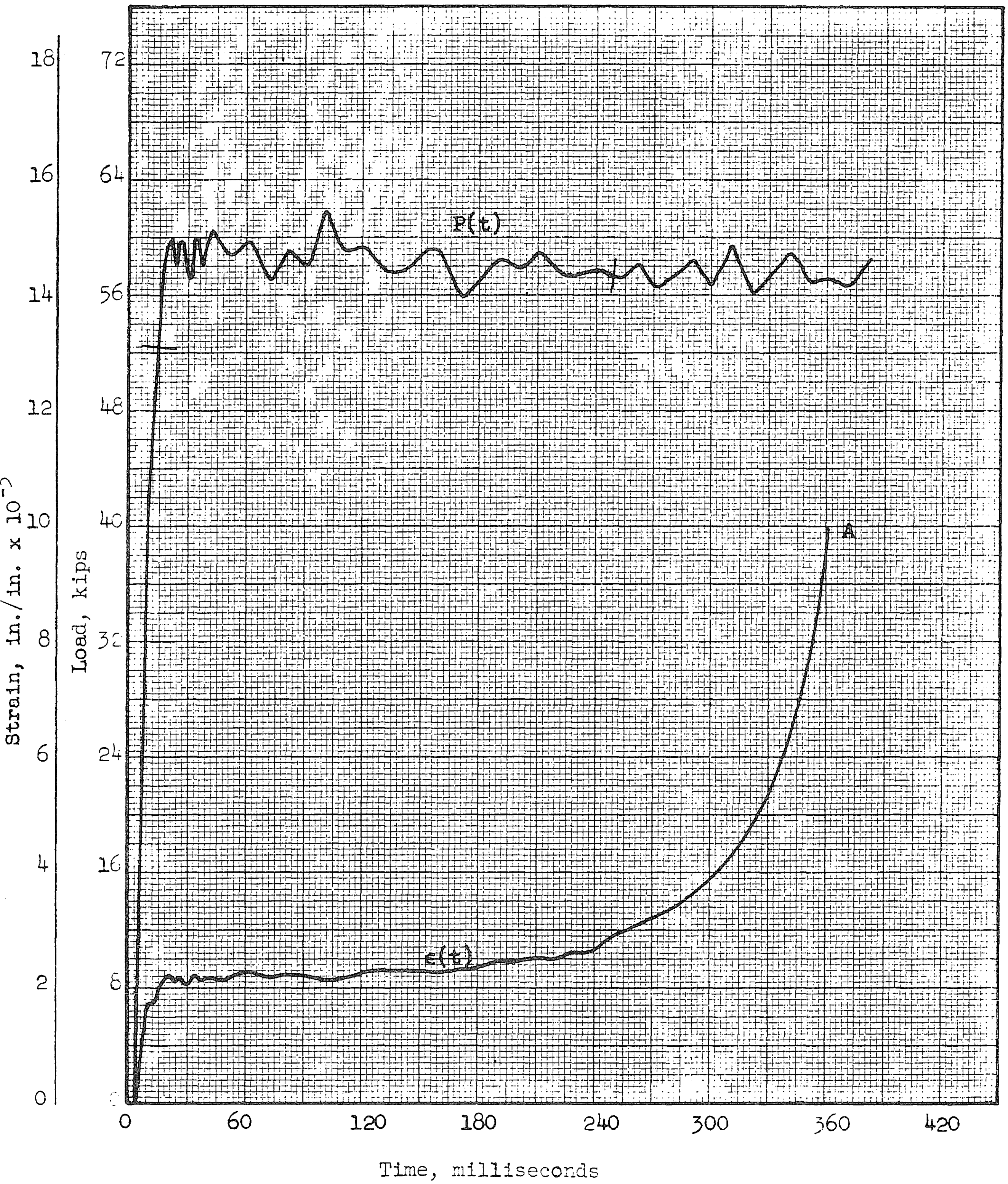

FIG. **A21a** LOAD AND STRAIN VS. TIME
SPECIMEN 9-48

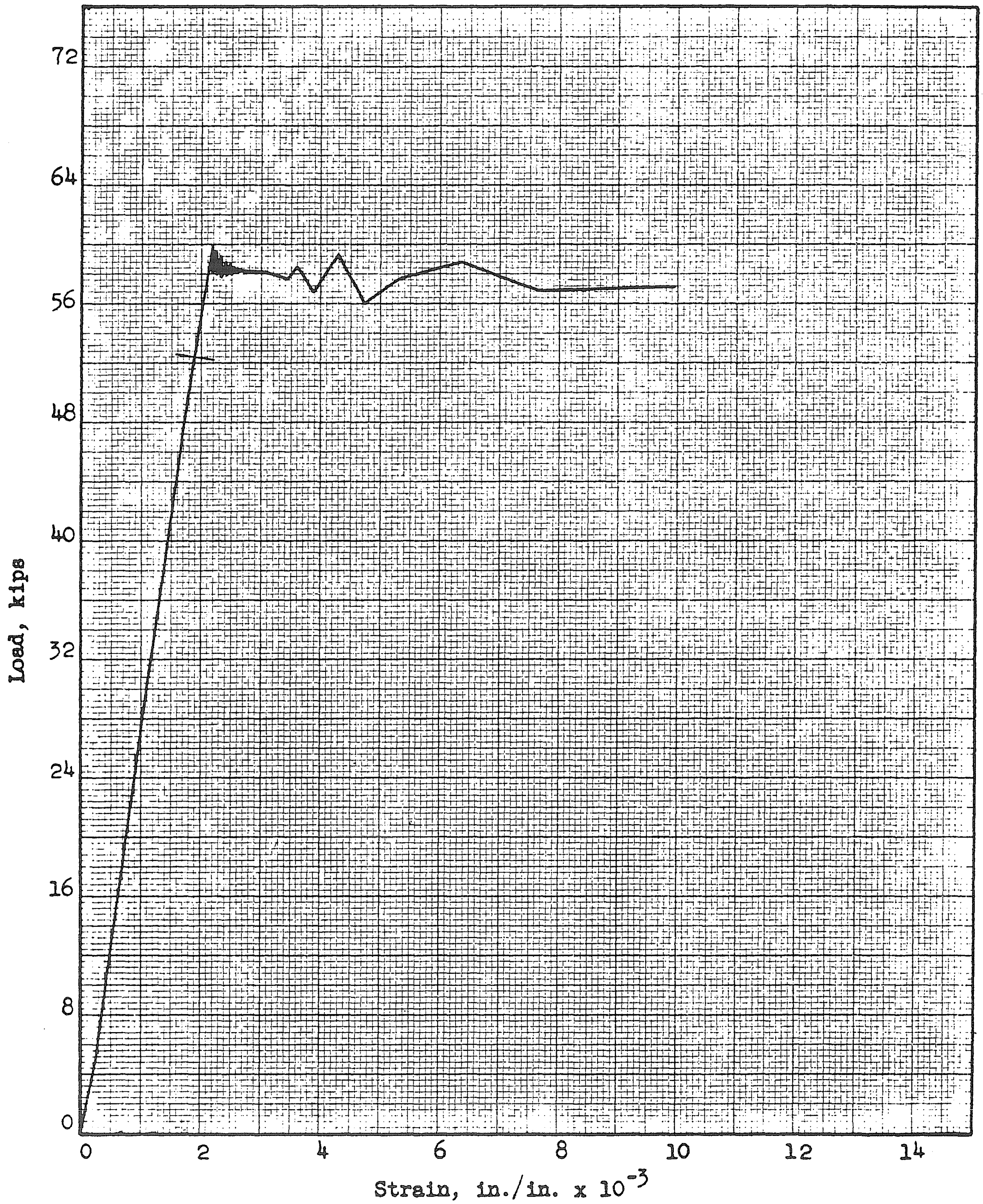

FIG. A21b LOAD VS. STRAIN
SPECIMEN 9-48

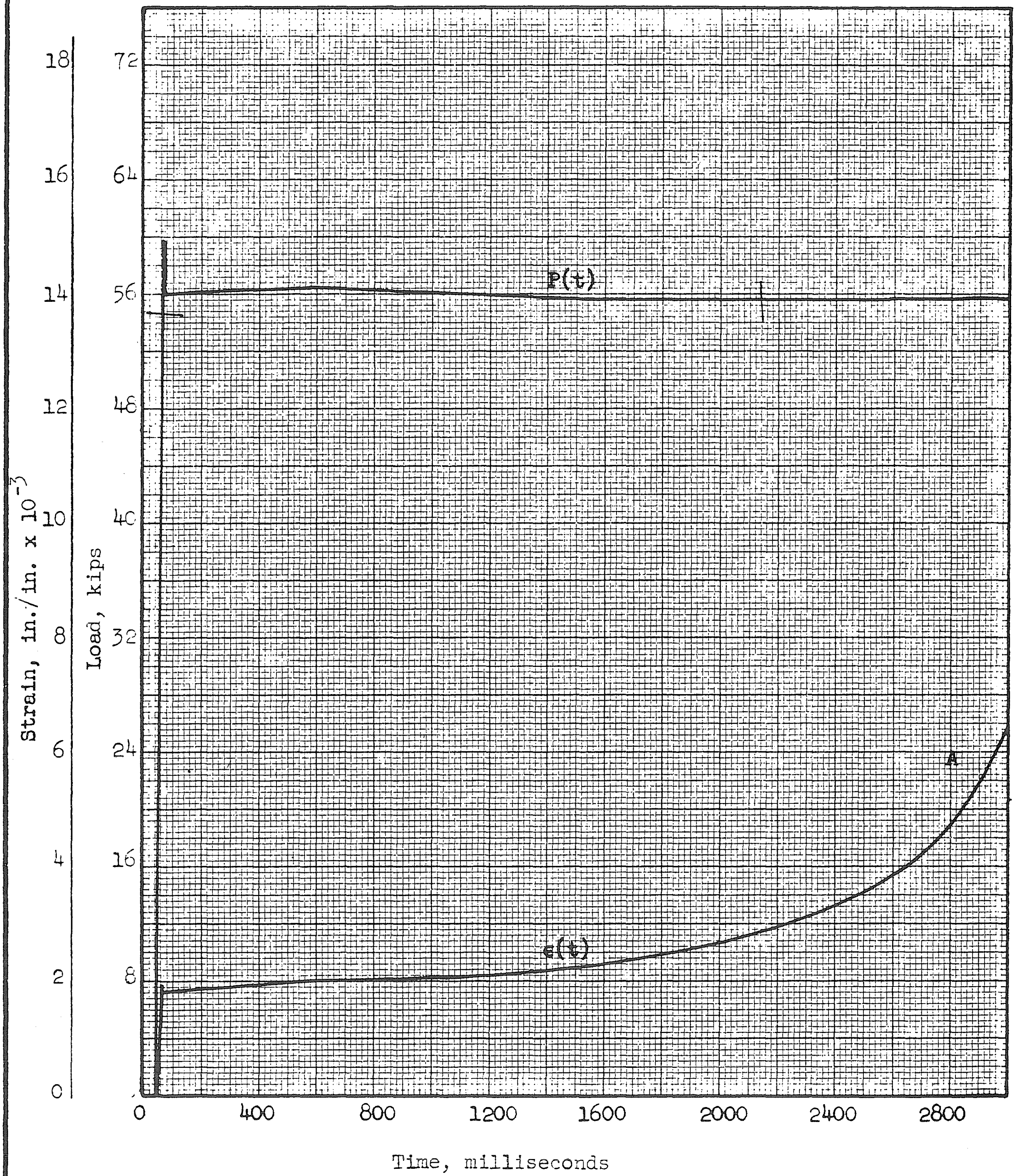

FIG. A22a LOAD AND STRAIN VS. TIME
SPECIMEN 9-51-1

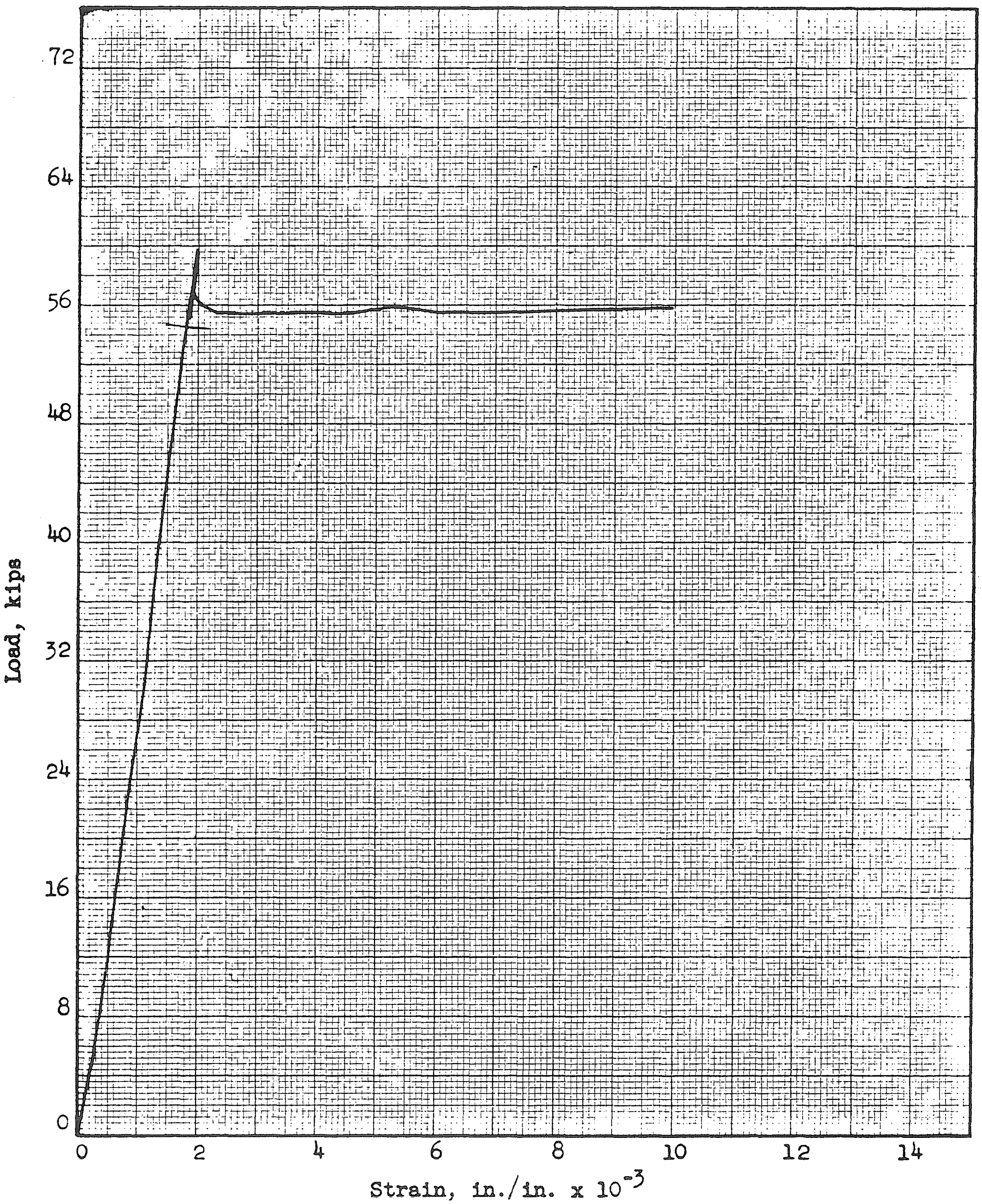

FIG. A22b LOAD VS. STRAIN
SPECIMEN 9-51-1

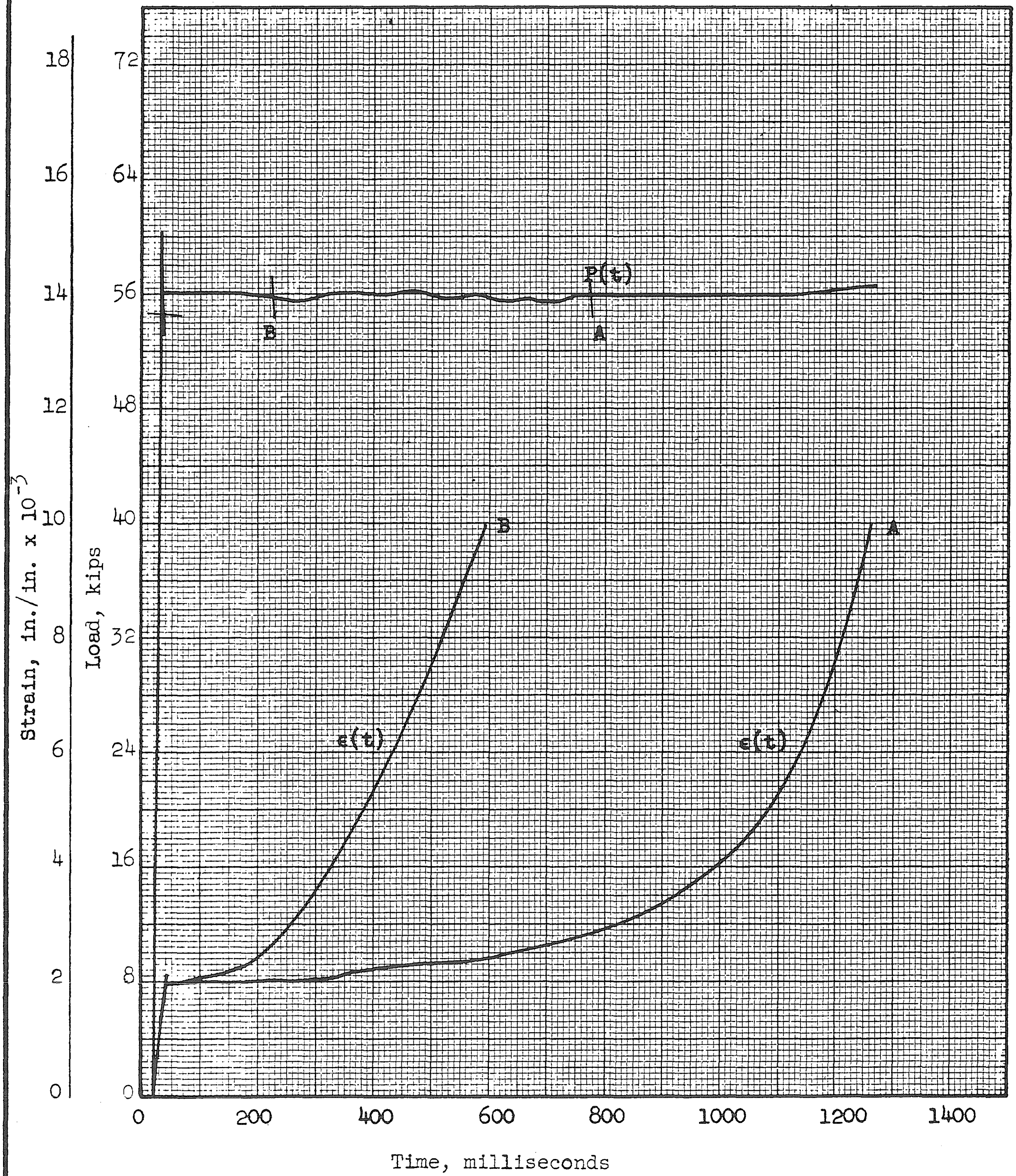

FIG. A23a LOAD AND STRAIN VS. TIME
SPECIMEN 9-51-2

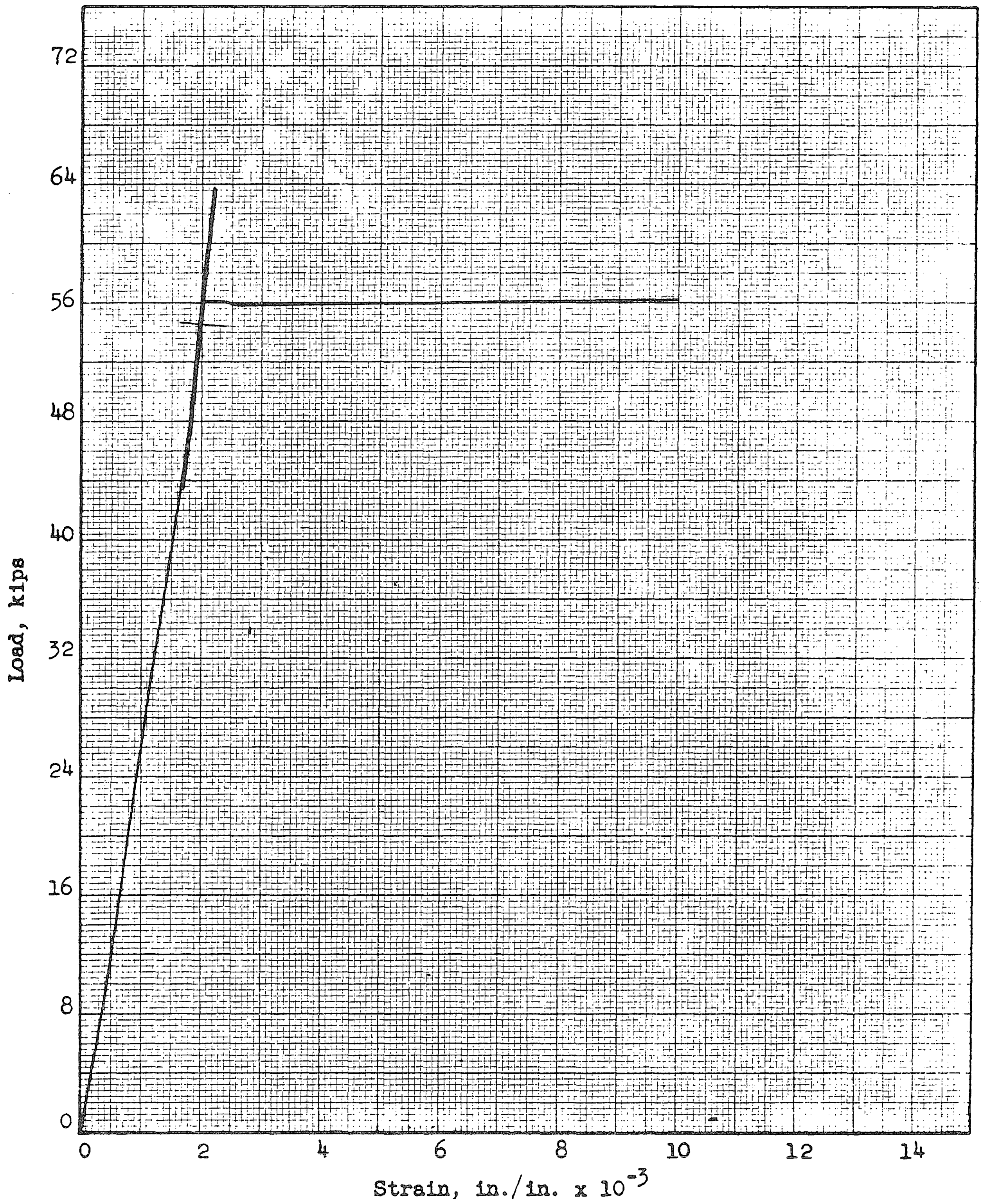

FIG. A23b LOAD VS. STRAIN
SPECIMEN 9-51-2

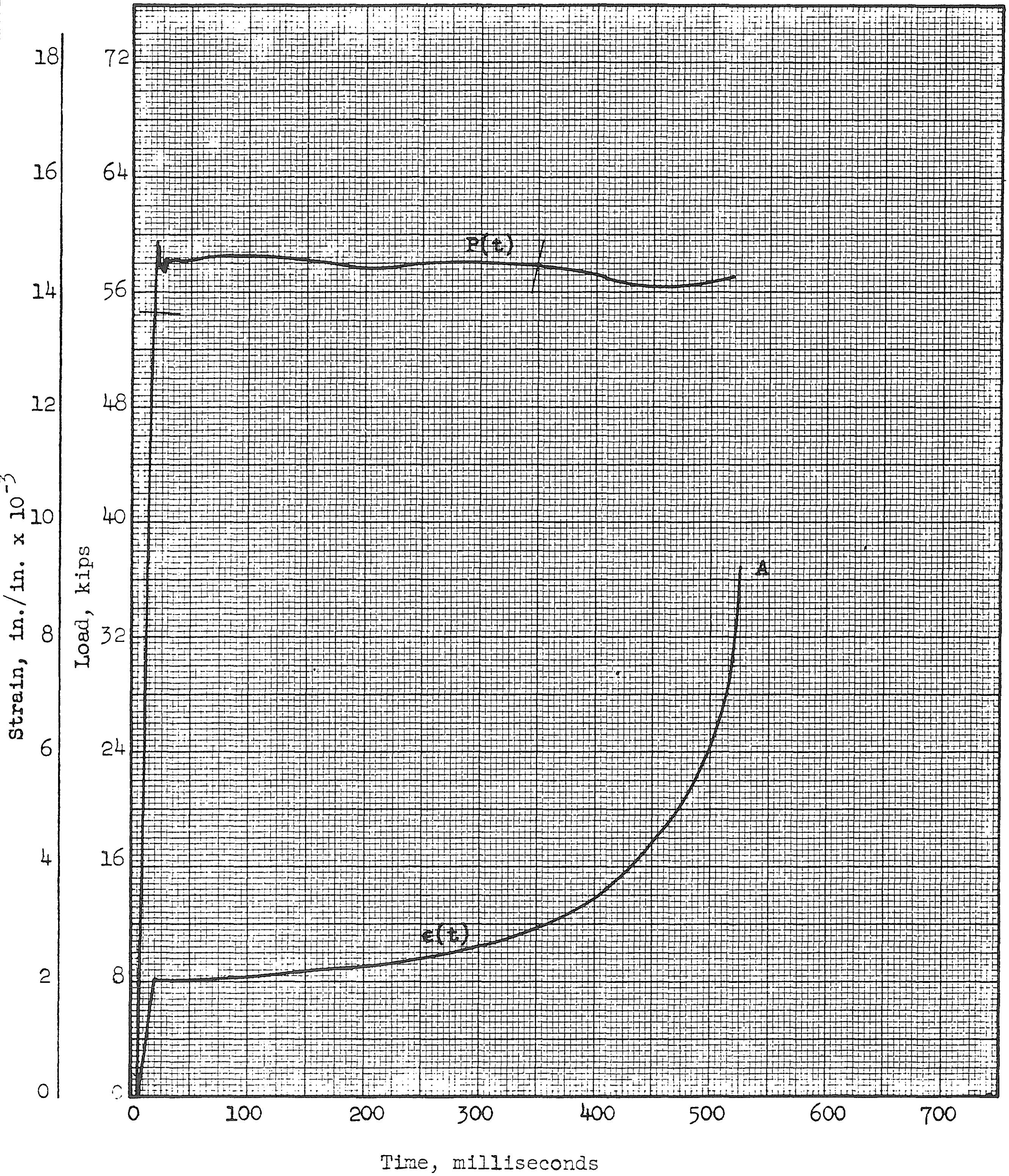

FIG. A24a LOAD AND STRAIN VS. TIME
SPECIMEN 9-51-3

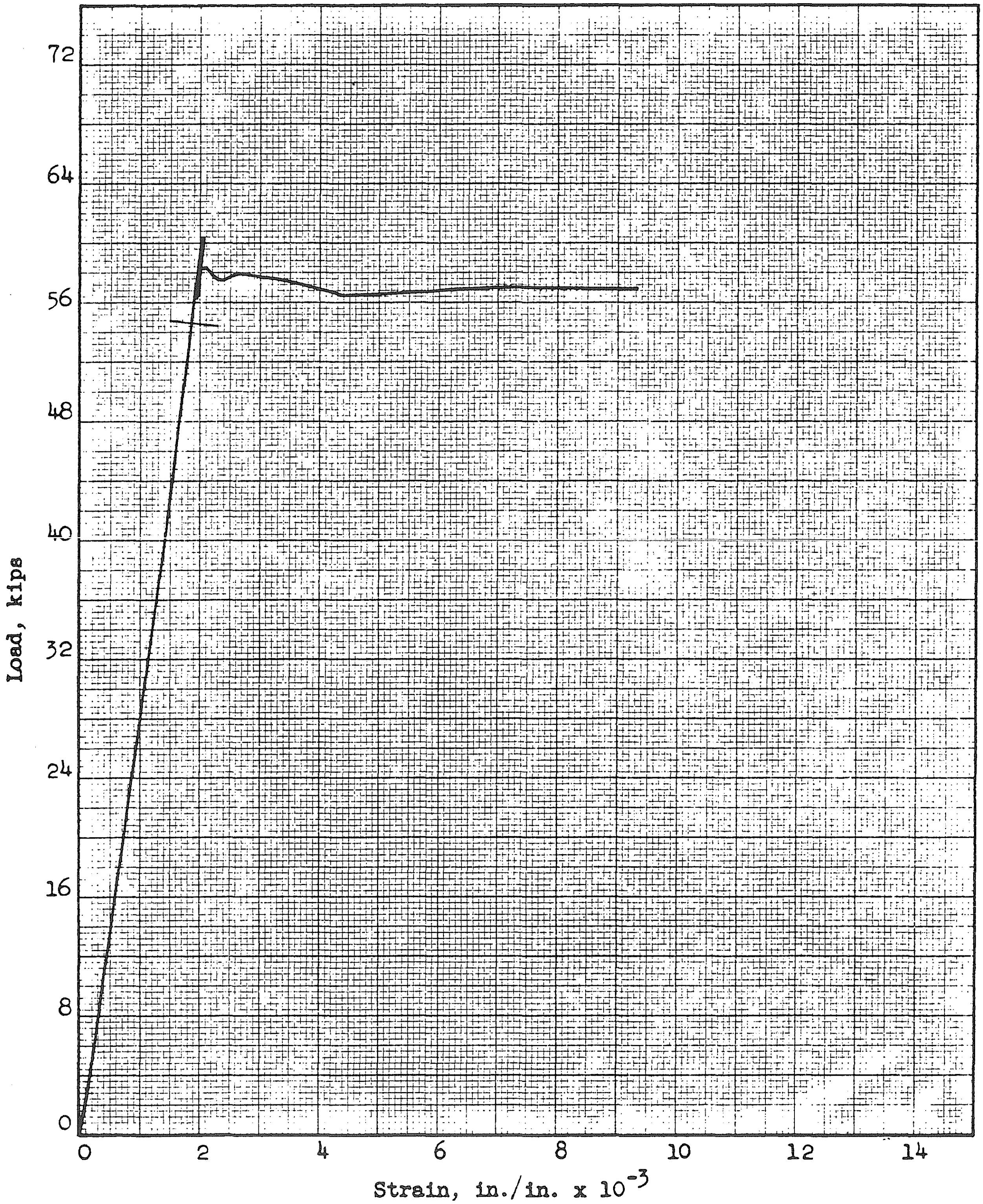

FIG. A24b LOAD VS. STRAIN
SPECIMEN 9-51-3

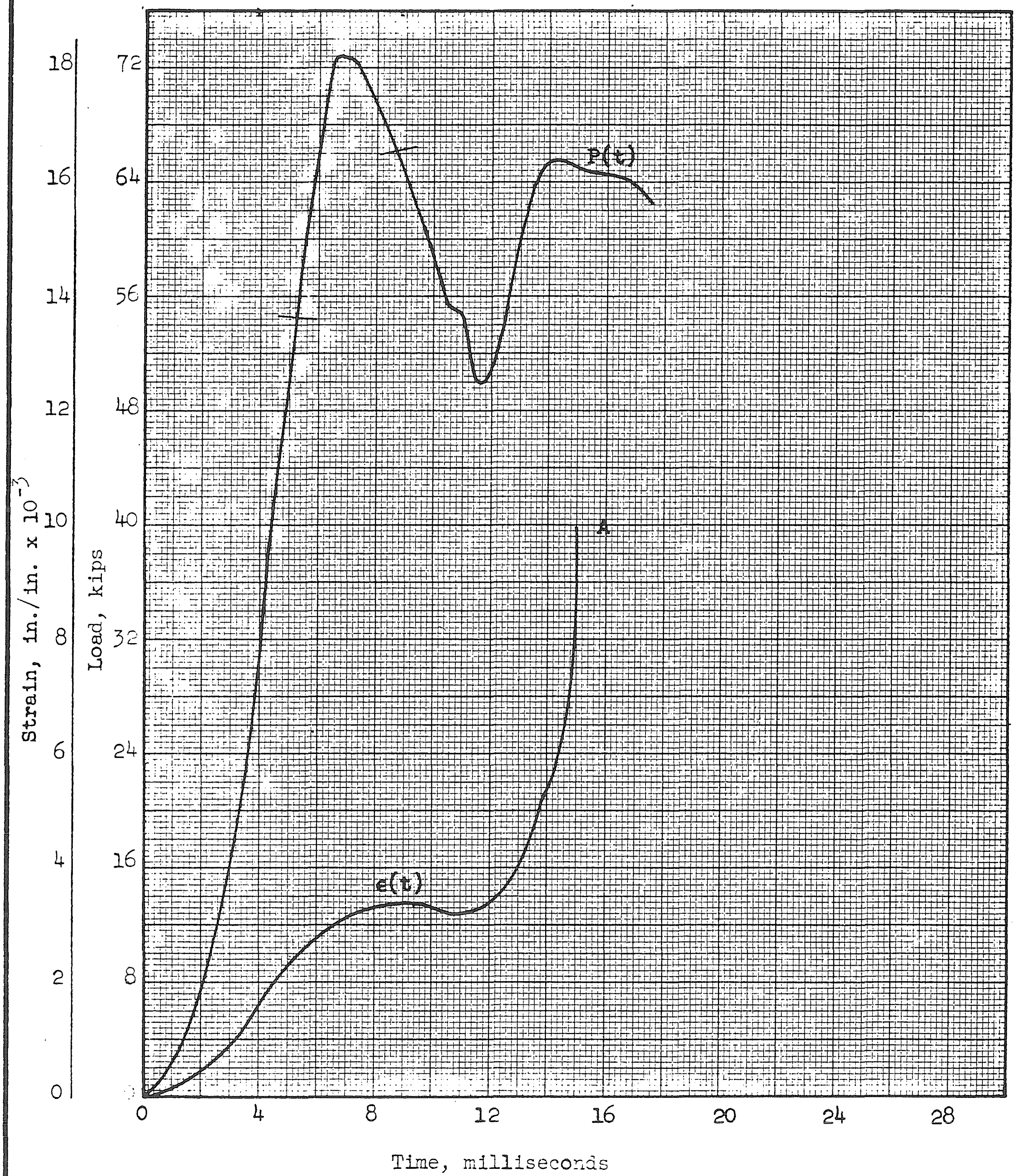

FIG. A25a LOAD AND STRAIN VS. TIME
SPECIMEN 9-51-4

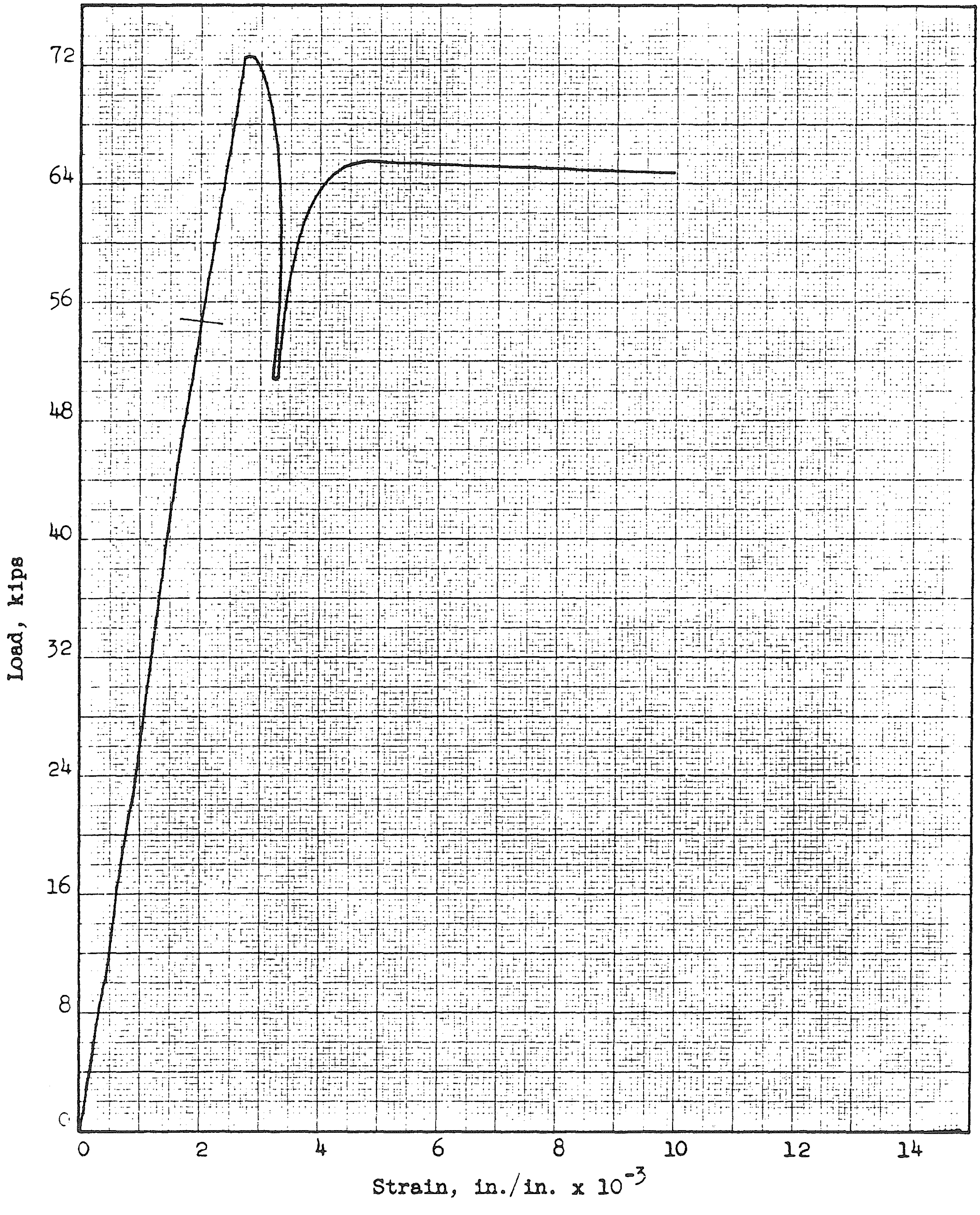

FIG. A25b LOAD VS. STRAIN
SPECIMEN 9-51-4

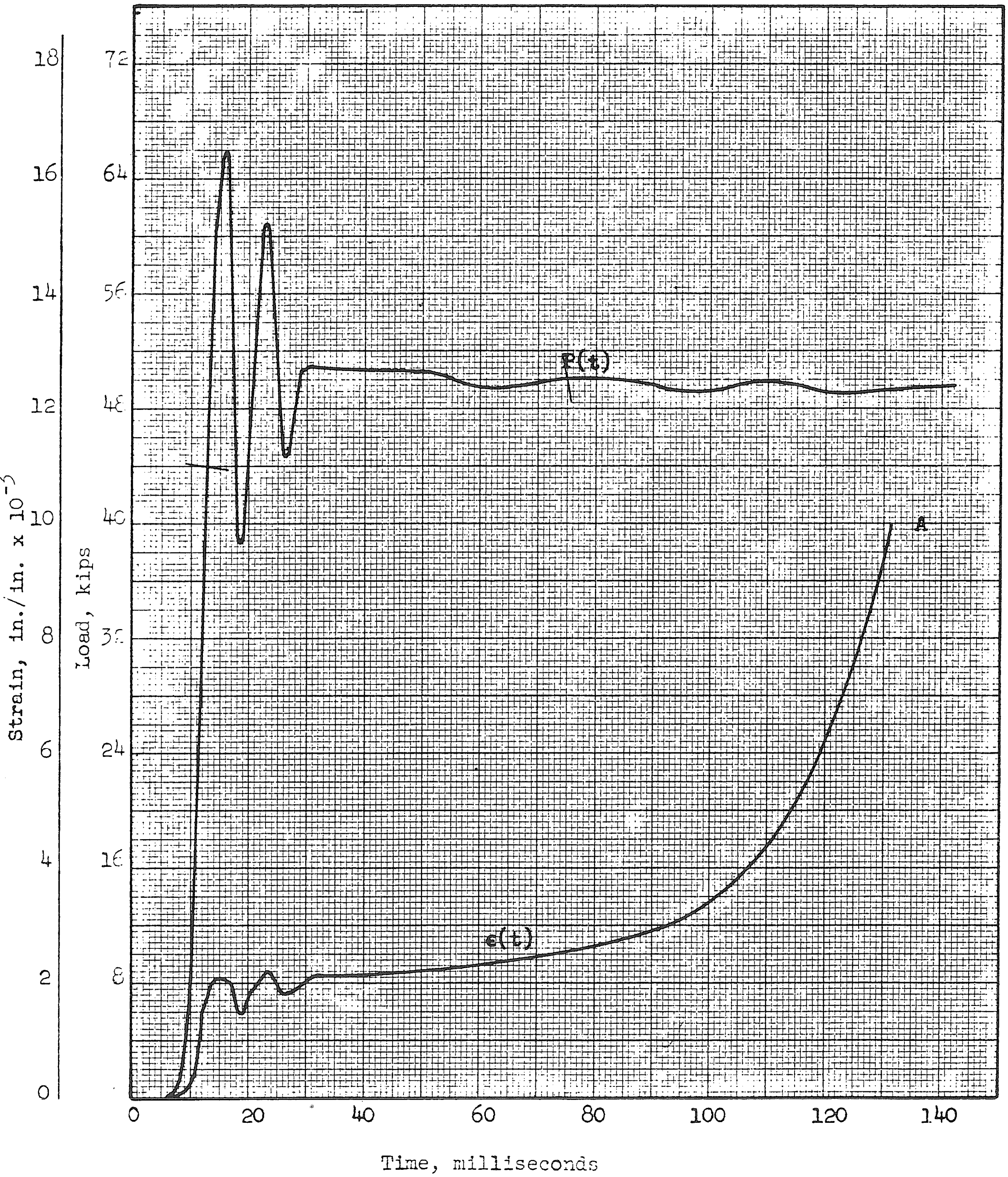

FIG. A26a LOAD AND STRAIN VS. TIME
SPECIMEN 9-69-2

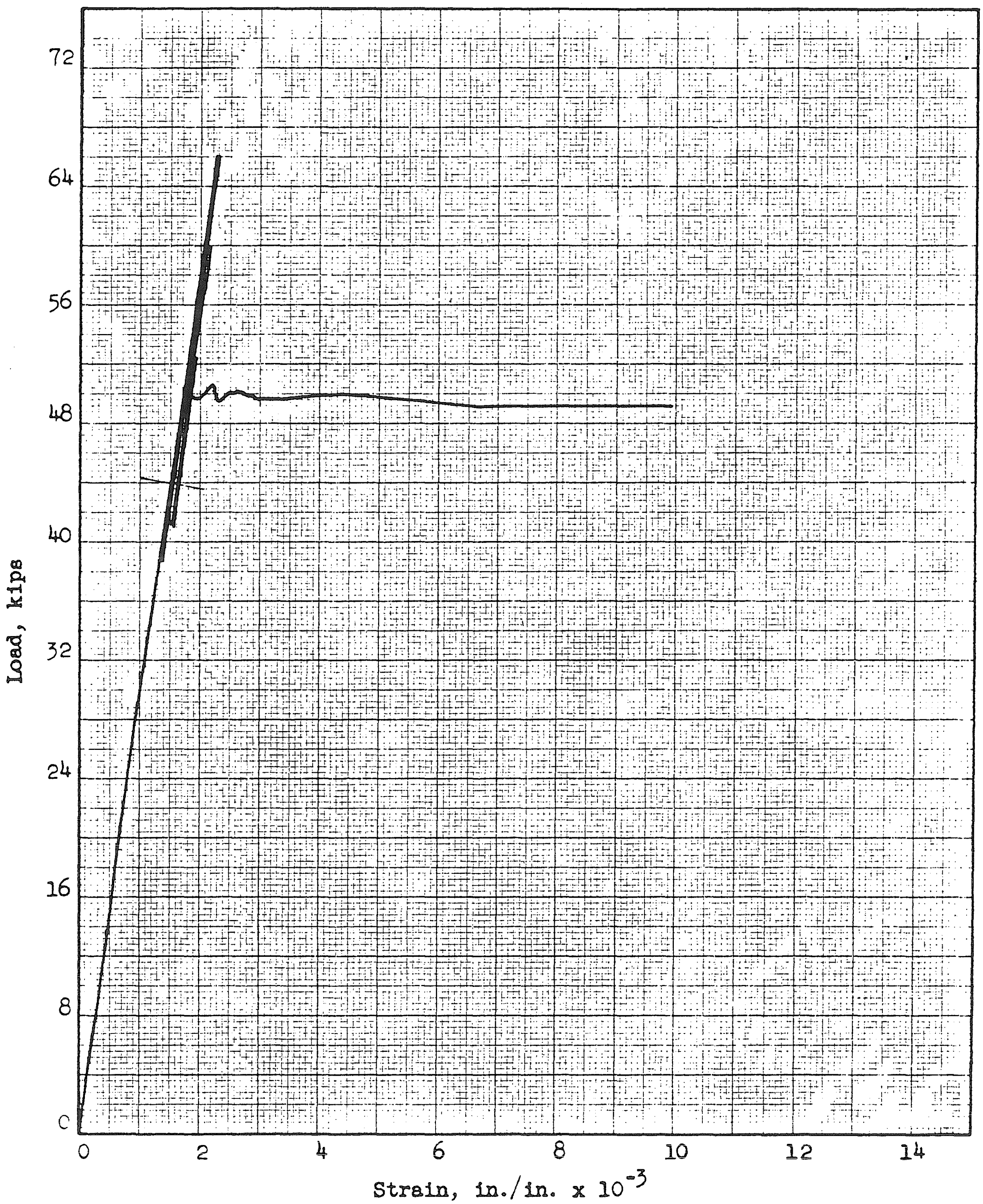

FIG. A26b LOAD VS. STRAIN
SPECIMEN 9-69-2

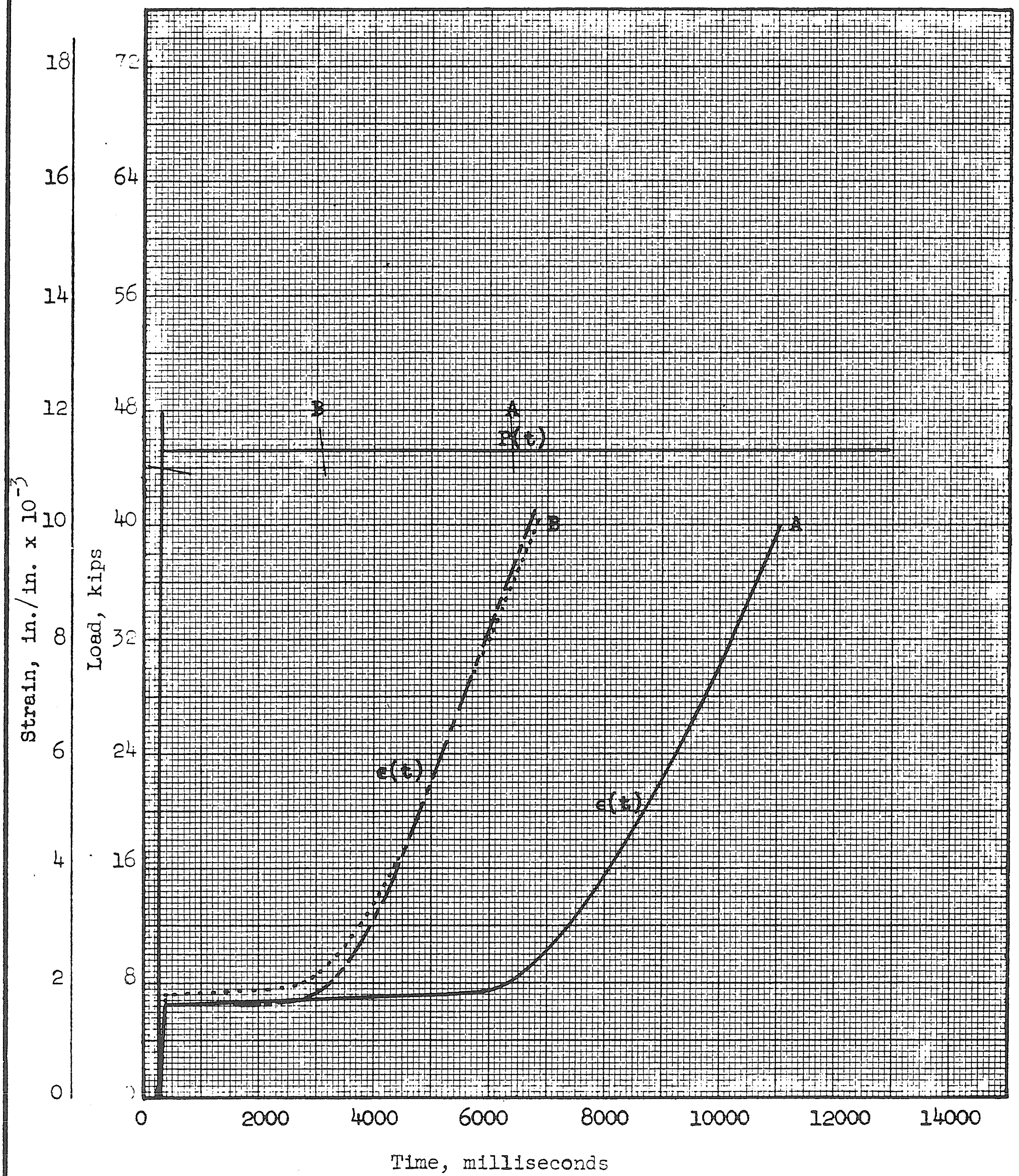

FIG. A27a LOAD AND STRAIN VS. TIME
SPECIMEN 9-69-4

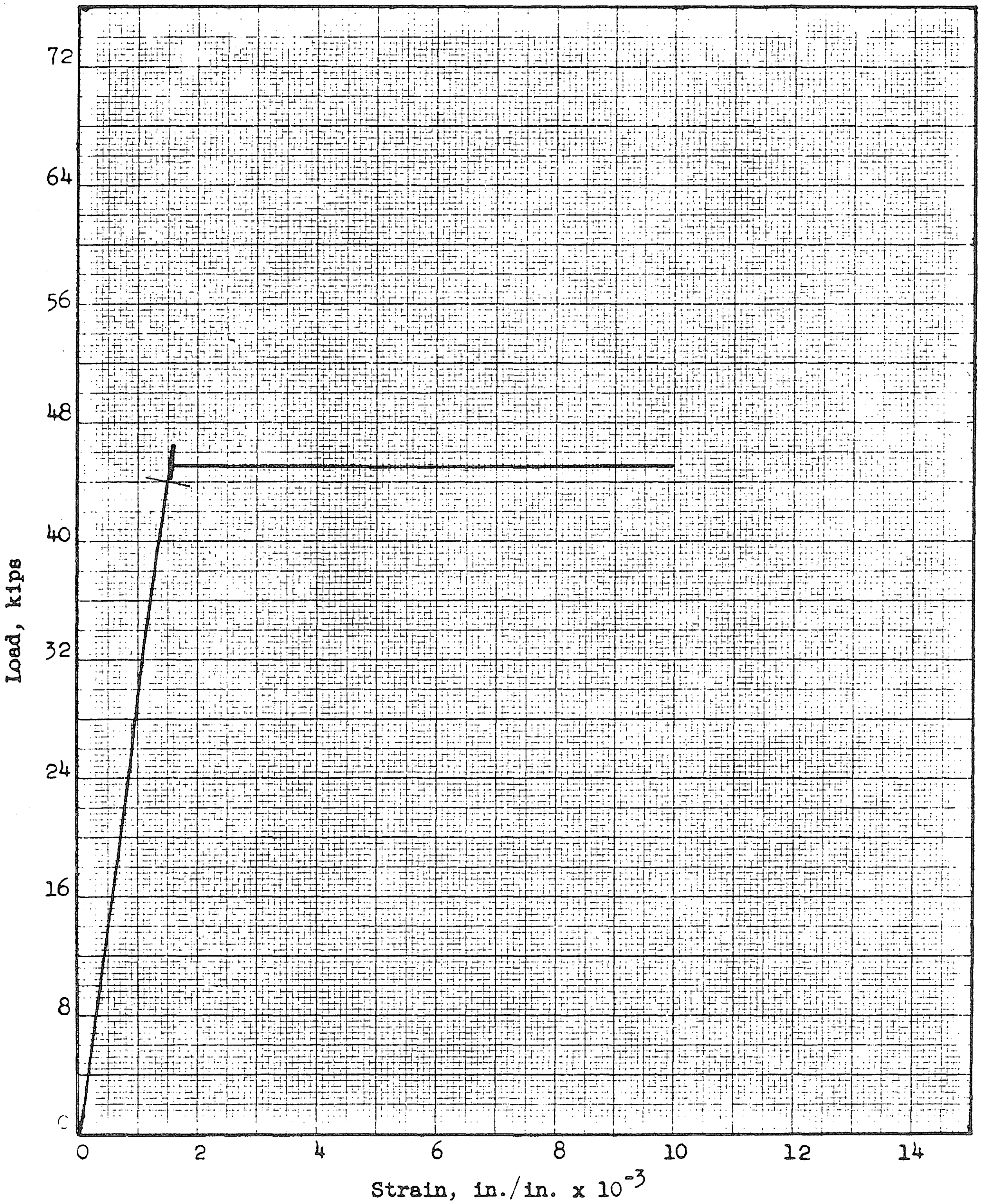

FIG. A27b LOAD VS. STRAIN
SPECIMEN 9-69-4

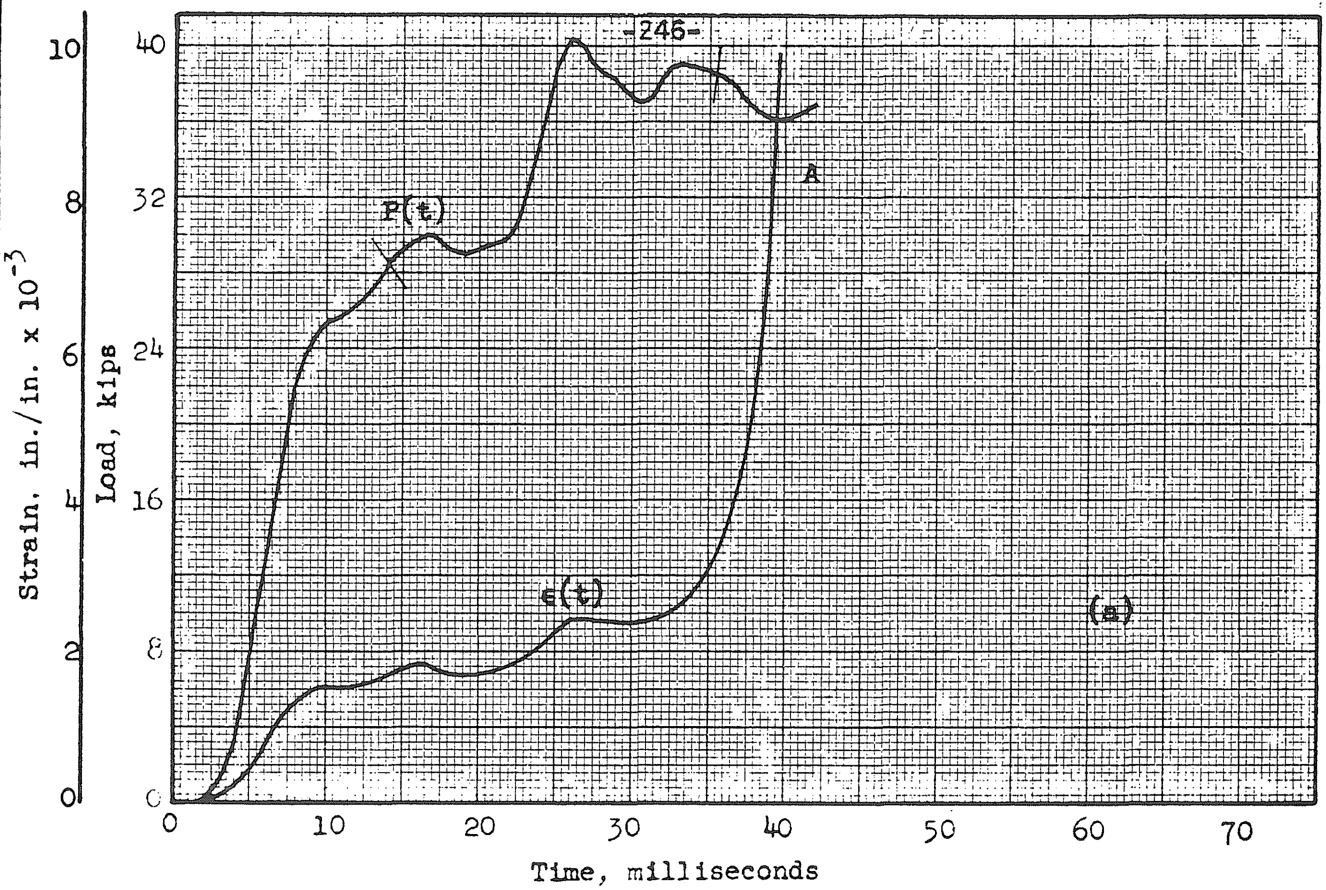

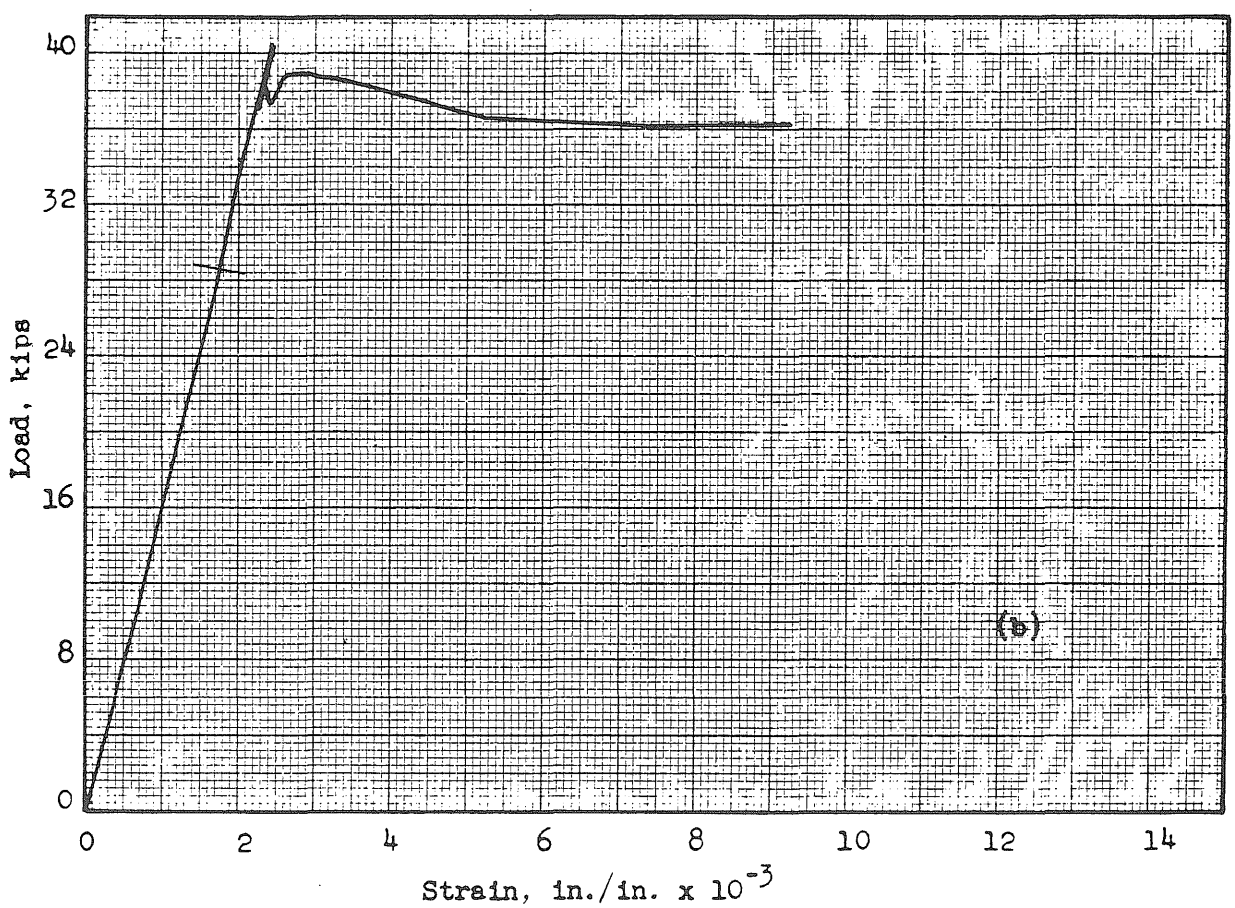

FIG. A28 LOAD AND STRAIN VS. TIME AND LOAD VS. STRAIN
SPECIMEN 7-9

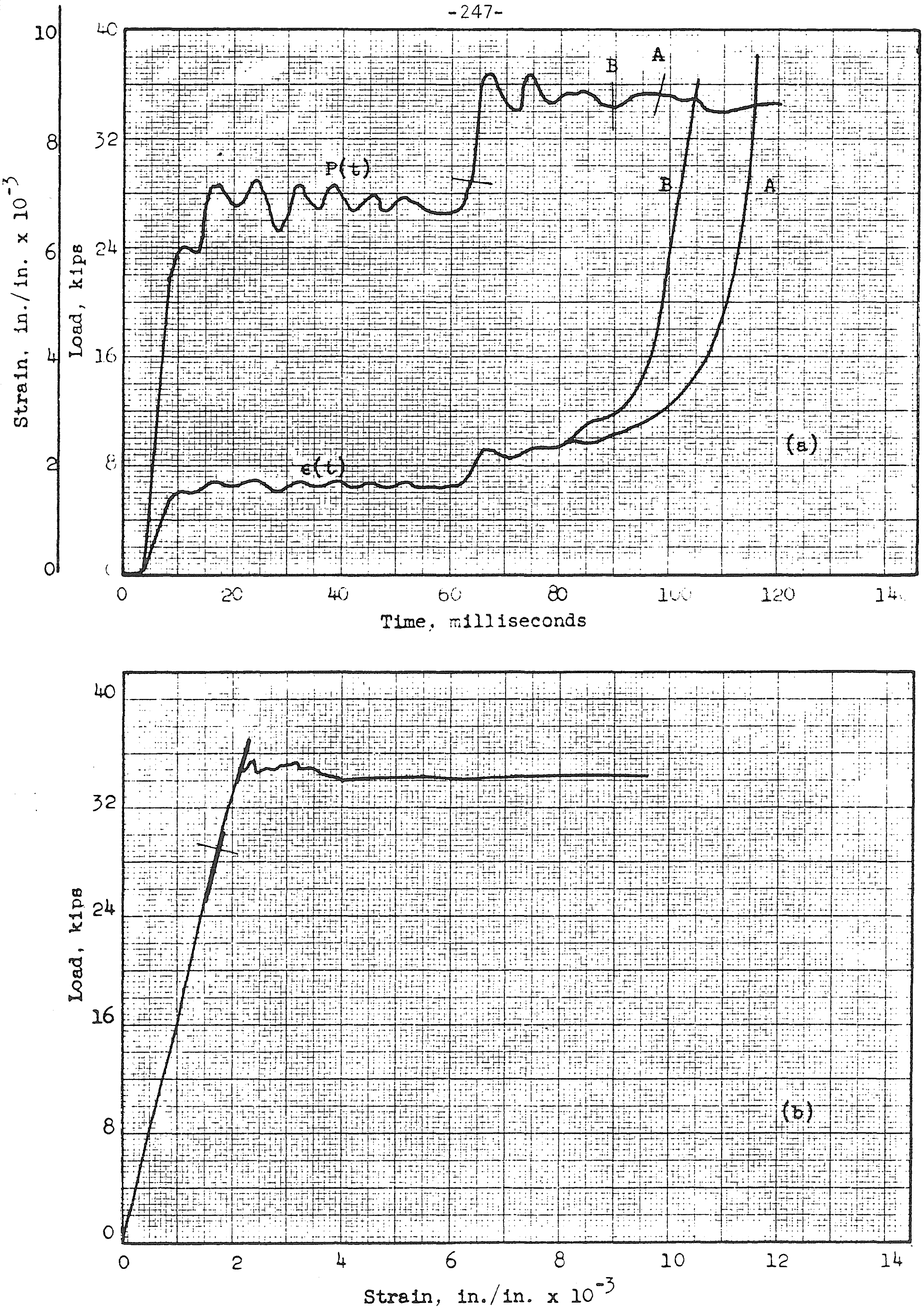

FIG. A29 LOAD AND STRAIN VS. TIME AND LOAD VS. STRAIN
SPECIMEN 7-10

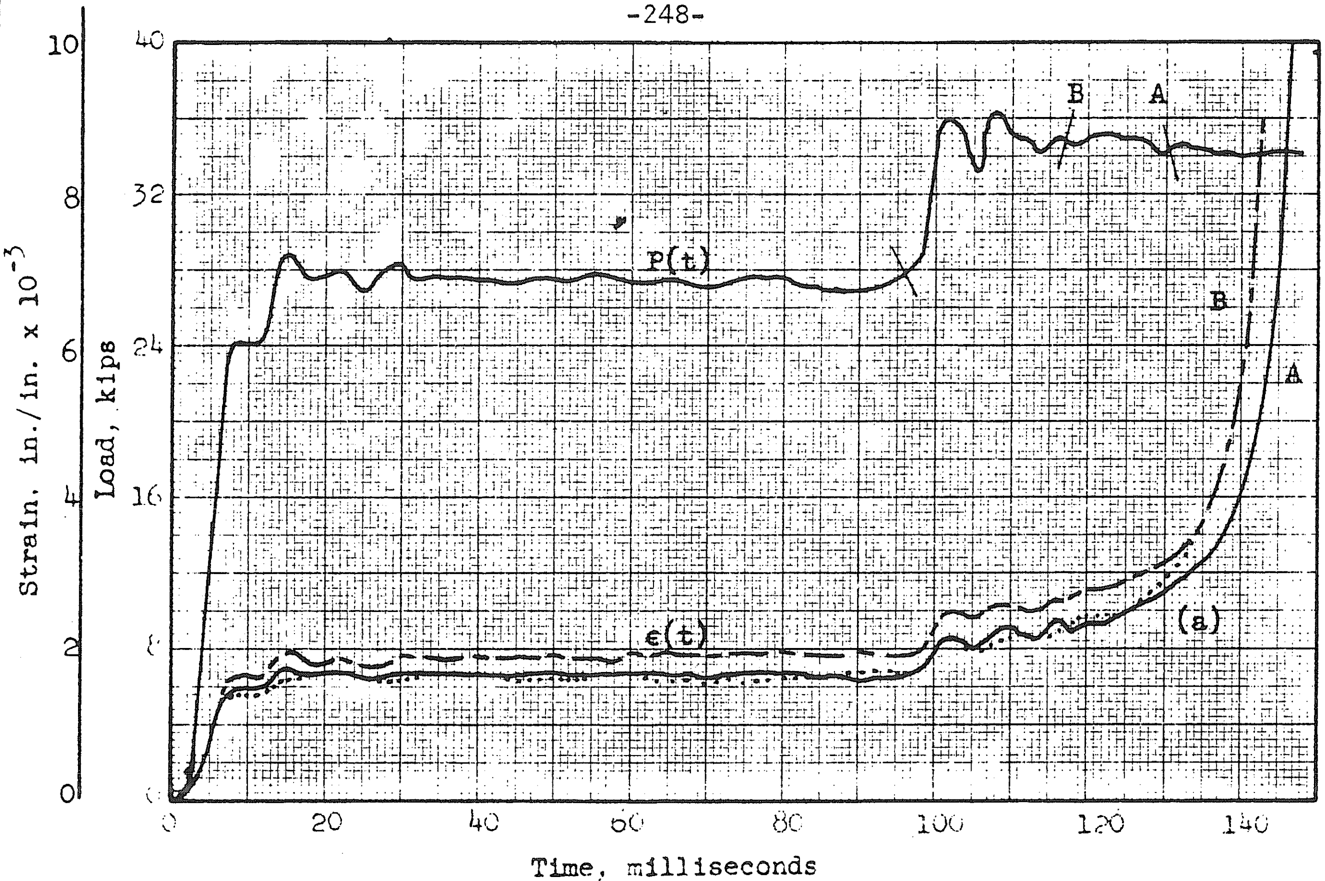

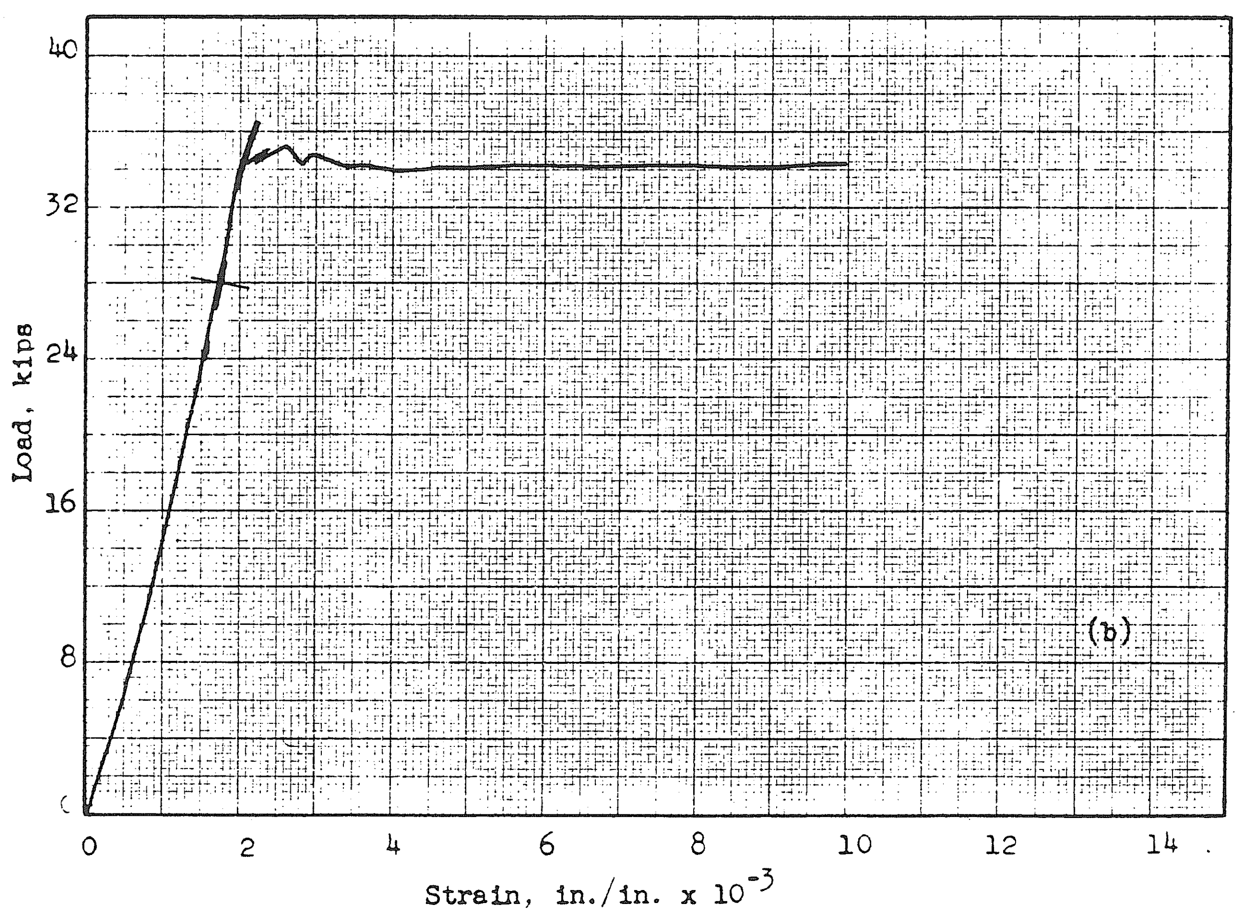

FIG. A30 LOAD AND STRAIN VS. TIME AND LOAD VS. STRAIN
SPECIMEN 7-18

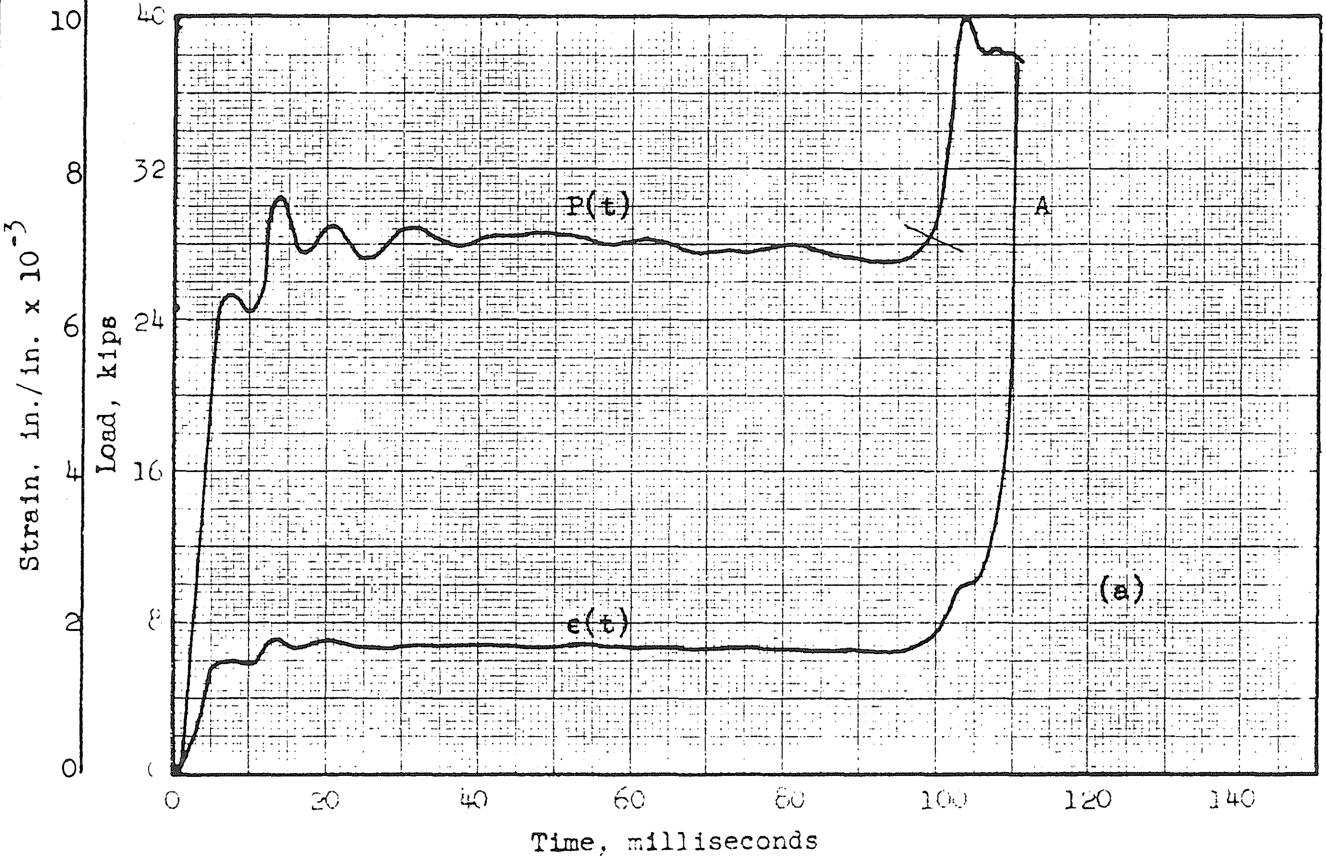

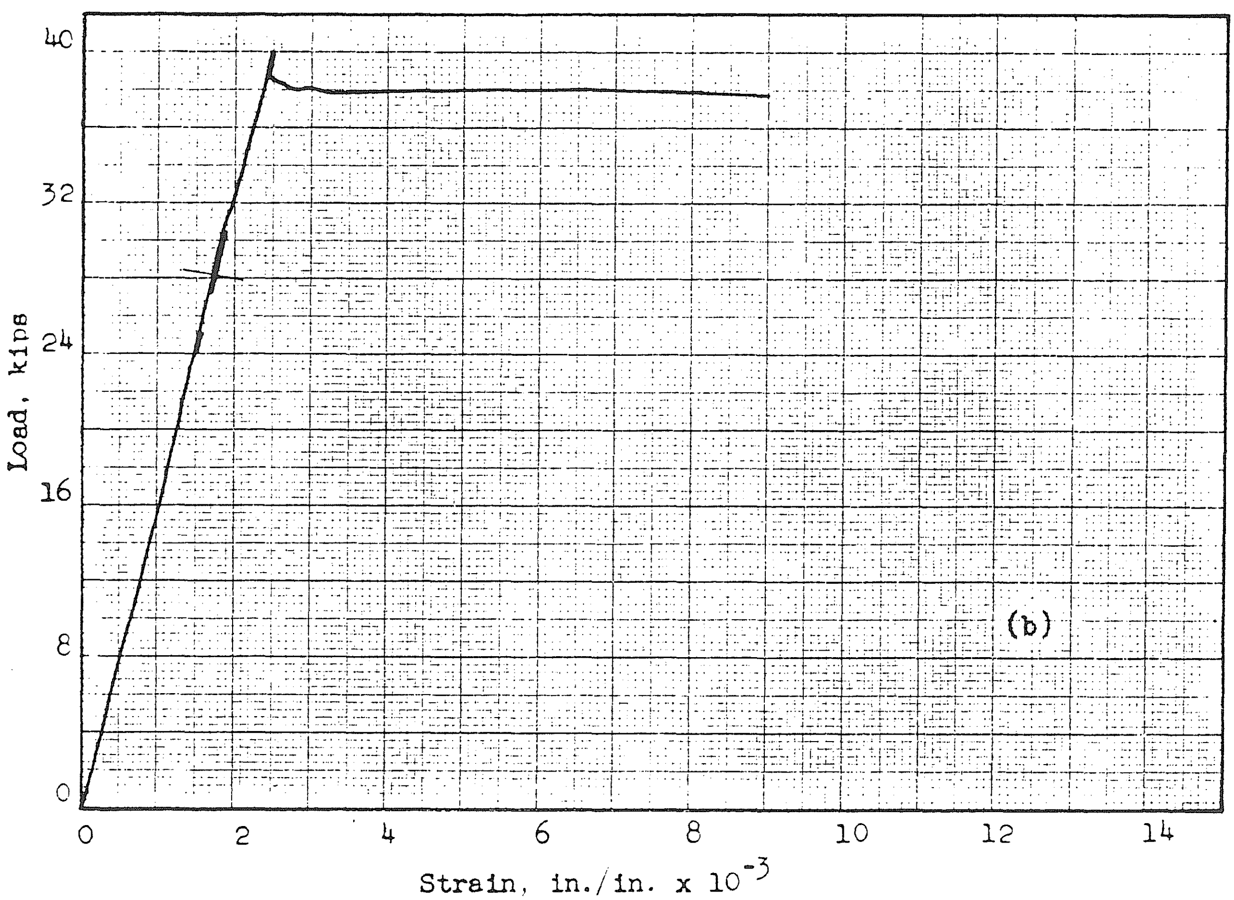

FIG. A31 LOAD AND STRAIN VS. TIME AND LOAD VS. STRAIN
SPECIMEN 7-23

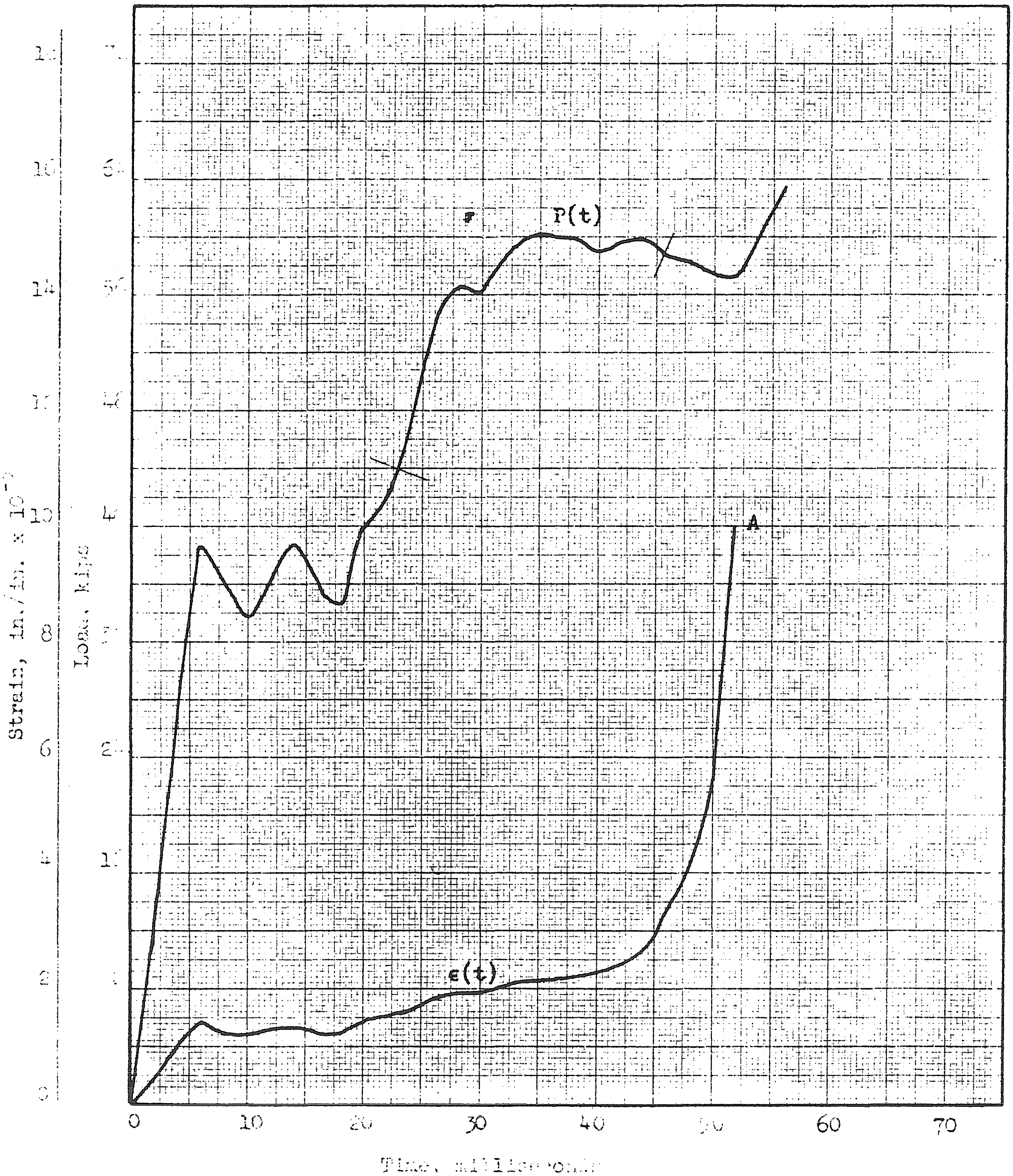

FIG. A32a LOAD AND STRAIN VS. TIME
SPECIMEN 9-69-1

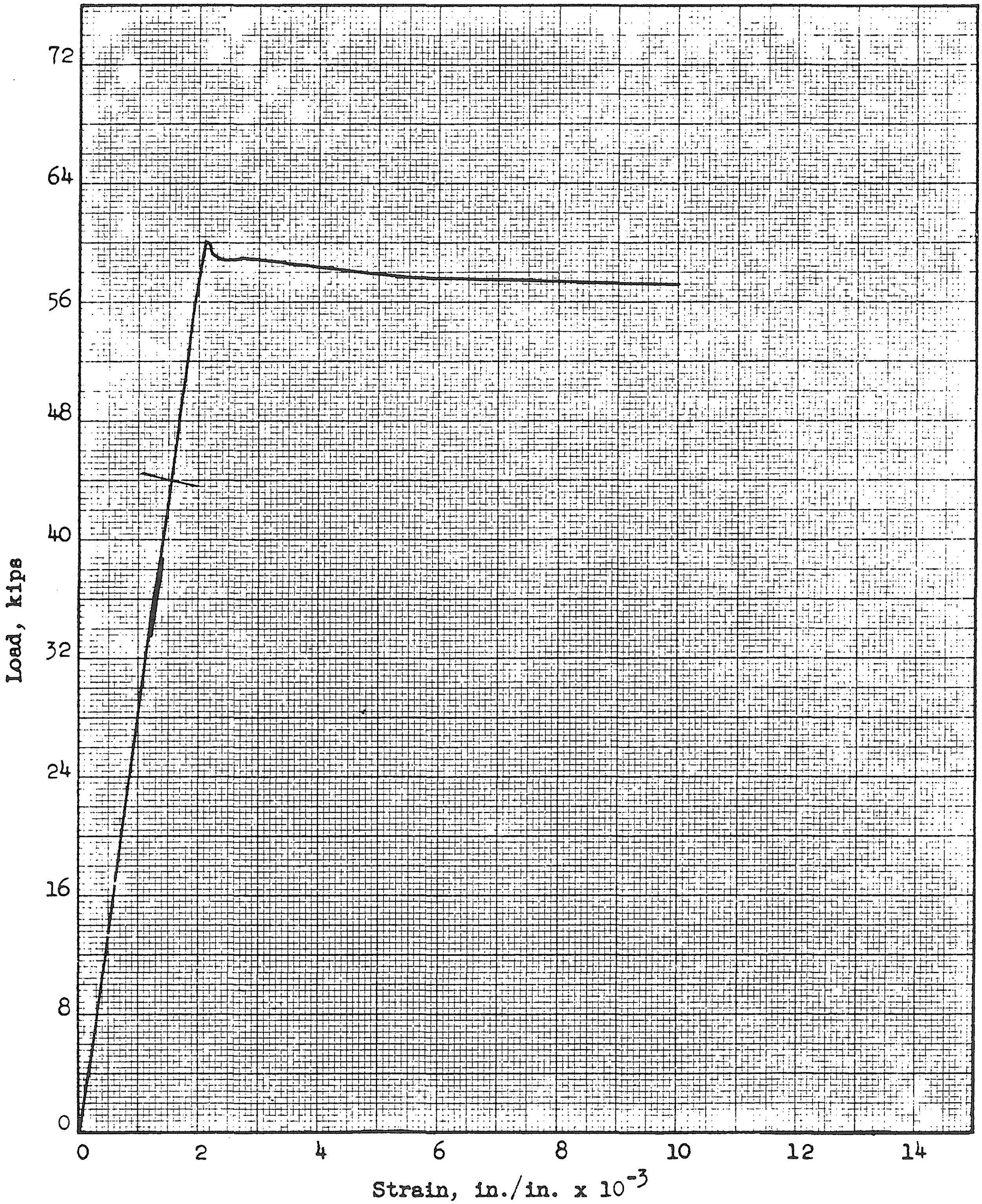

FIG. A32b LOAD VS. STRAIN
SPECIMEN 9-69-1

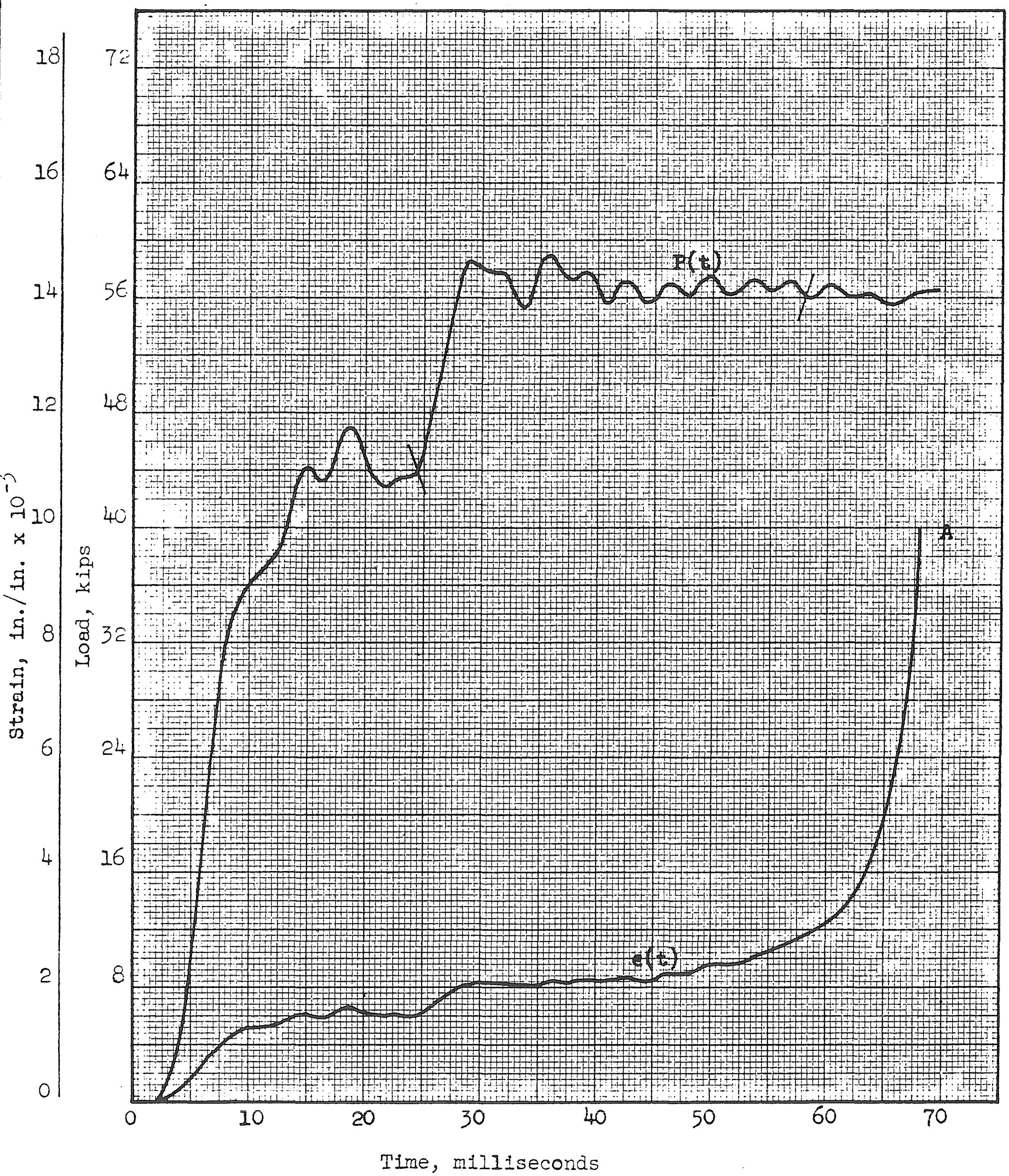

FIG. A33a LOAD AND STRAIN VS. TIME
SPECIMEN 9-69-3

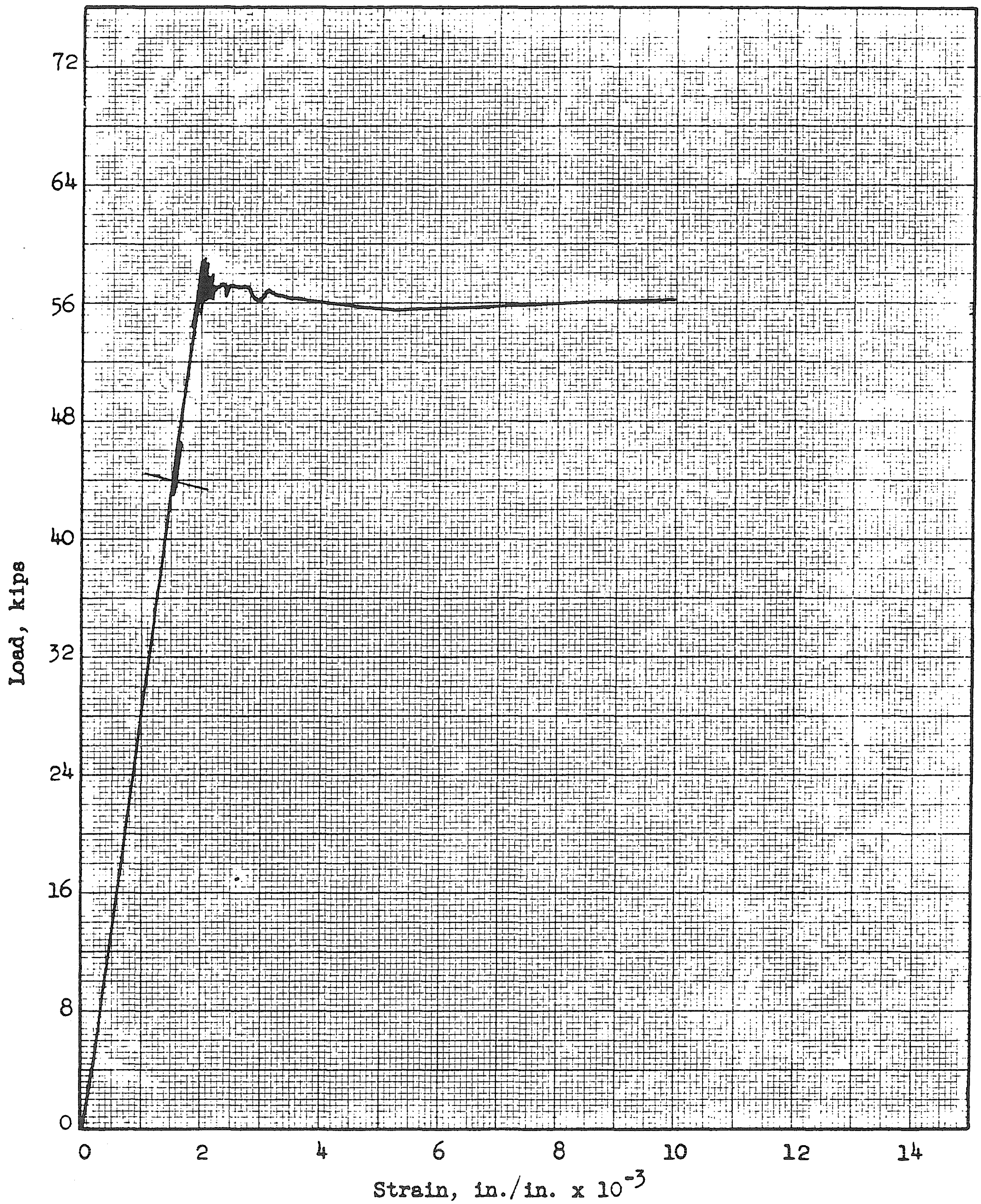

FIG. A33b LOAD VS. STRAIN
SPECIMEN 9-69-3

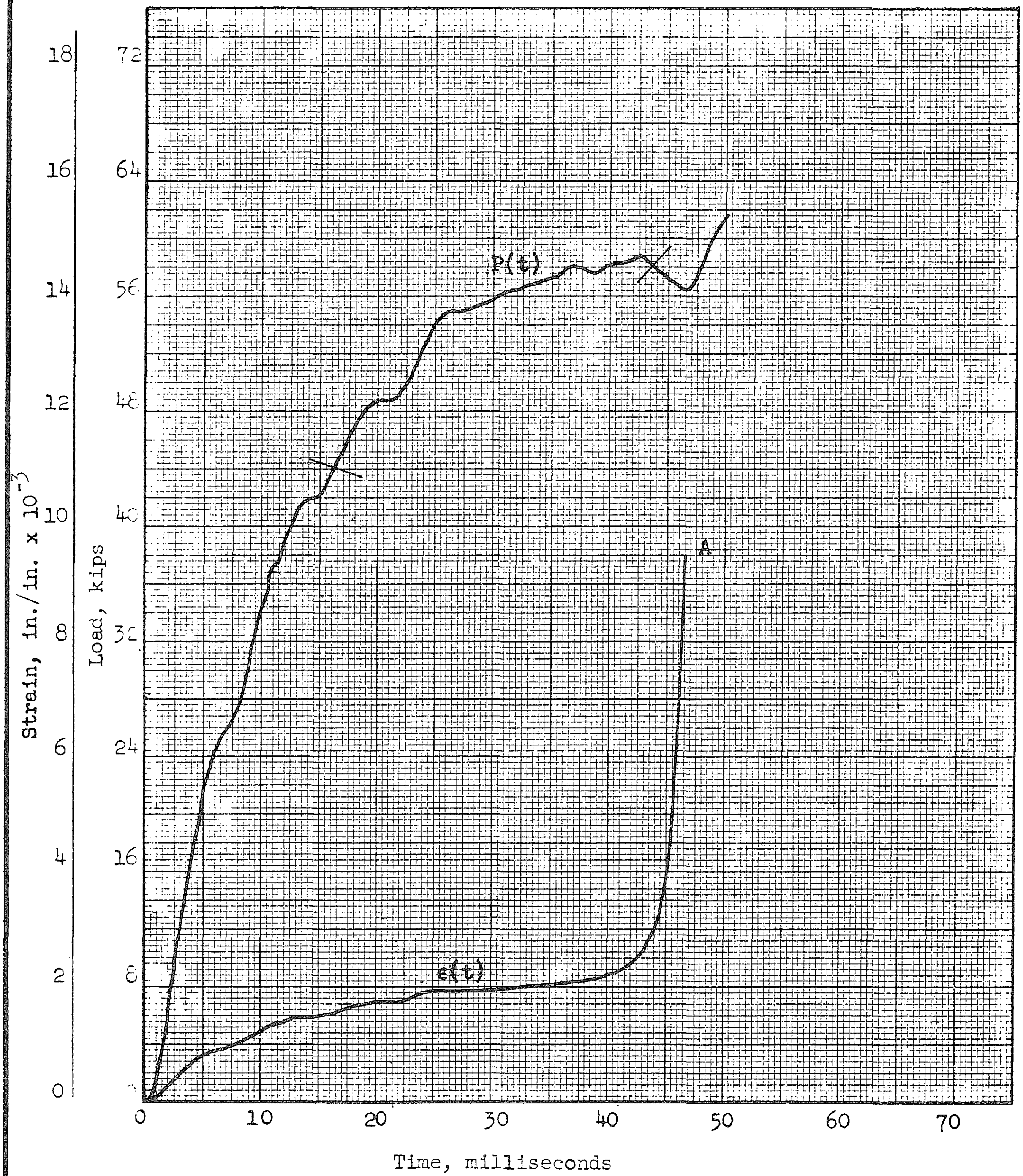

FIG. A34a LOAD AND STRAIN VS. TIME
SPECIMEN 9-61

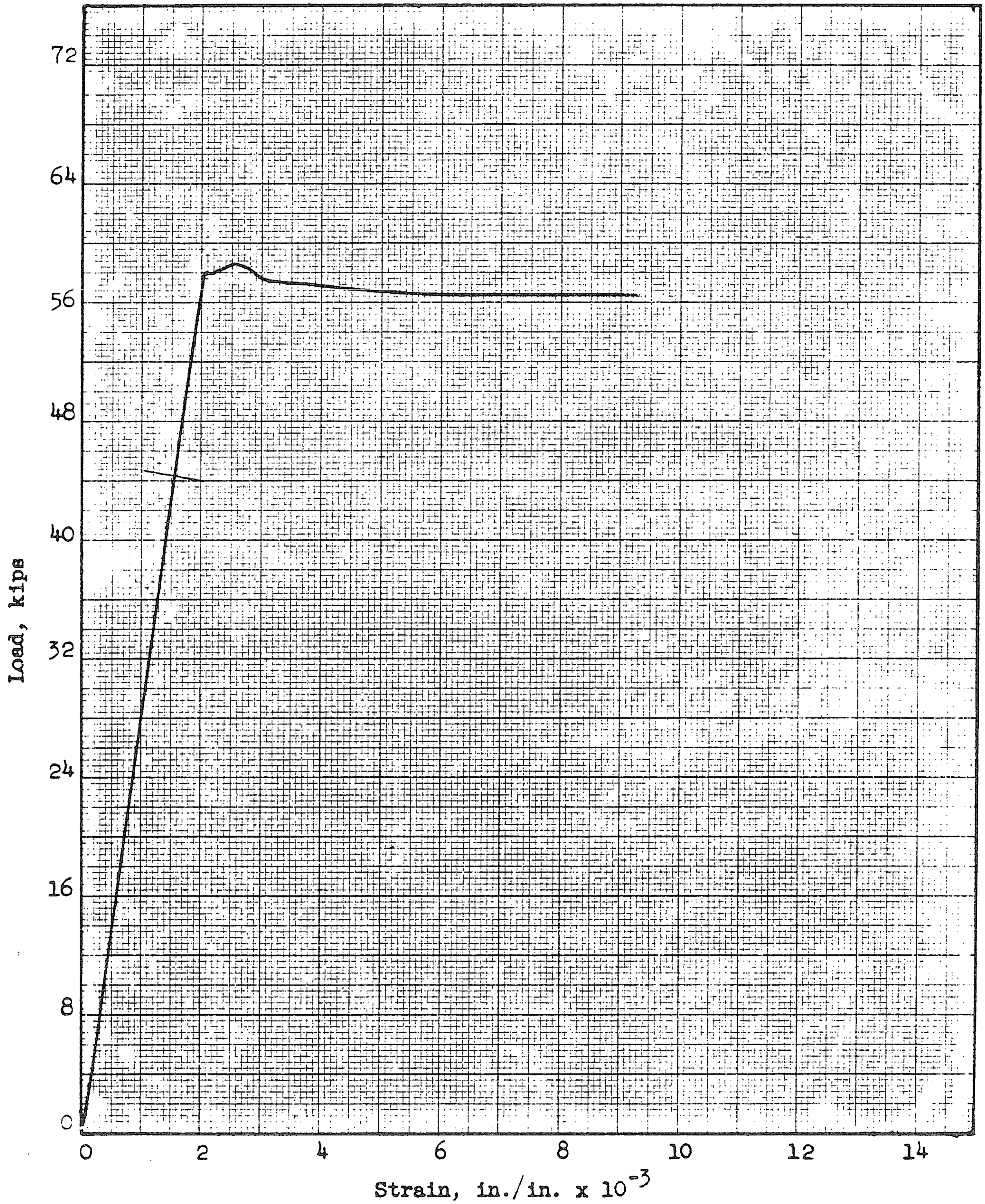

FIG. A34b LOAD VS. STRAIN
SPECIMEN 9-61

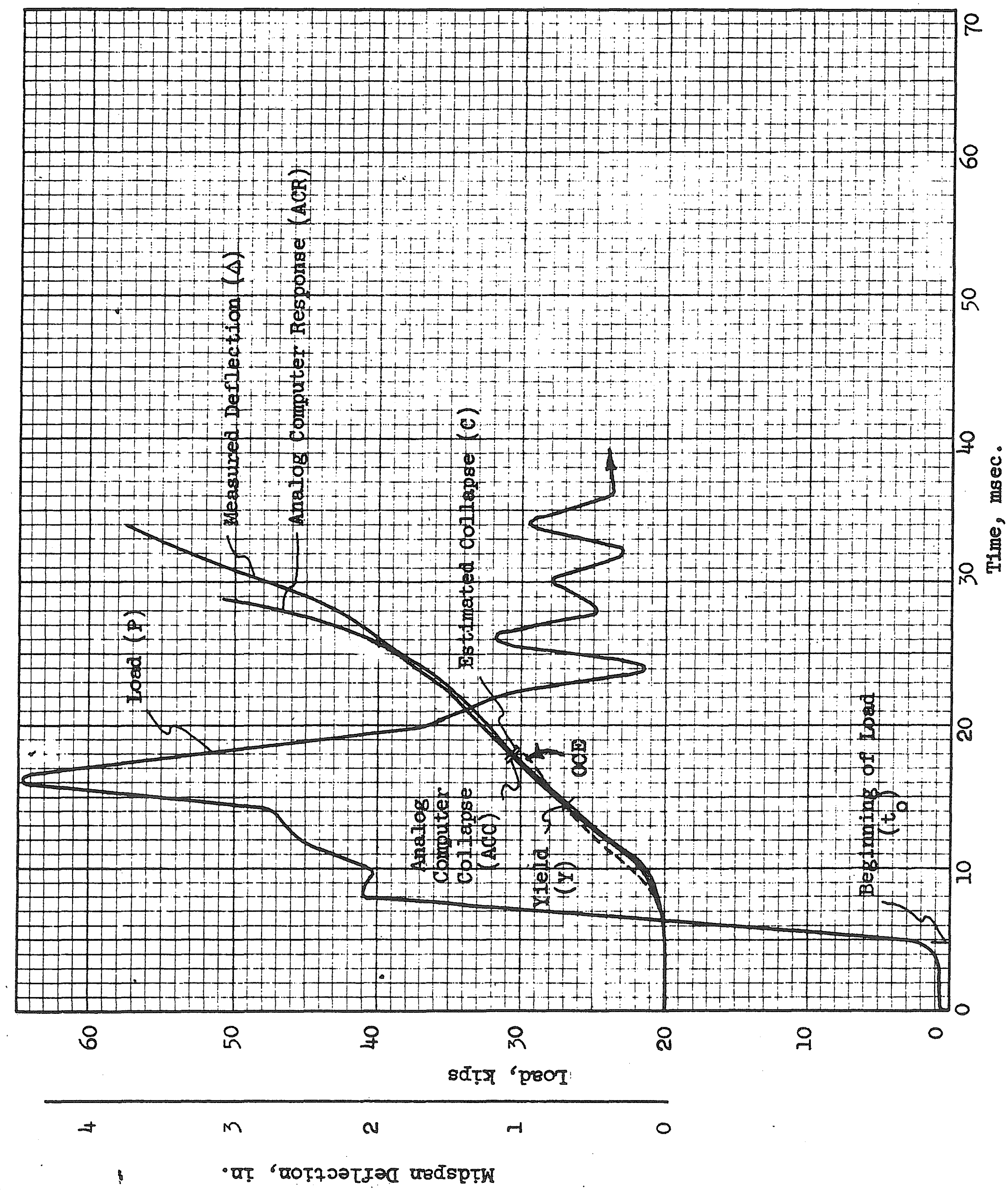

FIG. A35 LOAD AND RESPONSE, BEAM 2a1

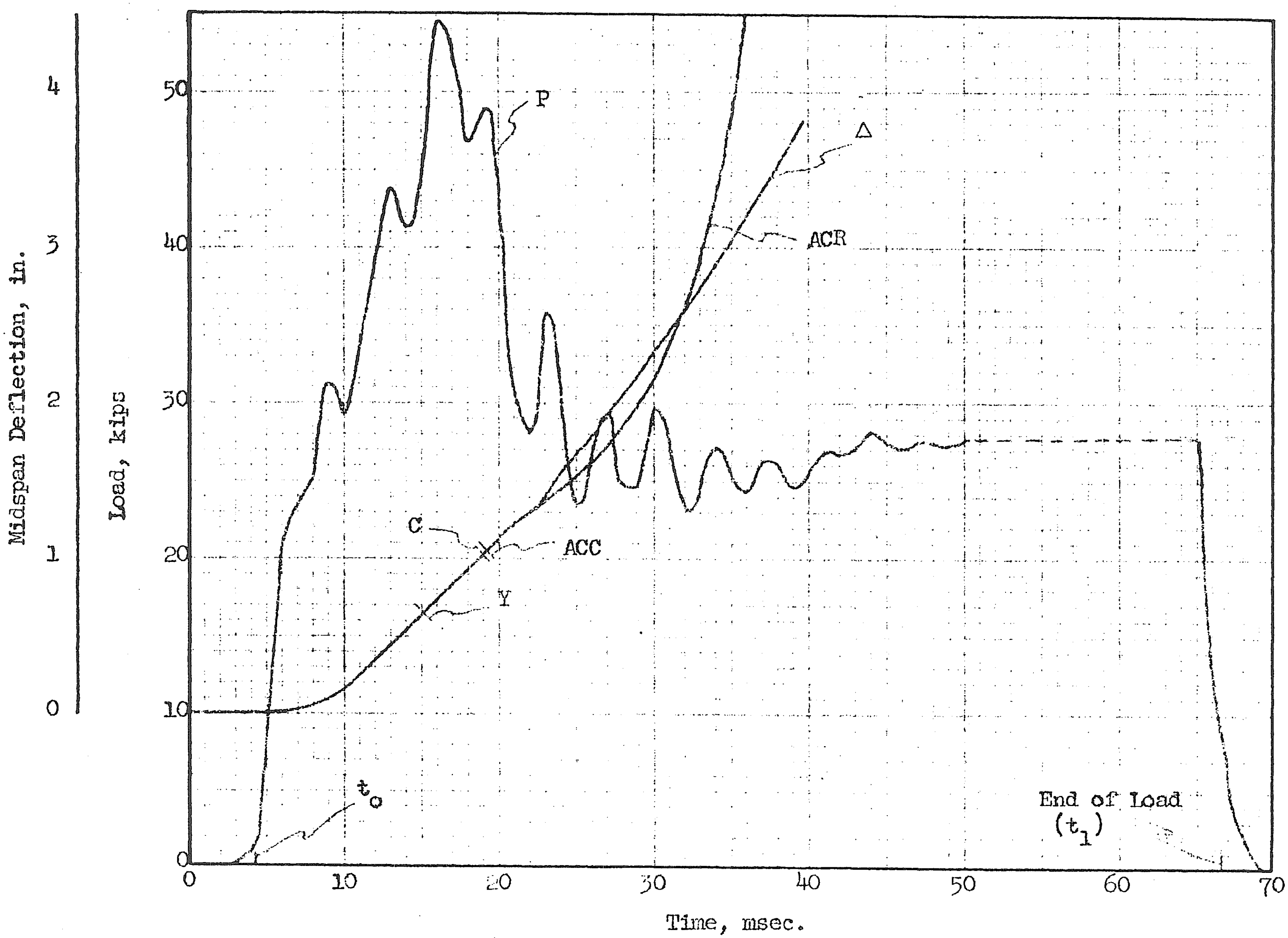

FIG. A36 LOAD AND RESPONSE, BEAM 2a2

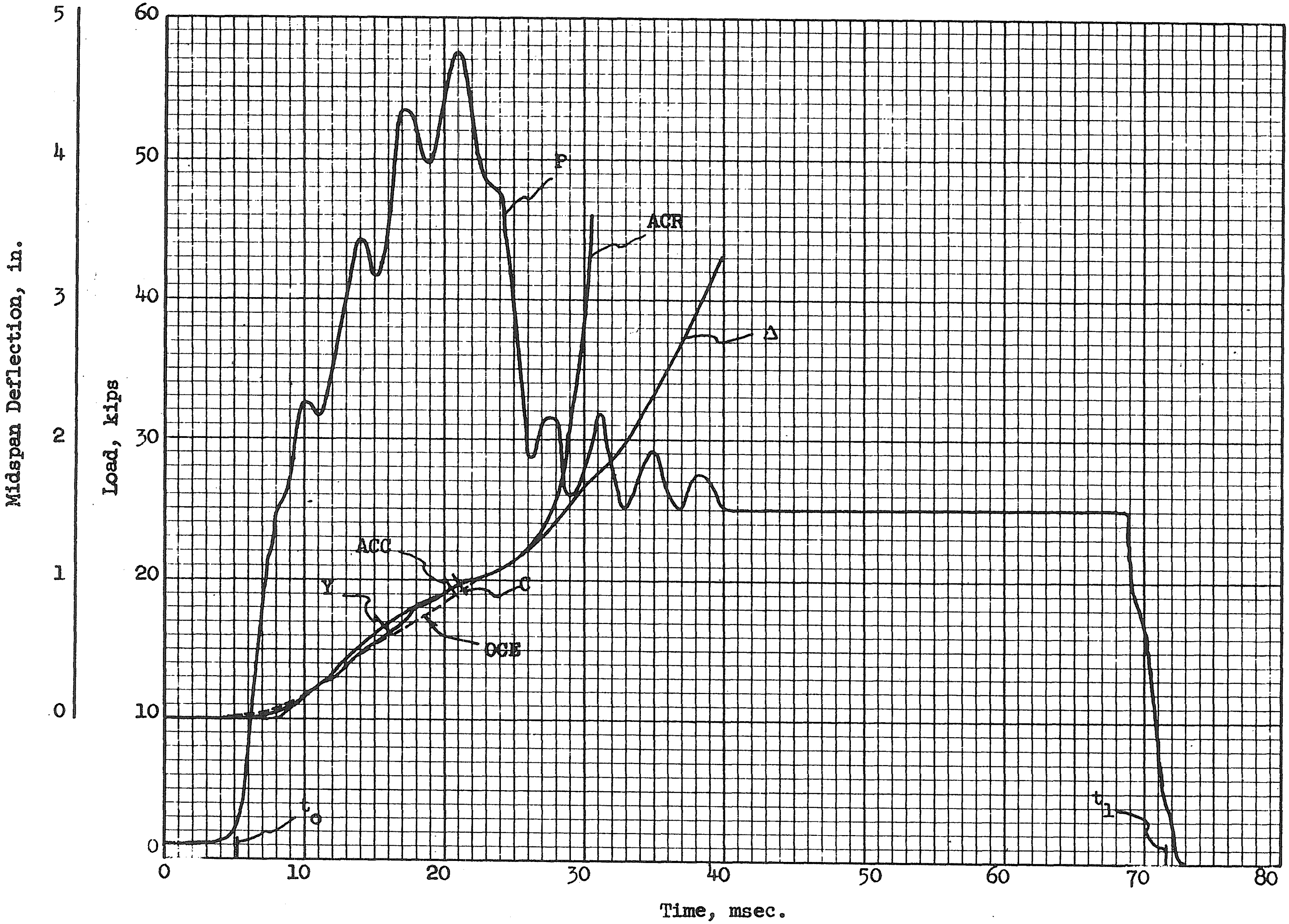

FIG. A37 LOAD AND RESPONSE, BEAM 2b2

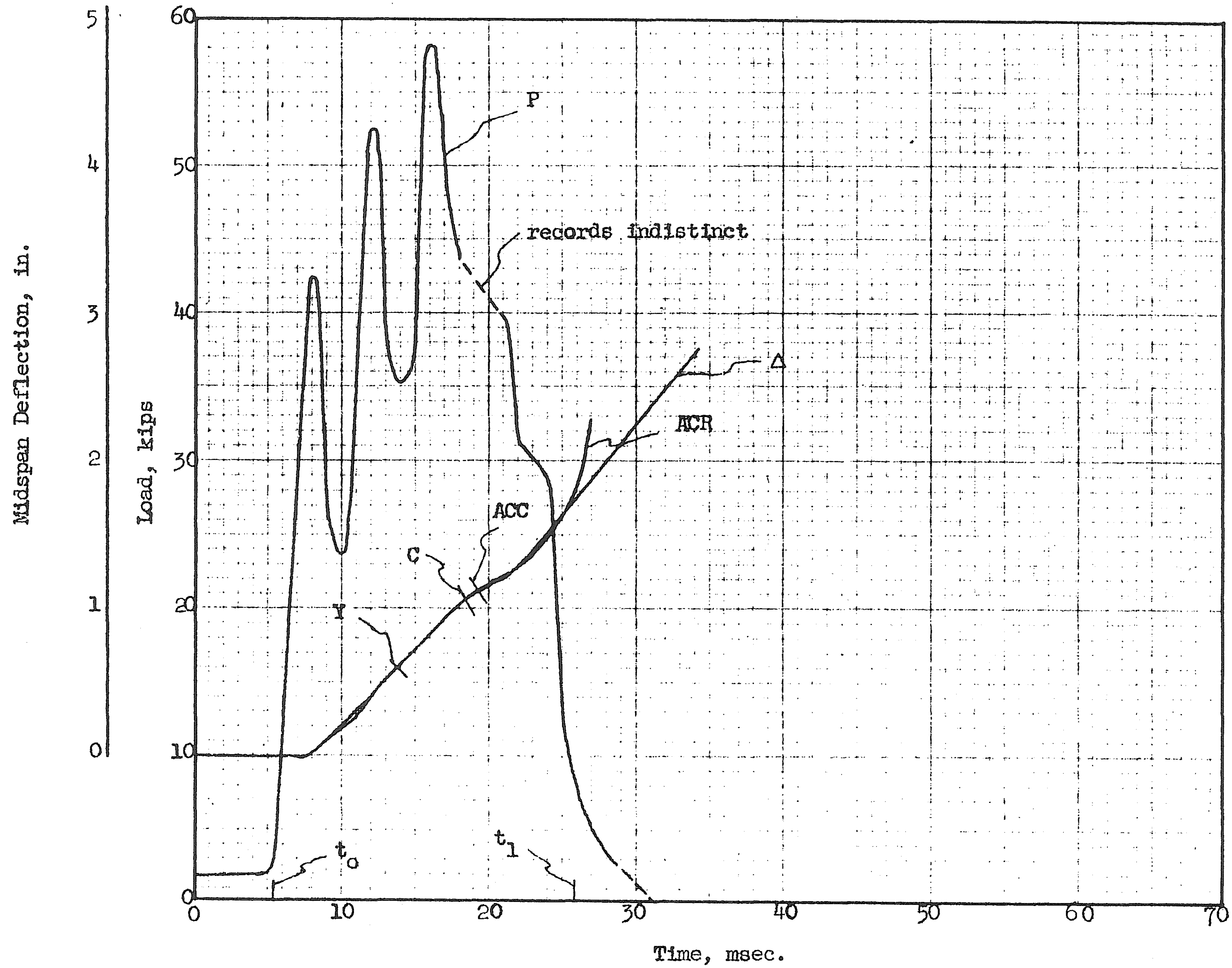

FIG. A38 LOAD AND RESPONSE, BEAM 2b3

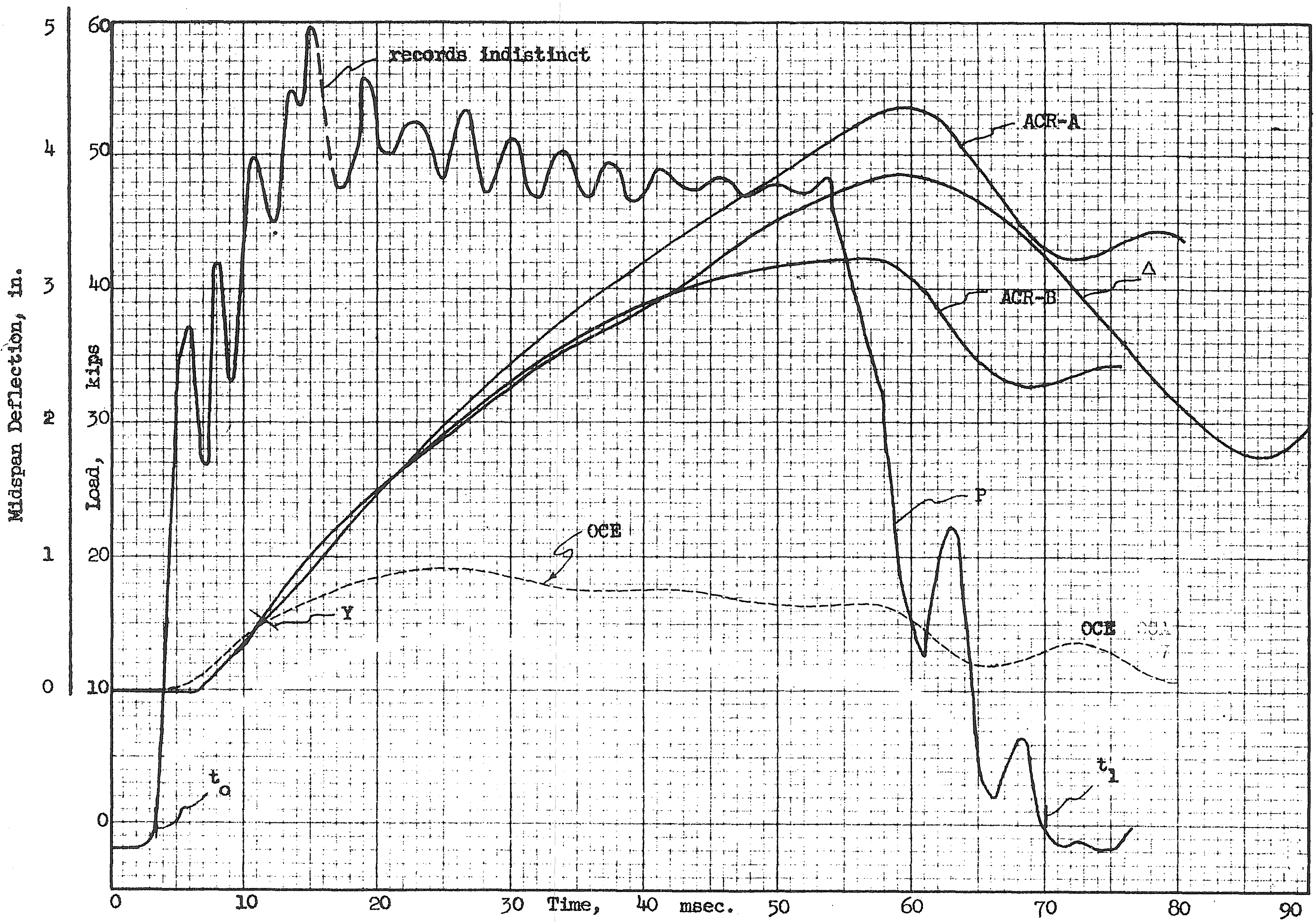

FIG. A39 LOAD AND RESPONSE, BEAM 3a2

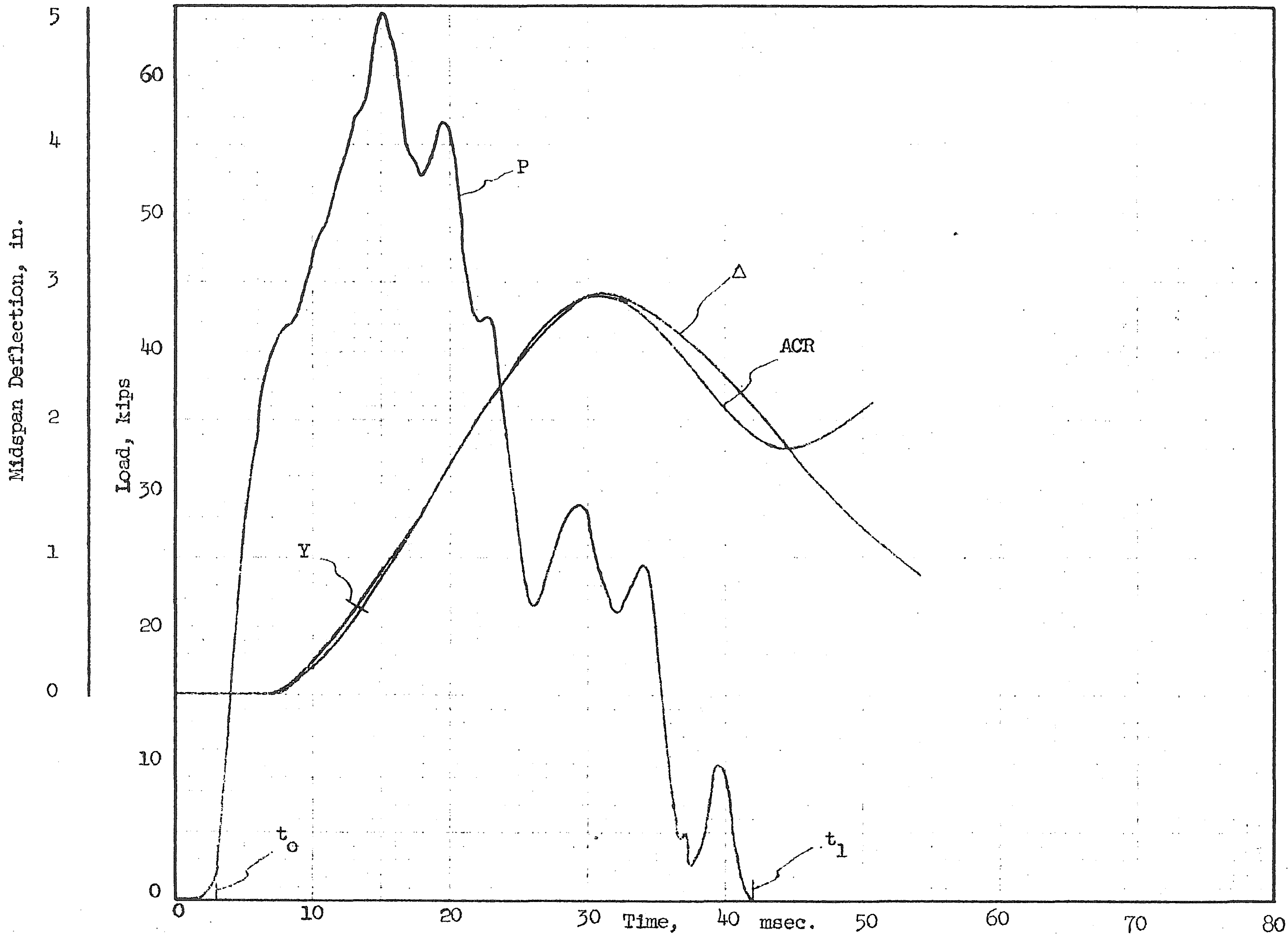

FIG. A40 LOAD AND RESPONSE, BEAM 3a3

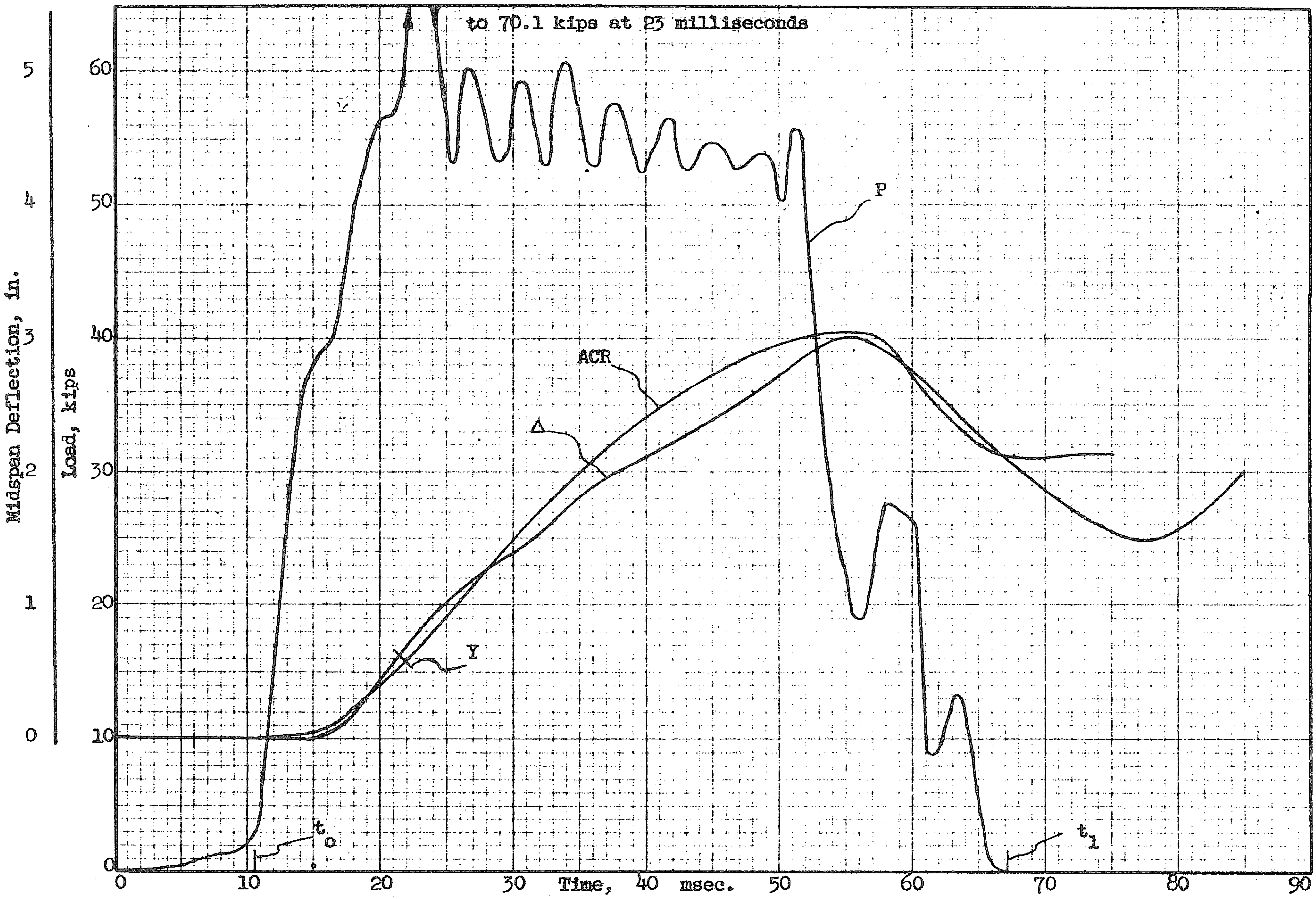

FIG. A41 LOAD AND RESPONSE, BEAM 3a4

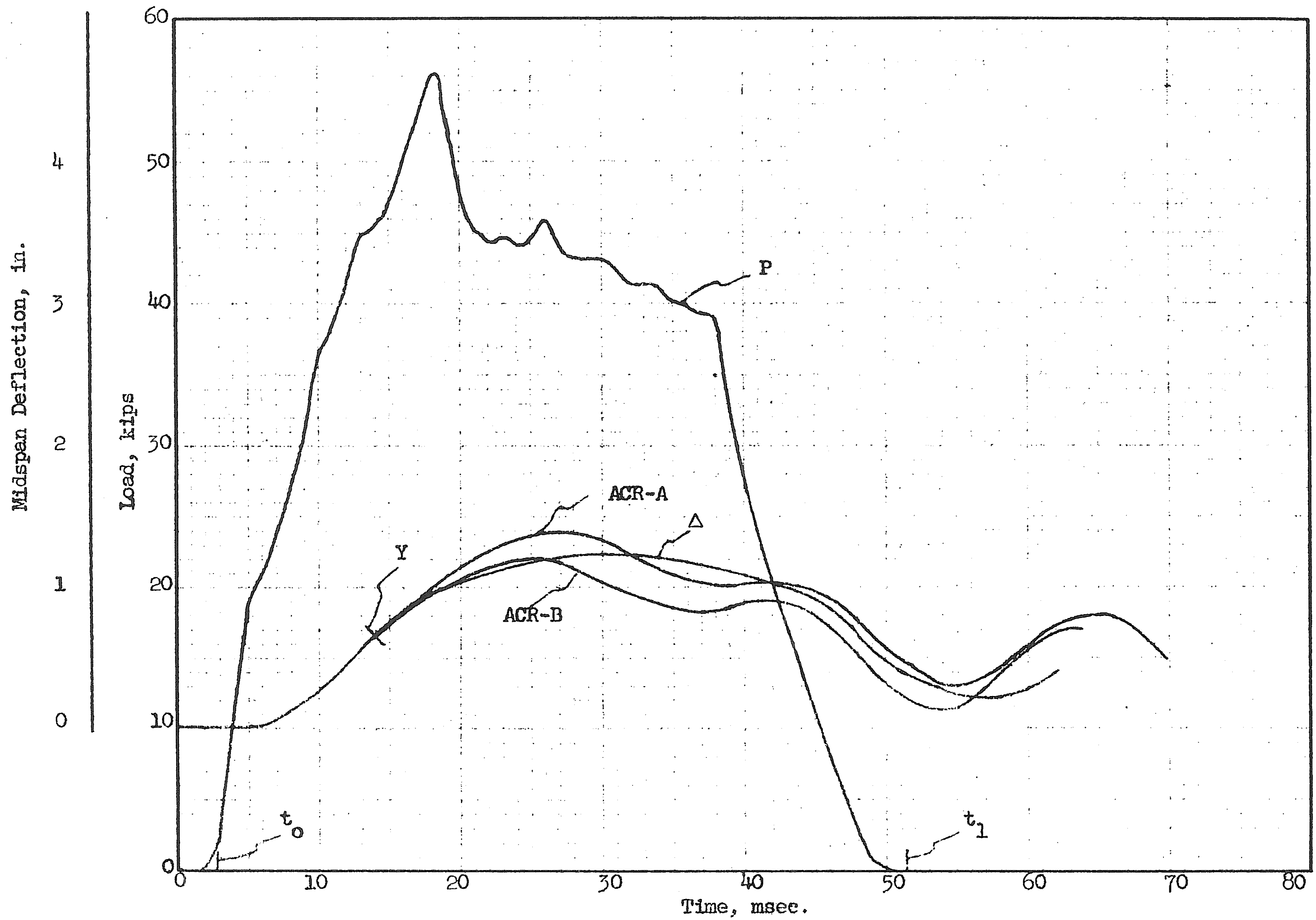

FIG. A42 LOAD AND RESPONSE, BEAM 3a5, BLOW 1

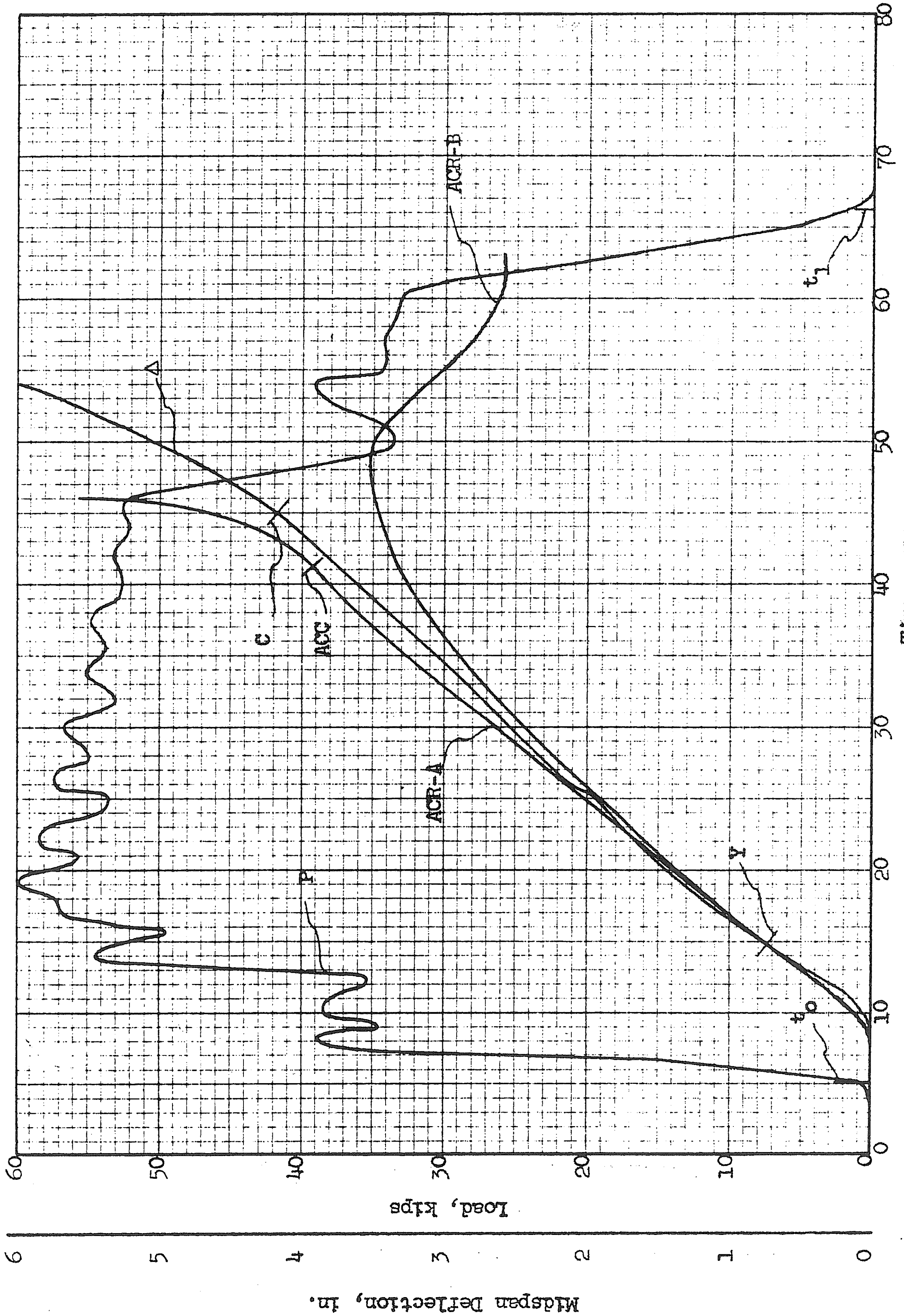

FIG. A43 LOAD AND RESPONSE, BEAM 3a5, BLOW 2

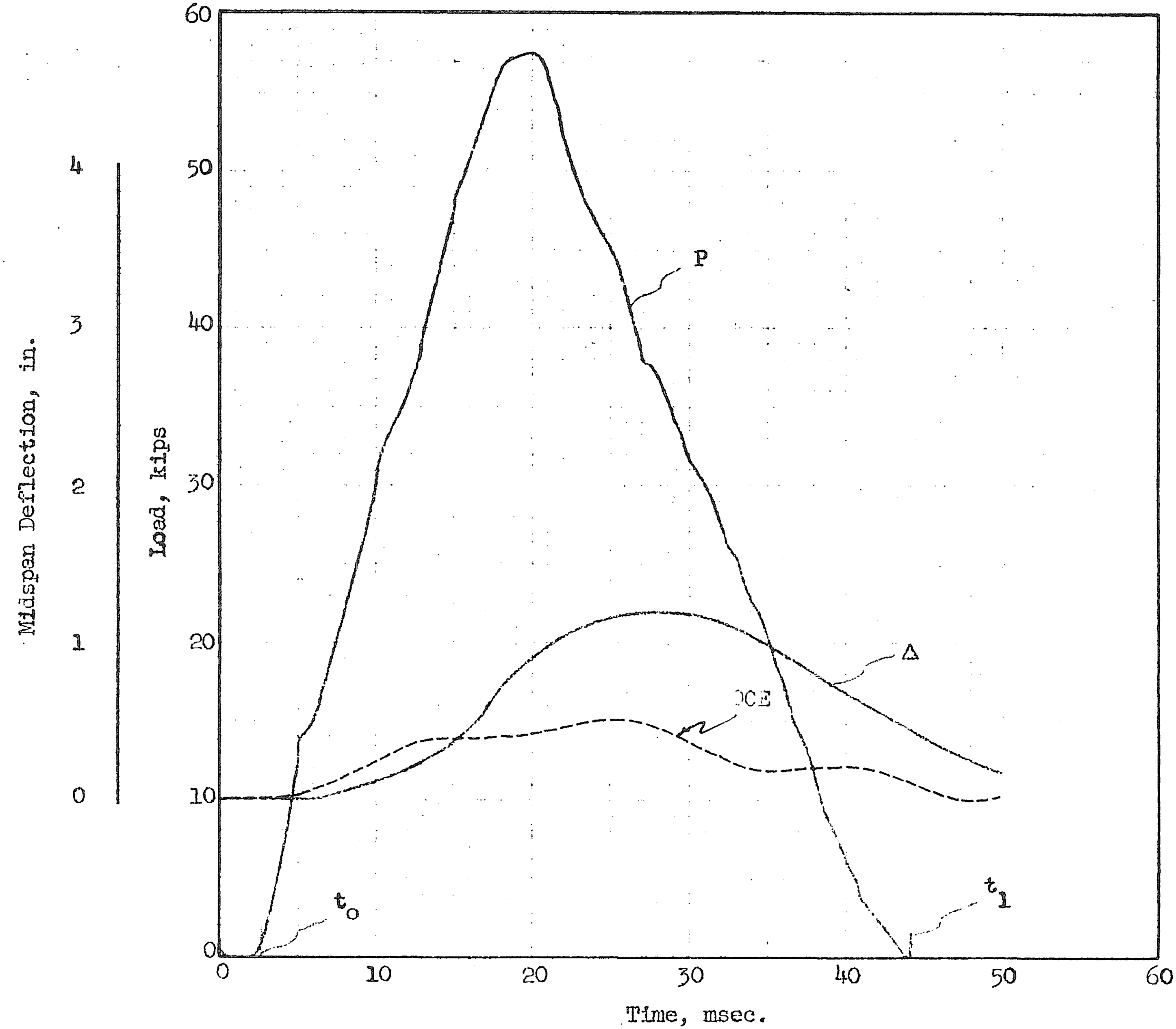

FIG. A44 LOAD AND RESPONSE, BEAM 3b2, BLOW 1

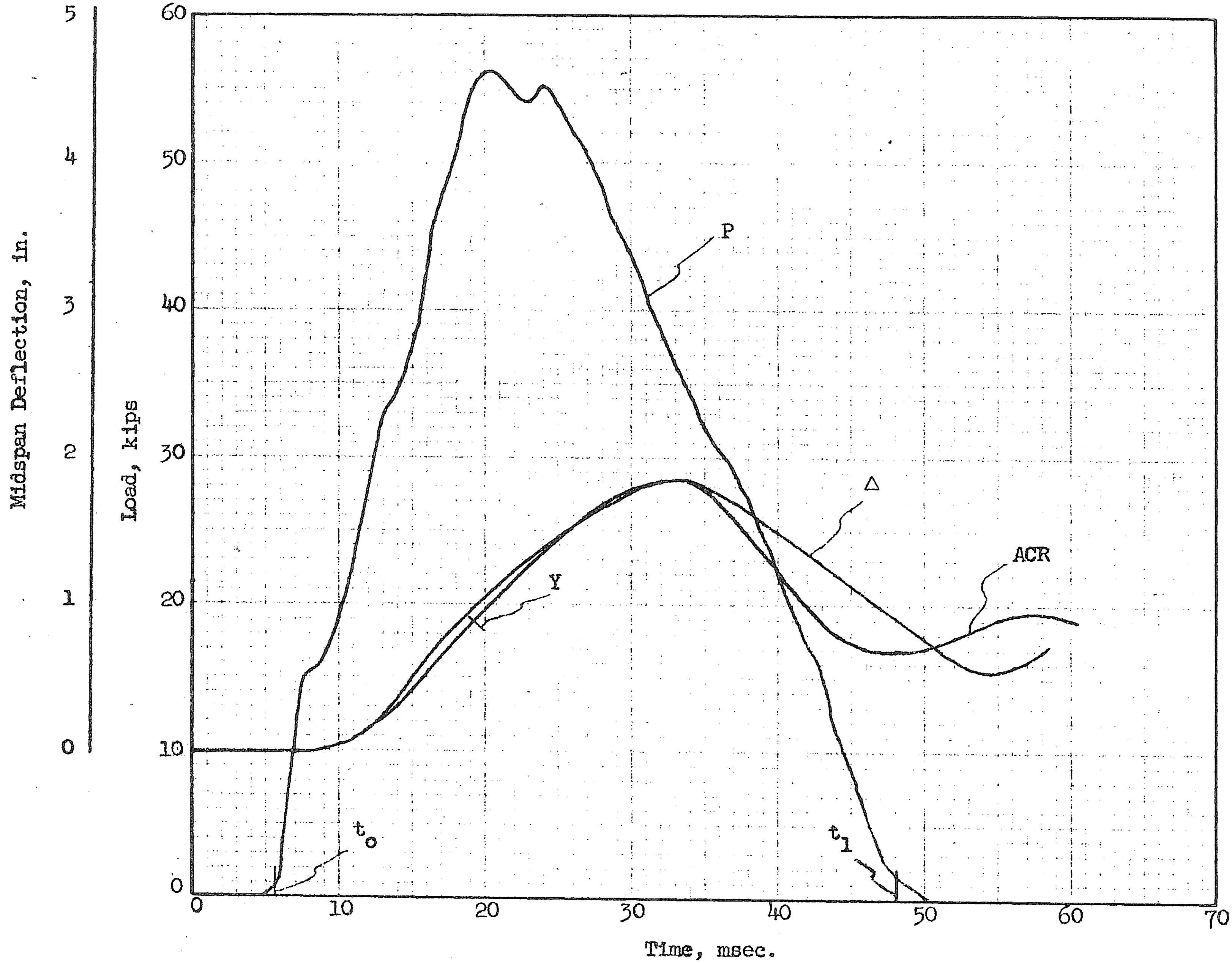

FIG. A45 LOAD AND RESPONSE, BEAM 3b2, BLOW 2

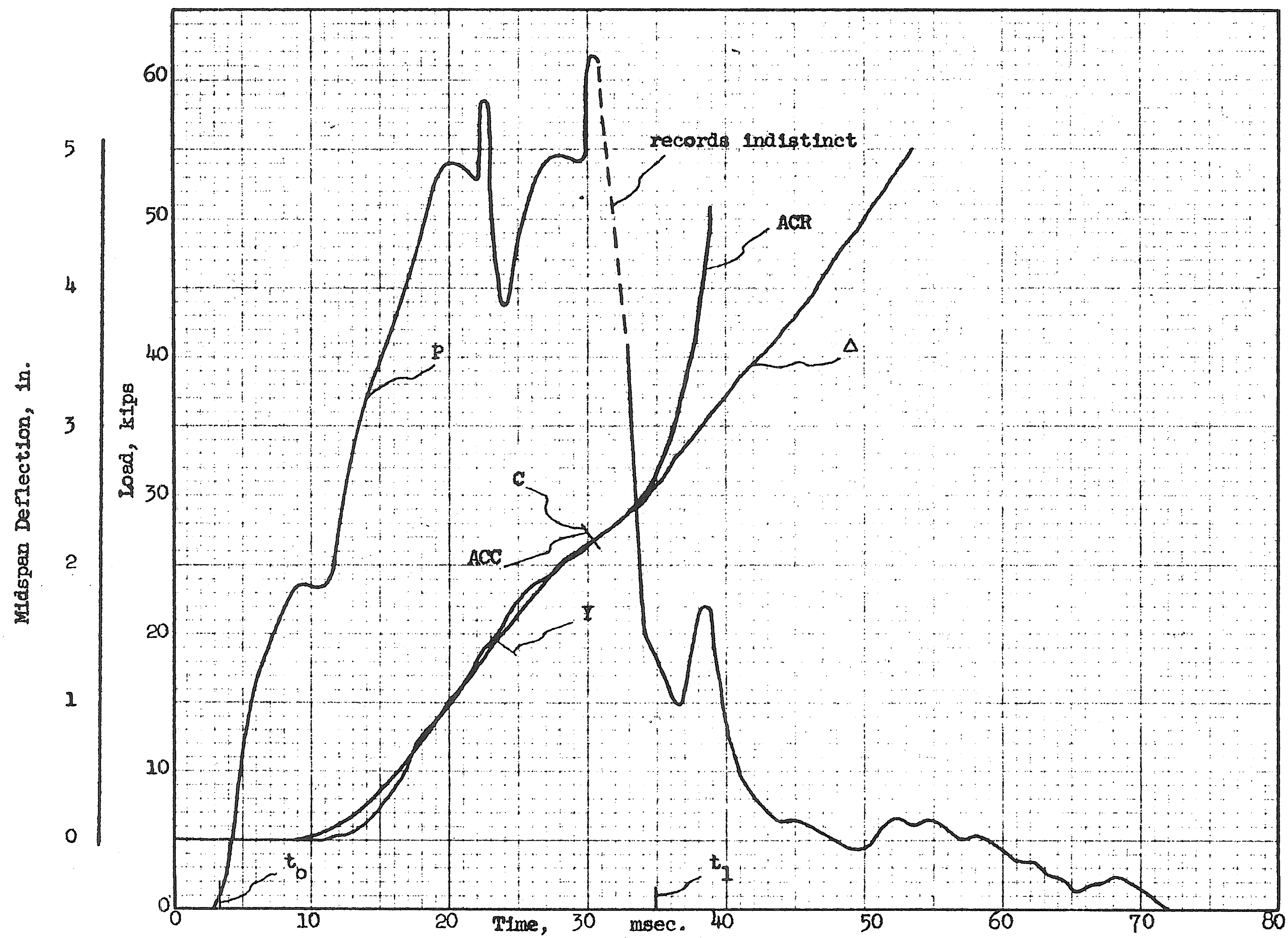

FIG. A46 LOAD AND RESPONSE, BEAM 3b2, BLOW 3

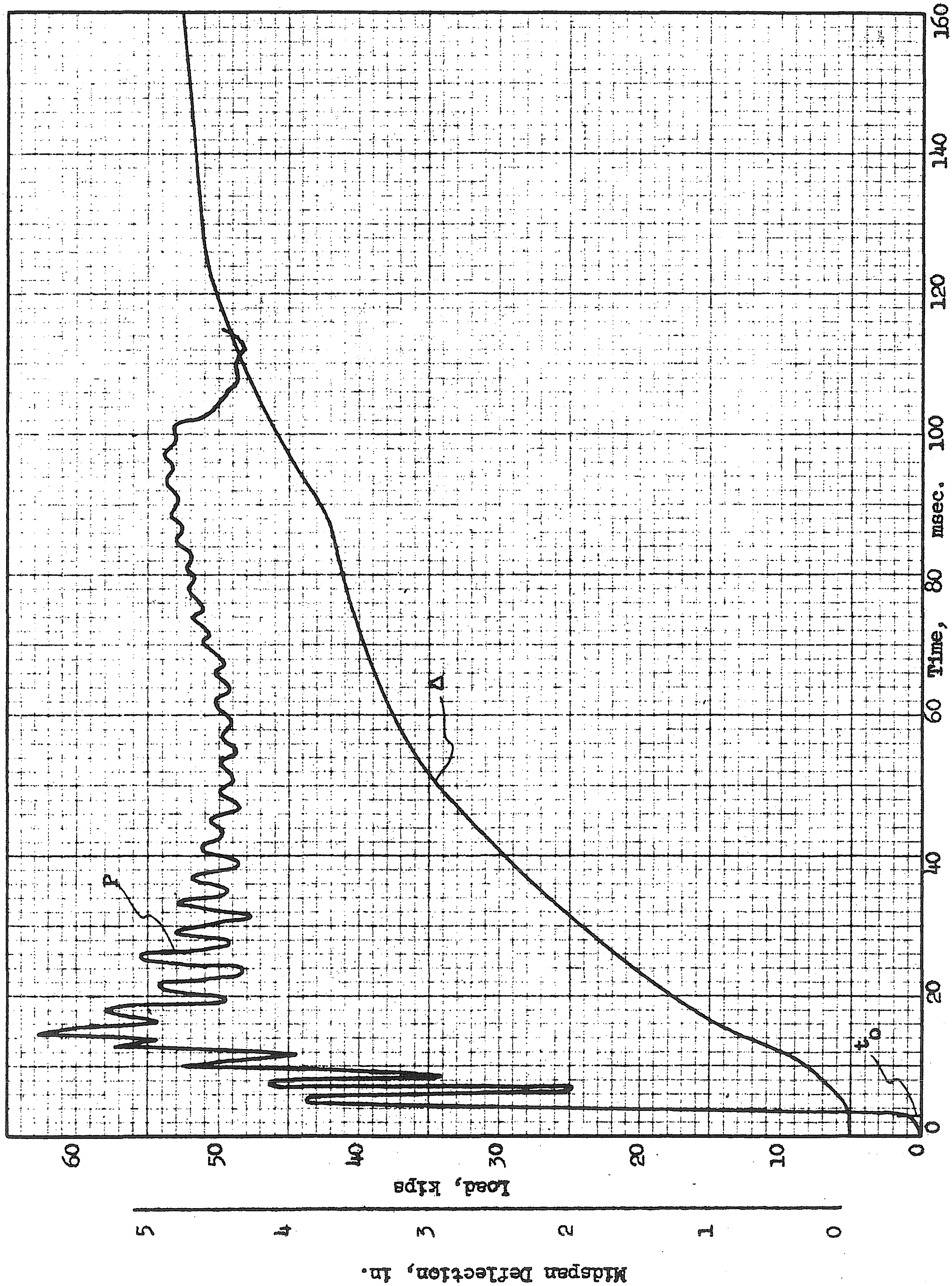

FIG. A47 LOAD AND RESPONSE, BEAM 3b3

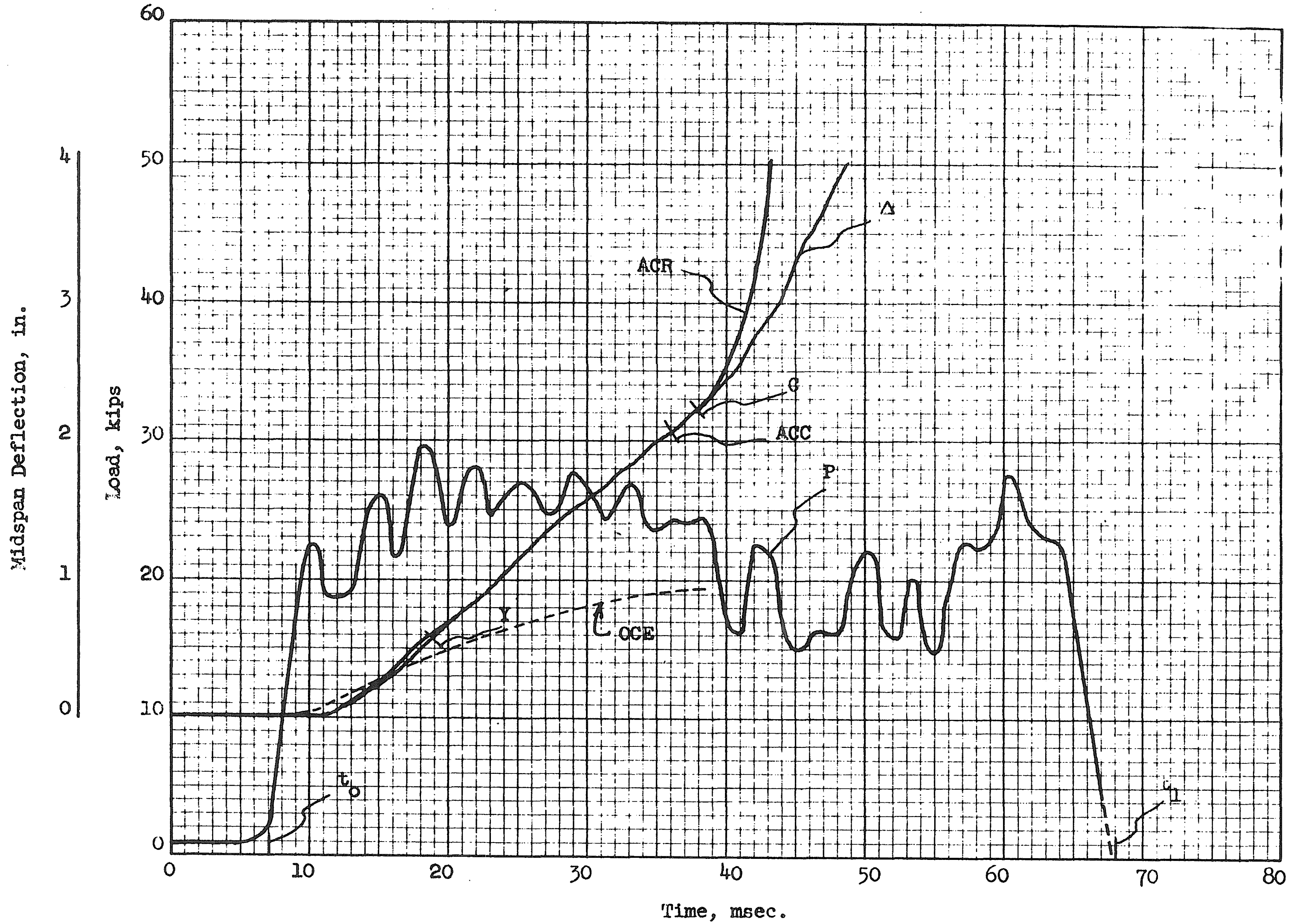

FIG. A48 LOAD AND RESPONSE, BEAM 4a1

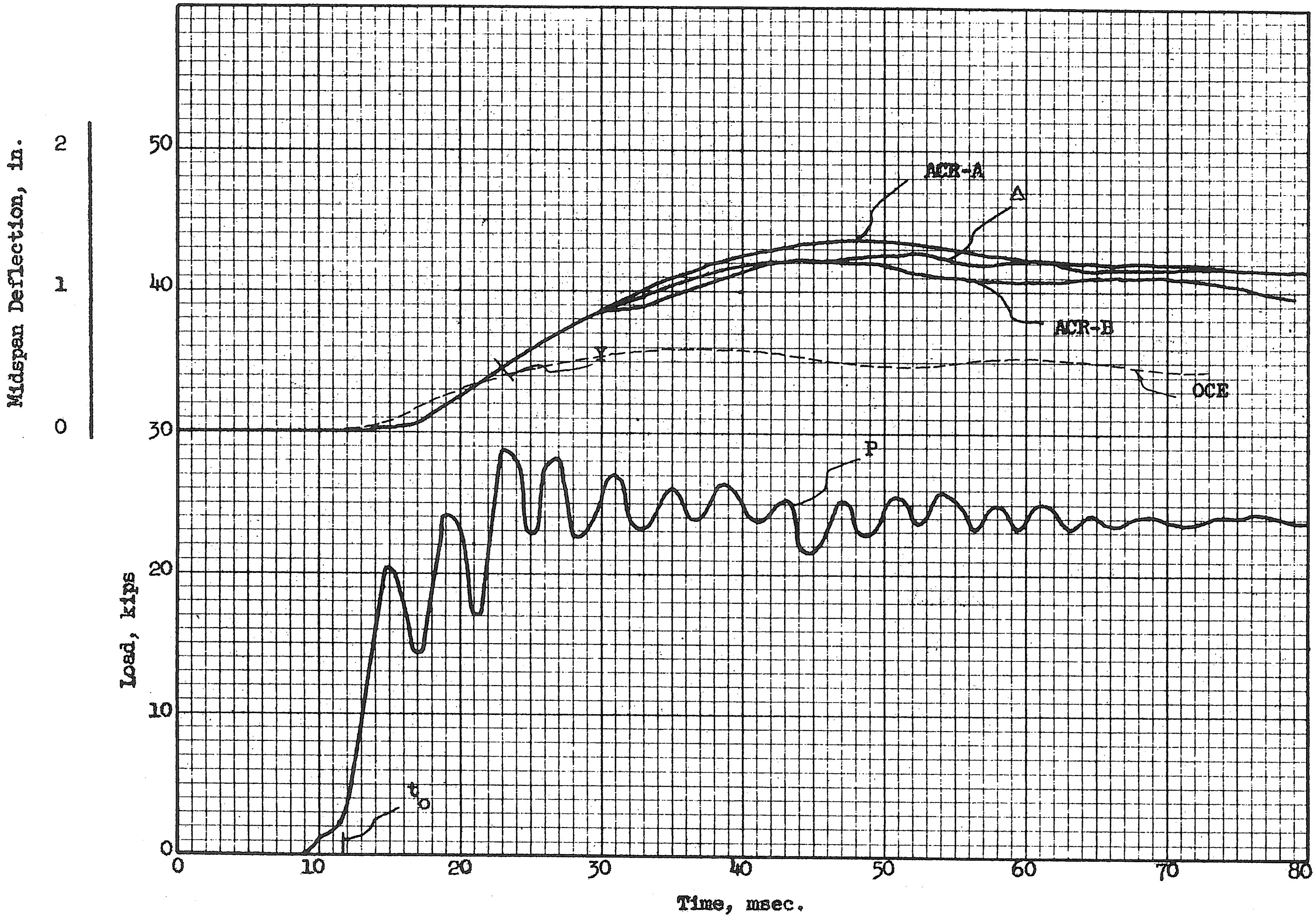

FIG.. A49 LOAD AND RESPONSE, BEAM 4a2, BLOW 1

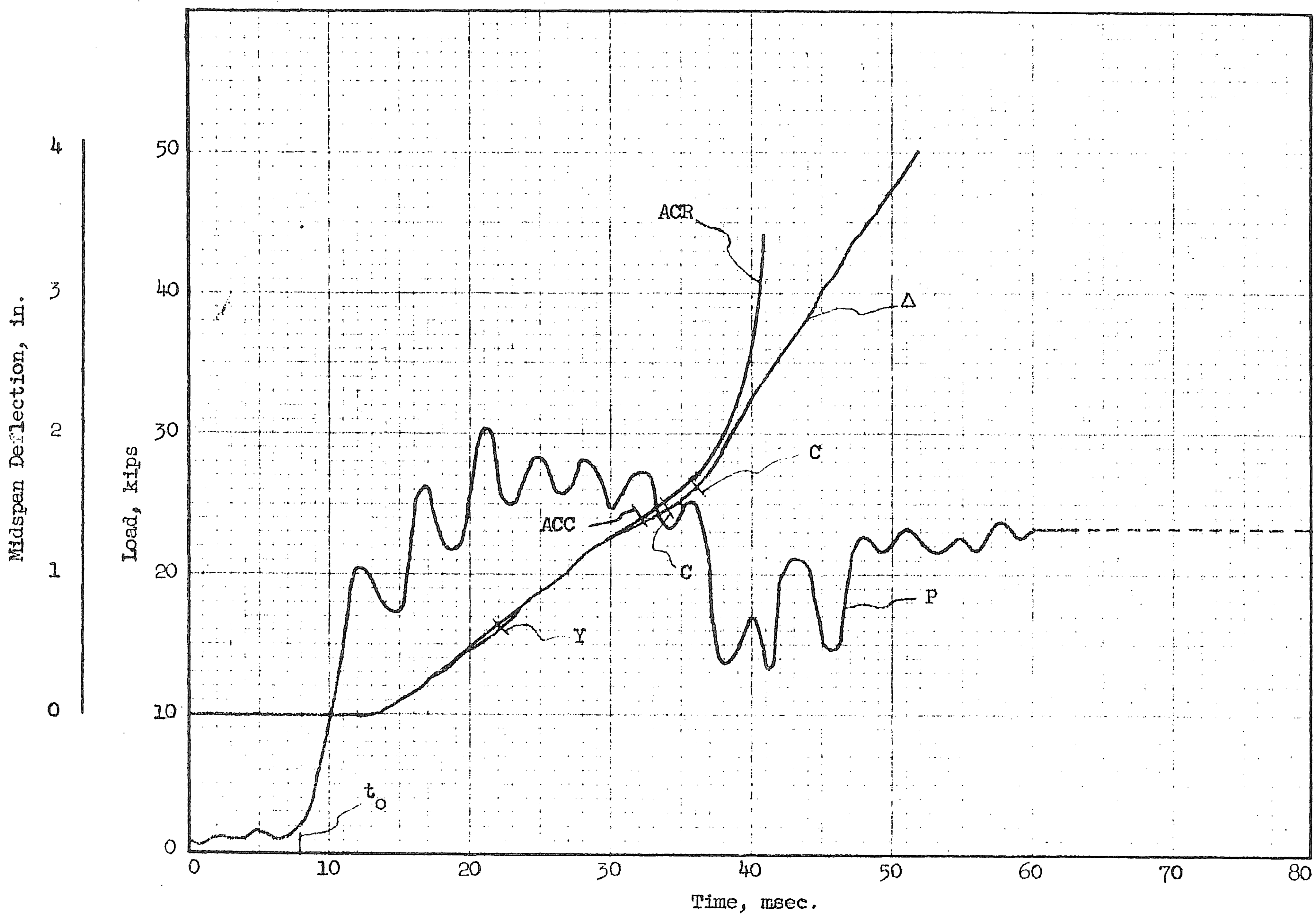

FIG. A50 LOAD AND RESPONSE, BEAM 4a2, BLOW 2

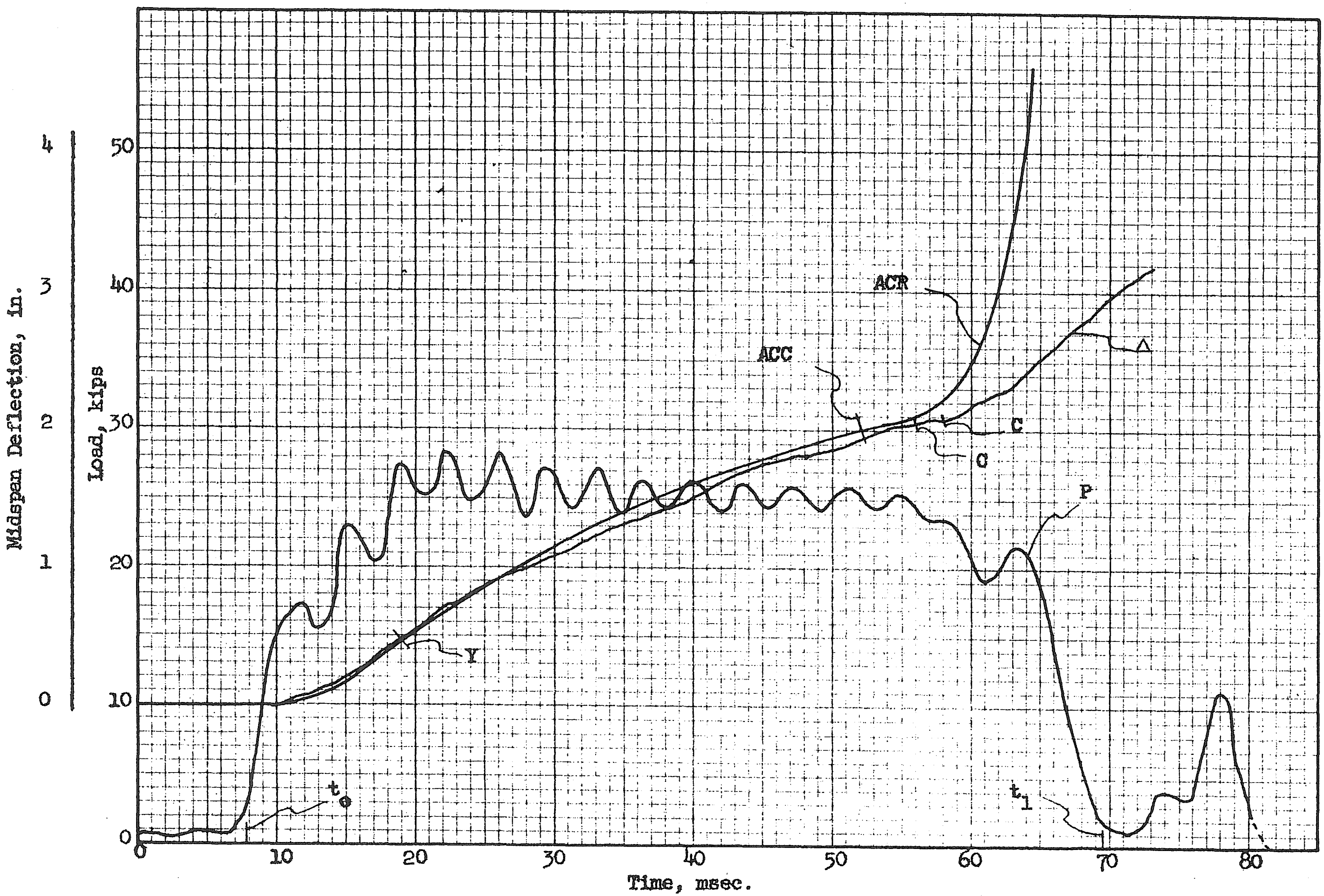

FIG. A51 LOAD AND RESPONSE, BEAM 4b3

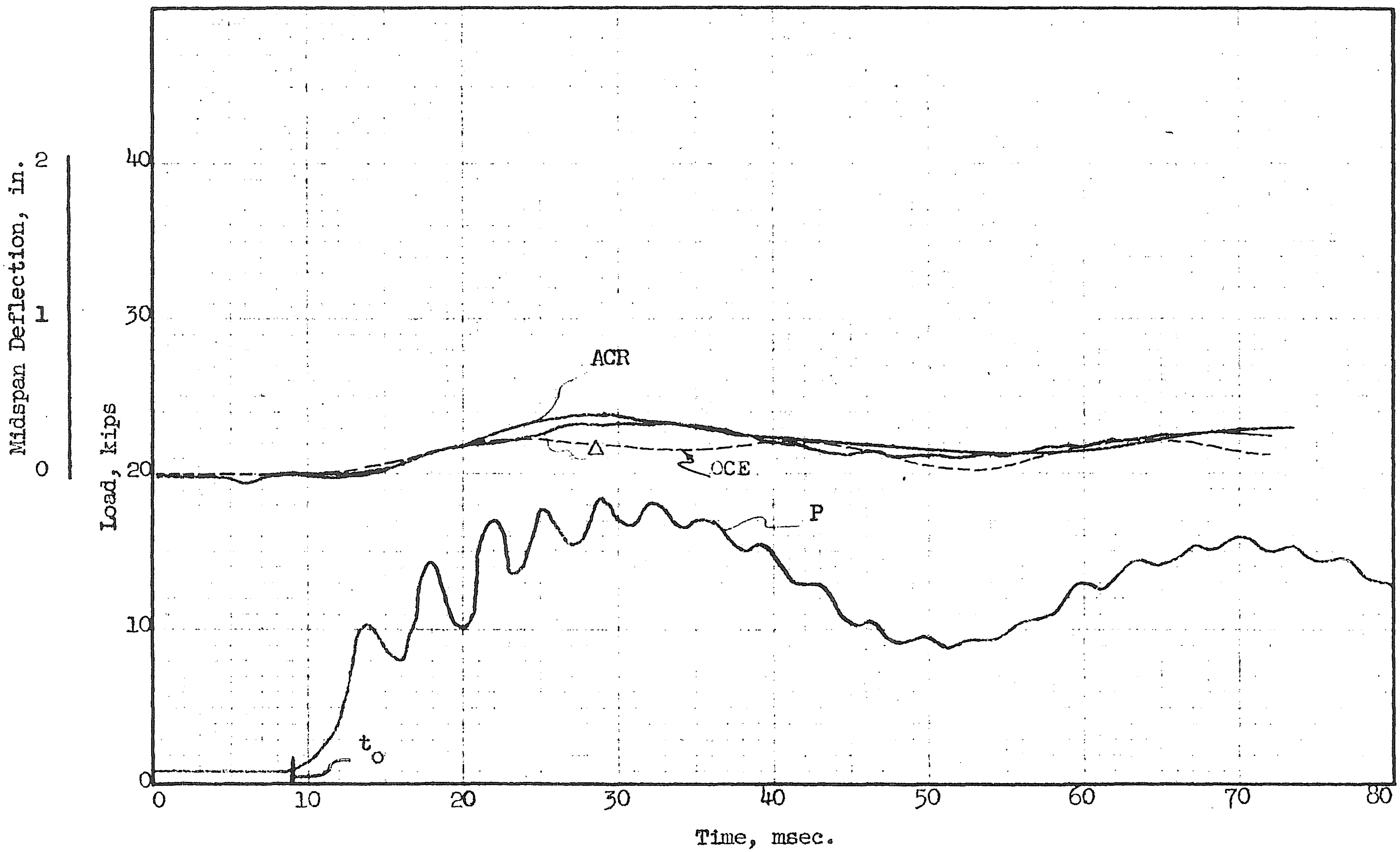

FIG. A52 LOAD AND RESPONSE, BEAM 4c2, BLOW 1

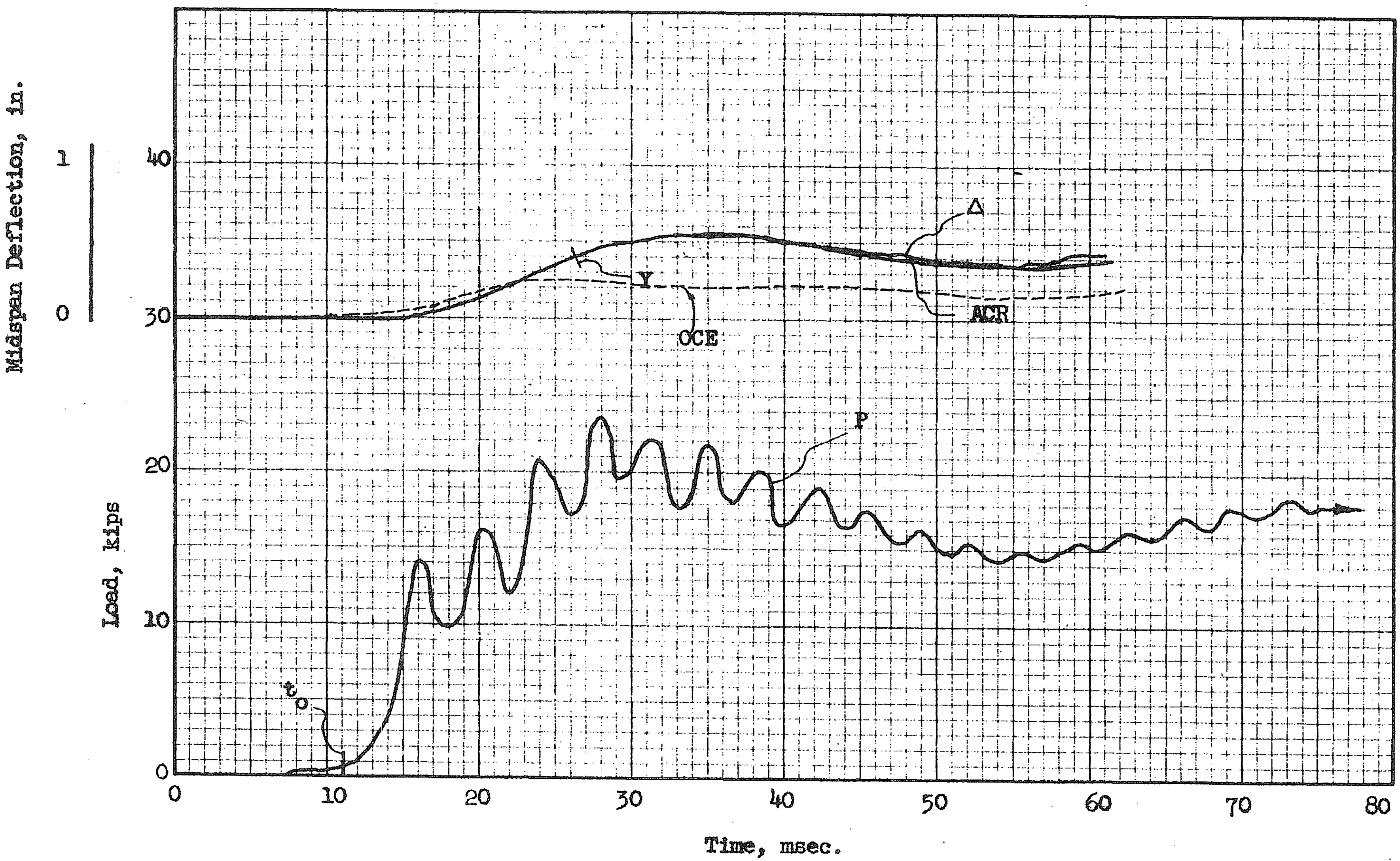

FIG. A53 LOAD AND RESPONSE, BEAM 4c2, BLOW 2

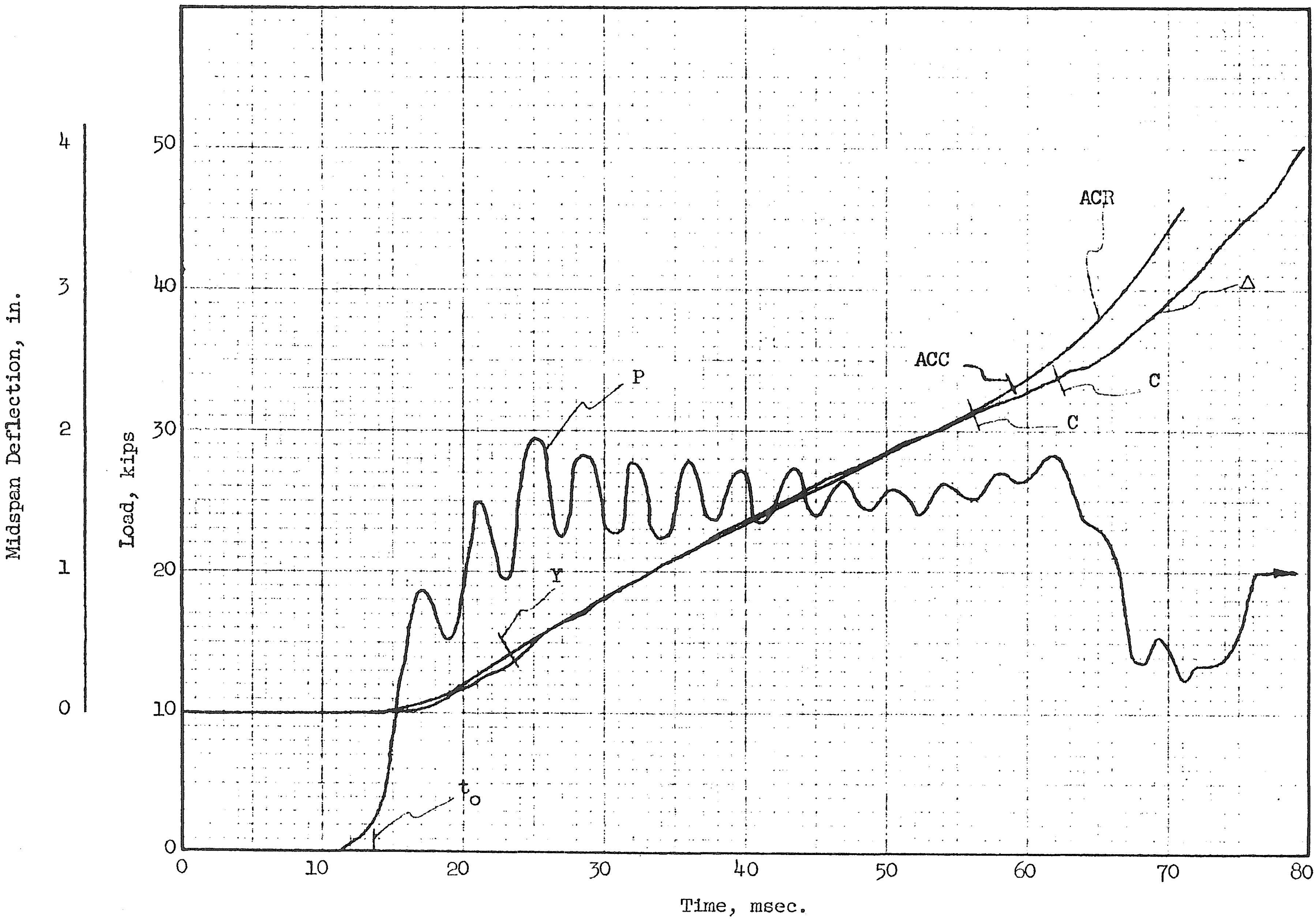

FIG. A54 LOAD AND RESPONSE, BEAM 4c2, BLOW 3

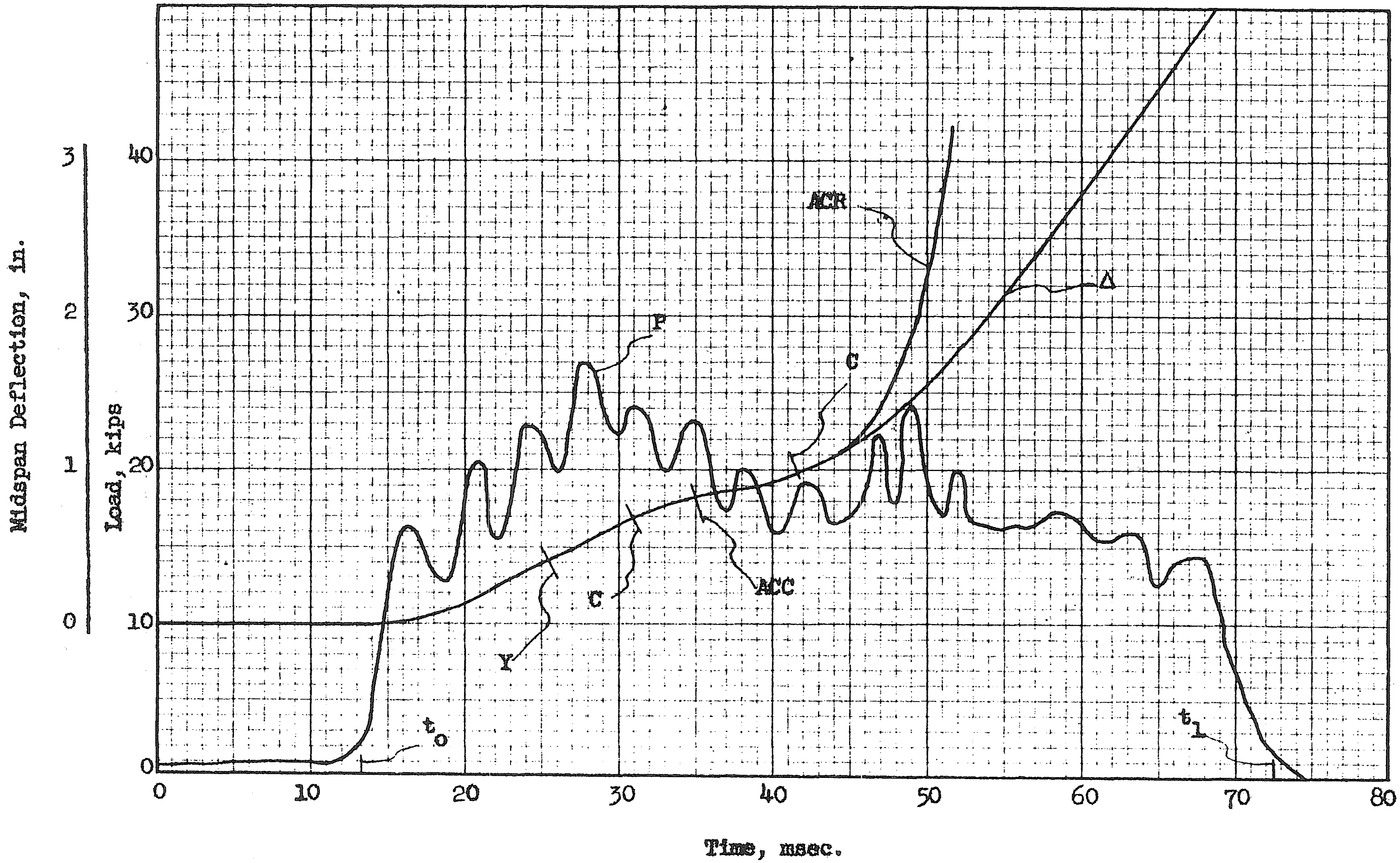

FIG. A55 LOAD AND RESPONSE, BEAM 4c3

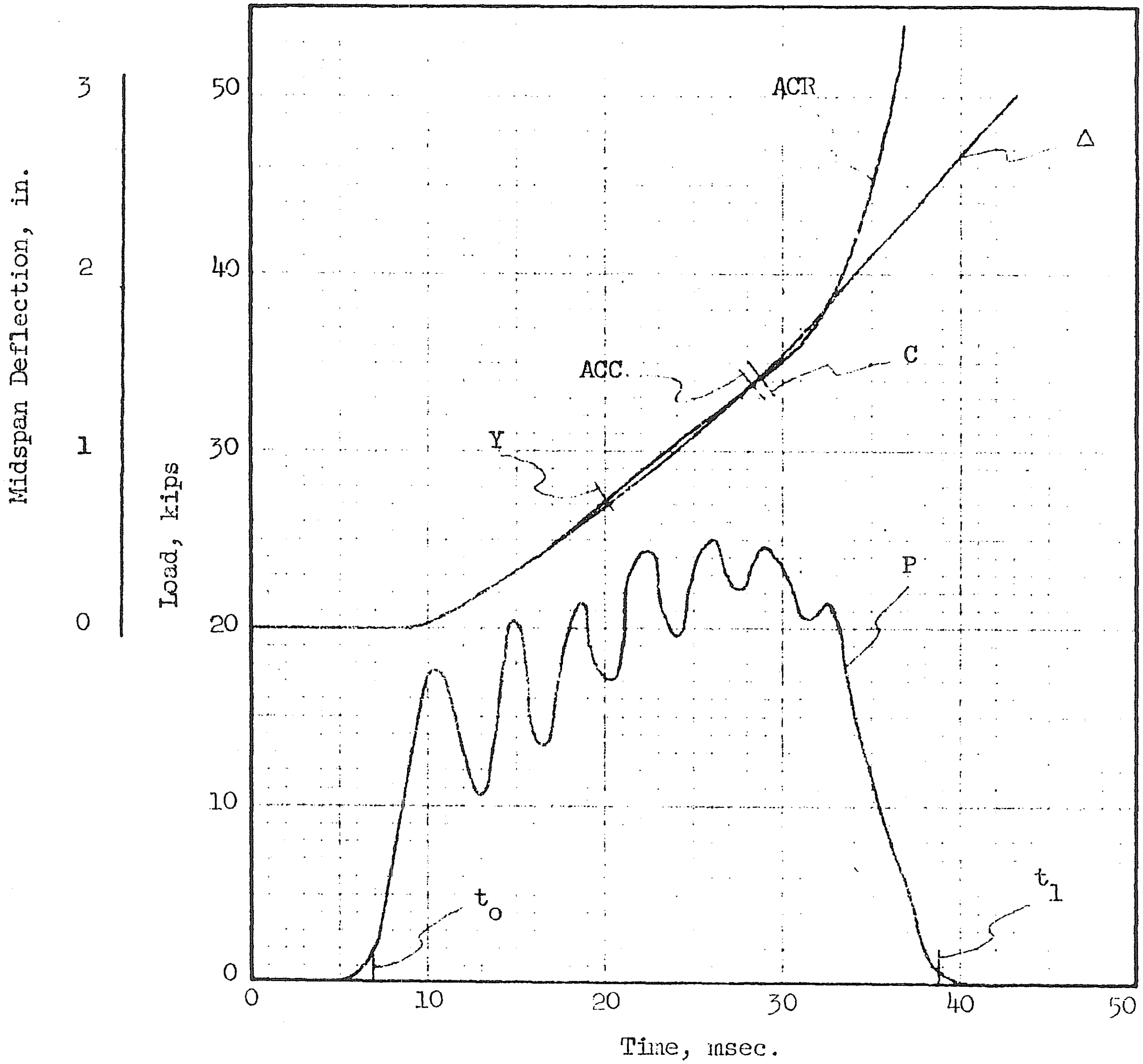

FIG. A56 LOAD AND RESPONSE, BEAM 5a1

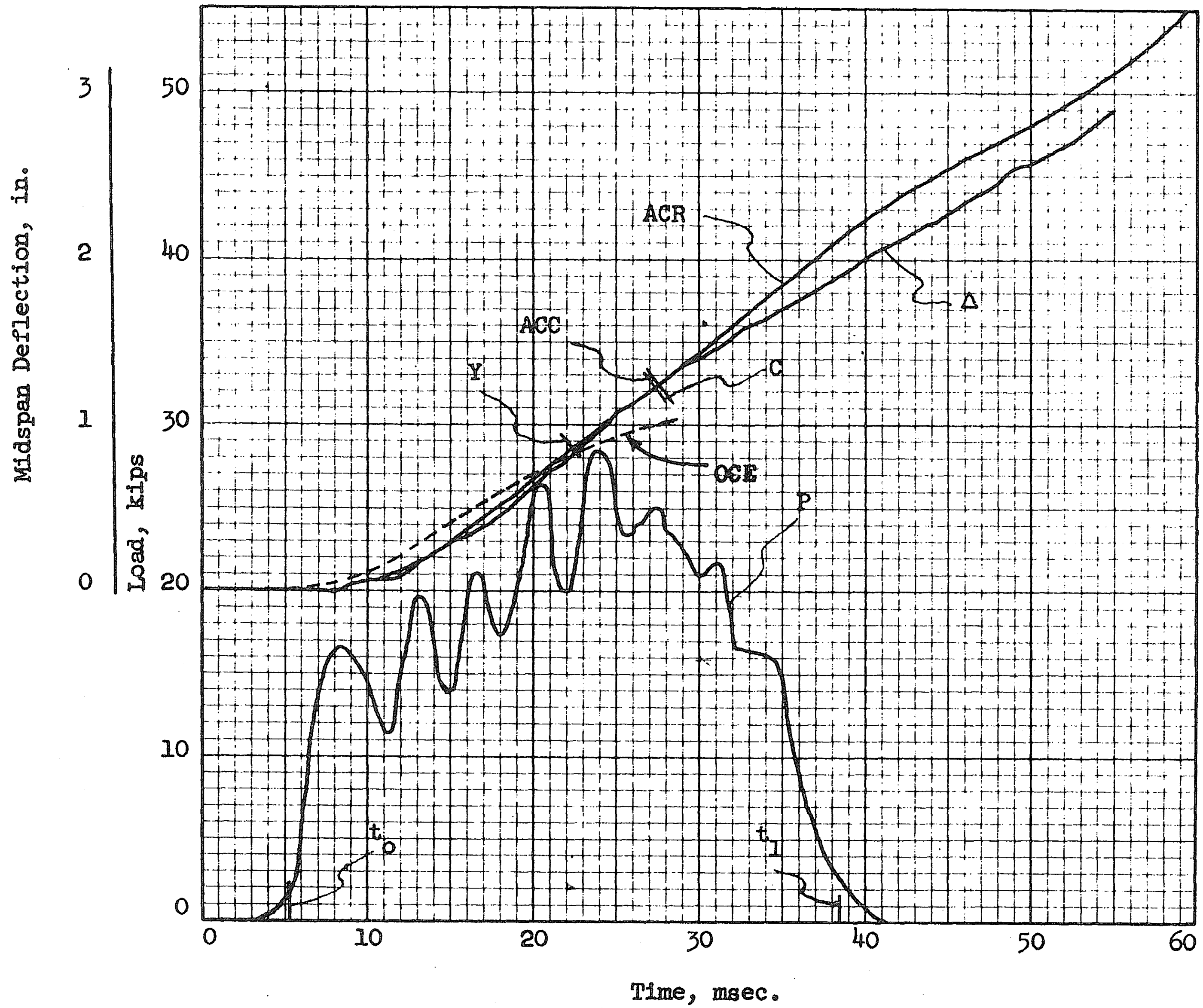

FIG. A57 LOAD AND RESPONSE, BEAM 5a2

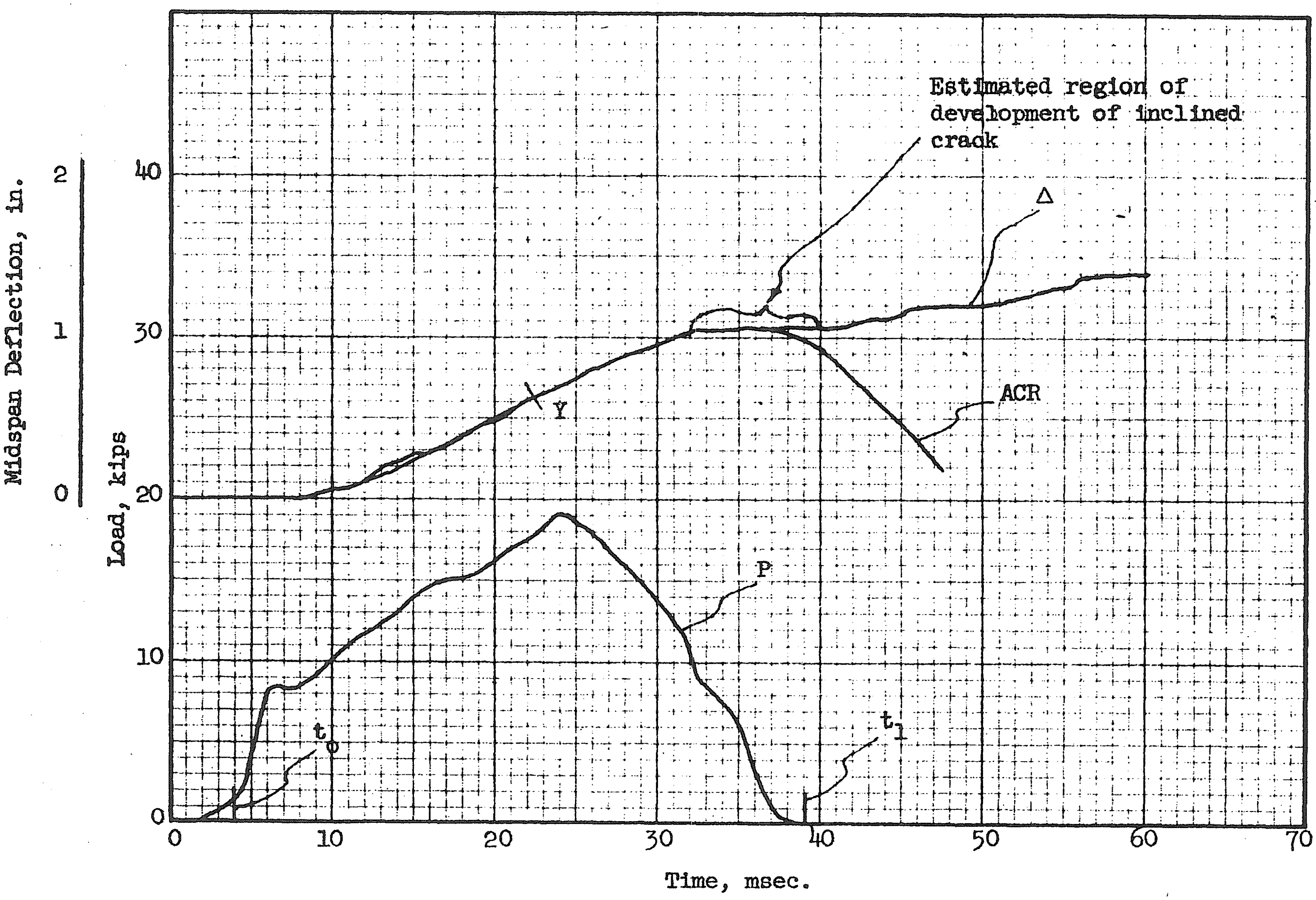

FIG. A58 LOAD AND RESPONSE, BEAM 5b3

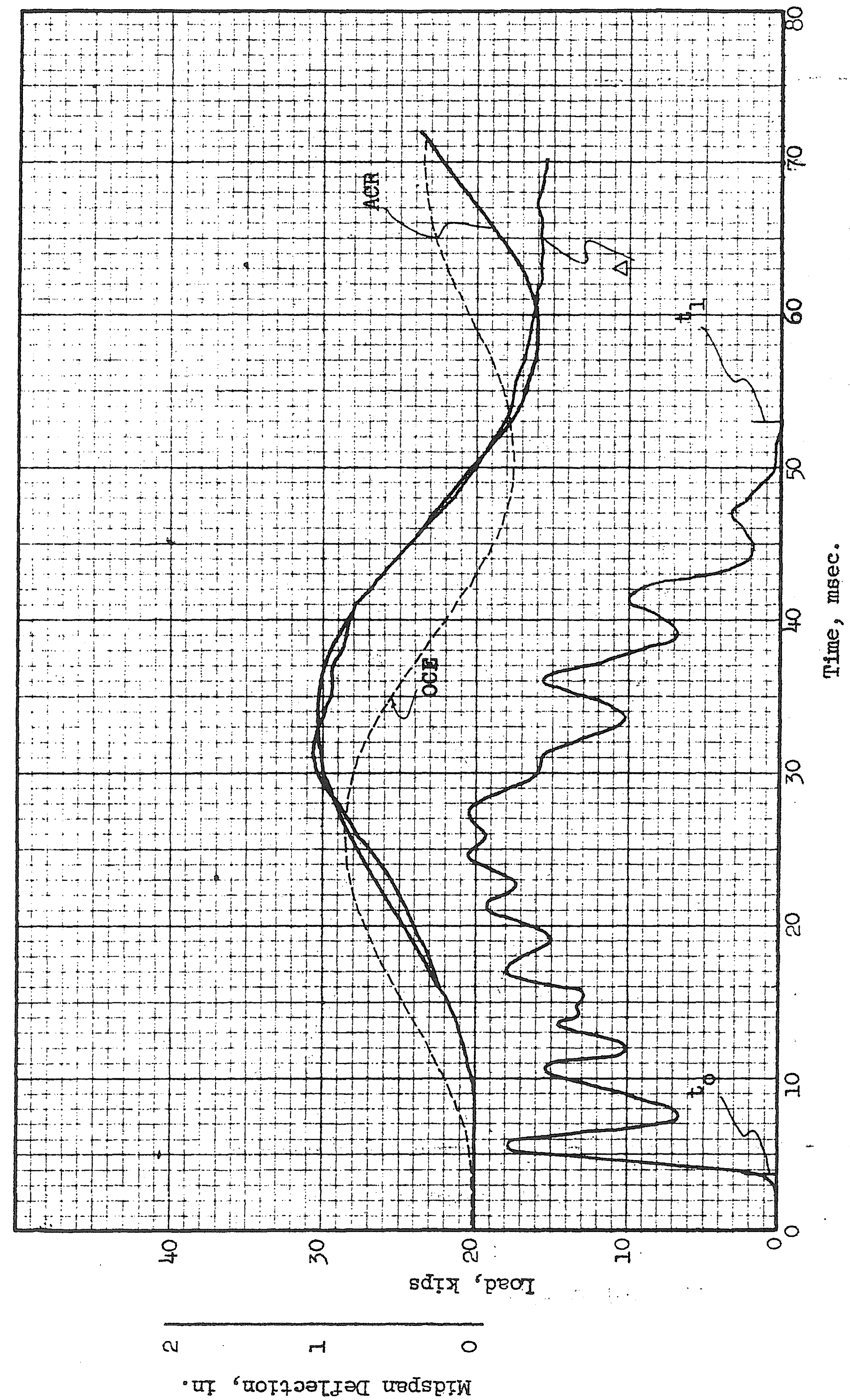

FIG. A59 LOAD AND RESPONSE, BEAM 5b4, BLOW 1

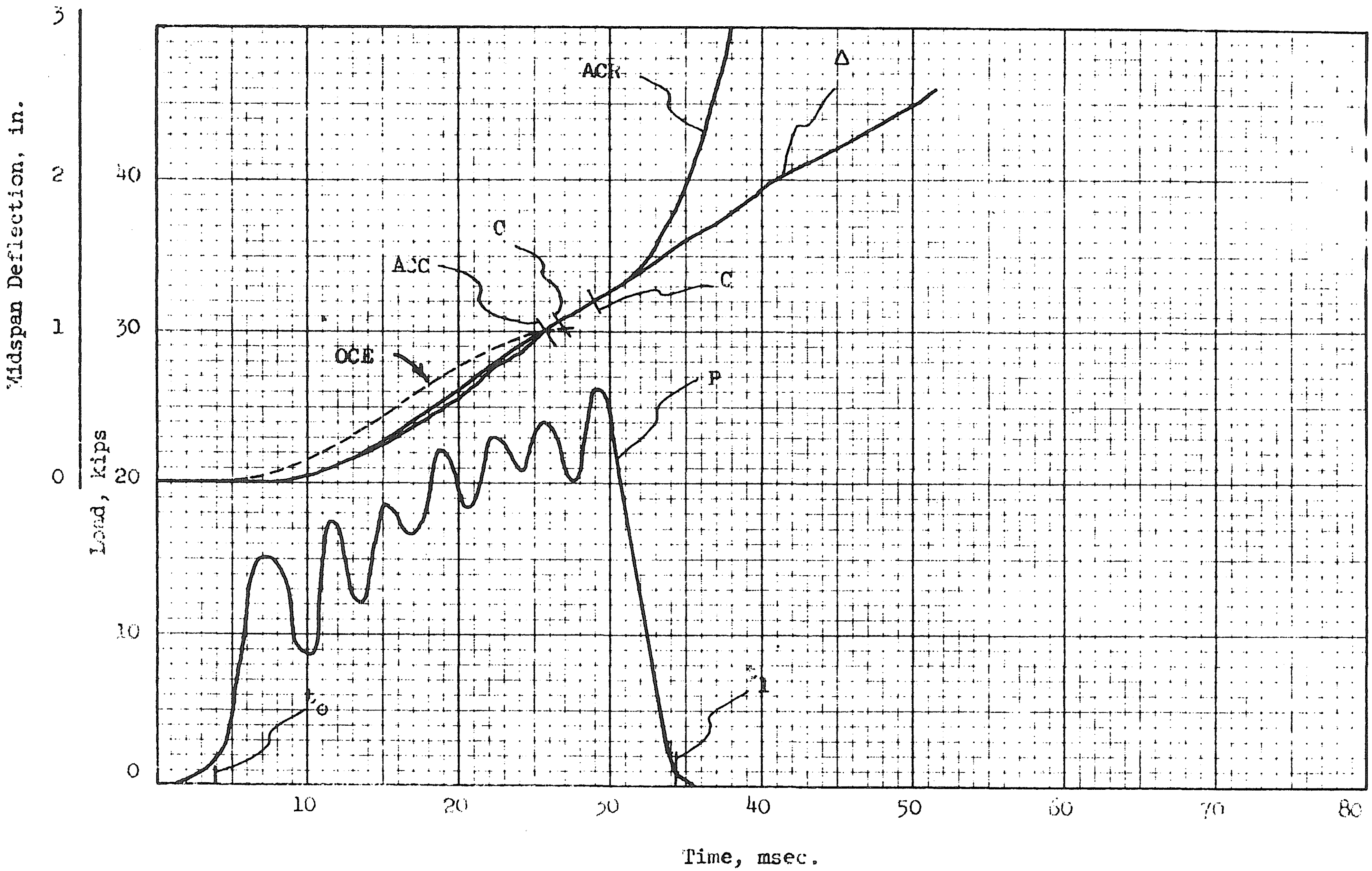

FIG. A60 LOAD AND RESPONSE, BEAM 5b4, BLOW 2

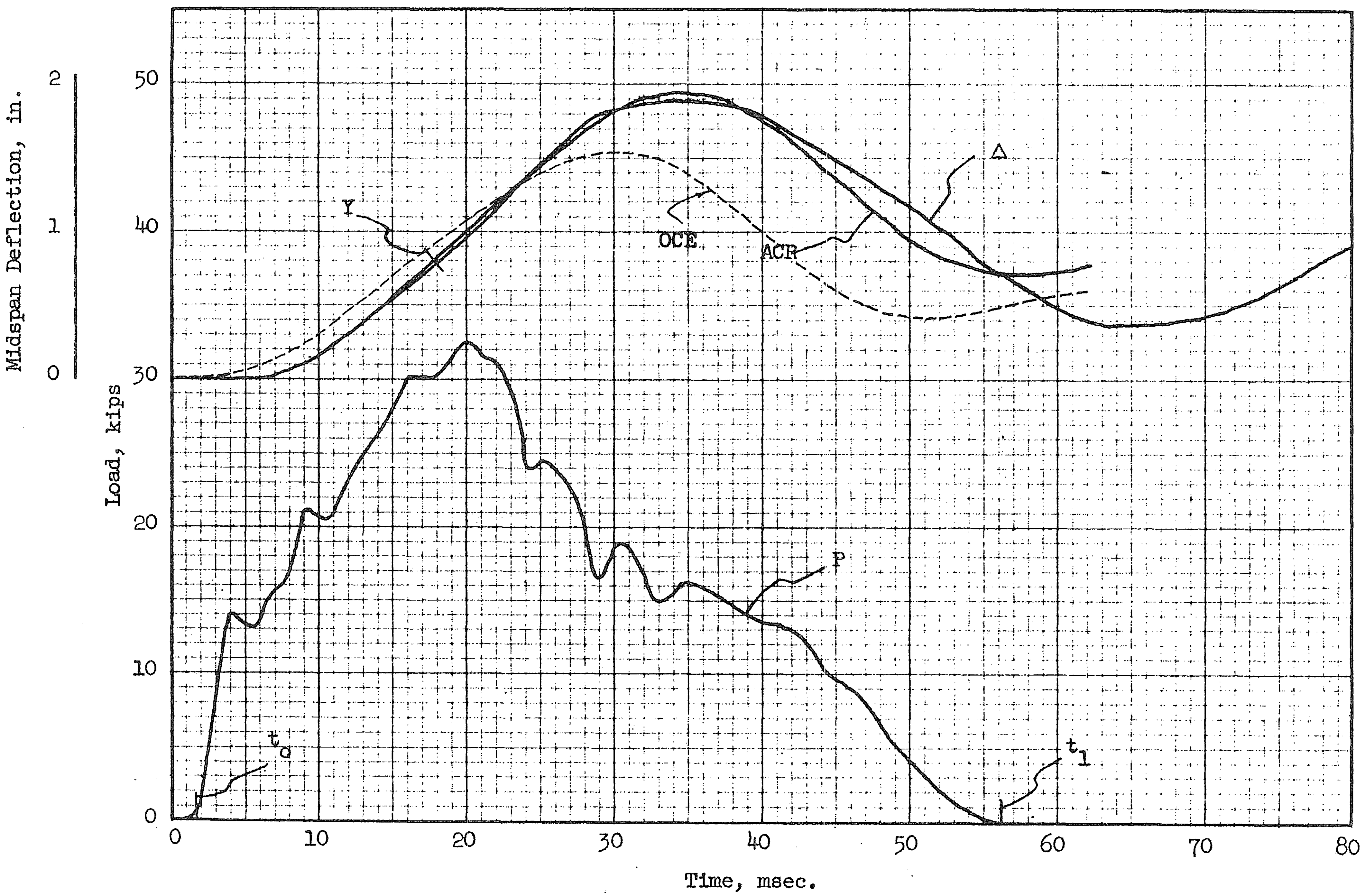

FIG. A61 LOAD AND RESPONSE, BEAM 6a1, BLOW 1

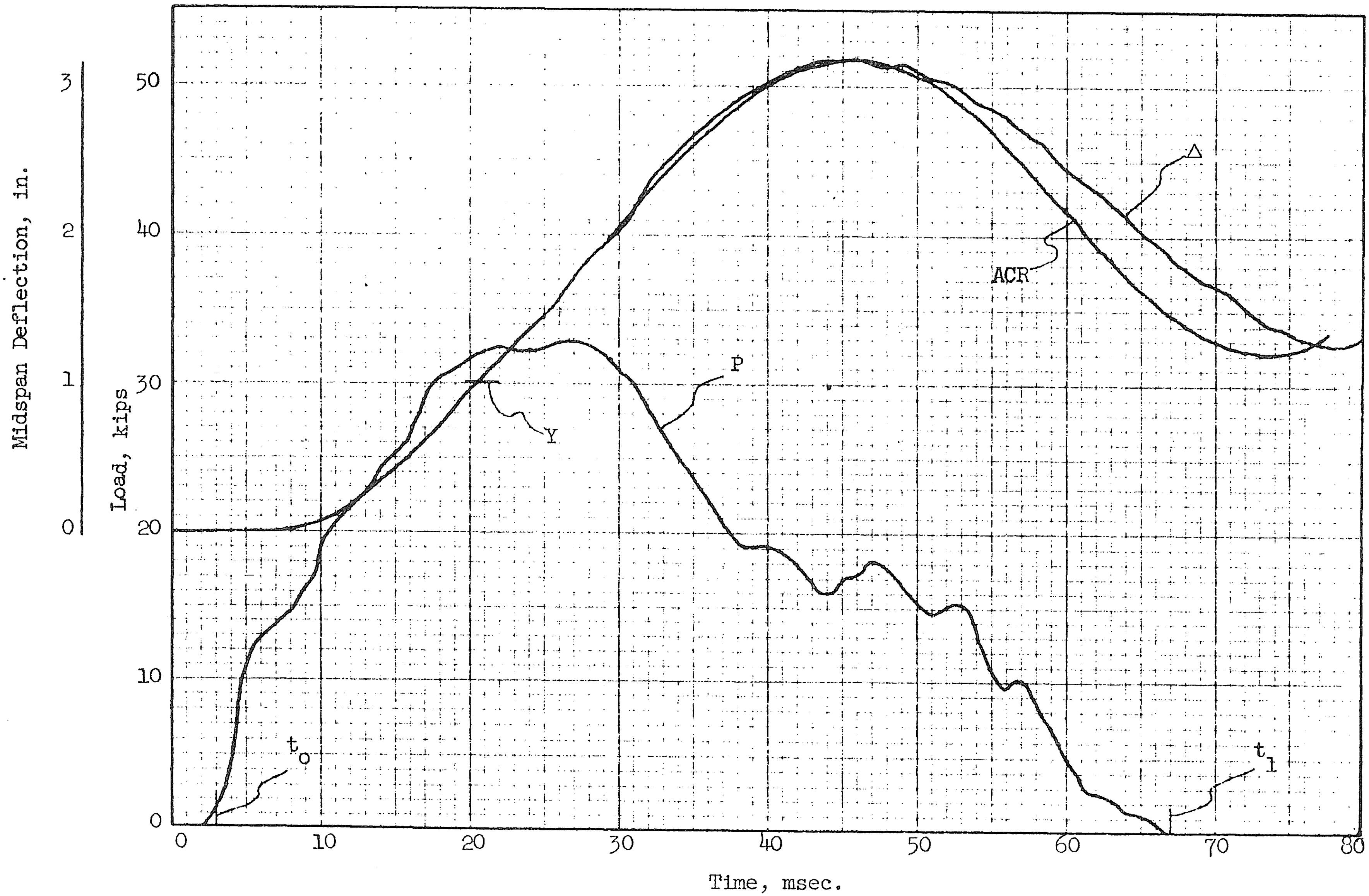

FIG. A62 LOAD AND RESPONSE, BEAM 6a1, BLOW 2

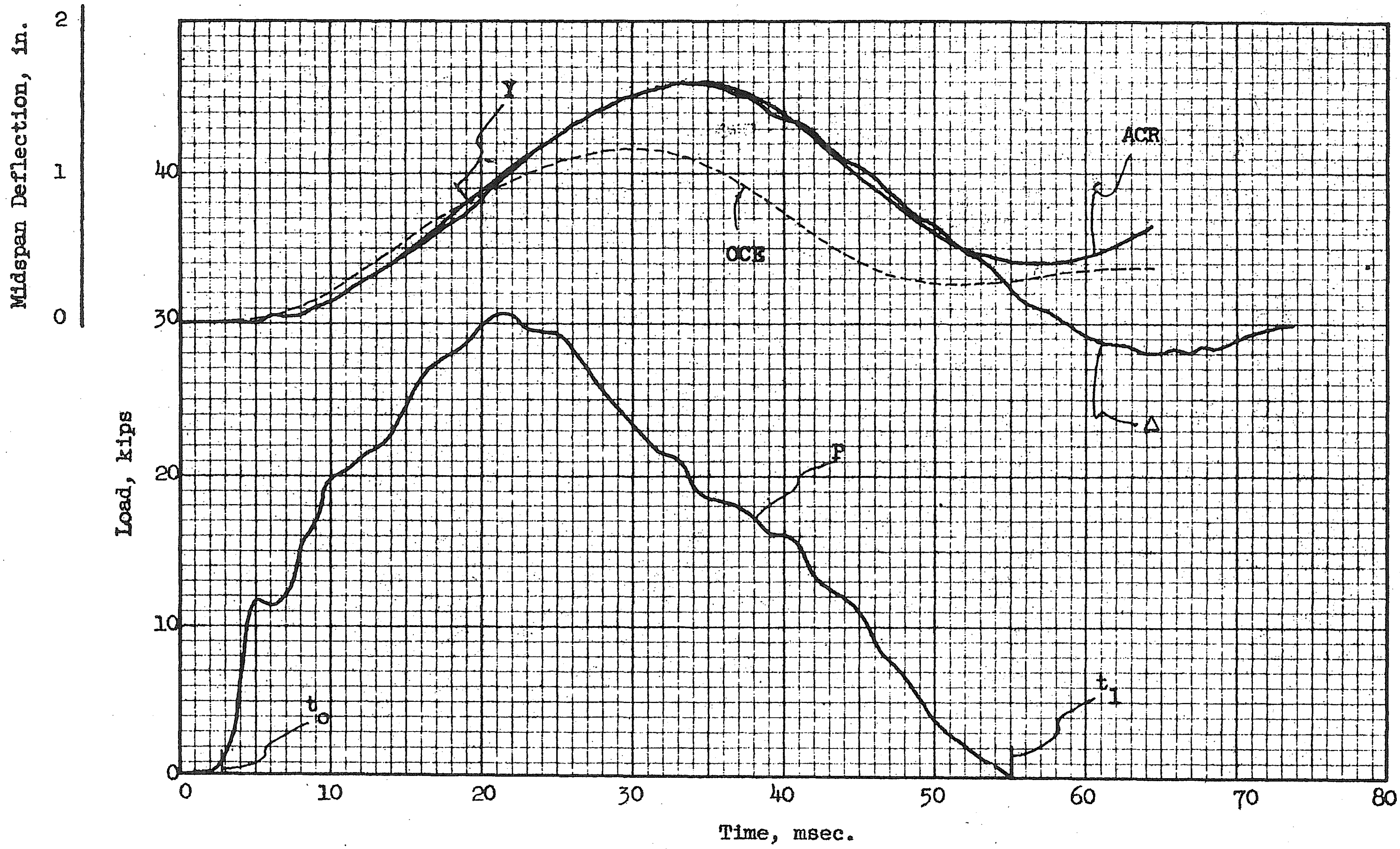

FIG. A63 LOAD AND RESPONSE, BEAM 6b2, BLOW 1

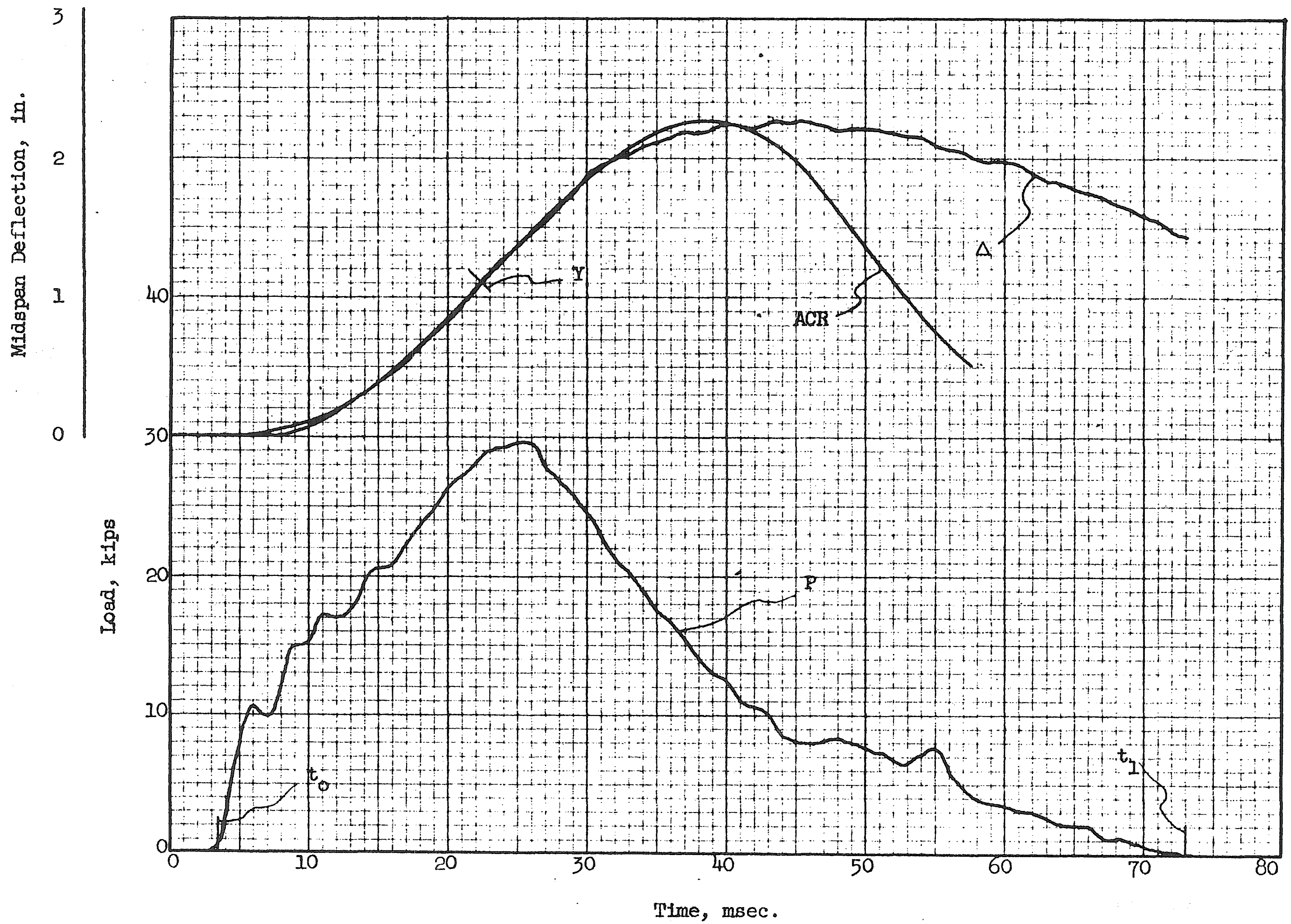

FIG. A64 LOAD AND RESPONSE, BEAM 6b2, BLOW 2

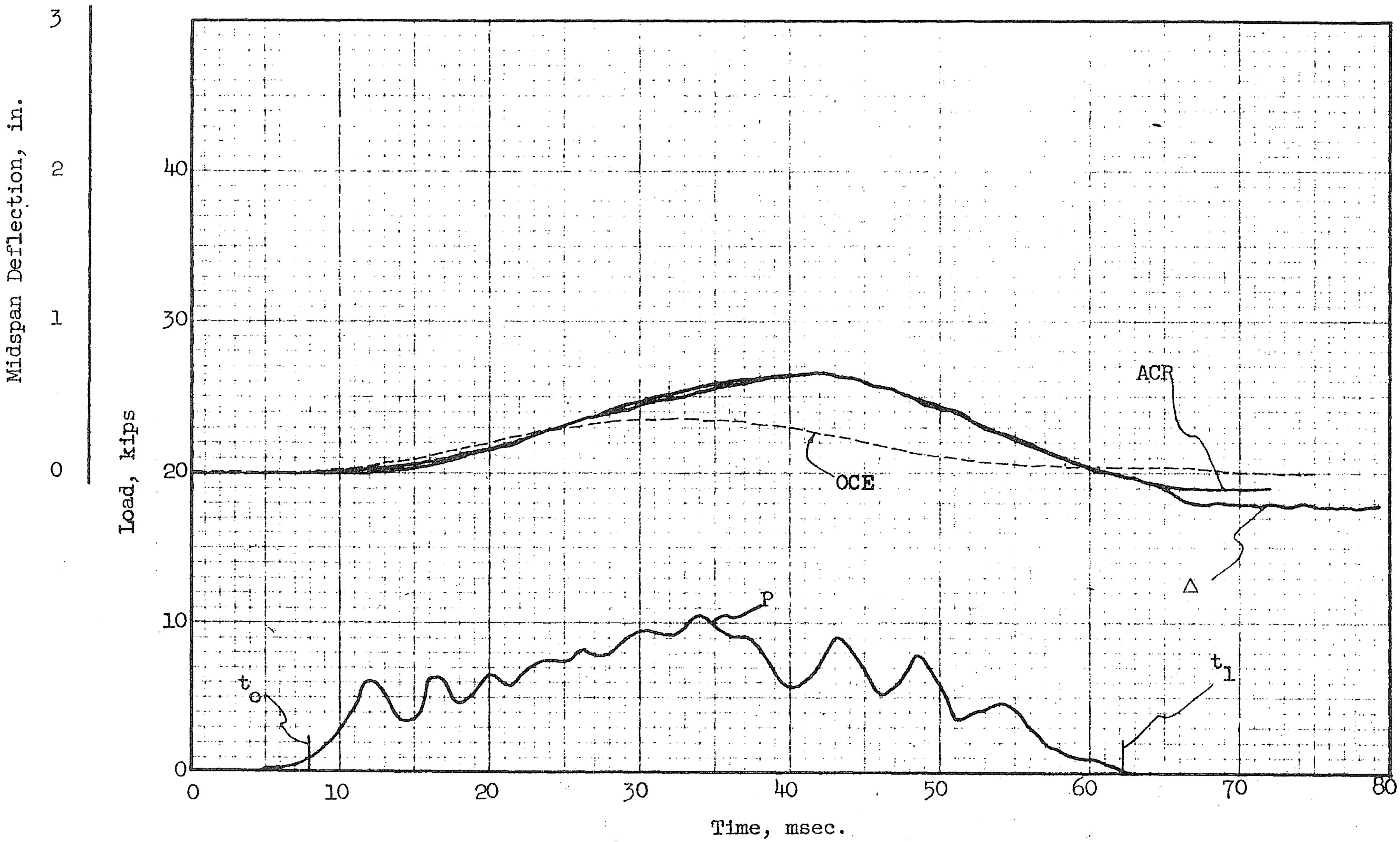

FIG. A65 LOAD AND RESPONSE, BEAM 7a2, BLOW 1

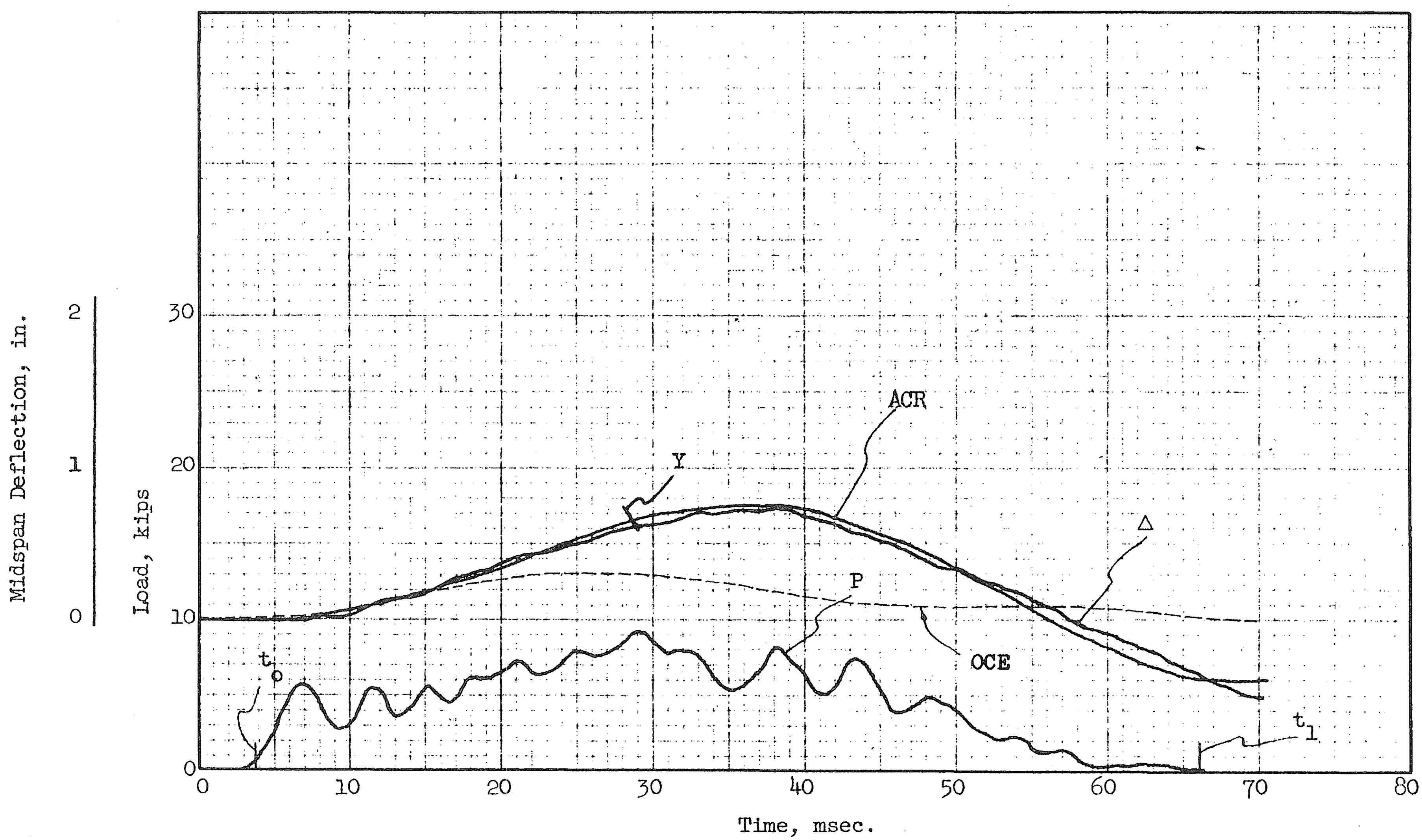

FIG. A66 LOAD AND RESPONSE, BEAM 7a2, BLOW 2

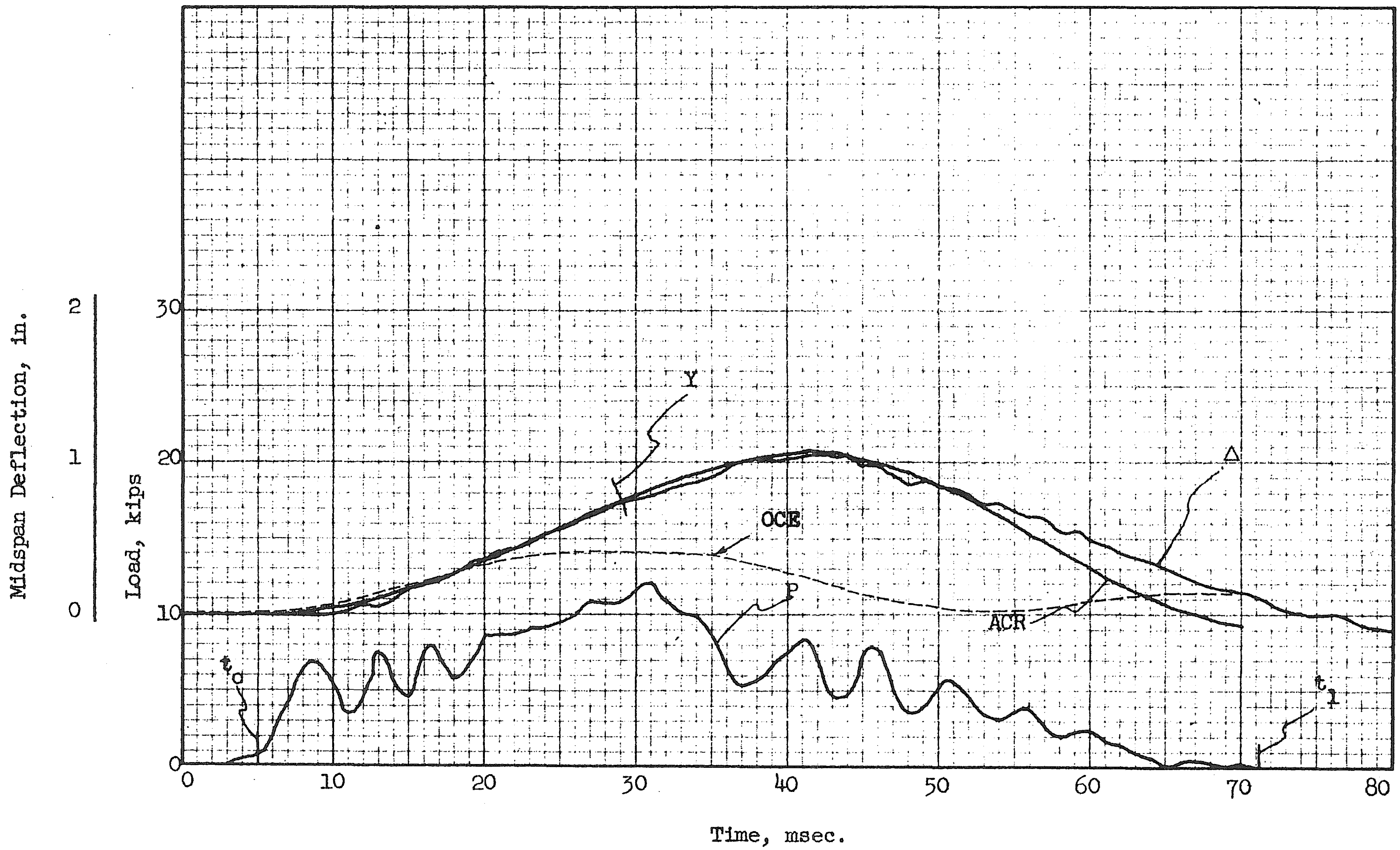

FIG. A67 LOAD AND RESPONSE, BEAM 7a2, BLOW 3

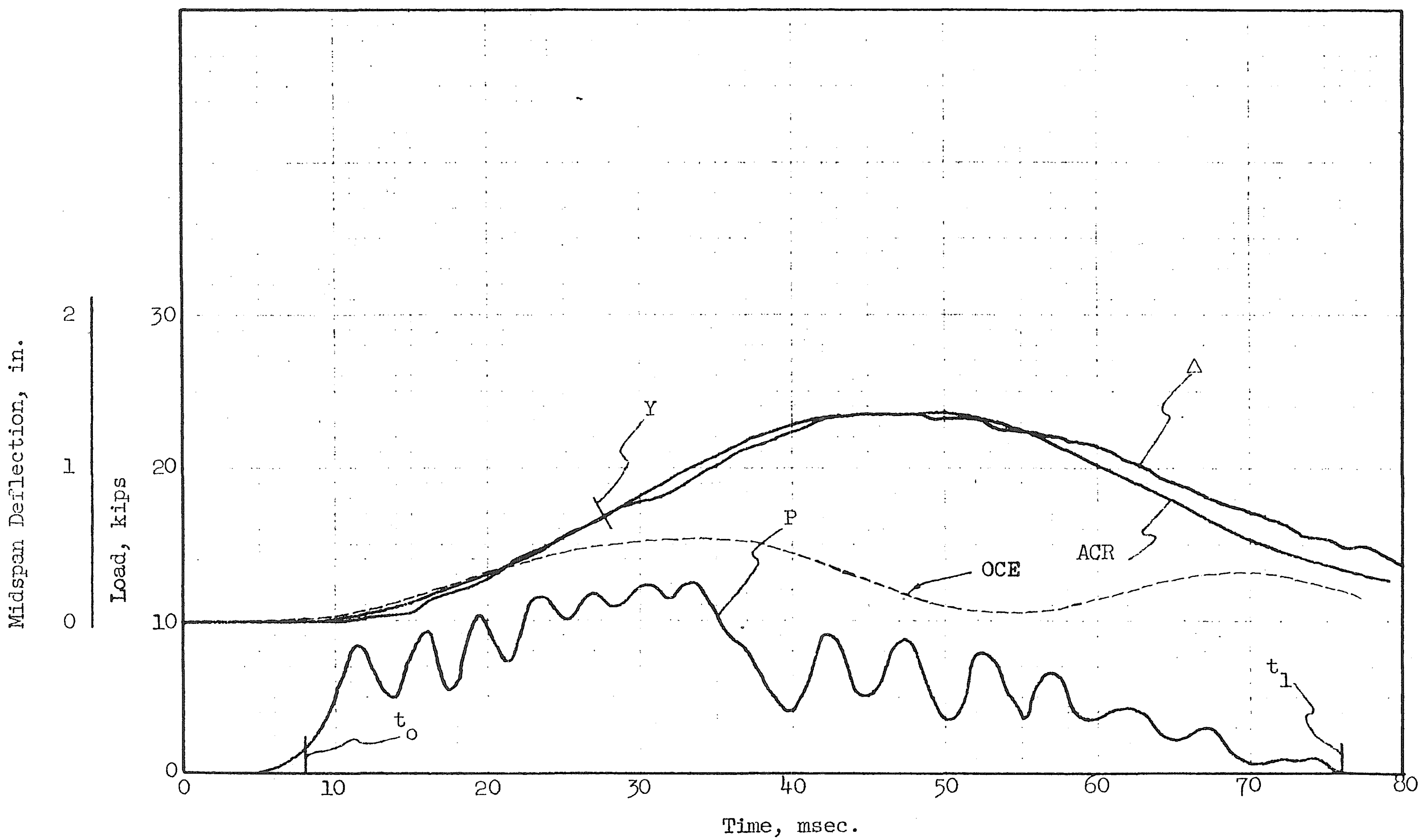

FIG. A68 LOAD AND RESPONSE, BEAM 7a2, BLOW 4

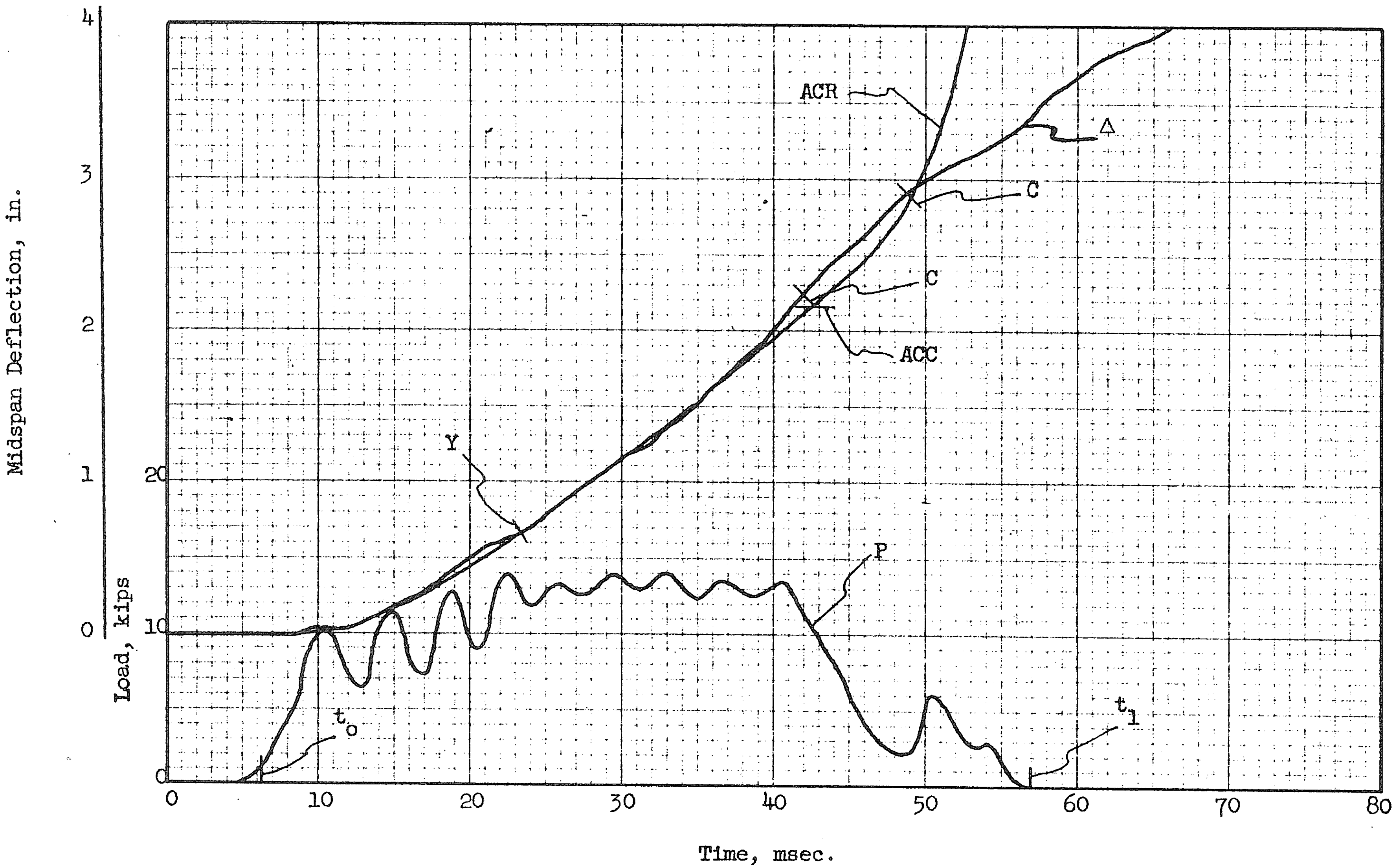

FIG. A69 LOAD AND RESPONSE, BEAM 7a2, BLOW 5

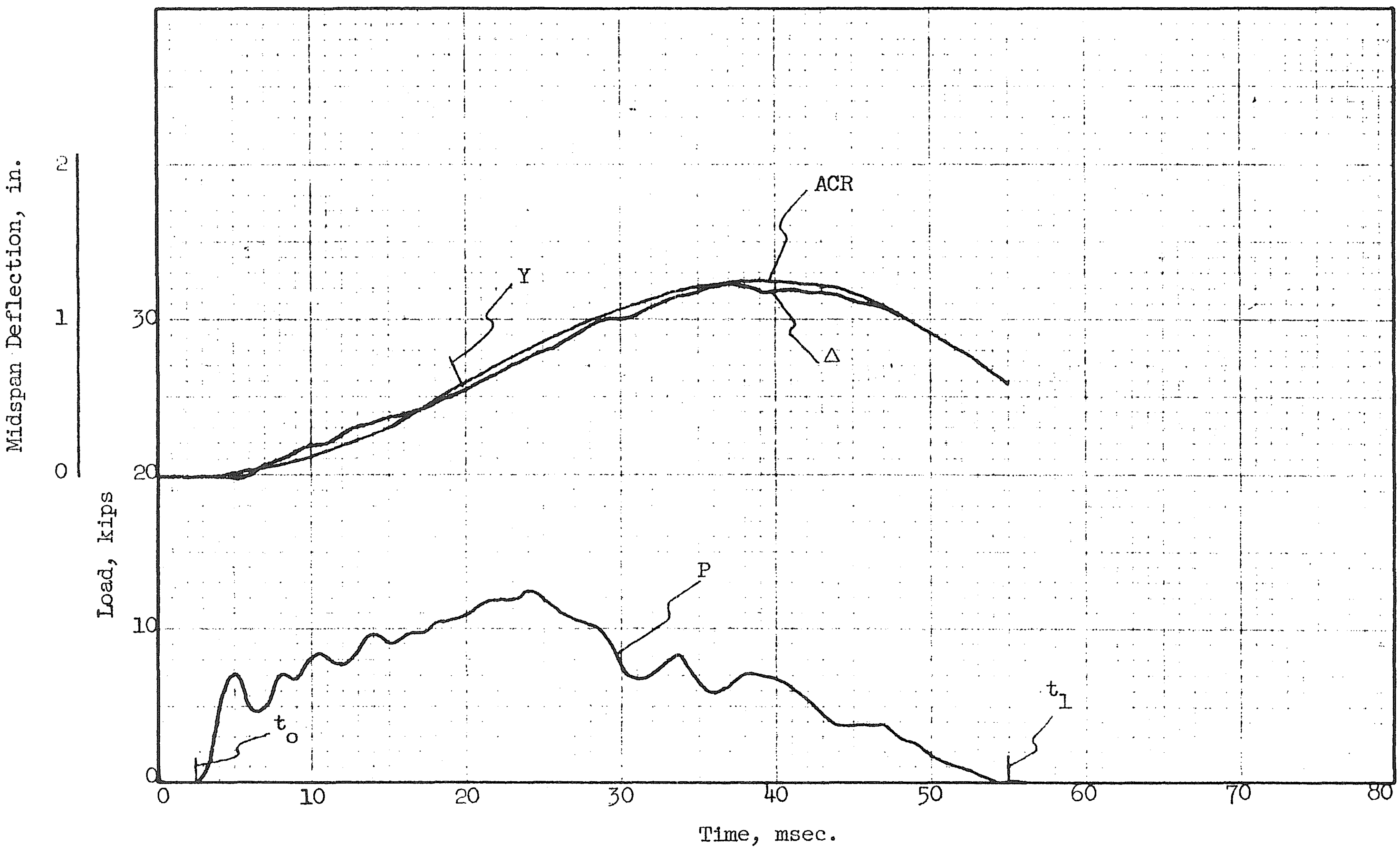

FIG. A70 LOAD AND RESPONSE, BEAM 7a3, BLOW 1

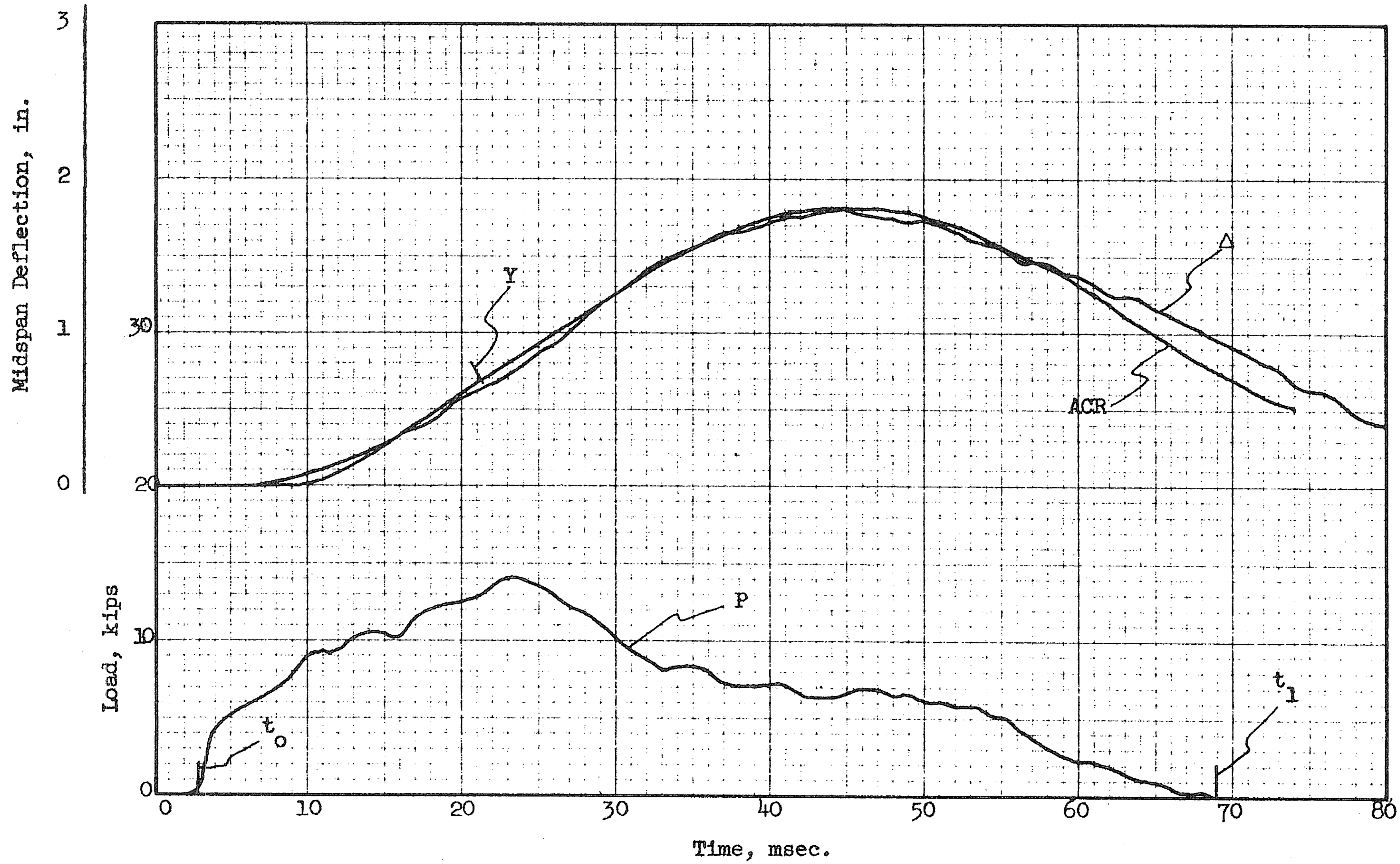

FIG. A71 LOAD AND RESPONSE, BEAM 7a3, BLOW 2

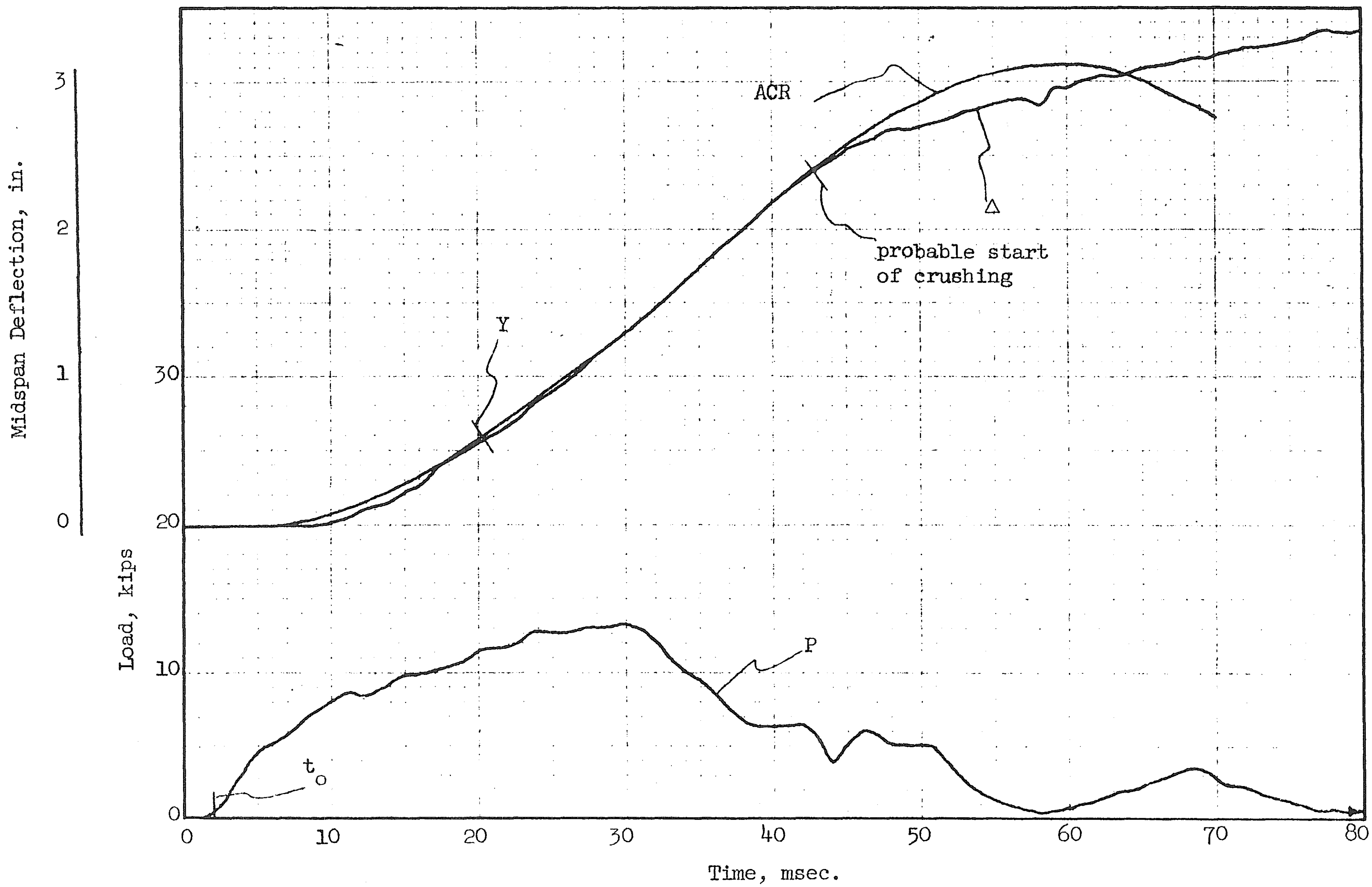

FIG. A72 LOAD AND RESPONSE, BEAM 7a3, BLOW 3

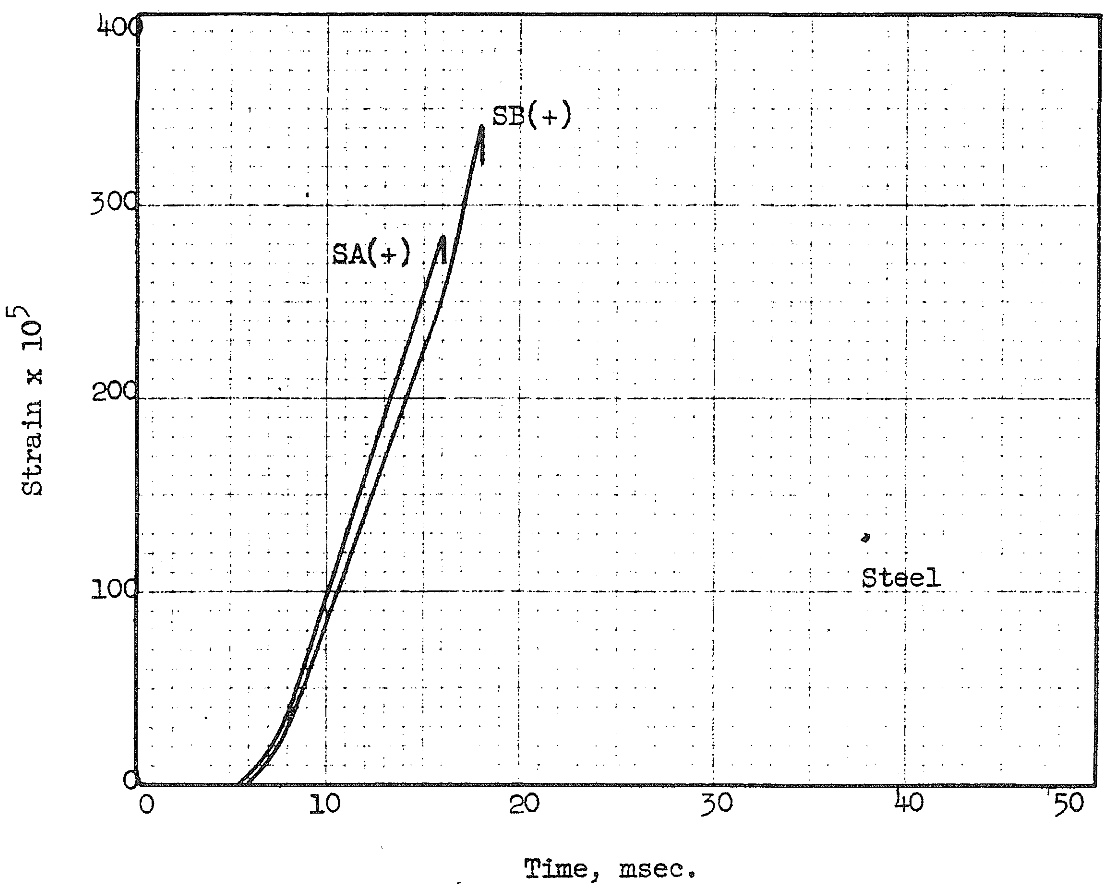

FIG. A73 STRAIN VS. TIME, BEAM 2al

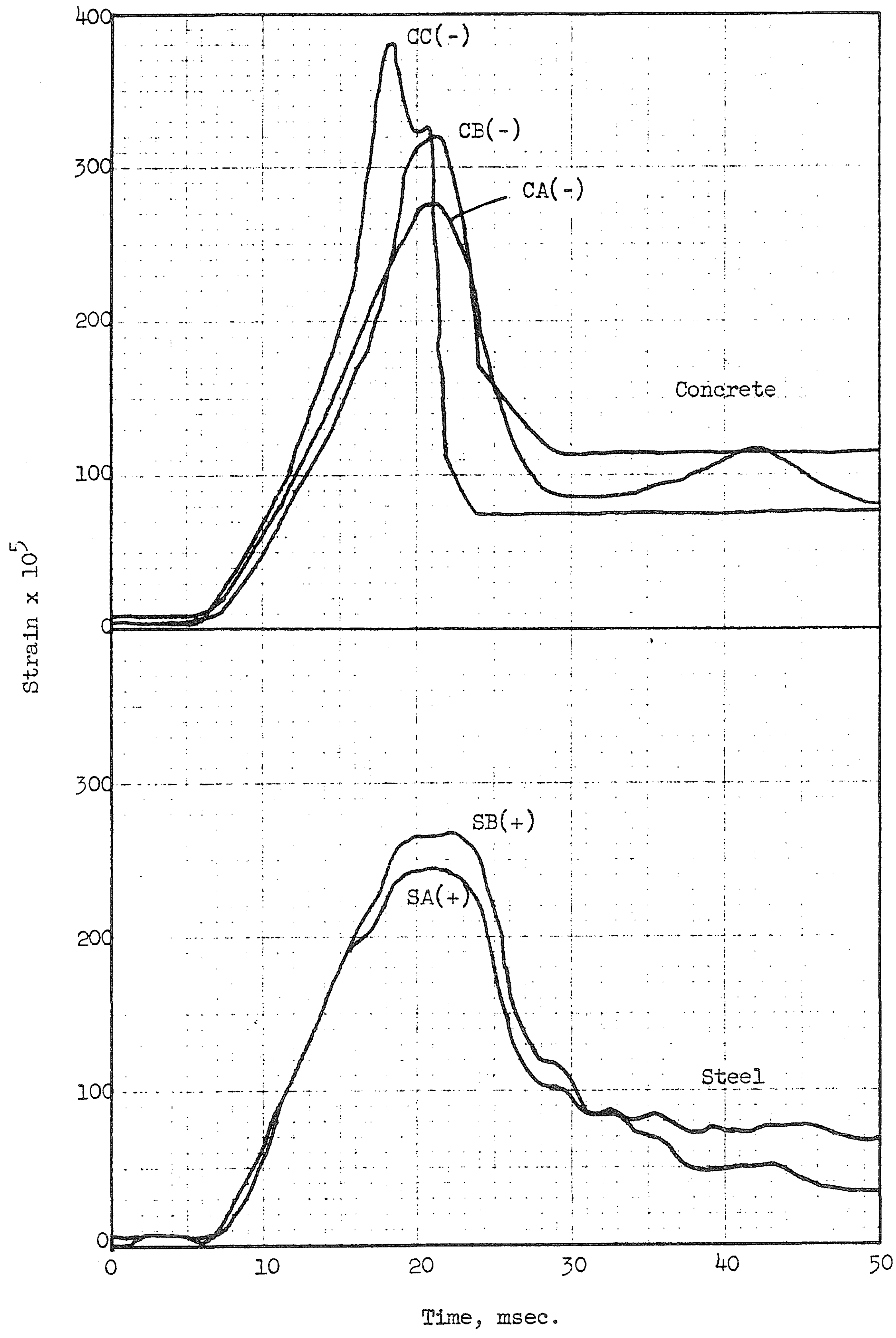

FIG. A74 STRAIN VS. TIME, BEAM 2b2

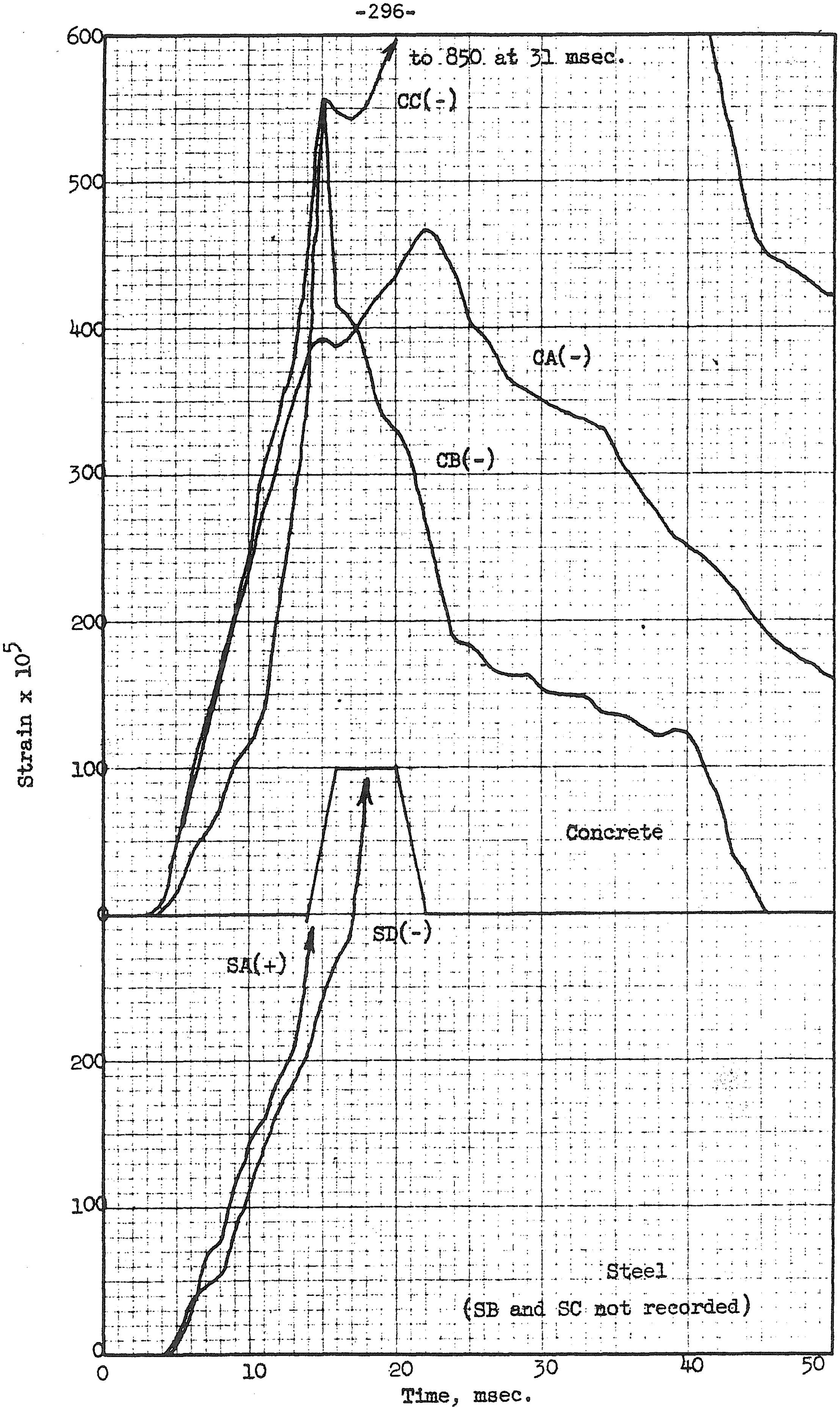

FIG. A75 STRAIN VS. TIME, BEAM 3a2

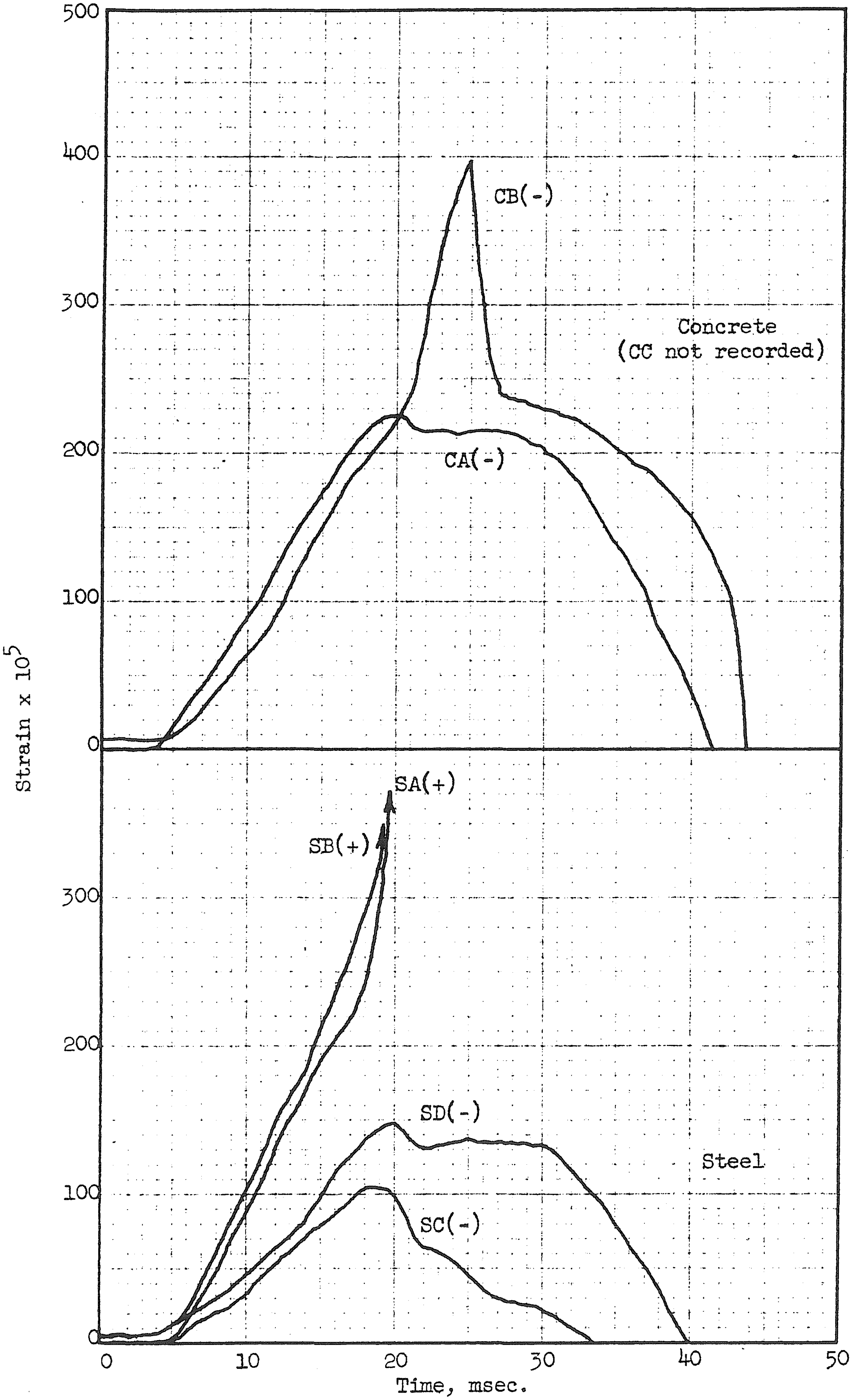

FIG. A76 STRAIN VS. TIME, BEAM 3b2, BLOW 1

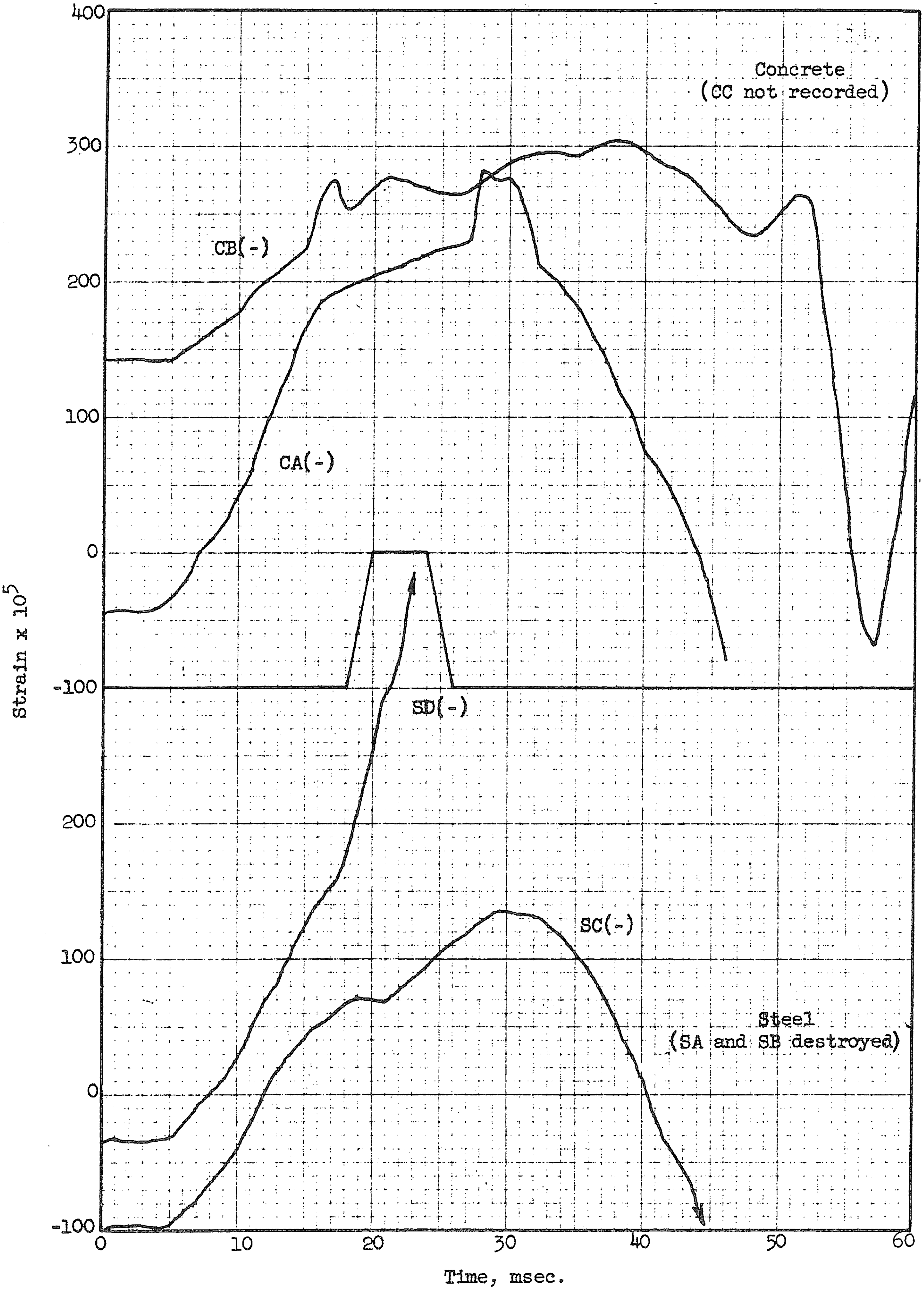

FIG. A77 STRAIN VS. TIME, BEAM 3b2, BLOW 2

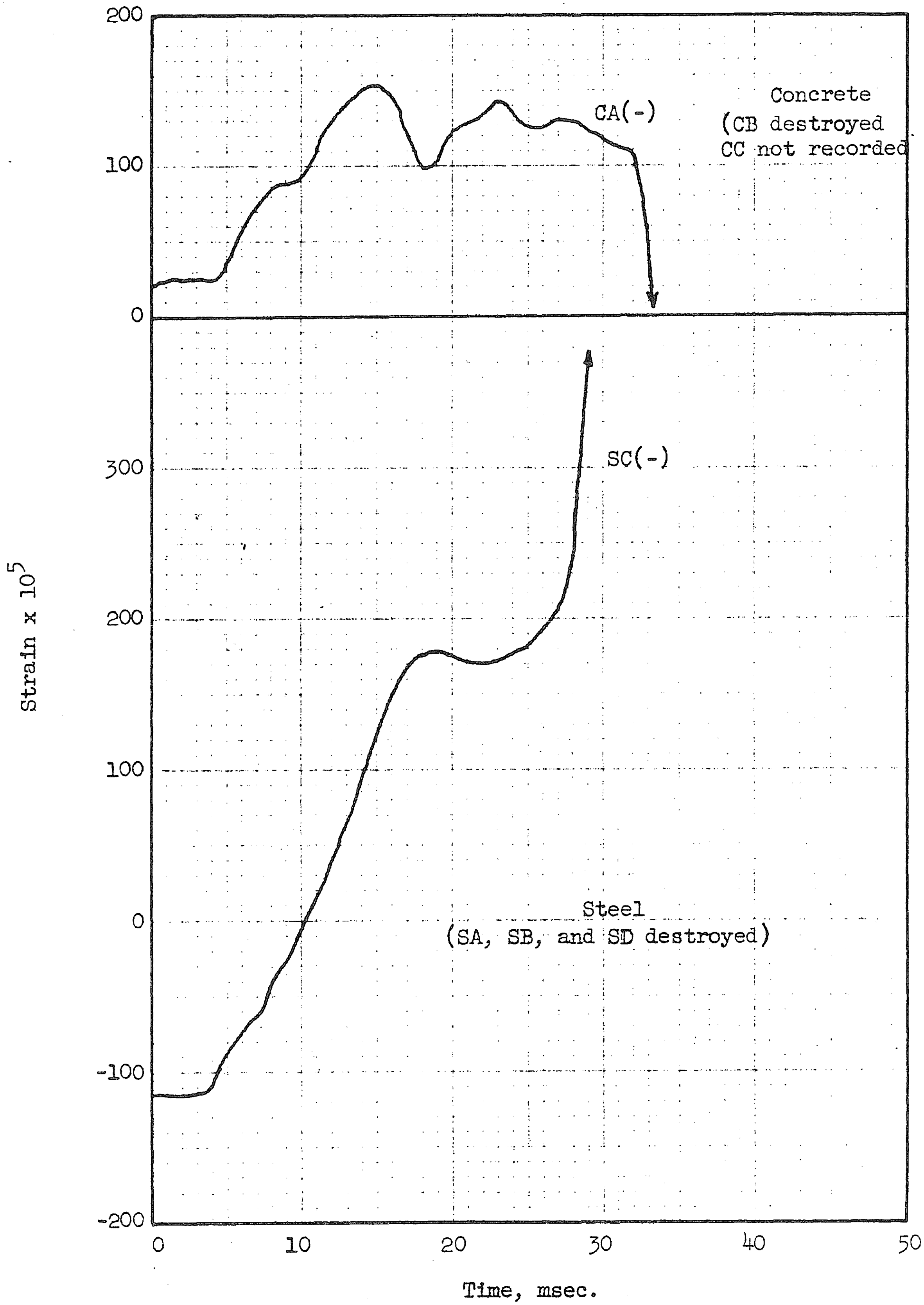

FIG. A78 STRAIN VS. TIME, BEAM 3b2, BLOW 3

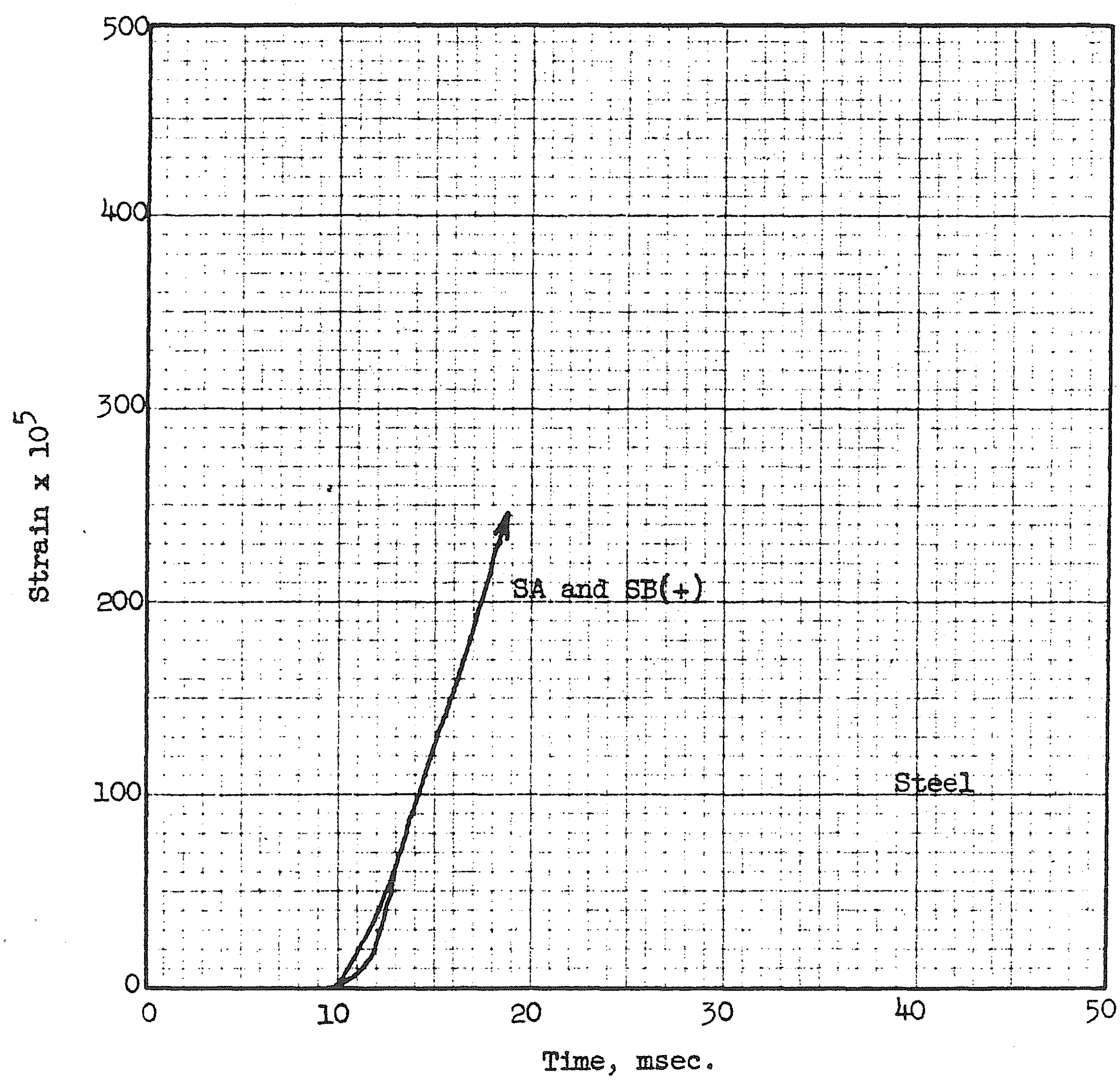

FIG. A79 STRAIN VS. TIME, BEAM 4a1

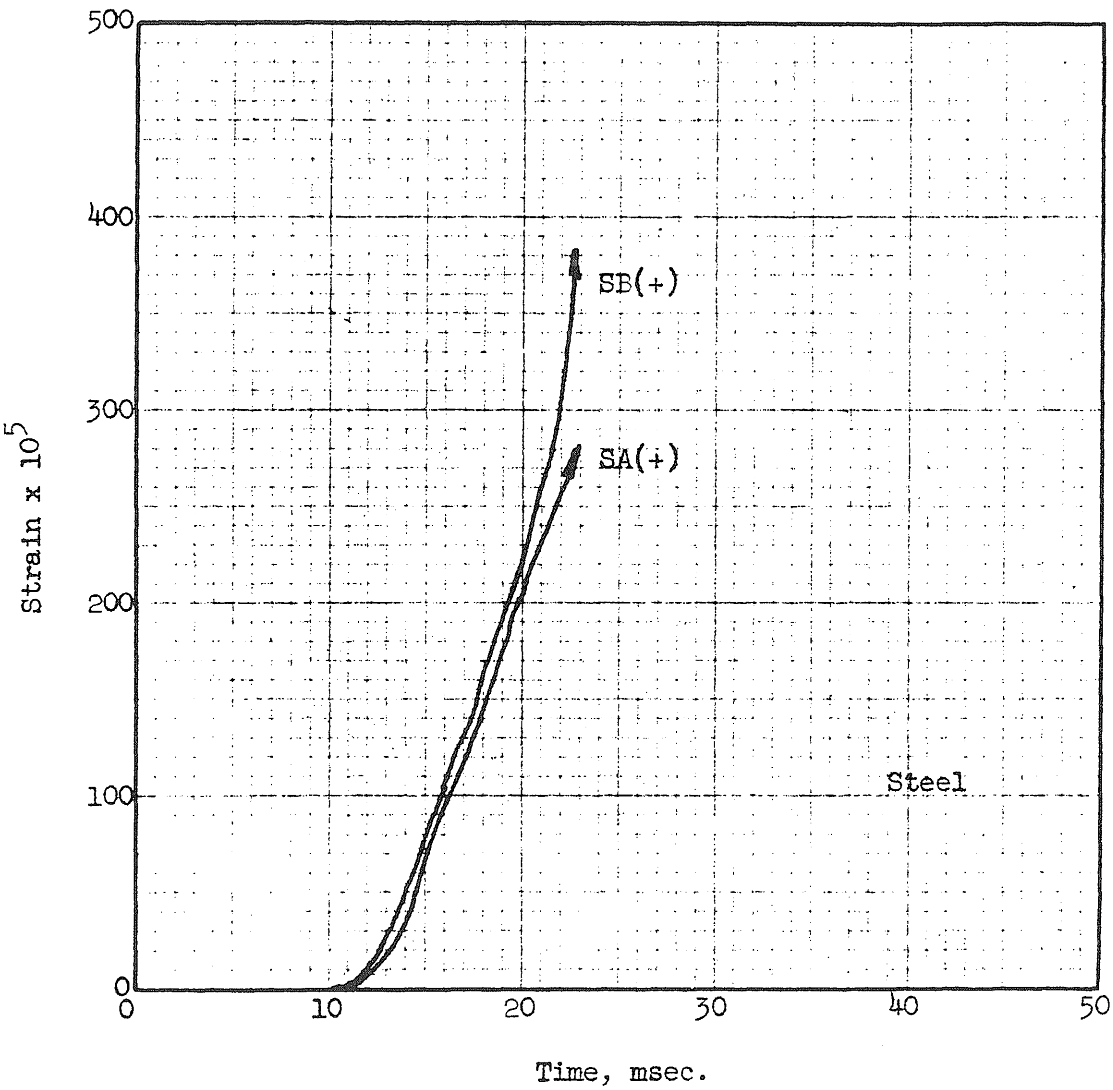

FIG. A80 STRAIN VS. TIME, BEAM 4a2, BLOW 1

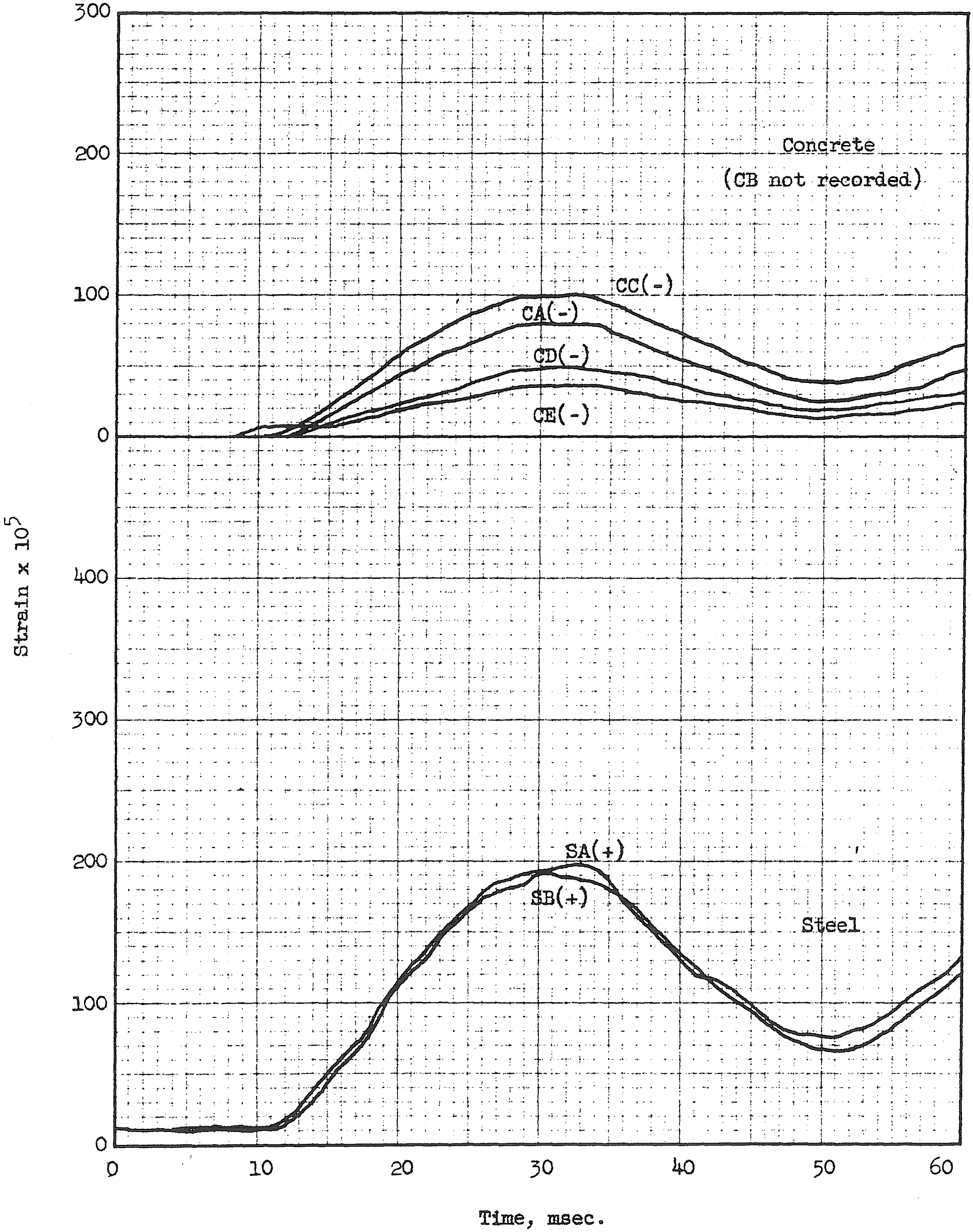

FIG. A81 STRAIN VS. TIME, BEAM 4c2, BLOW 1

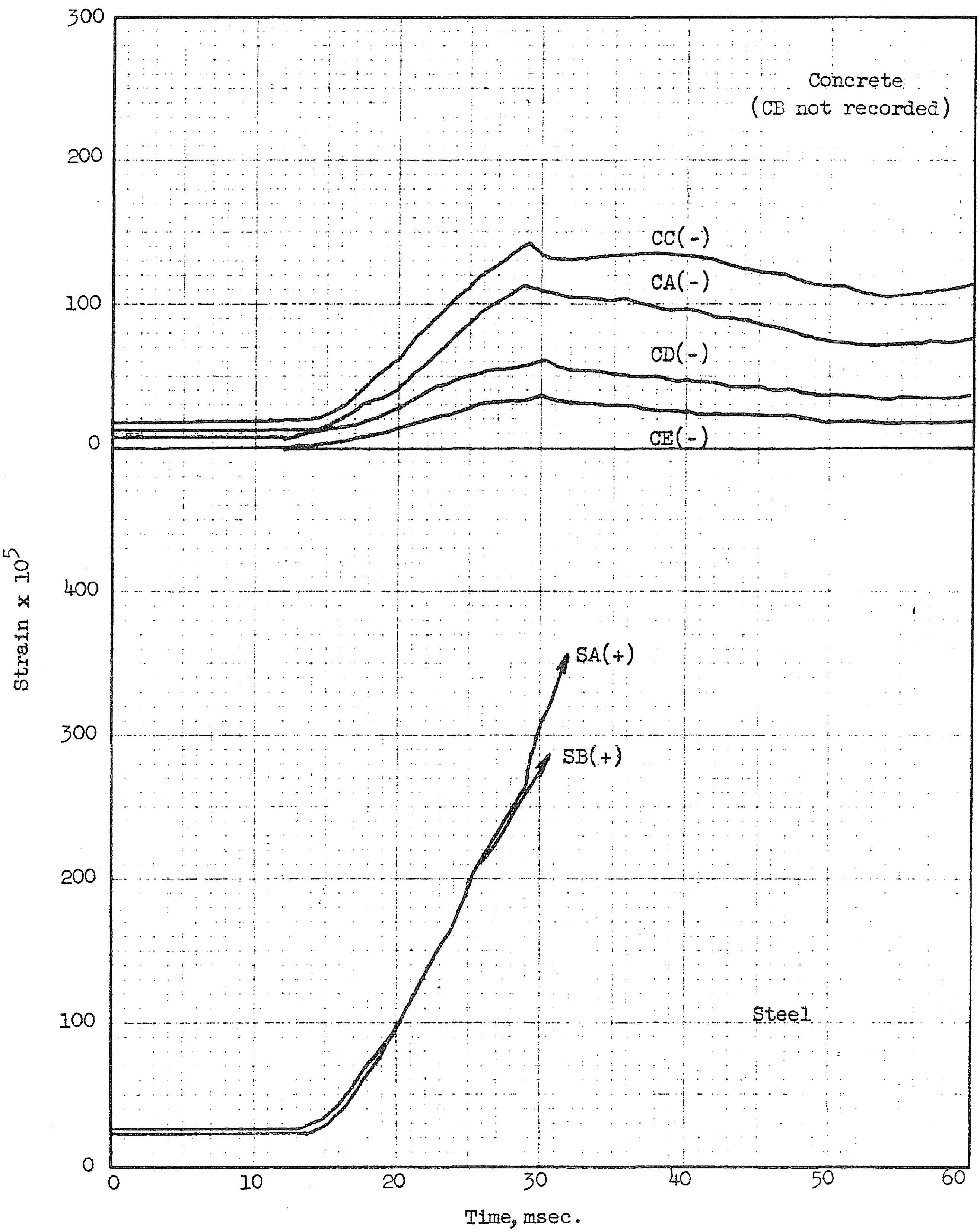

FIG. A82 STRAIN VS. TIME, BEAM 4c2, BLOW 2

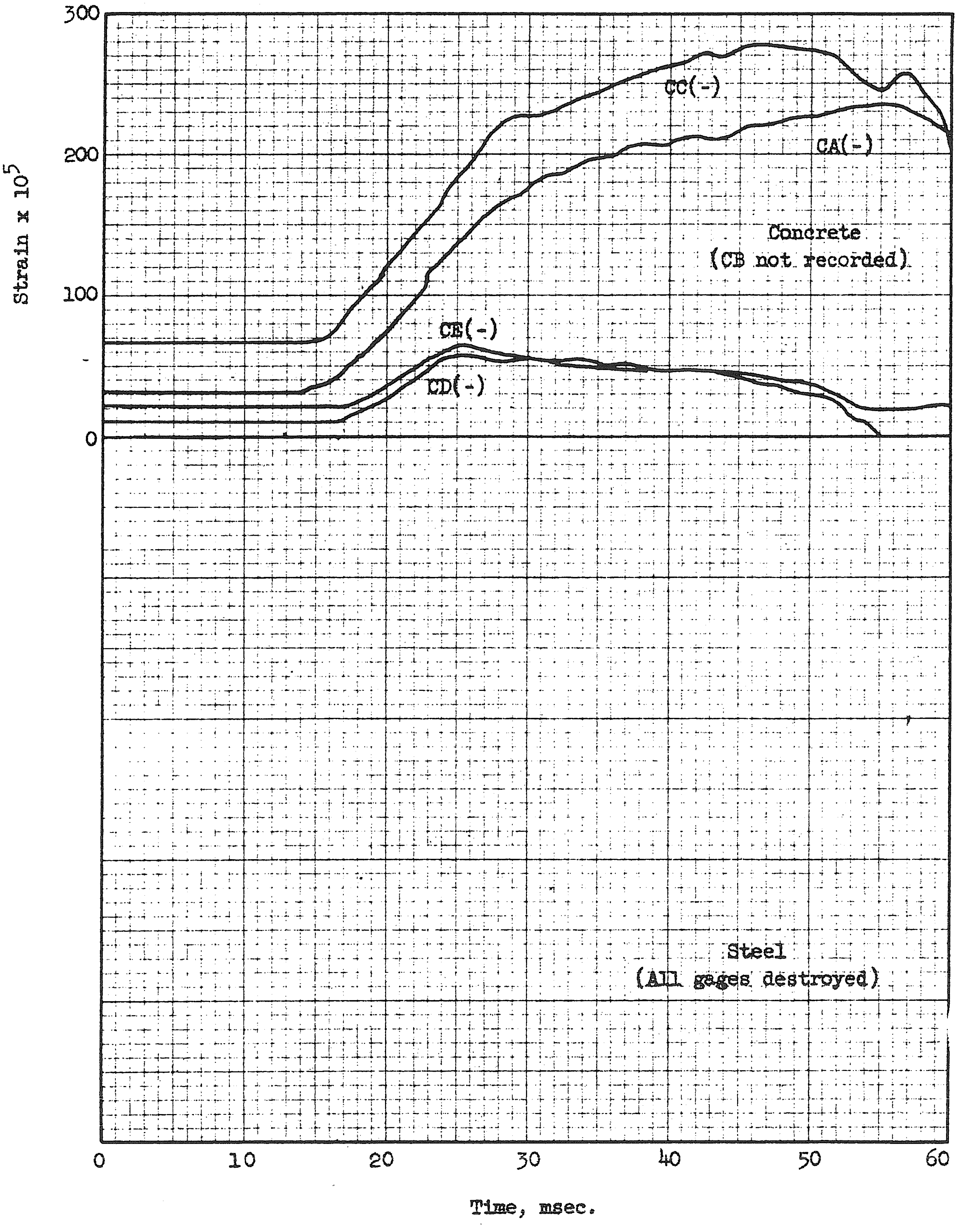

FIG. A83 STRAIN VS. TIME, BEAM 4c2, BLOW 3

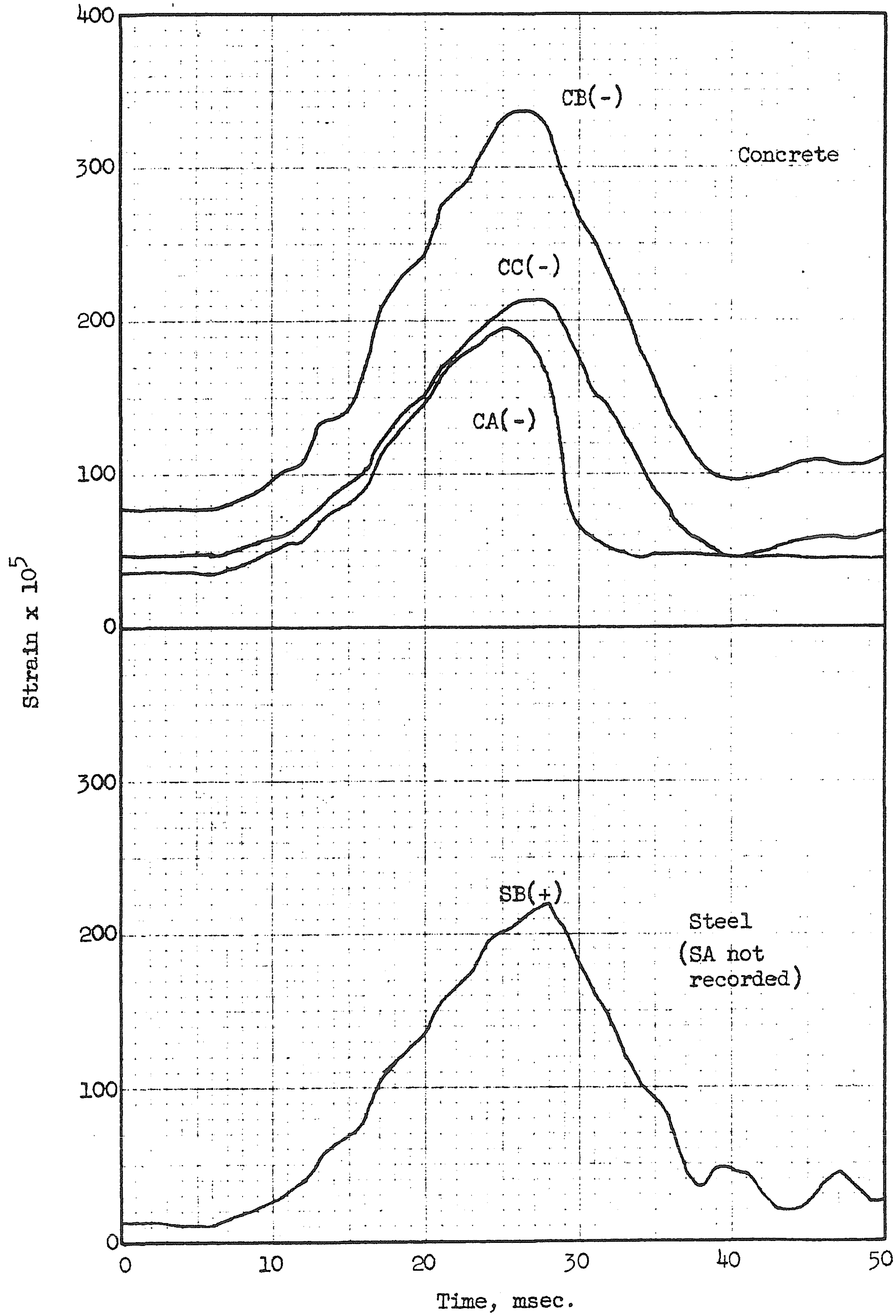

FIG. A84 STRAIN VS. TIME, BEAM 5a2

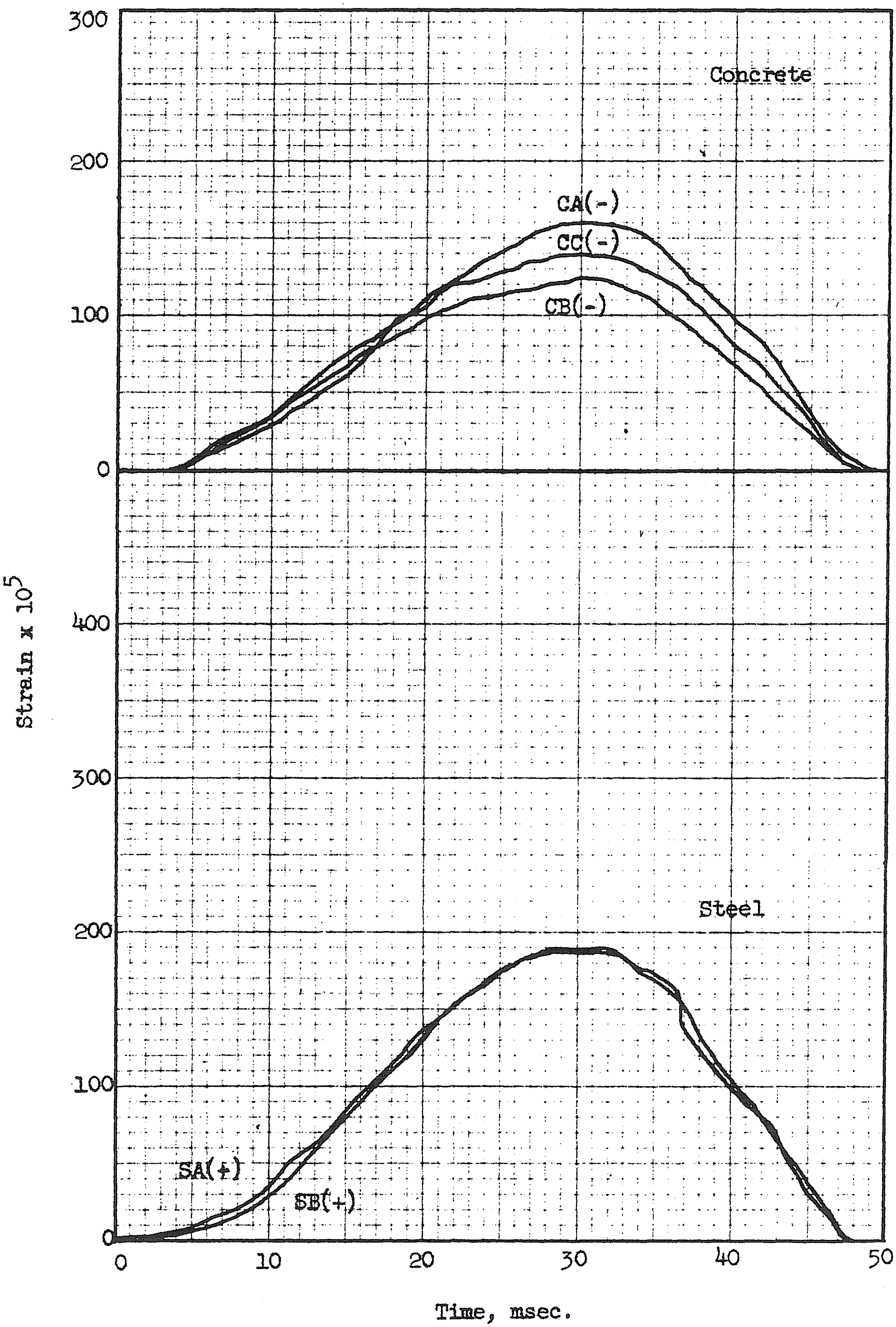

FIG. A85 STRAIN VS. TIME, BEAM 5b4, BLOW 1

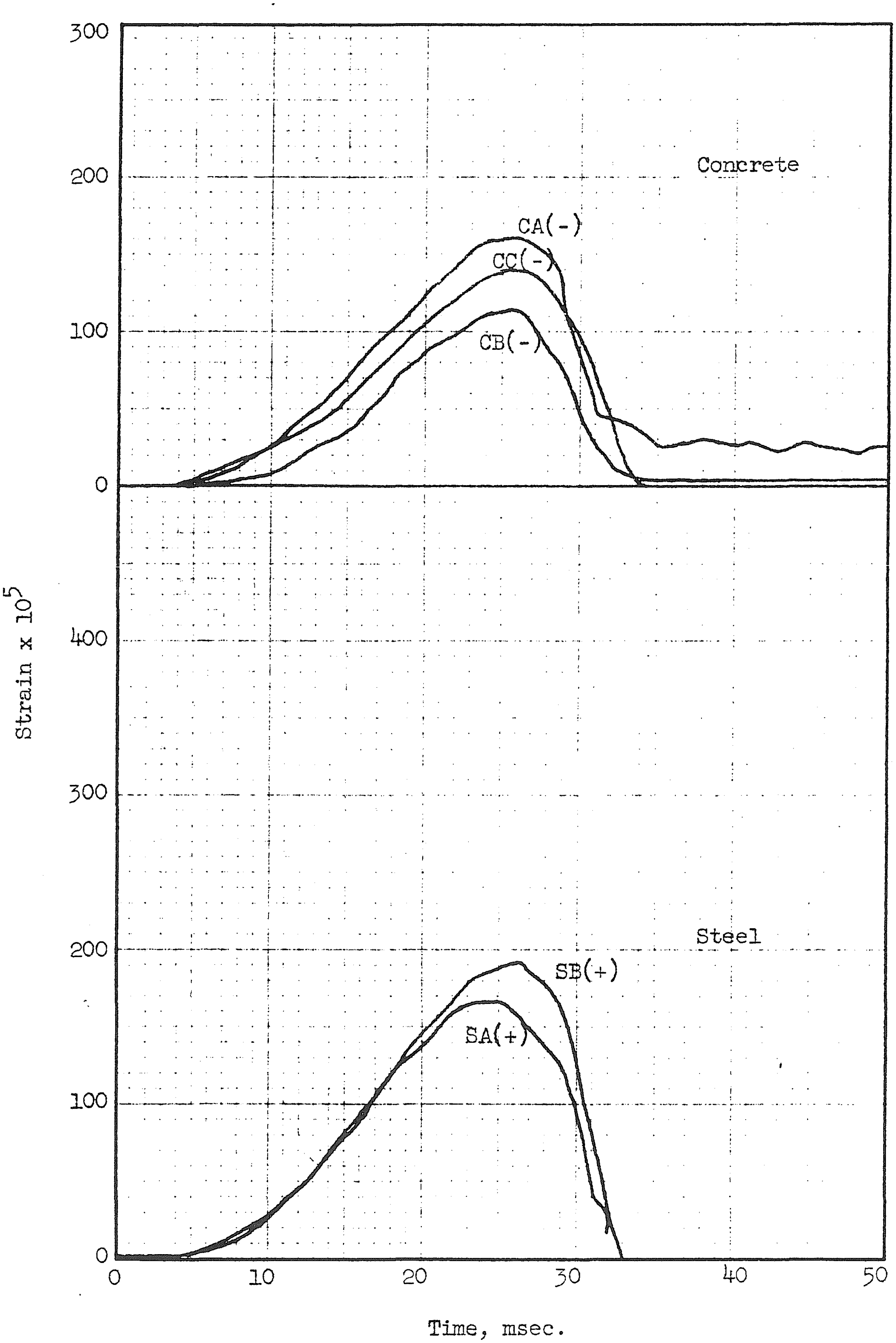

FIG. A86 STRAIN VS. TIME, BEAM 5b4, BLOW 2

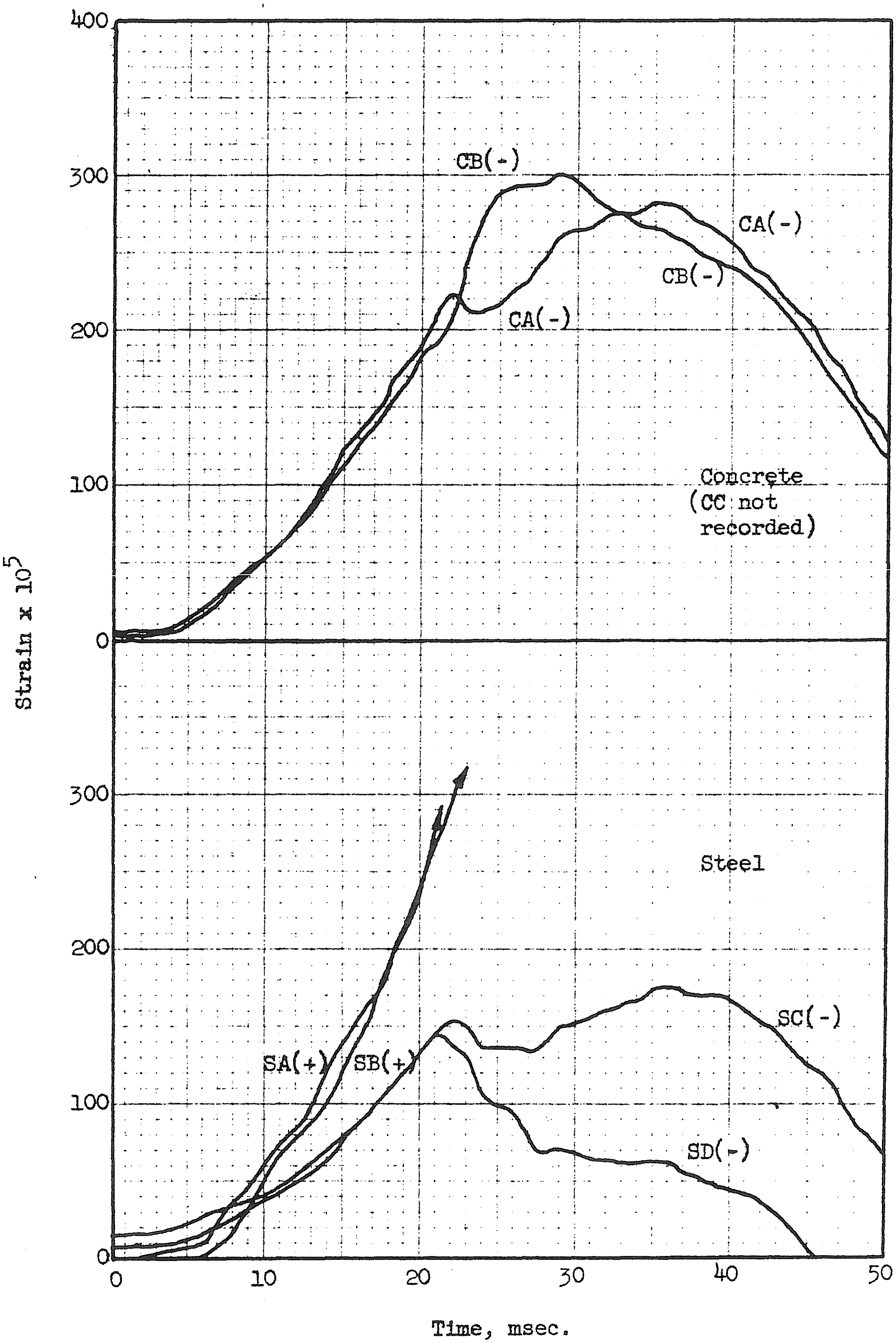

FIG. A87 STRAIN VS. TIME, BEAM 6a1, BLOW 1

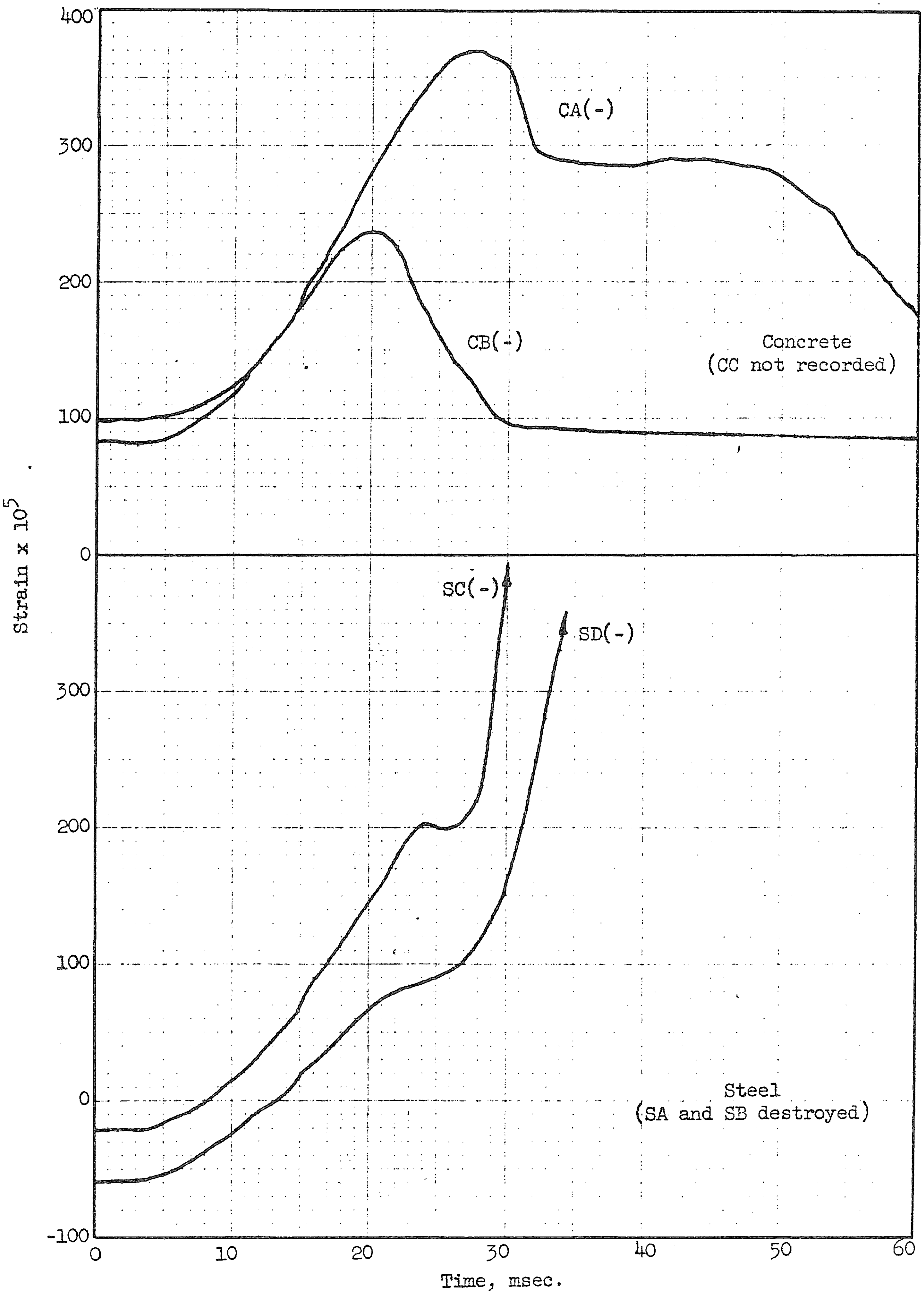

FIG. A88 STRAIN VS. TIME, BEAM 6a1, BLOW 2

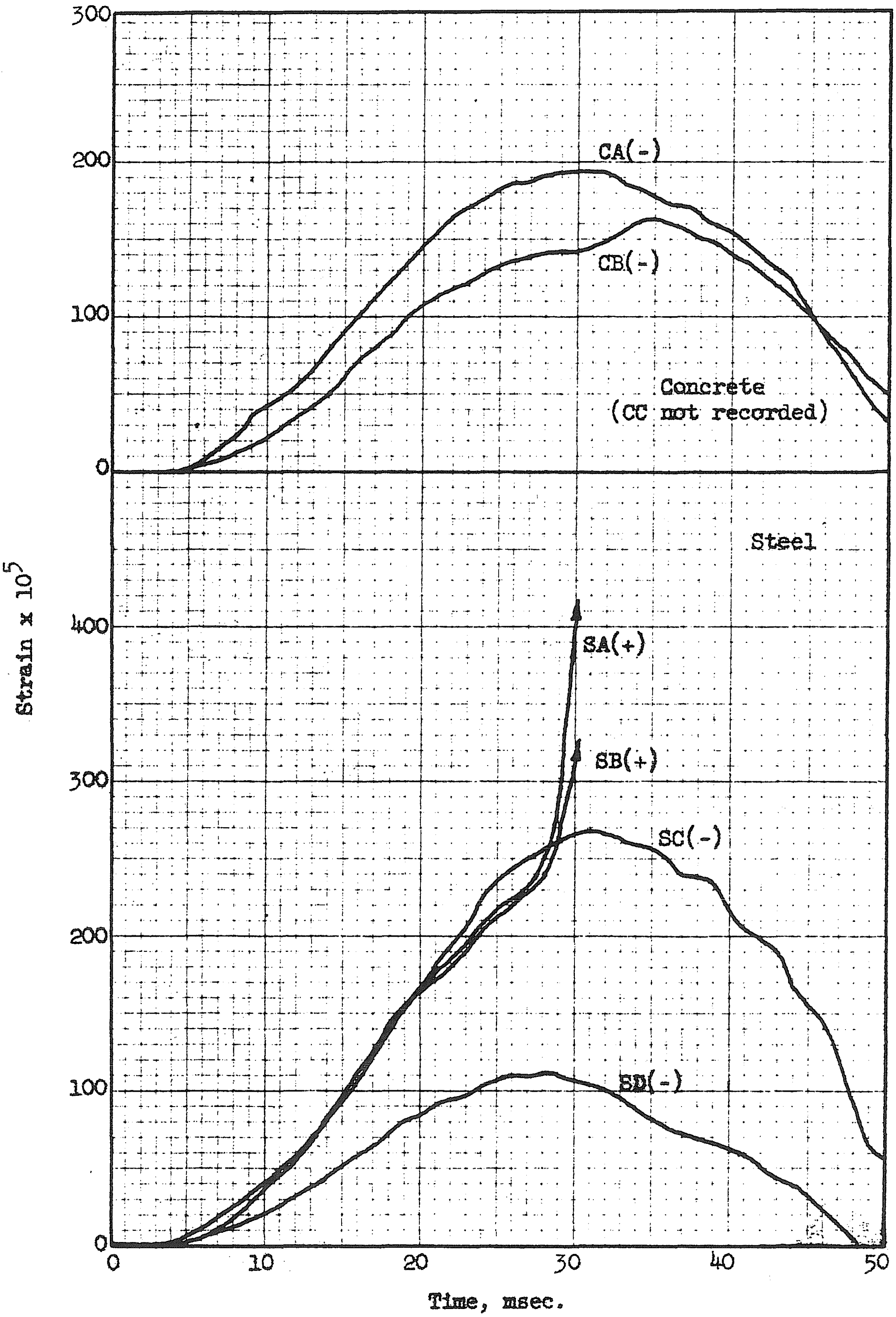

FIG. A89 STRAIN VS. TIME, BEAM 6b2, BLOW 1

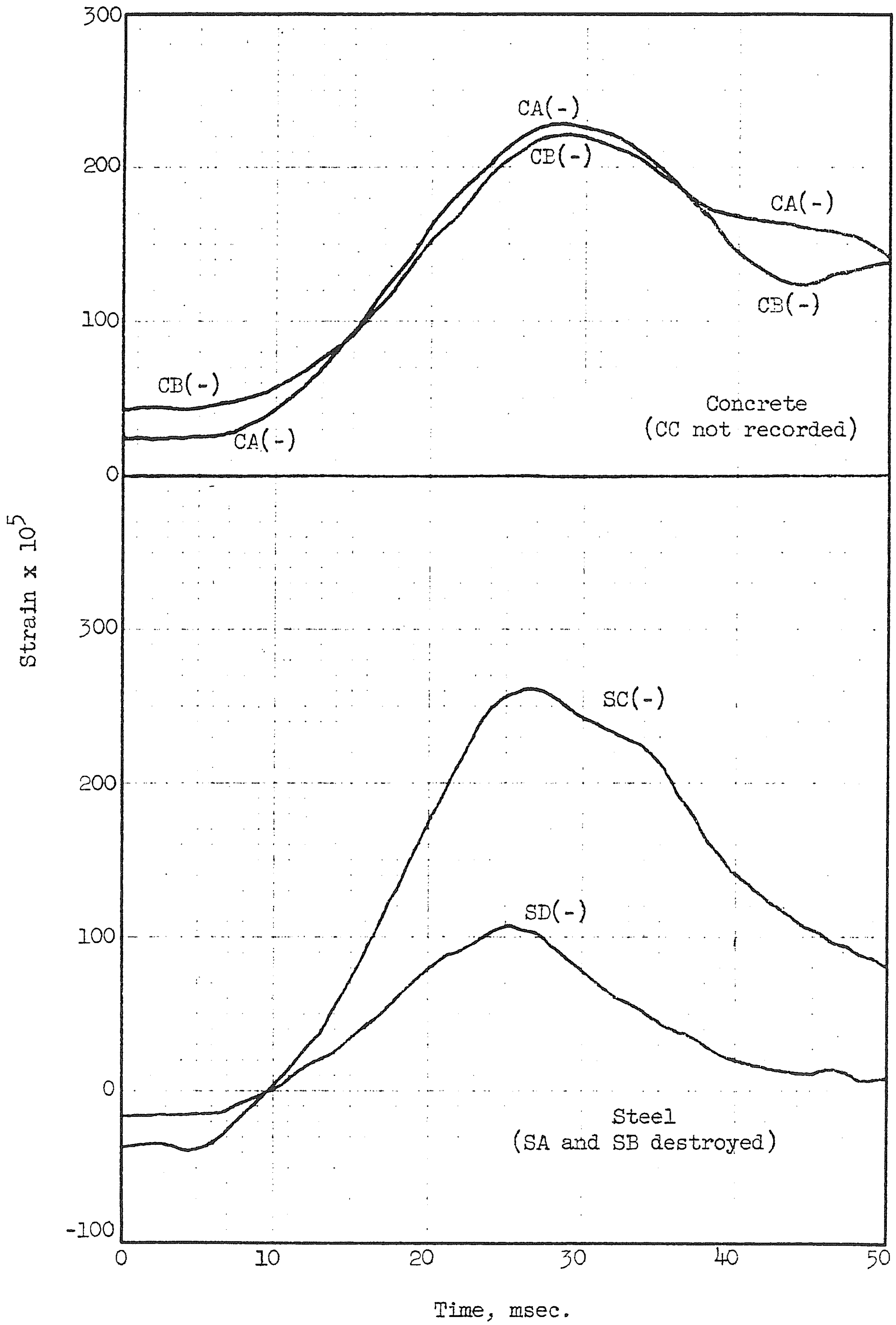

FIG. A90 STRAIN VS. TIME, BEAM 6b2, BLOW 2

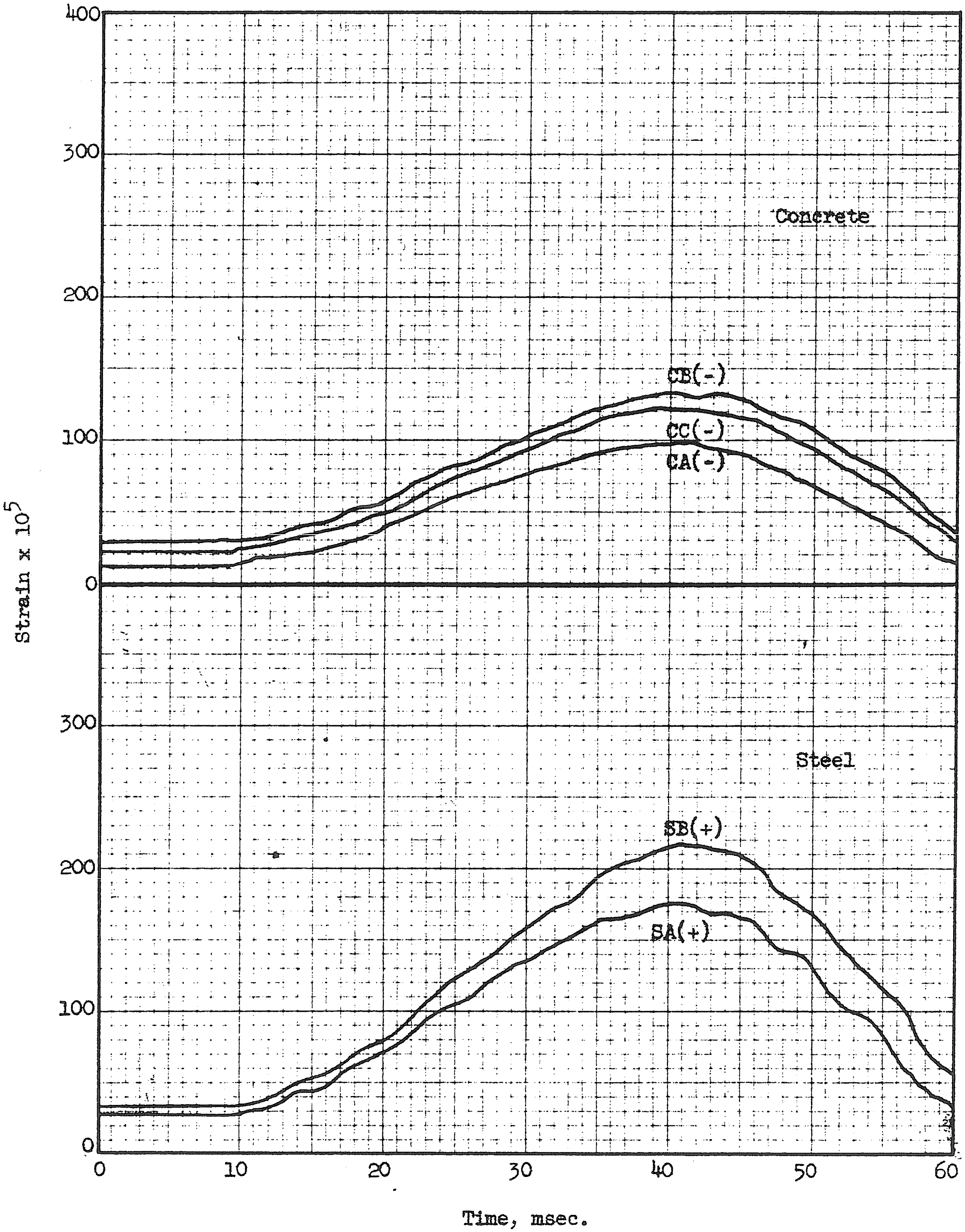

FIG. A91 STRAIN VS. TIME, BEAM 7a2, BLOW 1

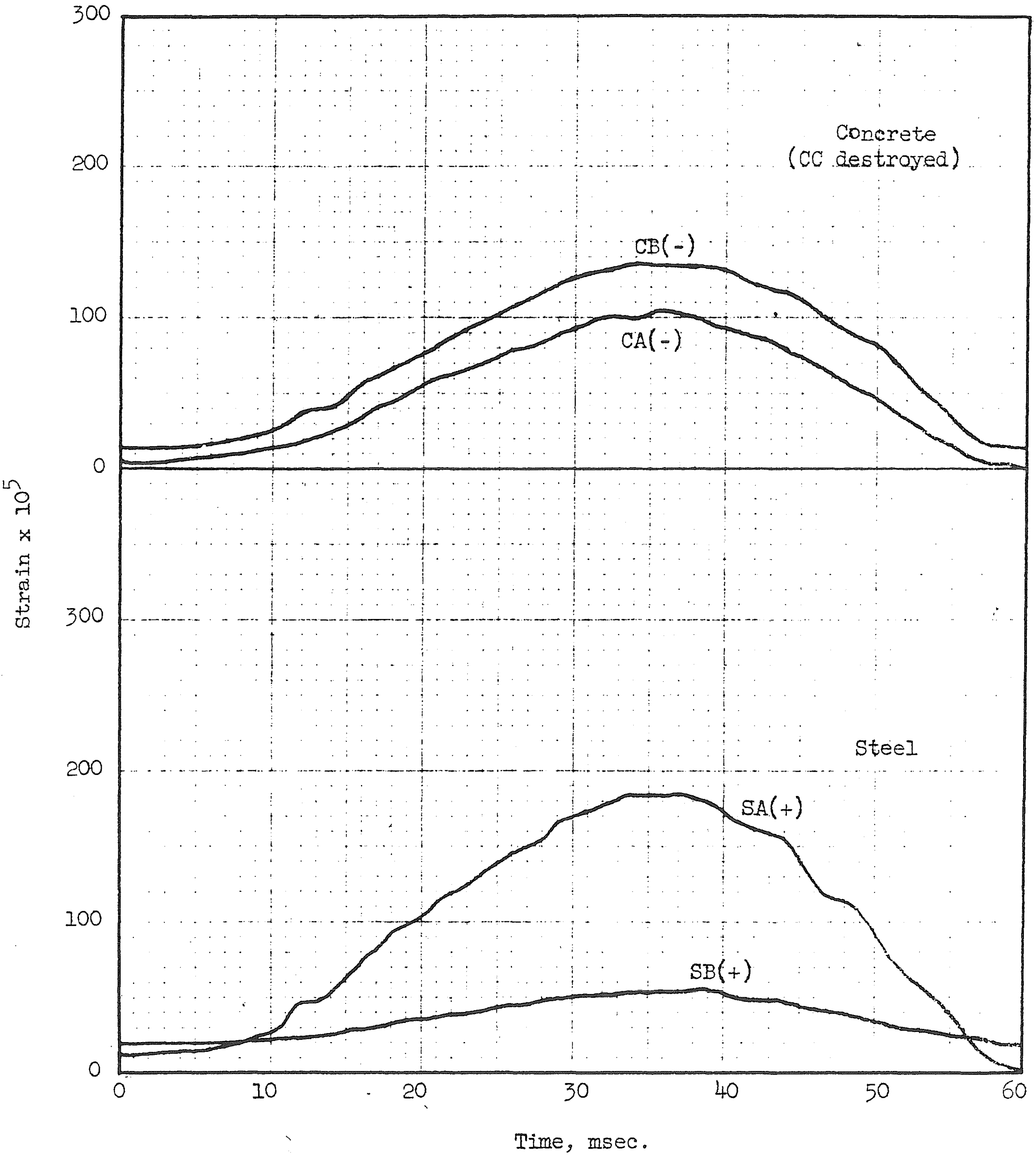

FIG. A92 STRAIN VS. TIME, BEAM 7a2, BLOW 2

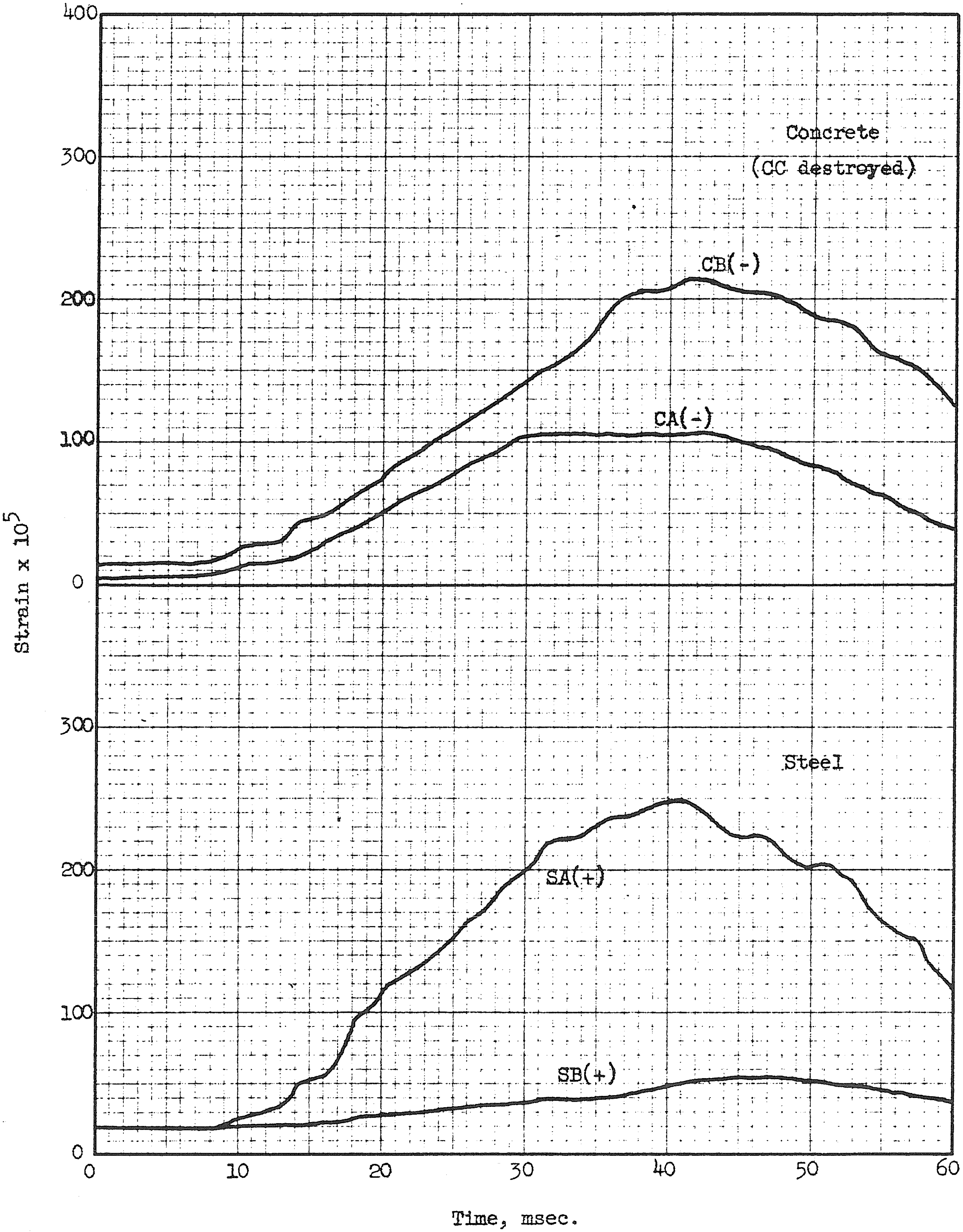

FIG. A93 STRAIN VS. TIME, BEAM 7a2, BLOW 3

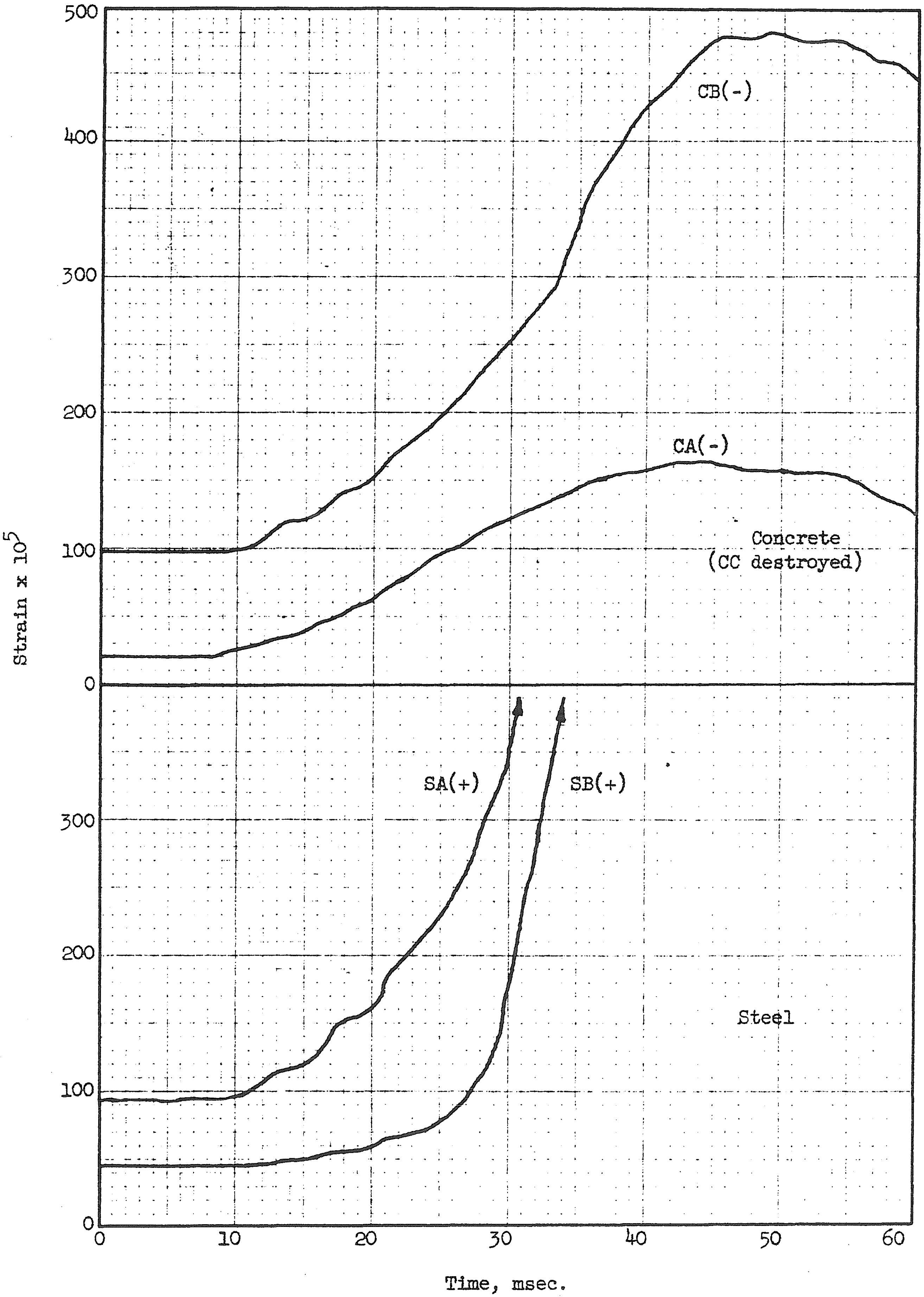

FIG. A94 STRAIN VS. TIME, BEAM 7a2, BLOW 4

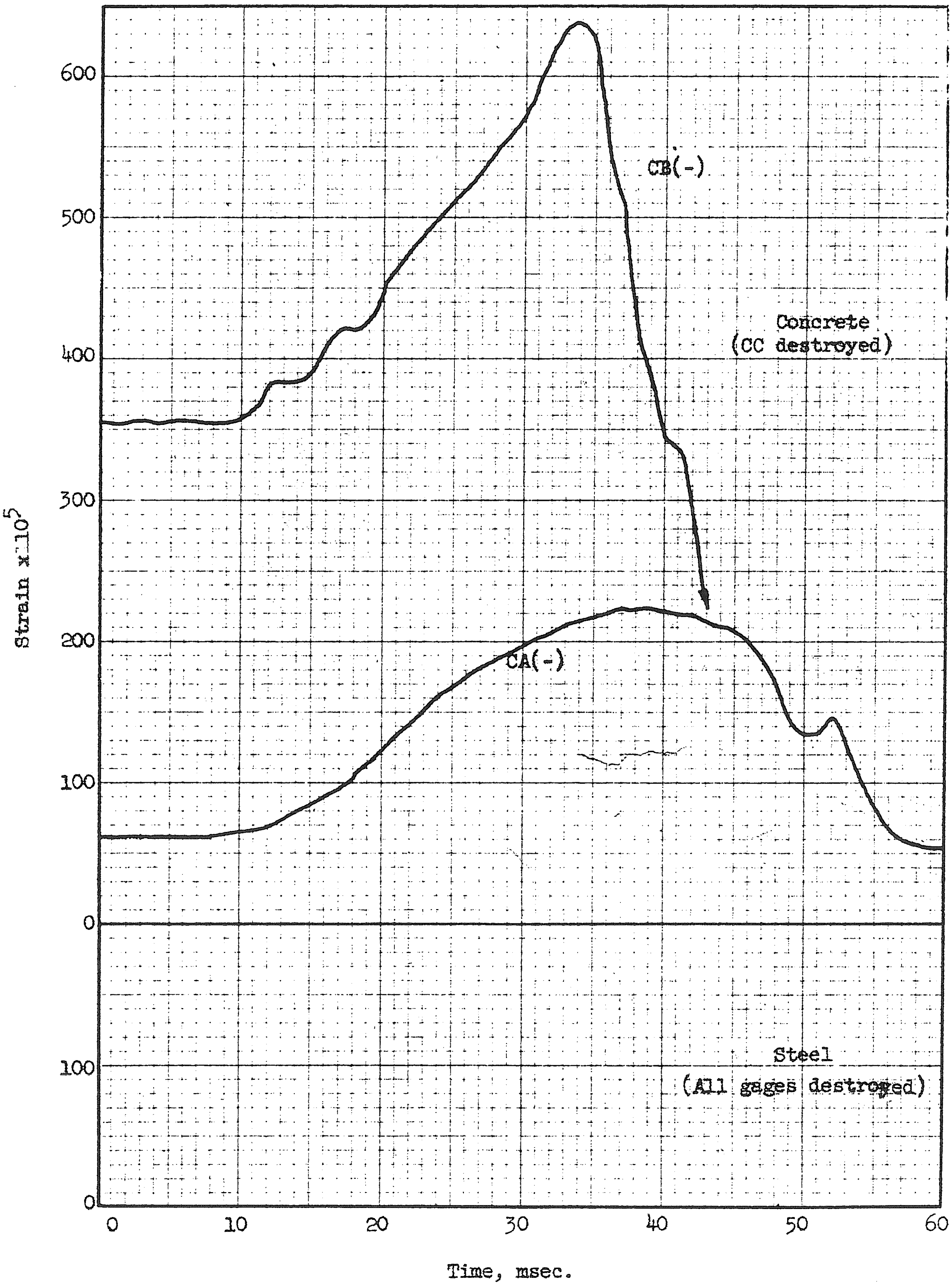

FIG. A95 STRAIN VS. TIME, BEAM 7a2, BLOW 5

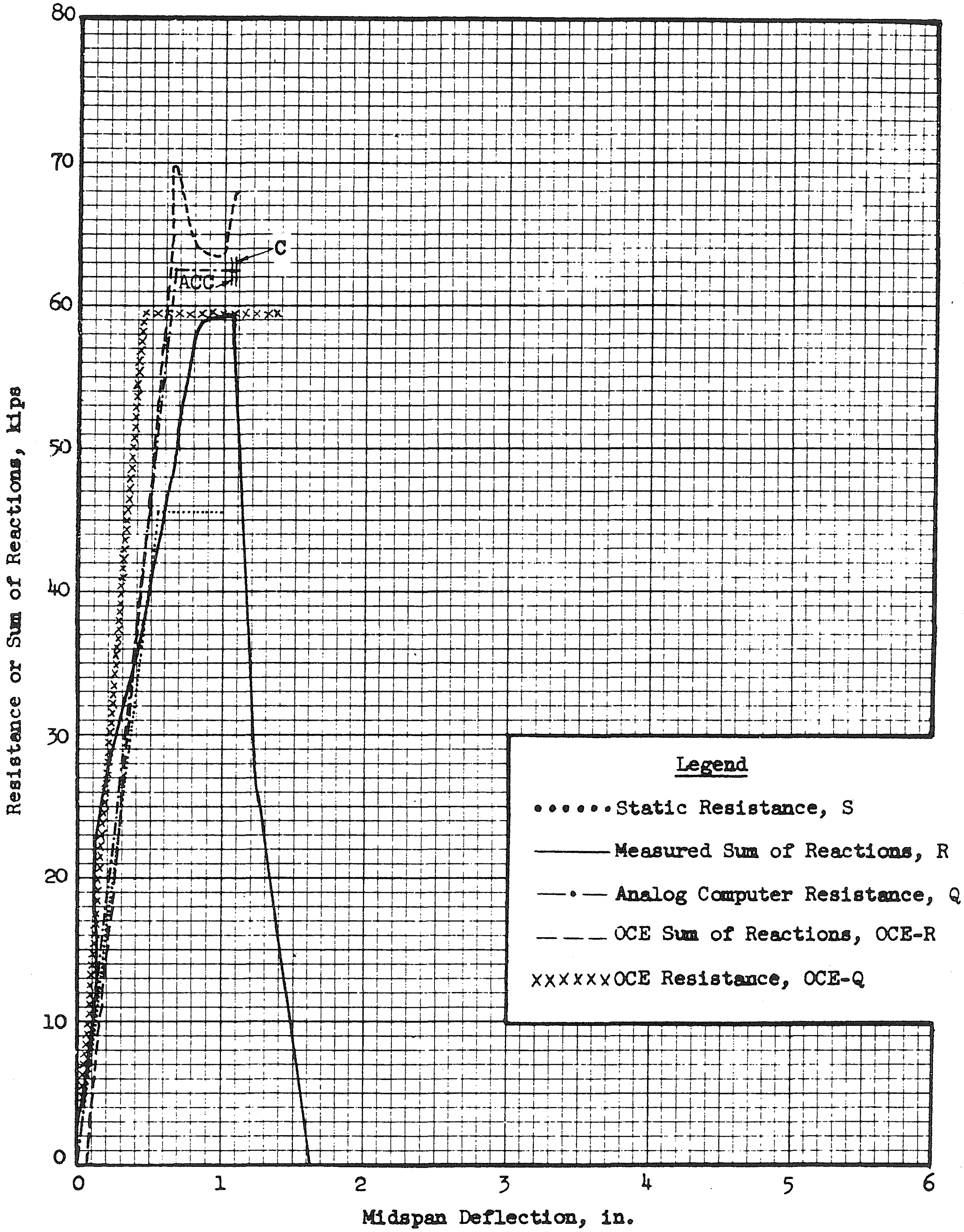

FIG. A96 RESISTANCE AND REACTION VS. DEFLECTION
BEAM 2al

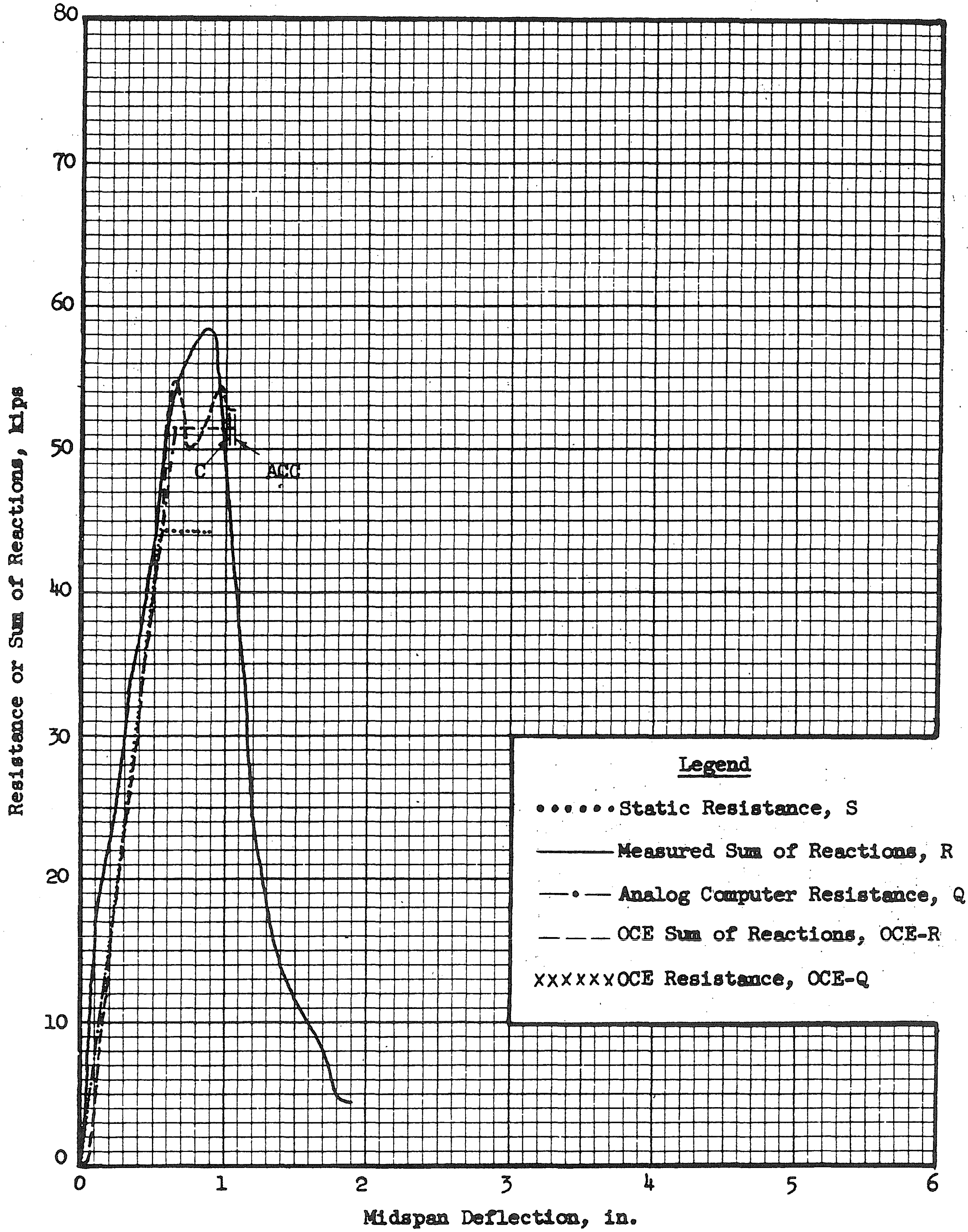

FIG. A97 RESISTANCE AND REACTION VS. DEFLECTION
BEAM 2a2

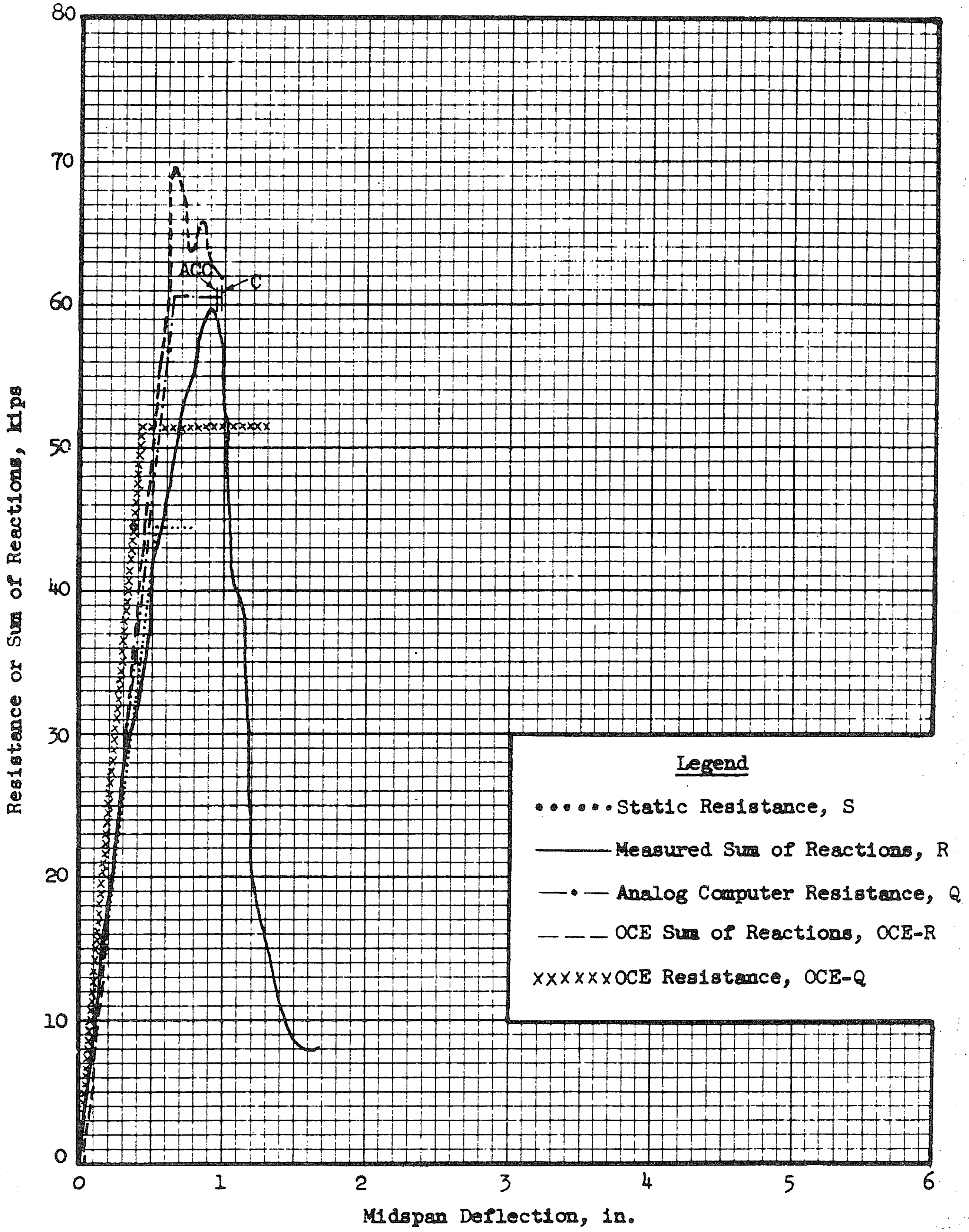

FIG. A98 RESISTANCE AND REACTION VS. DEFLECTION
BEAM 2b2

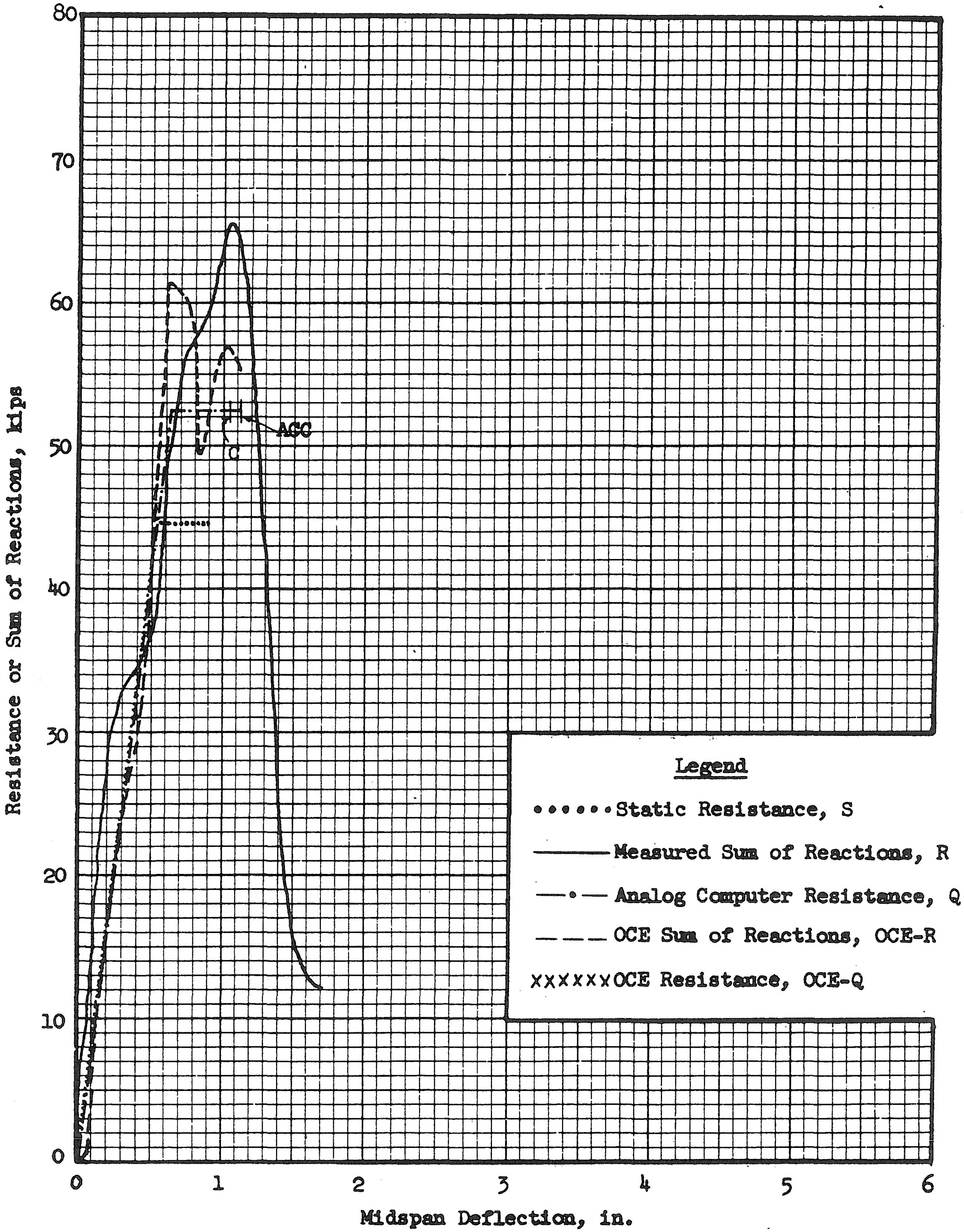

FIG. A99 RESISTANCE AND REACTION VS. DEFLECTION
BEAM 2b3

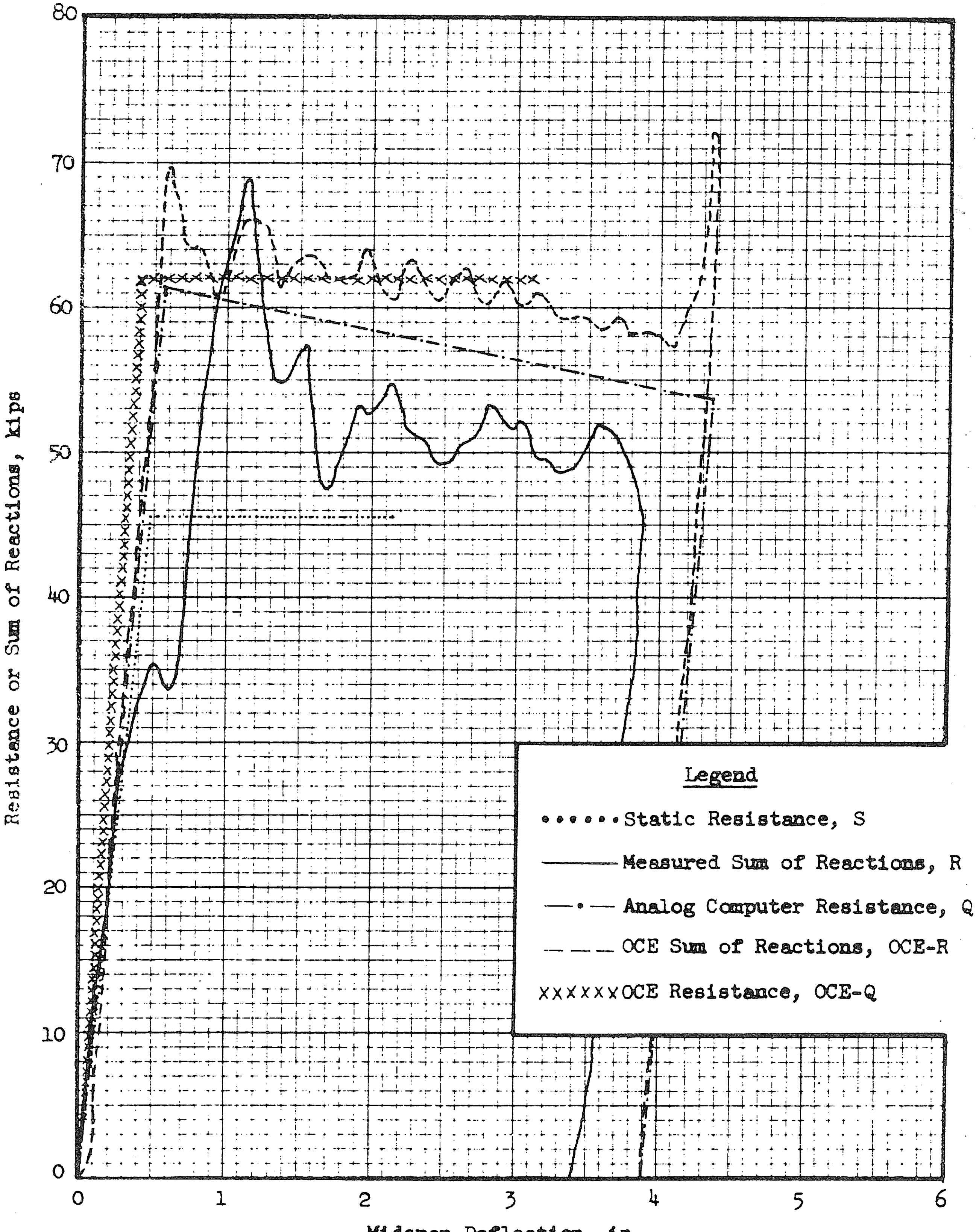

FIG. A100 RESISTANCE AND REACTION VS. DEFLECTION
BEAM 3a2

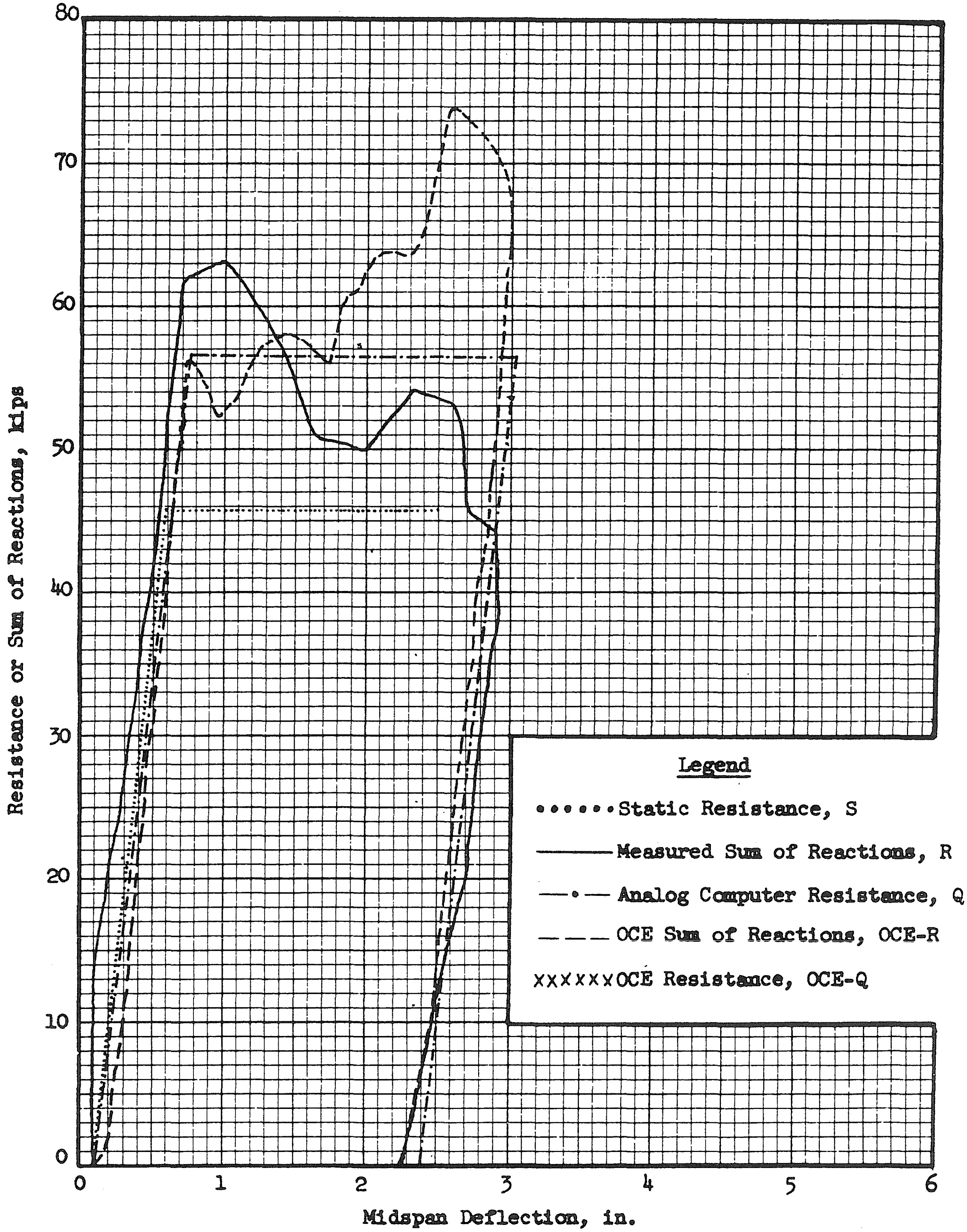

FIG. A101 RESISTANCE AND REACTION VS. DEFLECTION
BEAM 3a3

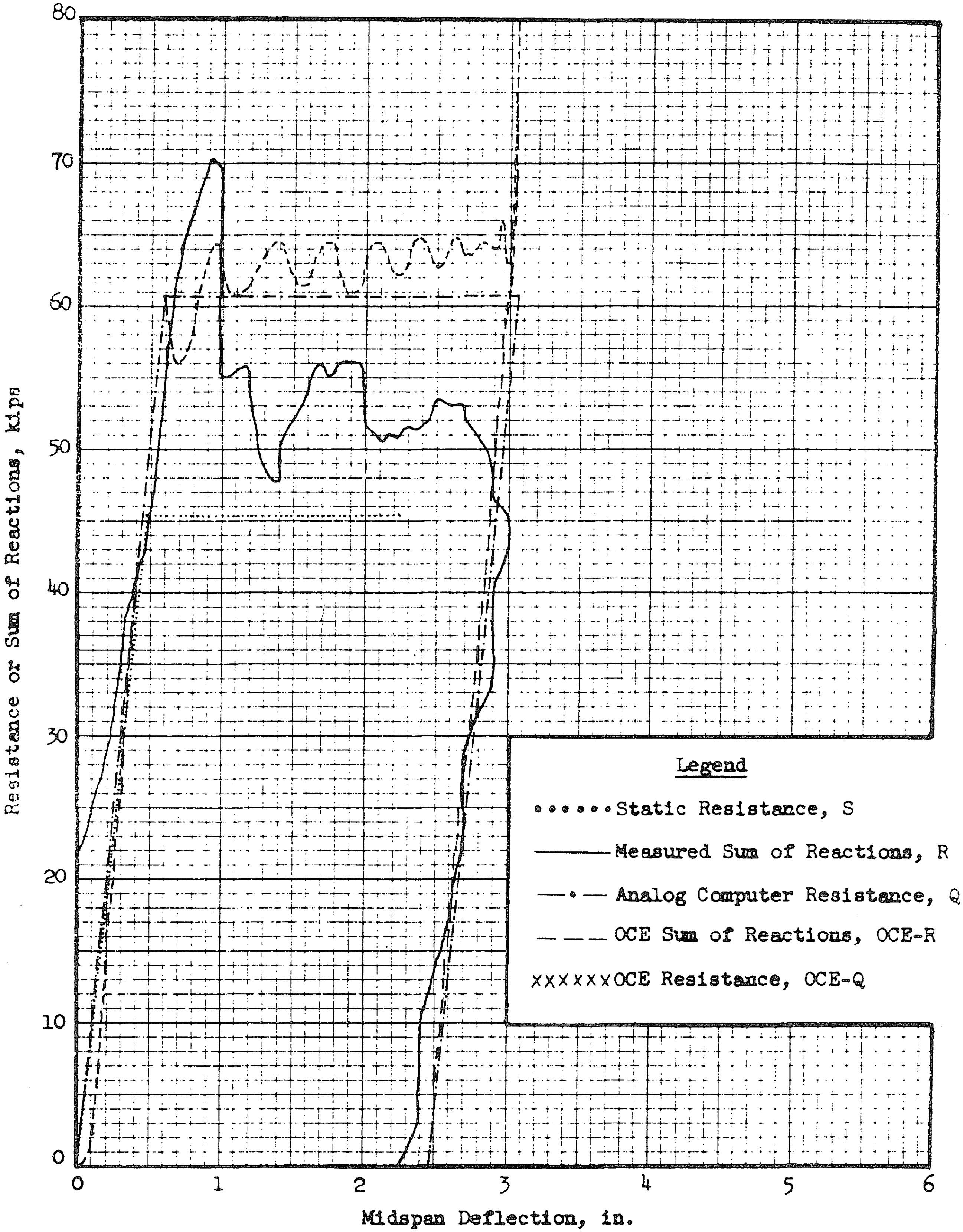

FIG. A102 RESISTANCE AND REACTION VS. DEFLECTION
BEAM 3a4

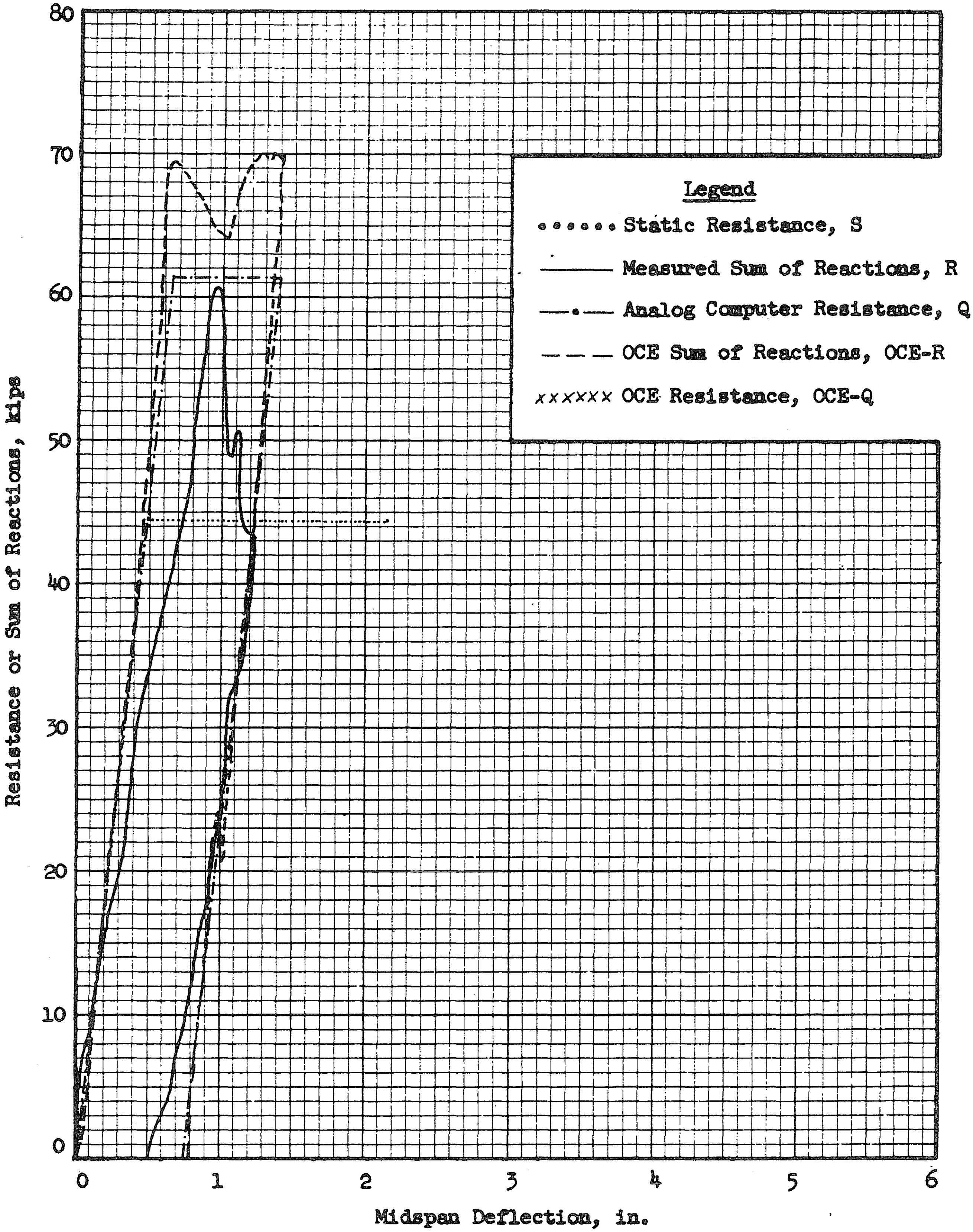

FIG. A103 RESISTANCE AND REACTION VS. DEFLECTION
BEAM 3a5, BLOW 1

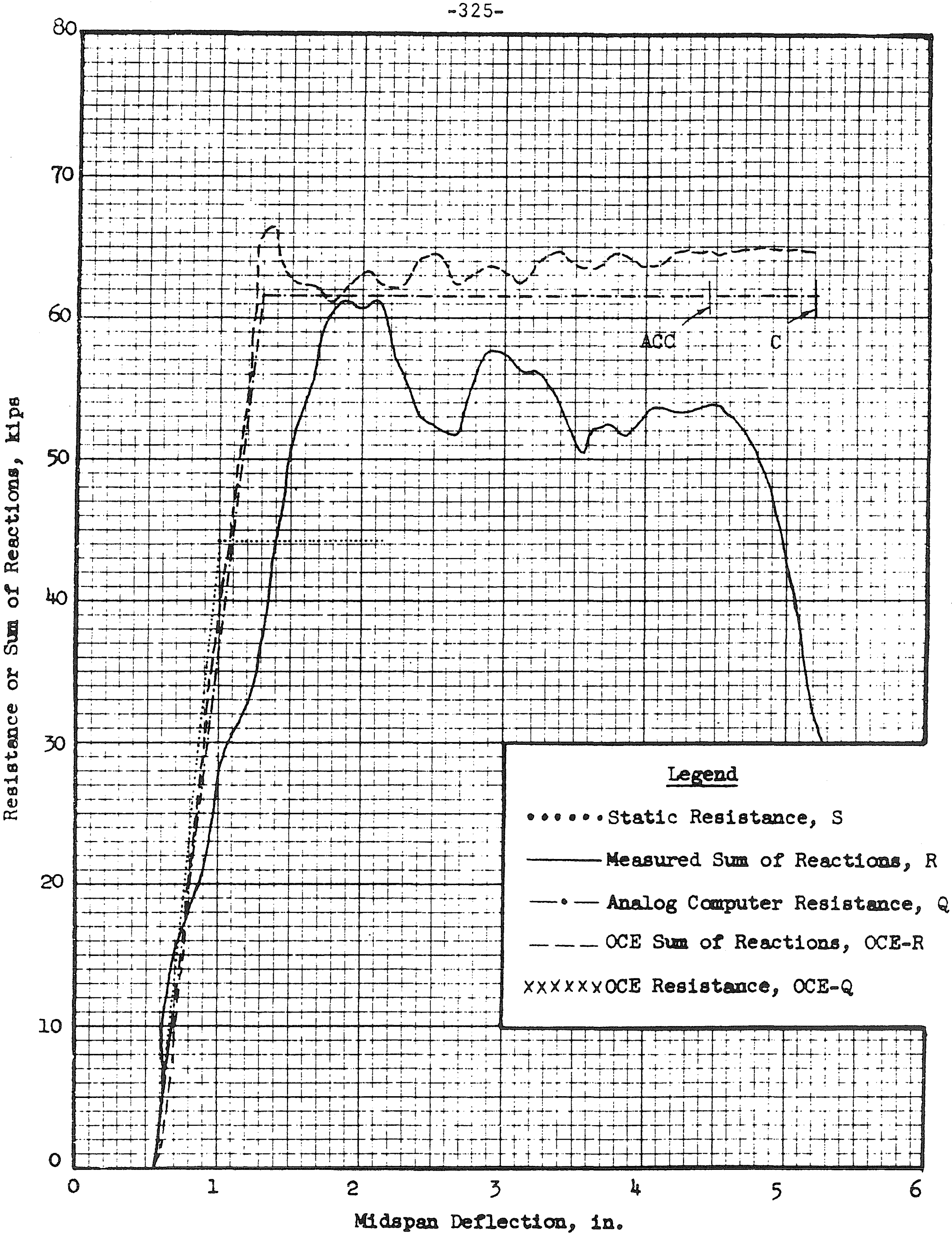

FIG. A104 RESISTANCE AND REACTION VS. DEFLECTION
BEAM 3a5, BLOW 2

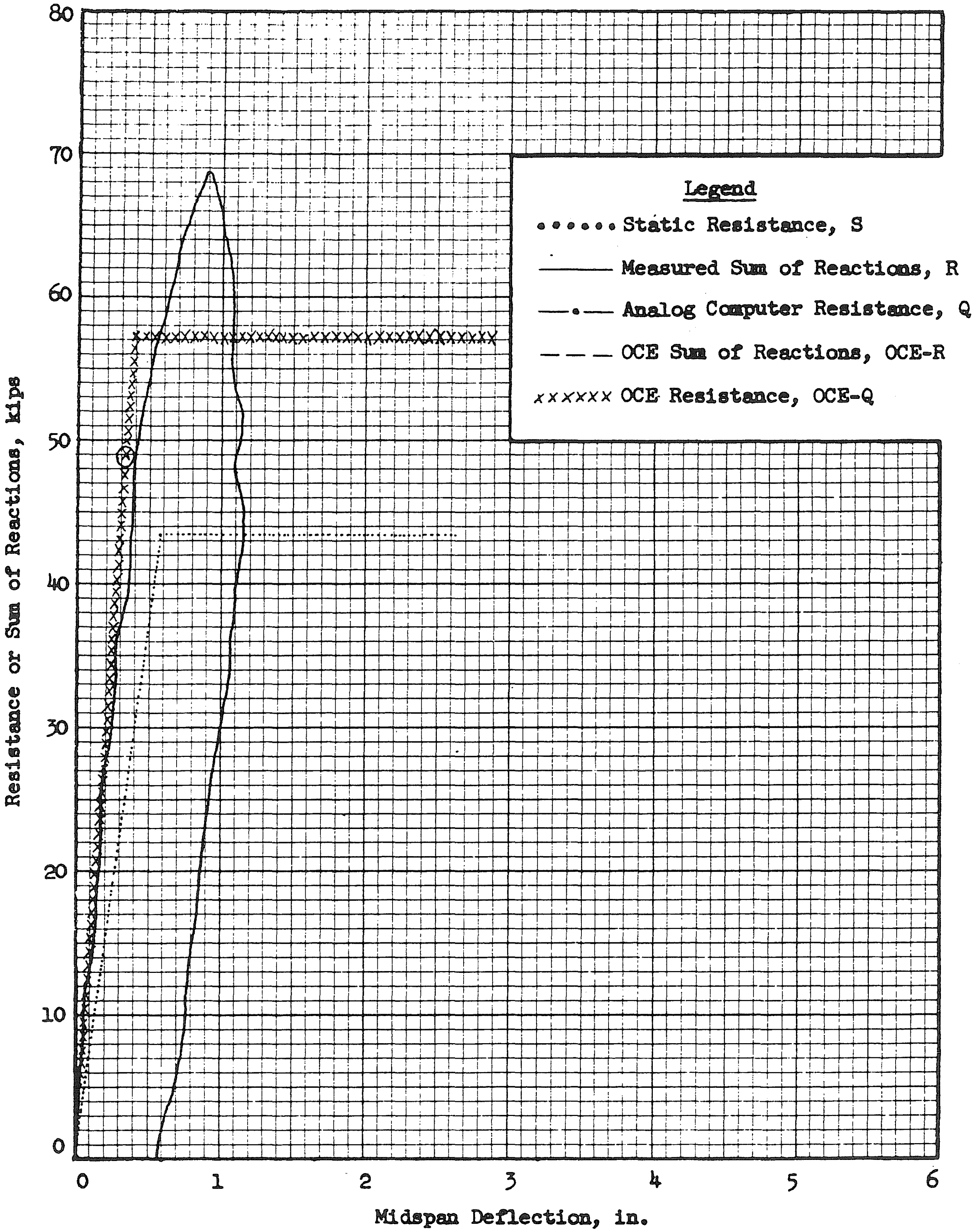

FIG. A105 RESISTANCE AND REACTION VS. DEFLECTION
BEAM 3b2, BLOW 1

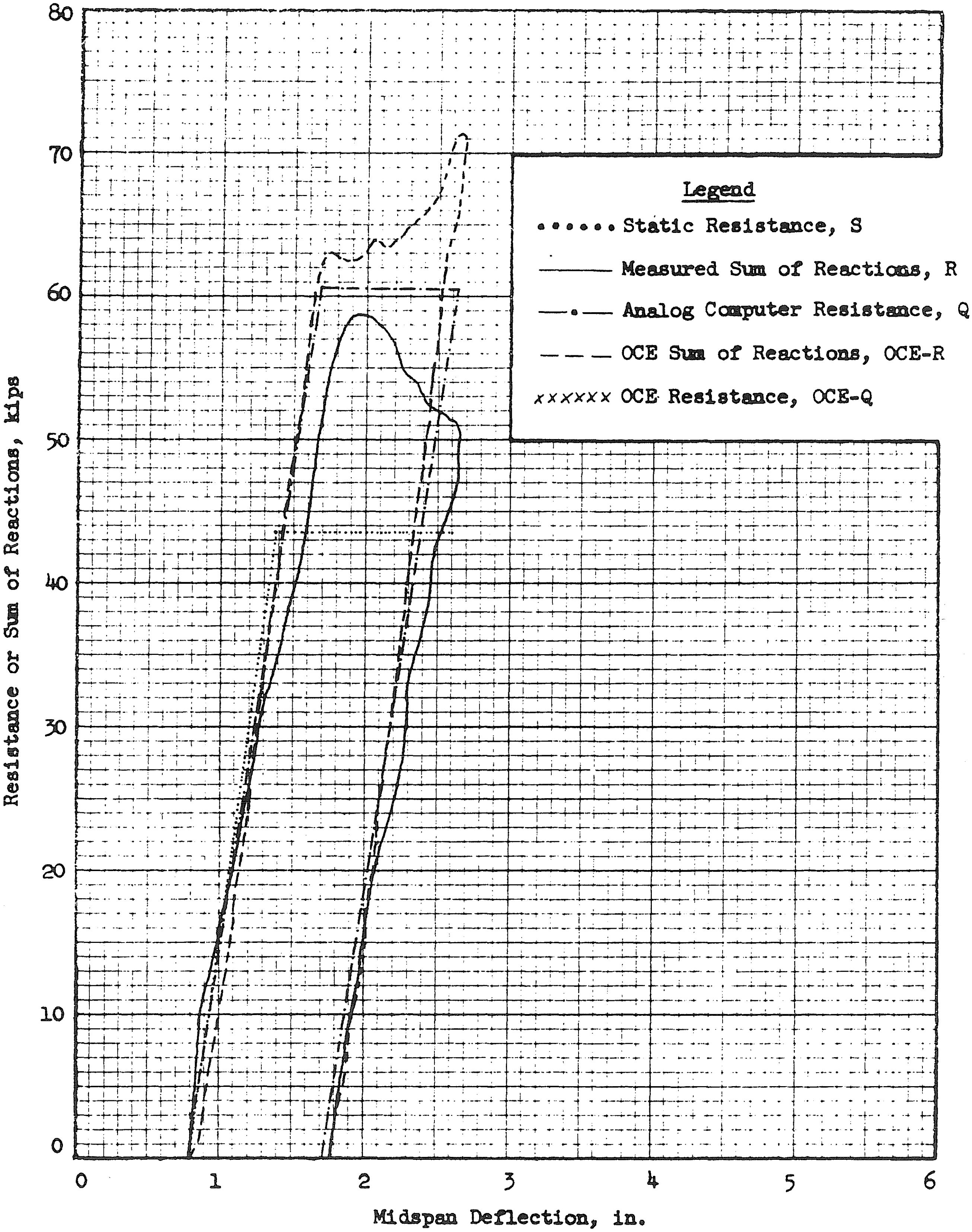

FIG. A106 RESISTANCE AND REACTION VS. DEFLECTION
BEAM 3b2, BLOW 2

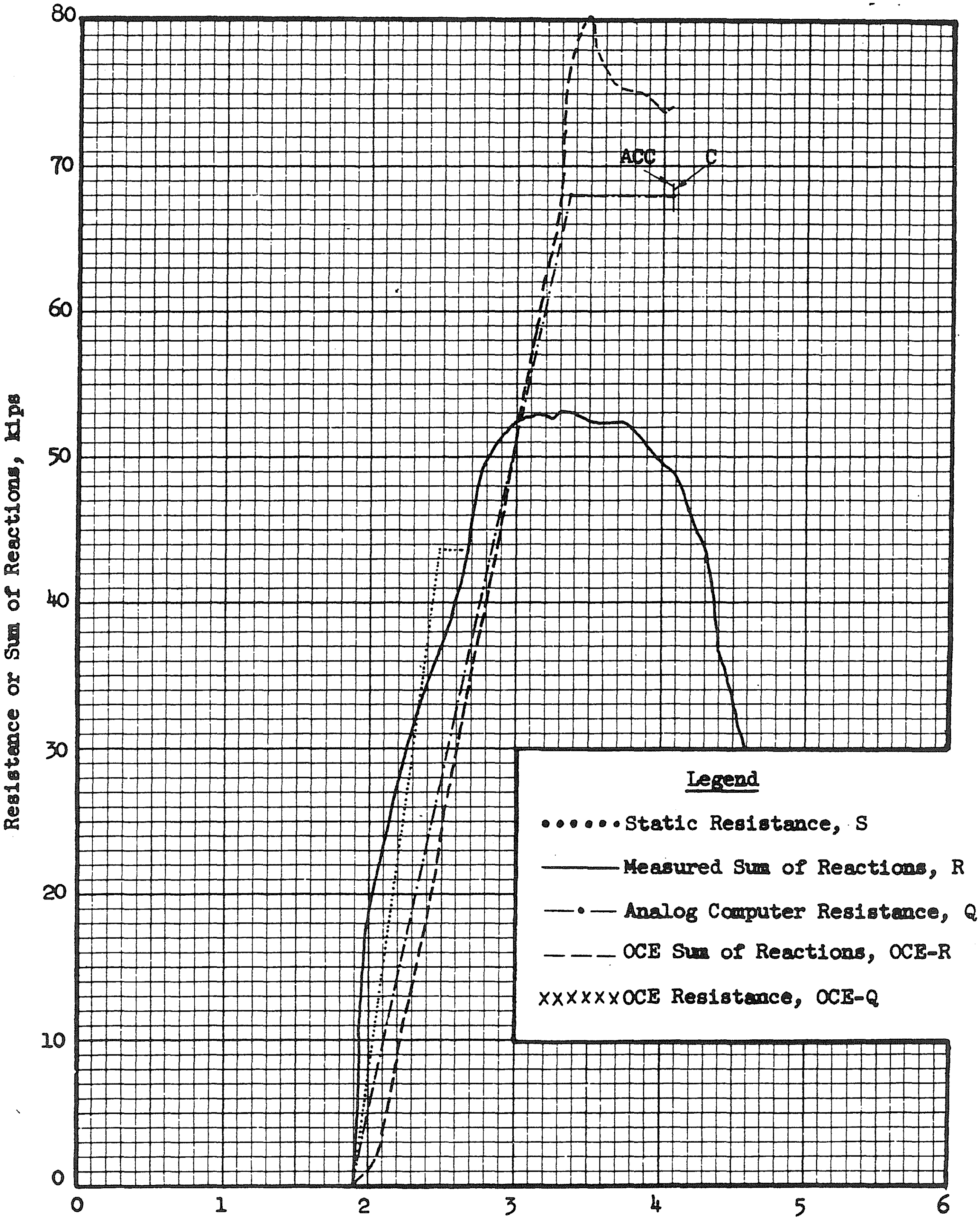

FIG. A107 RESISTANCE AND REACTION VS. DEFLECTION
BEAM 3b2, BLOW 3

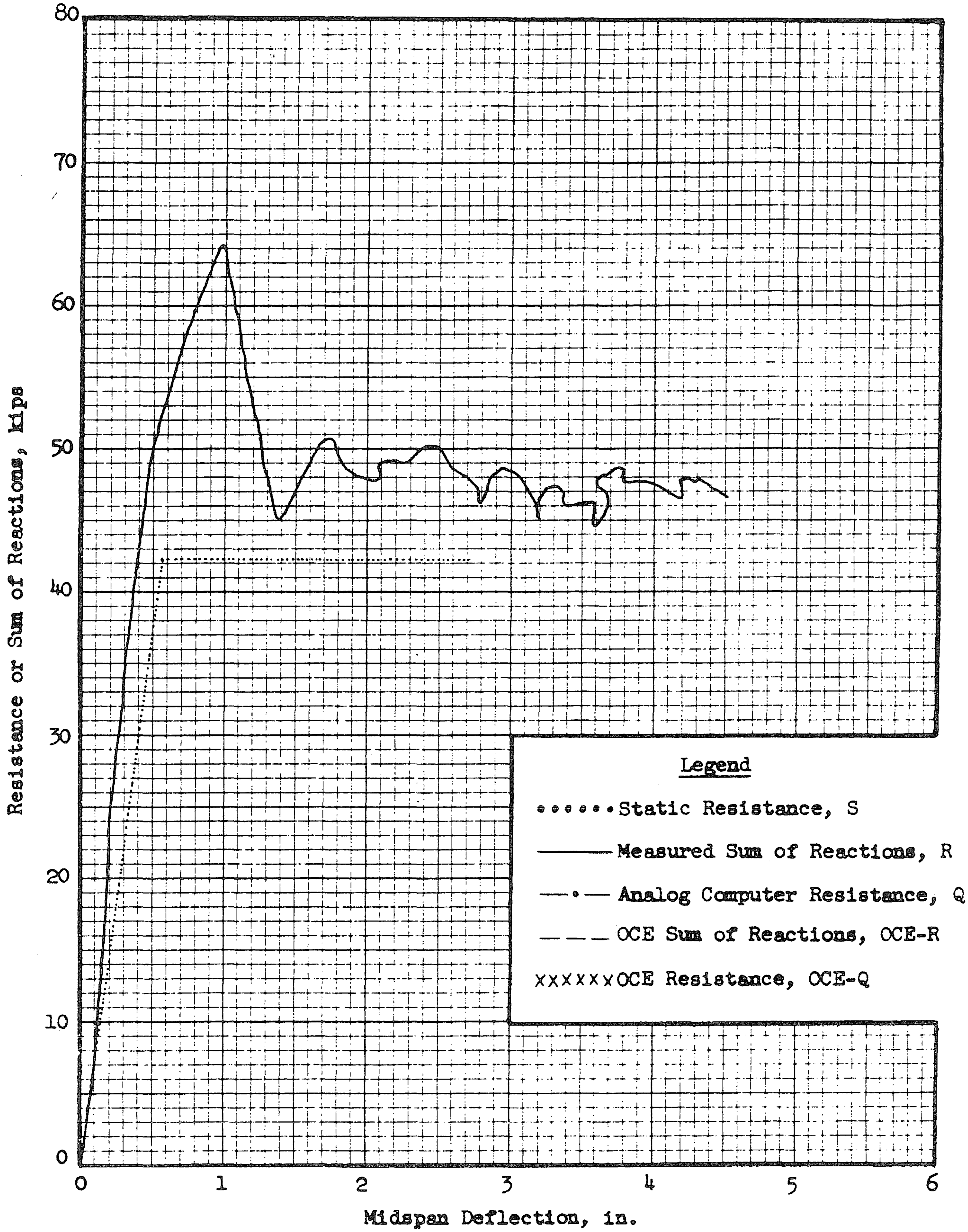

FIG. A108 RESISTANCE AND REACTION VS. DEFLECTION
BEAM 3b3

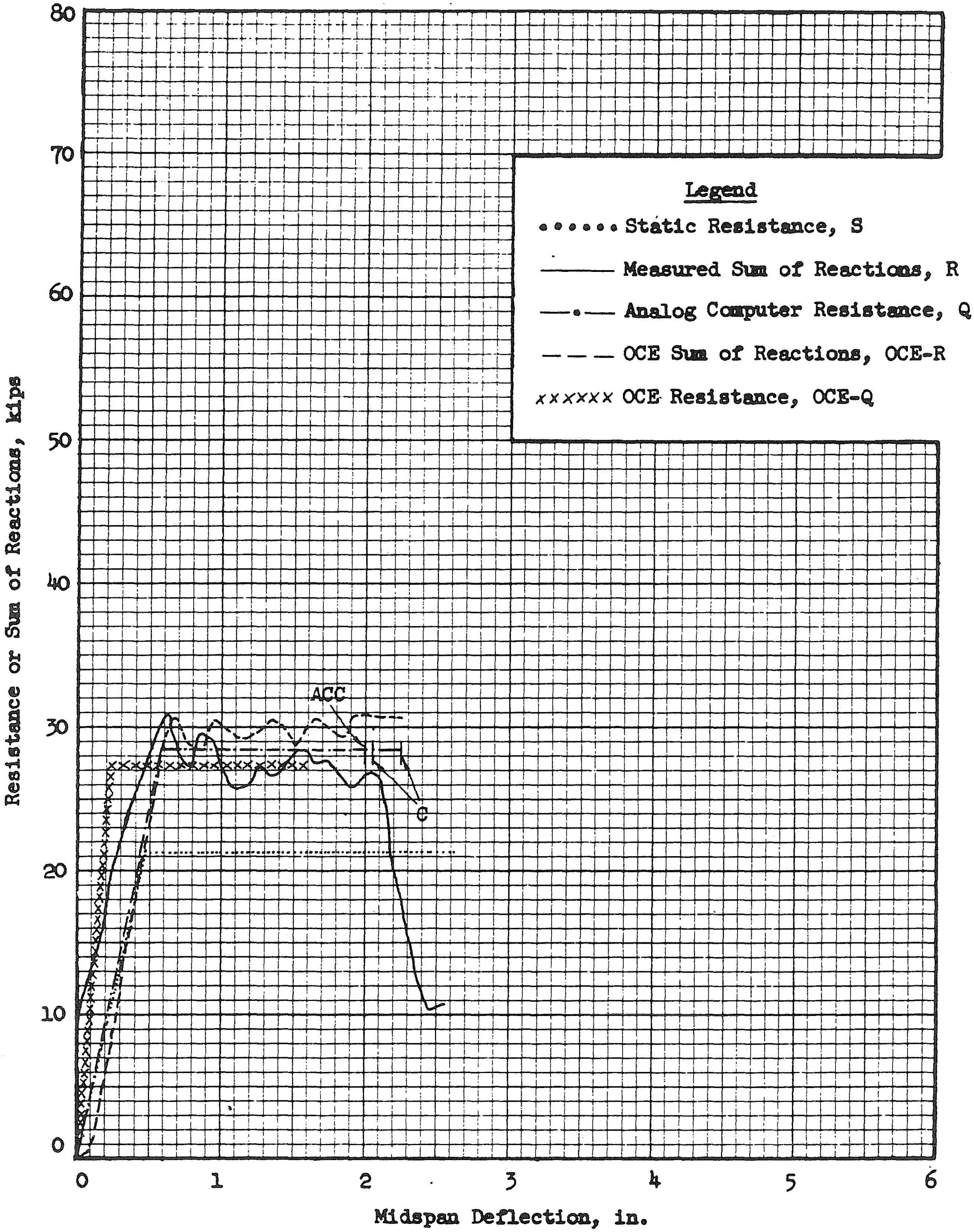

FIG. A109 RESISTANCE AND REACTION VS. DEFLECTION
BEAM 4a1

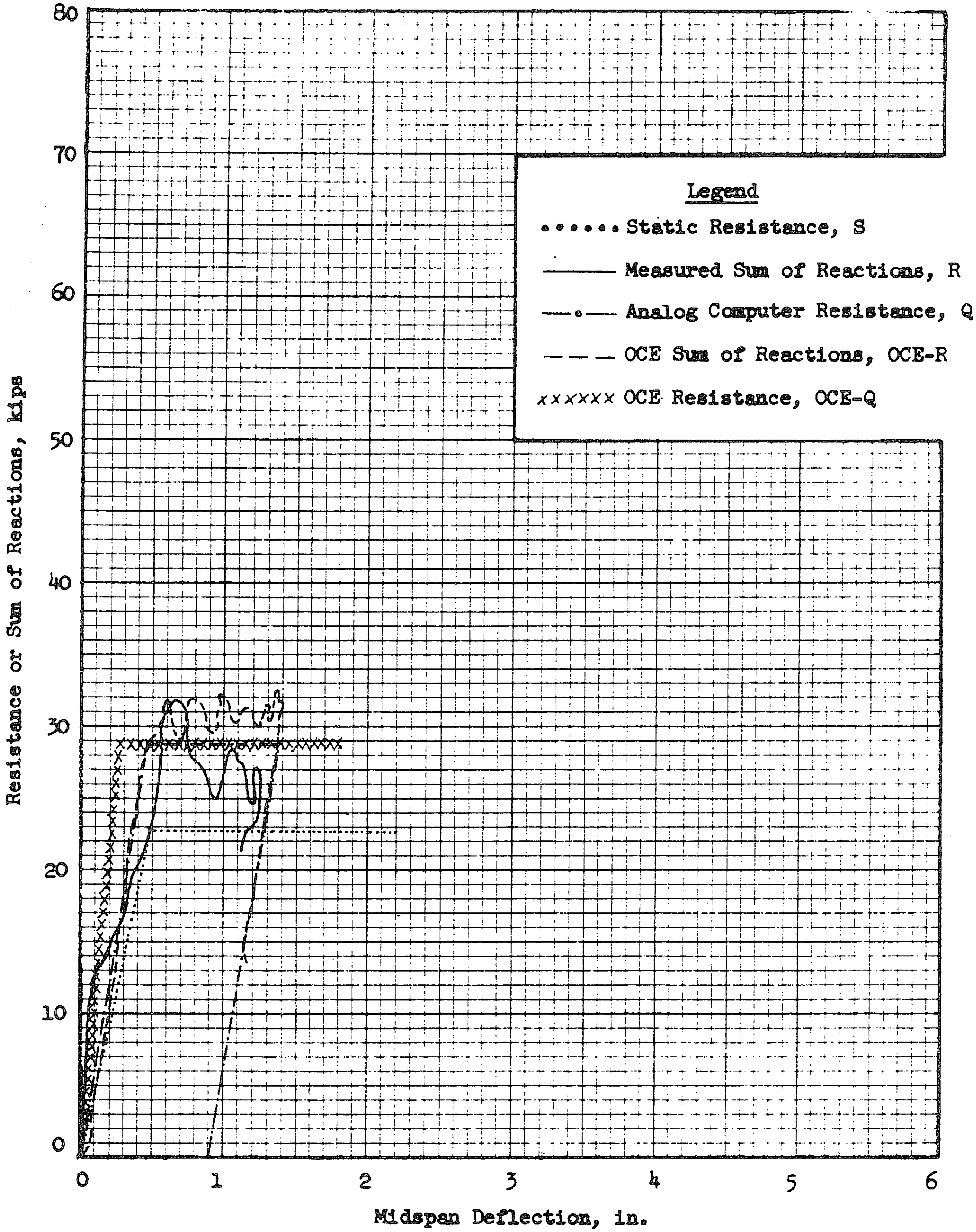

FIG. A110 RESISTANCE AND REACTION VS. DEFLECTION
BEAM 4a2, BLOW 1

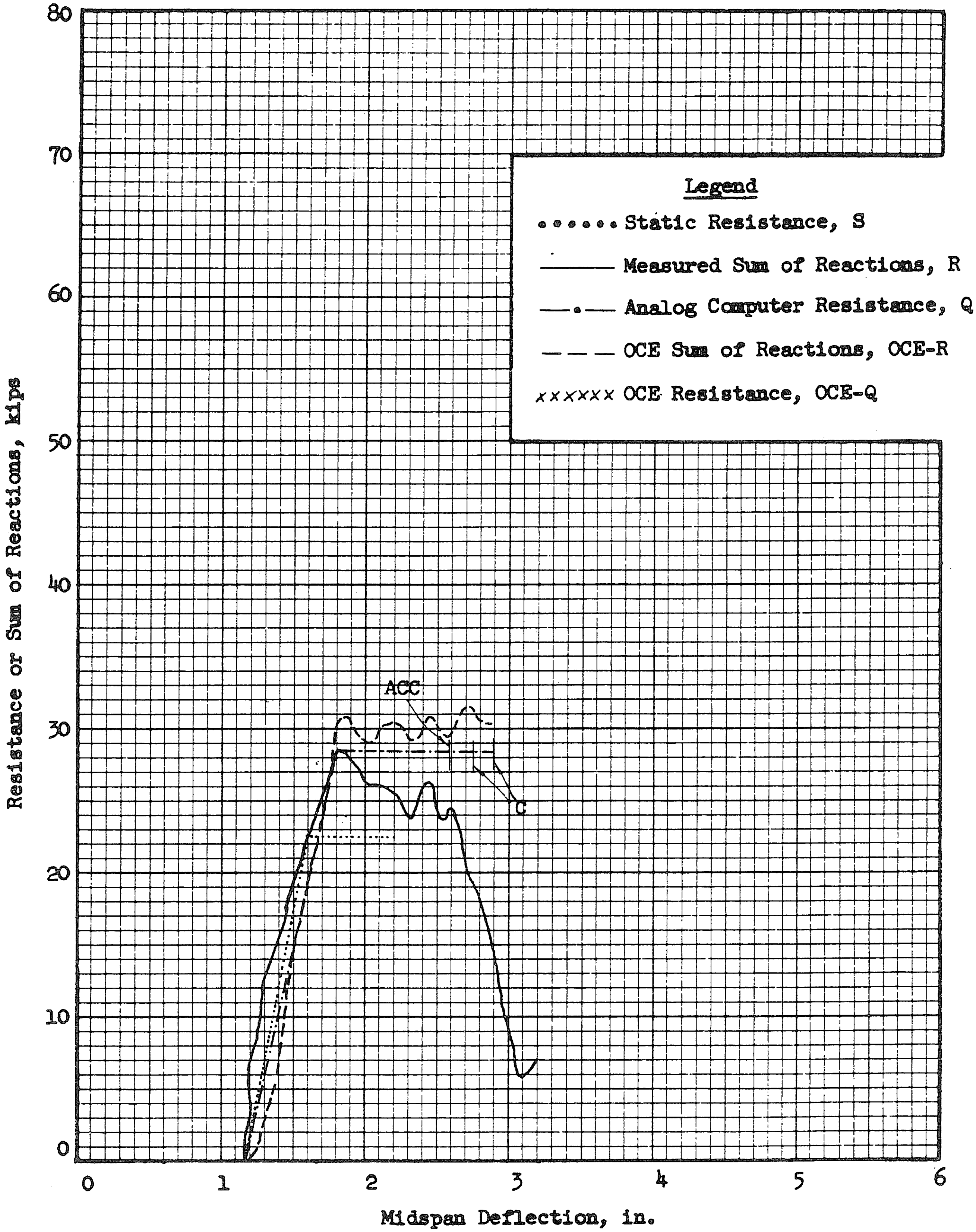

FIG. A111 RESISTANCE AND REACTION VS. DEFLECTION
BEAM 4a2, BLOW 2

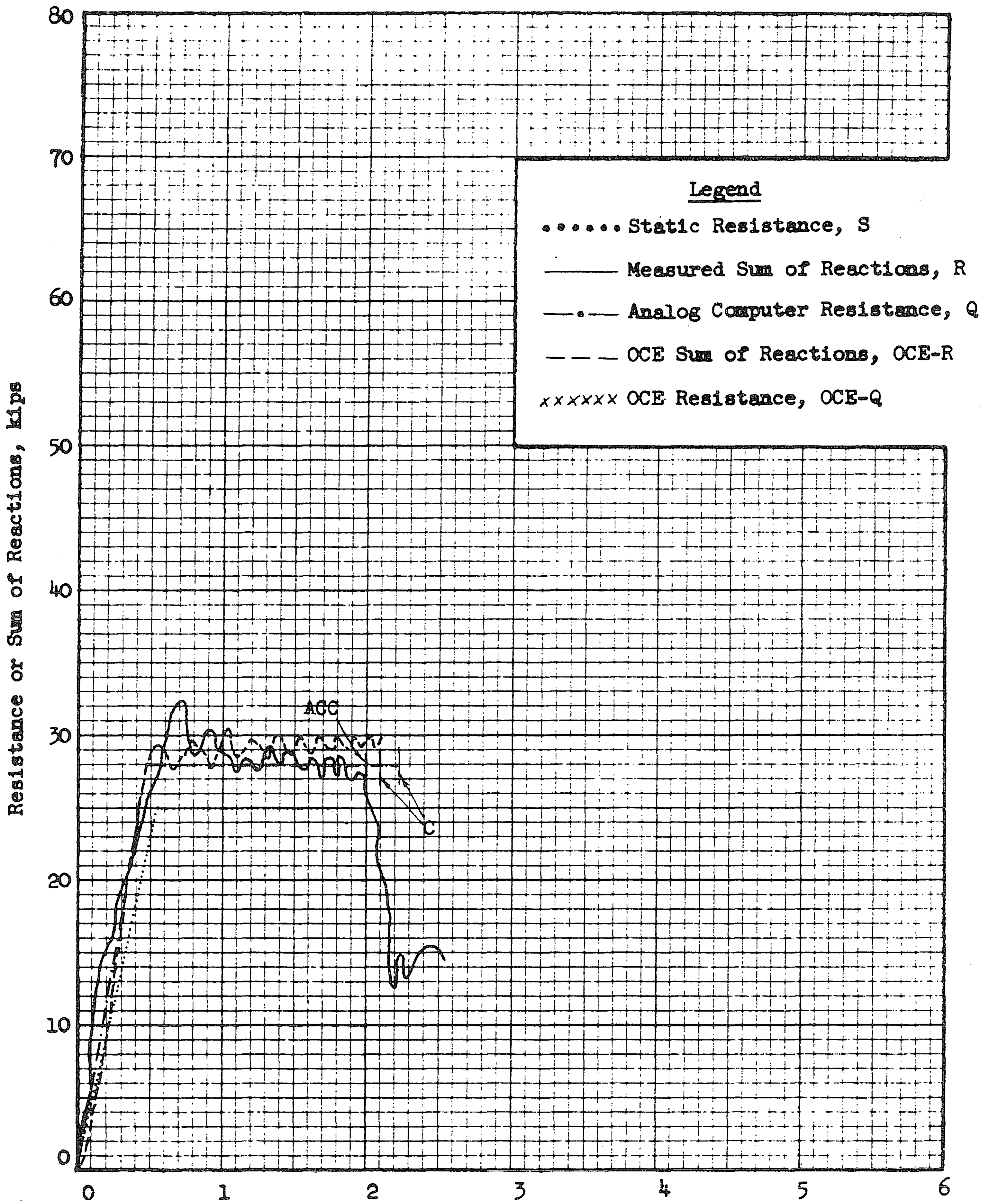

FIG. A112 RESISTANCE AND REACTION VS. DEFLECTION
BEAM 4b3

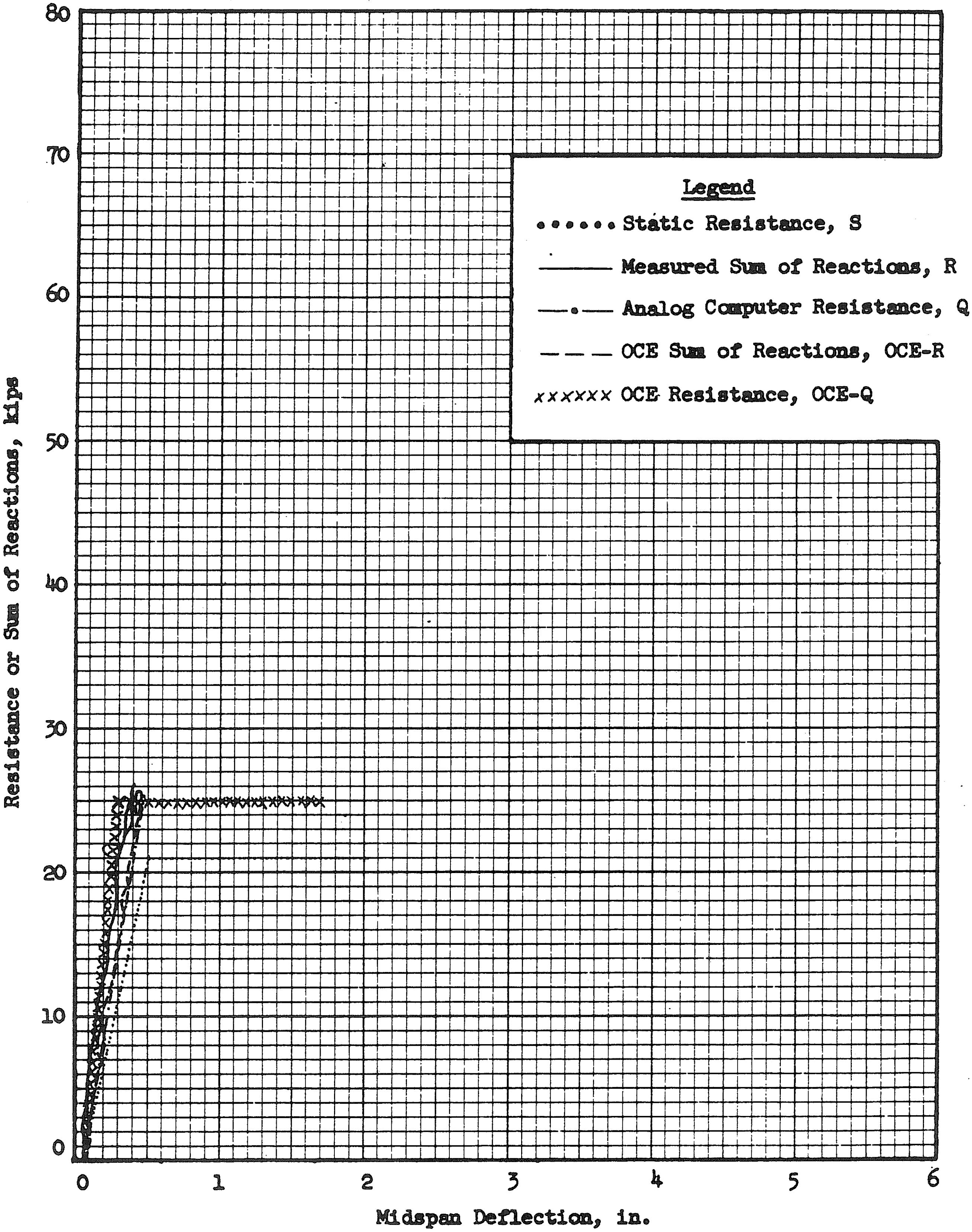

FIG. A113 RESISTANCE AND REACTION VS. DEFLECTION
BEAM 4c2, BLOW 1

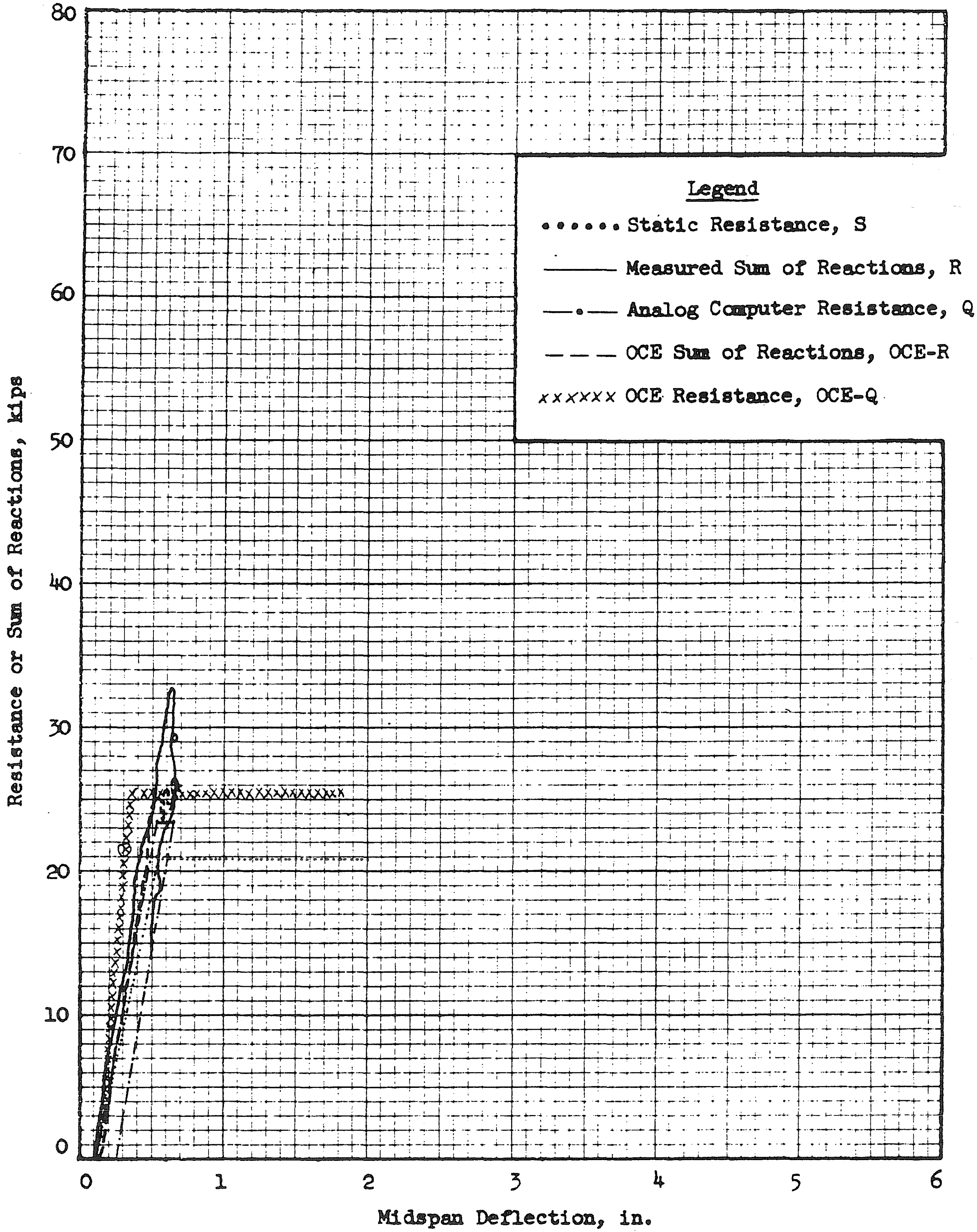

FIG. A114 RESISTANCE AND REACTION VS. DEFLECTION
BEAM 4c2, BLOW 2

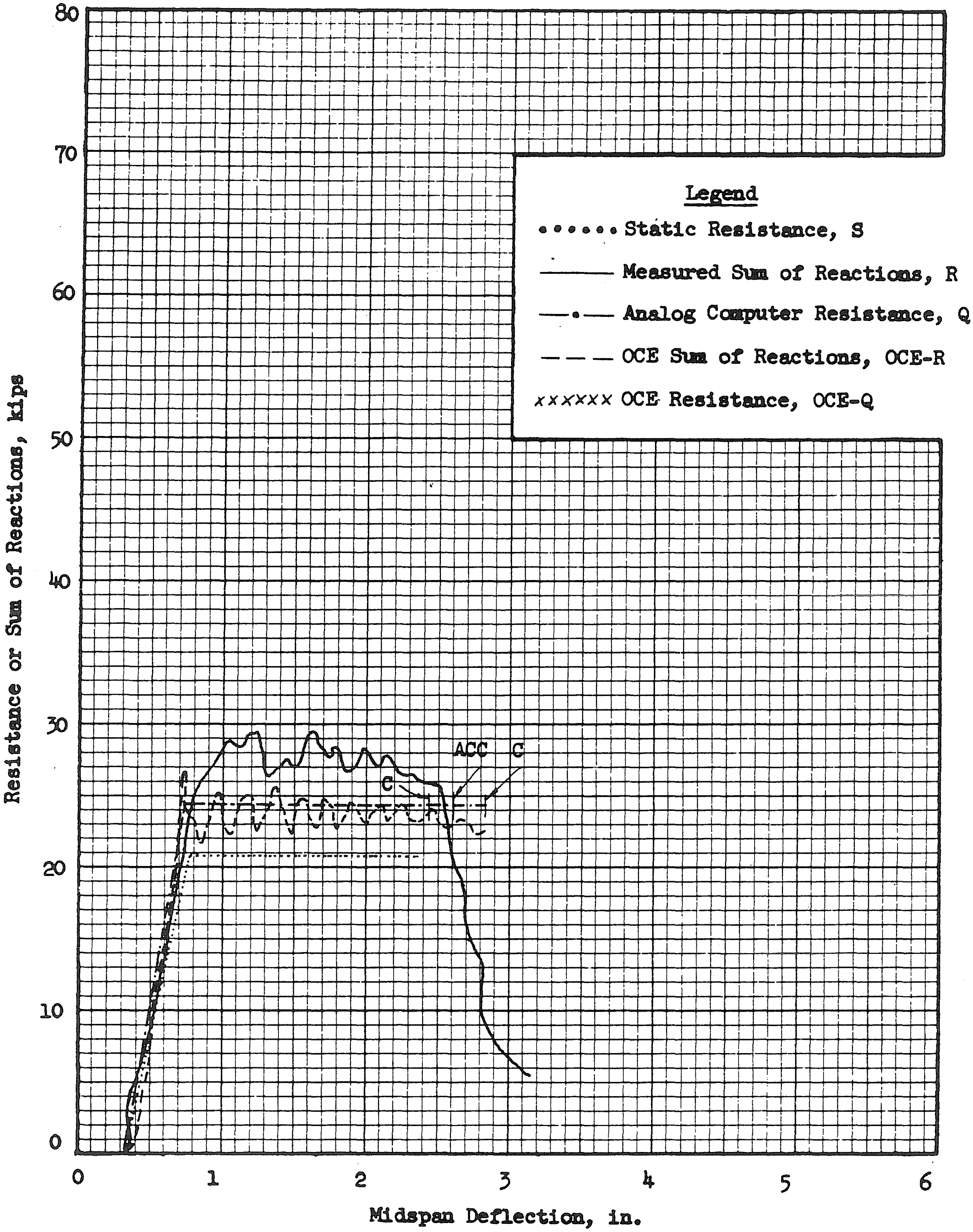

FIG. A115 RESISTANCE AND REACTION VS. DEFLECTION
BEAM 4c2, BLOW 3

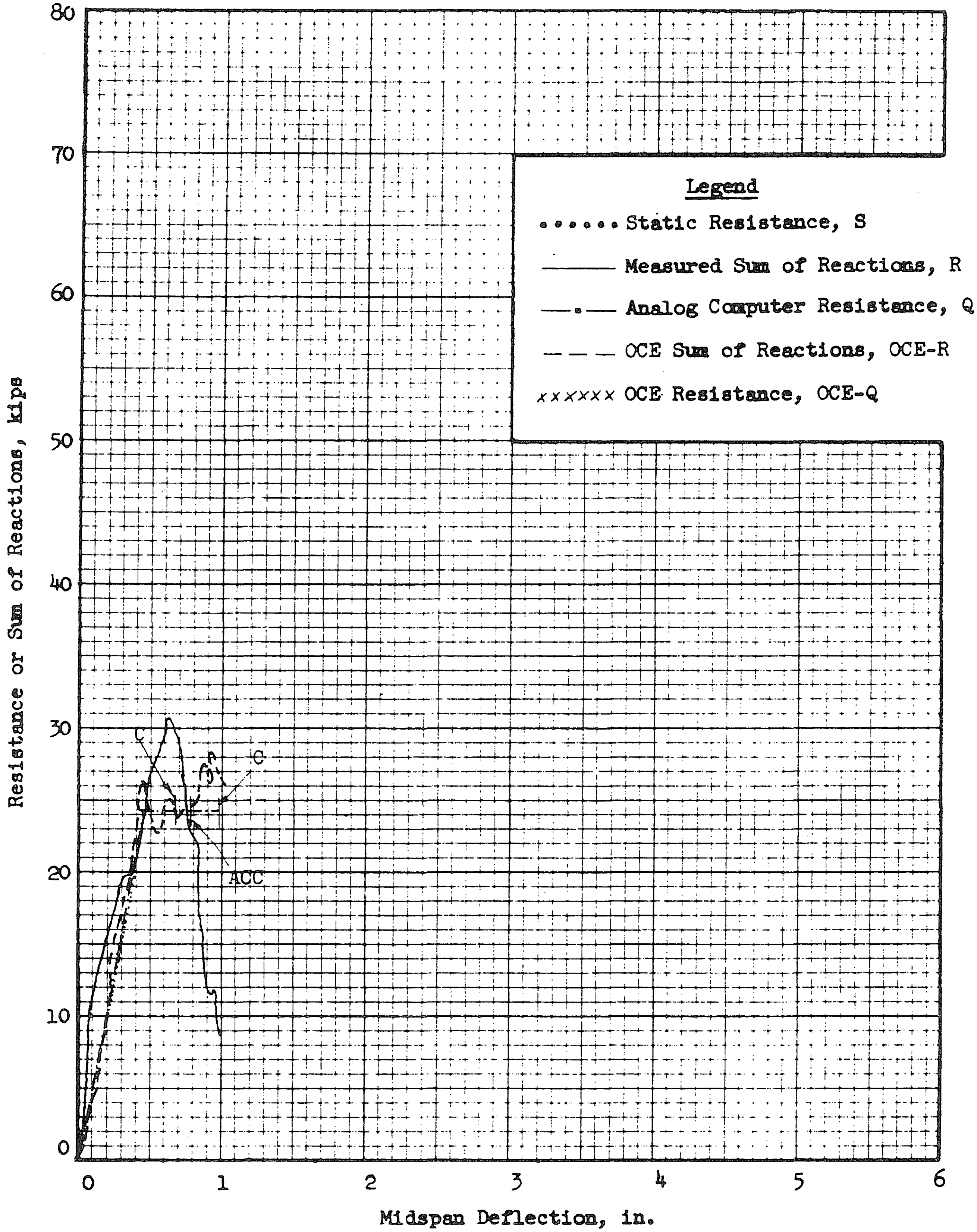

FIG. A116 RESISTANCE AND REACTION VS. DEFLECTION
BEAM 4c5

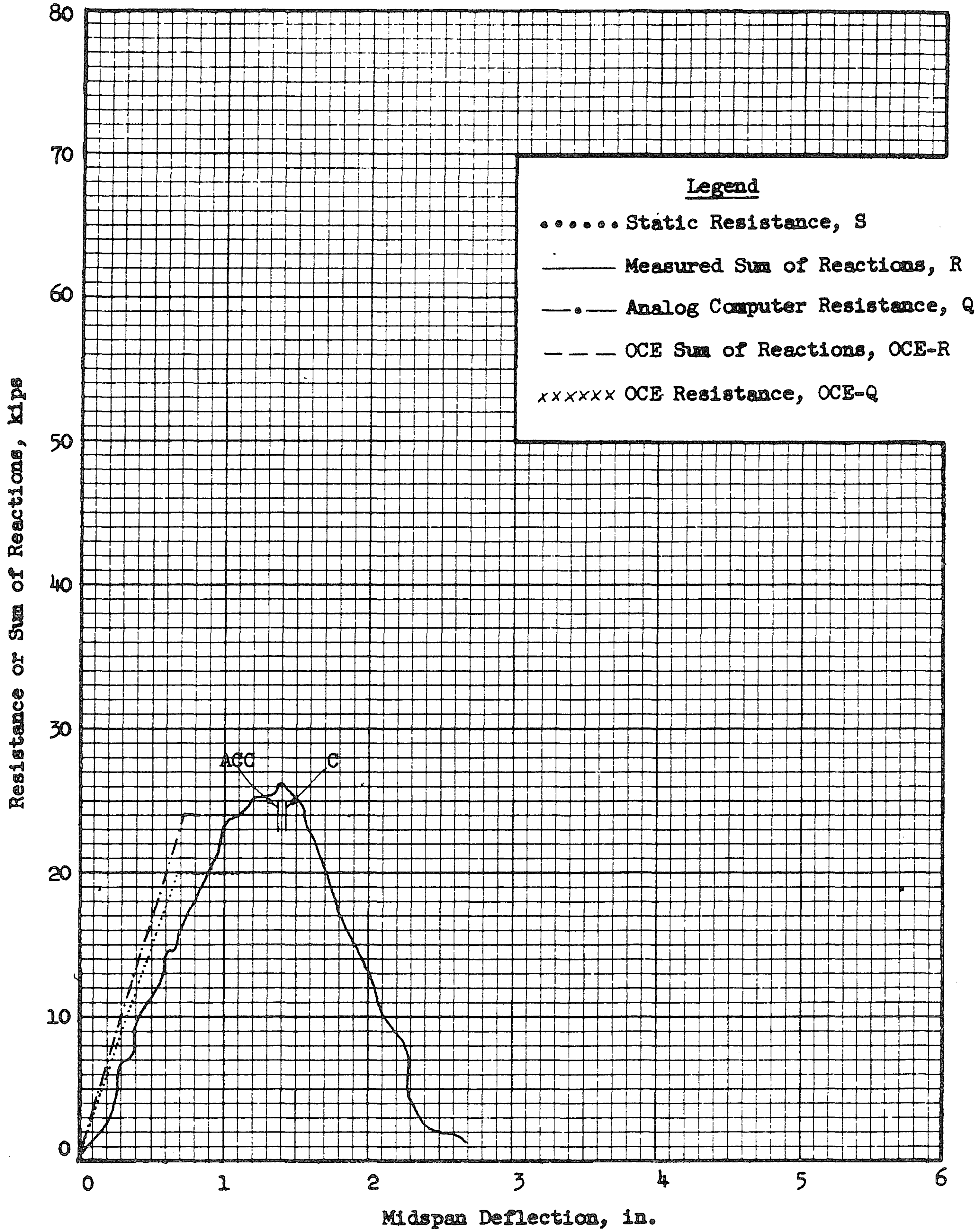

FIG. A117 RESISTANCE AND REACTION VS. DEFLECTION
BEAM 5a1

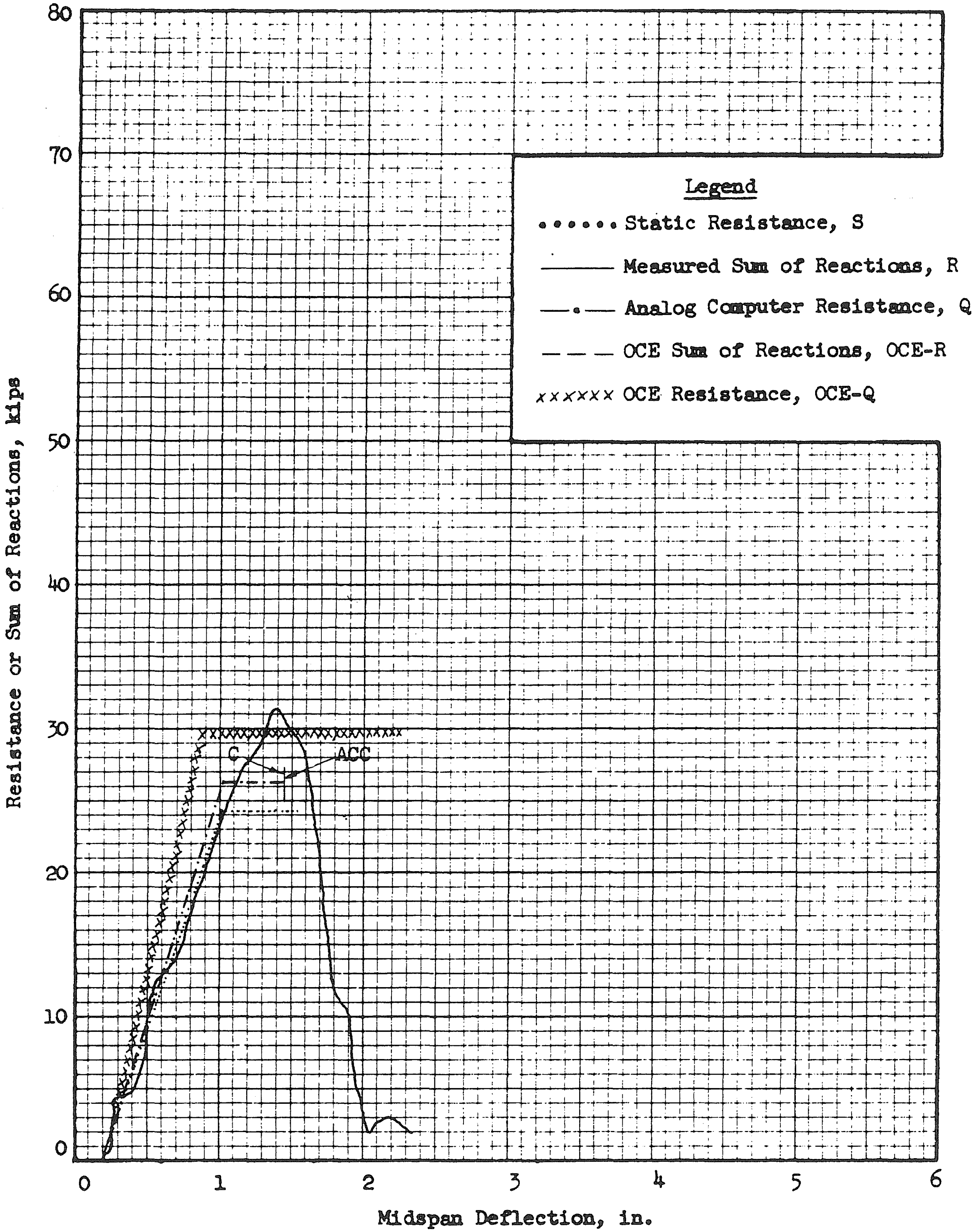

FIG. A118 RESISTANCE AND REACTION VS. DEFLECTION
BEAM 5a2

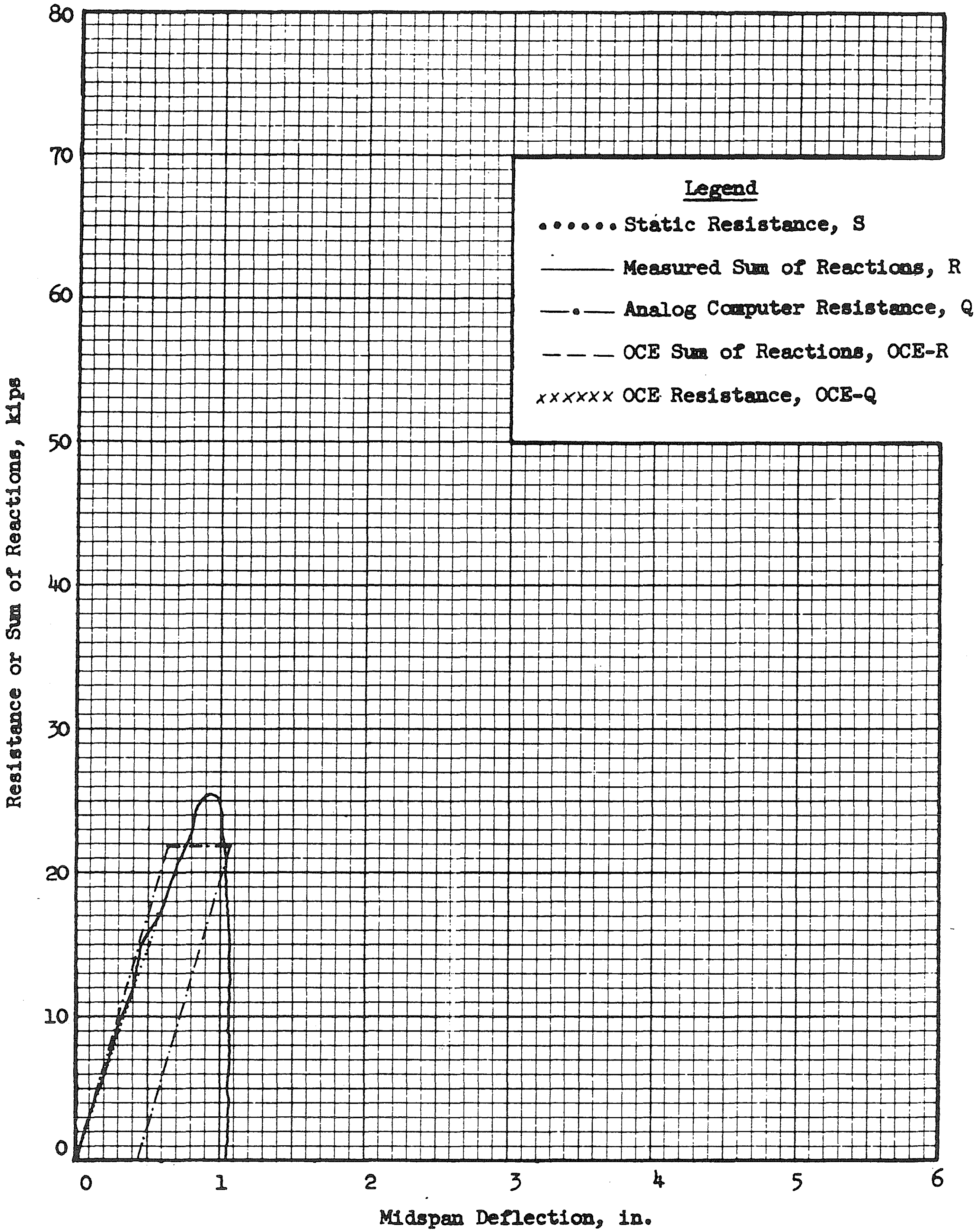

FIG. A119 RESISTANCE AND REACTION VS. DEFLECTION
BEAM 5b3

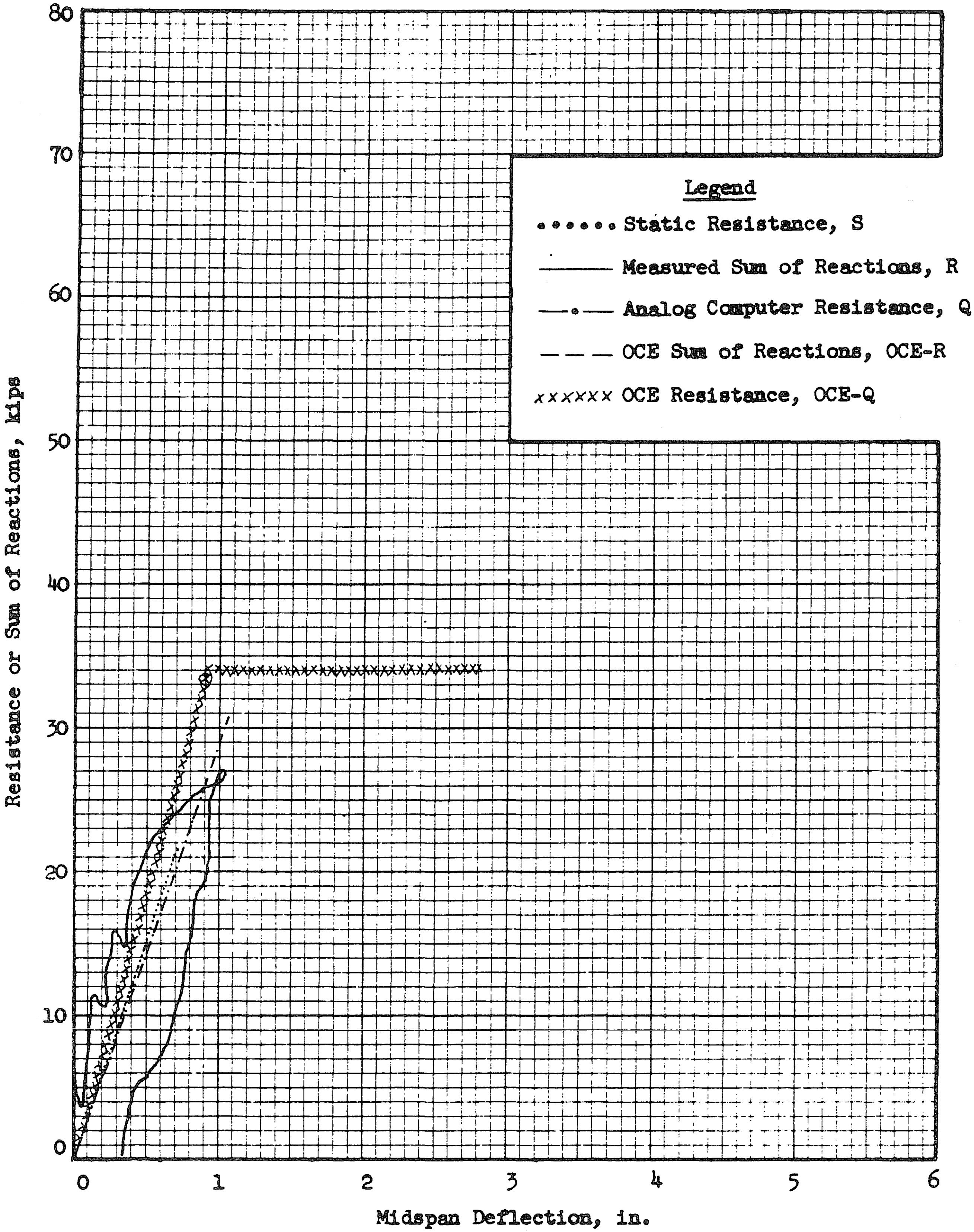

FIG. A120 RESISTANCE AND REACTION VS. DEFLECTION
BEAM 5b4, BLOW 1

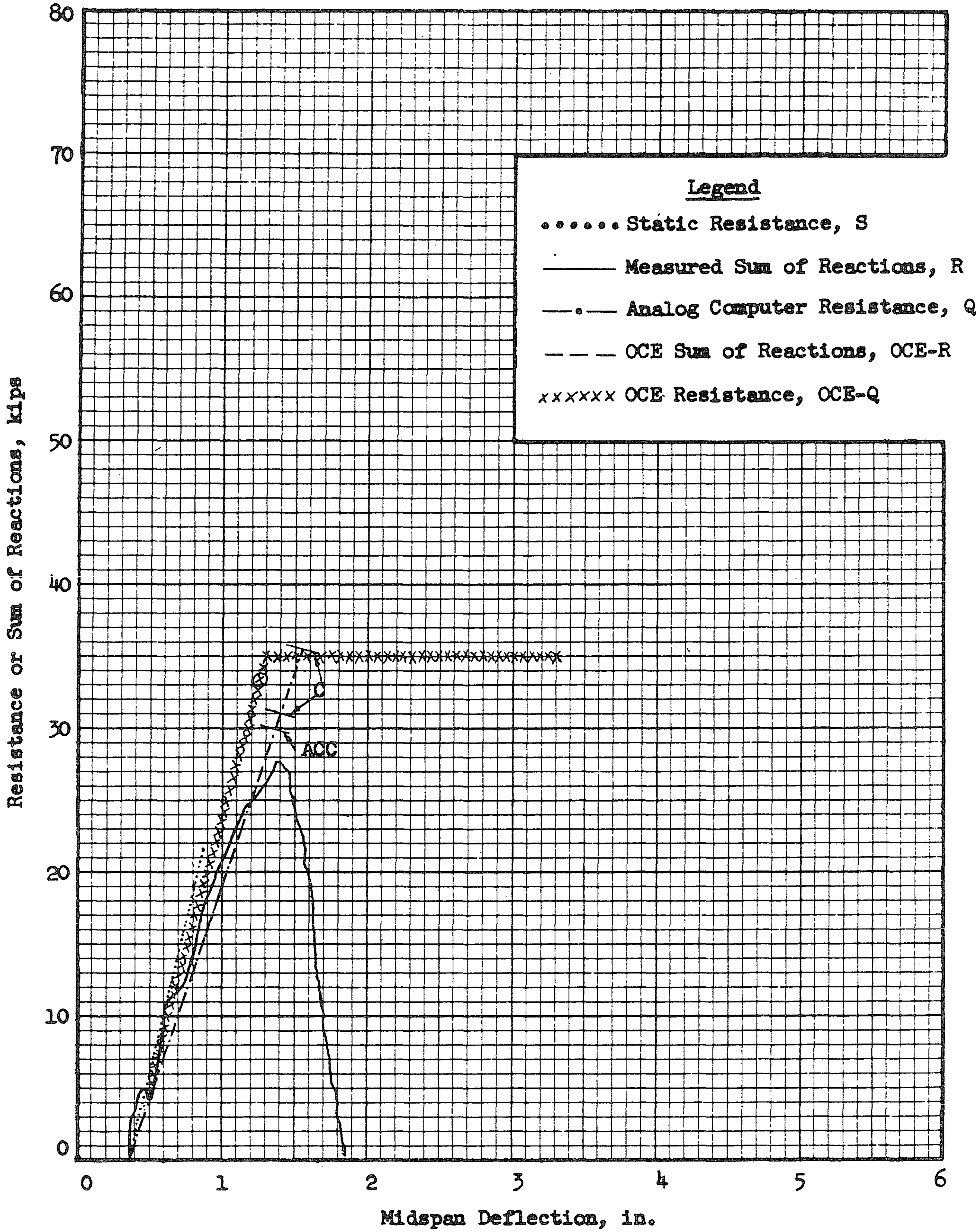

FIG. A121 RESISTANCE AND REACTION VS. DEFLECTION
BEAM 5b4, BLOW 2

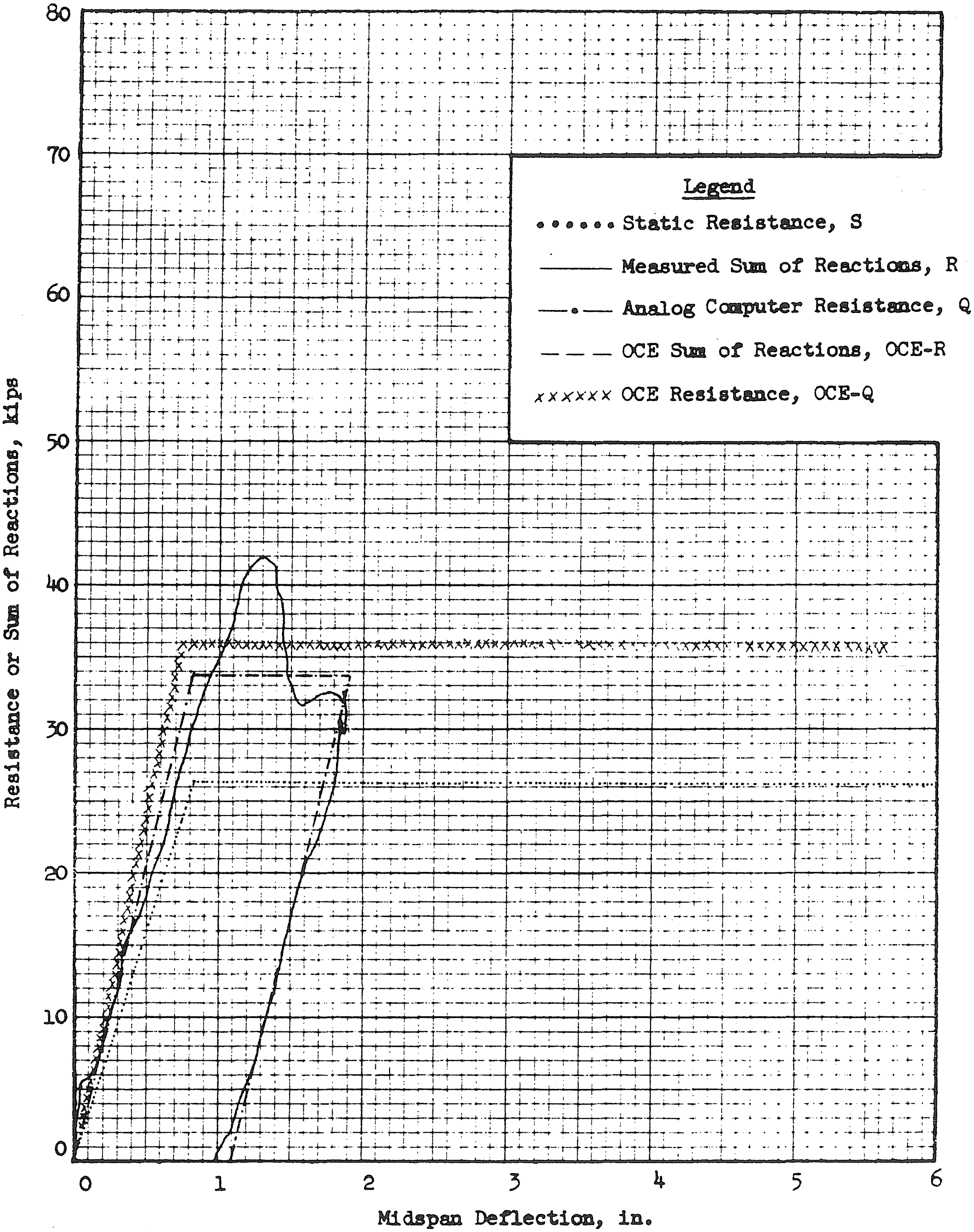

FIG. A122 RESISTANCE AND REACTION VS. DEFLECTION
BEAM 6a1, BLOW 1

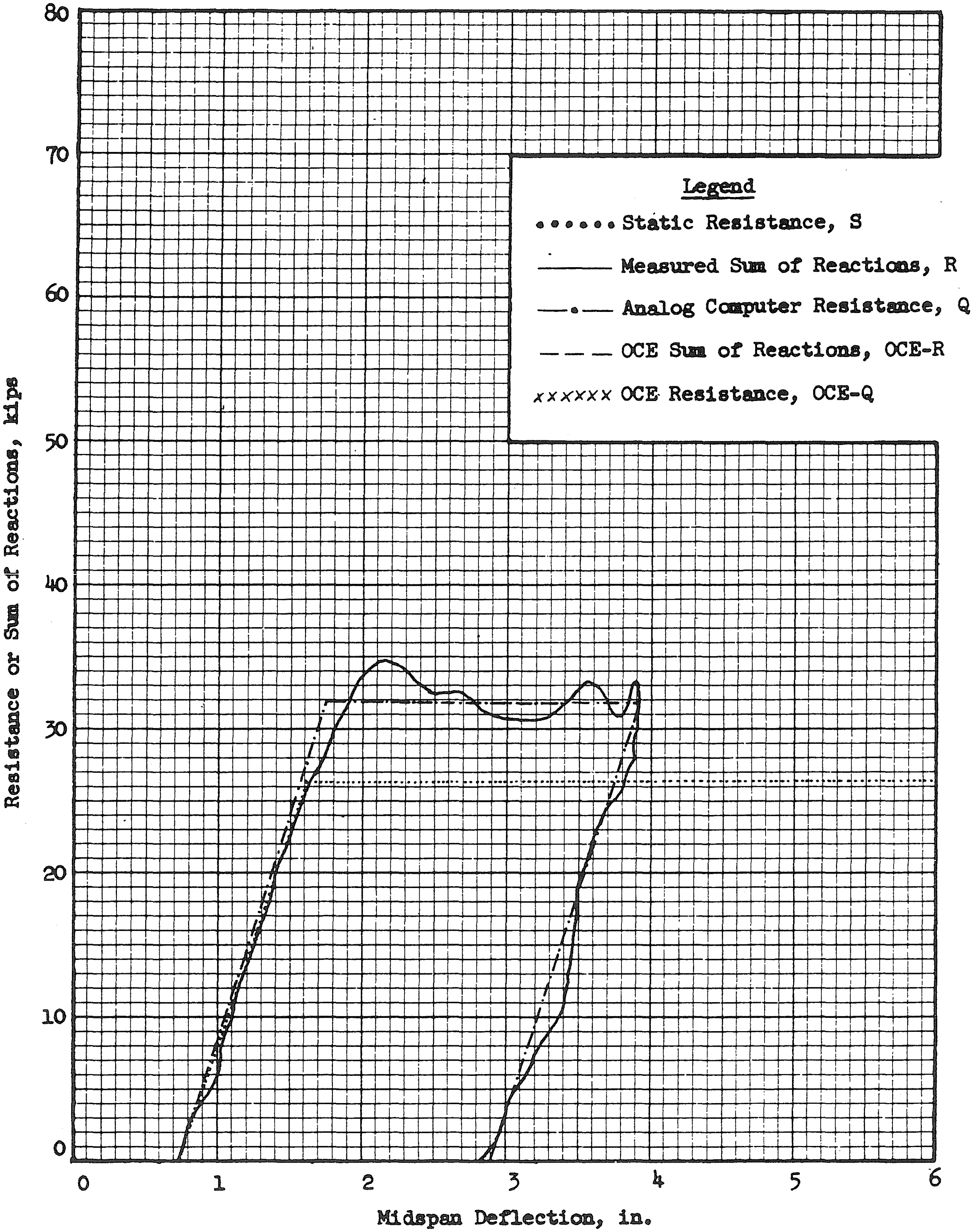

FIG. A123 RESISTANCE AND REACTION VS. DEFLECTION
BEAM 6a1, BLOW 2

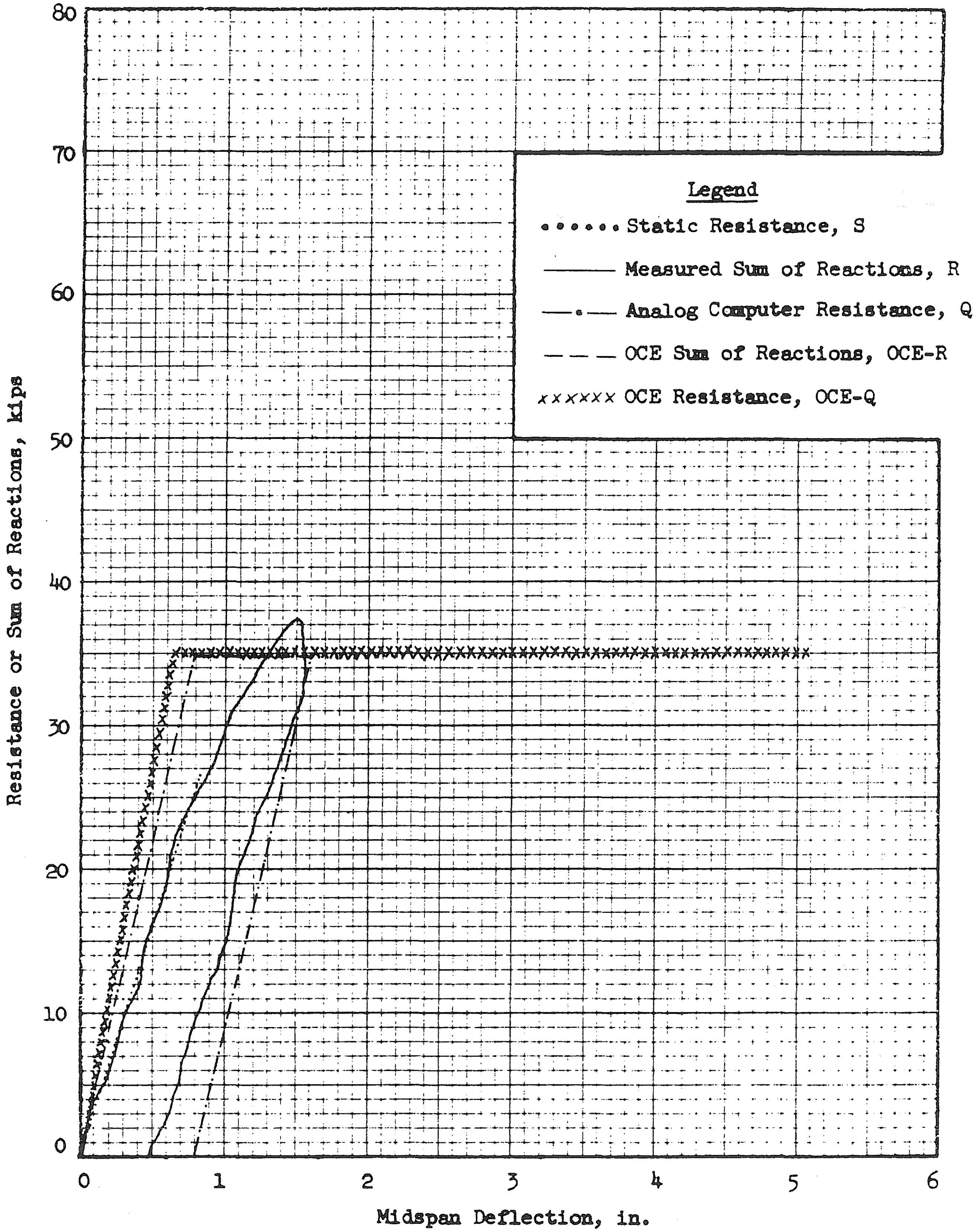

FIG. A124 RESISTANCE AND REACTION VS. DEFLECTION
BEAM 6b2, BLOW 1

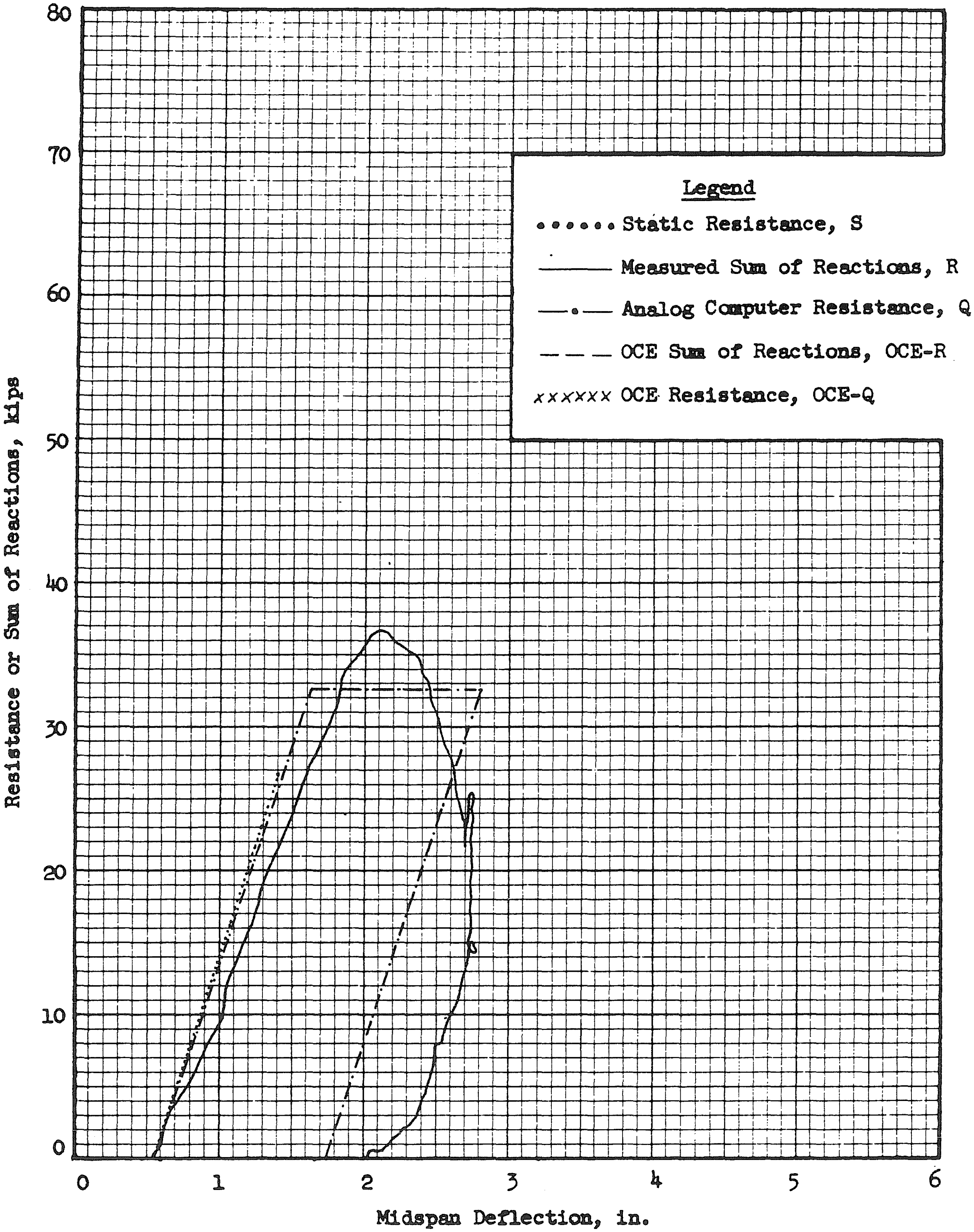

FIG. A125 RESISTANCE AND REACTION VS. DEFLECTION
BEAM 6b2, BLOW 2

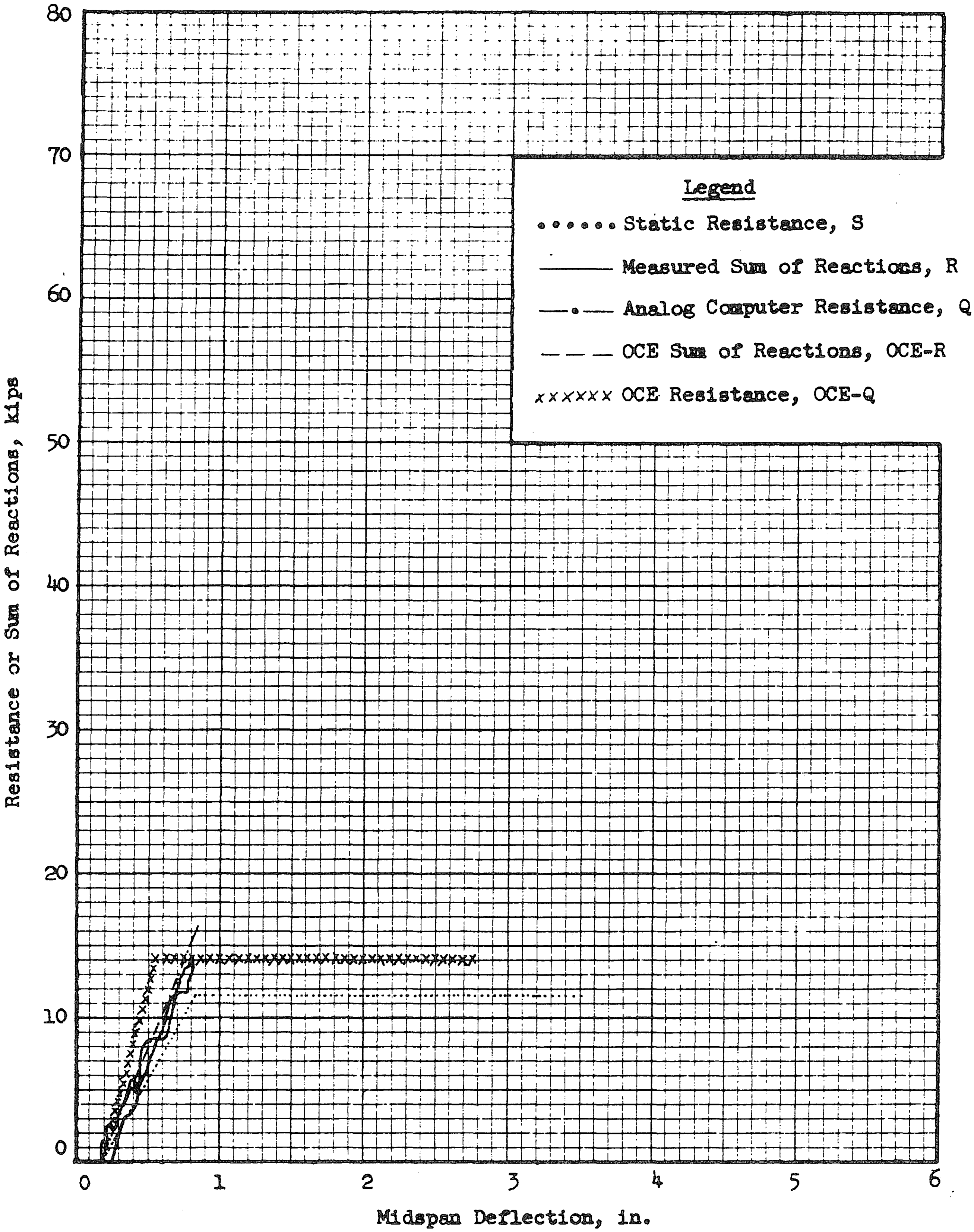

FIG. A126 RESISTANCE AND REACTION VS. DEFLECTION
BEAM 7a2, BLOW 1

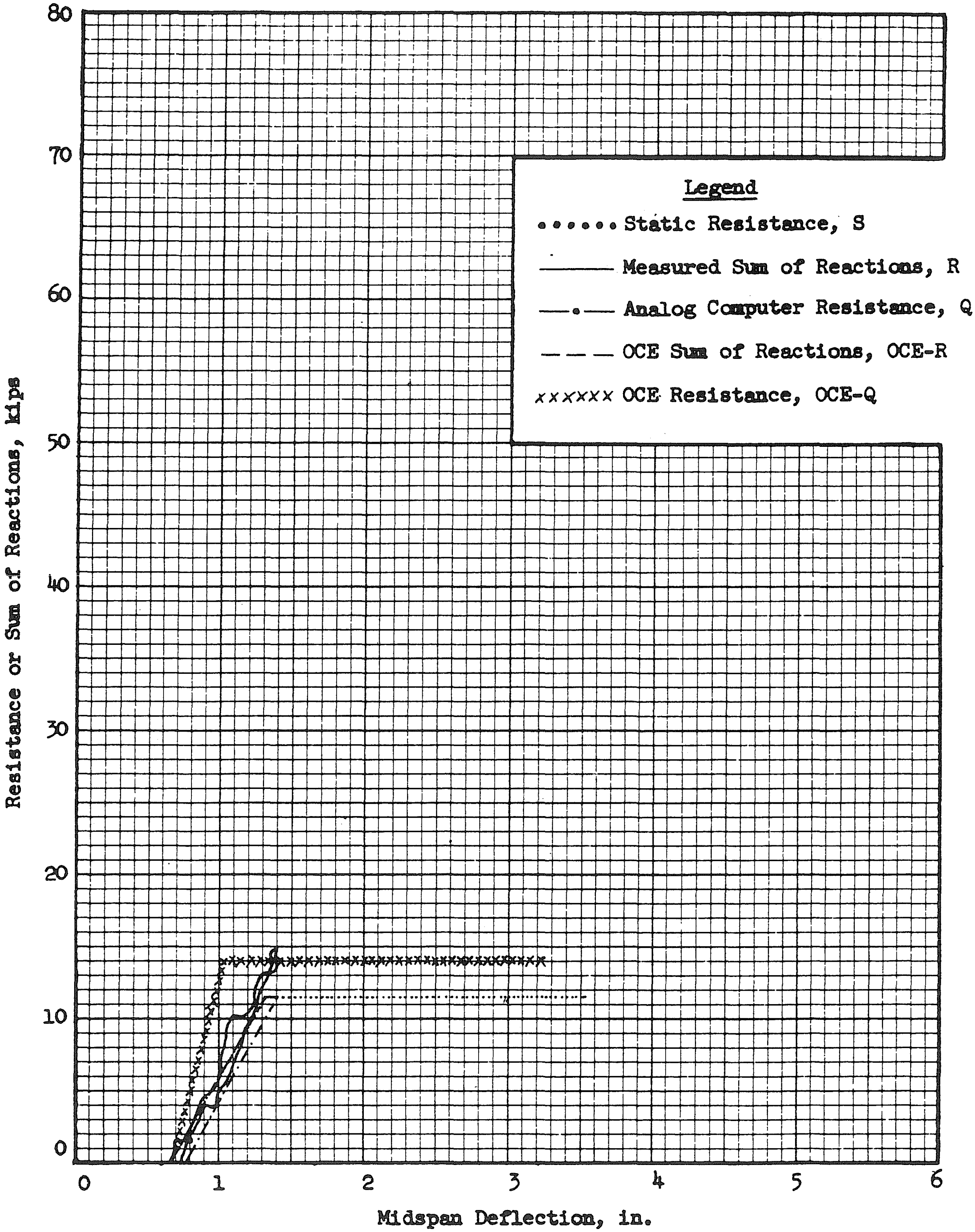

FIG. A127 RESISTANCE AND REACTION VS. DEFLECTION
BEAM 7a2, BLOW 2

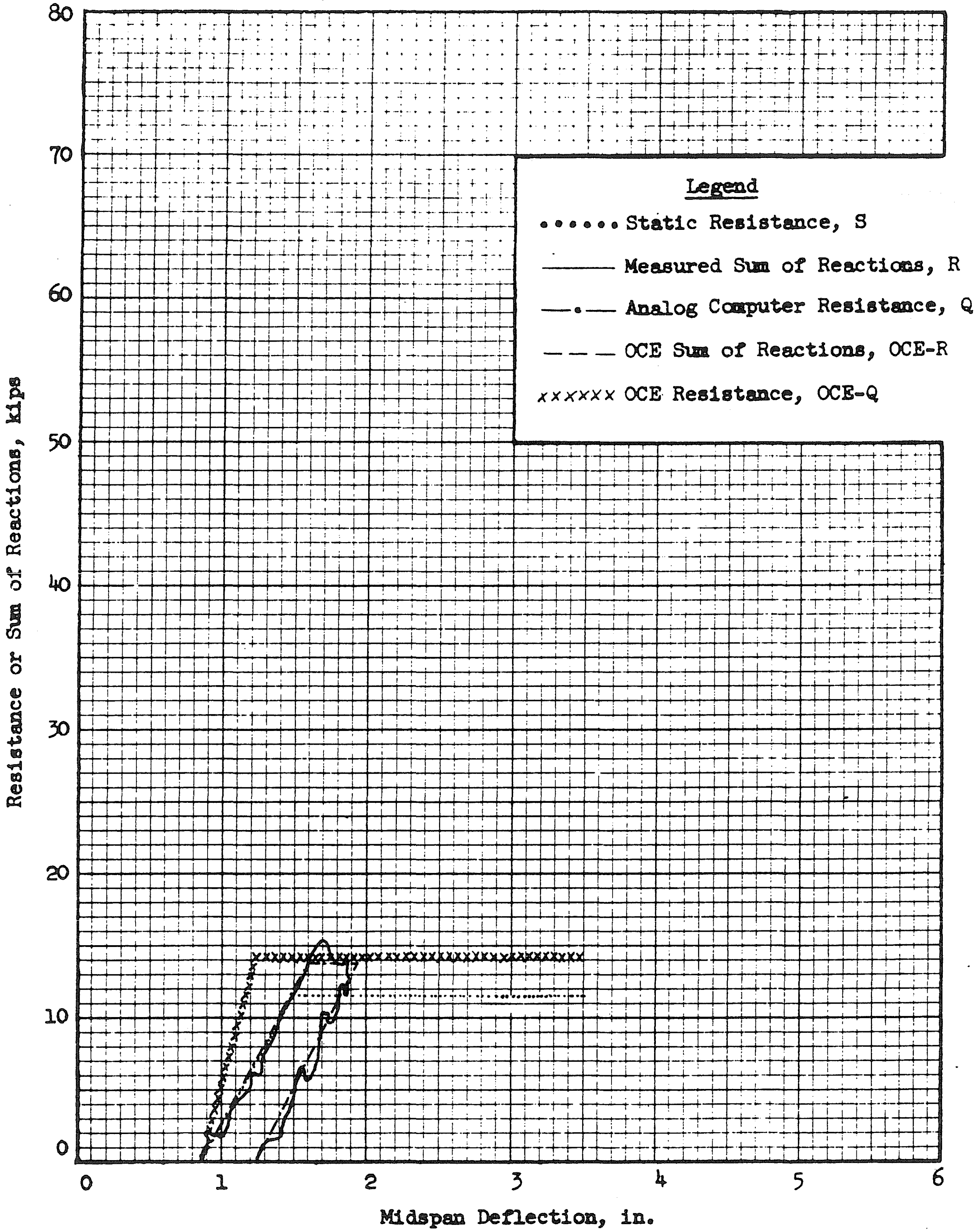

FIG. A128 RESISTANCE AND REACTION VS. DEFLECTION
BEAM 7a2, BLOW 3

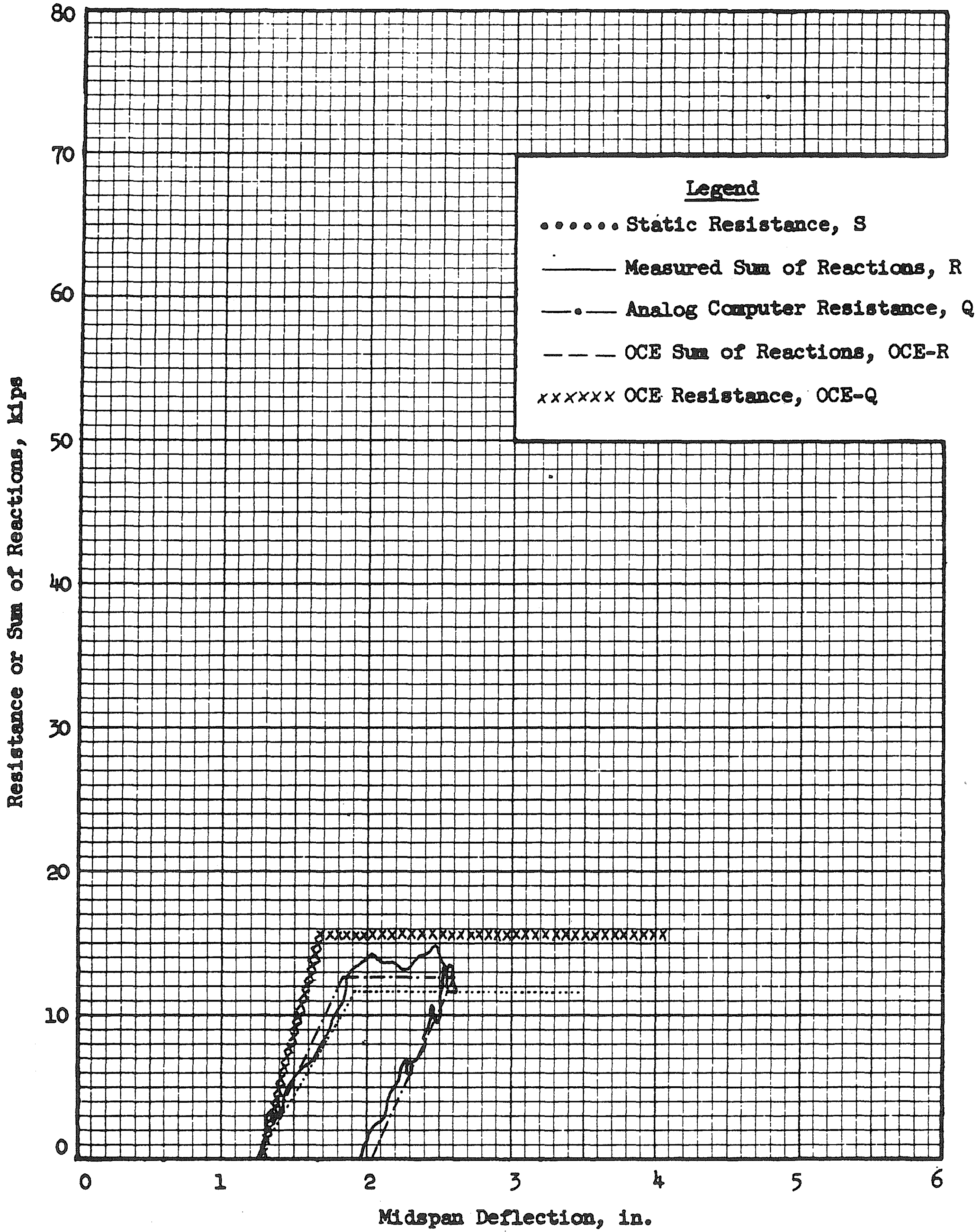

FIG. A129 RESISTANCE AND REACTION VS. DEFLECTION
BEAM 7a2, BLOW 4

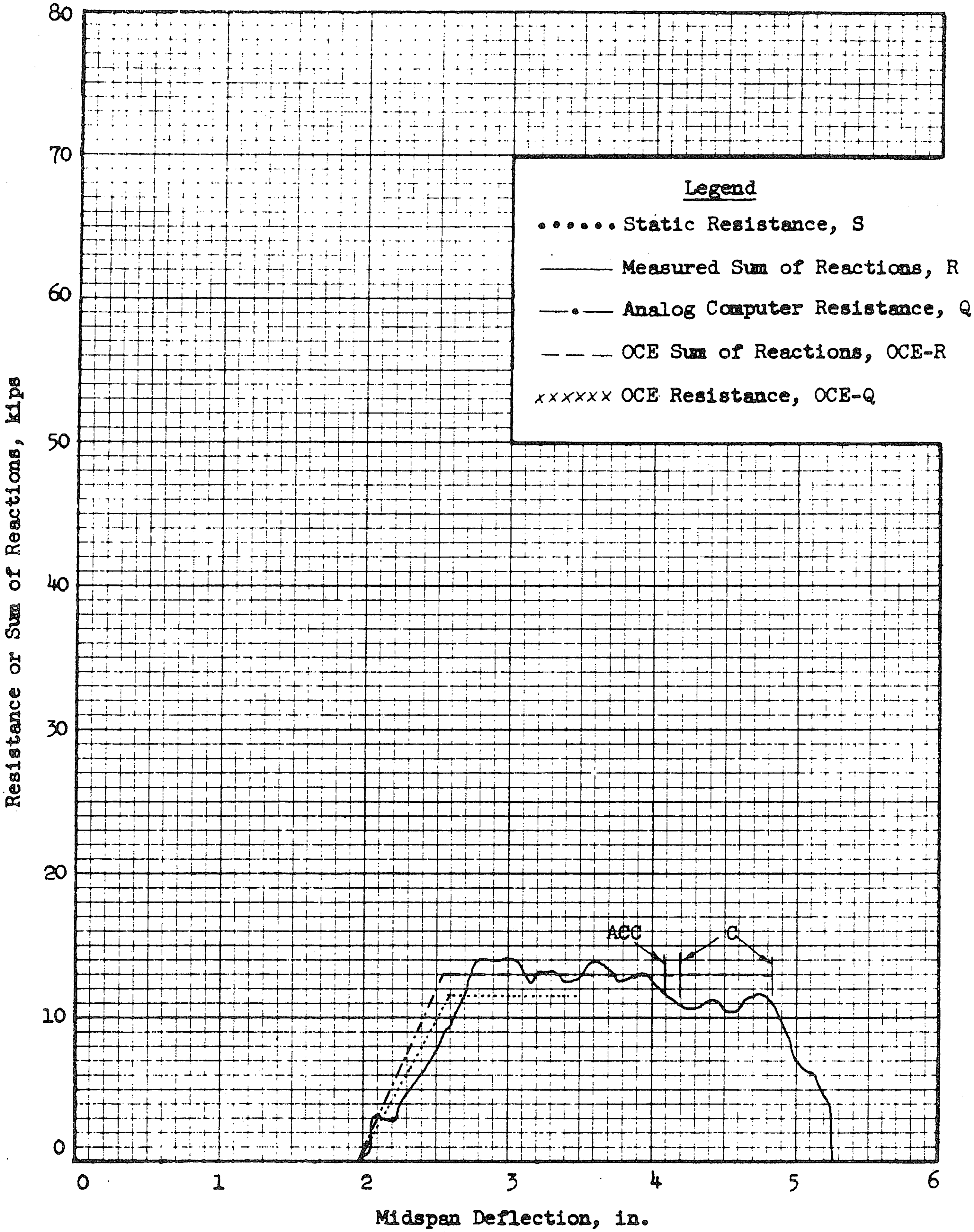

FIG. A130 RESISTANCE AND REACTION VS. DEFLECTION
BEAM 7a2, BLOW 5

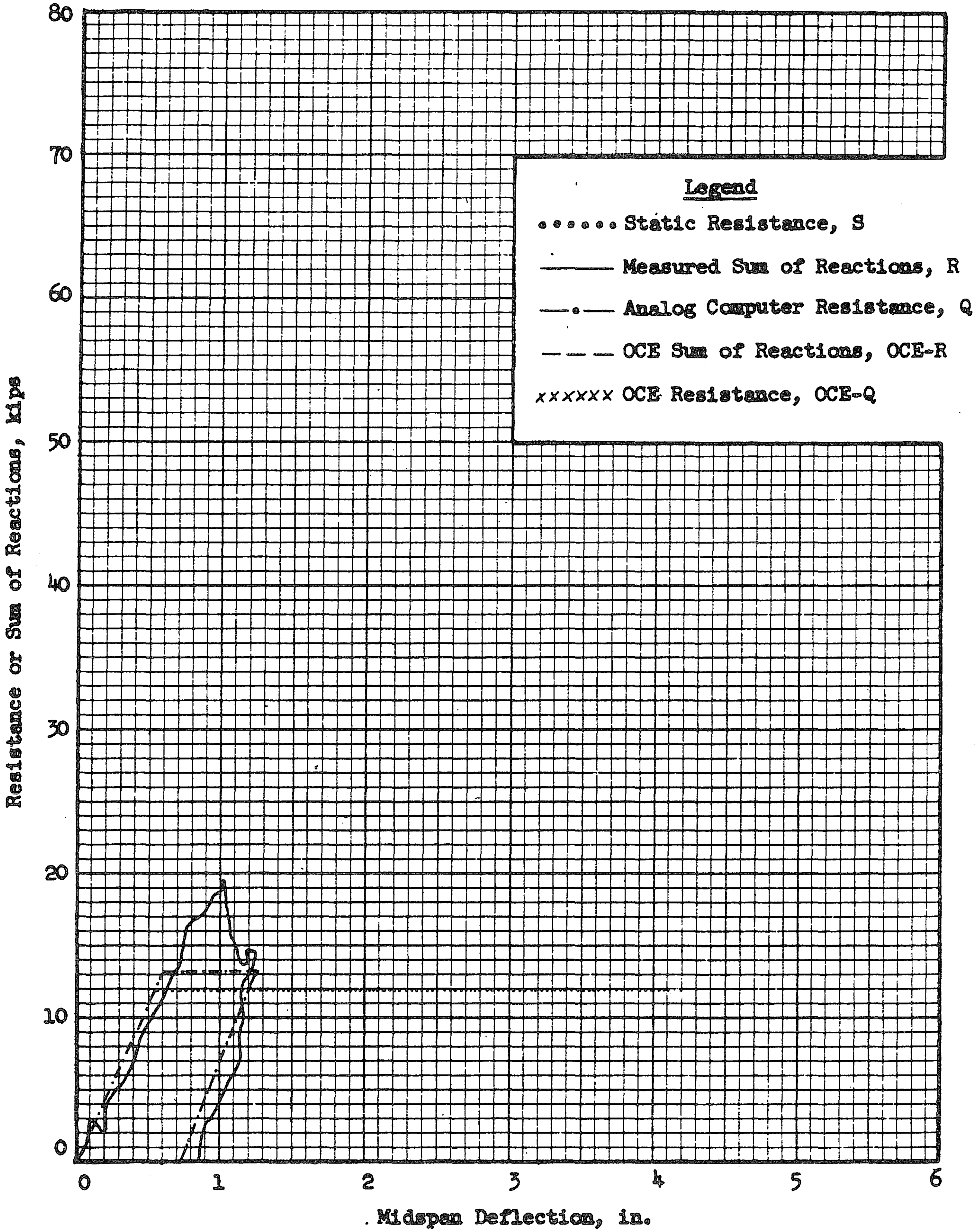

FIG. A131 RESISTANCE AND REACTION VS. DEFLECTION
BEAM 7a3, BLOW 1

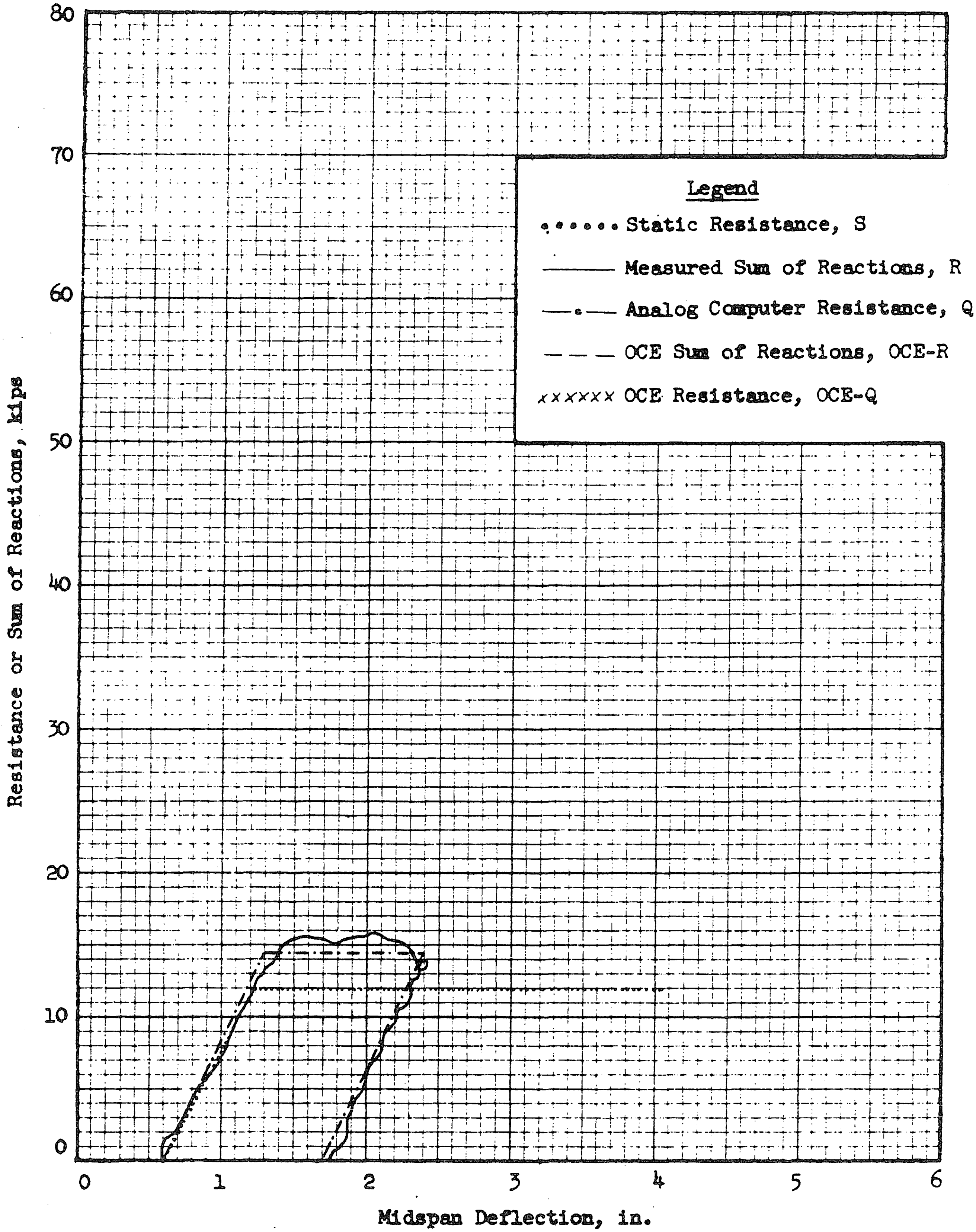

FIG. A132 RESISTANCE AND REACTION VS. DEFLECTION
BEAM 7a3, BLOW 2

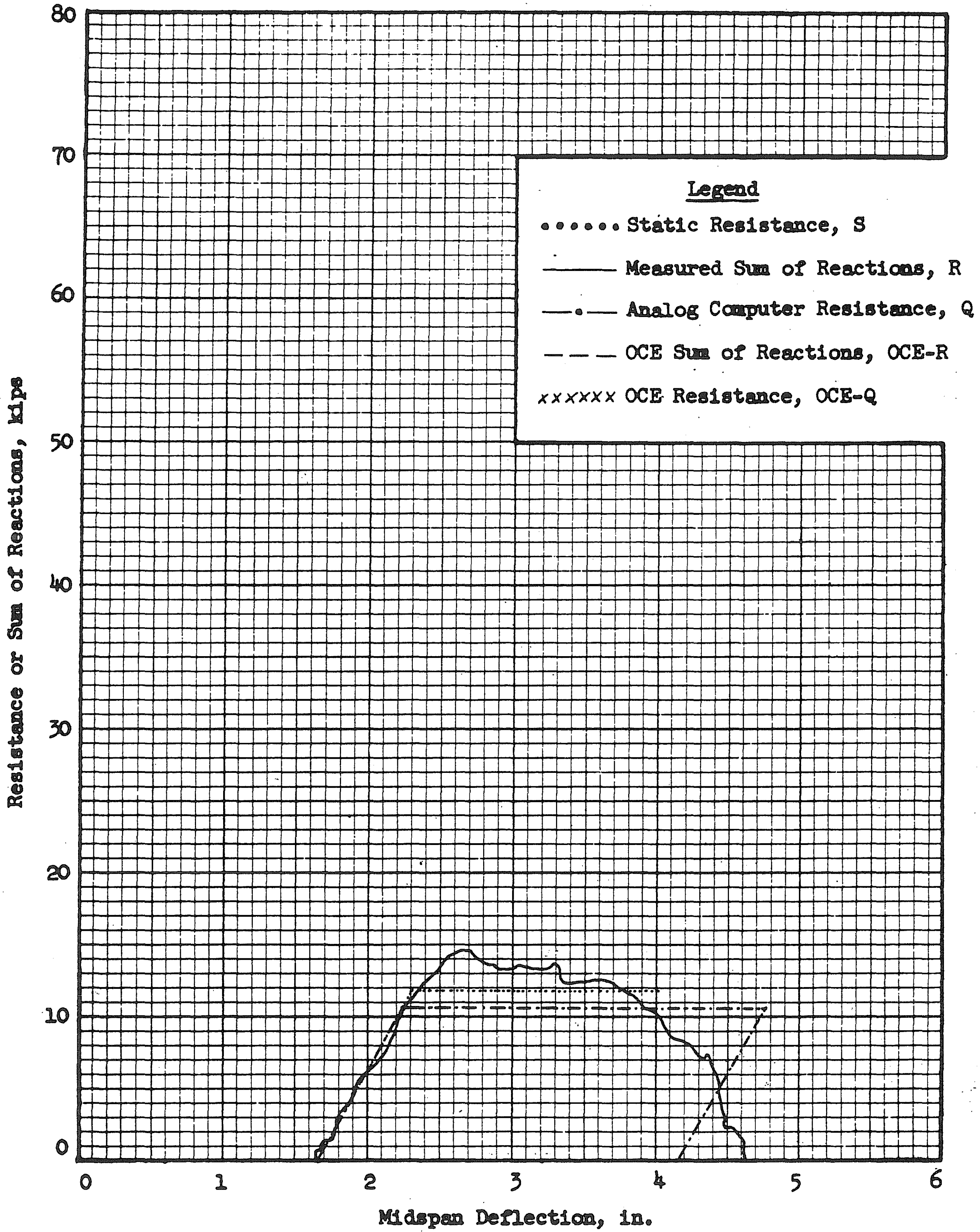

FIG. A133 RESISTANCE AND REACTION VS. DEFLECTION
BEAM 7a3, BLOW 3

DISTRIBUTION LIST FOR BLAST AND SHOCK R&D REPORTS

REVISED: 1 Aug 60

ADDRESSEE	NO OF CYS
ARMY	
Chief of Research and Development, DA, Washington 25, D.C., ATTN: Atomic Division	1
Chief of Engineers, DA, Washington 25, D.C., ATTN: ENGNB	1
Chief of Engineers, DA, Washington 25, D.C., ATTN: ENGEB	1
Commanding General, U. S. Continental Army Command, Ft. Monroe, Va.	1
President, U. S. Army Air Defense Board, Ft. Bliss, Texas	1
Commandant, Command & General Staff College, Ft. Leavenworth, Kansas, ATTN: Archives	1
Commandant, U. S. Army Air Defense School, Ft. Bliss, Texas, ATTN: Command & Staff Dept.	1
Director, Special Weapons Development, Hq CONARC, Ft. Bliss, Texas, ATTN: Chester I. Peterson	1
Commanding General, The Engineer Center, Ft. Belvoir, Va., ATTN: Asst. Commandant, Engineer School	1
Commanding Officer, Engineer Research & Development Lab., Ft. Belvoir, Va., ATTN: Chief, Tech. Support Branch	1
Commanding Officer, Transportation Research Command, Ft. Eustis, Va., ATTN: Chief, Tech. Information Div.	1
Commanding Officer, USA Signal R&D Lab., Ft. Monmouth, N. J., ATTN: Technical Documents Center, Evans Area	1
Commanding Officer, Chemical Warfare Lab., Army Chemical Center, Md., ATTN: Tech. Library	1
Director, Waterways Experiment Station, P. O. Box 631, Vicksburg, Miss. ATTN: Library	1
NAVY	
Director of Naval Intelligence, DN, Wash. 25, D.C., ATTN: OP-922V	1
Chief, Bureau of Ships, DN, Washington 25, D.C., ATTN: Code 372	1
Chief, Bureau of Ships, DN, Washington 25, D.C., ATTN: Code 423	1
Chief, Bureau of Yards & Docks, DN, Wash. 25, D.C., ATTN: D-400	1
Chief, Bureau of Yards & Docks, DN, Wash. 25, D.C., ATTN: D-440	1
Chief of Naval Research, DN, Wash. 25, D.C., ATTN: Code 811	1
Commander-in-Chief, U. S. Pacific Fleet, FPO, San Francisco, Calif.	1

ADDRESSEE	NO OF CYS
NAVY (Cont'd)	
Commander-in-Chief, U. S. Atlantic Fleet, U. S. Naval Base, Norfolk 11, Va.	1
Commandant of the Marine Corps, DN, Wash. 25, D.C., ATTN: Code A03H	4
President, U. S. Naval War College, Newport, R. I.	1
Superintendent, U. S. Naval Postgraduate School, Monterey, Calif.	1
Commanding Officer, Nuclear Weapons Training Center, Atlantic, Naval Base, Norfolk 11, Va., ATTN: Nuclear Warfare Dept.	1
Commanding Officer, U. S. Naval Schools Command, U. S. Naval Station, Treasure Island, San Francisco, Calif.	1
Commanding Officer, Nuclear Weapons Training Center, Pacific, Naval Station, North Island, San Diego 35, Calif.	2
Commanding Officer, U. S. Naval Damage Control Training Center, Naval Base, Philadelphia 12, Pa., ATTN: ABC Defense Course	1
Commanding Officer & Director, U. S. Naval Civil Engineering Lab., Port Hueneme, Calif., ATTN: Code L31	1
Director, U. S. Naval Research Lab., Washington 25, D.C.	1
Commanding Officer, U. S. Naval Radiological Defense Laboratory, San Francisco, Calif., ATTN: Tech. Information Division	1
Commanding Officer & Director, David W. Taylor Model Basin, Wash. 7, D. C., ATTN: Library	1
AIR FORCE	
Hq USAF (AFTAC) Washington 25, D.C.	1
Director of Research & Development, DCS/D, Hq USAF, Washington 25, D.C. ATTN: Guidance & Weapons Division	1
Air Force Intelligence Center, Hq USAF, ACS/I (AFCIN-3K2), Wash. 25, D.C.	1
Commander-in-Chief, Strategic Air Command, Offutt AFB, Nebraska, ATTN: OAWS	1
Commander, Tactical Air Command, Langley AFB, Va., ATTN: Document Security Branch	1
Director, Air University Library, Maxwell AFB, Alabama	2
Commander, Wright Air Development Center, Wright-Patterson AFB, Ohio ATTN: WCOSI	1

DIST LIST FOR BLAST &
SHOCK R&D REPORTS

ADDRESSEE AIR FORCE (Cont'd)	NO OF CYS
Commander, AF Special Weapons Center, Kirtland AFB, New Mexico, ATTN: Tech. Information Office	1
Commandant, USAF Institute of Technology, Wright-Patterson AFB, Ohio, ATTN: MCLI-ITRIDL	1
Commander, Ballistic Systems Division (BSD), P. O. Box 262, Inglewood, Calif.	1
Director, USAF Project RAND, Via: U. S. Air Force Liaison Office, The RAND Corporation, 1700 Main Street, Santa Monica, Calif.	1
Director of Civil Engineering, Hq USAF, Washington 25, D.C., ATTN: AFOCE	1
OTHERS	
Director of Defense Research & Engineering, Wash. 25, D. C., ATTN: Tech. Library	1
U. S. Documents Officer, Office of the United States National Military Representative-SHAPE, APO 55, New York, N. Y.	1
Commander-in-Chief, Pacific, Fleet Post Office, San Francisco, Calif.	1
Director, Weapons Systems Evaluation Group, OSD, Room 1E880, The Pentagon, Washington 25, D.C.	1
Commandant, Armed Forces Staff College, Norfolk 11, Va., ATTN: Library	1
Commander, Field Command, DASA, Sandia Base, Albuquerque, New Mexico	16
Commander, Field Command, DASA, Sandia Base, Albuquerque, New Mexico ATTN: Training Division	2
Chief, Defense Atomic Support Agency, Washington 25, D.C.	5
Commandant, Army War College, Carlisle Barracks, Pa., ATTN: Library	1
Commandant, National War College, Washington 25, D.C., ATTN: Class Rec. Library	1
Commandant, The Industrial College of the Armed Forces, Ft. McNair, Washington 25, D.C.	1
Officer-in-Charge, US Naval School, Civil Engineering Corps Officers, US Naval Construction Battalion, Port Hueneme, California.	1
Chief, Classified Technical Library, Technical Information Service, U.S. Atomic Energy Commission, Washington 25, D.C., ATTN: Mrs. Jean O'Leary	1

ADDRESSEE	OTHERS(Cont'd)	NO OF CYS
Dr. Robert J. Hansen, Division of Industrial Cooperation, Massachusetts Institute of Technology, 77 Massachusetts Ave., Cambridge, Mass.		1
Dr. Bruce G. Johnston, The University of Michigan, University Research Security Office, Lobby 1, East Engineering Bldg., Ann Arbor, Michigan		1
Sandia Corporation, Sandia Base, Albuquerque, New Mexico, ATTN: Classified Document Division (For M.L. Merritt)		1
Dr. Nathan M. Newmark, University of Illinois, Room 111, Talbot Lab., Urbana, Illinois		1
Commander, ASTIA, Arlington Hall Station, Arlington 12, Va., ATTN: TIPDR		15
Holmes & Narver Inc., AEC Facilities Division, 849 S. Broadway, Los Angeles 14, California.		1